UNIVERSIDADE FEDERAL DE JUIZ DE FORA - UFJF

INSTITUTO DE CIÊNCIAS EXATAS - ICE

PROGRAMA DE PÓS-GRADUAÇÃO EM FÍSICA

Alexander Bonila Rivera

Testing the fundamental physical properties of relic neutrinos using cosmological data

Juiz de Fora

2022

Alexander Bonila Rivera

Testing the fundamental physical properties of relic neutrinos using cosmological data

Tese apresentada ao Programa de Pós-Graduação em Física da Universidade Federal de Juiz de Fora, na área de física teórica, como requisito parcial para obtenção do título de Doutor em Física.

Orientador: Prof. Dr. Everton M. C. Abreu

Coorientador: Prof. Dr. Jorge Ananias Neto

Juiz de Fora

2022

Ficha catalográfica elaborada através do Modelo Latex do CDC da UFJF
com os dados fornecidos pelo(a) autor(a)

Bonilla Rivera, Alexander.

Testing the fundamental physical properties of relic neutrinos using cosmological data / Alexander Bonila Rivera. – 2022.

314 f. : il.

Orientador: Prof. Dr. Everton M. C. Abreu

Coorientador: Prof. Dr. Jorge Ananias Neto

Tese (Doutorado) – Universidade Federal de Juiz de Fora - UFJF, Instituto de Ciências Exatas - ICE. Programa de Pós-Graduação em Física, 2022.

1. Cosmic Neutrino Background. 2. Cosmological Lepton Asymmetry. 3. Cosmic Microwave Background. 4. Large Scale Structure. 5. Big Bang Nucleosyntesis. M. C. Abreu, Everton, orient. II. Neto, Jorge, A., coorientador. III. Título.

Alexander Bonilla Rivera

"Testing the fundamental physical properties of relic neutrinos using cosmological data"

Tese apresentada ao Programa de Pós-Graduação em Física da Universidade Federal de Juiz de Fora como requisito parcial à obtenção do título de Doutor em Física. Área de concentração: Física.

Aprovada em 20 de setembro de 2022.

BANCA EXAMINADORA

Prof. Dr. Everton Murilo Carvalho de Abreu - Orientador

Universidade Federal Rural do Rio de Janeiro

Prof. Dr. Jorge Ananias Neto - Coorientador

Universidade Federal de Juiz de Fora

Prof. Dr. Rafael da Costa Nunes

Universidade Federal do Rio Grande do Sul

Prof. Dr. Edesio Miguel Barboza Junior

Universidade do Estado do Rio Grande do Norte

Prof. Dr. Albert Carlo Rodrigues Mendes

Universidade Federal de Juiz de Fora

Prof. Dr. Gil de Oliveira Neto

Universidade Federal de Juiz de Fora

Juiz de Fora, 16/09/2022.

Documento assinado eletronicamente por **Everton Murilo Carvalho de Abreu**, **Usuário Externo**, em 20/09/2022, às 18:52, conforme horário oficial de Brasília, com fundamento no § 3º do art. 4º do Decreto nº 10.543, de 13 de novembro de 2020.

Documento assinado eletronicamente por **Edesio Miguel Barboza Junior**, **Usuário Externo**, em 20/09/2022, às 19:06, conforme horário oficial de Brasília, com fundamento no § 3º do art. 4º do Decreto nº 10.543, de 13 de novembro de 2020.

Documento assinado eletronicamente por **Jorge Ananias Neto**, **Professor(a)**, em 20/09/2022, às 19:07, conforme horário oficial de Brasília, com fundamento no § 3º do art. 4º do Decreto nº 10.543, de 13 de novembro de 2020.

Documento assinado eletronicamente por **Albert Carlo Rodrigues Mendes**, **Professor(a)**, em 20/09/2022, às 19:45, conforme horário oficial de Brasília, com fundamento no § 3º do art. 4º do Decreto nº 10.543, de 13 de novembro de 2020.

Documento assinado eletronicamente por **Rafael da Costa nunes**, **Usuário Externo**, em 21/09/2022, às 11:52, conforme horário oficial de Brasília, com fundamento no § 3º do art. 4º do Decreto nº 10.543, de 13 de novembro de 2020.

Documento assinado eletronicamente por **Gil de Oliveira Neto**, **Professor(a)**, em 21/09/2022, às 13:56, conforme horário oficial de Brasília, com fundamento no § 3º do art. 4º do Decreto nº 10.543, de 13 de novembro de 2020.

A autenticidade deste documento pode ser conferida no Portal do SEI-Ufjf (www2.ufjf.br/SEI) através do ícone Conferência de Documentos, informando o código verificador **0951741** e o código CRC **37BB0540**.

Dedico este trabalho em memória do meu pai Eduardo Bonilla Afanador
†23 Oct 2020

AGRADECIMENTOS

Em primeiro lugar, gostaria de agradecer ao meu amigo e colega Rafael Da Costa Nunes que me convidou para fazer parte deste programa de pós-graduação e a quem devo muito da orientação no início da minha carreira científica. Aos meus orientadores na UFJF e a UFRRJ, Jorge Ananias e Everton Abreu, pelos ensinamentos, incentivo e amizade. Agradeço a toda a minha família e amigos, de quem tenho recebido grande apoio nesta odisseia. A todos os funcionários e professores do programa de pós-gradução em física da UFJF. A todos os professores que tive em minha vida que contribuíram de forma direta ou indireta para minha formação. A cidade de Juiz de Fora e aos vários colegas que fiz aqui. Impossível lembrar e listar todos aqui, então fica aqui meu agradecimento a todos que conheci pelos bons momentos. Aos membros da banca que aceitaram o convite para participar dessa ocasião importante na minha formação profissional. A CAPES e FAPEMIG pela financiamento.

"The most incomprehensible thing about the universe is that it is comprehensible."

Albert Einstein

RESUMO

Nesta tese, investigamos as restrições observacionais no fundo de neutrinos cósmicos (CNB) dado pelo cenário estendido Λ CDM (Λ CDM $+N_{eff} + \sum m_\nu + c^2_{eff} + c^2_{vis} + \xi_\nu$), usando os últimos dados observacionais de *Planck* CMB (espectro de potência de temperatura, baixa polarização e reconstrução de lentes), oscilações acústicas bariônicas (BAOs), o novo valor local recente da constante de Hubble do *Telescópio Espacial Hubble* (*HST*) e informações da abundância de aglomerados de galáxias (GCs). Nós estudamos as restrições no background do CNB usando dados CMB + BAO + *HST* com e sem os dados de GC. Encontramos $\Delta N_{eff} = 0,614 \pm 0,26$ com um nível de confiança de 68 por cento quando os dados de GC são adicionados na análise. Não encontramos desvio significativo para a velocidade do som no quadro de repouso CNB. Também analisamos o caso particular Λ CDM $+N_{eff} + \sum m_\nu + \xi_\nu$ com os dados observacionais. Nesse cenário, encontramos $\Delta N_{eff} = 0,60 \pm 0,28$ a um nível de confiança de 68 por cento. Em ambos os cenários, não foram encontrados desvios médios para o parâmetro de degenerescência. Por outro lado, consideramos uma assimetria cosmológica leptônica na forma de neutrinos e impomos novas sensibilidades esperadas sobre tal assimetria através do parâmetro de degenerescência (ξ_ν) usando alguns configurações futuras do experimento CMB, como CORE e CMB-S4. Tomando o cenário padrão com três estados de neutrino, encontramos $\xi_\mu = 0,05 \pm 0,10\,(\pm\,0,04)$, de CORE (CMB-S4) em 95 por cento CL, respectivamente. Além disso, dentro deste cenário, avaliamos a escala de massa dos neutrinos, obtendo que o esquema de massa da hierarquia normal é privilegiado. Nossos resultados são uma atualização sobre a assimetria cosmológica leptônica e a escala de massa de neutrino neste contexto, a partir da qual pode trazer uma perspectiva sobre a hipótese nula para ξ_ν (e seus efeitos em ΔN_{eff}), onde talvez, ξ_ν pode assumir um valor não nulo de até 95 por cento CL de experiências futuras, como CMB-S4. Finalmente, consideramos a possibilidade de testar novas partículas leves termalizadas e também restringir possíveis interações de nova física de neutrinos de Dirac. Muitos modelos de neutrinos de Dirac que visam abordar a estabilidade de Dirac, a pequenez das massas de neutrinos ou a assimetria matéria-antimatéria do nosso Universo conferem os parceiros de quiralidade destros ν_R com interações adicionais que podem termalizá-los, como é o caso dos bósons Z' ultraleves. Discutimos modelos bem motivados para $U(1)_{B-L}$, através da medida do número efetivo de graus de liberdade relativísticos no Universo primitivo, N_{eff}. Consideramos uma extensão do modelo padrão de cosmologia, tipo ΛCDM + Σm_ν + $M_z^{'}$, onde $M_z^{'}$ é a massa do bóson Z'. Usando diferentes testes observacionais, descobrimos que $\sum m_\nu < 0.32$ eV, $M_{z'} < 17.2$ GeV and $m^{\rm eff}_{\nu,{\rm sterile}} < 0.47$ eV, que está dentro dos limites de estudos anteriores, incluindo os resultados de 2018 da colaboração *Planck*. Além disso, comparamos a sensibilidade do SPT-3G, Observatório Simons e CMB-S4 a outros experimentos, em particular o LHC.

Key-words: Fundo Cósmico Neutrino. Lepton Asymmetry. Fundo Cósmico de Microondas. bósons ultraleves.

ABSTRACT

In this thesis we investigate the observational constraints on the cosmic neutrino background (CNB) given by the extended ΛCDM scenario (ΛCDM $+N_{eff} + \sum m_\nu + c^2_{eff} + c^2_{vis} + \xi_\nu$) using the latest observational data from *Planck* CMB (temperature power spectrum, low-polarisation and lensing reconstruction), baryon acoustic oscillations (BAOs), the new recent local value of the Hubble constant from *Hubble Space Telescope* (*HST*) and information of the abundance of galaxy clusters (GCs). We study the constraints on the CNB background using CMB + BAO + *HST* data with and without the GC data. We find $\Delta N_{eff} = 0.614 \pm 0.26$ at 68 per cent confidence level when the GC data are added in the analysis. We do not find significant deviation for sound speed in the CNB rest frame. We also analyze the particular case ΛCDM $+N_{eff} + \sum m_\nu + \xi_\nu$ with the observational data. Within this scenario, we find $\Delta N_{eff} = 0.60 \pm 0.28$ at 68 per cent confidence level. In both the scenarios, no mean deviations are found for the degeneracy parameter. On the other hand, We consider a cosmological lepton asymmetry in the form of neutrinos and impose new expected sensitivities on such asymmetry through the degeneracy parameter (ξ_ν) by using some future CMB experiment configurations, such as CORE and CMB-S4. Taking the default scenario with three neutrino states, we find $\xi_\mu = 0.05 \pm 0.10\,(\pm 0.04)$, from CORE (CMB-S4) at 95 percent CL, respectively. Also, within this scenario, we evaluate the neutrino mass scale, obtaining that the normal hierarchy mass scheme is privileged. Our results are an update concerning on the cosmological lepton asymmetry and the neutrino mass scale within this context, from which can bring a perspective on the null hypothesis for ξ_ν (and its effects on ΔN_{eff}), where perhaps, ξ_ν may take a non-null value up to 95 percent CL from future experiments such as CMB-S4. Finally, we consider the possibility of testing new thermalized light particles and also constraints possible new-physics interactions of Dirac neutrinos. Many Dirac-neutrino models that aim to address the Dirac stability, the smallness of neutrino masses, or the matter–anti-matter asymmetry of our Universe confer the right-handed chirality partners ν_R with additional interactions that can thermalize them, which is the case of ultralight Z' bosons. We discuss well-motivated models for ν_R interactions such as gauged $U(1)_{B-L}$, through measure of the effective number of relativistic degrees of freedom in the early Universe, N_{eff}. We consider an extension of the standard model of cosmology, type ΛCDM + Σm_ν + $M_z^{'}$, where $M_z^{'}$ is the mass of the Z' boson. Using different observational tests, we found that $\sum m_\nu < 0.32$ eV, $M_{z'} < 17.2$ GeV and $m^{\rm eff}_{\nu,\rm sterile} < 0.47$ eV, which is within the limits of previous studies, including the 2018 results of the *Planck* collaboration. Furthermore, we compare the sensitivity of SPT-3G, Simons Observatory, and CMB-S4 to other experiments, in particular the LHC.

Key-words: Cosmic Neutrino Background. Lepton Asymmetry. Cosmic Microwave Background. ultralight bosons.

List of Publications

List of publications by the present author up to the date of submission of the thesis in chronological order. Total of 24 articles published, 10 as first author and current h-index = 13. This thesis is based on investigations [2], [10] and [15].

1. *Report of the Topical Group on Cosmic Probes of Fundamental Physics for Snowmass 2021.* Rana X. Adhikari et al. (**Alexander Bonilla**). (Sep 23, 2022). e-Print: 2209.11726 [hep-ph]

2. *Unveiling the nature of Dirac's neutrinos in light of the latest cosmological evidence: The case for dark radiation and PBH.* **Alexander Bonilla**. Send to Symmetry MDPI, Special Issue "Neutrino Physics and Symmetry".

3. *Cosmology with the Laser Interferometer Space Antenna (LISA).* LISA Cosmology Working Group. Pierre Auclair et al. (**Alexander Bonilla**) (Apr 11, 2022), e-Print: 2204.05434 [astro-ph.CO]

4. *Cosmology Intertwined: A Review of the Particle Physics, Astrophysics, and Cosmology Associated with the Cosmological Tensions and Anomalies.* Elcio Abdalla, Guillermo Franco Abellán, Amin Aboubrahim, Adriano Agnello, Ozgur Akarsu, et al. (**Alexander Bonilla**), (Mar 11, 2022) Contribution to: 2022 Snowmass Summer Study, e-Print: 2203.06142 [astro-ph.CO]

5. *Astrophysics with the Laser Interferometer Space Antenna (LISA).* LISA Astrophysics Working Group. Pau Amaro-Seoane, Jeff Andrews, Manuel Arca Sedda, Abbas Askar, Razvan Balasov, et al. (**Alexander Bonilla**), (Mar 11, 2022), e-Print: 2203.06016 [astro-ph.CO]

6. *Inferring $S_8(z)$ and $\gamma(z)$ with cosmic growth rate measurements using machine learning.* Felipe Avila, Armando Bernui, **Alexander Bonilla**, Rafael C. Nunes (Jan 19, 2022), e-Print: 2201.07829 [astro-ph.CO]

7. *Reconstruction of the dark sectors' interaction: A model-independent inference and forecast from GW standard sirens.* **Alexander Bonilla**(Juiz de Fora U.), Suresh Kumar(Kurukshetra U.), Rafael C. Nunes(Sao Jose, INPE), Supriya Pan(Presidency U., Kolkata), MNRAS, Volume 512, Issue 3, May 2022, Pages 4231–4238, e-Print: 2102.06149 [astro-ph.CO]

8. *Measurements of H0 and reconstruction of the dark energy properties from a model-independent joint analysis.* **Alexander Bonilla**, Suresh Kumar, Rafael C. Nunes (Nov 13, 2020). Published in: Eur.Phys.J.C 81 (2021) 2, 127, e-Print: 2011.07140 [astro-ph.CO]

9. *Forecasts on the speed of gravitational waves at high z.* **Alexander Bonilla**(Juiz

de Fora U.), Rocco D'Agostino(Naples U. and INFN, Naples), Rafael C. Nunes(Sao Jose, INPE), José C.N. de Araujo(Sao Jose, INPE) (Oct 12, 2019). Published in: JCAP 03 (2020) 015, e-Print: 1910.05631 [gr-qc]

10. *Cosmological considerations in Kaniadakis statistics.* Everton M.C. Abreu, Jorge Ananias Neto, Albert C.R. Mendes, **Alexander Bonilla**, Rodrigo M. de Paula (Dec 4, 2018). Published in: EPL 124 (2018) 3, 30003

11. *Forecast on lepton asymmetry from future CMB experiments.* **Alexander Bonilla**(Juiz de Fora U.), Rafael C. Nunes(Sao Jose, INPE), Everton M.C. Abreu(Rio de Janeiro Federal U. and Juiz de Fora U. and UFRJ, Rio de Janeiro) (Oct 15, 2018). Published in: Mon.Not.Roy.Astron.Soc. 485 (2019) 2, 2486-2491, e-Print: 1810.06356 [astro-ph.CO]

12. *Tsallis' entropy, modified Newtonian accelerations and the Tully-Fisher relation.* Everton M.C. Abreu(Rio de Janeiro Rural U. and Juiz de Fora U. and Rio de Janeiro Federal U.), Jorge Ananias Neto(Juiz de Fora U.), Albert C.R. Mendes(Juiz de Fora U.), **Alexander Bonilla**(Juiz de Fora U.), Rodrigo M. de Paula(Juiz de Fora U.) (Apr 14, 2018). Published in: EPL 124 (2018) 3, 30005, e-Print: 1804.06723 [hep-th]

13. *Constraints On Dark Energy Models From Galaxy Clusters and Gravitational Lensing Data.* **Alexander Bonilla**, Jairo E. Castillo (Nov 25, 2017). Published in: Universe 4 (2018) 1, 21, e-Print: 1711.09291 [astro-ph.CO]

14. *Accelerated cosmos in a nonextensive setup.* H. Moradpour(RIAAM, Maragha), **Alexander Bonilla**(Juiz de Fora U.), Everton M. C. Abreu(Juiz de Fora U. and Rio de Janeiro Rural U.), Jorge Ananias Neto(Juiz de Fora U.) (Nov 19, 2017). Published in: Phys.Rev.D 96 (2017) 12, 123504, e-Print: 1711.08338 [physics.gen-ph]

15. *Tsallis and Kaniadakis statistics from a point of view of the holographic equipartition law.* Everton M. C. Abreu, Jorge Ananias Neto, Albert C. R. Mendes, **Alexander Bonilla** (Nov 17, 2017). Published in: EPL 121 (2018) 4, 45002, e-Print: 1711.06513 [gr-qc]

16. *Probing the properties of relic neutrinos using the cosmic microwave background, the Hubble Space Telescope and galaxy clusters.* Rafael C. Nunes(Juiz de Fora U.), **Alexander Bonilla**(Juiz de Fora U.) (Oct 27, 2017). Published in: Mon.Not.Roy.Astron.Soc. 473 (2018) 4, 4404-4409, e-Print: 1710.10264 [astro-ph.CO]

17. *Holographic Dark Energy from Fluid/Gravity Duality Constraint by Cosmological Observations.* Behnam Pourhassan(Damghan U.), **Alexander Bonilla**(Juiz de Fora U.), Mir Faizal(Lethbridge U.), Everton M. C. Abreu(Juiz de Fora U. and Rio de Janeiro Rural U.) (Apr 6, 2017). Published in: Phys.Dark Univ. 20 (2018) 41-48, e-Print: 1704.03281 [hep-th]

18. *Observational Constraints on f(T) gravity from varying fundamental constants.* Rafael C. Nunes(Juiz de Fora U.), **Alexander Bonilla**(Distrital U., Bogota), Supriya Pan(IISER, Kolkata, Mohanpur), Emmanuel N. Saridakis(Baylor U. and Natl. Tech. U., Athens and Valparaiso U., Catolica) (Aug 5, 2016). Published in: Eur.Phys.J.C 77 (2017) 4, 230, e-Print: 1608.01960 [gr-qc]

19. *Exploring the Dark Universe: constraints on dynamical Dark Energy models from CMB, BAO and growth rate measurements.* **Alexander Bonilla Rivera**(Juiz de Fora U.), Jorge Enrique García-Farieta(Colombia, U. Natl.) (May 6, 2016). Published in: Int.J.Mod.Phys.D 28 (2019) 09, 1950118, e-Print: 1605.01984 [astro-ph.CO]

20. *Theoretical Foundations of PGWs Printed in the CMB and its Observational Status.* **Alexander Bonilla Rivera** (Jan 14, 2016). Contribution to: Second Workshop on Numerical and Observational Astrophysics, e-Print: 1601.03789 [astro-ph.CO]

21. *Constraints On Holographic Cosmological Models From Gamma Ray Bursts.* **Alexander Bonilla Rivera**, Jairo Ernesto Castillo Hernandez (Jan 2, 2016). Published in: Adv.Stud.Theor.Phys. 10 (2016) 33-43, e-Print: 1601.00183 [astro-ph.CO]

22. *Constraints on Holographic cosmologies from strong lensing systems.* Victor H. Cardenas(Valparaiso U.), **Alexander Bonilla**(Valparaiso U.), Veronica Motta(Valparaiso U.), Sergio del Campo(Valparaiso U., Catolica) (Oct 30, 2013). Published in: JCAP 11 (2013) 053, e-Print: 1310.8251 [astro-ph.CO]

23. *Cosmic slowing down of acceleration using fgas.* Victor H. Cardenas, Carla Bernal, **Alexander Bonilla** (Jun 4, 2013). Published in: Mon.Not.Roy.Astron.Soc. 433 (2013) 3534, e-Print: 1306.0779 [astro-ph.CO]

24. *Observación de lentes gravitatorias con ALMA.* **A. Bonilla** (Valparaiso U.), O. Toloza (Valparaiso U.), I. Fuentes (Valparaiso U.), V. Motta (Valparaiso U.). Published in: Bol.A.A.Astron. 54 (2011), 385-388

list of Figures

List of Figures

list of tables

List of Tables

List of Symbols

Certain symbols have more than one meaning, which depends on the context. These symbols are marked by "(context)"

a	Scale factor/scale-independent bias factor (context)
a_{lm}	Coefficients of the decomposition of Θ in spherical harmonics
a_{nr}	Scale factor at z_{nr}
a_0	Scale factor today (usually normalized to 1)
A_L	Phenomenological parameter governing the amplitude of CMB lensing
A_L	Amplitude of primordial scalar power spectrum
b	Galaxy bias
b_{auto}	Galaxy bias in auto-correlation
b_{cb}	Galaxy bias defined with respect to the cold dark matter+baryons fieldn
b_{cross}	Galaxy bias in cross-correlation
B_{ij}	Bayes factor of model i with respect to model j
b_m	Galaxy bias defined with respect to the total matter field
c	Scale-dependent bias factor in cross-correlation
c_s	Speed of sound
C_l^{BB}	CMB B-mode polarization anisotropy angular power spectrum
C_l^{EE}	CMB E-mode polarization anisotropy angular power spectrum
C_l^{TE}	CMB temperature-E-mode polarization anisotropy angular cross-power spectrum
C_l^{TT}	CMB temperature anisotropy angular power spectrum
$C_l^{\mathcal{K}g}$	CMB lensing convergence-galaxy angular cross-power spectrum
$C_l^{\phi\phi}$	CMB lensing potential power spectrum
c_ν	Neutrino speed
$\mathcal{C}$	Collision operator
d	Scale-dependent bias factor in auto-correlation
$\mathbf{d}$	Data
d_R^i	Right-handed down quark singlet
d_V	Volume distance
$d\sigma_T/d\Omega$	Thomson scattering differential cross section
D_l	$l(l+1)C_l$
e_R^i	Right-handed electron singlet
$\mathcal{E}(\mathbf{d})$	Bayesian evidence/marginal likelihood
$E(z)$	Normalized expansion rate $E(z) = H(z)/H_0$
f	Distribution function
f_{cb}	Growth rate of the cold dark matter+baryons power spectrum
f_m	Growth rate of the matter power spectrum
f_ν	Fraction of the matter density parameter in neutrinos $f_\nu = \Omega_\nu/\Omega_m$

g_i	Internal degrees of freedom of species i
g_*	Effective number of relativistic degrees of freedom
g_*^s	Effective number of entropy degrees of freedom
G_f	Fermi constant
$G_{\mu\nu}$	Einstein tensor
h	Reduced Hubble constant
$H(z)$	Hubble parameter at a given redshift z
H_0	Hubble parameter up today (Hubble constant)
K	FLRW metric curvature
k	wavenumber
k_{eq}	wavenumberof perturbation entering the horizon at z_{eq}
k_{fs}	Neutrino free-streaming wavenumber
k_n	Wavenumber of the n-th CMB acoustic peak
k_{nr}	Wavenumber of perturbation entering the horizon at z_{nr}
k_{sd}	Wavenumber at which scale-dependent bias becomes important
$L_L^{\hat{\imath}}$	Left-handed lepton doublet
$L_R^{\hat{\imath}}$	Rigth-handed lepton doublet
$\mathcal{L}$	Liouville operator
$\mathcal{L}(d \mid \theta)$	Likelihood
$\mathcal{L}_{SM}$	Liouville operator
l	Multipole
l_n	Multipole of the n-th CMB acoustic peak
m_i	Mass of species i
m_{ligth}	Mass of lightest neutrino eigenstate
m_s^{eff}	Effective sterile neutrino mass
$\sum m_\nu$	Sum of the three active neutrino masses
n_e	Number density of free electrons
n_i	Number density of species i
n_{run}	Running of the scalar spectral index $dn_s/dlnk$
n_s	Tilt of primordial scalar power spectrum (scalar spectral index)
N_{eff}	Effective number of relativistic degrees of freedom
N_*	Number of e-folds of cosmic inflation
p	Momentum/probability (context)
$p(\theta \mid d)$	Posterior distribution
$P_{cb}(k)$	Cold dark matter+baryons power spectrum
P_i	Pressure of species i
$P(k)$	Matter power spectrum
$P_g(k)$	Galaxy power spectrum
$P_{HF\nu}(k)$	Non-linear power spectrum from **Halofit** calibrated to massive neutrinos

$P_{mg}(k)$	Matter-galaxy cross-power spectrum
$P_{prim}(k)$	Primordial power spectrum of matter fluctuations
$P_{\mathcal{R}}(k)$	Primordial power spectrum of $\mathcal{R}$
$\mathcal{P}_{\mathcal{R}}$	Dimensionless primordial power spectrum of $\mathcal{R}$
P^{shot}	Shot noise
$\mathcal{P}_{\theta}$	Prior distribution
$Q_L^{\hat{\imath}}$	Left-handed quark doublet
R	Baryon-to-photon momentum density ratio
r	Tensor-to-scalar ratio evaluated at the pivot scale $k = 0.05\ Mpc^{-1}$
r_d	Damping scale
r_{fs}	Neutrino free-streaming horizon
r_s	Comoving sound horizon
s_i	Entropy density of species i
t	Time
T	Temperature of the Universe (photon temperature)
T_{CMB}	CMB temperature today
$T(k)$	Transfer function
$T_{\mu\nu}$	Stress-energy tensor
T_{ν}	Effective neutrino temperature
$T_{\nu,dec}$	Neutrino decoupling temperature
u_R^i	Right-handed up quark singlet
U_{ij}	Pontecorvo–Maki–Nakagawa–Sakata matrix
w	Dark energy equation of state
w_0	Dark energy EoS today (CPL parametrization)
w_a	Minus derivative of DE EoS with respect to scale factor (CPL parametrization)
$W^{\mathcal{K}}$	Kernel for CMB lensing
Y_{lm}	Spherical harmonics
Y_p	Primordial Helium fraction
z	Redshift
z_{dec}	Redshift of decoupling
z_{drag}	Redshift of baryon drag
z_{eff}	Effective redshift
z_{eq}	Redshift of matter-radiation equality
z_{nr}	Redshift of neutrino non-relativistic transition
z_{re}	Redshift of reionization
z_{Λ}	Redshift of matter-Λ equality
Γ	Reaction rate
δ	Dirac Delta
δ_i	Overdensity of species i

Δm^2_{21}	Solar mass-squared splitting
$\lvert\Delta m^2_{31}\rvert$	Atmospheric mass-squared splitting
η	Baryon-to-photon ratio
θ	Parameter vector
θ_d	Angular size of the damping scale
θ_n	Angular size of the n-th CMB acoustic peak
θ_s	Angular size of the first CMB acoustic peak
Θ	CMB temperature anisotropies/Heaviside step function (context)
$\mathcal{K}$	CMB lensing convergence
λ	Wavelength
λ_{fs}	Neutrino free-streaming scale
Λ	Cosmological constant
ν_i	Neutrino mass eigenstates ($i = 1, 2, 3$)
ν_α	Neutrino flavour eigenstates ($\alpha = \mathrm{e}, \mu, \tau$)
$\xi(r)$	Galaxy 2-point correlation function
ρ_{crit}	Critical energy density of the Universe today
ρ_i	Energy density of species i
σ_T	Thomson scattering cross section
σ_8	Amplitude of matter fluctuations averaged on a sphere of radius 8 h^{-1} Mpc
τ	Optical depth to reionization
ϕ	Inflaton/gravitational potential/lensing potential/quintessence field (context)
Φ	Higgs doublet
χ	Comoving distance to a given redshift
χ_h	Comoving particle horizon at a given redshift
χ_*	Comoving distance to z_{dec}
Ψ	Gravitational potential
ω_b	Physical density parameter of baryons
ω_c	Physical density parameter of cold dark matter
ω_K	Physical density parameter associated to curvature
ω_m	Physical density parameter of matter
ω_r	Physical density parameter of radiation
ω_γ	Physical density parameter of photons
ω_ν	Physical density parameter of neutrinos
ω_Λ	Physical density parameter of Λ
Ω_b	Density parameter of baryons
Ω_c	Density parameter of cold dark matter
Ω_K	Density parameter associated to curvature
Ω_m	Density parameter of matter
Ω_r	Density parameter of radiation

Ω_γ	Density parameter of photons
Ω_ν	Density parameter of neutrinos
Ω_Λ	Density parameter of Λ

List of Abbreviations

BAO	Baryon Acoustic Oscillations
BBN	Big Bang Nucleosynthesis
BE	Bose-Einstein
BOSS	Baryon Oscillation Spectroscopic Survey
BSM	Beyond the Standard Model
CDM	Cold Dark Matter
CKM	Cabibbo-Kobayashi-Maskawa
C.L.	Confidence level
CMB	Cosmic Microwave Background
CνB	Cosmic Neutrino Background
CPL	Chevallier-Polarski-Linder
COBE	Cosmic Background Explorer
DDE	Dynamical dark energy
DE	Dark Energy
DES	Dark Energy Survey
DESI	Dark Energy Spectroscopic Instrument
DM	Dark Matter
DR	Data Release
DUNE	Deep Underground Neutrino Experiment
eBOSS	Extended Baryon Oscillation Spectroscopic Survey
EISW	Early integrated Sachs-Wolfe
EoS	Equation of state
EW	Electro-weak
FD	Fermi-Dirac
FIRAS	Far Infrared Absolute Spectrophotometer
FKP	Feldman-Kaiser-Peacock
FLRW	Friedmann-Lemaître-Robertson-Walker
GR	General Relativity
GW	Gravitational Wave
HFI	High Frequency Instrument
IO	Inverted neutrino mass ordering
ISW	Integrated Sachs-Wolfe
KamLAND	Kamioka Liquid Scintillator Antineutrino Detector
LFI	Low Frequency Instrument
LISW	Late integrated Sachs-Wolfe
LSS	Large-scale structure
LSST	Large Synoptic Space Telescope

MCMC	Markov Chain Monte Carlo
MGS	Main Galaxy Sample
MSW	Mikheyev-Smirnov-Wolfenstein
NISDB	Neutrino-induced scale-dependent bias
NO	Normal neutrino mass ordering
NOνA	Neutrinos at the main injector off-axis νe appearance
NPDDE	Non-phantom dynamical dark energy
PCA	Principal component analysis
PMNS	Pontecorvo-Maki-Nakagawa-Sakata
QCD	Quantum chromodynamics
RHN	Right Hand Neutrinos
RSD	Redshift-space distortions
SDSS	Sloan Digital Sky Survey
SM	Standard Model of Particle Physics/Cosmology
SNe1a	Type 1a Supernovae
SNO	Sudbury Neutrino Observatory
T2K	Tokai to Kamioka
UV	Ultraviolet
WFIRST	Wide Field Infrared Survey Telescope
WMAP	Wilkinson Microwave Anisotropy Probe
ΛCDM	Λ-cold dark matter (standard model of cosmology)
2dfGRS	2-degree field galaxy redshift survey
6dFGS	6-degree field galaxy survey

Contents

Chapter 1

Introduction

"I have done a terrible thing, I have postulated a particle that cannot be detected."
– Wolfgang Pauli (after having postulated the existence of the neutrino, 1930)

1.1. Dark Universe, neutrinos and lepton asymmetry

The existence of a cosmic neutrino background (CνB), which comprises the so-called relic neutrinos, is a consequence of the thermal history of the universe where the neutrinos decouple from the rest of the cosmic plasma at $k_B T \sim$ MeV and start streaming freely. Unlike the cosmic microwave background (CMB), the CνB is yet to be detected directly, and such a direct detection proves to be difficult [211]. However, indirect measures have been established by using CMB as well as estimations from the primordial abundances of light elements. Recently, Follin et al. [212] have interpreted data about damping of acoustic oscillations of the CMB and they have demonstrated a detection of the temporal phase shift generated by neutrino perturbations. This detection is the most model-independent determination of the existence of CνB. The properties the massive neutrinos play an important role in the dynamics of the universe, inferring direct changes in important cosmological sources and, consequently, in the determination of cosmological parameters; see [261, 282, 294] for reviews. The effects of the relic neutrinos on the CMB and LSS are only gravitational, as they are decoupled (free-streaming particles) at the time of recombination and structure formation. The standard parameters that characterize these effects on cosmological sources are the effective number of species $N_{\rm eff}$ and the total neutrino mass $\sum m_\nu$. *Planck* team [213], within the ΛCDM + $\sum m_\nu$ model has constrained $\sum m_\nu < 0.194$ eV (from the CMB alone), and $N_{\rm eff} = 3.04 \pm 0.33$ at 95 per cent confidence

level (CL). The value of $N_{\rm eff}$ via theoretical calculations is well determined within the framework of the standard model, namely $N_{\rm eff} = 3.046$ [295]. The evidence of any positive deviation from this value can be a signal that the radiation content of the Universe is not only due to photons and neutrinos, but also to some extra relativistic relics, the so-called dark radiation in the literature, and parametrized by $\Delta N_{\rm eff} = N_{\rm eff} - 3.046$. However, two phenomenological parameters $c^2_{\rm eff}$ and $c^2_{\rm vis}$ are also introduced to infer properties of the CνB. Here, $c^2_{\rm eff}$ is the sound speed in the CνB rest frame and $c^2_{\rm vis}$ is the viscosity parameter, which parameterizes the anisotropic stress. The evolution of standard neutrinos (non-interacting free-streaming neutrinos) is obtained for $c^2_{\rm eff} = c^2_{\rm vis} = 1/3$. The $C\nu B$ properties, including constraints on $c^2_{\rm eff}$ and $c^2_{\rm vis}$, have been investigated via different methods and approaches [214–222]. It is important to mention that these parametrizations were strongly inspired by pioneer works about dark matter properties [223, 224]. From the temperature power spectrum (TT), the temperature-polarization cross spectrum (TE), the polarization power spectrum (EE) + low-polarization (lowP) + baryon acoustic oscillations (BAOs), the *Planck* collaboration [213] has constrained $c^2_{\rm eff} = 0.3242 \pm 0.0059$ and $c^2_{\rm vis} = 0.31 \pm 0.037$. Recently, within the ΛCDM $+c^2_{\rm eff} + c^2_{\rm vis} + \sum m_\nu$ model, [222] have reported the constraints $c^2_{\rm eff} = 0.309 \pm 0.013$ and $c^2_{\rm vis} = 0.54^{+0.17}_{-0.18}$ at 95 per cent CL from CMB + lensing + BAO data. In general terms, measuring a deviation from $(c^2_{\rm eff}, c^2_{\rm vis}) = 1/3$ can refute the null hypothesis that the relic neutrinos are relativistic and free-streaming. Another natural extension of the physics properties of the neutrino is to consider a certain degree of lepton asymmetry (a cosmological leptonic asymmetry), which is usually parametrized by the so-called degeneracy parameter $\xi_\nu = u_\nu / T_{\nu 0}$ [282, 304, 308, 310, 311], where u_ν is the neutrino chemical potential and $T_{\nu 0}$ is the current temperature of the CνB, such that $T_{\nu 0}/T_{CMB} = (4/11)^{1/3}$. The leptonic asymmetry also shifts the equilibrium between protons and neutrons at the Big Bang Nucleosynthesis (BBN) epoch, leading to indirect effects on the CMB anisotropy through the primordial helium abundance Y_{He}. The effects of the massive neutrinos and a leptonic asymmetry on BBN and CMB have been investigated in many studies [225, 226, 260, 273, 288, 289, 291–293, 301, 319]. Recently, a leptonic asymmetric model of cosmological data are reported at 95 per cent CL by [273].

The lepton asymmetry of the Universe, represented by neutrinos and anti-neutrinos, is nowadays one of the most weakly constrained cosmological parameter. Although the baryon number asymmetry is well measured from CMB constraints concerning the baryon density, the lepton asymmetry could be larger by many orders of magnitude and not of the same order as expected by the Big Bang BBN considerations. The presence of a large lepton asymmetry can be considered as an excess of the neutrinos over anti-neutrinos or vice-versa, which can be a requirement due to the charge neutrality of the Universe. Also it might possibly be hidden in the $C\nu B$, and can have imprints on cosmological observations. For instance, from CMB anisotropy [275,301], the large neutrino asymmetries

have consequences in the early Universe phase transitions, cosmological magnetic fields and dark matter relic density (see [307, 309, 312] for more details). Other effects due to the lepton asymmetry can be considered as changes in the decoupling temperature of $C\nu B$ [285, 290], the time equivalence between the energy densities of radiation and matter, the production of primordial light elements at BBN [306], an excess in the contribution of the total radiation energy density and the expansion rate of the Universe [286], photon decoupling [293], among others. These changes can affect the evolution of the matter density perturbations in the Universe, which effect not only on the CMB anisotropies, but also the formation, evolution and distribution of the large scale structure (LSS) of the Universe [295]. The LSS formation is more sensitive to the neutrino masses than CMB. The formation of the structures is driven by the cosmic expansion and self-gravity of matter perturbations, both affected by the massive neutrinos. Nevertheless, the relic neutrinos slow down the growth of structures due to their high thermal speeds, leading to a suppression of the total matter power spectrum [264]. On the other hand, the gravitational lensing of CMB and the integrated Sachs-Wolf effect are also modified by the presence of massive neutrinos [261]. The effect of massive neutrinos in the nonlinear growth structure regime has recently been studied by [321]. The properties of neutrinos are very important in the determination of the dynamics of the Universe inferring direct effects on cosmological sources, and consequently the estimation of cosmological parameters (see [261, 277, 280, 282, 287, 294, 296, 297, 313–318, 320]). Finally, and more important for the present thesis, is to consider the aforementioned cosmological lepton symmetry, which is another natural extension of the neutrino physics properties. As we already mentioned, this property is usually parameterized by the degeneracy parameter $\xi_\nu = u_\nu/T_{\nu 0}$, where $T_{\nu 0} \approx 1.9K$ [282, 304, 308, 310, 311]. We can assign to chemical potentials a label of its eigenstates of mass, such that $\{u_i\}$ is for neutrinos and $\{-u_i\}$ for anti-neutrinos. If the neutrinos are Majorana particles, then they must have $u_i = 0$, otherwise neutrinos are Dirac fermions. Thus, evidence on the null hypothesis is needed to answer this question [298]. The difference between $\{\xi_i\}$ and $\{-\xi_i\}$ determines the asymmetry between the density of neutrinos and anti-neutrinos. Then, the presence of a relevant and non-zero ξ_ν have some cosmological implications [260, 273, 288, 289, 291–293, 301, 304, 308, 310, 311, 319]. From the particle physics point of view, the lepton asymmetry measurement of the Universe is crucial to understand some of the particle physics processes that might have taken place in the early Universe at high energies, including the better constraint on models for the creation of matter-antimatter asymmetry in the Universe [263, 271, 274]. The tightest constraints on lepton asymmetry at present are commonly based on a combination of CMB data via constraints on the baryon density and measurements of the primordial abundances of light elements [278, 298, 311].

The Standard Model (SM) of particle physics is a very successful description of

the subatomic Universe, connecting the weak, strong, and electromagnetic forces to the framework of gauge symmetries. Only the latter two are unbroken symmetries, i.e., bring conserved quantum numbers, color, and electric charge, respectively.1 The search for additional forces has always driven particle physics but has so far not been successful, resulting in tight bounds either on the strength or range of the new force. Today's research focuses almost exclusively on spontaneously broken new gauge symmetries, mimicking the success of the electroweak theory. The only classically conserved quantities in the SM of particle physics are the Baryon and lepton numbers, considering that the lepton mixing pattern observed in neutrino oscillations proves the non-conservation of the individual lepton numbers $L_{e,\mu,\tau}$, or linear combinations thereof. Ignoring new forces that do not act on SM particles, e.g., unbroken hidden forces in the dark matter sector, it is clear that the only new exact symmetry can be a linear combination of B and L. Classical symmetries of the Lagrangian can be broken at the quantum level through triangle anomalies, which have to be canceled to obtain a valid quantum field theory. For B - L, the anomalies can be canceled simply by introducing three SM-singlet right-handed neutrinos ν_R, which automatically lead to massive active (Dirac) neutrinos, which is very convenient and welcome. Gauging any other linear combination X of B and L would require the introduction of chiral fermions charged under SU(2)L $\times$ U(1)Y and is by now possible only if X is spontaneously broken to generate fermion masses above (and disconnected from) the electroweak scale. $U(1)_{B-L}$ hence Presents itself as the only possible unbroken gauge symmetry acting on known particles beyond electromagnetism and color. This is further corroborated by the fact that we have yet to observe any B - L violating process despite extensive decades of searching, most prominently the search for $\Delta(B-L)=2$ neutrinoless double beta decay. Even the baryon asymmetry of our Universe is no argument for breaking B - L, because the Dirac nature of neutrinos gives rise to an elegant leptogenesis mechanism under the name of neutrinogenesis even for conserved B - L. This scenario has rarely been considered; new "fifth" forces coupled to baryon number, lepton number, or B - L have, of course, been studied before, but never as unbroken, and hence never with Dirac neutrinos. Therefore, exploring the implications of an unbroken $U(1)_{B-L}$ symmetry as an alternative point of view to direct searches for B - L violation is worthwhile. This last will be of great importance in the following, as the coupling to light right-handed neutrinos severely constrains the new force. We consider a generalized model UV-SM completion with the attributes of a $B-L$ model in addition to the charges from an alignment with SM hypercharge leading parameter β. This linear superposition has chiral anomalies cancellation predicting three RHNs (one per generation) and hence the same minimal particle content of the minimal $B-L$. This model will have a new framework with predictions testable in the current and subsequent experiments detecting neutrinos and dark matter interactions. Besides the $B-L$ motivations, as the presence of a neutrino mass generation mechanism and portals as Z', and leptogenesis scenarios, the U(1) model has an impact in explaining the

thermalization of new RHN. We expect additional dynamical behavior of an extended model ν_R describes crucial scenarios in the smallness of neutrino masses, generating the observed matter–anti-matter asymmetry of our Universe, and protecting the Dirac nature from quantum gravity. All of these new ν_R interactions will then face strong constraints from cosmic intensity experiments (like CMB-S4) that will make it difficult to see the portals like Z' in any other intensity (e.g., SHiP or DUNE) or energy frontier (e.g., LHC) complexes. We assume GR and the ΛCDM to do cosmological analyses. Besides, we consider that the reheating temperature of the Universe reached at least the mass of the Z' mediators that couple to RHS.

1.2. Outline of the thesis

In this thesis, we consider the extension of the minimal ΛCDM model, provided with some free parameters like the number of relativistic degrees of freedom in the early universe, the non-relativistic neutrino mass, the sound speed and the viscosity of the $C\nu B$; and so we derive observational constraints on the additional five neutrinos parameters that can characterize the properties of the cosmic neutrino background. For this purpose, we consider data from CMB observed by *Planck* 2015, BAOs, the recent local value of the Hubble constant from *Hubble Space Telescope* (*HST*) and information from the abundance of galaxy clusters (GCs), BBN, among other. In addition to this, we want to obtain new and precise limits on the cosmological lepton asymmetry, in terms of the degeneracy parameter ξ_ν, as well as the neutrino mass scale, considering the configurations of future CMB experiments such as CMB-CORE and CMB-S4. On the other hand, we also analyze the introduction of 1, 2 and 3 right-hand neutrinos, including the mass and the coupling of the Z' boson, as a particle that functions as a portal between the electromagnetic world and the dark sector.

To this end, in my thesis the first six chapters are a review that supports the main results of the last chapters and are organized as follows: In Chapter 2, I provide a review of the standard model of cosmology, starting with its foundations in general relativity and pointing towards currently significant observational tensions such as that of the Hubble parameter. In the Chapter 3, I briefly analyze the standard model of particle physics, with particular emphasis on neutrino physics, and its main problems in this scheme, which brings us to physics beyond the standard model in the leptonic sector. Next, in Chapter 4, I review the history of neutrinos in early times, as well as an interplay between the BBN epoch and recombination. In Chapter 5, I present a review of the anisotropies of the CMB, always emphasizing the implications of relativistic and massive neutrinos in

what will be used more forward as one of the main cosmological tests. Before reaching our main results, in the Chapter 6, I review the presence of neutrinos in the large-scale structure of the universe, emphasizing the suppression effects they produce in the power spectrum of matter. The heart of this thesis is Chapters 7, 8 & 9, where I addressed the main fundamental physical properties of relic neutrinos, analyzed in the light of the most recent observational evidence and future experiments and the introduction of right-hand neutrinos, and a new boson, which will provide a new portal between the light sector and the dark sector, namely the standard model of particle physics and the standard model of cosmology. Finally, in Chapter 10, I present the main conclusions of this thesis and provide an outlook for future work.

Chapter 2

Particle cosmology and beyond

"There are more things in heaven and earth, Horatio, than are dreamt of in your philosophy." – Hamlet to Horatio in Hamlet, William Shakespeare (1603)

In this chapter, I will review in some detail the physical foundations of the two pillars of physical cosmology, namely the standard model of cosmology and the standard model of particle physics, which together lead to the concept of particle cosmology, in both cases, making special emphasis on the fundamental physical properties of neutrinos in both cases, making special emphasis on the fundamental physical properties of neutrinos and on what is currently called physics beyond the standard model (particle/cosmology).

2.1. Fundamentals of General Relativity

The essence of the theory of general relativity (GR) is based on **Einstein's field equations** (EFE):

$$G_{\mu\nu} = \frac{8\pi G}{c^4} T_{\mu\nu} \ , \tag{2.1}$$

where $G_{\mu\nu}$ represents the Einstein tensor, which describes the geometric properties of spacetime, and $T_{\mu\nu}$ is the energy-momentum or stress-energy tensor, which includes contributions from the various sources of matter and energy, supported in the background of spacetime. G and c are Newton's constant of universal gravitation and the speed of light in vacuum, respectively. Starting from the principle of equivalence between inertial mass and gravitational mass ($m_G/m_I = 1$)[1], Einstein postulated the idea that gravitation is a

[1] The principle states that: a system immersed in a gravitational field is punctually indistinguishable from an accelerated non-inertial reference frame. Around 1889, Loránd Eötvös

manifestation of the curvature of space-time, and that this curvature would be determined by all forms of matter-energy.

Motivated by the geometrization of the force of gravity, Einstein's field equations can be obtained from the following well-motivated and established postulates:

1. **The spacetime variety**: Spacetime is constituted by all physical events, described by the pair $(\mathcal{M},\ \mathbf{g})$, where M is a smooth 4-dimensional manifold and $\mathbf{g}$ is a Lorentzian metric on $\mathcal{M}$.

   On the variety $\mathcal{M}$ are defined all the fields of matter considered, for example, the electromagnetic field, the neutrino field, scalar field,..., etc., which describe the content of matter in spacetime. The fields of matter obey equations expressed as relations between tensors on $\mathcal{M}$. The derivatives with respect to the coordinates are covariant derivatives, concerning the symmetric connection defined by the metric g. If we denote the fields of matter included in the theory by $\Psi^{\alpha}_{(i)\gamma}$, where the sub-index i denotes the different fields of matter, then the following two postulates about the nature of the fields $\Psi^{\alpha}_{(i)\gamma}$ are common to the special theory and the general theory of relativity:

2. **Local causality**: The equations that obey the fields of matter must be such that, if $\mathcal{U} \subset \mathcal{M}$ is a convex neighborhood and $p,\ q \in \mathcal{U}$, then a signal can be sent in $\mathcal{U}$ between p and q if and only if p and q can be joined by a $c^1 - curve$ contained in $\mathcal{U}$, whose tangent vector everywhere is different from zero and is like of time or like of light (This curve is called non-space like).

   Another equivalent way of establish the postulate, and more physically significant, can be given in terms of the Cauchy problem for fields of matter: Let $p \in \mathcal{U}$ such that every non-space curve through p intersects the surface as of space $x^0 = cte.$ inside $\mathcal{U}$. Let $\mathcal{F}$ be the set of points on the hypersurface $x^0 = cte.$, which can be reached by non-space curves in $\mathcal{U}$ through p. Then, it is required that the values of the material fields in p must be uniquely determined by the values of the field and its derivatives to a finite order on $\mathcal{F}$. That is, the equations of motion (differential equations) that determine the fields (laws of physics) involve derivatives up to a finite order n (usually up to order 2) have a unique solution, which is determined by the boundary conditions, that is, the value of the fields and their first $n-1$ derivatives, given on a hypersurface intersected by the cone of light passed from point p.

3. **Local energy conservation**: There is a symmetric tensor $T_{\mu\nu} = T_{\mu\nu}\left(\Psi_i, \nabla\Psi_i\right) = T_{\nu\mu}$ which is a function of the fields of matter and their derivatives, up to a finite order, such that:

established experimentally that there was no apparent difference between gravitational mass and inertial mass, with an accuracy of one part in 20 million.

a) $T_{\mu\nu} = 0$ over $\mathcal{U} \subset \mathcal{M}$ open, if and only if $\Psi_i = 0$ for all over $\mathcal{U}$.

b) $T^{\mu\nu}_{;\nu} = 0$

The first condition expresses that all fields of matter contribute to energy. From the second condition, if the space-time manifold admits a Killing **K** vector field then, we obtain a conservation law, since let be:

$$p^{\alpha} = T^{\alpha\beta}K_{\beta}, \tag{2.2}$$

the components of the vector **P** obtained by contracting the momentun-energy tensor with the Killing field, then

$$p^{\alpha}_{;\alpha} = T^{\alpha\beta}_{;\alpha}K_{\beta} + T^{\alpha\beta}K_{\beta;\alpha}, \tag{2.3}$$

since $T^{\mu\nu}_{;\nu} = 0$ and **K** satisfies the Killing equation, i.e., $K_{(\alpha;\beta)} = 0$. Thus, if $\mathcal{D}$ is a compact and orientable region, by Gauss's theorem we have that

$$\int_{\partial\mathcal{D}} P^{\alpha} d\sigma_{\alpha} = \int_{\mathcal{D}} P^{\alpha}_{;\alpha} dv = 0. \tag{2.4}$$

Therefore, this result can be interpreted physically, since the flow of the component of the momentun-energy tensor in the direction of the Killing field on a closed surface is canceled, which is the generalization of Noether's theorem, which states that to all symmetry corresponds a conservation law. In the particular case of the flat Lorentzian manifold, associated with the ten linearly independent Killing vectors are the ten usual conservation laws, for energy, momentum and total angular momentum.

Another no less important question are the equations of motion, which is represented by the **geodesic equation**, which in some coordinate basis is represented as:

$$\frac{d^2x^{\alpha}}{d\lambda^2} + \Gamma^{\alpha}_{\beta\gamma}\frac{dx^{\beta}}{d\lambda}\frac{dx^{\gamma}}{d\lambda} = 0, \tag{2.5}$$

where λ is known as the affine parameter of a geodesic curve and

$$\Gamma^{\alpha}_{\beta\gamma} = \frac{1}{2}g^{\alpha\mu}\left(\frac{\partial g_{\mu\beta}}{\partial x^{\gamma}} + \frac{\partial g_{\mu\gamma}}{\partial x^{\beta}} - \frac{\partial g_{\beta\gamma}}{\partial x^{\mu}}\right), \tag{2.6}$$

are known as Christoffel symbols, and $g_{\beta\gamma}$ is the metric tensor in some coordinate base. On the one hand, if we consider the causality postulate, it places the metric **g** apart from the other fields of matter on $\mathcal{M}$, given its special geometric character. on the other hand, the equivalence principle establishes the existence of an accelerated system where the gravitational field is not detected, that is, it is punctually null. This accelerated system

is precisely the one in which the Christoffel symbols of the metric cancel out, that is: $\Gamma^{\alpha}_{\beta\gamma}|_p = 0$. This fact, together with the fact that the Lagrangian must be a physical scalar independent of the chosen reference frame, means that the Lagrangian of the gravitational field cannot be formed exclusively from the metric tensor and the Christoffel symbols, since because this is null for the previously considered coordinate system, the variation would be identically null for all observers, which does not make physical sense.

The possibility of choosing an accelerated reference system where the Christoffel symbols are null implies that the Lagrangian of the relativistic gravitational field must be formed by derivatives of higher order than one of the metric tensor and, therefore, the equivalence principle implies that the Lagrangian must be some scalar related to curvature. Indeed, the most common way to write the Lagrangian of the gravitational field is:

$$\mathcal{L}_G = \frac{c^3}{16\pi G} R\sqrt{-g}, \tag{2.7}$$

where R is the Ricci scalar, $g = |g_{\mu\nu}|$ is the determinant of the metric tensor. On the other hand, the causality and conservation postulates do not tell us how to construct $T^{\mu\nu}$ for a set of given matter fields. However, there is a unique and well-defined way to calculate the momentum-energy tensor, if the equations of motion for the fields are derived from a Lagrangian, as is the case for the usual fields of matter and of physical interest.

Let $\mathcal{L}_M$ be the Lagrangian density, which is a function of the matter fields Ψ_i, their covariant derivatives, up to a finite order and of the metric. Then, the equations of motion of the fields are obtained from the action:

$$S = \int \mathcal{L}_M dv. \tag{2.8}$$

Demanding that S is stationary under variation of the fields within a compact 4-dimensional region $\mathcal{D}$, i.e., $\delta S = 0$. This condition leads to the Euler-Lagrange equations:

$$\frac{\partial \mathcal{L}_M}{\partial \Psi_i} - \frac{\partial \mathcal{L}_M}{\partial \left(\nabla \Psi_i\right)} = 0. \tag{2.9}$$

The momentun-energy tensor is obtained from the Lagrangian density $\mathcal{L}_M$, considering the variations of the action under changes in the metric:

$$T_{\mu\nu} \equiv \frac{2}{\sqrt{-g}} \frac{\delta S}{\delta g^{\mu\nu}}. \tag{2.10}$$

For example, a scalar field $\phi(x)$, which represents scalar particles of mass m, with no

charge and zero spin, is described by the Lagrangian density

$$\mathcal{L}_M = \frac{1}{2}\sqrt{-g}\left(g^{\mu\nu}\phi_{;\mu}\phi_{;\nu} - m^2\phi^2\right), \tag{2.11}$$

where units of $\hbar = 1$ and $c = 1$ have been used. The Euler-Lagrange equations for this system lead to the Klein-Gordon equation:

$$\left(\Box + m^2\right)\phi = 0, \tag{2.12}$$

where the D'alembertian is given by: $\Box\phi = g^{\mu\nu}\phi_{;\mu\nu}$, and the momentum-energy tensor is:

$$T_{\mu\nu} = \phi_{;\mu}\phi_{;\nu} - \frac{1}{2}g_{\mu\nu}\left(g^{\gamma\delta}\phi_{;\gamma}\phi_{;\delta} + m^2\phi^2\right). \tag{2.13}$$

So far the metric $\mathbf{g}$ has not been specified. In the special theory of relativity, which does not include gravitational effects, the metric is flat, i.e., $\mathbf{g} = \boldsymbol{\eta}$. As mentioned above, the force of gravity, due to its universal character, must be excluded as a field of forces in a flat space, if we want to maintain the idea that a free particle follows "straight lines" or that the speed of light in the vacuum is constant. To maintain the principle of relativity, that is, physics is the same for all observers, or equivalently, the laws of physics must be independent of the coordinate system, the field equations that determine the metric must be tensor relations, which involve matter through the momentun-energy tensor, if we want to maintain the equivalence principle, that is, if two fields of matter contribute the same energy density to a system, then the field equations for the metric must lead to same result. On the geometry side, as Hilbert suggested to Einstein, the only geometric object, except identities or multiples, which is determined by the metric tensor and first derivatives of its components, is the Riemann tensor, or tensors derived from them, and therefore the only possibility, is a linear combination of the Ricci tensor, the scalar curvature and a constant, proportional to the momentum-energy tensor, given the conditions imposed on it, which is symmetric and satisfies the principle of local conservation, so:

Einstein's field equations (2.1) and equations of motion (2.5) can be obtained from first principles through the well-known Einstein-Hiltber action:

$$S = \int \sqrt{-g}\left[\frac{1}{2\kappa}\left(R + \Lambda\right) + \mathcal{L}_M\right] d^4x, \tag{2.14}$$

where $\kappa = 8\pi G/c^4$, R is the Ricci scalar and in this case we include the effects of the cosmological constant Λ. Thus, the EFE including the cosmological constant take the form:

$$R_{\mu\nu} - \frac{1}{2}g_{\mu\nu}R + \Lambda g_{\mu\nu} = \frac{8\pi G}{c^4}T_{\mu\nu}\ , \tag{2.15}$$

where from Eq. (2.1)

$$G_{\mu\nu} = R_{\mu\nu} - \frac{1}{2} g_{\mu\nu} R \tag{2.16}$$

and $R_{\mu\nu}$ is the Ricci tensor. This is a system of 10 nonlinear coupled differential equations for the metric and its first derivatives. However, since the covariant divergence of each side of the equations (2.15) is satisfied independently:

$$\left(G^{\mu\nu} + \Lambda g^{\mu\nu}\right)_{;\nu} = \frac{8\pi G}{c^4} T^{\mu\nu}_{;\nu} = 0. \tag{2.17}$$

Then, the number of independent equations is reduced to six. This is the correct number of equations, since of the ten independent components of the metric tensor, four of them can be chosen arbitrarily, since it corresponds to the fact that the components of the metric tensor are unique, except for a coordinate transformation. Thus, Einstein's field equations (2.15) determine the metric tensor $g_{\mu\nu}$, depending on the physical system to analyze, i.e., neutron stars, black holes, solar system dynamics,...etc.

So far we have made very general considerations about the fields of matter and the geometry of space-time. In what follows, we are going to apply these fairly general considerations of the geometry of space-time and matter fields to our object of study of interest, namely the standard model of cosmology and neutrino matter fields. In cosmology, which is the metric which describes the universe and what is the matter content? It turns out that both questions are very difficult to answer and, indeed, there are no still clear answers, as we stressed in the following sections and next chapters.

2.1.1 Friedmann-Lemaître-Robertson-Walker metric

The metric used to describe the universe on large scales is the Friedmann-Lemaître-Robertson-Walker (FLRW) metric. The fundamental hypothesis on which the standard model of cosmology is based is the **cosmological principle**, which establishes that on a large scale the universe is homogeneous and isotropic. This means that the observed universe is the same for any observer, regardless of the point from which it is being observed or the direction, that is, on a large scale, the distribution of matter in the universe (the density of galaxies and their movement) is independent of the direction and the place from which it is observed. The cosmological hypothesis is based on observing the distribution of galaxies and cosmic background radiation. Einstein's field equations allow us to describe the geometry of space-time, determined by the distribution of matter in the universe. The simplest way to describe the distribution of matter in the universe that satisfies the cosmological principle is the model of the perfect fluid, where galaxies are the particles which constitutes the perfect fluid. As in fluid dynamics, where matter is

made up of particles, it is assumed that the observation scales are large enough so that the volume element contains a sufficient number of particles and the fluid, seen as a continuous distribution of matter, is a good approximation to describe the dynamics of this system. A more formal definition can be found in [194]. Before solving Einstein's equations for this model of the universe, the symmetry arguments established by the cosmological principle allow us to advance in the general form of the metric, independently of the explicit form of the momentum-energy tensor that describes the matter in the universe. To find the most general form of the metric that satisfies the cosmological principle, we will establish the following hypotheses, as a starting point:

1. Weyl's postulate: The universe lines of galaxies form a geodesic bundle $\{\Gamma\}$ that do not intersect and are orthogonal to a family of hypersurfaces $\{\Sigma\}$ as of space.
2. Each hypersurface $\{\Sigma\}$ has a time coordinate x^0.
3. Each hypersurface $\{\Sigma\}$ is locally isotropic.
4. Every pair of points on each hypersurface $\{\Sigma\}$ are equivalent.
5. The global metric and all the cosmic tensors such as the stress-energy one $T_{\mu\nu}$ are form-invariant with respect to the isometries of those subspaces.

We shall come back in a moment to maximally symmetric spaces. Roughly speaking, the second requirement above means that the matter quantities can depend only on the time.

The cosmological principle seems to be compatible with observations at very large scales. On a scale of about 100 h^{-1} Mpc the rms density fluctuations are at the level of $\sim$10% and on scales larger than 300 h^{-1} Mpc the distribution of both mass and luminous sources safely satisfies the cosmological principle of isotropy and homogeneity [206]. In a recent work [160] find that the quasar distribution is homogeneous on scales larger than 250 h^{-1} Mpc. Moreover, numerical relativity seems to indicate that the average evolution of a generic metric on large scale is compatible with that of FLRW metric [70]. The CfA2 redshift survey produce the first large area and moderately deep maps of large scale structure in the nearby universe, as well as the first crude but truly quantitative measurements of the 3-D clustering properties of galaxies. Redshifts are the simplest link to determine galaxy distances. This initial map was quite surprising, showing that the distribution of galaxies in space was anything but random, with galaxies actually appearing to be distributed on surfaces, almost bubble like, surrounding large empty regions, or "voids", where we can identify the "Great Wall", with the Coma cluster at the centre[2]. Drawn to the same scale is a small section of the Sloan Digital Sky Survey (SDSS) [1], in which an even larger "Sloan

[2] `http://tdc-www.harvard.edu/zcat/`

Great Wall" has been identified. This is one of the largest observed structures in the Universe, containing over 10,000 galaxies and stretching over more than 1.37 billion light years. The wedge of the 2dFGRS [2], which determined distances to more than 220,000 galaxies in the southern sky out to a depth of 2 billion light years. The SDSS has a similar depth but a larger solid angle and currently includes over 650,000 observed redshifts in the northern sky.

On the other hand, the mock galaxy surveys constructed using semianalytic techniques to simulate the formation and evolution of galaxies within the evolving dark matter distribution of the "Millennium" simulation [3] are made by selecting matching survey geometries and magnitude limits. The Illustris project is a large cosmological simulation of galaxy formation, completed in late 2013, using a state of the art numerical code and a comprehensive physical model[3]. In the Fig. 1, we can see the predicted large-scale structure of galaxies, which was studied for the first time with hydrodynamical simulations of this type thanks to their large enough volume. They form a cosmic web composed of gas and stars and feature galaxies at their intersections which not only match the shapes and sizes of real galaxies very well but also reproduce the observed spatial clustering pattern as seen in the newest data of extensive galaxy surveys. This match persists when the galaxies are separated into different subsamples according to color and stellar mass. Additionally, the simulations make precise forecasts about how the cosmic web, as traced by galaxies, evolves in time and relates to the underlying backbone of cosmic structure made up of dark matter. t is particularly fascinating that we can accurately predict the influence of supermassive black holes on the distribution of dark matter on large scales and therefore, the insights gained with IllustrisTNG are crucial for the reliable interpretation of future cosmological data that aim for precision tests of our cosmological model.

According to the cosmological principle, the constant-time spatial hypersurfaces are maximally symmetric.[4] A maximally symmetric space is completely characterised by one number only, i.e. its scalar curvature, which is also a constant. See [194, Chapter 13].

Let R be this constant scalar curvature. The Riemann tensor of a maximally symmetric D-dimensional space is written as:

$$R_{\mu\nu\rho\sigma} = \frac{R}{D(D-1)}(g_{\mu\rho}g_{\nu\sigma} - g_{\mu\sigma}g_{\nu\rho}) \ . \tag{2.18}$$

[3] `https://www.illustris-project.org/`

[4] This means that they possess 6 Killing vectors, i.e. there are six transformations which leave the spatial metric invariant [194].

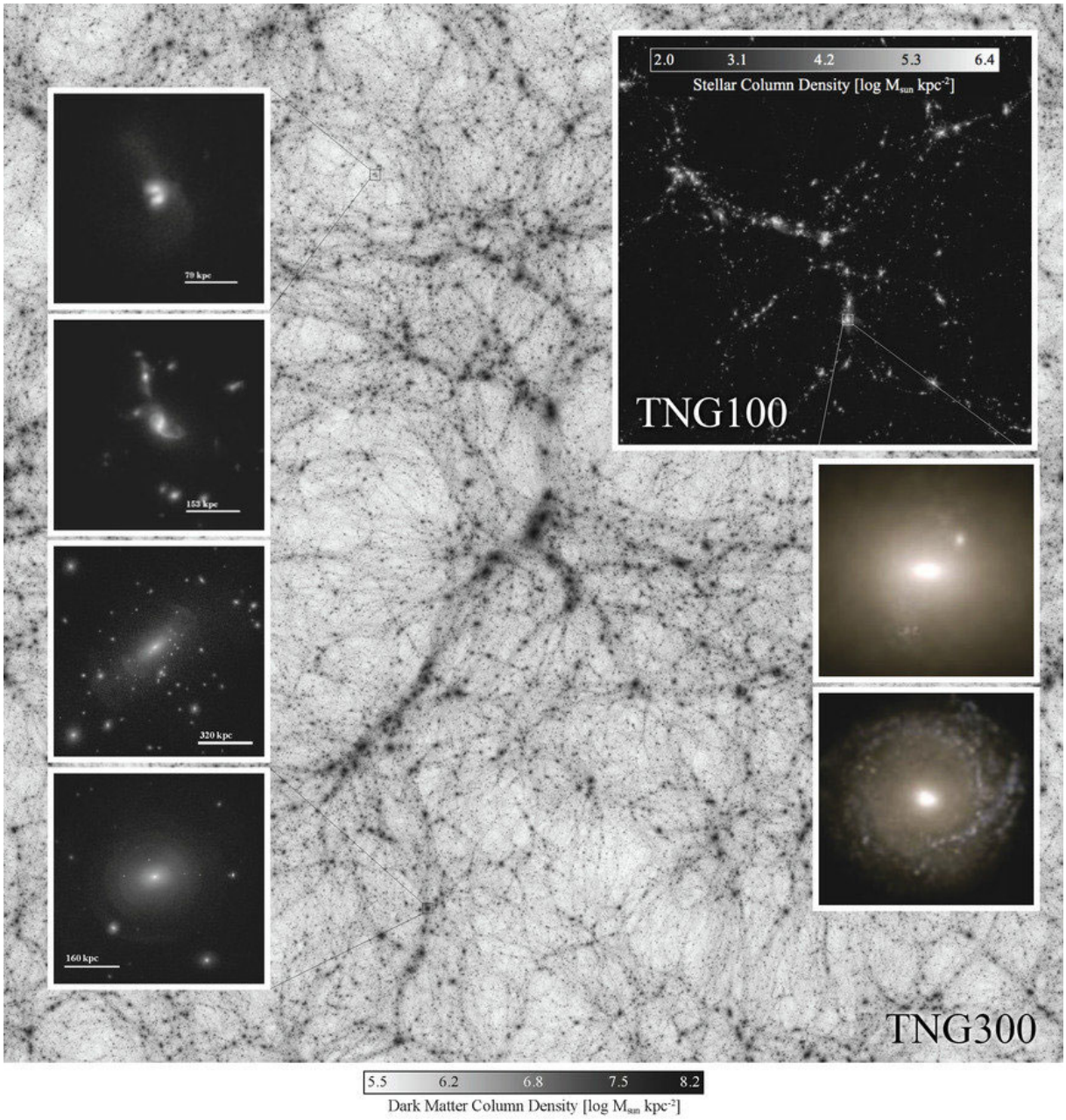

Figure 1 – LSS IllustrisTNG-Simulations. The gas velocity in a thin sílice of 100 physical Kilo-Parsecs, centered on the second most massive galaxy cluster in the TNG100 calculations. The image contrasts the gas motions in cosmic filaments against the fireball of motions triggered by the deep gravitational potential well and the supermassive Black hole sitting at its center. Where the image is black, the gas hardly moves, while White regions have velocities exceeding 1000 Km/s. CREDIT: ©ILLUSTRISTNG COLLABORATION

Contracting with $g^{\mu\rho}$ we get for the Ricci tensor:

$$R_{\nu\sigma} = \frac{R}{D} g_{\nu\sigma} \ , \tag{2.19}$$

and then R is the scalar curvature, as we stated, since $g^{\nu\sigma} g_{\nu\sigma} = D$. Since any given number can be negative, positive or zero, we have three possible maximally symmetric spaces. Now, focusing on the 3-dimensional spatial case:

1. $ds_3^2 = |d\mathbf{x}|^2 \equiv \delta_{ij} dx^i dx^j$, i.e. the Euclidean space. The scalar curvature is zero, i.e. the space is flat. This metric is invariant under 3-translations and 3-rotations.

2. $ds_3^2 = |d\mathbf{x}|^2 + dz^2$, with the constraint $z^2 + |\mathbf{x}|^2 = a^2$. This is a 3-sphere of radius a embedded in a 4-dimensional Euclidean space. It is invariant under the six 4-dimensional rotations.

3. $ds_3^2 = |d\mathbf{x}|^2 - dz^2$, with the constraint $z^2 - |\mathbf{x}|^2 = a^2$. This is a 3-hypersphere, or a hyperboloid, in a 4-dimensional pseudo-Euclidean space. It is invariant under the six 4-dimensional pseudo-rotations (i.e. Lorentz transformations).

Let us write in a compact form the above metrics as follows:

$$ds_3^2 = |d\mathbf{x}|^2 \pm dz^2 \ , \qquad z^2 \pm |\mathbf{x}|^2 = a^2 \ . \tag{2.20}$$

Differentiating $z^2 \pm |\mathbf{x}|^2 = a^2$, one gets:

$$z dz = \mp \mathbf{x} \cdot d\mathbf{x} \ . \tag{2.21}$$

Now put this back into ds_3^2:

$$ds_3^2 = |d\mathbf{x}|^2 \pm \frac{(\mathbf{x} \cdot d\mathbf{x})^2}{a^2 \mp |\mathbf{x}|^2} \ . \tag{2.22}$$

In a more compact form:

$$ds_3^2 = |d\mathbf{x}|^2 + K \frac{(\mathbf{x} \cdot d\mathbf{x})^2}{a^2 - K|\mathbf{x}|^2} \ , \tag{2.23}$$

with $K = 0$ for the Euclidean case, $K = 1$ for the spherical case and $K = -1$ for the hyperbolic case. The components of the spatial metric in Eq. (2.23) can be immediately read off and are:

$$g_{ij}^{(3)} = \delta_{ij} + K \frac{x_i x_j}{a^2 - K|\mathbf{x}|^2} \ . \tag{2.24}$$

Writing the metric (2.23) in spherical coordinates, we U use the fact that $|d\mathbf{x}|^2 = dr^2 + r^2 d\Omega^2$, where

$$d\Omega^2 \equiv d\theta^2 + \sin^2\theta d\phi^2 \ , \tag{2.25}$$

and making use of:

$$\mathbf{x} \cdot d\mathbf{x} = \frac{1}{2} d|\mathbf{x}|^2 = \frac{1}{2} d(r^2) = r dr \ . \tag{2.26}$$

we arrive at the following expression:

$$ds_3^2 = \frac{a^2 dr^2}{a^2 - Kr^2} + r^2 d\Omega^2 \tag{2.27}$$

If we normalise $r \to r/a$ in metric (2.27), we can write:

$$ds_3^2 = a^2 \left(\frac{dr^2}{1 - Kr^2} + r^2 d\Omega^2 \right) \ , \tag{2.28}$$

and letting a to be a function of time, we finally get the FLRW metric:

$$\boxed{ds^2 = -c^2 dt^2 + a^2(t) \left(\frac{dr^2}{1 - Kr^2} + r^2 d\Omega^2 \right).} \tag{2.29}$$

The time coordinate used here is called **cosmic time**, whereas the spatial coordinates are called **comoving coordinates**. For each t the spatial slices are maximally symmetric; $a(t)$ is called **scale factor**, since it tells us how the distance between two points scales with time. The FLRW metric was first worked out by Friedmann in [66] and [67] and then derived on the basis of isotropy and homogeneity by Robertson and Walker in [154], [155] and [189]. Lemaître's work [98] had been also essential to develop it.[5] A further comment concerning FLRW metric (2.29) is in order here. The dimension of distance is being carried by the scale factor a itself, since we rescaled the radius $r \to r/a$. Indeed, as we computed earlier, the spatial curvature is $R^{(3)} = 6K/a(t)^2$, also time-varying, and it is a real, dimensional number as it should be. A very useful form of rewriting FLRW metric (2.29) is via the **conformal time** η:

$$a d\eta = dt \qquad \Rightarrow \qquad \eta - \eta_i = \int_{t_i}^{t} \frac{dt'}{a(t')} \ . \tag{2.30}$$

[5] See also [99] for a recent republication and translation of Lemaître's 1933 paper.

As we shall see later, but as we already can guess from the above integration, $c(\eta - \eta_i)$ represents the comoving distance travelled by a photon between the times η_i and η, or t_i and t. The conformal time allows to rewrite FLRW metric (2.29) as follows:

$$ds^2 = a(\eta)^2 \left(-c^2 d\eta^2 + \frac{dr^2}{1 - Kr^2} + r^2 d\Omega^2 \right) \tag{2.31}$$

i.e. the scale factor has become a conformal factor (hence the name for η). Recalling the earlier discussion about dimensionality, if a has dimensions then $c\eta$ is dimensionless. On the other hand, if a is dimensionless, then η is indeed a time. Note also that metric (2.31) for $K = 0$ is Minkowski metric multiplied by a conformal factor.

Another useful way to write FLRW metric (2.29) is using the **proper radius**, which is defined as follows:

$$\mathcal{D}(t) \equiv a(t) r \ . \tag{2.32}$$

We shall discuss in more detail the proper radius, or proper distance, in Sec. 2.3.1. Using $\mathcal{D}$ instead of r, the FLRW metric (2.29) becomes:

$$ds^2 = -c^2 dt^2 \left(1 - H^2 \frac{\mathcal{D}^2/c^2}{1 - K\mathcal{D}^2/a^2} \right) - \frac{2H\mathcal{D} dt d\mathcal{D}}{1 - K\mathcal{D}^2/a^2} + \frac{d\mathcal{D}^2}{1 - K\mathcal{D}^2/a^2} + \mathcal{D}^2 d\Omega^2 \ , \tag{2.33}$$

where

$$\boxed{H \equiv \frac{\dot{a}}{a}} \tag{2.34}$$

is the **Hubble parameter**. The dot denotes derivation with respect to the cosmic time.

2.1.2 Christoffel symbols and geodesics

If we assume $K = 0$ in metric (2.29), rewrite it in Cartesian coordinates and calculate the Christoffel symbols, we have:

$$\Gamma^0_{00} = 0 \ , \qquad \Gamma^0_{0i} = 0 \ , \qquad \Gamma^0_{ij} = \frac{a\dot{a}}{c} \delta_{ij} \ , \qquad \Gamma^i_{0j} = \frac{H}{c} \delta^i{}_j \ . \tag{2.35}$$

We now use these in the geodesic equation (2.5):

$$\frac{dP^\mu}{d\lambda} + \Gamma^\mu_{\nu\rho} P^\nu P^\rho = 0 \ , \tag{2.36}$$

where $P^\mu \equiv dx^\mu/d\lambda$ is the four-momentum and λ is an affine parameter. For a particle of mass m, one has $\lambda = \tau/m$, where τ is the proper time. The norm of the four-momentum is:

$$\mathcal{P}^2 \equiv g_{\mu\nu} P^\mu P^\nu = -\frac{E^2}{c^2} + p^2 = -m^2 c^2 \ , \tag{2.37}$$

where we have defined the energy and the physical momentum (**proper momentum**):

$$\frac{E^2}{c^2} \equiv -g_{00}(P^0)^2 \ , \qquad p^2 \equiv g_{ij} P^i P^j \ , \tag{2.38}$$

and the last equality of Eq. (2.37), which applies only to massive particles, comes from:

$$\frac{ds^2}{d\lambda^2} = \frac{m^2 ds^2}{d\tau^2} = -m^2 c^2 \ , \tag{2.39}$$

since, by definition, $ds^2 = -c^2 d\tau^2$. We have recovered above the well-known dispersion relation of special relativity. The metric $g_{\mu\nu}$ used above is, in principle, general. But, of course, we now specialise it to the FLRW one.

For a photon, $m = 0$ and $E = pc$. The time-component of the geodesic equation is the following:

$$\frac{dP^0}{d\lambda} + \frac{a\dot{a}}{c} \delta_{ij} P^i P^j = 0 \ . \tag{2.40}$$

Introducing the proper momentum as defined in Eq. (2.38), one gets:

$$\frac{dp}{d\lambda} + H p^2 = 0 \ . \tag{2.41}$$

Therefore, we can write:

$$\frac{E_{\rm obs}}{E_{\rm em}} = \frac{a_{\rm em}}{a_{\rm obs}} \ . \tag{2.42}$$

On the other hand the photon energy is $E = hf$, with f its frequency. Therefore:

$$\frac{a_{\rm em}}{a_{\rm obs}} = \frac{E_{\rm obs}}{E_{\rm em}} = \frac{f_{\rm obs}}{f_{\rm em}} = \frac{\lambda_{\rm em}}{\lambda_{\rm obs}} = \frac{1}{1+z} \ . \tag{2.43}$$

This is the relation between the redshift and the scale factor. We have connected observation with theory. Usually, $a_{\rm obs} = 1$ and the above relation is simply written as $1 + z = 1/a$.

What does happen, on the other hand, to the energy of a massive particle? The time-geodesic equation for massive particles is identical to photons, but the dispersion relation is different, i.e., $E^2 = m^2c^4 + p^2c^2$. Therefore:

$$E = \sqrt{m^2c^4 + \frac{p_i^2 a_i^2 c^2}{a^2}} \,, \tag{2.44}$$

where p_i is some initial proper momentum, at the time t_i and $a_i = a(t_i)$. For $m = 0$ we recover the result already obtained for photons. For massive particles the above relation can be approximated as follows:

$$E = mc^2 \left(1 + \frac{p_i^2 a_i^2}{2a^2 m^2 c^2} + \dots\right) \,, \qquad (mc \gg p) \,, \tag{2.45}$$

i.e., performing the expansion for small momenta which is usually done in special relativity. The second contribution between parenthesis is the classical kinetic energy of the particle, whose average is proportional to $k_{\rm B}T$. Therefore:

$$T \propto a^{-1} \,, \text{ for relativistic particles,} \tag{2.46}$$

$$T \propto a^{-2} \,, \text{ for non-relativistic particles.} \tag{2.47}$$

We shall recover the above result also using the Boltzmann equation.

2.2. Friedmann equations

Given FLRW metric, Friedmann equations can be straightforwardly computed from the Einstein equations (2.15). If we calculate from FLRW metric 2.29 the components of the Ricci tensor, we have:

$$R_{00} = -\frac{3}{c^2}\frac{\ddot{a}}{a} \,, \qquad R_{0i} = 0 \,, \qquad R_{ij} = \frac{1}{c^2} g_{ij} \left(2H^2 + \frac{\ddot{a}}{a} + 2\frac{Kc^2}{a^2}\right) \,, \tag{2.48}$$

and the scalar curvature is:

$$R = \frac{6}{c^2}\left(\frac{\ddot{a}}{a} + H^2 + \frac{Kc^2}{a^2}\right) \,. \tag{2.49}$$

Finally, we compute the Einstein equations:

$$H^2 + \frac{Kc^2}{a^2} = \frac{8\pi G}{3c^2}T_{00} + \frac{\Lambda c^2}{3} \tag{2.50}$$

$$g_{ij}\left(H^2 + 2\frac{\ddot{a}}{a} + \frac{Kc^2}{a^2} - \Lambda c^2\right) = -\frac{8\pi G}{c^2}T_{ij} \tag{2.51}$$

These are called *Friedmann equations*. ¿But, which is stress-energy tensor $T_{\mu\nu}$ that we must use with Eqs. 2.50 and 2.51 and that are compatible with the cosmological principle?.

First, let me make some general considerations about fluid mechanics. The kinematical properties of a fluid element are determined by its velocity, acceleration, shear, and vorticity. All these quantities are defined in the space-time, and for convenience one uses comoving coordinates, that is Lagrangian coordinates that follow the flow motion or *Hubble flow* in our case. In principle, one splits the space-time structure into surfaces of simultaneity to rest frame observers, with a projected metric on the surface $h_{\mu\nu} = g_{\mu\nu} + u_\mu u_\nu$; where u^μ are the components of the four velocity $\mathbf{u}$. In this frame it is natural to define an expansion tensor $\Theta_{\mu\nu} = \nabla_{(\mu}u_{\nu)}$, and the vorticity tensor $\omega_{\mu\nu} = \nabla_{[\mu}u_{\nu]}$, where ∇ operates on the projected 3-D space. The trace of the expansion tensor is a scalar measure of the volume expansion, given by $\Theta = \nabla_\mu u^\nu$, and the shear tensor is the projected symmetric free-trace part of $\Theta_{\mu\nu}$ such that $\Theta_{\mu\nu} = \sigma_{\mu\nu} + \frac{1}{3}\Theta h_{\mu\nu}$. Accordingly, the energy-momentum tensor associated to the fluid can be separated into components parallel and orthogonal to the four velocity as:

$$T_{\mu\nu} = \rho u_\mu u_\nu + q_\mu u_\nu + q_\nu u_\mu + P h_{\mu\nu} + \pi_{\mu\nu}, \tag{2.52}$$

where $\rho = T_{\alpha\beta}u^\alpha u^\beta$ s the energy density that includes rest masses and possibly the internal energy, such as the chemical energy; $P = \frac{1}{3}h^{\alpha\beta}T_{\alpha\beta}$ is the pressure; $q_\mu = -h^\alpha_\mu T_{\alpha\nu}u^\nu$ is the momentum density or energy flux due to either diffusion or heat conduction;and $\pi_{\mu\nu} = [h^\alpha_{(\mu}h^\beta_{\nu)} - \frac{1}{3}h_{\mu\nu}h^{\alpha\beta}]T_{\alpha\beta}$ is thetrace-free anisotropic stress tensor due to viscosity. A perfect fluid is an non-viscous fluid with no heat conduction, that is, $q_\nu = 0$ and $\pi_{\mu\nu} = 0$. It is analogous to an ideal gas in standard thermodynamics.

keeping this in mind and having fixed the metric to be the FLRW one, we have some strong constraints:

- First of all: $G_{0i} = 0$ implies that $T_{0i} = 0$, i.e. there cannot be a flux of energy in any direction because it would violate isotropy;
- Second, since $G_{ij} \propto g_{ij}$, then $T_{ij} \propto g_{ij}$.
- Finally, since $G_{\mu\nu}$ depends only on t, then it must be so also for $T_{\mu\nu}$.

In terms of the full metric, it is a standard practice to represent the the stress-energy tensor as:

$$T_{\mu\nu} = \left(\rho + \frac{P}{c^2}\right) u_\mu u_\nu + P g_{\mu\nu} \tag{2.53}$$

where u_μ is the four-velocity of the fluid element, and taking into account the above constraints we arrive at:

$$T_{00} = \rho(t)c^2 = \varepsilon(t) \ , \qquad T_{0i} = 0 \ , \qquad T_{ij} = g_{ij} P(t) \ , \tag{2.54}$$

where $\rho(t)$ is the rest mass density, $\varepsilon(t)$ is the energy density and $P(t)$ is the pressure. Matter described by 2.53 is known as **perfect fluid**, that correctly describes fluids in the background geometry of the Universe. For more detail about the latter see [163] whereas for more detail about viscosity, heat fluxes and the imperfect fluids see e.g. [194] and [114]. Combine Eqs. 2.50, 2.51 and 2.54, the Friedmann equation becomes:

$$H^2 = \frac{8\pi G}{3}\rho + \frac{\Lambda c^2}{3} - \frac{K c^2}{a^2} \tag{2.55}$$

while the acceleration equation is the following:

$$\frac{\ddot{a}}{a} = -\frac{4\pi G}{3}\left(\rho + \frac{3P}{c^2}\right) + \frac{\Lambda c^2}{3} \tag{2.56}$$

In the Friedmann and acceleration equations, ρ and P are the total density and pressure. Hence, they can be written as sums of the contributions of the individual components:

$$\rho \equiv \sum_i \rho_i \ , \qquad P \equiv \sum_i P_i \ . \tag{2.57}$$

The contribution from the cosmological constant can be considered either geometrically or as a matter component with the following density and pressure:

$$\rho_\Lambda \equiv \frac{\Lambda c^2}{8\pi G} \ , \qquad P_\Lambda \equiv -\rho_\Lambda c^2 \ . \tag{2.58}$$

The scale factor a is, by definition, positive, but its derivative can be negative. This would represent a contracting universe. Note that the left hand side of the Friedmann equation (2.55) is non-negative. Therefore, $\dot{a}$ can vanish only if $K > 0$, i.e. for a spatially closed universe. This implies that, if $K \leqslant 0$ and if there exists an instant for which $\dot{a} > 0$, then the universe will expand forever.

2.2.1 Critical density and density parameters

Let us now rewrite Eq. (2.55) without incorporating Λ in the total density ρ:

$$H^2 = \frac{8\pi G\rho}{3} - \frac{Kc^2}{a^2} \ . \tag{2.59}$$

The value of the total ρ such that $K = 0$ is called **critical energy density** and has the following form:

$$\begin{aligned} \rho_{\rm cr} \equiv \frac{3H^2}{8\pi G} &= 1.88\ h^2\ 10^{-29}\ g/cm^3 && (2.60)\\ &= 1.053\ h^2\ 10^{-5}\ {\rm GeV/c^2\ cm^3} && (2.61)\\ &= 2.77\ h^{-1}\ 10^{11}\ M_\odot/(h^{-1}\ Mpc)^3 && (2.62)\\ &= 11.26\ h^2\ protons/m^3\ , && (2.63) \end{aligned}$$

where Eq. (2.60) represents its current value [13] and $M_\odot = 1.989 \times 10^{33} g$ is the solar mass unit. The critical density $\rho_{\rm cr}$ corresponds to approximately 6 protons per cubic meter, certainly a very dilute fluid. It turns out that $\rho_{\rm cr}(t_0)$ is very close to $\rho_{\rm cr}$, so that our universe is spatially flat. Such an extreme fine-tuning in K is a really surprising coincidence, known as the **flatness problem**. A possible solution is provided by the inflationary theory. Instead of densities, it is very common and useful to employ the density parameter Ω, which is defined as

$$\Omega \equiv \frac{\rho}{\rho_{\rm cr}} = \frac{8\pi G\rho}{3H^2} \tag{2.64}$$

i.e. the energy density normalised to the critical one. We can then rewrite Friedmann equation (2.55) as follows:

$$1 = \Omega - \frac{Kc^2}{H^2a^2} \ . \tag{2.65}$$

Defining

$$\Omega_K \equiv -\frac{Kc^2}{H^2a^2} \ , \tag{2.66}$$

i.e. associating the energy density

$$\rho_K \equiv -\frac{3Kc^2}{8\pi Ga^2} \ , \tag{2.67}$$

to the spatial curvature, we can recast Eq. 2.65 in the following simple form:

$$1 = \Omega + \Omega_K \ . \tag{2.68}$$

Therefore, the sum of all the density parameters, *the curvature one included*, is always equal to unity. In particular, if it turns out that $\Omega \simeq 1$, this implies that $\Omega_K \simeq 0$, i.e. the universe is spatially flat. From the latest Planck data [13] we know that:

$$\Omega_{K0} = 0.0008^{+0.0040}_{-0.0039} \tag{2.69}$$

at the 95 per cent CL. It is more widespread in the literature the normalisation of ρ to the *present-time* critical density, i.e.

$$\Omega \equiv \frac{\rho}{\rho_{\rm cr,0}} = \frac{8\pi G\rho}{3H_0^2} \tag{2.70}$$

because it leaves more evident the dependence on a of each material component. With this definition of Ω, Friedmann equation (2.55) is written as:

$$\frac{H^2}{H_0^2} = \sum_x \Omega_{x0} f_x(a) + \frac{\Omega_{K0}}{a^2} \ , \tag{2.71}$$

where $f_x(a)$ is a function which gives the a-dependence of the material component x and $f_x(a_0 = 1) = 1$. Consistently:

$$\sum_x \Omega_{x0} = 1 \tag{2.72}$$

also known as **closure relation**, taking into account that the equation (2.67) can be normalized and added like the rest of the species. We shall use the definition $\Omega_x \equiv \rho_x/\rho_{\rm cr,0}$ through this writing.

2.2.2 The energy conservation equation

The energy conservation equation can be written as

$$\nabla_\nu T^{\mu\nu} = 0 \tag{2.73}$$

is encapsulated in GR through the Bianchi identities. Therefore, it is not independent from the Friedmann equations 2.55 and 2.56. For the FLRW metric and a perfect fluid, it has a particularly simple form:

$$\dot{\rho} + 3H\left(\rho + \frac{P}{c^2}\right) = 0 \tag{2.74}$$

This is the $\mu = 0$ component of $\nabla_\nu T^{\mu\nu} = 0$ and it is also known from fluid dynamics as **continuity equation**.. This equation is actually not independent of the Friedmann and acceleration equations, but is required for consistency. It implies that the expansion of the universe (as specified by H(z)) can lead to local changes in the energy density. Note that there is no notion of conservation of "total energy," as energy can be interchanged between matter and the spacetime geometry. The continuity equation can be analytically solved if we assume an equation of state of the form $P = w\rho c^2$, with w constant. The general solution is:

$$\rho = \rho_0 a^{-3(1+w)} \qquad (w = \text{ constant}) \,, \tag{2.75}$$

where $\rho_0 \equiv \rho(a_0 = 1)$. There are three particular values of w which play a major role in cosmology:

- **Cold matter**: $w = 0$, i.e. $P = 0$, for which $\rho = \rho_0 a^{-3}$. The adjective cold refers to the fact that particles making up this kind of matter have a kinetic energy much smaller than the mass energy, i.e. they are non-relativistic. If they are thermally produced, i.e. if they were in thermal equilibrium with the primordial plasma, they have a mass much larger than the temperature of the thermal bath. We shall see this characteristic in more detail in Chapter 4. Cold matter is also called **dust** and it encompasses all the non-relativistic known elementary particles, which are overall dubbed **baryons** in the jargon of cosmology. If they exist, unknown non-relativistic particles are called **cold dark matter** (CDM).

- **Hot matter**: $w = 1/3$, i.e. $P = \rho/3$, for which $\rho = \rho_0 a^{-4}$. The adjective hot refers to the fact that particles making up this kind of matter are relativistic. For this reason they are known, in the jargon of cosmology, as **radiation** and they encompass not only the relativistic known elementary particles, but possibly the unknown ones (i.e. **hot dark matter**). The primordial neutrino background belonged to this class, but since neutrino seems to have a mass of approximately 0.1 eV, it is now cold. We shall see why in Chapter 4.

- **Vacuum energy**: $w = -1$, i.e. $P = -\rho$ and ρ is a constant. It behaves as the cosmological constant and provides the best (and the simplest) description that we have for dark energy, though plagued by the serious issues.

Similarly, it is sometimes useful to think of any nonzero spatial curvature as yet another component of the cosmological energy budget, obeying $w = -1/3$, so that $P = \rho/3$. It is not an energy density, of course; $\rho = \rho_0 a^{-2}$ is simply a convenient way to keep track of how much energy density is lacking, in comparison to a flat universe. The cosmic budget and evolution of energy density can be seen in the Fig. (4).

2.3. The standard model of cosmology

The most successful cosmological model is called ΛCDM and is made up of Λ, CDM, baryons and radiation (photons and massless neutrinos). The Friedmann equation for the ΛCDM model is the following:

$$H(z) = H_0\sqrt{\Omega_{\rm r0}(1+z)^4 + \Omega_{\rm m0}(1+z)^3 + \Omega_{\rm K0}(1+z)^2 + \Omega_\Lambda}\ . \tag{2.76}$$

We already saw in Eq. 2.69 the value of the spatial curvature contribution. From Ref. [13] here are the other ones:

$$\Omega_\Lambda = 0.6911 \pm 0.0062\ , \qquad \Omega_{\rm m0} = 0.3089 \pm 0.0062 \tag{2.77}$$

at 68 per cent CL, where $\Omega_{\rm m0} = \Omega_{\rm c0} + \Omega_{\rm b0}$, i.e. it includes the contributions from both CDM and baryons, since they have the same dynamics (i.e. they are both cold). It is however possible to disentangle them and one observes:

$$\Omega_{\rm b0}h^2 = 0.02230 \pm 0.00014\ , \qquad \Omega_{\rm c0}h^2 = 0.1188 \pm 0.0010 \tag{2.78}$$

also at 68 per cent CL. The radiation content, i.e. photons plus neutrinos, can be easily calculated from the temperature of the CMB, as we shall see in Chapter 4. It turns out that:

$$\Omega_{\gamma 0}h^2 \approx 2.47 \times 10^{-5}\ , \qquad \Omega_{\nu 0}h^2 \approx 1.68 \times 10^{-5} \tag{2.79}$$

Since $h = 0.68$, and recalling the closure relation of Eq. (2.72), we can conclude that today 69% of our universe is made of cosmological constant, 26% of CDM and 5% of baryons Fig. (2). Radiation and spatial curvature are negligible.

Later, we shall see that cosmological observables very often carry the imprint of particular length scales, in relation to specific physical effects responsible for shaping the observables themselves. For this reason, it is convenient to briefly recall basic concepts pertaining to distances in cosmology.

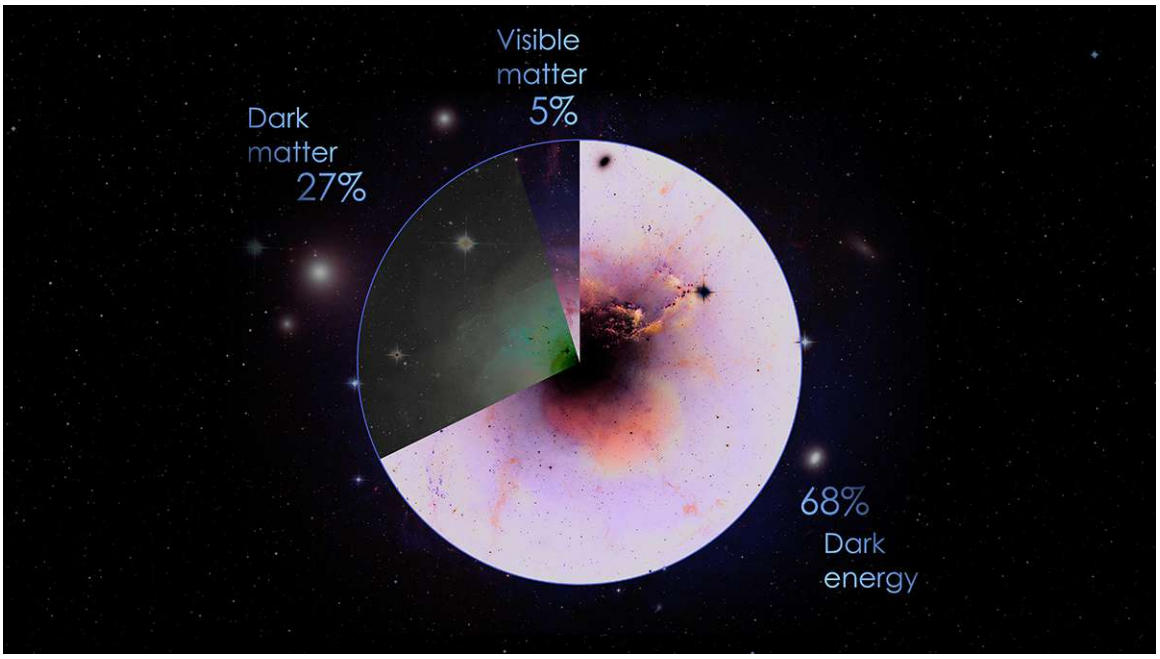

Figure 2 – Matter/energy composition of the Universe as it is currently conceived by the standard model of cosmology ΛCDM. Credits: `https://svs.gsfc.nasa.gov/12307`

2.3.1 Distances in cosmology

We present and discuss in this section the various notions of distance that are employed in cosmology. See e.g. [78] for a reference on the subject.

2.3.1.1 Comoving distance and proper distance

We have already encountered comoving coordinates in the FLRW metric 2.29 and the proper radius $\mathcal{D}(t) \equiv a(t)r$ in the FLRW metric 2.33. We must be clearer about the difference between the radial coordinate and the distance. They are equal only when $d\Omega = 0$. The comoving square infinitesimal distance is indeed, from FLRW metric 2.29 the following:

$$d\chi^2 = \frac{dr^2}{1 - Kr^2} + r^2 d\Omega^2 \ , \tag{2.80}$$

i.e. it has indeed a radial part, but also has a transversal part. So, if χ is the comoving distance between two points, the proper distance at a certain time t is $d(\chi, t) = a(t)\chi$. The comoving distance is a notion of distance which does not include the expansion of

the universe and thus does not depend on time. The proper distance is the distance that would be measured instantaneously by rulers. For example, imagine to extend a ruler between GN-z11 (the farthest known galaxy, $z = 11.09$) and us. Our reading at the time t would be the proper distance at that time. Suppose that $d\Omega = 0$. Then the comoving distance to an object with radial coordinate r is the following:

$$\chi = \int_0^r \frac{dr'}{1 - Kr'^2} = \begin{cases} \arcsin r \ , \ \text{for } K = 1 \ , \\ r \ , \ \text{for } K = 0 \ , \\ \text{arcsinh } r \ , \ \text{for } K = -1 \ . \end{cases} \tag{2.81}$$

Deriving d with respect to the time one gets:

$$\dot{d} = \dot{a}\chi = \frac{\dot{a}}{a} d = Hd \ , \tag{2.82}$$

which recovers the Hubble's law for $t = t_0$. Fig. (3)

2.3.1.2 Distances and horizons

For a photon, not unexpectedly,

$$d\chi = \frac{cdt}{a(t)} = cd\eta \ , \tag{2.83}$$

i.e. the comoving distance is equal to the conformal time, which we introduced in Eq. (2.30). We might say that the comoving distance is a *lookback conformal time*. By integrating $cdt/a(t)$ from $t_{\rm em}$ to t_0 we get the comoving distance from the source to us, or the conformal time spent by the photon travelling from the source to us:

$$\chi = \int_{t_{\rm em}}^{t_0} \frac{cdt'}{a(t')} = \int_a^1 \frac{cda'}{H(a')a'^2} \ . \tag{2.84}$$

For the dust-dominated case one has $H = H_0/a^{3/2}$ and the comoving distance as a function of the scale factor and of the redshift is:

$$\chi(a) = \frac{c}{H_0} \int_a^1 \frac{da'}{\sqrt{a'}} = \frac{2c}{H_0} \left(1 - \sqrt{a}\right) \ , \quad \chi(z) = \frac{2c}{H_0} \left(1 - \frac{1}{\sqrt{1+z}}\right) \ . \tag{2.85}$$

When $z \to 0$, $\chi \sim cz/H_0$. At the first order in the redshift, the lookback time distance is equivalent to the comoving one. When the lower integration limit in Eq. 2.84 is $a = 0$, i.e. the Big Bang, one defines the **comoving horizon** $\chi_{\rm p}$ (also known as **particle horizon** or **cosmological horizon**). This is the conformal time spent from the Big Bang until the

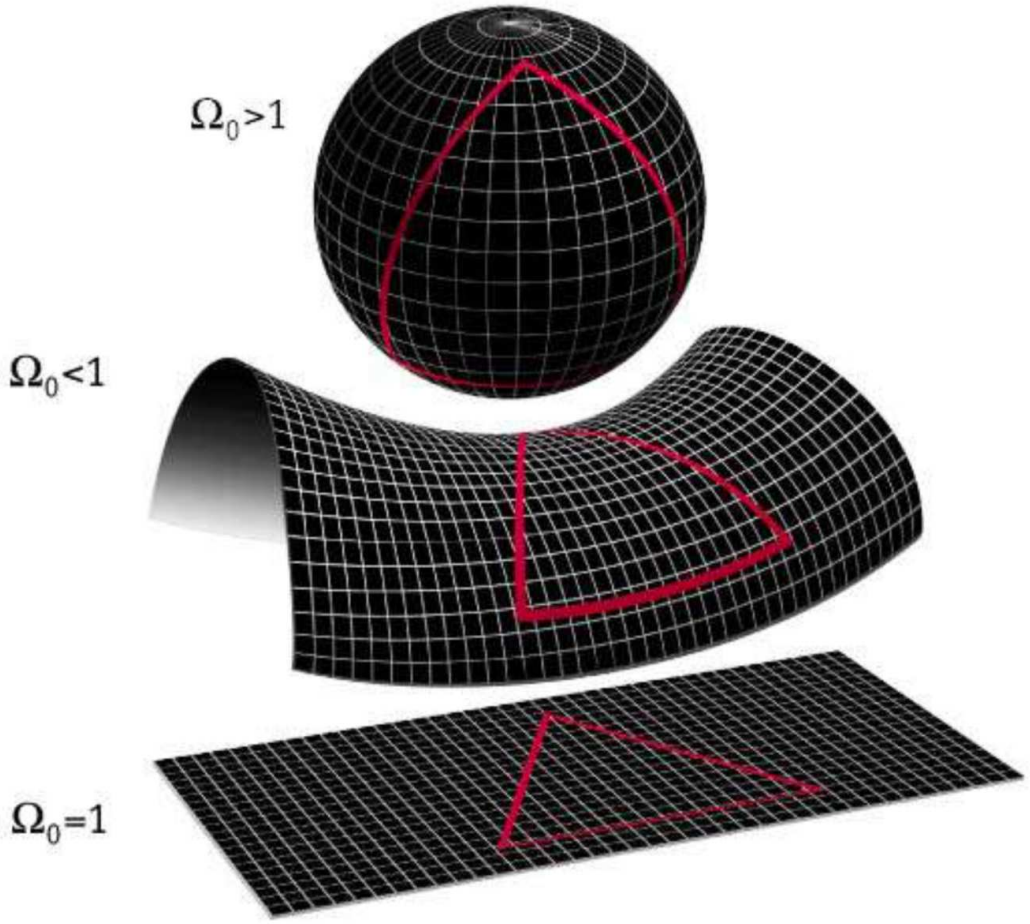

Figure 3 – Curvature of the Universe. The local geometry of the universe is determined by whether the density parameter Ω is greater than, less than, or equal to 1. From top to bottom: a spherical universe with $\Omega > 1$, a hyperbolic universe with $\Omega < 1$, and a flat universe with $\Omega = 1$. Credits: `https://wmap.gsfc.nasa.gov/universe/uni_shape.html`

cosmic time t or scale factor a. It is also the maximum comoving distance travelled by a photon (hence the name particle horizon) since the Big Bang and so it is the comoving size of the visible universe. In the dust-dominated case, using Eq. 2.85, with $a = 0$ or $z = \infty$ one obtains:

$$\chi_{\rm p} = c\eta_0 = \frac{2c}{H_0} \, . \tag{2.86}$$

Note that this is not the age of the universe, but three times its value. When the upper integration limit of Eq. 2.84 is infinite, one defines the **event horizon**:

$$\chi_{\rm e}(t) \equiv c\int_t^\infty \frac{dt'}{a(t')} = c\int_a^\infty \frac{da'}{H(a')a'^2} \, , \tag{2.87}$$

which of course makes sense only if the universe does not collapse. This represents the maximum distance travelled by a photon from a time t. If it diverges, then no event

horizon exists and therefore eventually all the events in the universe will be causally connected. This happens, for example, in the dust-dominated case:

$$\chi_{\mathrm{e}} = \frac{c}{H_0}\int_a^\infty \frac{da'}{\sqrt{a'}} = \infty \ . \tag{2.88}$$

But, in the de Sitter universe we have

$$\chi_{\mathrm{e}} = \frac{c}{H_0}\int_a^\infty \frac{da'}{a'^2} = \frac{c}{H_0 a} \ . \tag{2.89}$$

The proper event horizon for the de Sitter universe is a constant:

$$a\chi_{\mathrm{e}} = \frac{c}{H_0} \ . \tag{2.90}$$

2.3.1.3 The luminosity distance

The luminosity distance is a very important notion of distance for observation. It is based on the knowledge of the intrinsic luminosity L of a source, which is therefore called **standard candle**. Type Ia supernovae are standard candles, for example. Then, measuring the flux F of that source and dividing L by F, one obtains the square luminosity distance:

$$d_{\mathrm{L}}^2 \propto \frac{L}{F} \ . \tag{2.91}$$

Now, imagine a source at a certain redshift z with intrinsic luminosity $L = dE/dt$. The observed flux is given by the following formula:

$$F = \frac{dE_0}{dt_0 A_0} \ , \tag{2.92}$$

where A_0 is the area of the surface on which the radiation is spread:

$$A_0 = 4\pi a_0^2 \chi^2 \ , \tag{2.93}$$

i.e. over a sphere with the proper distance as the radius. We must use the proper distance, because this is the instantaneous distance between source and observer at the time of detection. Note that χ is the comoving distance between the source and us. We do not observe the same photon energy as the one emitted, because photons suffer from the cosmological redshift, thus:

$$\frac{dE}{dE_0} = \frac{a_0}{a} \ . \tag{2.94}$$

Finally, the time interval used at the source is also different from the one used at the observer location:

$$\frac{dt}{dt_0} = \frac{a}{a_0} \ . \tag{2.95}$$

We can easily show this by using FLRW metric with $ds^2 = 0$, i.e. $cdt = a(t)d\chi$. Consider the same $d\chi$ at the source and at the observer's location. Thus, $cdt = a(t)d\chi$ and $cdt_0 = a(t_0)d\chi$ and the above result follows. Putting all the contributions together, we get

$$F = \frac{dE_0}{dt_0 A_0} = \frac{a^2 dE}{a_0^2 dt 4\pi a_0^2 \chi^2} = \frac{dE}{dt 4\pi a_0^2 \chi^2 (1+z)^2} \ . \tag{2.96}$$

Hence, the luminosity distance is defined as:

$$d_{\mathrm{L}} \equiv a_0(1+z)\chi \tag{2.97}$$

From this formula and the observed redshifts of type Ia supernovae we can determine if the universe is in an accelerated expansion, in a model-independent way.

2.3.1.4 Angular diameter distance

The angular diameter distance is based on the knowledge of proper sizes. Objects with a known proper size are called **standard rulers**. Suppose a standard ruler of transversal proper size ds (small) to be at a redshift z and comoving distance χ. Moreover, this object has an angular dimension $d\phi$, also small. At a fixed time t, we can write the FLRW metric as:

$$ds^2 = a(t)^2 d\chi^2 \ . \tag{2.98}$$

Since the object is small and we are at the origin of the reference frame, the comoving distance χ is also the radial distance. Therefore, the transversal distance is:

$$ds = a(t)\chi d\phi \ . \tag{2.99}$$

Dividing the proper dimension of the object by its angular size provides us with the angular diameter distance:

$$d_{\mathrm{A}} = a(t)\chi \ . \tag{2.100}$$

For the case of a dust-dominated universe, one has:

$$d_{\rm A} = \frac{2c}{H_0}\left[\frac{1}{1+z} - \frac{1}{(1+z)^{3/2}}\right] . \tag{2.101}$$

In the limit of small z, we find $d_{\rm A} \sim cz/H_0$. All the distances that we defined insofar coincide at the first order expansion in z. Note the relation:

$$d_{\rm L} = (1+z)^2 d_{\rm A} , \tag{2.102}$$

known as **Etherington's distance duality** [63]. In gravitational lensing applications it is often necessary to know the angular-diameter distance between two sources at different redshifts (i.e. the angular-diameter distance between the lens and the background source).

2.3.2 History of the expansion and cosmography

The kinematics of the universe can be described through the Hubble parameter $H(t)$ and its dependence on time, i.e., the deceleration parameter $q(t)$. The information about the dynamics of the expansion can be obtained through these two parameters, which directly depends on the cosmological model.

2.3.2.1 The Hubble parameter and H_0 tension

Next we are going to deal with what is perhaps the most important cosmological parameter, namely the so-called *Hubble parameter* or rate of expansion today, $H_0 = \dot{a}/a(t_0)$. We can write the Hubble parameter in units of 100 km s^{-1} Mpc^{-1} , which can be used to estimate the order of magnitude for the present size (Hubble's horizon) and age of the universe

$$H_0 = 100h \text{ km s}^{-1} \text{ Mpc}^{-1} , \tag{2.103}$$

$$cH_0^{-1} = 3000h^{-1} \text{ Gyr} , \tag{2.104}$$

$$H_0^{-1} = 9.773h^{-1} \text{ Mpc} , \tag{2.105}$$

The parameter h has been measured to date $h = 0.7$ within 4%. When the Hubble parameter H is evaluated at the present time t_0, it becomes a number, whose value is

$$H_0 = 67.74 \pm 0.46 \text{ km s}^{-1} \text{ Mpc}^{-1} , \tag{2.106}$$

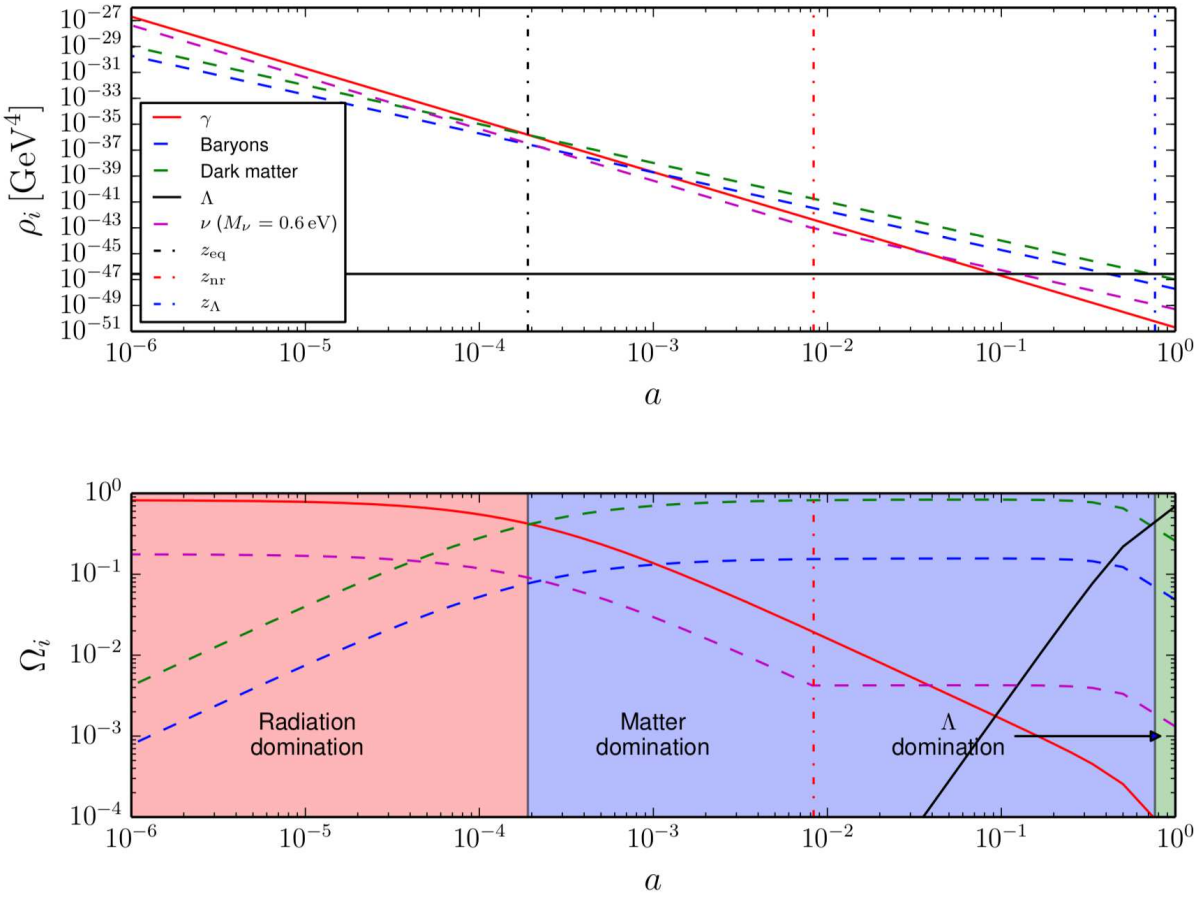

Figure 4 – Evolution of energy density and density parameters of the different species that constitute the cosmic budget. *Upper panel*: evolution of the energy densities ρ_i, in GeV^4, of photons (red solid curve), baryons (blue dashed curve), dark matter (green dashed curve), the cosmological constant (black solid curve), and massive neutrinos (with $M_\nu = 0.06eV$, purple dashed curve) as a function of scale factor a. The three vertical lines denote the redshift of matter-radiation equality (black dot-dashed line), the redshift of non-relativistic transition of massive neutrinos (red dot-dashed line), and the redshift of matter-Λ equality (blue dot-dashed line). *Lower panel*: evolution of the density parameters Ω_i for the various species, with the same color coding as the upper panel. In addition, the red, blue, and green shaded regions denote the eras of radiation, matter, and Λ domination (Figure obtained from [181]).

at the 68 per cent confidence level (CL), as reported by the Planck collaboration [13]. We will return to this topic later, regarding the tension between high and low redshift measurements.

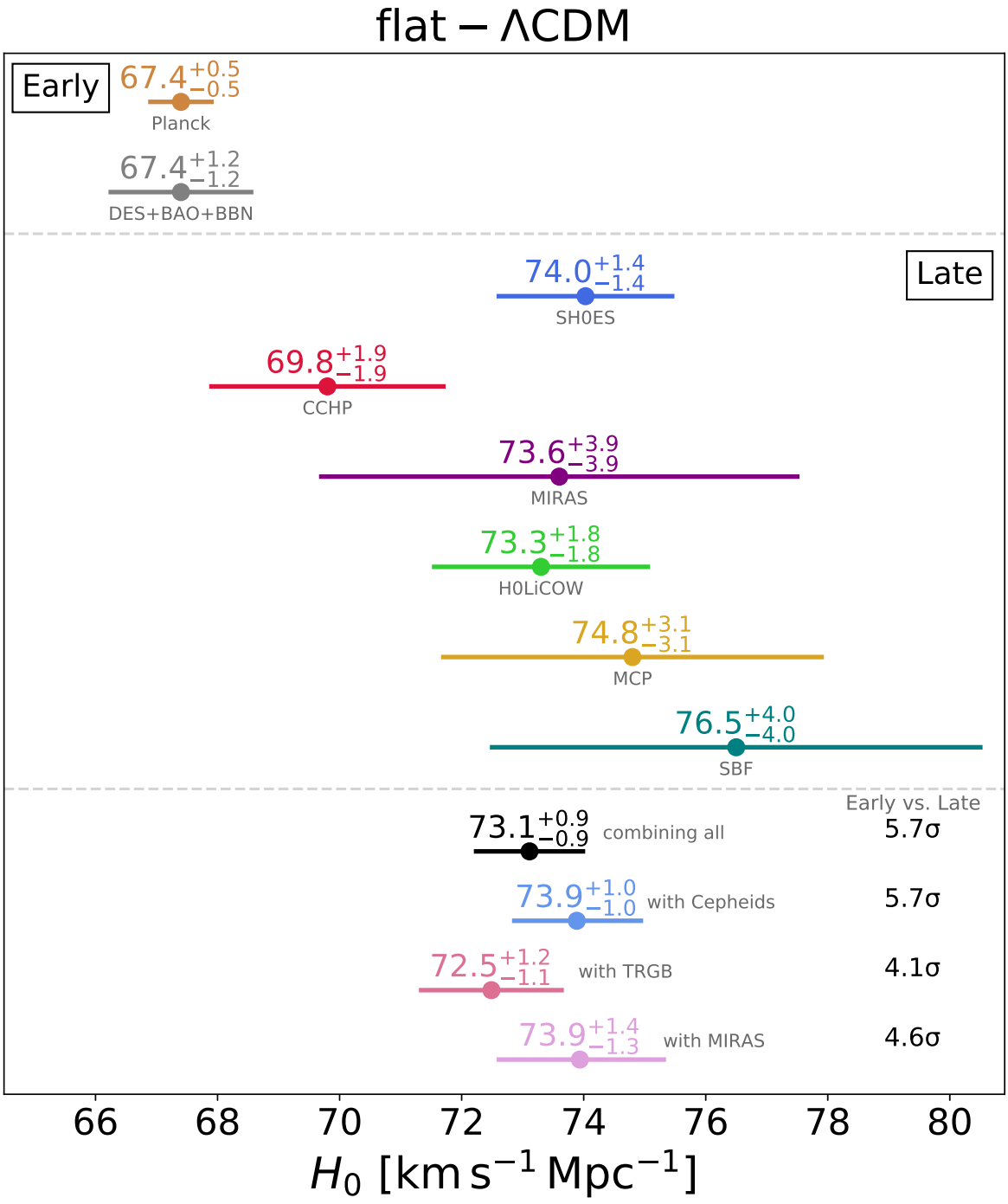

Figure 5 – Constraint on H_0 from different cosmological probes at 68% CL (Figure obtained from [416].

Another important issue has to do with the observational measurements of the Hubble parameter. The current cosmological test have provided a an impressive confirmation of the standard ΛCDM cosmological model, that has been constrained with

unprecedented accuracy. However, with the increase of the observational sensitivity a few statistically significant tensions between different independent cosmological datasets have emerged in recent years. Two important tensions to take into account are those of the measures of Hubble constant (H_0) and the amplitude or rateof the growth of structure (σ_8), the first that we will deal with in this chapter and the second in the chapter **??**. The 2018 legacy release from the Planck satellite [1] of the Cosmic Microwave Background (CMB) anisotropies,together with the latest Atacama Cosmology Telescope (ACT-DR4) [16] and South Pole Telescope (SPT-3G) [17] measurements, have provided a fantastic confirmation of the standard Λ Cold Dark Matter (ΛCDM) cosmological model. However, the improvement of the methods and the reduction of the uncertainties on the estimated cosmological parameters have seen the emergence of statistically significant tensions in the measurement of various quantities between the CMB data and model independent cosmological probes. The most statistically significant tension is in the estimation of the Hubble constant H_0 between the CMB, assuming a ΛCDM model, and the direct local distance ladder measurements. In particular, the Planck collaboration finds $H_0 = 67.27 \pm 0.60 km/s/Mpc$. This constraint is in tension at about 4.4σ with the 2019 SH0ES collaboration (R19) constraint, $H0 = 74.03 \pm 1.42 km/s/Mpc$, based on the analysis of the Hubble Space Telescope observations using 70 long-period Cepheids in the Large Magellanic Cloud.

As shown in Fig. 5, preferring smaller values, we have the early universe estimates of H_0, as obtained by Planck or by ACT+WMAP5 ($H0 = 67.6 \pm 1.1 km/s/Mpc$), and their combination with Baryon Acoustic Oscillation (BAO) data, the Y1 measurements of the Dark Energy Survey, supernovae from the Pantheon catalog, and a prior on the baryon density derived from measurements of primordial deuterium assuming standard Big Bang Nucleosynthesis (BBN). A reanalysis of the BOSS full shape data, as well as BAO+BBN from BOSS and eBOSS provides $H_0 = 67.35 \pm 0.97 km/s/Mpc$, while SPTpol finds $H_0 = 71.3 \pm 2.1 km/s/Mpc$. In contrast, standard distance ladder and time delay distances agree on a low-z high-H0 value, as the SH0ES estimate18 $H_0 = (73.5 \pm 1.4) km/s/Mpc$, and the H0LiCOW inferred value $H_0 = 73.3^{+1.7}_{-1.8} km/s/Mpc$, based on strong gravitational lensing effects on quasar systems. However, the strong lensing TDCOSMO+SLACS sample prefers $H0 = 67.4^{+4.1}_{-3.2} km/s/Mpc$. Then, we have the reanalysis of the Cepheid data by using Bayesian hyper-parameters, the local determination of H_0 considering the cosmographic expansion of the luminosity distance, the independent determination of H_0 based on the Tip of the Red Giant Branch, and that obtained by using the Surface Brightness Fluctuations method, or the Cosmic Chronometers. Finally, a larger value for H_0 is preferred by MIRAS (variable red giant stars), by STRIDES, using the Infrared or Baryonic Tully–Fisher relation, or by Standardized Type II supernovae. There is no single type of systematic measurement error in Cepheids which could solve the H_0 crisis, as speculated in ? (e.g., it would not work for Cepheids calibrated in NGC 4258), and in any

case it could not explain the final result from the Maser Cosmology Project, completely independent from these considerations, that finds $H0 = 73.9 \pm 3.0 km/s/Mpc$. If the late universe estimates are averaged in different combinations, these H_0 values disagree between 4.5σ and 6.3σ with those from Planck.

On the other hand, prospects for measuring H_0 with astrophysical neutrinos from supernovae are already present in the literature [334]. A core-collapse supernova (CCSNe) emits almost all its binding energy in the form of neutrinos. Observations of these neutrinos can provide crucial information on both the dynamics of CCSNe and the properties of neutrinos, including the neutrino lifetimes, magnetic moments, and the number of neutrino species. To date, we have only observed neutrinos from one CCSN: SN1987A [335], in the Large Magellanic Cloud. In spite of the limited statistics, these provided priceless information and solidified the current understanding of the dynamics of CCSNe. Galactic CCSNe, however, are very rare; their rate is, on average, around one to three per century. There is, however, an additional, strongly related but continuous source of astrophysical neutrinos: the diffuse supernova background (DSNB). The DSNB consists of neutrinos and antineutrinos emitted cumulatively from all past CCSNe in the observable Universe. The DSNB, composed of neutrinos coming from all possible CCSNe at redshifts z<5, is sensitive to the low redshift expansion of the Universe. Therefore, measurements of the DSNB serve as unique tools to constrain the underlying six- parameter ΛCDM cosmology using neutrinos. More statistics allow one to consider more ambitious measurements. HK and Theia, after a decade of running, can provide a "neutrino-measurement" of the expansion rate of the universe.

2.3.2.2 The cosmic time

The unit of measure of the Hubble constant is an inverse time:

$$H_0 = 3.24\ h \times 10^{-18}\ \mathrm{s}^{-1}\ , \tag{2.107}$$

whose inverse gives the order of magnitude of the age of the universe:

$$\frac{1}{H_0} = 3.09\ h^{-1} \times 10^{17}\ \mathrm{s} = 9.78\ h^{-1}\ \mathrm{Gyr}\ , \tag{2.108}$$

and multiplied by c gives the order of magnitude of the size of the visible universe, i.e. the Hubble radius that we have already seen in Eq. (2.104) but evaluated at the present time $t = t_0$:

$$\frac{c}{H_0} = 9.27\ h^{-1} \times 10^{25}\ \mathrm{m} = 3.00\ h^{-1}\ \mathrm{Gpc}\ . \tag{2.109}$$

But what does "present time" t_0 mean? Time flows, therefore t_0 cannot be a constant! That is true, but if we compare a time span of 100 years (the span of some human lives) to the age of the universe (about 14 billion years), we see that the ratio is about 10^{-8}. Since this is pretty small, we can consider t_0 to be a constant, also referred to as the age of the universe.[6] We can calculate it as follows:

$$t_0 = \int_0^{t_0} dt = \int_0^1 \frac{da}{\dot{a}} = \int_0^1 \frac{da}{H(a)a} = \int_0^\infty \frac{dz}{H(z)(1+z)} \,. \tag{2.110}$$

The integration limits of Eq. (2.110) deserve some explanation. We assumed that $a(t = 0) = 0$, i.e. the Big Bang. This condition is not always true, since there are models of the universe, e.g. the de Sitter universe, for which a vanishes only when $t \to -\infty$. The other assumption is that $a(t_0) = 1$. This is a pure normalisation, done for convenience, which is allowed by the fact that the dynamics is invariant if we multiply the scale factor by a constant. Recall that, in cosmology, when a quantity has subscript 0, it usually means that it is evaluated at $t = t_0$.

Let us now calculate the age of the universe for the ΛCDM model. Using Eq. 2.110, we get:

$$t_0 = \frac{1}{H_0} \int_0^1 da \frac{a}{\sqrt{\Omega_\Lambda a^4 + \Omega_{\mathrm{m}0} a + \Omega_{\mathrm{r}0} + \Omega_{K0} a^2}} \,. \tag{2.111}$$

Using the numbers shown insofar, we get upon numerical integration:

$$t_0 = \frac{0.95}{H_0} = 13.73 \text{ Gyr} \tag{2.112}$$

The value reported by [13] is 13.799 ± 0.021 at 68% confidence level. Note how $H_0 t_0 \approx 1$. This fact has been dubbed **synchronicity problem** by [19]. As one can see, in presence of Λ the dimensionless age of the universe reaches values larger than unity. This, mathematically, is due to the a^4 factor multiplying Ω_Λ in Eq. (2.111). Note that we can obtain the observed value $H_0 t_0 \approx 0.95$ also in absence of a cosmological constant and for a curvature-dominated universe, i.e. $\Omega_{K0} \approx 0.97$.

[6] Pretty much the same happens with the redshift. A certain source has redshift z which, actually, is not a constant but varies slowly. This is called **redshift drift** and it was first considered by Sandage and McVittie in [159] and [124]. Applications of the redshift drift phenomenon to gravitational lensing are proposed in [146].

2.3.2.3 The deceleration parameter

Let us focus now on Eq. 2.56. It contains $\ddot{a}$, so it describes how the expansion of the universe is accelerating or . The key-point is that if the right hand side of Eq. 2.56 is positive, i.e. $\rho + 3P/c^2 < 0$, then $\ddot{a} > 0$. There exists a parameter, named *deceleration parameter*, with which to measure the entity of the acceleration. It is defined as follows:

$$q \equiv -\frac{\ddot{a}a}{\dot{a}^2} \tag{2.113}$$

In [153] and [144] analysis based on type Ia supernovae observation have shown that $q_0 < 0$, i.e. the deceleration parameter is negative and therefore the universe is in a state of accelerated expansion.

Chapter 3

Neutrinos in the standard model of particle physics

"Dear Radioactive Ladies and Gentlemen." – Pauli's letter of the 4th of December 1930 (in his letter, Pauli refers to his new proposed particle, the "neutron". Apparently, Fermi clarified that he was talking about a different particle which he referred to as neutrino ("little neutral one").)

Physics at very small scales deals with the study of the elementary constituents of matter as produced in particle accelerators or within astrophysical and cosmological environments. In broad terms, particle physics seeks to determine the properties of the Universe at large scales, starting from the attophysics[1], describing the interactions among quarks and leptons, the basic building blocks of matter. The underlying theory is the so-called standard model (SM) of particle physics, which puts together quantum mechanics and Einstein's relativity along with the principle of gauge invariance. These basic pillars constitute the three revolutions in physics that took place in the past century. The SM of particles physics describes the electromagnetic, weak and strong interactions among the elementary constituents of matter in terms of a quantum field theory merging quantum mechanics with special relativity and incorporating interactions via gauge symmetry. In this picture, all basic forces other than gravity are mediated by the exchange of intermediate vector bosons associated with the SM gauge symmetry group $SU(3)_c \otimes SU(2)_L \otimes U(1)_Y$, that is, the photon, the gluons and the weak gauge bosons $W^{\pm}$ and Z. Its theoretical formulation was developed between the middle and the end of the twentieth century, and

[1] By atto we mean length scales of the order of $10^{-18}m$, where the electroweak force operates, which is set by the rest mass of the weak vector bosons which is roughly 100 GeV. This length scale would be the distance where a Yukawa force is mediated by the weak vector bosons. The magnitude of weak length scale was initially inferred by the Fermi constant measured by neutron and muon decay.

its current form has gained general acceptance after the experimental confirmation of the existence of quarks towards the middle of the 70s. Quarks carry colour and hence couple to gluons, while leptons do not. Today we know for certain that there are three types or 'generations' of elementary constituents of matter. The current formulation is based on a particular type of quantum field theory known as gauge theories. Such theories are described by a Lagrangian invariant under local transformations generated by the elements of symmetry groups (or product of symmetry groups). To ensure gauge invariance is necessary to include vector fields known as gauge fields into the Lagrangian (more precisely, derivatives are converted to covariant derivatives involving these gauge fields). Each symmetry group of the Lagrangian can then be interpreted as describing a force between particles, whose force carriers are the gauge fields.

The gauge bosons associated with the electroweak $SU(2)_L \otimes U(1)_Y$ part of the symmetry are the photon and $W^{\pm}$, Z gauge bosons. The latter was directly produced for the first time at CERN (the European Organization for Nuclear Research)[2] in 1983. On the other hand, the gluons are associated with the $SU(3)$ colour symmetry and were discovered at DESY (German Electron Synchrotron)[3]. For the gauge bosons and fermions to gain mass, the gauge symmetry must be spontaneously broken to the subgroup $SU(3)_c \otimes U(1)_q$, where SU(3)c describes the strong colour force, which holds the quarks together in the nucleus. In contrast, $U(1)_Q$ represents the long-range electromagnetic force between charged particles. The formulation of the spontaneous gauge symmetry-breaking mechanism was first proposed by Englert, Brout, Higgs, Guralnik, Hagen, and Kibble, which we will refer to as the Higgs mechanism. This mechanism predicts the existence of a physical elementary scalar particle, the so-called Higgs boson. Its recent discovery by the ATLAS and CMS experiments at the Large Hadron Collider (LHC) at CERN constituted an outstanding achievement in particle physics and a triumph for elementary particle theory, and it was awarded the 2013 physics Nobel Prize. While the mass ~ 125 GeV and current data on decay branching ratios seem, in general, to be in accordance with expectations, a better understanding of its properties from further data will be required to underpin the nature of the associated dynamics and possibly uncover new principles in nature.

The group $SU(3)_c \otimes SU(2)_L \otimes U(1)_Y$ is not believed to be the ultimate theory of elementary particle interactions. However, it is accepted as a good approximation at energy scales below a few hundred gigaelectronvolts (GeV). For example, supersymmetry or strong dynamics has been suggested to explain the naturalness of the electroweak breaking mechanism. While we wait for positive signs of new physics, such as supersymmetry, in the next run of the LHC, we turn to the neutrino sector, which provides one of the most solid present-day pieces of evidence for physics beyond the SM.

[2] `https://home.cern/`

[3] `https://www.desy.de/index_eng.html`

3.0.1 Brief history of neutrinos

Among the elementary building blocks of matter, neutrinos are unique in that they do not carry an electric charge and, as a result, interact only weakly; hence their experimental elusiveness. Neutrinos may pass through ordinary matter almost unaffected. As a result, they constitute a unique probe of the very early Universe, and the precise determination of their properties may hold the clue for what lies beyond the SM of particle physics. Neutrinos come from 'natural' sources such as nuclear fusion inside the Sun, cosmic ray interactions in the Earth's atmosphere, the Earth's natural radioactivity, supernova explosions, not to mention neutrinos produced primordially in the Big Bang itself (see Figure 6). The latter is the subject of this thesis.

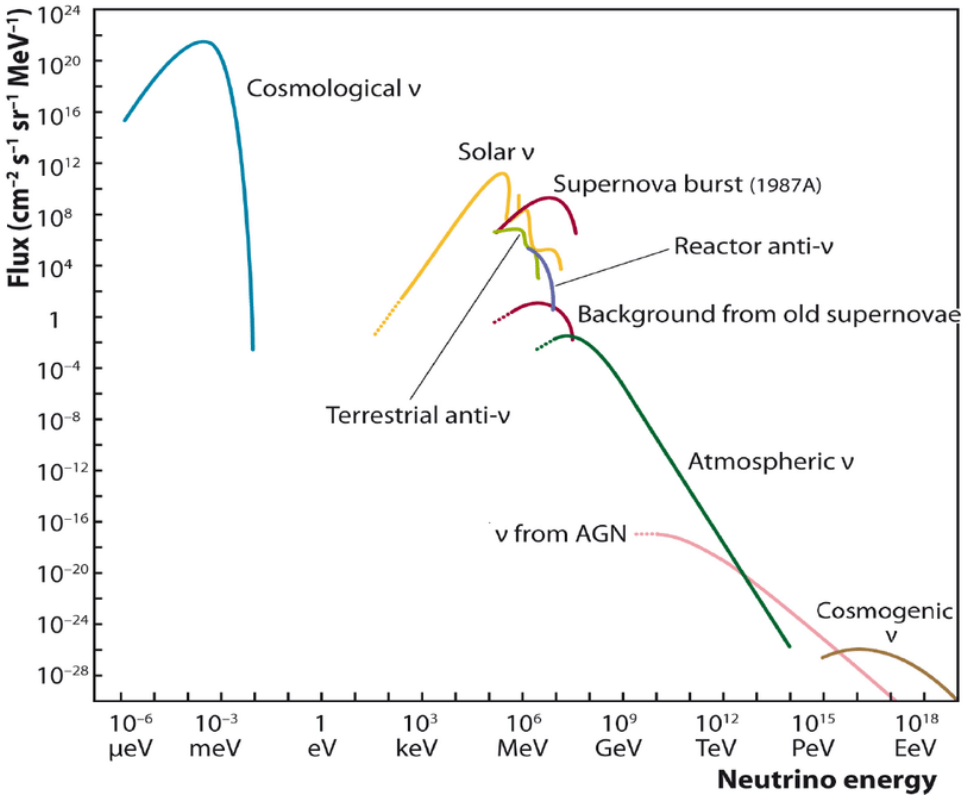

Figure 6 – Fluxes of different terrestrial, astrophysical and cosmic sources

There is one neutrino 'flavour' within each SM generation. The first neutrino ν_e was discovered in nuclear reactors in 1956 [322], while the ν_μ [323] and the ν_τ [324] were discovered in particle accelerators in 1961 and 2000, respectively. Three neutrino species also fit well with the good measurement of the Z-boson 'invisible' width at LEP and the primordial abundance of helium in the early Universe [325]. The Sun and most visible stars produce their energy by converting hydrogen to helium and are copious sources of neutrinos. Pontecorvo was the first to speculate that such neutrinos might be detectable through

radiochemical means in a large volume of chlorine-bearing liquid [326]. In 1964, Bahcall and Davis argued that a solar neutrino experiment would be feasible in a large enough detector volume placed deep underground to reduce cosmic-ray-associated backgrounds [327]. In the late 1960s, Ray Davis proposed his pioneer geochemical experiment at Homestake [328], which captured fewer neutrinos than expected in the standard solar model. Understanding the observed solar neutrino deficit remained a challenge until its final resolution over ten years ago, which gave us irrefutable proof for the existence of neutrino mass, a possibility always present ever since Pauli proposed the neutrino idea in order to account for energy conservation in nuclear beta decays. However, the success of the V–A hypothesis [329] in accounting for the observed parity violation in the weak interaction [330] was taken as an indication for massless neutrinos and incorporated into the manifestly chiral formulation of the $SU(3)_c \otimes SU(2)_L \otimes U(1)_Y$ theory.

The 1980s saw a prosperous period in neutrino physics. On the theory side, motivated by the idea of grand unification, one started to question the assumption of lepton (and baryon) number conservation. The unification idea inspired the seesaw mechanism as a way to understand the tiny neutrino masses as resulting from the exchange of superheavy 'messengers,' either fermions (type I seesaw) or triplet scalars (type II seesaw). The multi-generation description of the gauge group seesaw mechanism was formulated to describe the phenomenology of neutrino oscillations, leading to the current form of the lepton mixing matrix, presented in terms of θ_{12}, θ_{23} and θ_{13} of the mixing angles θ_{ij} as well as Dirac and Majorana CP phases affecting oscillations and lepton number violation processes, respectively. The last ingredient required to describe neutrino propagation was the accurate description of matter effects present in the interior of the Sun and the Earth, formulated by Mikheev, Smirnov, and Wolfenstein.

On the other hand, from the experimental point of view, start using water Cherenkov detectors, which lays the groundwork for the historic detection of neutrinos from SN1987a in the Large Magellanic Cloud. Through the measures of the zenith angle dependence and recoil energy spectrum of solar neutrinos, the observational bases are established of the long-standing problem of solar neutrinos indicated by geochemical experiments since Homestake. Besides, the observations of neutral current neutrino interactions on deuterium at the Sudbury Neutrino Observatory (SNO)[4] offer strong evidence for solar ν_e flavour conversions, also contributing to the determination of the oscillation parameters. The last piece of the solar neutrino puzzle had to wait to confirm the oscillation hypothesis by the nuclear reactor experiment KamLAND[5]. This experiment measured the flux of electron anti-neutrinos ($\bar{\nu}_e$) from distant nuclear reactors in Japan and the spectrum distortion, matching the one expected from large mixing angle oscillations. This last was crucial to

[4] `https://sno.phy.queensu.ca/`

[5] Kamioka Liquid Scintillator Antineutrino Detector - `https://www.awa.tohoku.ac.jp/kamland/`

exclude non-standard solutions, thus establishing the robustness of large-angle oscillations driven by θ_{12}.

Cosmic ray interactions with atomic nuclei in the Earth's atmosphere produce particle showers, resulting in (anti)neutrinos. Large underground experiments such as IMB, MACRO, and Kamiokande-II indicated a deficit in the muon- to-electron neutrino event ratio. The elucidation of this 'anomaly' had to wait till the commissioning of the Super-K experiment, which gave a very high statistics measurement over a wide energy range from hundreds of mega-eV to a few tera-eV. It showed that the observed deficit in the μ-like atmospheric events is due to ν_μ oscillations driven by θ_{23}, a discovery later confirmed by accelerator experiments such as K2K[6] and MINOS[7].

Recent reactor experiments, especially at Daya Bay, have observed the disappearance of electron-anti-neutrinos at a distance of about 2 km from the reactors, providing a robust determination of the third neutrino mixing angle θ_{13}, also seen at accelerator experiments such as T2K.This last opens the door to a new generation of oscillation experiments, probing CP violation in neutrino oscillations and may shed light on flavor mystery.

confirmation of the oscillation hypothesis by experiments based on reactors and accelerators. Dedicated fits indicate a pattern of mixing angles quite different from the Cabibbo–Kobayashi–Maskawa (CKM) matrix, which characterizes quark mixing. Altogether, the discovery of neutrino oscillations constitutes a historic landmark in particle physics, which not only implies new physics but is also likely to pave the way for a deep understanding of the flavour puzzle. In particular, lepton flavour violation may also be seen in the charged lepton sector, irrespective of neutrino mass, bringing complementary information. Moreover, there is likely total lepton number violation, as highlighted in the modern gauge theoretical formulation of neutrino masses. Proving the Majorana nature of neutrinos requires searching for lepton number violation processes such as neutrinoless double-beta decay.

3.0.2 Neutrinos in the SM

The SM of particles physics is a chiral gauge theory formulated in terms of separate left- and right-handed chiral components of the fermion matter fields. The mathematical description of the SM is based on the gauge group $SU(3)_c \otimes SU(2)_L \otimes U(1)_Y$, where the $SU(3)_c$ part describes the strong force (specifically the theory of quantum chromodynamics - QCD), whereas the $SU(2)_L \otimes U(1)_Y$ part describes the electro-weak (EW) interactions.

[6] KEK to Kamioka (Long-baseline Neutrino Oscillation Experiment) - `https://neutrino.kek.jp/`

[7] Main Injector Neutrino Oscillation Search - `https://news.fnal.gov/2005/03/minos-neutrino-experiment-launched-fermilab/`

In a rather symbolic form, which has many things in the background, the SM of particles physics Lagrangian is given by:

$$\mathcal{L}_{SM} = -\frac{1}{4}F_{\mu\nu}F^{\mu\nu} + i\bar{\Psi}\gamma^{\mu}D_{\mu}\Psi + D_{\mu}\Phi D^{\mu}\Phi - V(\Phi) - Y^{ij}\bar{\Psi}_i\Phi\Psi_j. \tag{3.1}$$

The first term includes the kinetic part for the gauge fields (through their field-strengths $F_{\mu\nu}$), the second term contains the kinetic part for the matter fields (denoted by Ψ) and their couplings to the gauge fields. The third term is the kinetic part for the Higgs field Φ (and specifies its interactions with gauge bosons), whereas the fourth term is the Higgs potential which gives rise to the Higgs mechanism and hence to EW symmetry breaking, wherein the $SU(2)_L \otimes U(1)_Y$ symmetry is broken down to the $U(1)_{EM}$ subgroup [8].

The matter content of the SM is arranged into left-handed $SU(2)$ quark doublets [$Q_L^i = (u_L^i,\, d_L^i)$, with $_L$ standing for left-handed and i = 1, 2, 3 running over the three generations] and lepton doublets [$L_L^i = (e_L^i,\, \nu_L^i)$], and right-handed singlets u_R^i, d_R^i, and e_R^i. The last term in Eq. (3.1) is the Yukawa interaction term, which couples the left-handed fermion doublets with the right-handed fermion singlets through the Higgs doublet. Upon EW symmetry breaking, the Yukawa interaction term gives mass to the charged leptons and quarks. Surprisingly, the SM matter content does not include right-handed neutrino fields ν_R^i. Therefore, the Yukawa interaction term cannot generate masses for the neutrinos. This last is no coincidence; instead, it occurs by construction. When the SM was formulated, there only existed upper limits on ν_e of about 200 eV, much smaller than the next lightest known fermion, the electron whose mass is about 0.5 MeV. Therefore, the SM was constructed to accommodate massless neutrinos. However, in 1998, the SuperKamiokande[9] atmospheric neutrino experiment detected neutrino oscillations, it became clear that the picture has to be extended to allow for neutrino masses. Several approaches to give mass to neutrinos in Beyond the Standard Model (BSM) scenarios exist. Nevertheless, the absence of a mechanism for providing mass to the neutrinos is among the most critical shortcomings of the SM. Conversely, the observation that neutrinos have mass is the only direct evidence for physics beyond the Standard Model, presumably operating at excessively high energy scales (which could explain the smallness of neutrino masses). As such, no doubt shedding light on the neutrino mass scale would open the door towards new physics, and the impact such a feat would have cannot be understated. Unveiling the neutrino mass scale, mass ordering, is one of the key targets of several experimental efforts, both in the laboratory and in cosmology.

[8] With $_{EM}$ standing for "Electromagnetism".
[9] `http://www-sk.icrr.u-tokyo.ac.jp/sk/index-e.html`

Family			T	T_3	Q
$\begin{pmatrix} \nu_{\mathrm{e}} \\ \mathrm{e} \end{pmatrix}_L$	$\begin{pmatrix} \nu_{\mu} \\ \mu \end{pmatrix}_L$	$\begin{pmatrix} \nu_{\tau} \\ \tau \end{pmatrix}_L$	$1/2$	$+1/2$	0
				$-1/2$	-1
$\nu_{\mathrm{e}R}$	$\nu_{\mu R}$	$\nu_{\tau R}$	0	0	0
e_R	μ_R	τ_R	0	0	-1
$\begin{pmatrix} \mathrm{u} \\ \mathrm{d} \end{pmatrix}_L$	$\begin{pmatrix} \mathrm{c} \\ \mathrm{s} \end{pmatrix}_L$	$\begin{pmatrix} \mathrm{t} \\ \mathrm{b} \end{pmatrix}_L$	$1/2$	$+1/2$	$+2/3$
				$-1/2$	$-1/3$
u_R	c_R	t_R	0	0	$+2/3$
d_R	s_R	b_R	0	0	$-1/3$

Table 3 – The weak-isospin structure of the fermions in the SM. L and R stand for left-handed and right-handed fermions, T and T_3 are the total weak-isospin and its third component, and Q is the electric charge. Note that the results presented in this report are insensitive to, and independent of, any small ($<$ MeV) neutrino masses.

Neutrinos play a special role in the electro-weak theory $SU(2)_L \otimes U(1)_Y$. While the left-handed neutrinos are part of the doublets $SU(2)_L$:

$$L_i = \begin{pmatrix} \nu_{l_i} \\ l_i \end{pmatrix}_L, \qquad l_i = \{e, \mu, \tau\}, \tag{3.2}$$

right-handed neutrinos are $SU(2)$ singlets. Since the electromagnetic charge and the hypercharge $U(1)$ differ by the value of the third weak isospin component:

$$Q = T_3 + Y, \tag{3.3}$$

where we can see that the right-handed neutrinos $(\nu_{l_i})_R$ do not carry quantum numbers $SU(2) \otimes U(1)$ (See Tab. 3). This has two important implications:

- The neutrinos seen experimentally are those produced by weak interactions. These are purely left-handed.
- Since we cannot infer the existence of right-handed neutrinos from weak processes, the presence of $(\nu_{l_i})_R$ can only be seen indirectly, most likely through the existence of masses for the neutrinos. However, the mass of the neutrinos does not necessarily imply the existence of right-handed neutrinos.

Let's briefly summarize what we know about left-handed neutrino thanks to weak interactions. In the electro-weak theory these neutrinos couple to the Z boson:

$$\mathcal{L}_{Z\nu\bar{\nu}} = \frac{e}{2\cos\theta_w \sin\theta_w} Z^\mu \left[J_\nu^{NC}\right]_\nu , \tag{3.4}$$

where

$$\left[J_\nu^{NC}\right]_\nu = \sum_i (\bar{\nu_{l_i}})_L \gamma_\nu (\nu_{l_i})_L. \tag{3.5}$$

Precise studies of the shape of the Z line allow us to determine the number of neutrino species i, since as this number increases, the total width of the Z also increases. Each type of neutrino (assumed its mass $m_{\nu_i} \ll M_z/2$) contributes in the same way way to the width of Z. The decay width into neutrinos (anti-neutrinos) is given by:

$$\Gamma(Z \to \nu_{l_i}\bar{\nu_{l_i}}) = \frac{\sqrt{2}G_F M_z^3}{24\pi}\rho, \tag{3.6}$$

where G_F is the Fermi constant determined in the muon decay and $\rho = (2g_A^l)^2$ is related to the axial coupling of charged leptons with Z. Doing use of $g_A^l = -0.50102 \pm 0.00030$, which is the mean of the results obtained by the four collaborations of LEP[10] (Namely: ALEPH, DELPHI, L3 and OPAL)[11] and SLD[12]. Thus, we have that, numerically:

$$\Gamma_\nu \equiv \Gamma(Z \to \nu_{l_i}\bar{\nu_{l_i}}) = (167.06 \pm 0.22) MeV. \tag{3.7}$$

With this, the number of different neutrino species, N_ν, can be derived from precision measurements of the full width of Z and its partial widths in hadrons and leptons, using the relation:

$$\Gamma_{tot} = \Gamma_{had} + 3\Gamma_{lep} + N_\nu \Gamma_\nu, \tag{3.8}$$

where $\Gamma_{tot} = (2.4939 \pm 0.0024)$ GeV, $\Gamma_{had} = (1.7423 \pm 0.0023)$ GeV, $\Gamma_{lep}(83.90 \pm 0,1)$ MeV and from the so-called invisible width of Z, we get $\Gamma_{inv} = N_\nu \Gamma_\nu = (499.9 \pm 3.4)$ MeV. So in this way, we can deduce the number of species of relativistic neutrinos:

$$N_\nu = 2.992 \pm 0.020, \tag{3.9}$$

[10] The Large Electron-Positron Collider. `https://home.cern/science/accelerators/large-electron-positron-collider`

[11] For an extensive review of these projects, you can visit the hompage of *The LEP Electroweak Working Group* `http://lepewwg.web.cern.ch/lepewwg/`

[12] `https://www-sld.slac.stanford.edu/sldwww/sld.html`

which reinforces the idea of three generations of leptons and establishes at the same time the existence of 3 active neutrinos, (See Fig. 7). It is possible to obtain a more precise value of N_ν using other information derivable from the Z line. The cross section for $e^+e^- \to hadrons$ can be expressed in terms of three factors: a peak cross section:

$$\sigma_0 = \frac{12\pi\Gamma_{lep}\Gamma_{had}}{\Gamma_{tot}^2 M_z^2} \tag{3.10}$$

a Breit–Wigner factor:

$$BW(s) = \frac{s\Gamma_{tot}^2}{(s - M_z^2)^2 + \frac{s^2\Gamma_{tot}^2}{M_z^2}} \tag{3.11}$$

and a bremsstrahlung correction of the initial state $[1 - \delta_{QED}(s)]$, with:

$$\sigma_{had} = \sigma_0 BW(s)[1 - \delta_{QED}(s)] \tag{3.12}$$

The value of σ_0 can be extracted from the analysis of the effective section for the process $e^+e^- \to hadrons$ in LEP:

$$\sigma_0 = (41.491 \pm 0.058)nb. \tag{3.13}$$

This can be combined with the LEP results for the ratio of hadronic to leptonic partial widths of Z, as:

$$R_l = \frac{\Gamma_{had}}{\Gamma_{lep}} = 20.765 \pm 0.026, \tag{3.14}$$

with which a value for the number of active neutrinos can be deduced, as:

$$N_\nu = \frac{\Gamma_{inv}}{\Gamma_\nu} = \frac{\Gamma_{lep}}{\Gamma_\nu}\left(\frac{\Gamma_{tot}}{\Gamma_{lep}} - \frac{\Gamma_{had}}{\Gamma_{lep}} - 3\right) = \frac{\Gamma_{lep}}{\Gamma_\nu}\left(\sqrt{\frac{12\pi R_l}{\sigma_0 M_Z^2}} - R_l - 3\right). \tag{3.15}$$

In the SM, the quotient Γ_{lep}/Γ_ν is known very precisely:

$$\frac{\Gamma_{lep}}{\Gamma_\nu} = 1.991 \pm 0.001. \tag{3.16}$$

Using this value, together with the experimentally determined Z boson mass, $M_Z = (91.1867 \pm 0.0021)$ GeV, and the values of σ_0 and R_l measured at LEP (See [331]), we obtain:

$$N_\nu = 2.994 \pm 0.011; \qquad \Gamma_{inv} = (500.1 \pm 1.9)MeV. \tag{3.17}$$

values that are consistent with those obtained previously but a factor of two more precise. If we use the width of the Z boson ($\Gamma_z = 2.4952 \pm 0.0023$ GeV - See Fig. 7), we get:

$$N_\nu = 2.9840 \pm 0.0082, \tag{3.18}$$

which is in agreement with the three observed generations of fundamental fermions, but with an accuracy of 0.3% (For a comprehensive review of the results of this project, see [331]). On the other hand, the coupling of the $W^\pm$ bosons to the charged leptonic currents is analogous to that of the Z and the neutrinos. Again, only left-handed neutrinos are involved. We have:

$$\mathcal{L}_{Wl_{\nu_l}} = \frac{e}{\sqrt{2}\sin\theta_w}\left[W_+^\mu J_{\mu-}^{lep} + W_-^\mu J_{\mu+}^{lep}\right], \tag{3.19}$$

where

$$J_{\mu-}^{lep} = (J_{\mu+}^{lep})^\dagger = \sum_i \bar{l}_{iL}\gamma_\nu \nu_{l_iL}. \tag{3.20}$$

The states of the previous equation are not in general eigenstates of mass, since the generation of mass can mix fermions of the same charge with each other. However, we can always diagonalize the charged lepton mass matrix by a unit transformation:

$$l_L = U^l \tilde{l}_L; \qquad l_R = U^l \tilde{l}_R. \tag{3.21}$$

After this transformation, we have:

$$J_{\mu-}^{lep} = (J_{\mu+}^{lep})^\dagger = \sum_{ij} \overline{\tilde{l}_{iL}}\gamma_\nu (U^l)_{ij}^\dagger \nu_{l_jL} = \sum_i \overline{\tilde{l}_{iL}}\gamma_\nu (U^l)_{ij}^\dagger \tilde{\nu}_{l_jL}, \tag{3.22}$$

where

$$\tilde{\nu}_{lL} = (U^l)^\dagger \nu_{lL}. \tag{3.23}$$

Since U^l is unitary, the neutral current $[J_\mu^{CN}]_\nu$ is identical to the one expressed in terms of ν_{lL} or $\tilde{\nu}_{lL}$. Normally, the $\tilde{\nu}_{l_jL}$ states are called *eigenstates of the weak interaction*, since they are produced in the decays of a W^+ associated with a charged lepton $\tilde{l}_i$ of defined mass. For simplicity in the notation we will remove the tilde from $\tilde{l}_{iL}$ and $\tilde{\nu}_{iL}$ from now

on, understanding that the states now called ν_{l_iL} are those produced by weak interactions. Similarly the charged leptons l_i are the states associated with the diagonal mass matrix:

$$M_l = \begin{pmatrix} m_e & & \\ & m_\mu & \\ & & m_\tau \end{pmatrix}. \tag{3.24}$$

We will return to this topic in the subsection 3.0.2.4.

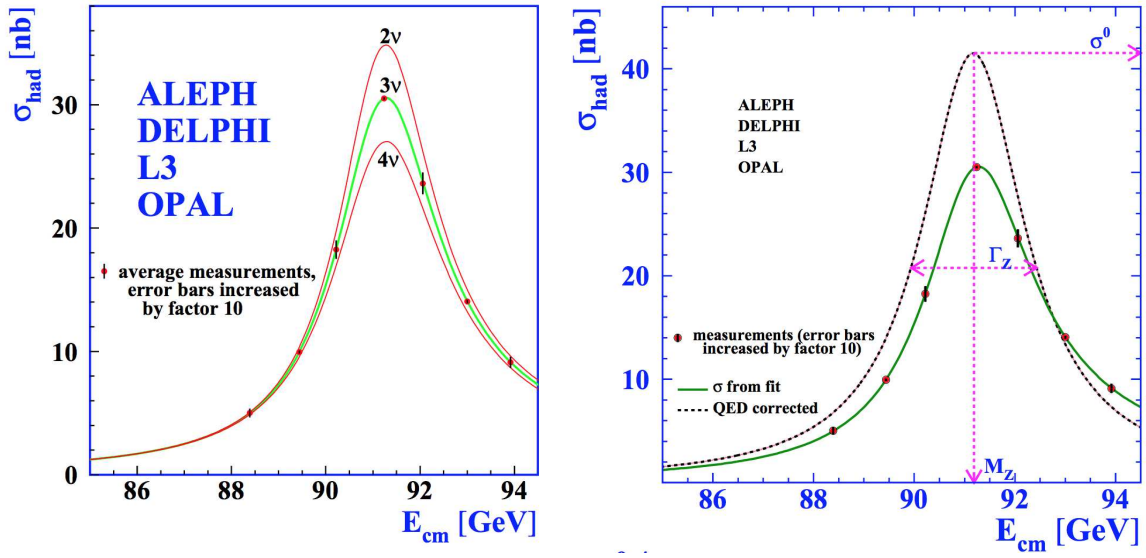

Figure 7 – *Left Panel.* Measurements of the hadron production cross-section around the Z resonance. The curves indicate the predicted cross-section for two, three and four neutrino species with SM couplings and negligible mass. *Right Panel.* Average over measurements of the hadronic cross-sections by the four experiments, as a function of centre-of-mass energy. The full line represents the results of model-independent fits to the measurements. Correcting for QED photonic effects yields the dashed curves, which define the Z parameters (Obtained from [331]).

3.0.2.1 Massive neutrinos

We saw in the last section that SM predicts massless neutrinos, making them essentially different from other fermions, such as the charged leptons and quarks, which are known to have masses. SM has also been highly successful in explaining the various low weak energy processes involving charged and neutral current interactions. For a long time, therefore, there was a substantial prejudice among some theorists that neutrinos are indeed massless. Many BSM scenarios that became extremely popular were, in fact, closely related to the neutrino's lack of mass. The situation has now changed drastically. There is convincing evidence for neutrino masses for several experiments described below and in subsequent sections. The landscape of particle physics has been altered for every discovery.

For a good reason, the neutrinos are now on the same footing as quarks, a fact anticipated by people who believed in quark lepton symmetry more literally than just as a token indicated by the weak interactions; but more importantly, it is giving new and exciting clues to the directions of new physics BSM. Our current understanding of neutrinos has changed dramatically in the past sixteen years. Thanks to many neutrino oscillation experiments involving solar, atmospheric, accelerator, and reactor (anti)-neutrinos, we have learned that neutrinos produced in a well-defined flavor eigenstate can be detected, after propagating a macroscopic distance, as a different flavor eigenstate. The simplest interpretation of this phenomenon is that, like all charged fermions, the neutrinos have mass and that, similar to quarks, the neutrino weak, or flavor, eigenstates are different from neutrino mass eigenstates, i.e., neutrinos mix. This new state of affairs has also raised many other issues which did not exist for massless neutrinos: For example:

- Massive Dirac neutrinos, like charged leptons and quarks, can have nonzero magnetic dipole moments, and massive Dirac and Majorana neutrinos can have nonzero transition dipole moments.
- The heavier neutrinos decay into lighter ones, like charged leptons and quarks.
- Most important, the neutrinos can be either Majorana or Dirac fermions (see next section for more details).

Learning about all these possibilities can bring our knowledge of neutrinos to the same level as that of charged leptons and quarks, which may also lead to a plethora of laboratory, astrophysical and cosmological consequences. More importantly, knowing the properties of neutrinos in detail can also play a crucial role in clarifying the model for new physical laws beyond those embodied in the Standard Model. One may also consider the possibility that there could be new neutrino species beyond the three known ones, for example, the sterile neutrino.

In addition to being a question whose answer would be a revolutionary milestone pointing to unexpected new physics, it may also become a necessity if the LSND[13] results are confirmed by the MiniBooNE[14] experiment, now in progress at Fermilab. This would, undoubtedly, be a second revolution in our thinking about neutrinos and the nature of unification. The existence of neutrino masses qualifies as the first evidence of new physics beyond the Standard Model. The answers to the neutrino-questions mentioned above will add substantially to our knowledge about the precise nature of this new physics and, in turn, about the nature of new forces beyond the Standard Model. They also have the

[13] Liquid Scintillating Neutrino Detector (LSND). `http://www.nu.to.infn.it/exp/all/lsnd/`
[14] `https://microboone.fnal.gov/`

potential to unravel some of the deepest and most long-standing mysteries of cosmology and astrophysics, such as the origin of matter, the origin of the heavy elements, and, perhaps, even the nature of dark energy.

We carry out this survey to show how the different experimental results expected in the coming decades can elucidate the nature of neutrinos and our search for new physics. In particular, we would like to know:

- the implications of neutrinos for such longstanding ideas as grand unification, supersymmetry, string theory, extra dimensions, etc.
- the implications of the possible existence of additional neutrino species for physics and cosmology.
- and whether neutrinos have anything to do with the origin of the observed matter-antimatter asymmetry in the universe and, if so, whether there is any way to determine this via low-energy experiments.

Once the answers to these questions are at hand, we will have considerably narrowed the choices of new physics, providing a giant leap in our understanding of the physical Universe.

3.0.2.2 Why neutrino mass necessarily means physics beyond the SM?

Up to date, neutrino oscillations are the only evidence for the existence of physics BSM of particle physics. It is imperative to decode the type of new physics indicated by existing observational data; to predict the signals of new physics that might appear in future projects, we need to make forecasts. We need to understand how they fit into the different schemes delineated for various reasons, including the issue of hierarchy problem and gauge coupling unification. In the SM, the quarks and leptons transform as: $Q_L(3,2,1/3)$, $u_R(3,1,4/3)$, $d_R(3,1,-2/3)$, $L(1,2,-1)$, $E_R(1,1,-2)$. The Higgs boson h^0, responsible for electroweak symmetry breaking, transforms as $(1,2,+1)$. The electroweak symmetry $SU(2)_L \otimes U(1)_Y$ is broken by the vacuum expectation of the Higgs doublet $\langle\Phi\rangle = v/\sqrt{2} \approx 246/\sqrt{2}$ GeV, which makes that $W^{\pm}$ and Z gauge bosons and electrically charged fermions acquire mass. *The reason neutrinos do not get mass as a result of the Higgs mechanism is that the right-handed neutrino ν_R was not included in the list of fermions in the Standard Model; as a result, there is no coupling of the form $\eta_\nu \bar{L} H \nu_R$ that could have given mass to the neutrinos after symmetry breaking.*

The apparently simple way to understand the mass of neutrinos would be to extend the standard model to include ν_R. This would also be desirable from the point of view of making the quark lepton model symmetric. There are two problems with this naively trivial modification:

- One is that by quark-lepton symmetry, one would expect the neutrino masses arising from the Yukawa coupling $\eta_\nu \bar{L} H \nu_R$ to be of the same order as the quark and charged leptons. Observational limits show that the masses of neutrinos are at least 10^6 times smaller than the smallest masses of quarks and leptons. Therefore, a non-zero neutrino mass suggests not only the existence of right-handed neutrinos (of which there would be three if they correspond to the usual generations) but also new physics that will allow us to understand why $M_\nu \lll m_{q,l}$. The seesaw mechanism provides a plausible basis for this understanding since it uses the fact that, among the known fermions, only neutrinos can have Majorana mass terms.

- The other problem with introducing a set of right-handed neutrino fields is that they are SM gauge singlets. This means that, as far as the symmetries of the Standard Model are concerned, a Majorana mass for the ν_R fields is allowed. If such a mass term is present, however, the neutrino masses are not simply given by the $\eta_\nu v$ but are determined by a more complicated function of $\eta_\nu v$ and the Majorana masses of the right-handed neutrinos. To avoid the presence of a Majorana mass for the right-handed neutrinos, one must impose an extra symmetry to the SM Lagrangian, a very nontrivial modification of what is traditionally referred to as the SM electroweak interactions.

3.0.2.3 Absolute mass of neutrinos

The study of solar and atmospheric neutrinos wrote an important chapter in particle physics, leading to the discovery of neutrino oscillations, which are a quantum-mechanical phenomenon, as they propagate, change the flavor, and thus confirm that they have mass. Oscillations of neutrinos do not probe the absolute neutrino mass, nor are they currently sensitive to the hierarchy order of the neutrino states. Currently, there are three realistic ways to probe the absolute neutrino mass:

- *Measuring the shape of the end-point of the spectrum in tritium beta decays*: The simplest way to directly measure the neutrino's mass is using beta decays. The neutrino mass can be determined by observing the shape of the end-point (18.6 keV) of the single beta-decay spectrum with sufficient precision. One method used to precisely measure the beta-decay spectrum relies on a spectrometer to precisely select high-energy electrons from single β-decay of molecular tritium ($T_2 \rightarrow^3 HeT^+ + e^- + \bar{\nu}_e$)

(See Fig. 8). The most recent experiment to use this technique is KATRIN[15], which placed a limit of $m_\nu < 0.9$ eV at 90% CL (where m_ν is the effective electron antineutrino mass), and combining this result with the first neutrino mass campaign ($m_\nu < 1.1$ eV at 90% CL), they find an upper limit of $m_\nu < 0.8$ eV at 90% CL, which constitutes the first direct measure of the neutrino mass with sub-eV sensitivity (0.7 ev at 90% CL) [332]. The final goal of KATRIN is to reach a sensitivity of 0.2 eV at 90% CL (see Fig. 9). The measurement principle to derive a model-independent[16] neutrino mass is the high precision measurement of the kinetic energy of the beta electron from the Tritium beta decay. In the beta decay of Tritium to Helium, an electron and anti-neutrino are released ($^3H \rightarrow^3 He + e^- + \bar{\nu}_e$). They share together the released transition energy, which is distributed to their kinetic energies, the rest mass of the electron, and -if the neutrino is massive- also to the rest mass of the neutrino. The subtle effect of the neutrino rest mass on the kinetic energy of the electron is largest when the neutrino is non-relativistic, i.e., at the endpoint of the electron energy spectrum. Therefore, a precision measurement of the electron energy very close to its endpoint gives information on the neutrino mass. In principle, every beta decaying isotope could be used. However, Tritium is an excellent candidate for this experiment, due to the very low end-point energy of Tritium decay, the effect of massive neutrinos on the electron's kinetic energy is more significant. On top of that, Tritium has a simple nuclear structure with one proton and two neutrons. This means no nuclear energy dependant corrections must be applied to the beta spectrum and calculated from the first principles of the well-proven V-A theory[17].

- *The search for neutrinoless double-beta decay* $\beta\beta0\nu$: Two-neutrino double-beta decay ($2\nu\beta\beta$) is the second-order (in the Fermi constant G_F) weak interaction process, by which two neutrons in a nucleus are converted to protons, plus two electrons plus two-electron anti-neutrinos, $(A, Z) \rightarrow (A, Z + 2) + 2e + 2\nu_e$. This rare process has been detected in a few nuclei, conserving the lepton number ($L = L_e + L_\nu + L_\tau$). On the other hand, neutrinoless double-beta decay $0\nu\beta\beta$ is a variety of double-beta decay expected to occur if neutrinos are Majorana (if there are no conserved leptons numbers)[18]. Its amplitude is proportional to an effective mass parameter $\langle m_{\beta\beta} \rangle$ as a function of the lightest neutrino mass $m_{lightest}$.

[15] Karlsruhe Tritium Neutrino Experiment (KATRIN) - `https://www.katrin.kit.edu/`

[16] This method is independent of any cosmological model and of the mass nature of the neutrino, i.e. it may be a lepton of Majorana or Dirac type.

[17] "Vector minus axial", a theory of weak interaction.

[18] The problem of the nature of massive neutrinos ν_i (Dirac or Majorana?) is one of the most fundamental problem of neu- trino physics. In order to reveal the nature of neutrinos with definite masses it is necessary to study processes in which the total lepton number L is violated.

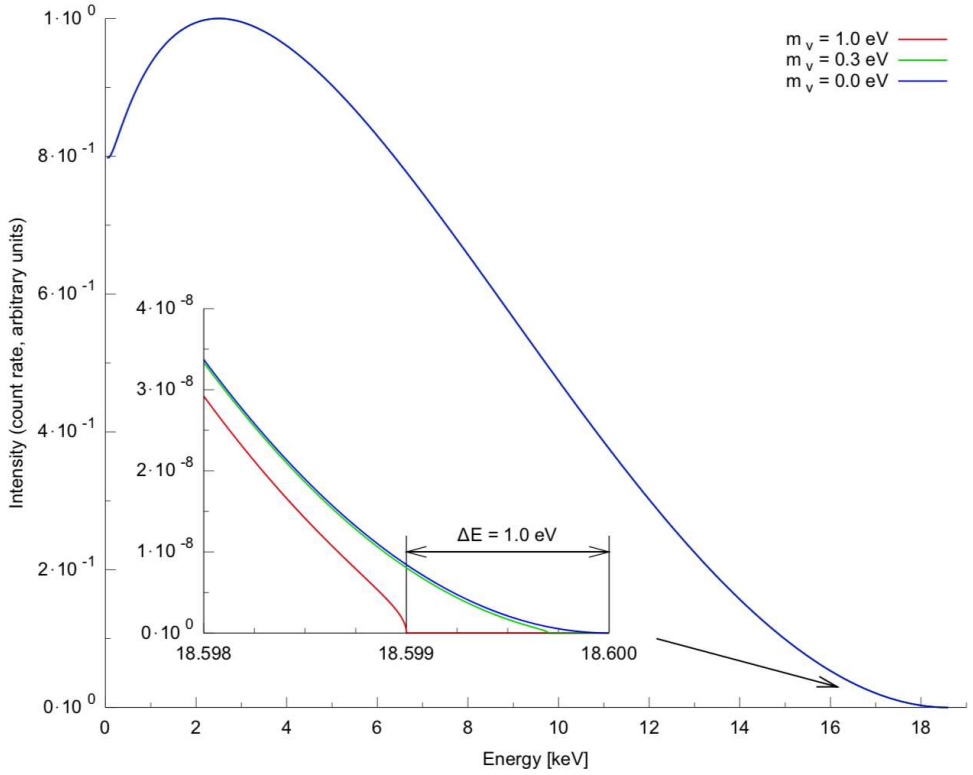

Figure 8 – Energy spectrum of tritium beta decay used by the KATRIN neutrino experiment. The neutrino mass is measured by analysing the end-point of the spectrum. In this plot three possible graphs are shown for massless, light and heavy neutrinos.

- *Measurements of temperature anisotropies in the CMB*: The hot, dense conditions of the early universe included a thermal background of photons and free electrons in the plasma. Photons streamed freely as the plasma cooled and the density of free electrons plummeted, and the mean free path became larger than the extent of the observable universe. Today we observe these photons as the CMB. These same hot and dense conditions led to a cosmic neutrino background ($C\nu B$) that contributes nearly as much as photons to the total energy density in the early universe. The neutrinos began to stream freely at $k_B T \approx 1 MeV$ and continue to flow freely through the cosmos to this day. Unlike with photons, direct detection of the $C\nu B$ is exceedingly difficult. Authors at [212], present the first detection of the temporal phase shift generated by neutrino perturbations during the acoustic oscillation phase of cosmological evolution, and find an amplitude of this effect consistent with the standard value associated with the three known neutrino species (see Fig. 10).

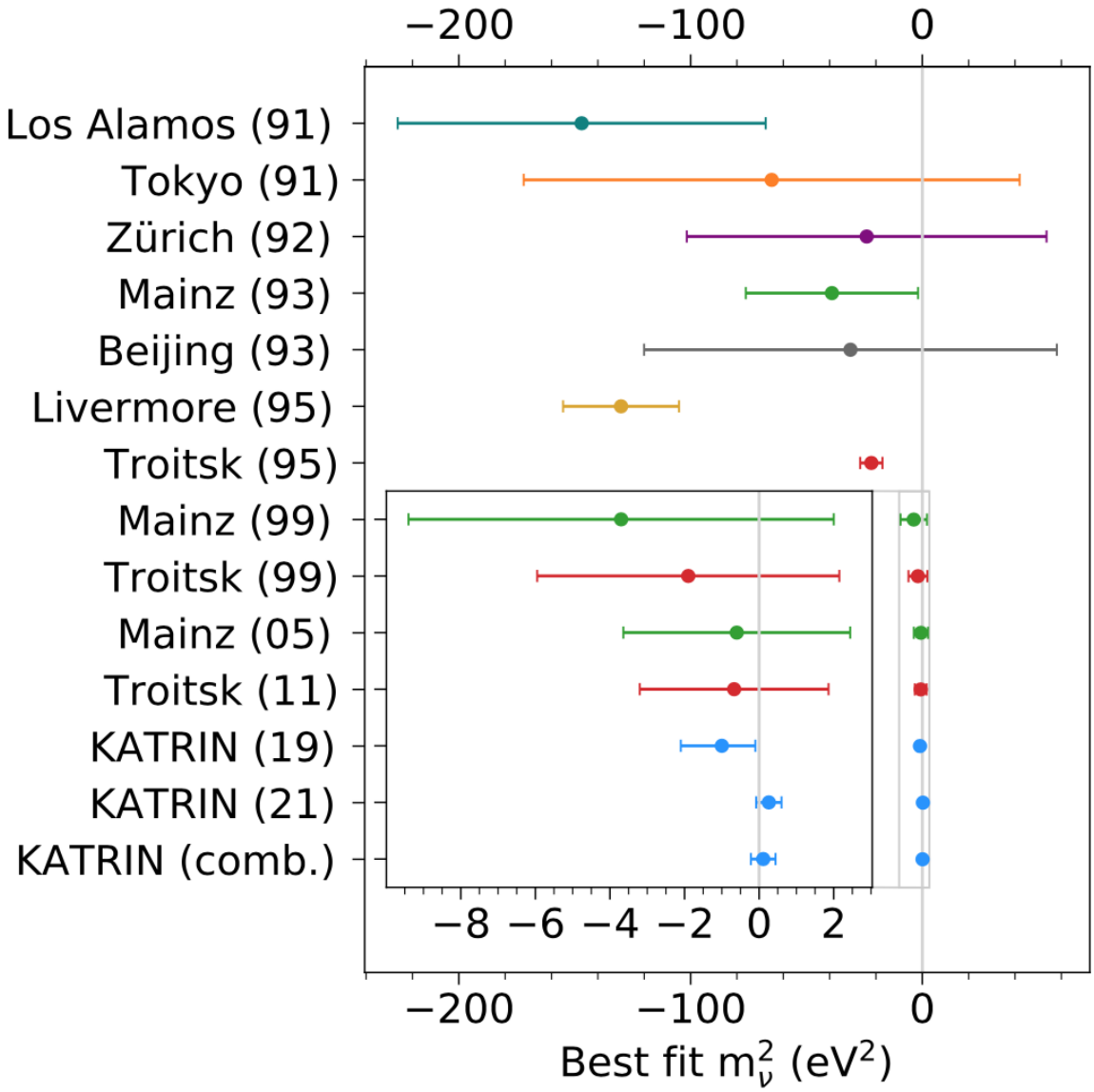

Figure 9 – Comparison of best-fit values and uncertainties with previous neutrino mass experiments (See [332] and the references therein).

One of the main objectives of the present thesis deals precisely with this last point, namely, to use the data of the CMB anisotropies to obtain limits on the number of relativistic species (3 generations of active neutrinos and something more) and the absolute mass value of neutrinos in the very low energy regime. This summarizes our summary of the experimental status of neutrino physics. Now we turn to theory, starting with the origin of neutrino mass and then moving to the structure of neutrino mixing and its theoretical basis.

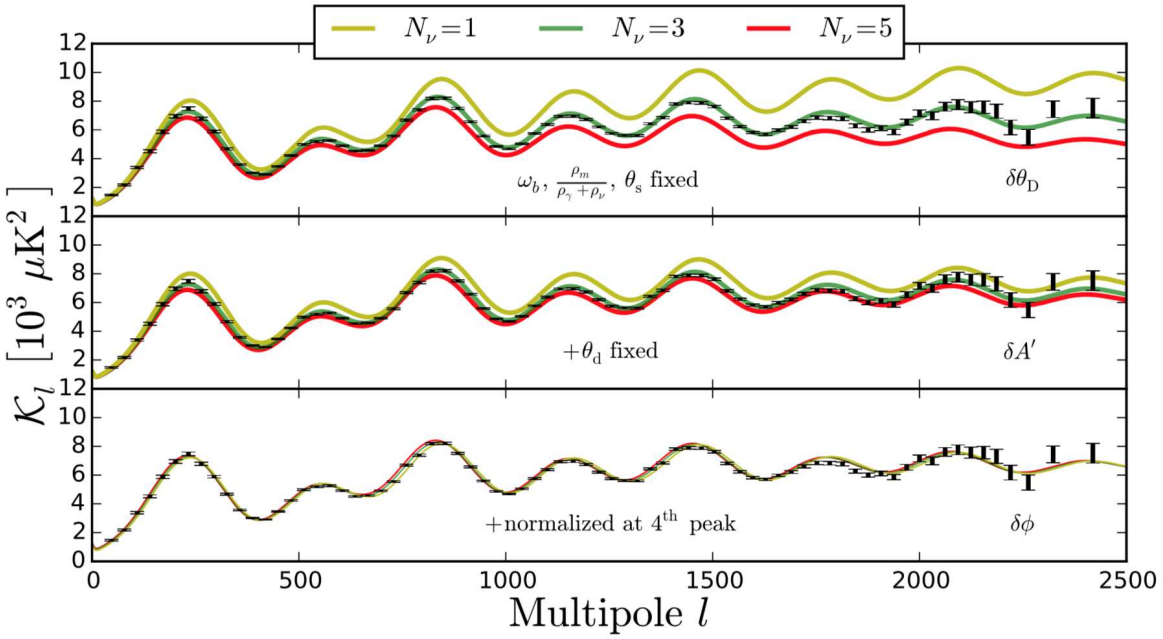

Figure 10 – Undamped power spectra $\mathcal{K}_l$ with different values of N_ν. Figure obtained from Follin et al. [212].

3.0.2.4 Dirac and Majorana masses

The fact that the neutrino has no electric charge endows it with specific properties not shared by the charged fermions of the Standard Model. One can write two kinds of Lorentz invariant mass terms for the neutrino, Dirac, and Majorana masses, whereas, for the charged fermions, conservation of electric charge allows only Dirac-type mass terms. In the four component notation for describing fermions, commonly used for writing the Dirac equation for the electron, the Dirac mass has the form $\bar{\nu}\nu$, connecting fields of opposite chirality. In contrast, the Majorana mass is of the form $\nu_L^T C^{-1}\nu_L$ connecting fields of the same chirality, where ν_L is the four-component spinor and C^{-1} is the charge conjugation matrix. *In the first case, the fermion ν is different from its antiparticle, whereas in the latter case, it is its own antiparticle.* A Majorana neutrino implies a whole new class of experimental signatures, the most prominent among them being the process of neutrinoless double-beta decay of heavy nuclei $0\nu\beta\beta$. Since $0\nu\beta\beta$ arises due to the presence of neutrino Majorana masses, a measurement of its rate can provide exact information about neutrino masses and mixing, provided:

- one can satisfactorily eliminate other contributions to this process that may arise from other interactions in a full beyond-the-standard-model theory, as we discuss below.

- one can precisely estimate the values of the nuclear matrix elements associated with

the $0\nu\beta\beta$ in question.

The expressions for the Dirac and Majorana mass terms clarify that a theory forbids Majorana masses for a fermion only if there is an additional global symmetry under which it has a nonzero charge. As noted above, for charged fermions such as the electron and the muon, Majorana mass-terms are forbidden because they have a nonzero electric charge, and the theory has electromagnetic U(1) invariance, and hence, all charged fermions are Dirac fermions. On the other hand, a Lagrangian with both Majorana and Dirac masses describes, necessarily, a pair of Majorana fermions, irrespective of how small the Majorana mass term is (although it may prove very difficult to address whether the fermion is of the Dirac or the Majorana type when the Majorana mass-term is significantly smaller than the Dirac mass term). Hence, since the neutrino has no electric charge, the "simplest" theories predict that the neutrino is a Majorana fermion meaning that a Majorana neutrino is more natural (or requires fewer assumptions) than a Dirac neutrino.

Let us return to the mass diagonalization problems for the leptonic sector (see subsection 3.0.2). As we saw in the SM building, the three flavor neutrinos, ν_e,ν_μ,ν_τ, complete the spectrum of elementary particles of the SM. Every neutrino is the partner of a charged lepton (electron, muon, tau), connected to it by the weak interaction. These interactions all fall within the context of the general gauge theory of $SU(2)_L \otimes U(1)_Y$. This easily divides the types of possible neutrino interactions into three broad categories:

- *Charged Current (CC)*: The first type of interaction is mediated by exchanging a charged W boson. The leptonic charged weak current, j^μ_W, is given by the form:

$$j^\mu_W = 2 \sum_{\alpha=e,\nu,\tau} \bar{\nu}_{\alpha,L} \gamma^\mu l_{\alpha,L}. \tag{3.25}$$

  These previously defined components enter directly into the Lagrangian:

$$\mathcal{L}_{\mathcal{CC}} = -\frac{g}{2\sqrt{2}} \left(j^\mu_W W_\mu + j^{\mu,\dagger}_W W^\dagger_\mu \right) \tag{3.26}$$

  via their coupling to the heavy gauge boson field $W^\pm$. Though the charged leptonic fields are of a definite mass eigenstate, this is not necessarily so for the neutrino fields, giving rise to the well-known phenomena of neutrino oscillations.

- *Neutral Current (NC)*: The second type of interaction, known as the neutral current (NC) exchange, is similar in character to the charged current case. The leptonic neutral current term, j^μ_Z, is given by:

$$j^\mu_Z = 2 \sum_{\alpha=e,\nu,\tau} g^\nu_L \bar{\nu}_{\alpha,L} \gamma^\mu \nu_{\alpha,L} + g^f_L \bar{l}_{\alpha,L} \gamma^\mu l_{\alpha,L} + g^f_R \bar{l}_{\alpha,R} \gamma^\mu l_{\alpha,R}, \tag{3.27}$$

which describes the exchange of the neutral boson, Z^0. Here, $\nu_{\alpha,L(R)}$ and $l_{\alpha,L(R)}$ correspond to the left (rigth) neutral and charged leptonic fields, while g_L^{ν}, g_L^f and g_R^l represent the fermion left and right- handed couplings. The corresponding Lagrangian is then:

$$\mathcal{L}_{\mathcal{NC}} = -\frac{g}{2\cos\theta_W} j_Z^{\mu} Z_{\mu}, \tag{3.28}$$

where Z_{μ} represent the heavy gauge boson field, whilw θ_W is the Weinberg mixing angle. Historically, the neutrino-lepton CC and NC interactions had been used to study the nature of the weak force in great detail.

- *CC + NC*: We now turn our attention to the last possible type of interaction, where the charged current and neutral current amplitudes interfere with one another. Such a combined exchange is realized in $\nu_e + e \rightarrow \nu_e + e$ scattering. One remarkable feature of neutrino-electron scattering is that it is highly directional. The outgoing electron is emitted at small angles concerning the incoming neutrino direction. A simple kinematic argument shows that indeed $E_e\theta_e^2 \leq 2m_e$. This remarkable feature has been exploited extensively in various neutrino experiments, particularly solar neutrino detection. The Kamiokande neutrino experiment was the first to use this reaction to reconstruct ^8B neutrino events from the sun and point back to the source. The Super-Kamiokande experiment later expanded the technique, creating a photograph of the sun using neutrinos[19]. Other solar experiments later used the method, such as SNO and BOREXINO.

3.0.3 Neutrino oscillations

Neutrinos do not decay, but they do change the flavor. This last is known as neutrino oscillation, and it is due to an odd quantum property of the particles. Each of the three neutrino flavors is a superposition mixture of three quantum states with different masses, which we label ν_1, ν_2, and ν_3. Think of it as like the (x,y,z) coordinates on the surface of a sphere: the total "position" on the sphere's surface is the neutrino flavor, but the "coordinates" are the hidden mass states. However, it does not stick to one spot: the state of the neutrino travels across the sphere's surface, eventually coming back to its starting point (hence the name "oscillation"). In less abstract terms, this means that as a neutrino propagates, it changes from one flavor to another. The following sections will discuss the theoretical approaches and implications of this change for experiments.

[19] The fact that such a picture was taken underground during both day and night is also quite remarkable - `http://www-sk.icrr.u-tokyo.ac.jp/`

3.0.3.1 Neutrino mass and mixing matrix

Is possible to articulate all neutrino interactions within this simple framework:

$$\mathcal{L} \supset \sum_{\alpha=e,\nu,\tau} \left[\bar{\nu}_\alpha i \not{\partial} \nu_\alpha + \frac{g}{\sqrt{2}} \left(\bar{\nu}_{\alpha,L} \gamma^\mu l_{\alpha,L} W_\mu^+ + h.c. \right) + \frac{g}{2\cos\theta_w} \bar{\nu}_{\alpha,L} \gamma^\mu \nu_{\alpha,L} Z_\mu \right] - \sum_{\alpha,\beta=e,\nu,\tau} \left(\bar{\nu}_{\alpha,L} m_{\alpha\beta} \nu_{\beta,R} + h.c \right), \tag{3.29}$$

Neutrino masses, whether Dirac or Majorana, imply lepton mixing. Note that only left-handed neutrinos couple to the weak gauge bosons $W^\pm$ and Z^0. The Dirac and Majorana mass term:

$$-\mathcal{L}_m^{Dirac} = \sum_{\alpha,\beta=e,\nu,\tau} \left(\bar{\nu}_{\alpha,L} m_{\alpha\beta} \nu_{\beta,R} + h.c \right), \tag{3.30}$$

$$-\mathcal{L}_m^{Majorana} = \frac{1}{2} \sum_{\alpha,\beta=e,\nu,\tau} \left(\bar{\nu}_{\alpha,L} m_{\alpha\beta} \nu_{\beta,L} + h.c \right), \tag{3.31}$$

is in general off-diagonal (i.e. m can be non-zero even if $\alpha \neq \beta$). This means that the flavor eigenstates or interaction eigenstates ν_α ($\alpha = e, \mu, \tau$) do not have a definite mass. In the Dirac case, the mass matrices can be diagonalized by a bi-unitary rotation:

$$m = U m_{Dirac} V^\dagger, \tag{3.32}$$

where $m_{Diac} = diag(m_1, m_2, m_3)$ is diagonal matrix and U and V are unitary matices, while in the Majorana case, the neutrino mass matrix, being symmetric, can be taken to a diagonal form by:

$$m = U^\dagger m_{Majorana} U^*, \tag{3.33}$$

where $m_{Majorana} = diag(m_1, m_2, m_3)$ is diagonal matrix. we can define the neutrino mass eigenstates as:

$$\nu_{j,L} \equiv \sum_\alpha U_{\alpha,j}^* \nu_{\alpha,L} \tag{3.34}$$

$$\nu_{j,R} \equiv \sum_\alpha V_{\alpha,j}^* \nu_{\alpha,R}. \tag{3.35}$$

Then, the Dirac and Majorana mass term can be rewritten as:

$$-\mathcal{L}_m^{Dirac} = \sum_{\alpha=e,\nu,\tau} \left(\bar{\nu}_{\alpha,L} m_\alpha \nu_{\alpha,R} + h.c \right) \tag{3.36}$$

$$-\mathcal{L}_m^{Majorana} = \sum_{\alpha=e,\nu,\tau} \left(\bar{\nu}_{\alpha,L} m_\alpha \nu_{\alpha,L} + h.c\right). \tag{3.37}$$

The unitary 3×3 mixing matrix U, is known as *Pontecorvo-Maki-Nakagawa-Sakata* (PMNS) mixing matrix. A standard parametrization of the mixing matrices for Dirac, U_{PMNS}, and Majorana, $\tilde{U}_{PMNS}$, is:

$$U_{PMNS} = \begin{pmatrix} 1 & 0 & 0 \\ 0 & c_{23} & s_{23} \\ 0 & -s_{23} & c_{23} \end{pmatrix} \begin{pmatrix} c_{13} & 0 & -s_{13}e^{-i\delta} \\ 0 & 1 & 0 \\ -s_{13}e^{i\delta} & 0 & c_{13} \end{pmatrix} \begin{pmatrix} c_{12} & s_{12} & 0 \\ -s_{12} & c_{12} & 0 \\ 0 & 0 & 1 \end{pmatrix}, \tag{3.38}$$

$$\tilde{U}_{PMNS} = U_{PMNS}\left(\theta_{12}, \theta_{13}, \theta_{23}, \delta\right) \begin{pmatrix} 1 & 0 & 0 \\ 0 & e^{i\alpha_1} & 0 \\ 0 & 0 & e^{i\alpha_2} \end{pmatrix}, \tag{3.39}$$

where, in general $\theta_{ij} \in [0, \pi/2]$ and $\delta, \alpha_1, \alpha_2 \in [0, 2\pi]$. On the other hand, $s_{12} = \sin\theta_{12}$, $s_{12} = \sin\theta_{12}$, δ is the CP-violating phase, and the extra phases $\alpha_{1,2}$, only come into play in double-beta decay.

3.0.3.2 Oscillations in vacuum

The most spectacular implication of neutrino masses and mixings is the macroscopic quantum phenomenon of neutrino oscillations, first introduced by B. Pontecorvo [333]. The Nobel prize in 2015 has been awarded to T. Kajita (from the SuperKakiokande collaboration) and A. B. McDonald (from the SNO collaboration) for the discovery of neutrino oscillations, which shows that neutrinos have a mass (See Fig. 11). We have seen that the neutrino flavour fields (ν_e, ν_μ, ν_τ) that couple via CC to the leptons(e, μ, τ) are unitary combinations of the mass eigenstates fields (ν_1, ν_2, ν_3):

$$\begin{pmatrix} \nu_e \\ \nu_\mu \\ \nu_\tau \end{pmatrix} = U_{PMNS}(\theta_{12}, \theta_{13}, \theta_{23}, Phases) \begin{pmatrix} \nu_1 \\ \nu_2 \\ \nu_3 \end{pmatrix}. \tag{3.40}$$

In a neutrino oscillation experiment, neutrinos are produced by a source (e.g., pion or μ decays, nuclear reactions,..., etc.) and are detected some macroscopic distance, L, away from the production point. They are produced and detected via weak processes in combination with a given lepton flavour in flavour states. As these states propagate undisturbed in space-time from the production to the detection regions, the different mass eigenstates, having slightly different phase velocities, pick up different phases, resulting in a non-zero probability that the state that arrives at the detector is in a different flavour

combination to the one initially produced. The probability for this flavour transition oscillates with the distance traveled. Two ingredients are mandatory for this phenomenon to take place:

- Neutrinos must keep quantum coherence in propagation over macroscopic distances, which is only possible because they are so weakly interacting.
- There is sufficient uncertainty in momentum at production and detection so that a coherent flavour state can be produced[20].

In addition to this, there are two types of experiments that can be envisaged:

- Appearance experiments, where one searches for the appearance of states with a new flavour in a beam. Such experiments are, by necessity, particularly sensitive to mixing parameters.
- Disappearance experiments, where one looks for the disappearance of neutrinos of the initial flavour from a beam. Such experiments might involve, in particular, electron neutrinos in case there is not sufficient energy available to create neutrinos of another kind. Such is the situation with reactor-produced neutrinos and solar neutrinos, whose energy is far below the rest masses of the charged μ– and τ-leptons. These kinds of the experiment are particularly sensitive to small energies and therefore also to small mass values.

For solar neutrinos, only experimental situation 2 is feasible for energetic reasons. In the scheme with neutrino mixing, the neutrino flavour states are coherent superpositions of the state vectors of neutrinos with different masses. Since $|\nu_i\rangle$ are mass eigenstates, their propagation can be described by plane wave solutions of the form:

$$|\nu_i(t)\rangle = e^{-iE_i(\mathbf{p})(t-t_0)}\,|\nu_i(0)\rangle \tag{3.41}$$

where $E_i = \sqrt{p_i^2 + m_i^2}$ is the energy of the mass-eigenstate i, t is the time from the start of the propagation t_0 and $\mathbf{p}$ is the three-dimensional momentum. The probability that at time t the state is in flavour β is:

$$P(\nu_\alpha \to \nu_\beta)(t) = |\langle\nu_\beta|\nu_\alpha(t)\rangle|^2 = |\sum_i U_{\beta i}U^*_{\alpha i}e^{-iE_i(p)(t-t_0)}|^2, \tag{3.42}$$

[20] If the momentum uncertainty is sufficiently small, one could kinematically distinguish the mass eigenstate (produced/detected)

where we have used the orthogonality relation $\langle \nu_i(\mathbf{p}) | \nu_j(\mathbf{p}) \rangle = \delta_{ij}$. In the ultrarelativistic limit, $|\mathbf{p_i}| = p_i \gg m_i$, we can approximate the energy as:

$$E_i(\mathbf{p}) - E_j(\mathbf{p}) \simeq \frac{1}{2} \frac{m_i^2 - m_j^2}{|\mathbf{p}|}, \tag{3.43}$$

and $L \simeq (t - t_0)$, and so we arrive at the master formula for neutrino oscillation, as:

$$P(\nu_\alpha \to \nu_\beta) = \sum_{i,j} U^*_{\alpha i} U_{\beta i} U_{\alpha j} U^*_{\beta j} e^{-i \frac{\Delta m^2_{ij} L}{2|\mathbf{p}|}}, \tag{3.44}$$

where $\Delta m^2_{ij} = m_i^2 - m_j^2$, $U_{\alpha i}$ are the elements of the PMNS matrix, L is the baseline and $|\mathbf{p}|$ is the neutrino momentum. There are many ways to derive this formula. The simplest way in most textbooks uses simple quantum mechanics, where neutrinos are treated as plane waves. A slightly more rigorous method treats neutrinos as wave packets. Finally, it is also possible to derive it from QFT, where neutrinos are treated as intermediate virtual states. The different methods make more or less explicit the necessary primary conditions of neutrino oscillations mentioned above. Let us analyze more closely the master formula (3.44). The probability is a superposition of oscillatory functions of the baseline with wavelengths that depend on the neutrino mass differences $\Delta m^2_{ij} = m_i^2 - m_j^2$, $U_{\alpha i}$, and amplitudes that depend on different combinations of the mixing matrix elements. Defining $W^{ij}_{\alpha\beta} \equiv \left[U^*_{\alpha i} U_{\beta i} U_{\alpha j} U^*_{\beta j} \right]$ and using the unitarity of the mixing matrix, we can rewrite the probability in the more familiar form:

$$P(\nu_\alpha \to \nu_\beta) = \delta_{\alpha\beta} - 4 \sum_{j>i} Re \left[W^{ij}_{\alpha\beta} \right] \sin^2 \left(\frac{\Delta m^2_{ij} L}{4 E_\nu} \right) \mp \sum_{j>i} Im \left[W^{ij}_{\alpha\beta} \right] \sin^2 \left(\frac{\Delta m^2_{ij} L}{2 E_\nu} \right) \tag{3.45}$$

, where the $\mp$ refers to neutrino/antineutrino and $|\mathbf{p}| \simeq E_\nu$. We refer to an *appearance* or *disappearance* oscillation probability when the initial and final flavours are different ($\alpha \neq \beta$) or the same ($\alpha = \beta$), respectively. Note that oscillation probabilities show the expected GIM[21] suppression of any flavor-changing process: they vanish if the neutrinos are degenerate. In the simplest case of two-family mixing, the mixing matrix depends on just one mixing angle:

$$U_{PMNS} = \begin{pmatrix} \cos\theta & \sin\theta \\ -\sin\theta & \cos\theta \end{pmatrix}, \tag{3.46}$$

[21] In quantum field theory, the GIM mechanism (or Glashow–Iliopoulos–Maiani mechanism) is the mechanism by which neutral currents that change flavor are suppressed.

and there is only one mass square difference Δm^2. The oscillation probability of Eq. (3.45) simplifies to the well-known expression where we have introduced convenient physical units:

$$P(\nu_\alpha \to \nu_\beta) = \sin^2 2\theta \sin^2 \left(1.27 \frac{\Delta m^2(eV^2) L(km)}{E_\nu(GeV)}\right), \qquad \alpha \neq \beta. \tag{3.47}$$

$$P(\nu_\alpha \to \nu_\alpha) = 1 - P(\nu_\alpha \to \nu_\beta). \tag{3.48}$$

The probability is the same for neutrinos and antineutrinos because there cannot be CP violation when there are only two families. Indeed CPT implies that the disappearance probabilities are the same for neutrinos and antineutrinos, and therefore according to Eq. (3.47) the same must hold for the appearance probability. The latter is a sinusoidal function of the distance between source and detector, with a period determined by the oscillation length:

$$L_{osc} = \pi \frac{E_{\nu(GeV)}}{1.27 \Delta m^2(eV^2)}, \tag{3.49}$$

which is proportional to the neutrino energy and inversely proportional to the neutrino mass square difference. The amplitude of the oscillation is determined by the mixing angle and it is maximal for $\sin^2 2\theta = 1$ or $\theta = \pi/4$. In many neutrino oscillation experiments, the baseline is not varied, but the oscillation probability can be measured as a function of the neutrino energy. In this case, the position of the first maximum contains information on the mass splitting:

$$E_{max}(GeV) = 1.27 \frac{\Delta m^2(eV^2) L(km)}{\pi/2}. \tag{3.50}$$

An optimal neutrino oscillation experiment in a vacuum is such that the ratio of the neutrino energy and baseline length is tunned to be the same order as the mass splitting, $E/L \sim \Delta m^2$. If $E/L \gg \Delta m^2$, the oscillation phase is small and the oscillation probability depends on the combination $P(\nu_\alpha \to \nu_\beta) \propto \sin^2 2\theta (\Delta m^2)^2$, and the mixing angle and mass splitting cannot be disentangled. The opposite limit $E/L \ll \Delta m^2$ is the fast oscillation regime, where one can only measure an energy or baseline-smeared oscillation probability:

$$\langle P(\nu_\alpha \to \nu_\beta) \rangle \simeq \frac{1}{2} \sin^2 2\theta. \tag{3.51}$$

It is interesting to note that this averaged oscillation regime gives the same result as the flavour transition probability in the case of incoherent propagation ($L \gg L_{coh}$), such that:

$$P(\nu_\alpha \to \nu_\beta) = |U_{\alpha i} U_{\beta i}|^2 = 2 \cos^2\theta \sin^2\theta = \frac{1}{2} \sin^2 2\theta. \tag{3.52}$$

Flavour transitions via incoherent propagation are sensitive to mixing but not neutrino mass splitting. The 'smoking gun' for neutrino oscillations is not the flavour transition, which can occur in the presence of neutrino mixing without oscillations, but the peculiar L/E_ν dependence. An optimal experiment that intends to measure both the mixing and the mass splitting requires running $E/L \sim \Delta m^2$.

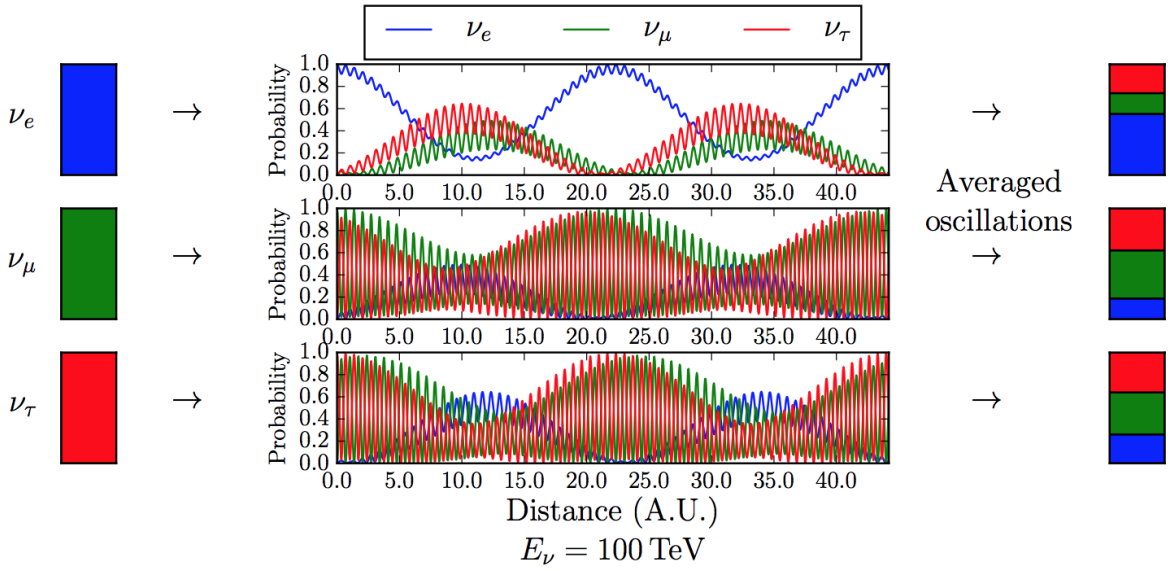

Figure 11 – The oscillation of a 100 TeV neutrino that starts out in an initial flavor state of ν_e, ν_μ, or ν_τ from top to bottom. The best-fit oscillation parameters from [30] are used. The right-most panels show the oscillation-averaged transition probability to ν_e in blue, ν_μ in green, ν_τ in red. Distances are shown in astronomical units, illustrating a 100 TeV neutrino would undergo many oscillations if it originated outside the Solar System.

3.0.3.3 Oscillations in matter

Up to now, we have considered the propagation of massive neutrinos in a vacuum. We have seen that the flavor content of the neutrino beam in a vacuum is determined by the neutrino mass-squared differences Δm^2 and elements of the neutrino mixing matrix U_{PMNS}. As was first shown by Wolfenstein, in the case of matter, neutrino masses and mixing and the coherent scattering of neutrinos in the matter must be taken into account. The electron number density determines the contribution of the coherent scattering into the Hamiltonian. Suppose the electron density depends on the distance (as in the case of the sun). In that case, the transition probabilities between different flavor neutrinos can have resonance character (MSW effect)[22]. When neutrinos propagate in the matter (Earth, sun, etc.), their propagation is modified owing to coherent forward scattering on electrons and nucleons. First of all, if it is a ν_e, if and only if it can exchange a W boson

[22] The Mikheyev–Smirnov–Wolfenstein effect (often referred to as matter effect) is a particle physics process which can act to modify neutrino oscillations in matter.

with an electron. This gives rise to an extra potential energy of interaction V_W. Clearly this extra energy would be proportional to the Fermi coupling constant G_F and coming from $\nu_e - e$ scattering it would also be proportional to the number of electrons per unit volume N_e. Thus, from the standard model we have:

$$V_W = +\sqrt{2}G_F N_e. \tag{3.53}$$

Second, a neutrino in matter can exchange a Z boson with an electron, proton, or neutron with the medium. The standard model tells us that any flavour can do it and that the amplitude is independent of that flavour. Likewise, it tells us that the couples to the electron and the positron at zero momentum transfer are equal and opposite. Assuming then that the matter through which the neutrino travels is electrically neutral, the contributions of the scattering with the electron and the proton with the neutrino through the exchange of Z cancel each other. Therefore, the exchange of one Z gives rise only to a neutrino flavour-independent interaction potential V_Z that depends only on N_n, the number of neutrons per unit volume, such that:

$$V_Z = -\sqrt{2}G_F N_n. \tag{3.54}$$

The standard model interactions do not change the flavor of the neutrino. Therefore, unless hypothetical non-standard-model flavor-changing interactions are at work, the observation of neutrino flavor change implies a mass for the neutrino and mixing even as neutrinos pass through matter. And that, as for V_W, this interaction energy changes sign if we change neutrinos by antineutrinos. In the case of two flavours, the effective mass and mixing angle have relatively simple expressions:

$$\Delta\tilde{m}^2 = \sqrt{\left(\Delta m^2 \cos 2\theta \mp 2\sqrt{2}EG_F N_e\right)^2 + \left(\Delta m^2 \sin 2\theta\right)^2} \tag{3.55}$$

where the sign $\mp$ corresponds to neutrinos/antineutrinos. In the sun the density of electrons is not constant. However, if the variation is sufficiently slow, the eigenstates will change slowly with the density, and we can assume that the neutrino produced in an eigenstate in the center of the sun, remains in the same eigenstate along the trajectory. This is the so-called *adiabatic approximation.*

In the Standard Model neutrinos have always been treated as massless particles and it is only the discovery of neutrino oscillations which has given us any evidence to suggest otherwise. The fact that any oscillations occur means that one of the Δm^2_{ij}, implying that at least one of the neutrino masses must also be non-zero. In fact, since all of the mass splittings are measured to be non-zero at least two of the masses are required

to be non-zero. However, as discussed in the last section, oscillations are insensitive to the absolute values of the neutrino masses and can only observe the differences between them. At present the masses have proven to be so small that they are inaccessible to current experiments. The end-point of tritium beta-decay in the Troitzk experiment sets the world's most stringent limit: $m_{\nu_e} < 2.05eV$ at 95% CL. Though it should be noted that the mass measured here, m_{ν_e} , is that of a flavour state, and therefore represents a combination of the three mass states it contains.

Even with the mass differences we can measure, thus far it has not been possible to determine the sign of Δm^2_{31}. The two possibilities are referred to as the "normal" ($\Delta m^2_{31} > 0$) and "inverted" ($\Delta m^2_{31} < 0$) hierarchies, and amount to a choice between which of the mass states is largest:

- Normal Hierarchy Ordering (NO): $m_3 > m_2 > m_1$
- Inverted Hierarchy Ordering (IO): $m_2 > m_1 > m_3$

The difficulty in determining the sign is essentially caused by the uncertainties on Δm^2_{23} and Δm^2_{31} being larger than the size of Δm^2_{21}, and therefore the sign has a negligible effect on the oscillation probabilities compared to current experimental uncertainties. It is only matter effects in solar neutrino oscillations that have allowed us to determine the sign of Δm^2_{21}.

With the last results in mind, we review the current and most updated predictions test of parameters in PMNS matrix. The results are obtained in the global neutrino oscillations fit and they are summarized in Tab. (4), for normal (NO) and inverted (IO) mass ordering. Some comments are in order. First we note that the improved precision on θ_{13} follows mainly from the Daya Bay data. Thanks to the combination of T2K neutrino and antineutrino data, exist now an improved sensitivity to CP violation. Indeed, T2K is the first experiment showing a sensitivity on its own, excluding some values of δ before combining with reactor data.

3.1. Neutrinos in cosmology and big questions

When we introducing massive neutrinos inside the image of the standard model of cosmology (Λ+CDM), and allowing for a more general DE component with constant EoS w, with density parameter Ω_{DE}, equation (2.76) becomes:

$$E(a) = \sqrt{\Omega_{\rm r0}a^{-4} + \Omega_{\rm m0}a^{-3} + \Omega_{\rm K0}a^{-2} + \Omega_X e^{\int_0^1 \frac{da'}{a'}[1+w(a')]} + \Omega_\nu(a)}\ , \tag{3.56}$$

Parameter	Best fit $\pm 1\sigma$	2σ range	3σ range
Δm^2_{21} $[10^{-5} eV^2]$	7.56 ± 0.19	7.20 - 7.95	7.05 - 8.14
$\lvert\Delta m^2_{31}\rvert$ $[10^{-5} eV^2]$ (NO)	2.55 ± 0.04	2.47 - 2.63	2.43 - 2.67
$\lvert\Delta m^2_{31}\rvert$ $[10^{-5} eV^2]$ (IO)	2.49 ± 0.04	2.41 - 2.57	2.37 - 2.61
$\sin^2\theta_{12}/10^{-1}$	$3.21^{+0.18}_{-0.16}$	2.89 - 3.59	2.73 - 3.79
$\theta_{12}/^\circ$	$34.5^{+1.1}_{-1.0}$	32.5 - 36.8	31.5 - 38.0
$\sin^2\theta_{23}/10^{-1}$ (NO)	$4.30^{+0.20}_{-0.18}$	3.98 - 4.78	3.84 - 6.35
$\theta_{23}/^\circ$	41.0 ± 1.1	39.1 - 43.7	38.3 - 52.8
$\sin^2\theta_{23}/10^{-1}$ (IO)	$5.96^{+0.17}_{-0.18}$	4.04 - 4.56	3.88 - 6.38
$\theta_{23}/^\circ$	50.5 ± 1.0	39.5 - 42.5	38.5 - 53.0
$\sin^2\theta_{13}/10^{-1}$ (NO)	$2.155^{+0.090}_{-0.075}$	1.98 - 2.31	1.89 - 2.39
$\theta_{13}/^\circ$	$8.44^{+0.18}_{-0.15}$	8.10 - 8.70	7.90 - 8.90
$\sin^2\theta_{13}/10^{-1}$ (IO)	$2.140^{+0.082}_{-0.085}$	1.97 - 2.30	1.98 - 2.39
$\theta_{13}/^\circ$	$8.41^{+0.16}_{-0.17}$	8.00 - 8.70	7.90 - 8.90
δ/π (NO)	$1.40^{+0.31}_{-0.20}$	0.85 - 1.95	0.00 - 2.00
$\delta/^\circ$	252^{+56}_{-36}	153 - 351	0 - 360
δ/π (IO)	$1.44^{+0.26}_{-0.23}$	1.01 - 1.93	0.00 - 0.17
$\delta/^\circ$	259^{+47}_{-41}	182 - 347	0 - 31

Table 4 – Updated fits to parameters of the mixing matrix.

where $E(a) = H(a)/H_0$ and $\Omega_\nu(a) = \rho_\nu(a)/\rho_{cr}$ denotes the neutrino energy density as a function of scale factor ($a = 1/(1+z)$). In equation (3.56), we have not specified a functional form for $\Omega_\nu(a)$ since neutrinos behave as radiation (or hot dark matter at late times) in the early Universe and matter (dust) at late times, implying that the scaling of their energy density with z is non-trivial. Nevertheless, as anticipated earlier we know that in the very early Universe, when neutrinos behave as radiation:

$$\Omega_\nu \propto (1+z)^4, \tag{3.57}$$

whereas at very late times, when neutrinos behave as matter, such that:

$$\Omega_\nu \propto (1+z)^3. \tag{3.58}$$

With this in mind, we only need a couple of details to know exactly which are the analytical expressions that correspond to each energy domain, namely:

- We know from Eq. 3.0.2, that there are three generations of active neutrinos, which in their primordial form, are known to contribute significantly to the radiation

content, through the number of degrees of freedom of relativistic species N_ν, such that: $\rho_{rad} \propto \rho_{phot} + \rho_\nu(N_\nu)$.

- Regarding the contribution of promondial neutrinos to the density content of matter, we know that at least one species of the three active neutrinos ceases to be relativistic and acquires mass as the universe evolves. However, we need the Boltzman equation to know the energy density that contributes to the matter content of the universe, such that: $\rho_{m0} \propto \rho_{DM} + \rho_{Baryons} + \rho_\nu$.

These aspects will be covered in the next chapter (Chap. (4)), where we will deal with the solution to Boltzman's equation for different types of species, which constitute the matter and energy content of the universe, including relativistic and non-relativistic neutrinos, which we will call hereafter hereafter as: Cosmic Neutrino Background ($C\nu B$).

To finish this chapte, let us consider that many of the keys to the new physics come from cosmology, which has made fast progress over the last few years. For example, it is truly remarkable that about 5% of the entire Universe consists of stuff we know, and all the rest remains a complete mystery, dubbed dark matter and dark energy. For example, we mention dark matter, whose exact nature remains elusive, despite solid evidence in favor of its existence, ever since the pioneering observations of the astronomer Fritz Zwicky in the 1930s. Dark matter neither emits nor scatters light or other electromagnetic radiation; hence it cannot be detected directly by optical or radio astronomy. Nevertheless, most of the matter in the Universe is indeed non-luminous, and its existence is also inferred by modeling structure formation and galaxy evolution. However, we still do not know its composition. Viable dark matter particle physics candidates must be electrically neutral and provide the correct relic abundance, hence they must be stable over cosmological time scales. The most popular candidate is a weakly interacting massive particle (WIMP), the lightest supersymmetric particle in models with conserved R-parity. Although neutrinos cannot provide the required amount of dark matter, the physics through which they acquire their small masses may be closely connected, providing a fascinating link between neutrinos and early Universe cosmology. One exciting possibility is that dark matter is stabilized by a remnant of the flavour symmetry, which explains the oscillation pattern. Many other types of relations between dark matter and neutrinos can be considered. Another open issue in cosmology is the understanding of the matter-antimatter asymmetry. An attractive mechanism is to generate a primordial lepton–anti-lepton asymmetry through the out-of-equilibrium CP-violating decays of the messenger particles responsible for neutrino mass. This would take place very early on in the evolution of the Universe, while subsequent non-perturbative processes would convert the lepton number (B-L) asymmetry into a baryon asymmetry. In such a leptogenesis picture, neutrinos are responsible for the origin of matter. To sum up, over the last century, neutrinos have provided a crucial

tool in our understanding of weak interactions and guidance in formulating today's SM of particle physics. It is not risky to imagine that they may also help in directing us towards the 'theory of everything that lies ahead. Among the challenges in present-day particle physics, many are coming from the neutrino sector. Some of them are as follows:

1. **The Nature of Neutrinos.** *Is lepton number violated in nature? Are neutrinos their own anti-particles?.* The observation of neutrinoless double beta decay ($\beta\beta_{0\nu}$) would provide the answer and many experiments are going on.

2. **The Origin of Neutrino Mass.** *Why are neutrinos so light when compared the other elementary fermions? Is this a hint for some sort of unifica- tion of the gauge interactions? Are neutrino masses a low-scale phenomenon?*

3. **The Pattern of Neutrino Mixing.** Why are lepton mixing angles so differ- ent from the CKM mixing angles? Is there an underlying symmetry of flavour?

4. **Probing Non-standard Neutrino Interactions.** *Is there lepton flavour violation beyond that seen in oscillations? Do they show up in neutrino propa- gation?*

5. **Charged Lepton Flavour Violation and CP Violation.** *Do processes such as $\mu \longrightarrow e + \gamma$ take place? Is leptonic CP violated? Does lepton flavour violation take place at LHC energies?.* This would be truly complementary to the oscillation studies.

6. **Probing Neutrinos at High Energy Accelerators.** *Can neutrino properties be probed at LHC energies and higher? Is tera-eV scale supersymmetry the origin of neutrino mass?*

7. **Neutrino Cosmology.** Owing to their weak interaction, neutrinos constitute an ideal probe of the early Universe, and may shed light on the origin of dark matter. *Can the origin of dark matter and neutrino mass be related?*

These are some of the challenges of today, which should inspire our research efforts in search of clues to the theory of tomorrow and which are the guide to address this thesis, from a theoretical-observational perspective.

Chapter 4

Neutrinos in the early ages

"Cosmology brings us face to face with the deepest mysteries, questions that were once treated only in religion and myth." – Carl Sagan in Cosmos: A Personal Voyage, Episode 10: "The Edge of Forever" (1980)

In this Chapter we discuss the application of Boltzmann equation in cosmology. In particular, we address Big Bang Nucleosynthesis (BBN), recombination of protons and electrons in neutral hydrogen atoms and the relic abundance of CDM (see [57], [92] and [26]).

4.1. Thermal equilibrium and Boltzmann equation

We have encountered in the previous Chapter the continuity equation (2.74):

$$\dot{\varepsilon} + 3H(\varepsilon + P) = 0 \,, \tag{4.1}$$

where recall that the dot represents derivation with respect to the cosmic time. Surprisingly, it is possible to obtain the continuity equation by using the first and second law of thermodynamics, i.e.

$$TdS = PdV + dU \,, \tag{4.2}$$

where T is the temperature, S is the entropy, V is the volume and U is the internal energy

of the cosmic fluid. Now, assuming adiabaticity, i.e. $dS = 0$, and writing $U = \varepsilon V$, one gets

$$PdV + d(\varepsilon V) = 0 \qquad \Rightarrow \qquad V d\varepsilon + (\varepsilon + P)dV = 0 \, . \tag{4.3}$$

In using Eq. (4.2), we have made a very strong assumption: the evolution of the universe is an adiabatic reversible transformation, i.e. at each instant the universe is in an equilibrium state. In some instances we can trust this assumption and it gives the correct continuity equation. In particular, we will see that Eq. (4.1) can be obtained from Boltzmann equation assuming no interactions among particles or assuming a very high rate of interactions so that thermal equilibrium is reached. The latter instance can be mathematically represented as follows:

$$\Gamma \gg H, \tag{4.4}$$

i.e. *the interaction rate is much larger than the Hubble rate*, where the interaction rate is defined as follows:

$$\Gamma \equiv n\sigma v_{\rm rel} \tag{4.5}$$

where n is the particle number density of projectiles, $v_{\rm rel}$ is the relative velocity between projectile and targets and σ is the cross section. Equation (4.4) can also be rephrased as the fact that the mean-free-path is much smaller than the Hubble radius. In this situation, particles interact so frequently that they do not even care about the cosmological expansion and any fluctuation in their energy density is rapidly smoothed out, thus recovering thermal equilibrium. It is important to make distinction between *kinetic equilibrium* and *chemical equilibrium*. When $\Gamma \gg H$ refers to a process of the type:

$$1 + 2 \leftrightarrow 3 + 4 \, , \tag{4.6}$$

i.e. we have four different particle species which transform into each other in a balanced way, then we have *chemical equilibrium*. This can be also reformulated as:

$$\mu_1 + \mu_2 = \mu_3 + \mu_4 \tag{4.7}$$

where the μ's are the chemical potentials. On the other hand, when $\Gamma \gg H$ refers to a reaction such as a scattering:

$$1 + 2 \leftrightarrow 1 + 2 \, , \tag{4.8}$$

then we have *kinetic equilibrium*. Kinetic or chemical equilibrium (or both) imply thermal equilibrium. In general, it is possible for a species to break chemical equilibrium and still remain in kinetic, therefore thermal, equilibrium with the rest of the cosmic plasma through scattering processes.[1] Note that Γ is different for different fundamental interactions and for different particle species masses. Therefore, the above condition (4.4) is valid for all the known (and perhaps unknown) particles in the very early universe but is broken at different times for different species. This is the essence of the *thermal history of the universe*. So, at the very beginning (we are talking about tiny fractions of seconds after the Big Bang) all the particles were in thermal equilibrium in a primordial soup, the *primordial plasma*. When for a species, the condition $\Gamma \sim H$ is reached, it decouples from the primordial plasma. If it does this by breaking the chemical equilibrium, then it is said to freeze out and attains some fixed abundance.[2] When we want to explicitly calculate the residual abundance of some species, we have to track its evolution until $\Gamma \sim H$. In this instance, equilibrium thermodynamics fails and we are compelled to use Boltzmann equation. For example, we shall use Boltzmann equation when analysing the formation of light elements during BBN, the recombination of protons and electrons in neutral hydrogen atoms and the relic abundance of CDM. The fundamental interactions which characterise the above-mentioned processes compel some particles to react and transform into others and vice-versa, such as in Eq. (4.6). When $\Gamma \gg H$ these reactions take place with equal probability in both directions, hence the $\leftrightarrow$ symbol, but when $\Gamma \sim H$ eventually one direction is preferred over the other. This is the characteristic of irreversibility which demands the use of Boltzmann equation.

4.2. The entropy density

For many of the forthcoming purposes the hypothesis of thermal equilibrium is suitable and very useful. As we have stated at the beginning of this chapter, it is justified in those instances in which the interaction rate among particles is much higher than the expansion rate. In these cases, one can use equilibrium thermodynamics and a very useful quantity is the entropy density:

$$s \equiv \frac{S}{V} \,, \tag{4.9}$$

because, as we will show in a moment, sa^3 is conserved. In thermal equilibrium, we can

[1] This occurs in some DM particle models. For example a $m = 100$ GeV WIMP chemically decouples at 5 GeV and kinetically decouples at 25 MeV. See e.g. [151].

[2] It attains a fixed abundance if it is a stable particle, of course. If not it disappears.

cast the thermodynamical relation (4.2) in the following form:

$$TdS = Vd\varepsilon + (\varepsilon + P)dV = V\frac{d\varepsilon}{dT}dT + (\varepsilon + P)dV \ , \tag{4.10}$$

because the energy density (and also the pressure) only depends on the temperature T. The integrability condition applied to Eq. (4.10) yields to:

$$\frac{\partial^2 S}{\partial T \partial V} = \frac{\partial^2 S}{\partial V \partial T} \quad \Rightarrow \quad T\frac{dP}{dT} = \varepsilon + P \ . \tag{4.11}$$

Bosons and fermions in thermal equilibrium are distributed according to the Bose-Einstein and Fermi-Dirac distributions:

$$f_{\rm BE} = \frac{1}{\exp\left(\frac{E-\mu}{k_{\rm B}T}\right) - 1} \ , \qquad f_{\rm FD} = \frac{1}{\exp\left(\frac{E-\mu}{k_{\rm B}T}\right) + 1} \tag{4.12}$$

We now prove Eq. (4.11) in another way, assuming a distribution function of the type $f = f(E/T)$. We first must know how to calculate dP/dT. Call $E/T = x$ and $f' \equiv df/dx$. Then:

$$df = f'dx = \frac{f'}{T}dE - \frac{f'E}{T^2}dT \ . \tag{4.13}$$

Comparing this with

$$df = \frac{\partial f}{\partial E}dE + \frac{\partial f}{\partial T}dT \ , \tag{4.14}$$

we can establish that

$$\frac{\partial f}{\partial T} = -\frac{E}{T}\frac{\partial f}{\partial E} \ . \tag{4.15}$$

Now we use this result into:

$$\frac{dP}{dT} = g_{\rm s}\int \frac{d^3\mathbf{p}}{(2\pi\hbar)^3}\frac{\partial f}{\partial T}\frac{p^2c^2}{3E} \ , \tag{4.16}$$

and obtain

$$\frac{dP}{dT} = -g_{\rm s}\int \frac{d^3\mathbf{p}}{(2\pi\hbar)^3}\frac{E}{T}\frac{\partial f}{\partial E}\frac{p^2c^2}{3E} \ . \tag{4.17}$$

Now we introduce spherical coordinates in the proper momentum space:

$$d^3\mathbf{p} = p^2 dp d^2\hat{p} \ , \tag{4.18}$$

and use the dispersion relation $E^2 = p^2c^2 + m^2c^4$ in order to write

$$\frac{\partial f}{\partial E} = \frac{\partial f}{\partial p}\frac{dp}{dE} = \frac{\partial f}{\partial p}\frac{E}{pc^2} \ . \tag{4.19}$$

Equation (4.17) thus becomes:

$$\frac{dP}{dT} = -g_{\rm s}\int \frac{p^2 dp d^2\hat{p}}{(2\pi\hbar)^3}\frac{E}{T}\frac{\partial f}{\partial p}\frac{p}{3} \ . \tag{4.20}$$

Integrating by parts:

$$\frac{dP}{dT} = -g_{\rm s}\,\frac{4\pi}{(2\pi\hbar)^3}\frac{Ep^3}{3T}f\Big|_0^\infty + g_{\rm s}\int \frac{dpd^2\hat{p}}{(2\pi\hbar)^3}\frac{1}{3T}f\left(3p^2E + p^3\frac{pc^2}{E}\right) \ , \tag{4.21}$$

where we have used again $dE/dp = pc^2/E$. The first contribution vanishes for $p \to \infty$, since $f \to 0$, i.e. there are no particles with infinite momentum. Recovering the momentum volume $d^3\mathbf{p}$, we get:

$$\frac{dP}{dT} = g_{\rm s}\int \frac{d^3\mathbf{p}}{(2\pi\hbar)^3}\frac{1}{T}f\left(E + \frac{p^2c^2}{3E}\right) \quad \Rightarrow \frac{dP}{dT} = \frac{\varepsilon + P}{T} \tag{4.22}$$

as we wanted to show. We now prove that the temperature derivative of the pressure is the entropy density. Substituting Eq. (4.11) into Eq. (4.10), i.e.

$$TdS = d(\varepsilon V) + PdV = d[(\varepsilon + P)V] - VdP \ , \tag{4.23}$$

one gets

$$dS = \frac{1}{T}d[(\varepsilon + P)V] - V\frac{\varepsilon + P}{T^2}dT = d\left[\frac{(\varepsilon + P)V}{T}\right] \ , \tag{4.24}$$

i.e. up to an additive constant:

$$s \equiv \frac{S}{V} = \frac{\varepsilon + P}{T} \ . \tag{4.25}$$

Taking into account the chemical potential μ, the thermodynamical relation (4.2) becomes

$$TdS = d(\varepsilon V) + PdV - \mu d(nV) \ , \tag{4.26}$$

and the entropy density is redefined as

$$s \equiv \frac{S}{V} = \frac{\varepsilon + P - \mu n}{T} \tag{4.27}$$

Using the continuity equation and/or Eq. (4.2), we can show that sa^3 is a constant:

$$\frac{d}{dt}(sa^3) = 0 \tag{4.28}$$

i.e. the entropy density is proportional to $1/a^3$.

4.3. Photons

In these notes we use "photons" as synonym of CMB, though this is not correct since there exist photons whose origin is not cosmological, e.g. those produced in our Sun as well as in other stars or emitted by hot interstellar gas. These say non-cosmological photons contribute at least one order of magnitude less than CMB photons [41] so our sloppiness is partially justified. Assuming a vanishing chemical potential since $\mu/(k_{\rm B}T) < 9 \times 10^{-5}$, as reported by [65], the Bose-Einstein distribution for photons becomes:

$$f_\gamma = \frac{1}{\exp\left(\frac{E}{k_{\rm B}T}\right) - 1} = \frac{1}{\exp\left(\frac{pc}{k_{\rm B}T}\right) - 1} \ , \tag{4.29}$$

where we have used the dispersion relation $E = pc$. Taking into account the chemical potential is important in order to study distortions in the CMB spectrum, which is a very recent and promising research field [44], [43]. Let us calculate the photon energy density:

$$\varepsilon_\gamma = 2 \int \frac{d^3\mathbf{p}}{(2\pi\hbar)^3} \frac{pc}{\exp\left(\frac{pc}{k_{\rm B}T}\right) - 1} \ , \tag{4.30}$$

where the factor 2 represents the two states of polarisation of the photon. The angular part can be readily integrated out, giving a factor 4π. We are left then with:

$$\varepsilon_\gamma = \frac{c}{\pi^2\hbar^3} \int_0^\infty dp \frac{p^3}{\exp\left(\frac{pc}{k_{\rm B}T}\right) - 1} \ . \tag{4.31}$$

Let us do the substitution $x \equiv pc/(k_{\rm B}T)$. We obtain:

$$\varepsilon_\gamma = \frac{c}{\pi^2\hbar^3} \left(\frac{k_{\rm B}T}{c}\right)^4 \int_0^\infty dx \frac{x^3}{e^x - 1} \ . \tag{4.32}$$

The integration is proportional to the Riemann ζ function, which has the following integral representation:

$$\zeta(s) = \frac{1}{\Gamma(s)} \int_0^\infty dx \frac{x^{s-1}}{e^x - 1} = \frac{1}{(1 - 2^{1-s})\Gamma(s)} \int_0^\infty dx \frac{x^{s-1}}{e^x + 1} \ , \tag{4.33}$$

where $\Gamma(s)$ is Euler gamma function. In alternative, a possible way to perform the integration is the following. Let I_- be:

$$I_- \equiv \int_0^\infty dx \frac{x^3}{e^x - 1} = \int_0^\infty dx \frac{e^{-x} x^3}{1 - e^{-x}} \ . \tag{4.34}$$

Now use the geometric series in order to write

$$\frac{1}{1 - e^{-x}} = \sum_{n=0}^{\infty} e^{-nx} \ , \tag{4.35}$$

and substitute this in the integral I_-:

$$I_- = \sum_{n=0}^{\infty} \int_0^\infty dx \ e^{-(n+1)x} x^3 \ . \tag{4.36}$$

Integrate the above equation three times by part and show that:

$$I_- = 6 \sum_{n=1}^{\infty} \frac{1}{n^3} \int_0^\infty dx \ e^{-nx} \ . \tag{4.37}$$

Integrate again and find:

$$I_- = 6 \sum_{n=1}^{\infty} \frac{1}{n^4} \equiv 6\zeta(4) = \frac{\pi^4}{15} \ , \tag{4.38}$$

in agreement with Eq. (4.33). Therefore, the photon energy density is the following:

$$\varepsilon_\gamma = \frac{\pi^2}{15 \hbar^3 c^3} (k_{\rm B} T)^4 \ . \tag{4.39}$$

This is the Stefan-Boltzmann law, of the black-body radiation. From the continuity equation we know that $\varepsilon_\gamma = \varepsilon_{\gamma 0}/a^4$ so that we can infer that

$$T = \frac{T_0}{a} \ , \qquad T_0 = 2.725 \text{ K} \tag{4.40}$$

i.e. the temperature of the photons decreases with the inverse scale factor. This is a result that we will prove also using the Boltzmann equation (indeed the continuity equation that provides $\varepsilon_\gamma = \varepsilon_{\gamma 0}/a^4$ *is* a way of writing the Boltzmann equation). In the above equation (4.40), the value of T_0 is the measured one of the CMB. Knowing this value, we can estimate the photon energy content today (and thus at any times):

$$\Omega_{\gamma 0} = \frac{\varepsilon_{\gamma 0}}{\varepsilon_{\rm cr0}} = \frac{8\pi^3 G}{45 \hbar^3 c^3 H_0^2 c^2} (k_{\rm B} T_0)^4 \ . \tag{4.41}$$

Using $H_0 = 100\ h$ km s^{-1} Mpc^{-1} and the known constants of nature, we obtain:

$$\Omega_{\gamma 0} h^2 = 2.47 \times 10^{-5} \ . \tag{4.42}$$

The photon number density is calculated as follows:

$$n_\gamma = \frac{1}{\pi^2 \hbar^3} \int_0^\infty dp \frac{p^2}{\exp\left(\frac{pc}{k_{\rm B}T}\right) - 1} \ . \tag{4.43}$$

Making the usual substitution $x \equiv pc/(k_{\rm B}T)$ and using Eq. (4.33) we get:

$$n_\gamma = \frac{(k_{\rm B}T)^3}{\pi^2 \hbar^3 c^3} \int_0^\infty dx \frac{x^2}{e^x - 1} \Rightarrow n_\gamma = \frac{2\zeta(3)}{\pi^2 \hbar^3 c^3} (k_{\rm B}T)^3, \tag{4.44}$$

and after replacing in the physical constants, the photon number density today is $n_{\gamma 0} = 411$ cm^{-3}.

4.4. Neutrinos

The same comment made at the beginning of the previous section also applies here: with "neutrinos" we mean the cosmological, or primordial, ones and not those produced e.g. in supernovae explosions. The massless neutrino energy density also scales as $\varepsilon_\nu = \varepsilon_{\nu 0}/a^4$, as the photons energy density, but since neutrinos are fermions we need now to employ the Fermi-Dirac distribution.

$$\varepsilon = \frac{c}{2\pi^2 \hbar^3} \left(\frac{k_{\rm B}T}{c}\right)^4 g_{\rm s} \int_0^\infty dx \frac{x^3}{e^x + 1} \ . \tag{4.45}$$

Since neutrinos are spin 1/2 fermions, then $g_\nu = 2$, where g_ν is the neutrino $g_{\rm s}$. On the other hand, neutrinos are particles which interact only via weak interaction and this violates parity. In other words, only left-handed neutrinos can be detected. *Right-handed neutrinos*, if they exist, would interact only via gravity and via the *seesaw mechanism* with the left-handed neutrino [69]. Right-handed neutrinos are also called *sterile neutrinos* and are advocated as possible candidates for DM [59]. Let I_+ be the integral in Eq. (4.45):

$$I_+ \equiv \int_0^\infty dx \frac{x^3}{e^x + 1} \ . \tag{4.46}$$

Using Eq. (4.33), we have:

$$I_+ = (1 - 2^{-3}) I_- = \frac{7}{8} I_- \ , \tag{4.47}$$

i.e. the difference between bosons and fermions energy densities per spin state is simply a factor 7/8. Taking into account that $I_- = \pi^4/15$, the neutrino energy density (4.45) is:

$$\varepsilon_\nu = \frac{7}{8} N_\nu g_\nu \frac{\pi^2}{30\hbar^3 c^3} \left(k_{\rm B} T_\nu\right)^4 \tag{4.48}$$

where N_ν is the number of neutrino families, which, as we saw in chapter (2), is equal to 3 active neutrinos, from the point of view of particle physics (see Eq. (3.9)). Of course, an equivalent expression holds true for antineutrinos.

4.4.1 Temperature of the massless neutrino thermal bath

As we have seen in Eq. (4.28), for a species in thermal equilibrium its entropy density s is proportional to $1/a^3$. Moreover, if that species is relativistic then its temperature T scales as $1/a$. Therefore, for a relativistic species in thermal equilibrium $s \propto T^3$. Since photons and neutrinos do not interact, it is reasonable to ask whether the temperatures of the photon thermal bath and of the neutrino thermal bath are the same. We cannot observe the neutrino thermal bath today, but we can indeed predict different temperatures. When the temperature of the photon thermal bath was sufficiently high, positron-electron annihilation and positron-electron pair production were balanced reactions:

$$e^+ + e^- \leftrightarrow \gamma + \gamma \; . \tag{4.49}$$

In order to produce e^+-e^- pairs, the photons must have temperature of the order of 1 MeV at least. Therefore, when the temperature of the photon thermal bath drops below that value, the above reactions are unbalanced and more photons are thus injected in the thermal bath. For this reason we expect the photon temperature to drop more slowly than $1/a$ and then to be different from the neutrino temperature. We now quantify this difference using the conservation of sa^3. For a relativistic bosonic species (such as the photon), the entropy density is:

$$s_{\rm boson} = \frac{\varepsilon + P}{T} = \frac{4\varepsilon}{3T} = g_{\rm s} \frac{2\pi^2 k_{\rm B}^4}{45\hbar^3 c^3} T^3 \tag{4.50}$$

whereas for a relativistic fermion species (such as the neutrino), the entropy density is:

$$s_{\rm fermion} = \frac{7}{8} g_{\rm s} \frac{2\pi^2 k_{\rm B}^4}{45\hbar^3 c^3} T^3 \tag{4.51}$$

Therefore, at a certain scale factor a_1 earlier than e^--e^+ annihilation, the entropy density is:

$$s(a_1) = \frac{2\pi^2 k_{\rm B}^4}{45\hbar^3 c^3} T_1^3 \left[2 + \frac{7}{8}(2+2) + \frac{7}{8} N_\nu \left(g_\nu + g_\nu\right)\right] , \tag{4.52}$$

where we have left explicit all the degrees of freedom, i.e. 2 for the photons, 2 for the electrons, 2 for the positrons, g_ν for the neutrinos and g_ν for the antineutrinos. Moreover, we have assumed the same temperature T_1 for photons and neutrinos because they came from the original thermal bath (the Big Bang). At a certain scale factor a_2 after the annihilation the entropy density is:

$$s(a_2) = \frac{2\pi^2 k_{\rm B}^4}{45\hbar^3 c^3} \left(2T_\gamma^3 + \frac{7}{4} N_\nu g_\nu T_\nu^3\right) , \tag{4.53}$$

where we have now made distinction between the two temperatures. Equating

$$s(a_1) a_1^3 = s(a_2) a_2^3 , \tag{4.54}$$

we obtain

$$(a_1 T_1)^3 \left[2 + \frac{7}{4}\left(N_\nu g_\nu + 2\right)\right] = (a_2 T_\nu)^3 \left[2\left(\frac{T_\gamma}{T_\nu}\right)^3 + \frac{7}{4} N_\nu g_\nu\right] . \tag{4.55}$$

Since $(a_1 T_1)^3 = (a_2 T_\nu)^3$, because the neutrino temperature did not change its $\propto 1/a$ behaviour, we are left with:

$$\boxed{\frac{T_\nu}{T_\gamma} = \left(\frac{4}{11}\right)^{1/3} \approx 0.714} \tag{4.56}$$

Therefore, since the CMB temperature today is of $T_{\gamma 0} = 2.725$ K, we expect a thermal neutrino background of temperature $T_{\nu 0} \approx 1.945$ K. Remarkably, the result of Eq. (4.56) does not depend on the neutrino g_ν. Let us open a brief parenthesis in order to justify the procedure that we have used in order to determine the result in Eq. (4.56). We saw that for a single species in thermal equilibrium sa^3 is conserved because of the continuity equation. However, during electron-positron annihilation the continuity equation *does not* hold true neither for photons nor for electron and positron, i.e.

$$\dot{\varepsilon}_\gamma + 4H\varepsilon_\gamma = +\Gamma_{\rm ann} , \tag{4.57}$$

$$\dot{\varepsilon}_e + 3H(\varepsilon_e + P_e) = -\Gamma_{\rm ann} , \tag{4.58}$$

where $\Gamma_{\rm ann}$ is the e^--e^+ annihilation rate. Therefore, we cannot use the constancy of sa^3 for each of these species separately. However, we can and did use it for the *total*, since the sum of the two above equations gives:

$$\dot{\varepsilon}_{\rm tot} + 3H(\varepsilon_{\rm tot} + P_{\rm tot}) = 0 \; . \tag{4.59}$$

In other words, the continuity equation always applies if one suitably extends the set of species, ultimately because of Bianchi identities. Using Eq. (4.56), the neutrino and antineutrino energy densities can be thus related to the photon energy density as follows:

$$\varepsilon_\nu = \varepsilon_{\bar{\nu}} = \frac{7}{8}\frac{N_\nu g_\nu}{2}\left(\frac{4}{11}\right)^{4/3}\varepsilon_\gamma \tag{4.60}$$

where we have left unspecified the value of the neutrino degeneracy g_ν and the number of neutrino families N_ν. The total radiation energy content can thus be written as

$$\varepsilon_{\rm r} \equiv \varepsilon_\gamma + \varepsilon_\nu + \varepsilon_{\bar{\nu}} = \varepsilon_\gamma\left[1 + \frac{7}{8}N_\nu g_\nu\left(\frac{4}{11}\right)^{4/3}\right] \; . \tag{4.61}$$

The Planck collaboration [13] has put the constraint

$$N_{\rm eff} \equiv N_\nu g_\nu = 3.04 \pm 0.33 \tag{4.62}$$

at 95% CL. Therefore, three neutrino families ($N_\nu = 3$) and one spin state for each neutrino ($g_\nu = 1$) are values which work fine. Calculating the neutrino + antineutrino number density today is straightforward:

$$n_\nu = \frac{N_\nu g_\nu}{\pi^2\hbar^3}\int_0^\infty dp \frac{p^2}{\exp\left(\frac{pc}{k_{\rm B}T_\nu}\right)+1} \; , \tag{4.63}$$

where now the subscript ν indicates both neutrinos and antineutrinos. Making the usual substitution $x \equiv pc/(k_{\rm B}T_\nu)$, we get:

$$n_\nu = \frac{N_\nu g_\nu (k_{\rm B}T_\nu)^3}{\pi^2\hbar^3c^3}\int_0^\infty dx \frac{x^2}{e^x+1} = \frac{N_\nu g_\nu (k_{\rm B}T_\nu)^3}{\pi^2\hbar^3c^3}\frac{3\zeta(3)\Gamma(3)}{2} = \frac{3\zeta(3)N_\nu g_\nu (k_{\rm B}T_\nu)^3}{2\pi^2\hbar^3c^3} \; . \tag{4.64}$$

Taking into account (4.56), we obtain

$$\boxed{n_\nu = \frac{3}{11}N_\nu g_\nu n_\gamma} \tag{4.65}$$

4.4.2 Massive neutrinos

The 2015 Nobel Prize in Physics has been awarded to Takaaki Kajita and Arthur B. McDonald *for the discovery of neutrino oscillations, which shows that neutrinos have mass*. Indeed, neutrino flavours oscillate among the leptonic families (electron, muon and tau), e.g. an electronic neutrino can turn into a muonic one and a tau one, depending on its energy and on how far it travels (see section (3.0.3)). The most stringent constraints on neutrino mass do not come from particle accelerators but cosmology: $\sum m_\nu < 0.194$ eV at 95% CL from the Planck collaboration [13]. The neutrino mass is thus very small and this does not change relevantly the early history of the universe whereas it has some impact at late-times for structure formation [101]. Using Eq. (**??**) and the FD distribution, the massive neutrino energy density can be calculated as follows:

$$\varepsilon_\nu = \int \frac{d^3\mathbf{p}}{(2\pi\hbar)^3} \frac{\sqrt{p^2c^2 + m_\nu^2 c^4}}{\exp\left[\sqrt{p^2c^2 + m_\nu^2 c^4}/(k_\mathrm{B}T)\right] + 1} \,, \tag{4.66}$$

where we are assuming $g_\mathrm{s} = 1$. Actually, Eq. (4.66) is valid for any fermion (or boson, if we have the -1 at the denominator), provided we can neglect the chemical potential. For this reason, we drop the subscript ν and consider a generic species of mass m, fermion or boson, in order to make more general statements. Rewrite Eq. (4.66) as follows:

$$\varepsilon = \frac{mc^2}{2\pi^2\hbar^3} \int_0^\infty dp\, p^2 \frac{\sqrt{p^2/(m^2c^2) + 1}}{\exp\left[A\sqrt{p^2/(m^2c^2) + 1}\right] \pm 1} \,, \qquad A \equiv \frac{mc^2}{k_\mathrm{B}T} \,, \tag{4.67}$$

and calling $x \equiv A\sqrt{p^2/(m^2c^2) + 1}$, the above integration (B.12) becomes:

$$\varepsilon = \frac{m^4c^5}{2\pi^2\hbar^3A^4} \int_A^\infty dx\, \frac{x^2\sqrt{x^2 - A^2}}{e^x \pm 1} = \frac{(k_\mathrm{B}T)^4}{2\pi^2\hbar^3c^3} \int_A^\infty dx\, \frac{x^2\sqrt{x^2 - A^2}}{e^x \pm 1} \,. \tag{4.68}$$

Note the lower integration limit.

4.4.3 Relativistic and non-relativistic regimes of particles in thermal equilibrium

Unfortunately, the above integral in Eq. (4.68) cannot be solved analytically. When $A \ll 1$, i.e. the thermal energy is much larger than the mass energy, the integral in Eq. (4.68) can be expanded as follows:

$$\int_A^\infty dx\, \frac{x^2\sqrt{x^2 - A^2}}{e^x - 1} = \frac{\pi^4}{15} - \frac{\pi^2A^2}{12} + \mathcal{O}(A^3) \,, \tag{4.69}$$

$$\int_A^\infty dx\, \frac{x^2\sqrt{x^2 - A^2}}{e^x + 1} = \frac{7\pi^4}{120} - \frac{\pi^2A^2}{24} + \mathcal{O}(A^3) \,. \tag{4.70}$$

The zero-order terms recovers the result of Eq. (4.39), for photons, and of Eq. (4.48), obtained for massless neutrinos. In general, we can state that *particles with mass m in thermal equilibrium at temperature T behave as relativistic particles when $mc^2 \ll k_{\rm B}T$*. The opposite limit $mc^2 \gg k_{\rm B}T$ is much trickier to investigate analytically, so we shall do it numerically. Calling $x \equiv A\sqrt{p^2/(m^2c^2)+1}$, the number density can be written as:

$$n = \frac{m^3c^3}{2\pi^2\hbar^3A^3}\int_A^\infty dx\ \frac{x\sqrt{x^2-A^2}}{e^x \pm 1}\ . \tag{4.71}$$

The ratio $\varepsilon/(nmc^2)$ can be written as:

$$\gamma \equiv \frac{\varepsilon}{(nmc^2)} = \frac{1}{A}\frac{\int_A^\infty dx\ \frac{x^2\sqrt{x^2-A^2}}{e^x\pm 1}}{\int_A^\infty dx\ \frac{x\sqrt{x^2-A^2}}{e^x\pm 1}}\ , \tag{4.72}$$

where γ is indeed some sort of averaged Lorentz factor since it is the ratio of the energy density to the mass energy density. The behaviour of γ as function of A is shown in Fig. 12.

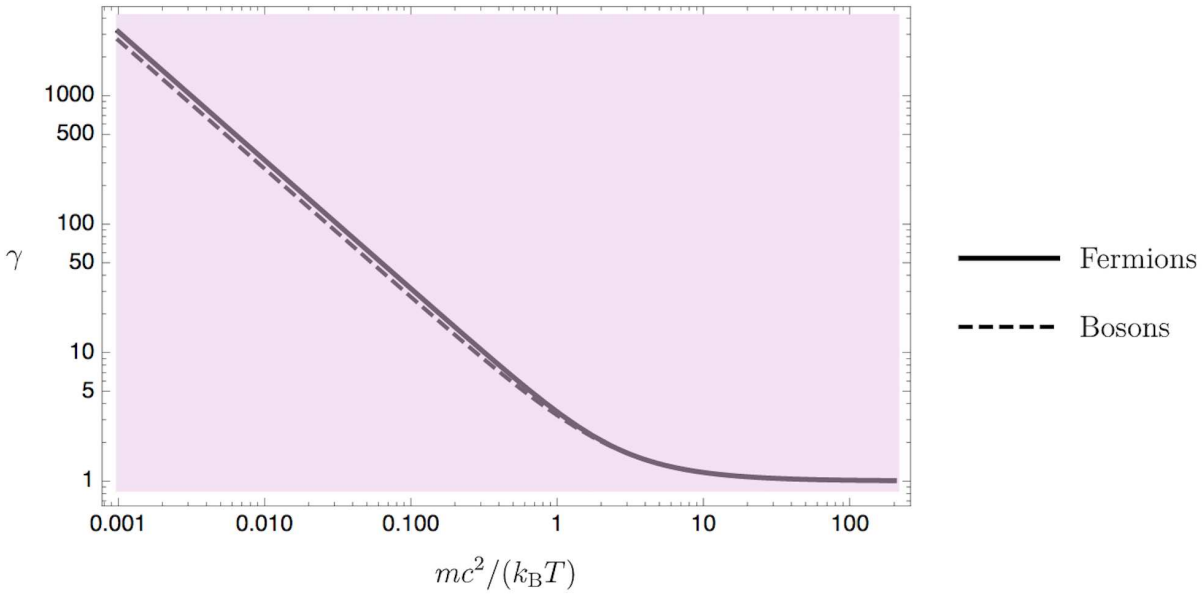

Figure 12 – Plot of γ as function of A. The solid line is for fermions whereas the dashed one for bosons.

From Fig. 12 we can infer that $\varepsilon/(nmc^2) \approx 1$ when $mc^2 \gg k_{\rm B}T$ and therefore the particle becomes non-relativistic since all its energy is mass energy. In general, we can state that *particles with mass m in thermal equilibrium at temperature T behave as non-relativistic particles when $mc^2 \gg k_{\rm B}T$*. The transition relativistic $\rightarrow$ non-relativistic takes place for $k_{\rm B}T \approx 10mc^2$. Now, suppose that a single family of neutrinos and antineutrinos became

non-relativistic only recently, what would be their energy density and density parameter today? Being non-relativistic, we can write their energy density as follows:

$$\varepsilon_{m_\nu} = \rho_\nu c^2 = n_\nu m_\nu c^2 \ , \tag{4.73}$$

and thus the density parameter today is:

$$\Omega_{m_\nu 0} = \frac{8\pi G n_{\nu 0} m_\nu}{3H_0^2} \ . \tag{4.74}$$

Using Eq. (4.65) and the result for $n_{\gamma 0}$, Eq. (4.74) can be written as:

$$\Omega_{m_\nu 0} = \frac{1}{94.22h^2} g_\nu \frac{m_\nu c^2}{\text{eV}} \tag{4.75}$$

.

Thus, the contribution of massive neutrinos to the present-day critical energy density is given by:

$$\Omega_{\nu 0} = \frac{\sum m_\nu}{94.22h^2}, \tag{4.76}$$

which we had studied in the Chapter 4 (see Eq. (4.75)). From Eq. (4.75) to Eq. (4.76) we use: $c = 1$, $g_\nu = 1$ and $m_\nu = \sum m_\nu$, with which we take into account natural physical units, the degrees of freedom and the three active neutrinos. In this way we can know exactly what is the contribution of the $C\nu B$ (see Eq. (3.58)) to the dimensionless density of matter and so our Eq. (3.56) takes the form:

$$E(z) = \sqrt{\Omega_{\text{r}0} a^{-4} + \Omega_{\text{m}0} a^{-3} + \Omega_{\text{K}0} a^{-2} + \Omega_X e^{\int_0^1 \frac{da'}{a'}[1+w(a')]} + \Omega_{\nu 0} a^{-3}} \ , \tag{4.77}$$

Later, we shall see that cosmological observables very often carry the imprint of particular length scales, in relation to specific physical effects responsible for shaping the observables themselves (Chapter 6 and 5).

4.4.4 Matter-Radiation equality

The epoch, or instant, at which the energy density of matter (i.e. baryons plus CDM) equals the energy density of radiation (i.e. photons plus neutrinos) is particularly

important from the point of view of the evolution of perturbations, as we shall see in Chapter 6. From Eq. (4.61) we have that:

$$\boxed{\Omega_{\rm r0} = \Omega_{\gamma 0}\left[1 + \frac{7}{8}N_{\rm eff}\left(\frac{4}{11}\right)^{4/3}\right]} \tag{4.78}$$

In order to calculate the scale factor $a_{\rm eq}$ of the equality we only need to solve the following equation:

$$\frac{\Omega_{\rm r0}}{a_{\rm eq}^4} = \frac{\Omega_{\rm m0}}{a_{\rm eq}^3} \ , \tag{4.79}$$

which gives

$$a_{\rm eq} = \frac{\Omega_{\rm r0}}{\Omega_{\rm m0}} = \frac{\Omega_{\gamma 0}}{\Omega_{\rm m0}}\left[1 + \frac{7}{8}N_{\rm eff}\left(\frac{4}{11}\right)^{4/3}\right] \ . \tag{4.80}$$

Using Eq. (4.42) and $N_{\rm eff} = 3$ one obtains:

$$\boxed{a_{\rm eq} = \frac{4.15 \times 10^{-5}}{\Omega_{\rm m0}h^2}} \qquad \Rightarrow \qquad \boxed{1 + z_{\rm eq} = 2.4 \times 10^4 \ \Omega_{\rm m0}h^2} \tag{4.81}$$

What does happen to the equality redshift $z_{\rm eq}$ if one of the neutrino species has mass $m_\nu \neq 0$?. If that neutrino species becomes non-relativistic *after* the equality epoch, then the above calculation still holds true. Therefore, let us assume that the neutrino species becomes non-relativistic, thereby counting as matter, before the equality. Since there is more matter and less radiation we expect the equality to take place earlier, i.e.

$$a_{\rm eq} = \frac{3.59 \times 10^{-5}}{(\Omega_{\rm m0} + \Omega_{m_\nu 0})h^2} \quad 1 + z_{\rm eq} = 2.79 \times 10^4 \ (\Omega_{\rm m0} + \Omega_{m_\nu 0})h^2 \ . \tag{4.82}$$

Since $T = T_0(1+z)$, the photon temperature at equality is:

$$T_{\gamma,{\rm eq}} = 2.79 \times T_0 \cdot 10^4 \ (\Omega_{\rm m0} + \Omega_{m_\nu 0})h^2 = 7.60 \times 10^4 \ (\Omega_{\rm m0} + \Omega_{m_\nu 0})h^2 \ {\rm K} \ . \tag{4.83}$$

Using Eq. (4.56), the temperature of neutrinos at equality is:

$$T_{\nu,{\rm eq}} = 5.43 \times 10^4 \ (\Omega_{\rm m0} + \Omega_{m_\nu 0})h^2 \ {\rm K} \ . \tag{4.84}$$

The neutrino mass energy $m_\nu c^2$ has to be larger than $k_{\rm B}T_{\nu,{\rm eq}}$ in order for the above calculation to be consistent. This yields:

$$m_\nu c^2 > 5.43 \ k_{\rm B} \times 10^4 \ (\Omega_{\rm m0} + \Omega_{m_\nu 0})h^2 \ {\rm K} = 4.68 \ (\Omega_{\rm m0} + \Omega_{m_\nu 0})h^2 \ {\rm eV} \ . \tag{4.85}$$

Using $\Omega_{\rm m0}h^2 = 0.14$ and Eq. (4.75) we get $m_\nu c^2 > 0.69$ eV, which is incompatible with the constraint $\sum m_\nu < 0.194$ found by the Planck collaboration.

4.5. Boltzmann equation

Here is the main character of this Chapter: Boltzmann equation. It is very simple to write:

$$\frac{df}{dt} = C[f] \,, \tag{4.86}$$

but nonetheless very meaningful, as we shall appreciate. Here f is the one-particle distribution function and $C[f]$ is the collisional term, i.e. a functional of f describing the interactions among the particles constituting the system under investigation. The one-particle distribution is a function of time t, of the particle position $\mathbf{x}$ and of the particle momentum $\mathbf{p}$. In turn, also $\mathbf{x}$ and $\mathbf{p}$ are functions of time, because of the particle motion. Therefore, the total time derivative can be written as:

$$\frac{df}{dt} = \frac{\partial f}{\partial t} + \frac{d\mathbf{x}}{dt}\cdot\nabla_{\mathbf{x}} f + \frac{d\mathbf{p}}{dt}\cdot\nabla_{\mathbf{p}} f = \frac{\partial f}{\partial t} + \mathbf{v}\cdot\nabla_{\mathbf{x}} f + \mathbf{F}\cdot\nabla_{\mathbf{p}} f \equiv \hat{L}(f) \,, \tag{4.87}$$

where $\mathbf{v}$ is the particle velocity and $\mathbf{F}$ is the force acting on the particle. The operator $\hat{L}$ acting on f is similar to the convective derivative used in fluid dynamics and is also called *Liouville operator*. If interactions are absent, then

$$\frac{df}{dt} = 0 \,, \tag{4.88}$$

is the collisionless Boltzmann equation, or Vlasov equation. It represents mathematically the fact that the number of particles in a phase space volume element does not change with the time. Note that we are starting here with the non relativistic version of the Boltzmann equation. We shall see it later in the general relativistic case and cosmology. The collisionless Boltzmann equation is a direct consequence of Liouville theorem:

$$\frac{d\rho(t, \mathbf{x}_i, \mathbf{p}_i)}{dt} = 0 \,, \qquad i = 1, \cdots, N \tag{4.89}$$

where $\rho(\mathbf{x}_i, \mathbf{p}_i, t)$ is the N-particle distribution function, i.e.

$$\rho(t, \mathbf{x}_i, \mathbf{p}_i) d^N\mathbf{x} d^N\mathbf{p} \,, \tag{4.90}$$

is the probability of finding our system of N particles in a small volume $d^N\mathbf{x}d^N\mathbf{p}$ of the phase space centred in $(\mathbf{x}_i, \mathbf{p}_i)$. If the particles are not interacting, then the probability of finding N particles in some configuration is the product of the single probabilities. That is, the positions in the phase space of the individual particles are independent events. Therefore:

$$\rho \propto f^N \ , \qquad \frac{d\rho}{dt} = N f^{N-1} \frac{df}{dt} \ , \tag{4.91}$$

and using Liouville theorem (4.89) one obtains the collisionless Boltzmann equation (4.88).

4.5.1 Boltzmann equation in General Relativity and Cosmology

In GR the distribution function must be expressed covariantly as $f = f(x^\mu, P^\mu)$, and the total derivative of f cannot be taken with respect to the time because this would violate the general covariance of the theory. The total derivative of f is taken with respect to an affine parameter λ, as follows:

$$\frac{df}{d\lambda} = \frac{\partial f}{\partial x^\mu}\frac{dx^\mu}{d\lambda} + \frac{\partial f}{\partial P^\mu}\frac{dP^\mu}{d\lambda} \ . \tag{4.92}$$

The geometry enters through the derivative of the four-momentum, which can be expressed via the geodesic equation:

$$\frac{dP^\mu}{d\lambda} + \Gamma^\mu_{\nu\rho} P^\nu P^\rho = 0 \ , \tag{4.93}$$

so that

$$\frac{df}{d\lambda} = P^\mu \frac{\partial f}{\partial x^\mu} - \Gamma^\mu_{\nu\rho} P^\nu P^\rho \frac{\partial f}{\partial P^\mu} \equiv \hat{L}_{\rm rel}(f) \ , \tag{4.94}$$

where we have defined the relativistic Liouville operator $\hat{L}_{\rm rel}$. It might seem that in the relativistic case we have gained one variable, i.e. P^0, but this is not so because P^0 is related to the spatial momentum P^i via the relation $g_{\mu\nu}P^\mu P^\nu = -m^2c^2$. For this reason, we can reformulate the Liouville operator as follows:

$$\frac{df}{d\lambda} = P^\mu \frac{\partial f}{\partial x^\mu} - \Gamma^i_{\nu\rho} P^\nu P^\rho \frac{\partial f}{\partial P^i} \ , \tag{4.95}$$

i.e. by considering $f = f(x^\mu, P^i)$.

4.5.2 Collisionless Boltzmann equation in relativistic cosmology

When we couple Eq. (4.95) with FLRW metric, we must take into account that f cannot depend on the position x^i, because of homogeneity and isotropy. The collisionless Boltzmann equation thus becomes:

$$P^0 \frac{\partial f}{\partial t} - \Gamma^i_{\nu\rho} P^\nu P^\rho \frac{\partial f}{\partial P^i} = 0 \, . \tag{4.96}$$

Considering the spatially flat case $K = 0$, the above equation (4.96) can be cast as follows:

$$\frac{\partial f}{\partial t} - 2HP^i \frac{\partial f}{\partial P^i} = 0 \, . \tag{4.97}$$

Again, because of isotropy, f cannot depend on the direction of P^i, but only on its modulus $P^2 = \delta_{ij} P^i P^j$. For a generic function $f = f(x^2)$, we have:

$$x^i \frac{\partial f}{\partial x^i} = x \frac{\partial f}{\partial x} \, , \tag{4.98}$$

with $x^2 \equiv \delta_{ij} x^i x^j$. Therefore, we can write

$$\frac{\partial f}{\partial t} - 2HP \frac{\partial f}{\partial P} = 0 \, . \tag{4.99}$$

We can see that the solution of the above equation is a generic function:

$$f = f(a^2 P) = f(ap) \, , \tag{4.100}$$

where in the second equality we have used the definition of the proper momentum. The Boltzmann equation written using the proper momentum has the following form:

$$\boxed{\frac{\partial f}{\partial t} - Hp \frac{\partial f}{\partial p} = 0} \tag{4.101}$$

4.5.3 Moments of the collisionless Boltzmann equation

Taking moments of the Boltzmann equation means to integrate it in the momentum space, weighed with powers of the proper momentum. This method is due to Grad [72]. For example, the moment zero of Eq. (4.101) is the following:

$$\int \frac{d^3\mathbf{p}}{(2\pi\hbar)^3} \left(\frac{\partial f}{\partial t} - Hp \frac{\partial f}{\partial p} \right) = 0 \, . \tag{4.102}$$

Using the definition of the particle number density (**??**), we can see that Eq. (4.102) becomes:

$$\dot{n} + 3Hn = 0 \quad \Rightarrow \quad \frac{1}{a^3}\frac{d(na^3)}{dt} = 0 \tag{4.103}$$

The particle number na^3 is conserved. This is an expected result since we have considered a collisionless Boltzmann equation, i.e. absence of interactions and thus no source of creation or destruction of particles. Weighing Eq. (4.101) with the energy and integrating in the momentum space we get:

$$\dot{\varepsilon} - H \int \frac{d^3\mathbf{p}}{(2\pi\hbar)^3} pE(p)\frac{\partial f}{\partial p} = 0 \ . \tag{4.104}$$

Integrate by parts the above equation and show that it becomes:

$$\dot{\varepsilon} + 3H\left(\varepsilon + P\right) = 0 \ , \tag{4.105}$$

i.e. the continuity equation. Weighing Boltzmann equation (4.101) with $\hat{p}^i$ will always result in an identity, because of isotropy. We can show this as follows:

$$\int \frac{d^3\mathbf{p}}{(2\pi\hbar)^3}\hat{p}^i\left(\frac{\partial f}{\partial t} - Hp\frac{\partial f}{\partial p}\right) = \int d^2\hat{p}\ \hat{p}^i \int \frac{dp\ p^2}{(2\pi\hbar)^3}\left(\frac{\partial f}{\partial t} - Hp\frac{\partial f}{\partial p}\right) = 0 \ . \tag{4.106}$$

Since $f = f(ap)$ then only the integration in p contains f and the angular integration is just a multiplicative factor, then, we can see that:

$$\int d^2\hat{p}\ \hat{p}^i = 0 \ , \tag{4.107}$$

and thus Eq. (4.106) is an identity.

4.6. Big-Bang Nucleosynthesis

The BBN is the formation of the primordial light elements, mainly helium. It took place at a temperature (photon temperature) of about 0.1 MeV, which corresponds to a redshift $z \approx 10^9$. In order to investigate the BBN, we need to know the characters of the story. At temperatures say larger than 1 MeV the primordial plasma was formed by photons, electrons, positrons, neutrinos, antineutrinos, protons and neutrons. We have already seen how photons, electrons, positrons, neutrinos, antineutrinos interact among each other, so now we focus on protons and neutrons. Their interactions relevant to BBN are the following:

$$n \leftrightarrow p + e^- + \bar{\nu}_e \qquad \text{(beta decay)} \,, \tag{4.108}$$

$$p + e^- \leftrightarrow \nu_e + n \qquad \text{(electron capture)} \,, \tag{4.109}$$

$$p + \bar{\nu}_e \leftrightarrow e^+ + n \qquad \text{(inverse beta decay)} \,. \tag{4.110}$$

As we have seen, at a temperature of about 1 MeV neutrinos decouple. Therefore, the β-decay reaction in Eq. (4.108) (from left to right) takes over and the number of neutrons starts to diminish. On the other hand, they can also be captured by protons and form deuterium nuclei. The BBN is essentially a competition in capturing neutrons before they decay.

4.6.1 The baryon-to-photon ratio

A very important number for BBN and cosmology is the *baryon-to-photon ratio* η_b, which we have already encountered at the beginning of this chapter. It is defined as follows:

$$\boxed{\eta_\mathrm{b} \equiv \frac{n_\mathrm{b}}{n_\gamma} = 5.5 \times 10^{-10} \left(\frac{\Omega_{\mathrm{b}0} h^2}{0.020}\right)} \tag{4.111}$$

i.e. as the ratio between the number of baryons and the number of photons. We have defined it via number densities, which individually are time-dependent quantities but whose ratio is fixed since both scales as $1/a^3$. The above numbers in Eq. (4.111) can be found as follows:

$$\eta_\mathrm{b} = \frac{n_\mathrm{b}}{n_\gamma} = \frac{\varepsilon_{\mathrm{b}0}}{m_\mathrm{b} c^2 n_{\gamma 0}} \,, \tag{4.112}$$

where we have assumed the baryons to be nonrelativistic, which is indeed the case at the temperatures we are dealing with ($k_\mathrm{B} T \sim$ MeV) since the proton mass is of the order of 1 GeV. Using Eq. (4.39) and Eq. (4.44), we can write

$$\frac{n_{\gamma 0}}{\varepsilon_{\gamma 0}} = \frac{30\zeta(3)}{\pi^2 k_\mathrm{B} T_0} \,. \tag{4.113}$$

Therefore,

$$\eta_\mathrm{b} = \frac{\pi^4 k_\mathrm{B} T_0 \varepsilon_{\mathrm{b}0}}{30\zeta(3) m_\mathrm{b} c^2 \varepsilon_{\gamma 0}} = \frac{\pi^4 k_\mathrm{B} T_0 \Omega_{\mathrm{b}0}}{30\zeta(3) m_\mathrm{b} c^2 \Omega_{\gamma 0}} \,, \tag{4.114}$$

where in the last equality we have multiplied and divided by the present critical energy density in order for the density parameters to appear. The fact that there is a billion

photon for each proton and electron is very important for the following reason. Even if the temperature of the thermal bath is lower than the binding energy of deuterium, i.e. 2.2 MeV, there are still many photons with energy higher than 2.2 MeV which are able to break newly formed deuterium nuclei. This is also known as *deuterium bottleneck*. As Kolb and Turner comment in their book [92, page 92], it is not deuterium's fault if BBN takes place at temperature much smaller than 2.2 MeV. Rather, the very high entropy of the universe, i.e. the smallness of $\eta_{\rm b}$, is the culprit.

4.6.2 The deuterium bottleneck

The deuterium bottleneck is the situation in which newly formed deuterium nuclei are destroyed by photons. With no deuterium available, BBN cannot take place. Let us start considering the reaction:

$$p + n \leftrightarrow D + \gamma \ , \tag{4.115}$$

at chemical equilibrium. Using Saha equation (**??**), we have

$$\frac{n_D n_\gamma}{n_D^{(0)} n_\gamma^{(0)}} = \frac{n_p n_n}{n_p^{(0)} n_n^{(0)}} \ . \tag{4.116}$$

Neglecting the photon chemical potential, i.e. $n_\gamma = n_\gamma^{(0)}$, and using Eq. (**??**) we obtain:

$$\frac{n_D}{n_p n_n} = \frac{n_D^{(0)}}{n_p^{(0)} n_n^{(0)}} = \frac{g_D}{g_p g_n} \left(\frac{2\pi\hbar^2 m_D}{m_p m_n k_{\rm B} T} \right)^{3/2} e^{-(m_D - m_p - m_n)c^2/(k_{\rm B}T)} \ . \tag{4.117}$$

The deuterium has spin 1, whereas protons and neutrons have spin 1/2. Therefore,

$$\frac{n_D}{n_p n_n} = \frac{3}{4} \left(\frac{2\pi\hbar^2 m_D}{m_p m_n k_{\rm B} T} \right)^{3/2} e^{B_D/(k_{\rm B}T)} \ , \tag{4.118}$$

where $B_D = 2.22$ MeV is the deuterium binding energy. We can write the masses ratio as follows:

$$\frac{m_D}{m_p m_n} = \frac{m_p + m_n - B_D/c^2}{m_p m_n} = \frac{1}{m_n} + \frac{1}{m_p} - \frac{B_D}{m_p m_n c^2} \ . \tag{4.119}$$

Introducing the neutron-proton mass difference [203]:

$$Q \equiv (m_n - m_p)c^2 = 1.239 \text{ MeV} \ , \tag{4.120}$$

we can write

$$\frac{m_D}{m_p m_n} = \frac{1}{m_p(1+Q/m_pc^2)} + \frac{1}{m_p} - \frac{B_D}{m_p^2(1+Q/m_pc^2)c^2} \ . \tag{4.121}$$

Since $Q/m_pc^2 \sim B_D/m_pc^2 \sim 10^{-3}$, we approximate:

$$\frac{m_D}{m_p m_n} \approx \frac{2}{m_p} \ . \tag{4.122}$$

Moreover, being $n_n = n_p = n_\mathrm{b}$, we can write:

$$\frac{n_D}{n_\mathrm{b}} = \frac{3}{4} n_\mathrm{b} \left(\frac{4\pi\hbar^2}{m_p k_\mathrm{B} T} \right)^{3/2} e^{B_D/(k_\mathrm{B}T)} \ , \tag{4.123}$$

i.e. we obtain a deuterium-to-baryon ratio which defines how many baryons exist that are deuterium nuclei. Dealing with the n_b on the right hand side as follows:

$$n_\mathrm{b} = \eta_\mathrm{b} n_\gamma = \eta_\mathrm{b} n_\gamma^{(0)} = 2\eta_\mathrm{b} \frac{(k_\mathrm{B}T)^3}{\pi^2\hbar^3c^3} \ , \tag{4.124}$$

where we have used Eq. (**??**) for the photon number density, we get

$$\frac{n_D}{n_\mathrm{b}} = \frac{12}{\sqrt{\pi}} \eta_\mathrm{b} \left(\frac{k_\mathrm{B}T}{m_pc^2} \right)^{3/2} e^{B_D/(k_\mathrm{B}T)} \ . \tag{4.125}$$

As long as $k_\mathrm{B}T \gg B_D$ the relative deuterium abundance is completely negligible since it is exponentially suppressed. However, even when $k_\mathrm{B}T \sim B_D$ the relative abundance is very small, because of the prefactor η_b. This is the deuterium bottleneck. Typically, the temperature T_BBN at which the BBN starts is the one at which the bottleneck is overcome. This is because, as numerical calculations show, once deuterium is formed it rapidly combines into Helium. So, we define T_BBN as the one for which $n_D = n_\mathrm{b}$:

$$\log\left(\frac{12}{\sqrt{\pi}} \eta_\mathrm{b} \right) + \frac{3}{2} \log\left(\frac{k_\mathrm{B}T_\mathrm{BBN}}{m_pc^2} \right) = -\frac{B_D}{k_\mathrm{B}T_\mathrm{BBN}} \ . \tag{4.126}$$

Numerically solving this equation, one finds

$$\boxed{k_\mathrm{B}T_\mathrm{BBN} \approx 0.07 \text{ MeV}} \tag{4.127}$$

Note that we can use Saha equation only until chemical equilibrium holds true. When the reaction $p + n \leftrightarrow D + \gamma$ unbalances and deuterium is formed, we must use the full Boltzmann equation (**??**). However, it can be shown numerically that the two equations provide compatible results up to the moment in which the equilibrium is broken. Therefore,

Saha equation is an useful tool for estimating *when* the equilibrium is broken but, of course, if one needs precise results one should solve the full Boltzmann equation.

4.6.3 Neutron abundance

After the deuterium bottleneck is overcome, BBN takes place in the following chain reactions:

$$p + n \to D + \gamma \,, \tag{4.128}$$

$$D + D \to {}^3\mathrm{He} + n \,, \tag{4.129}$$

$$D + {}^3\mathrm{He} \to {}^4\mathrm{He} + p \,. \tag{4.130}$$

In the following, we shall assume that the three above reactions take place instantaneously and the neutrons are captured in Helium nuclei. This is not what occurred, of course, but it turns out to be a good approximation which allows us to perform easy calculations. Note that Lithium ^{3}Li is also produced, but in tiny fraction (one billionth of the hydrogen abundance). However, measuring its abundance in the universe is a very important independent measure of $\Omega_{\mathrm{b}0}$. The main prediction of BBN is on the abundance of ^{4}He because this is the element which is mostly formed, due to both its high binding energy per nucleon, which is about 7 MeV, see Fig. 13, but also to the fact that there is not much time for forming heavier nuclei since the thermal bath is rapidly cooling and η_{b} is so small.

Our objective is thus to determine the neutron abundance at T_{BBN}. This is done considering two reactions. The electron capture:

$$p + e^- \leftrightarrow n + \nu \,, \tag{4.131}$$

and the β-decay:

$$n \leftrightarrow p + e^- + \bar{\nu} \,. \tag{4.132}$$

The β-decay will provide just an exponential suppression on the abundance predicted by the the electron capture. Therefore, we focus on the latter. For temperature $k_{\mathrm{B}}T \gg 1$ MeV, protons and neutrons are in chemical equilibrium:

$$\frac{n_p}{n_n} = \frac{n_p^{(0)}}{n_n^{(0)}} = \left(\frac{m_p}{m_n}\right)^{3/2} e^{(m_n - m_p)c^2/(k_{\mathrm{B}}T)} \sim e^{Q/(k_{\mathrm{B}}T)} \,, \tag{4.133}$$

where $Q = 1.239$ MeV, see Eq. (4.120). When $k_{\mathrm{B}}T \gg Q$, the mass difference between protons and neutrons is irrelevant, and therefore they are in chemical equilibrium. When $k_{\mathrm{B}}T$ drops below Q nature starts to favor protons because they are energetically more

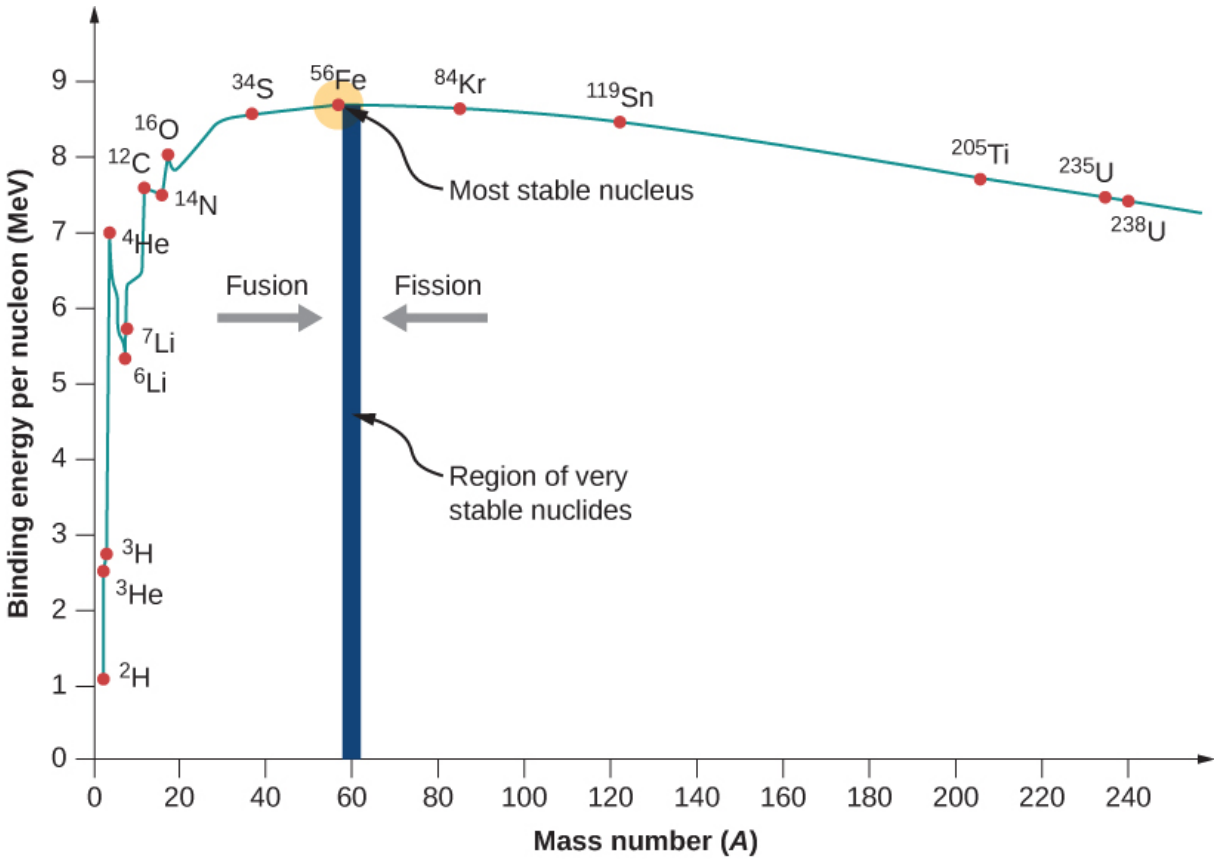

Figure 13 – Binding energy per nucleon. Figure taken from `https://phys.libretexts.org/Bookshelves/University_Physics/`.

"economic" and neutrons start to disappear. However, as we mentioned earlier, out of equilibrium we cannot use Saha equation but have to solve the full Boltzmann equation:

$$\frac{1}{a^3}\frac{d(n_n a^3)}{dt} = n_n^{(0)} n_l^{(0)} \langle \sigma v \rangle \left(\frac{n_p n_l}{n_p^{(0)} n_l^{(0)}} - \frac{n_n n_l}{n_n^{(0)} n_l^{(0)}} \right) , \tag{4.134}$$

where we have denoted with the subscript l the leptons, either electron or neutrino, involved in the electron capture process. We assume their chemical potentials to be zero and simplify Eq. (4.134) as follows:

$$\frac{1}{a^3}\frac{d(n_n a^3)}{dt} = n_l^{(0)} \langle \sigma v \rangle \left(\frac{n_p n_n^{(0)}}{n_p^{(0)}} - n_n \right) . \tag{4.135}$$

Let us define the neutron abundance and the scattering rate as follows:

$$X_n \equiv \frac{n_n}{n_n + n_p} , \qquad n_l^{(0)} \langle \sigma v \rangle \equiv \lambda_{np} . \tag{4.136}$$

Note that Eq. (4.135) can be cast, using Eq. (4.136), as follows:

$$\frac{dX_n}{dt} = \lambda_{np}\left[(1-X_n)e^{-Q/(k_{\rm B}T)} - X_n\right] \ . \tag{4.137}$$

In order to solve (numerically) Eq. (4.137), we introduce the variable:

$$x \equiv \frac{Q}{k_{\rm B}T} \ . \tag{4.138}$$

The time derivative of $x \equiv Q/(k_{\rm B}T)$ can be cast as follows:

$$\frac{dx}{dt} = Hx = x\sqrt{\frac{8\pi G\varepsilon}{3c^2}} \ . \tag{4.139}$$

Since we are deep in the radiation-dominated era, we can write the energy density of Eq. (4.139) as follows:

$$\boxed{\varepsilon = \frac{\pi^2(k_{\rm B}T)^4}{30(\hbar c)^3}g_*} \tag{4.140}$$

where *the effective number of relativistic degrees of freedom* is

$$g_* \equiv \sum_{i=\rm bosons} g_i + \frac{7}{8}\sum_{i=\rm fermions} g_i \ , \tag{4.141}$$

where recall the 7/8 factor coming from Eq. (4.47). The effective number of relativistic degrees of freedom is actually a function of the temperature, since it decreases when a certain species becomes non-relativistic. For temperature larger than 1 MeV g_* is roughly a constant and its value is:

$$g_* = 2 + \frac{7}{8}(3+3+2+2) = 10.75 \ , \tag{4.142}$$

where we have considered two degrees of freedom coming from the photons, 3 + 3 coming from neutrinos and anti-neutrinos and 2 + 2 coming from electrons and positrons. We have considered just a single spin state for each neutrino and anti-neutrino. The Hubble parameter can thus be cast in the following form:

$$H^2 = \frac{8\pi G}{3c^2}\frac{\pi^2(k_{\rm B}T)^4}{30(\hbar c)^3}g_* = \frac{4\pi^3 G g_* Q^4}{45c^2(\hbar c)^3}\frac{1}{x^4} \ , \tag{4.143}$$

where $H(x=1) = 1.13s^{-1}$ and the Eq. (4.137) can be cast as:

$$\frac{dX_n}{dx} = \frac{x\lambda_{np}}{H(x=1)}\left[e^{-x} - X_n(1+e^{-x})\right] \ . \tag{4.144}$$

We only need a last piece of information, i.e. the interaction rate λ_{np}:

$$\lambda_{np} = \frac{255}{\tau_n x^5}(12 + 6x + x^2) \ , \tag{4.145}$$

where $\tau_n = 886.7$s, is the neutron lifetime. The above scattering rate can be found in [26]. We can now solve numerically Eq. (4.144) together with Eq. (4.145). The initial condition on X_n is of course $X_n(x \to 0) = 1/2$, as we can see from the Saha equation (4.133). We plot the evolution of X_n in Fig. 14.

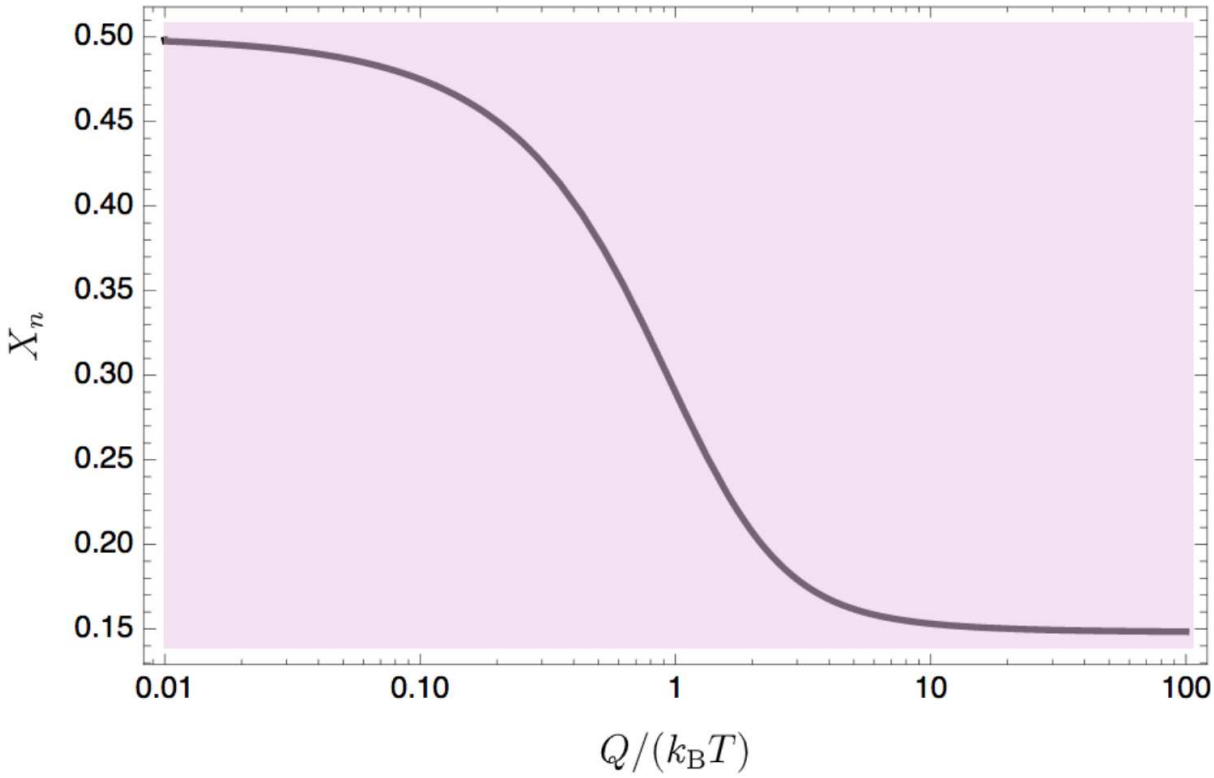

Figure 14 – Evolution of X_n from Eq. (4.144).

As we can appreciate from Fig. 14, $X_n \to 0.15$ as $x \to \infty$. This number is not a very good approximation of the residual abundance of neutrons at $T_{\rm BBN}$ because there are other relevant processes which contribute to deplete or enhance the number of neutrons. Namely:

$$n \to p + e^- + \bar{\nu} \ , \tag{4.146}$$

$$n + p \to D + \gamma \ , \tag{4.147}$$

i.e. the β-decay and the neutron-proton capture. These processes lower the number of

free neutrons. The Helium-3 formation:

$$D + D \rightarrow {}^3\mathrm{He} + n \ , \tag{4.148}$$

puts back into play another neutron and the Helium-4 formation:

$${}^3\mathrm{He} + D \rightarrow {}^4\mathrm{He} + p \ , \tag{4.149}$$

reinserts into play another proton, which helps in capturing neutrons, thus lowering their number. The right way to calculate the abundances of the light elements produced during BBN is to consider all the coupled Boltzmann equations for all the relevant reactions taking place. This is, of course, done numerically and the standard code is Wagoner's one [188] (there has been refinements since then). We now show that correcting $X_n = 0.15$ by taking into account only the β-decay gives a result which is in surprising agreement with the more reliable one which takes into account all the reactions. What we have to do is to weigh $X_n = 0.15$ with $\exp(-t_{\mathrm{BBN}}/\tau_n)$,[3] where t_{BBN} is the time corresponding to $k_{\mathrm{B}}T_{\mathrm{BBN}} = 0.07$ MeV, i.e. the time at which BBN starts. Moreover, we suppose that at this time all the free neutrons are immediately captured and produce Helium-4. Thereby, estimating X_n gives a direct estimation of $X_{^4\mathrm{He}}$. At $k_{\mathrm{B}}T_{\mathrm{BBN}} = 0.07$ MeV, electrons and positrons have already annihilated. Therefore, the effective relativistic degrees of freedom are:

$$g_* = 2 + \frac{7}{8}\left(\frac{4}{11}\right)^{4/3} 6 \approx 3.36 \ , \tag{4.150}$$

where we have taken into account the temperature difference between photons and neutrinos. Since $T \propto 1/a$ and in the radiation-dominated epoch $a \propto \sqrt{t}$, we can relate time and temperature as follows:

$$\frac{1}{4t^2} = H^2 = \frac{4\pi^3 G (k_{\mathrm{B}}T)^4}{45c^2(\hbar c)^3} g_* \ , \tag{4.151}$$

and from the Eq. (4.151), we obtain:

$$t = 271 \left(\frac{0.07 \text{ MeV}}{k_{\mathrm{B}}T}\right)^2 \text{ s} \ . \tag{4.152}$$

Therefore, the expected abundance of neutrons at $k_{\mathrm{B}}T_{\mathrm{BBN}} = 0.07$ MeV is:

$$X_n(T_{\mathrm{BBN}}) = 0.15 \cdot e^{-271/886.7} \approx 0.11 \ . \tag{4.153}$$

[3] This exponential weight comes from Poisson distribution, which governs stochastic processes such as the β-decay.

Assuming that all the neutrons end up in Helium-4 nuclei, we have the prediction:

$$Y_P \equiv 4X_{^4\mathrm{He}} \equiv \frac{4n_{^4\mathrm{He}}}{n_\mathrm{b}} = 2X_n(T_\mathrm{BBN}) = 0.22\ . \tag{4.154}$$

The factor 4 comes from the fact that Y_P is a mass fraction and each Helium-4 nucleus contains 4 baryons. We have also assumed $m_\mathrm{b} = m_p = m_n$. The more accurate numerical result is [92]:

$$Y_P = 0.2262 + 0.0135 \log\left(\frac{\eta_\mathrm{b}}{10^{-10}}\right)\ , \tag{4.155}$$

which is in very good agreement with our "back-of-the-envelope" calculation. In Fig. 15 the time-evolution plots of the mass fractions of various elements are displayed.

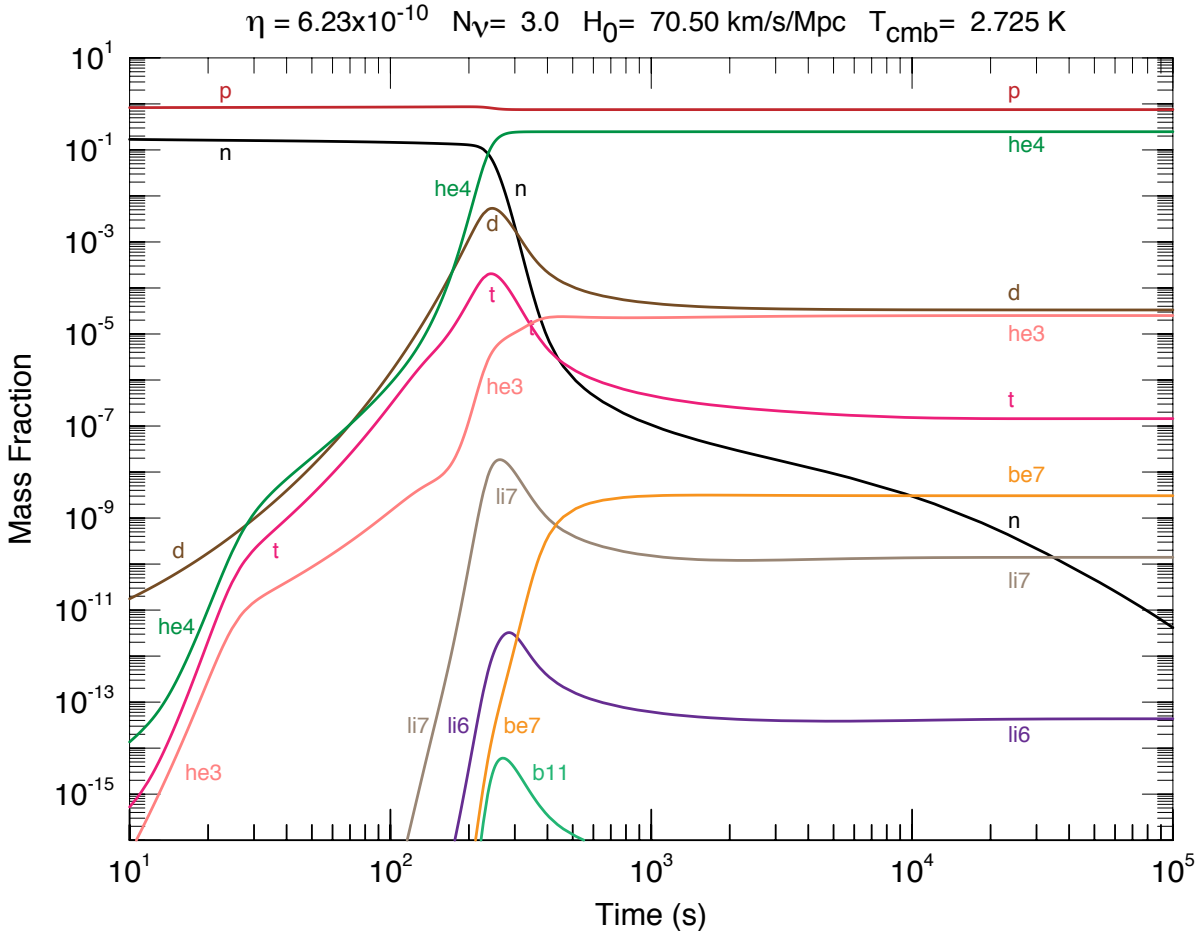

Figure 15 – Time-evolution of the mass fraction of various elements. Figure taken from `http://cococubed.asu.edu/images/net_bigbang/bigbang_time_2010.pdf`.

4.7. Recombination and decoupling

Recombination is the process by which neutral hydrogen is formed via combination

of protons and electrons. *Decoupling* is generally refered to be the epoch when photons stop to interact with free electrons and their mean free path becomes larger than the Hubble radius and we are able to detect them as CMB coming from the *last scattering surface*. For the two events, the relevant interactions are:

$$p + e^- \leftrightarrow H + \gamma \,, \tag{4.156}$$

$$e^- + \gamma \leftrightarrow e^- + \gamma \qquad \text{(Compton/Thomson scattering)} \,. \tag{4.157}$$

Recombination and decoupling temporally occur close to each other for the following reason. At sufficiently low temperatures, which we will calculate, photons are no more able to break hydrogen atoms and so these start to form in larger number (recombination). Being captured in hydrogen atoms, the number of free electrons dramatically drops and the Thomson scattering rate goes to zero (decoupling). The seminal paper on recombination is [139]. In order to determine the epoch of recombination, let us use again Saha equation:

$$\frac{n_e n_p}{n_H} = \frac{n_e^{(0)} n_p^{(0)}}{n_H^{(0)}} \,. \tag{4.158}$$

Let us assume neutrality of the universe, i.e. $n_e = n_p$ and define the free electron fraction:

$$X_e \equiv \frac{n_e}{n_e + n_H} = \frac{n_p}{n_p + n_H} \,, \tag{4.159}$$

If we consider that the degeneracy of the hydrogen atom, in the state $1s$, is $g_{1s} = 4$ (it has two hyperfine states, one of spin 0 and the other of spin 1), then Saha equation can be written (using Eq. (**??**)), as:

$$\frac{X_e^2}{1 - X_e} = \frac{1}{n_e + n_H} \left(\frac{m_e m_p k_{\rm B} T}{2 m_H \pi \hbar^2} \right)^{3/2} e^{-(m_e + m_p - m_H)c^2/(k_{\rm B} T)} \,. \tag{4.160}$$

Consider the contribution at the denominator of the right hand side as:

$$n_e + n_H = n_{\rm b} = \eta_{\rm b} n_\gamma = \eta_{\rm b} \frac{2\zeta(3)}{\pi^2 \hbar^3 c^3} (k_{\rm B} T)^3 \approx 10^{-9} \frac{(k_{\rm B} T)^3}{\hbar^3 c^3} \,. \tag{4.161}$$

Look at the first equality as follows: the total electron number is made up of those which are free plus those which have already been captured. Moreover, the total electron number density is the same as the baryon number density because electrons *are* baryons

(in the jargon of cosmology). We again neglect the mass difference elsewhere than at the exponential, and write:

$$\frac{X_e^2}{1-X_e} \approx 10^9 \left(\frac{m_e c^2}{2\pi k_{\rm B} T}\right)^{3/2} \exp\left(-\frac{13.6 \text{ eV}}{k_{\rm B} T}\right) , \tag{4.162}$$

where we used

$$\varepsilon_0 \equiv (m_e + m_p - m_H)c^2 = 13.6 \text{ eV} , \tag{4.163}$$

i.e. the ionisation energy of the hydrogen atom. The high photon-to-baryon number delays recombination as well as it delayed BBN. Indeed, when $k_{\rm B}T = 13.6$ eV, we get from Eq. (4.162):

$$\frac{X_e^2}{1-X_e} \approx 10^{15} , \tag{4.164}$$

From which one gets that $X_e \approx 1$. This means that even when the energy of the thermal bath drops below the ionisation energy of the hydrogen atom, still no hydrogen is formed and the electrons remain free. This, again, happens because there are still many photons with energy much higher than 13.6 eV. As we already mentioned, Saha equation works until chemical equilibrium is maintained. In Tab. 5 we show numerical calculations of X_e from Eq. (4.162) in order to have a hint about the time of recombination.

$k_{\rm B}T$ [eV]	X_e
0.5	1
0.38	0.995
0.36	0.970
0.34	0.819
0.32	0.434
0.30	0.137
0.29	0.067
0.25	0.001

Table 5 – Free electron fraction at different photon temperatures.

From Tab. 5 we see that the free electron fraction falls abruptly at about $k_{\rm B}T \approx 0.30$ eV.

In Fig. 16 we numerically solve Saha equation (4.162) and use both $k_{\rm B}T$ and the redshift as variables.

In order to accurately calculate X_e, we need to use the full Boltzmann equation (**??**), which for recombination becomes:

$$\frac{1}{a^3}\frac{d(n_e a^3)}{dt} = n_e^{(0)} n_p^{(0)} \langle \sigma v \rangle \left(\frac{n_H n_\gamma}{n_H^{(0)} n_\gamma^{(0)}} - \frac{n_e n_p}{n_e^{(0)} n_p^{(0)}}\right) . \tag{4.165}$$

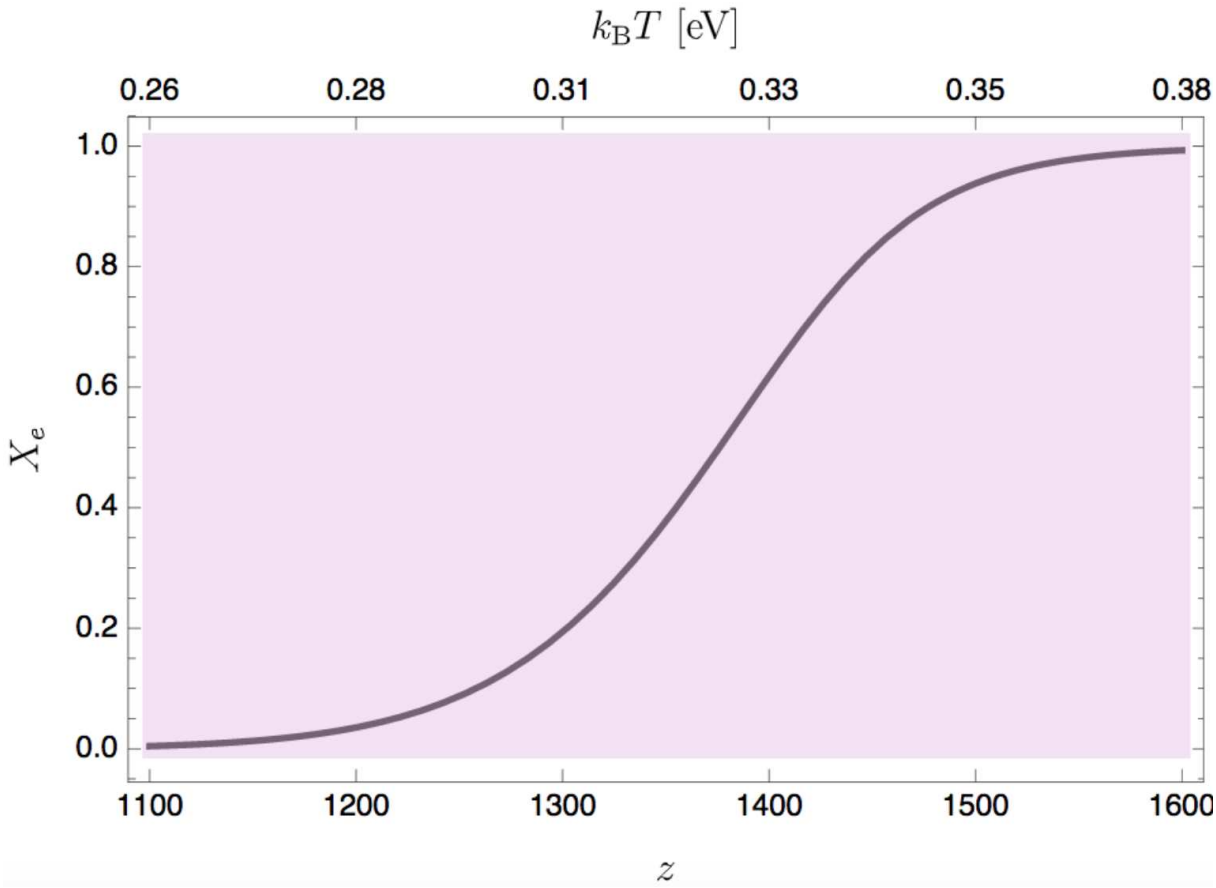

Figure 16 – Numerical solution of the Saha equation (4.162).

We assume $n_\gamma = n_\gamma^{(0)}$ and $n_e = n_p$ again. Therefore,

$$\frac{1}{a^3}\frac{d(n_e a^3)}{dt} = \langle\sigma v\rangle \left[n_H \left(\frac{m_e k_{\rm B} T}{2\pi\hbar^2}\right)^{3/2} e^{-\varepsilon_0/(k_{\rm B}T)} - n_e^2 \right] . \tag{4.166}$$

Introducing now the free electron fraction X_e defined in Eq. (4.159), we get:

$$\frac{dX_e}{dt} = \langle\sigma v\rangle \left[(1-X_e) \left(\frac{m_e k_{\rm B} T}{2\pi\hbar^2}\right)^{3/2} e^{-\varepsilon_0/(k_{\rm B}T)} - X_e^2 n_b \right] . \tag{4.167}$$

As we did for BBN in Eq. (4.124), we can replace $n_{\rm b}$ with:

$$n_{\rm b} = 2\eta_{\rm b} \frac{(k_{\rm B}T)^3}{\pi^2\hbar^3 c^3} . \tag{4.168}$$

Now we need the fundamental physics of the capture process. It is given by:

$$\langle\sigma v\rangle \equiv \alpha^{(2)} = 9.78\, \alpha^2 \frac{\hbar^2}{m_e^2 c} \left(\frac{\varepsilon_0}{k_{\rm B}T}\right)^{1/2} \log\left(\frac{\varepsilon_0}{k_{\rm B}T}\right) , \tag{4.169}$$

where $\alpha = 1/137$ is the fine structure constant. The superscript (2) serves to indicate that the best way to form hydrogen is not via the capture of an electron in the $1s$ state, because this generates a 13.6 eV photon which ionises another newly formed H. The efficient way to form hydrogen is to form it in a excited state. When it relaxes to the ground state, the photons emitted have not enough energy to ionise other hydrogen atoms. For example, an electron captured in the $n = 2$ state generates a 3.4 eV photon. Subsequently, when the electron falls in the ground state, the hydrogen releases another 10.2 eV photon. Neither of the two photons has sufficient energy for ionising another hydrogen atom in the ground state. We now solve numerically Eq. (4.167) together with Eq. (4.124) and Eq. (4.169). We use the redshift as independent variable:

$$\frac{dX_e}{dt} = \frac{dX_e}{dz}\frac{dz}{dt} = -\frac{dX_e}{dz}H(1+z) \ , \tag{4.170}$$

and the following Hubble parameter:

$$\frac{H^2}{H_0^2} = \Omega_{\rm m0}(1+z)^3 + \Omega_{\rm r0}(1+z)^4 + \Omega_\Lambda \ , \tag{4.171}$$

where for $z \approx 1100$ is the matter contribution the dominant one. Therefore, we rewrite Eq. (4.167) as follows:

$$\frac{dX_e}{dz} = -\frac{\langle\sigma v\rangle}{H(1+z)}\left[(1-X_e)\left(\frac{m_e k_{\rm B} T}{2\pi\hbar^2}\right)^{3/2} e^{-\varepsilon_0/(k_{\rm B}T)} - X_e^2 n_{\rm b}\right] \ , \tag{4.172}$$

also taking into account that the photon temperature T scales as:

$$T = T_0(1+z) \ , \tag{4.173}$$

with $T_0 = 2.725$ K.

In Fig. 17 we show the numerical solution of the Boltzmann equation (4.172), compared with the solution of the Saha equation (4.162). Note how the two solutions are compatible for high redshifts, but that of the Boltzmann equation predicts a residual free electron fraction of about $X_e \approx 10^{-3}$. At the same time of recombination the decoupling of photons from electron takes place. As we anticipated, this happens because very few free electrons remain after hydrogen formation and therefore photons are free to propagate undisturbed and seen by us as the CMB.

Decoupling

As we have already mentioned at the beginning of this chapter, roughly speaking in the expanding universe any kind of reaction stops occurring when its interaction rate Γ

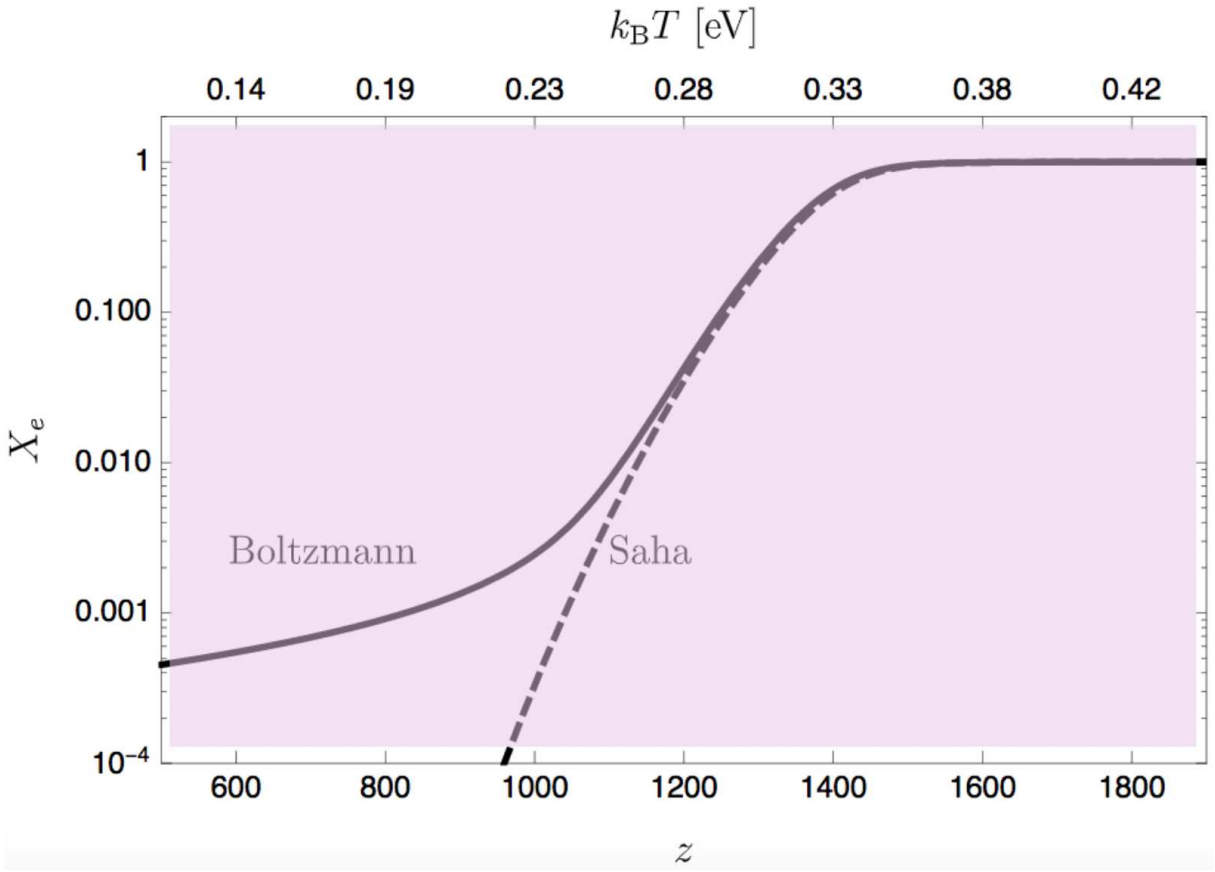

Figure 17 – Solid line: numerical solution of the Boltzmann equation (4.172). Dashed line: solution of the Saha equation (4.162).

becomes of the order of H. In the case of photons and electrons, the relevant process is Thomson scattering, for which:

$$\Gamma_{\rm T} = n_e \sigma_{\rm T} c = X_e n_{\rm b} \sigma_{\rm T} c \,, \tag{4.174}$$

where n_e is the free-electron number density, which we have written as $X_e n_{\rm b}$ because we have neglected the Helium abundance. The baryon number density can be expressed as

$$n_{\rm b} = \frac{\rho_{\rm b}}{m_{\rm b}} = \frac{3H_0^2 \Omega_{\rm b0}}{8\pi G m_p a^3} \,, \tag{4.175}$$

where we have identified $m_{\rm b} = m_p$ since it is the proton mass that dominates the baryon energy density. We can see that:

$$\frac{\Gamma_{\rm T}}{H} = \frac{n_e \sigma_{\rm T} c}{H} = 0.0692\ h \frac{X_e \Omega_{\rm b0} H_0}{H a^3} \,. \tag{4.176}$$

As for H, we consider a matter plus radiation universe, for which:

$$H^2 = H_0^2 \frac{\Omega_{\rm m0}}{a^3} \left(1 + \frac{a_{\rm eq}}{a}\right) \,. \tag{4.177}$$

Using the above Hubble parameter we obtain:

$$\frac{\Gamma_{\rm T}}{H} = 113 X_e \left(\frac{\Omega_{\rm b0}h^2}{0.02}\right)\left(\frac{0.15}{\Omega_{\rm m0}h^2}\right)^{1/2}\left(\frac{1+z}{1000}\right)^{3/2}\left(1+\frac{1+z}{3600}\frac{0.15}{\Omega_{\rm m0}h^2}\right)^{-1/2} . \qquad (4.178)$$

The decoupling redshift $z_{\rm dec}$ is defined to be that for which $\Gamma_{\rm T} = H$. Note that in the above equation X_e is a function of the redshift, which we have plotted in Fig. 17. On the other hand, X_e drops abruptly during recombination, so that the factor 113 is easily overcome. For this reason recombination and decoupling take place at roughly the same time.

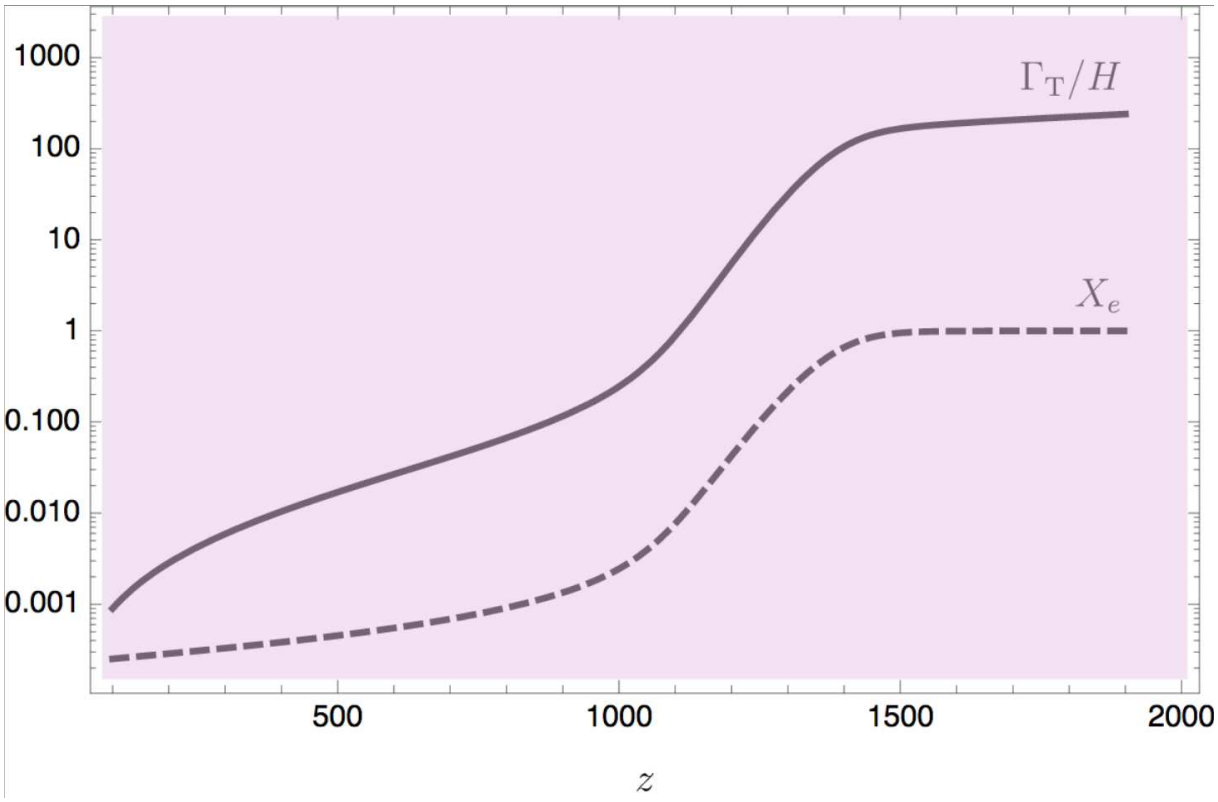

Figure 18 – Solid line: numerical solution of the ratio $\Gamma_{\rm T}/H$ of Eq. (4.178). Dashed line: numerical solution of Eq. (4.172) for X_e.

Now imagine that no recombination takes place, i.e. $X_e = 1$. The above equation then gives the decoupling redshift:

$$1 + z_{\rm dec} = 43\left(\frac{0.02}{\Omega_{\rm b0}h^2}\right)^{2/3}\left(\frac{\Omega_{\rm m0}h^2}{0.15}\right)^{1/3} . \qquad (4.179)$$

This is the freeze-out redshift of the electrons, i.e. eventually photons and electrons do not interact anymore because they are too diluted by the cosmological expansion. This would happen for a redshift 42. This number is important because of the following. Well

after decoupling, ultraviolet light emitted by stars and gas is able to ionise again hydrogen atoms. This phase is called *reionisation*. If the latter ocurred for redshifts smaller than 42, the newly freed electron would not interact with photons because they are too much diluted by the cosmological expansion. Indeed, reionization takes place for $z_{\rm reion} \approx 10$, so that the CMB spectrum is poorly affected.

Chapter 5

Neutrinos in the CMB epoch

Long the realm of armchair philosophers, the study of the origins and evolution of the universe became a physical science with falsifiable theories

—Wayne Hu, PhD Thesis

In this Chapter we attack the hierarchy of Boltzmann equations that we have found for photons and present an approximate, semi-analytic solution which will allow us to understand the temperature correlation in the CMB sky and its relation with the cosmological parameters. Our scope is to understand the features of the angular, temperature-temperature power spectrum in Fig. 19. Note that in this plot the definition

$$\mathcal{D}_\ell^{TT} \equiv \frac{\ell(\ell+1)C_{TT,\ell}}{2\pi} \,, \tag{5.1}$$

is used. We shall see the reason for the $\ell(\ell+1)$ normalisation, whereas the $C_{TT,\ell}$'s are given as functions of the multipole moments of the temperature distribution and the primordial power spectrum for scalar perturbations. In Fig. 19 we can also see data points up to $\ell \approx 2500$. What can we say from this number about the angular sensitivity of *Planck*? It can be roughly computed as follows. For a given $\ell_{\rm max}$ how many realisations of $a_{\ell m}$ do we have?. For each ℓ we have $2\ell + 1$ possible values of m, thus that:

$$N_{\ell_{\rm max}} = \sum_{\ell=0}^{\ell_{\rm max}} (2\ell+1) = (\ell_{\rm max}+1)^2 \,. \tag{5.2}$$

The full sky has:

$$4\pi \text{ rad}^2 = \frac{4}{\pi}(180 \text{ deg})^2 \approx 41000 \text{ deg}^2 \,. \tag{5.3}$$

If an experiment has sensitivity of 7 deg, then we can have at most

$$\frac{4}{\pi}(180/7)^2 \approx 842\ , \tag{5.4}$$

pieces of independent information and therefore we can determine as many $a_{\ell m}$. This gives $\ell_{\rm max} \approx 28$ and it was the sensitivity of *CoBE*. For *Planck*, the angular sensitivity was of 5 arcmin, which corresponds to

$$\frac{4}{\pi}(180 \times 60/5)^2 \approx 10^6\ , \tag{5.5}$$

pieces of independent information and then to $\ell_{\rm max} = 2436$. In this Chapter we omit the superscript S referring to the scalar perturbations contribution to Θ, since most of the time we shall discuss of it. We shall only use T in order to distinguish the tensor contribution.

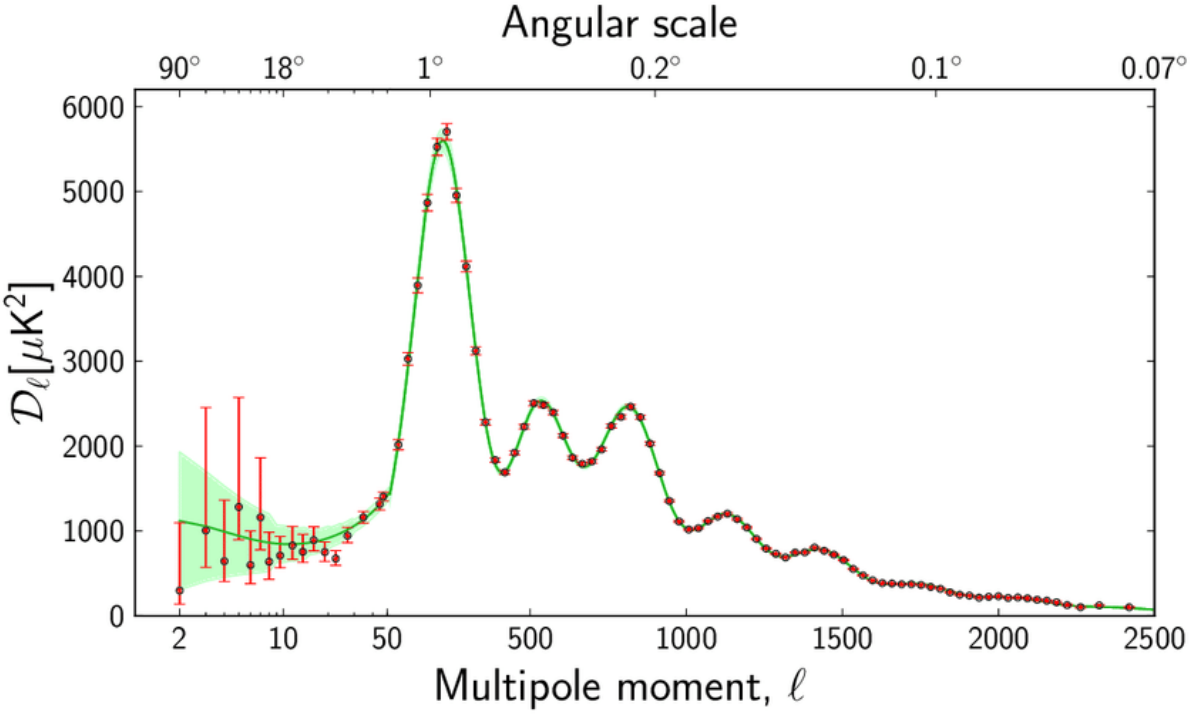

Figure 19 – CMB TT power spectrum. The green solid line is the best fit ΛCDM model and the data (red points) are from Planck.

5.1. Free-streaming

It is convenient to start neglecting the collisional term in the Boltzmann equation and considering thus the phase of photon *free-streaming*. We can write for scalar

perturbations:

$$\left(\frac{\partial}{\partial\eta}+\frac{dx^i}{d\eta}\frac{\partial}{\partial x^i}\right)(\Theta+\Psi)=\Psi'-\Phi'\ . \tag{5.6}$$

As we know from Boltzmann equation, the differential operator on the left hand side is a convective derivative, i.e. a derivative along the photon path:

$$\frac{d}{d\eta}(\Theta+\Psi)=\Psi'-\Phi'\ , \tag{5.7}$$

whose inversion is the basis of the *line-of-sight integration* approach to CMB anisotropies [166], which is an alternative to attacking the hierarchy of coupled Boltzmann equations (which still must be attacked but can be truncated at much lower ℓ's) as it was done e.g. in [113]. For time-independent potentials, as they are in the matter-dominated epoch, the collisionless Boltzmann equation for photons tells us that $\Theta+\Psi$ is constant along the photons paths, i.e. along our past light-cone, since recombination. Recall that the scalar-perturbed metric that we are using is given by:

$$ds^2=-a^2(\eta)(1+2\Psi)d\eta^2+a^2(\eta)(1+2\Phi)\delta_{ij}dx^idx^j\ . \tag{5.8}$$

Inside a potential well, Ψ is negative. In order to be convinced of this one has just to think about the Newtonian limit and realise that 2Ψ is the Newtonian gravitational potential, hence negative. So, since $\Theta+\Psi$ stays constant, we have that:

$$\Theta(\eta_*,\mathbf{x}_*,\hat{p})+\Psi(\eta_*,\mathbf{x}_*)=\Theta(\eta_0,\mathbf{x}_0,\hat{p})+\Psi(\eta_0,\mathbf{x}_0)\ . \tag{5.9}$$

where on the left hand side we have chosen the quantities at recombination whereas on the right hand side we have chosen the present time. Note that $\mathbf{x}_0$, is where our laboratory (the CMB experiment) is, i.e. Earth, and as such is fixed. Therefore, since we can only detect photons on our past light-cone, and those from CMB comes from a fixed comoving distance $r_*=\eta_0-\eta_*$, we have that:

$$\mathbf{x}_*=\mathbf{x}_0-r_*\hat{p}\ . \tag{5.10}$$

Note that $\hat{p}$ is the photon direction and so it is opposite to the direction of the line of sight $\hat{n}=-\hat{p}$. So, the only independent variables are 2, the components of $\hat{p}$. They become just a single one, μ, because of the way in which we factorise the azimuthal dependence (and assuming axial symmetry). The potential $\Psi(\eta_0,\mathbf{x}_0)$ is usually neglected, or incorporated

in the potential at recombination, since it is not detectable. As it is well known, classically only potential differences are physically meaningful. The above equation then tells us that:

$$\Theta(\eta_*, \mathbf{x}_0 - r_*\hat{p}, \hat{p}) + \Psi(\eta_*, \mathbf{x}_0 - r_*\hat{p}) = \Theta(\eta_0, \mathbf{x}_0, \hat{p}) \ , \tag{5.11}$$

i.e. the observed temperature fluctuation (on the right hand side) accounts for the energy loss due to climbing out the potential well or falling down a potential hill. This is the so-called **Sachs-Wolfe effect** [157]. Writing the above equation in Fourier modes, we have:

$$\int \frac{d^3\mathbf{k}}{(2\pi)^3}\Theta(\eta_0, \mathbf{k}, \hat{p})e^{i\mathbf{k}\cdot\mathbf{x}_0} = \int \frac{d^3\mathbf{k}}{(2\pi)^3}\left[\Theta(\eta_*, \mathbf{k}, \hat{p}) + \Psi(\eta_*, \mathbf{k})\right] e^{i\mathbf{k}\cdot(\mathbf{x}_0 - r_*\hat{p})} \ . \tag{5.12}$$

We can set now $\mathbf{x}_0 = 0$, without losing of generality, and manifest the dependences as k and μ, the former since we normalise to the scalar primordial mode $\alpha(\mathbf{k})$, and the latter since we are considering axisymmetric scalar perturbations. Hence we have for the Fourier modes:

$$\Theta(\eta_0, k, \mu) = \left[\Theta(\eta_*, k, \mu) + \Psi(\eta_*, k)\right] e^{-ik\mu r_*} \ . \tag{5.13}$$

Using the partial wave expansion, we get:

$$\Theta_\ell(\eta_0, k) = \frac{1}{(-i)^\ell}\int_{-1}^{1}\frac{d\mu}{2}\mathcal{P}_\ell(\mu)\left[\Theta(\eta_*, k, \mu) + \Psi(\eta_*, k)\right] e^{-ik\mu r_*} \ , \tag{5.14}$$

and using the relation:

$$\int_{-1}^{1}\frac{d\mu}{2}\ \mathcal{P}_\ell(\mu)e^{-ik\mu r_*} = (-i)^\ell j_\ell\left(kr_*\right) \ , \tag{5.15}$$

we can write:

$$\Theta_\ell(\eta_0, k) = \Psi(\eta_*, k)j_\ell(kr_*) + \frac{1}{(-i)^\ell}\int_{-1}^{1}\frac{d\mu}{2}\mathcal{P}_\ell(\mu)\Theta(\eta_*, k, \mu)e^{-ik\mu r_*} \ . \tag{5.16}$$

Using again the partial wave expansion, we can write the above formula as:

$$\begin{aligned}\Theta_\ell(\eta_0, k) &= \Psi(\eta_*, k)j_\ell(kr_*) \\ +\frac{1}{(-i)^\ell}\sum_{\ell'}(-i)^{\ell'}(2\ell'+1)\Theta_{\ell'}(\eta_*, k)&\int_{-1}^{1}\frac{d\mu}{2}\mathcal{P}_\ell(\mu)\mathcal{P}_{\ell'}(\mu)e^{-ik\mu r_*} \ .\end{aligned} \tag{5.17}$$

We shall see later that, because of tight-coupling, the monopole and the dipole contribute the most at recombination. Hence, we can write, truncating the summation at $\ell' = 1$:

$$\Theta_\ell(\eta_0, k) = (\Theta_0 + \Psi)(\eta_*, k) j_\ell(kr_*) + \frac{3\Theta_1(\eta_*, k)}{(-i)^{\ell-1}} \int_{-1}^{1} \frac{d\mu}{2} \mathcal{P}_\ell(\mu) \mu e^{-ik\mu r_*} \ . \tag{5.18}$$

The integral can be performed as follows:

$$\int_{-1}^{1} \frac{d\mu}{2} \mathcal{P}_\ell(\mu) \mu e^{-ik\mu r_*} = i \frac{d}{d(kr_*)} \int_{-1}^{1} \frac{d\mu}{2} \mathcal{P}_\ell(\mu) e^{-ik\mu r_*} = \frac{1}{i^{\ell-1}} \frac{d}{d(kr_*)} j_\ell\left(kr_*\right) \ . \tag{5.19}$$

The same technique can be used, in principle, to calculate the integral for any ℓ': for each power of μ one gains a derivative of the spherical Bessel function. Recalling the formula [11]:

$$\frac{dj_\ell(x)}{dx} = j_{\ell-1}(x) - \frac{\ell+1}{x} j_\ell(x) \ , \tag{5.20}$$

we can write:

$$\begin{aligned} \Theta_\ell(\eta_0, k) = (\Theta_0 + \Psi)(\eta_*, k) j_\ell(kr_*) \\ +3\Theta_1(\eta_*, k) \left[j_{\ell-1}(kr_*) - \frac{\ell+1}{kr_*} j_\ell(kr_*) \right] \ . \end{aligned} \tag{5.21}$$

So, the spherical Bessel functions start to appear. We have obtained the above free-streaming solution neglecting the potentials derivatives in Eq. (5.7). Taking them into account is not difficult, since an additional piece containing the integration of the potential derivatives would appear in Eq. (5.13):

$$\Theta(\eta_0, k, \mu) = \left[\Theta(\eta_*, k, \mu) + \Psi(\eta_*, k)\right] e^{-ik\mu r_*} + \int_{\eta_*}^{\eta_0} d\eta \, (\Psi' - \Phi')(\eta, k) e^{-ik\mu(\eta_0 - \eta)} \ . \tag{5.22}$$

The exponential factor in the integral comes from the Fourier transform of the potentials and from considering:

$$\mathbf{x} = \mathbf{x}_0 - (\eta_0 - \eta)\hat{p} \ , \tag{5.23}$$

at any given time η along the photon trajectory (this is the "line of sight", in practice). Performing again the expansion in partial waves, we get:

$$\begin{aligned} \Theta_\ell(\eta_0, k) = (\Theta_0 + \Psi)(\eta_*, k) j_\ell(kr_*) \\ +3\Theta_1(\eta_*, k) \left[j_{\ell-1}(kr_*) - \frac{\ell+1}{kr_*} j_\ell(kr_*) \right] \\ + \int_{\eta_*}^{\eta_0} d\eta \, [\Psi'(\eta, k) - \Phi'(\eta, k)] j_\ell(kr) \ , \end{aligned} \tag{5.24}$$

where

$$r \equiv \eta_0 - \eta \, . \tag{5.25}$$

As we are going to see, the first two terms of the above formula contains the *primary anisotropies* of the CMB, which are the *acoustic oscillations* and the *Doppler effect*. The $\Psi(\eta_*, k)$ contribution in the first term is, as we have already anticipated, the **Sachs-Wolfe effect**. The last term is the **Integrated Sachs-Wolfe** (ISW) effect [157] and contributes only when the gravitational potentials are time-varying. This happens, when radiation and DE are relevant. For this reason the ISW effect is usually separated in the early-times one, due to a small presence of radiation still at decoupling, and in the late-times one, due to DE. Once we know all the contributions of the above formula, we can provide the prediction on the $C^S_{TT,\ell}$ spectrum. The presence of the spherical Bessel function is interesting for two reasons, which we display in Fig. 20 for the arbitrary choice $\ell = 10$.

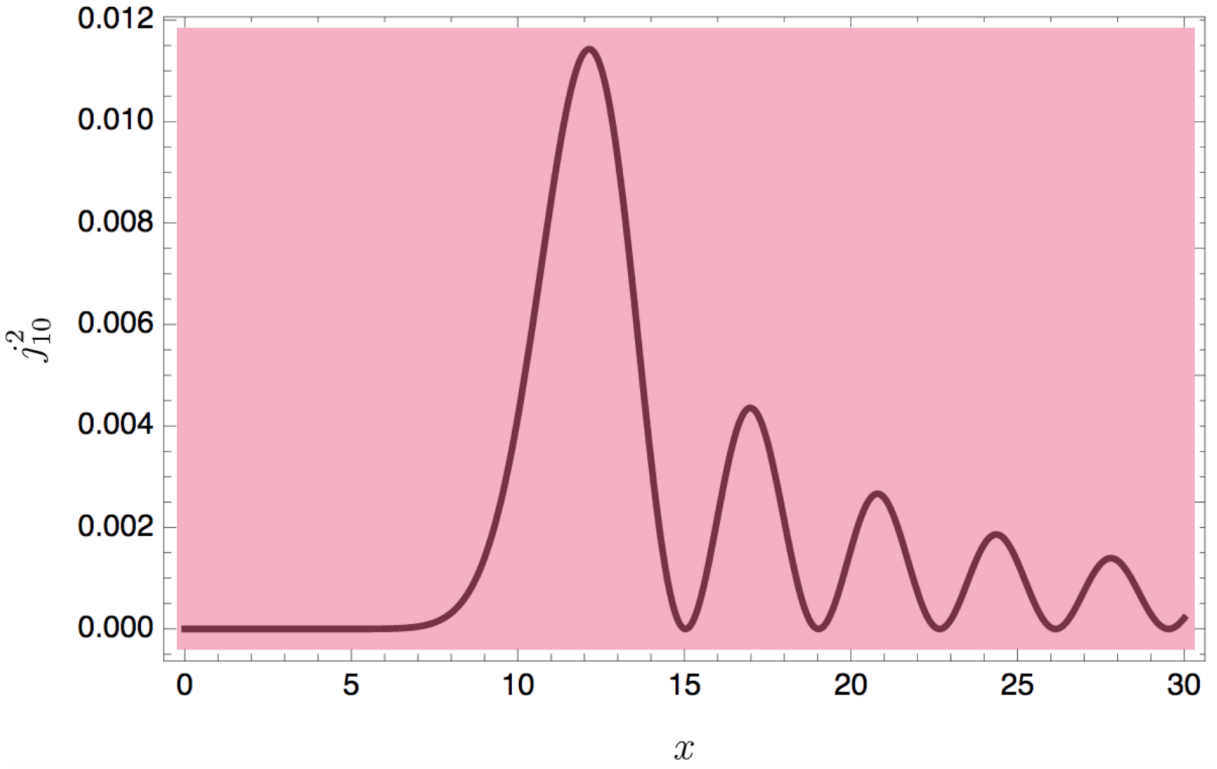

Figure 20 – Evolution of the spherical Bessel function $j^2_{10}(x)$.

We have chosen to plot the squared spherical Bessel function because it is the relevant window function when computing the C_ℓ's, as we shall see briefly. First, the maximum value is attained roughly when $x \approx \ell$ and for $x < \ell$ the spherical Bessel function is practically vanishing. Therefore, for a given multipole ℓ the scale which contribute most

for the observed anisotropy is:

$$k \approx \frac{\ell}{\eta_0 - \eta_*} \, . \tag{5.26}$$

The second reason of interest is that the spherical Bessel function goes to zero for large x. This means that scales such that $kr_* \gg 1$ do not contribute to the observed anisotropy. Physically, this is an effect due to the free-streaming phase for which, on very small scales, hot and cold photons mix up destroying thus the anisotropy. We have thus seen that the predicted anisotropy today is given by formula Eq. (5.24). We have now to justify the fact of considering only the monopole and the dipole at recombination. We shall commence in the next section discussing very large scales. In principle, Eq. (5.24) has the very same form for neutrinos, but with an initial conformal time η_i which is well anterior to η_*, since neutrinos do not interact and therefore they only free-stream (at least for temperatures of the primordial plasma below 1 MeV).

5.2. Anisotropies on large scales

On large scales, i.e. $k\eta \ll 1$, the relevant equations are:

$$\delta_\gamma' = -4\Phi' \, , \quad \delta_\nu' = -4\Phi' \, , \quad \delta_{\rm c}' = -3\Phi' \, , \quad \delta_{\rm b}' = -3\Phi' \, , \tag{5.27}$$

i.e. only the monopoles are relevant. Since we want to describe CMB, let us focus on the photon density contrast, which can be written as:

$$\delta_\gamma(k,\eta) = 4\Theta_0(k,\eta) \, , \tag{5.28}$$

introducing the monopole of the temperature fluctuation. The equation $\Theta_0' = -\Phi'$ can be immediately integrated, obtaining:

$$\Theta_0(k,\eta) = -\Phi(k,\eta) + C_\gamma(k) \, . \tag{5.29}$$

For the adiabatic primordial mode, the only which we are going to consider is $C_\gamma(k) = \Phi_{\rm P}(k) - \Psi_{\rm P}(k)/2$, and thus:

$$\Theta_0(k,\eta) = -\Phi(k,\eta) + \Phi_{\rm P}(k) - \frac{1}{2}\Psi_{\rm P}(k) \, . \tag{5.30}$$

We can consider the gravitational potentials to be equal in modulus and on large scales $\Phi(k,\eta)$ is independent of time and since recombination $\eta_* \gg \eta_{\rm eq}$ takes place well after

radiation-matter equality, we know that $\Phi(k,\eta_*) = 9\Phi_{\rm P}(k)/10$, i.e. the value of the gravitational potential drops of 10% in passing through radiation-matter domination. Therefore:

$$\Theta_0(k,\eta_*) = \frac{3}{5}\Phi_{\rm P}(k) = \frac{2}{3}\Phi(k,\eta_*) = -\frac{2}{3}\Psi(k,\eta_*) \; . \tag{5.31}$$

As we saw earlier in Eq. (5.24), the observed anisotropy is not $\Theta_0(k,\eta_*)$ but $\Theta_0(k,\eta_*) + \Psi(k,\eta_*)$, because of the gravitational redshift. Again, this is the Sachs-Wolfe effect, amounting to a shift in the photons frequency when they decouple from the baryonic plasma depending whether they are in a well or hill of the gravitational potential. So, we have from Eq. (5.31) that:

$$(\Theta_0 + \Psi)(k,\eta_*) = \frac{1}{3}\Psi(k,\eta_*) \; . \tag{5.32}$$

On the other hand, for $\delta_{\rm c}$ we know that

$$\delta_{\rm c}(k,\eta) = -3\Phi(k,\eta) + \frac{9\Phi_{\rm P}(k)}{2} \; , \tag{5.33}$$

again assuming adiabatic primordial modes. Using again $\Phi(k,\eta_*) = 9\Phi_{\rm P}(k)/10$, we get:

$$\delta_{\rm c}(k,\eta_*) = 2\Phi(k,\eta_*) = -2\Psi(k,\eta_*) \; . \tag{5.34}$$

The fluctuations in CDM contribute more in generating the potential wells than photons, a factor 2 against a factor $-2/3$. Combining the two equations:

$$(\Theta_0 + \Psi)(k,\eta_*) = -\frac{\delta_{\rm c}(k,\eta_*)}{6} \tag{5.35}$$

This result tells us that on large scales colder spots represent larger overdensities, a counter-intuitive result. One expects hotter photons the deeper the well is and in fact this is the case with just $\Theta_0(k,\eta_*)$, since we have:

$$\Theta_0(k,\eta_*) = -\frac{2}{3}\Psi(k,\eta_*) = \frac{\delta_{\rm c}(k,\eta_*)}{3} \; , \tag{5.36}$$

i.e. the larger the CDM overdensity, the larger the well and $\Theta_0(k,\eta_*)$ are. However, photons' response to the gravitational potential is only a factor $-2/3$ whereas the gravitational redshift adds a Ψ contribution, changing thus the sign of the observed anisotropy. In the limit of $\delta_{\rm c} \to -1$, one gets $(\Theta_0 + \Psi)(k,\eta_*) \to 1/6$, so cosmic voids correspond to hot spots! The results found here are valid only on large scales, i.e. for $k\eta_* \ll 1$, scales much larger than the horizon at recombination, which has an angular size of approximatively 1 degree.

Moreover, they also depend on the choice of initial conditions. We have opted for the adiabatic ones, as usual.

Let us use the theoretical prediction on the $C^S_{TT,\ell}$, together with the first contribution only from Eq. (5.24). The latter approximation is justified by the fact that we are considering large scales, hence the dipole contribution is negligible and the ISW effect is vanishing because the potentials are constant. Since:

$$(\Theta_0 + \Psi)(k, \eta_*) = \frac{1}{3}\Psi(k, \eta_*) = -\frac{1}{3}\Phi(k, \eta_*) = -\frac{3}{10}\Phi_{\rm P}(k) = -\frac{1}{5}\mathcal{R}(k) \ , \tag{5.37}$$

the transfer function is just the constant $-1/5$ (recall that we are neglecting the neutrino fraction R_ν) and thus the angular power spectrum is:

$$C^S_{TT,\ell}({\rm SW}) = \frac{4\pi}{25}\int_0^\infty \frac{dk}{k}\Delta^2_{\mathcal{R}}(k) j^2_\ell(k\eta_0) \ , \tag{5.38}$$

since $\eta_* \ll \eta_0$. Note that $k\eta_* \ll k\eta_0$ and we have seen in Fig. 20 that the spherical Bessel function contributes the most about $k\eta_0 \approx \ell$. Thus, for small ℓ, i.e. large angular scales, $k\eta_0$ is small and $k\eta_*$ is very small, where in fact $|\,(\Theta_0 + \Psi)\,(k, \eta_*)|^2$ is constant. In other words, the above approximation is valid for small ℓ, typically $\ell \lesssim 30$. In the above integral we can look at $j^2_\ell(k\eta_0)$ as a very peaked window function and approximate it as:

$$C^S_{TT,\ell}({\rm SW}) \approx \frac{4\pi}{25}\Delta^2_{\mathcal{R}}(\ell/\eta_0)\int_0^\infty \frac{dk}{k} j^2_\ell(k\eta_0) \ . \tag{5.39}$$

Using the result:

$$\int_0^\infty \frac{dx}{x} j^2_\ell(x) = \frac{1}{2\ell(\ell+1)} \ , \tag{5.40}$$

we have then:

$$\frac{\ell(\ell+1)C^S_{TT,\ell}({\rm SW})}{2\pi} \approx \frac{1}{25}\Delta^2_{\mathcal{R}}(\ell/\eta_0) \ . \tag{5.41}$$

Hence, for a scale-invariant spectrum $n_S = 1$ the combination $\ell(\ell+1)C^S_{TT,\ell}({\rm SW})$ is constant and it is called **Sachs-Wolfe plateau**. This also explains why CMB power spectra are usually presented with the $\ell(\ell+1)$ normalisation, as in Fig. 19. If $n_S \neq 1$, then $\ell(\ell+1)C^S_{TT,\ell}({\rm SW})$ is proportional to ℓ^{n_S-1}, i.e. the **primordial tilt** in the power spectrum leaves its mark in a tilted plateau for small ℓ.

5.3. Tight-coupling and acoustic oscillations

We have seen that in order to determine the prediction on the present time $C_{TT,\ell}$'s we need to know what happens at recombination. We devote this section to such purpose, showing that the monopole and the dipole contribute the most. Let us recover here the hierarchy of Boltzmann equations for the Θ_ℓ's, not taking into account polarisation:

$$(2\ell+1)\Theta'_\ell + k[(\ell+1)\Theta_{\ell+1} - \ell\Theta_{\ell-1}] = (2\ell+1)\tau'\Theta_\ell \ , \qquad (\ell > 2) \ , \tag{5.42}$$

$$10\Theta'_2 + 2k\,(3\Theta_3 - 2\Theta_1) = 10\tau'\Theta_2 - \tau'\Pi \ , \tag{5.43}$$

$$3\Theta'_1 + k(2\Theta_2 - \Theta_0) = k\Psi + \tau'\,(3\Theta_1 - V_{\rm b}) \ , \tag{5.44}$$

$$\Theta'_0 + k\Theta_1 = -\Phi' \ , \tag{5.45}$$

where recall that $\delta_\gamma = 4\Theta_0$ and $3\Theta_1 = V_\gamma$. The best way to deal with these equations is to solve them numerically by using Boltzmann codes such as CAMB or CLASS, but in this way the physics behind the $C_{TT,\ell}$'s remains hidden or unclear. For this reason we attack these equations in an approximate fashion, but analytically. We take the limit $-\tau' \gg \mathcal{H}$, which is called **tight-coupling** (TC) approximation. This limit physically means that the Thomson scattering rate between photons and electrons is much larger than the Hubble rate until recombination and then drops abruptly since the free electron fraction X_e goes to zero very rapidly, as we have seen when studying thermal history in Chapter 4. We shall first consider the case of **sudden recombination**, where all the photons last scatter at the same time. It is a fair approximation, though unrealistic. From the definition of the optical depth:

$$\tau \equiv \int_\eta^{\eta_0} d\eta'\ n_e \sigma_{\rm T} a \ , \tag{5.46}$$

show that $\tau \propto 1/\eta^3$ when matter dominates and $\tau \propto 1/\eta$ when radiation dominates. We can be more quantitative and write:

$$-\tau' = n_e\sigma_{\rm T}a = n_{\rm b}\sigma_{\rm T}a = \frac{\rho_{\rm b}}{m_{\rm b}}\sigma_{\rm T}a \ , \tag{5.47}$$

where we have used the definition of τ and assumed to be in an epoch before recombination, so that we can approximate n_e with $n_{\rm b}$, since all the electrons are free. Introducing the baryon density parameter and using $m_{\rm b} = 1$ GeV, the mass of the proton, show that:

$$-\tau' \approx 1.46 \times 10^{-19}\frac{\Omega_{\rm b0}h^2}{a^2}\ {\rm s}^{-1} \ . \tag{5.48}$$

Now we need to compare this scattering rate with the Hubble rate, in order to check the goodness of the TC approximation. Assuming matter-domination and using the conformal

time Friedmann equation (this because τ' is derived with respect to the conformal time), we have:

$$\mathcal{H} = H_0\sqrt{\Omega_{\rm m0}}a^{-1/2} \approx 3.33\times 10^{-18}h\sqrt{\Omega_{\rm m0}}\ a^{-1/2}\ {\rm s}^{-1}\ . \tag{5.49}$$

Therefore, the ratio:

$$\frac{-\tau'}{\mathcal{H}} = 0.044\ \frac{\Omega_{\rm b0}h^2}{\sqrt{\Omega_{\rm m0}h^2}}a^{-3/2}\ , \tag{5.50}$$

diverges for $a\to 0$ as expected (though the formula should be generalised to the case of radiation-domination), so if it is sufficiently big at recombination then the TC approximation would be reliable. Substituting the *Planck* values $\Omega_{\rm b0}h^2 = 0.022$ and $\Omega_{\rm m0}h^2 = 0.12$ one gets at recombination, i.e. for $a = 10^{-3}$:

$$\frac{-\tau'}{\mathcal{H}} \approx 10^2\ . \tag{5.51}$$

This means that the scattering rate is much larger than the Hubble rate even at recombination as long as there are free electrons around and thus we are going to use the tight-coupling approximation with reliability. Let us see in detail how the TC limit works. Let us compare in the hierarchy for $\ell\geq 2$ the terms Θ'_ℓ and $k\Theta_\ell$ with $\tau'\Theta_\ell$, which have all the same dimensions of inverse time. There are two physical time scales in our problem, one is given by the expansion rate and the other by the scattering rate, hence

$$\Theta'_\ell \propto \mathcal{H}\Theta_\ell, \tau'\Theta_\ell\ , \tag{5.52}$$

from a dimensional analysis. However, the mode for which $\Theta'_\ell\propto\tau'\Theta_\ell$ implies that $\Theta_\ell\propto\exp\tau$ and hence diverges at early times, which is unacceptable for a small fluctuation. We then dismiss this mode as unphysical and take into account just that for which $\Theta'_\ell\propto\mathcal{H}\Theta_\ell$, which is small compared to $\tau'\Theta_\ell$. Now, let us inspect the ratio

$$\frac{-\tau'}{k}\ . \tag{5.53}$$

This is the number of collisions which take place on a scale $1/k$. Hence, this number is very large, provided that we consider sufficiently large scales, i.e. small k. If the scale is too small, i.e. large k, then the TC approximation does not work well and we must take into account the multipole moments for $\ell\geq 2$. We will see this when investigating the **diffusion damping** or **Silk damping** effect. From the above analysis, for sufficiently large scales we can conclude then that $\Theta_\ell\approx 0$ for $\ell\geq 2$. Sufficiently large means much larger than the mean free path $-1/\tau'$ which is approximately of the order of 10 Mpc at

recombination. This number can be computed from Eq. (5.48) and is a comoving scale; the physical one is divided by a factor a thousand and so it is 10 kpc. Finally, note that $\Theta_\ell \sim \tau'/k\Theta_{\ell-1}$. Therefore, considering smaller and smaller scales makes necessary to include higher and higher order multipoles. Eliminating all the multipoles $\ell \geq 2$, the relevant equations are just the following two:

$$\Theta_0' + k\Theta_1 = -\Phi' \,, \tag{5.54}$$

$$3\Theta_1' - k\Theta_0 = k\Psi + \tau' \left(3\Theta_1 - V_\mathrm{b}\right) \,, \tag{5.55}$$

i.e. the TC approximation allows us to treat photons as a fluid until recombination. Note the coupling to baryons via the baryon velocity V_b. Thus, we need also the equations for baryons:

$$\delta_\mathrm{b}' + kV_\mathrm{b} = -3\Phi' \,, \tag{5.56}$$

$$V_\mathrm{b}' + \mathcal{H}V_\mathrm{b} = k\Psi + \frac{\tau'}{R}(V_\mathrm{b} - 3\Theta_1) \,, \tag{5.57}$$

where we have introduced $R \equiv 3\rho_\mathrm{b}/4\rho_\gamma$, i.e. the baryon density to photon density ratio. This number can be cast as:

$$R = \frac{3\Omega_{\mathrm{b}0}}{4\Omega_{\gamma 0}} a \approx 600a \,, \tag{5.58}$$

using the usual values and it grows from zero at early times to $R_* \approx 0.6$ at recombination. So it is small, but not that negligible. Let us rewrite the velocity equation for baryons in the following way:

$$V_\mathrm{b} = 3\Theta_1 + \frac{R}{\tau'}\left(V_\mathrm{b}' + \mathcal{H}V_\mathrm{b} - k\Psi\right) \,. \tag{5.59}$$

We can solve this equation via successive approximation, exploiting the fact that $R < 1$ before recombination. That is, assume the expansion:

$$V_\mathrm{b} = V_\mathrm{b}^{(0)} + RV_\mathrm{b}^{(1)} + R^2 V_\mathrm{b}^{(2)} + \dots \,. \tag{5.60}$$

The solution for $R = 0$ simply gives $V_\mathrm{b}^{(0)} = 3\Theta_1$, which we have used in order to investigate the primordial modes. This solution is reliable well before recombination, say at $a = 10^{-7}$ for example, because $R \approx 6 \times 10^{-5}$ there, but it is not satisfactory at recombination and we shall take into account the first order in R in the above expansion.

5.3.1 The acoustic peaks for $R = 0$

Let us start with the simple case of $R = 0$, which amounts to neglect baryons. Combine the photon Eqs. (5.54)-(5.55) with the zeroth-order TC condition $V_{\rm b} = 3\Theta_1$ and find the following second-order equation for Θ_0:

$$\Theta_0'' + \frac{k^2}{3}\Theta_0 = -\frac{k^2\Psi}{3} - \Phi'' \ . \tag{5.61}$$

We have here already the first fundamental piece of physics of the CMB. This is the equation of motion of a driven harmonic oscillator where instead of the position we have the monopole of the temperature fluctuation and the driving force is given by the gravitational potential. This equation describe **acoustic oscillations** of the baryon-photon fluid until recombination. After recombination we expect to observe these fluctuations in the $C_{TT,\ell}$'s, using the free-streaming formula (5.24), and in fact we do, cf. Fig. 19. Note that these oscillations are in the baryon-photon fluid and therefore affect also baryons. We therefore expect to see oscillations in the baryon distribution after recombination, called **baryon acoustic oscillations** (BAO), and detected by Eisenstein and collaborators in 2005 [61]. The BAO are the manifestation of a special length, the sound horizon at recombination, in the correlation function of galaxies which appears as a bump, i.e. an excess probability. In the Fourier space, i.e. for the power spectrum, a given scale is represented with various oscillations. BAO and weak gravitational lensing are among the main observables on which current and future experiments (such as *Euclid* and *LSST*) are based. Combine Eqs. (5.56) and (5.57) and the TC condition $V_{\rm b} = 3\Theta_1$ and find the following equation for $\delta_{\rm b}$:

$$\delta_{\rm b}' = 3\Theta_0' \ . \tag{5.62}$$

Hence, the same oscillatory solution of Θ_0 holds true for $\delta_{\rm b}$. Now, consider the fact that close to recombination CDM is already dominating and thus the potentials are equal and constant at all scales. We get:

$$\Theta_0'' + \frac{k^2}{3}\Theta_0 = -\frac{k^2\Psi}{3} \ . \tag{5.63}$$

This equation can be put in the following form:

$$(\Theta_0 + \Psi)'' + \frac{k^2}{3}(\Theta_0 + \Psi) = 0 \ , \tag{5.64}$$

where we have used the constancy of Ψ. Note how the observed temperature fluctuation, used in Eq. (5.24), has appeared. The solution is:

$$(\Theta_0 + \Psi)(\eta, k) = A(k) \sin\left(\frac{k\eta}{\sqrt{3}}\right) + B(k) \cos\left(\frac{k\eta}{\sqrt{3}}\right) \ , \tag{5.65}$$

with the driving potential, i.e. CDM, providing just an offset for the oscillations. At recombination we have

$$(\Theta_0 + \Psi)(\eta_*, k) = A(k) \sin\left(\frac{k\eta_*}{\sqrt{3}}\right) + B(k) \cos\left(\frac{k\eta_*}{\sqrt{3}}\right) \ , \tag{5.66}$$

with peaks and valleys in the temperature fluctuations given by this combination of sine and cosine, therefore dependent on the functions $A(k)$ and $B(k)$. Inserting these formula into Eq. (5.24) in order to compute the $\Theta_\ell(\eta_0, k)$ (the anisotropies today) and to compute the $C_{TT,\ell}$'s, we are able to explain the **acoustic oscillations** feature of the CMB TT spectrum, of Fig. 19. The functions $A(k)$ and $B(k)$ are determined by the initial condition, i.e. for $k\eta_* \ll 1$:

$$(\Theta_0 + \Psi)(k\eta_* \ll 1) \sim A(k)\frac{k\eta_*}{\sqrt{3}} + B(k) \ . \tag{5.67}$$

Hence, if we choose adiabatic modes, we must put $A(k) = 0$. So, considering different initial conditions changes the position of the acoustic peaks and observation allows to test the choice made. As we saw, Planck limits the presence of isocurvature modes to a few percent. With $A(k) = 0$, i.e. for adiabatic perturbations, using the large-scale solution that we found in Eq. (5.37), we have:

$$(\Theta_0 + \Psi)(\eta_*, k) = -\frac{1}{5}\mathcal{R}(k)T(k) \cos\left(\frac{k\eta_*}{\sqrt{3}}\right) \ , \tag{5.68}$$

where $T(k)$ is the transfer function of $\Theta_0 + \Psi$. It can be shown that it is limited to a range 0.4-2, approximately. See [131]. The extrema of the effective temperature fluctuations are thus given by:

$$\frac{k\eta_*}{\sqrt{3}} = n\pi \ , \qquad (n = 1, 2, \dots) \ , \tag{5.69}$$

where the odd values provide peaks, corresponding to the highest temperature fluctuations and thus to scales at which photons are maximally compressed and hot, whereas the even values provide throats, corresponding to the lowest temperature fluctuations and thus to scales at which photons are maximally rarefied and cold. In the spectrum, cf. Fig. 19, only peaks appear because of the quadratic nature of the $C_{TT,\ell}$'s as functions of the Θ_ℓ's, but

it should be clear that the first and the third peaks are compressional. From Eqs. (5.54) and (5.68), we can determine easily the dipole contribution:

$$\Theta_1(\eta_*, k) = -\frac{\Theta_0'(\eta_*, k)}{k} = -\frac{1}{5\sqrt{3}}\mathcal{R}(k)T(k)\sin\left(\frac{k\eta_*}{\sqrt{3}}\right) , \tag{5.70}$$

where we are still continuing in keeping the potentials constant. Substituting this equation and Eq. (5.68) into Eq. (5.24) in order to compute the angular power spectrum, we get:

$$C_{TT,\ell} = \frac{4\pi}{25}\int_0^\infty \frac{dk}{k}\Delta^2_{\mathcal{R}}(k)\left[\cos\left(\frac{k\eta_*}{\sqrt{3}}\right)j_\ell(k\eta_0) + \sqrt{3}\sin\left(\frac{k\eta_*}{\sqrt{3}}\right)\frac{dj_\ell(k\eta_0)}{d(k\eta_0)}\right]^2 , \tag{5.71}$$

where the derivative of the spherical Bessel function is given in Eq. (5.20). We have put $T(k) = 1$ here for simplicity. We can manipulate analytically this integral following the technique used in [133] and [131]. In these references, baryon loading and diffusion damping are taken into account but here we just tackle a simpler case. The idea is to avoid the oscillatory nature of the Bessel function and of the trigonometric ones (which are also problematic from a numerical perspective) by approximating $j_\ell(x)$ as follows, for large ℓ:

$$j_\ell(x) \approx \begin{cases} 0 , & (x < \ell) , \\ \frac{1}{\sqrt{x}(x^2-\ell^2)^{1/4}}\cos\left[\sqrt{x^2-\ell^2} - \ell\arccos(\ell/x) - \pi/4\right] , & (x > \ell) . \end{cases} \tag{5.72}$$

This approximation is identical either for $j_\ell(x)$ and for $j_{\ell-1}(x)$, since we are assuming ℓ to be large. Hence, when we deal with the derivative of the spherical Bessel function in Eq. (5.71), we can factorise a $j^2_\ell(x)$ and we can approximate the squared cosine coming from the above approximation with its average, i.e. a factor 1/2. We thus have the following integration:

$$C_{TT,\ell} = \frac{2\pi\Delta^2_{\mathcal{R}}}{25}\int_{\ell/\eta_0}^\infty \frac{dk}{k^2\eta_0\sqrt{(k\eta_0)^2-\ell^2}}\left[\cos\left(\frac{k\eta_*}{\sqrt{3}}\right) + \sqrt{3}\left(1-\frac{\ell}{k\eta_0}\right)\sin\left(\frac{k\eta_*}{\sqrt{3}}\right)\right]^2 , \tag{5.73}$$

where we have already assumed a scale-invariant spectrum, for simplicity. Using now the variable

$$x \equiv \frac{k\eta_0}{\ell} , \tag{5.74}$$

we can write:

$$\ell^2 C_{TT,\ell} = \frac{2\pi\Delta^2_{\mathcal{R}}}{25}\int_1^\infty \frac{dx}{x^2\sqrt{x^2-1}}\left[\cos(\ell\varrho x) + \sqrt{3}\frac{x-1}{x}\sin(\ell\varrho x)\right]^2 , \tag{5.75}$$

where note the appearance of the factor ℓ^2 on the left hand side and we have defined the quantity:

$$\varrho \equiv \frac{\eta_*}{\sqrt{3}\eta_0} \, . \tag{5.76}$$

Now, developing the square and using the trigonometric formulae:

$$\cos^2\alpha = \frac{1+\cos 2\alpha}{2} \, , \qquad \sin^2\alpha = \frac{1-\cos 2\alpha}{2} \, , \qquad 2\sin\alpha\cos\alpha = \sin 2\alpha \, , \tag{5.77}$$

we can write:

$$\ell^2 C_{TT,\ell} = \frac{2\pi\Delta^2_{\mathcal{R}}(k)}{25}\int_1^\infty \frac{dx}{x^2\sqrt{x^2-1}} \left[\frac{x^2+3(x-1)^2}{2x^2} + \frac{x^2-3(x-1)^2}{2x^2}\cos\left(2\ell\varrho x\right) + \frac{\sqrt{3}(x-1)}{x}\sin\left(2\ell\varrho x\right)\right] \, . \tag{5.78}$$

Now, let us treat separately the three integrands. The first, non-oscillatory one is simplest one:

$$N \equiv \int_1^\infty \frac{dx}{x^2\sqrt{x^2-1}}\frac{x^2+3(x-1)^2}{2x^2} = 3\left(1-\frac{\pi}{4}\right) \, , \tag{5.79}$$

but also the less interesting. The oscillatory ones can be dealt with following [131]. Define:

$$O_1 \equiv \int_1^\infty \frac{dx}{\sqrt{x-1}}\frac{x^2-3(x-1)^2}{2x^4\sqrt{x+1}}\cos\left(2\ell\varrho x\right) \, , \tag{5.80}$$

then solving the problem in [131, page 383], we can use the formula:

$$\int_1^\infty \frac{dx}{\sqrt{x-1}} f(x)\cos(bx) \approx f(1)\sqrt{\frac{\pi}{b}}\cos(b+\pi/4) \, , \tag{5.81}$$

for large values of b and a slowly varying $f(x)$. A similar result holds true also for the sine function. Using this formula we have then:

$$O_1 = \frac{1}{2\sqrt{2}}\sqrt{\frac{\pi}{2\ell\varrho}}\cos(2\ell\varrho+\pi/4) \, , \tag{5.82}$$

whereas for the integral containing the sine:

$$O_2 \equiv \int_1^\infty \frac{dx}{\sqrt{x-1}}\frac{\sqrt{3}(x-1)}{x^3\sqrt{x+1}}\sin\left(2\ell\varrho x\right) \approx 0 \, , \tag{5.83}$$

since $f(1) = 0$ here. The contribution O_2 comes from the cross product between the monopole and the dipole terms and it is usually neglected in the calculations. We have explicitly shown why here. Gathering the N and O_1 contributions, we plot the sum $N + O_1$ in Fig. **??**. In order to make this plot, we have used $a \propto \eta^2$, since we are in the matter-dominated epoch, and thus we have evaluated ϱ as follows:

$$\varrho = \frac{\eta_*}{\sqrt{3}\eta_0} = \frac{1}{\sqrt{3(1+z_*)}} = \frac{1}{\sqrt{3000}} \approx 0.0183 \; . \tag{5.84}$$

The agreement between the plots of Fig. 19 is poor but at least we have understood how the acoustic oscillations free-stream until today and are seen in the CMB TT power spectrum. There are several feature missing in Fig. **??**: there are too many peaks, their relative height diminishes too slowly and the overall trend does not decay as in Fig. 19. The reason is that we have neglected baryons and diffusion damping, which we are going to tackle in the next sections.

5.3.2 Baryon loading

The oscillations in Eq. (5.64) take place with frequency $k/\sqrt{3}$, i.e. as if the speed of sound was $1/\sqrt{3}$, i.e. the speed of sound of a pure photon fluid. We have been too radical in assuming $V_\mathrm{b} = 3\Theta_1$ in the equation for baryons. In fact we saw that this assumption is equivalent to say that $R = 0$, i.e. the baryon density is negligible with respect to the photon one. That is why photons do not feel baryons at all and baryons fluctuations oscillate in the same way as photons do. We now take into account R up to first-order. If we consider $V_\mathrm{b}^{(0)} = 3\Theta_1$ substituted in Eq. (5.59) we get up to order R:

$$V_\mathrm{b} = 3\Theta_1 + \frac{R}{\tau'}\left(3\Theta_1' + 3\mathcal{H}\Theta_1 - k\Psi\right) \; . \tag{5.85}$$

Combine the above equation and Eqs. (5.54)-(5.55) in order to find the following second-order equation for Θ_0:

$$\Theta_0'' + \mathcal{H}\frac{R}{1+R}\Theta_0' + \frac{k^2}{3(1+R)}\Theta_0 = -\frac{k^2\Psi}{3} - \Phi'' - \mathcal{H}\frac{R}{1+R}\Phi' \; . \tag{5.86}$$

Now the speed of sound, i.e. the quantity multiplying k^2, has been reduced:

$$c_s^2 = \frac{1}{3(1+R)} \; . \tag{5.87}$$

The extreme of the temperature fluctuation at recombination are now expected to be slightly changed, since:

$$\frac{k\eta_*}{\sqrt{3(1+R)}} = n\pi \ , \qquad (n = 1, 2, \dots) \ , \tag{5.88}$$

is now the condition defining them. Moreover, baryons are also responsible for the damping term $\mathcal{H}R\Theta_0'/(1+R)$, hence we also expect the extrema to have less and less amplitude. These features translate, once free-streamed,[1] in a relative suppression of the second peak with respect to the first one, as seen in Fig. 19. This effect is due to the **baryon loading** and it is also called **baryon drag**. Physically, baryons are heavy and prevent the oscillations in Θ_0 to be symmetric, favouring compression over rarefaction. Since $R \propto a$, then we have that:

$$R' = \mathcal{H}R \ . \tag{5.89}$$

Let us write Eq. (5.86) in the following form:

$$\left(\frac{d^2}{d\eta^2} + \frac{R'}{1+R}\frac{d}{d\eta} + k^2 c_s^2\right)(\Theta_0 + \Phi) = \frac{k^2}{3}\left(\frac{\Phi}{1+R} - \Psi\right) \ . \tag{5.90}$$

The above equation cannot be solved analytically, but we can use a semi-analytic approximation, provided by [79]. Let us employ the WKB method and use the following ansatz:

$$(\Theta_0 + \Phi)(\eta, k) = A(\eta)e^{iB(\eta,k)} \ , \tag{5.91}$$

where $A(\eta)$ and $B(\eta, k)$ are functions to be determined via Eq. (5.90). Substituting this ansatz into the homogenous part of Eq. (5.90) and find the following couple of equations, by separately equating the real and imaginary parts to zero:

$$-A(B')^2 + A'' + \frac{R'}{1+R}A' + k^2 c_s^2 A = 0 \ , \tag{5.92}$$

$$2B'A' + AB'' + \frac{R'}{1+R}AB' = 0 \ . \tag{5.93}$$

In the first equation, let us neglect the second and the third term with respect to the first one. That is, the oscillations provide almost at any time (except at the extrema) a

[1] To "free-stream" means to calculate the $C_{TT,\ell}$'s weighting the solution at recombination with the spherical Bessel function of Eq. (5.24).

much larger derivative than that of the amplitude or R. Then, the first equation is readily solved as:

$$\boxed{B(\eta, k) = k \int_0^\eta c_s(\eta') d\eta' \equiv k r_s(\eta)} \tag{5.94}$$

where in the last step we have defined the **sound horizon**, i.e. the conformal distance travelled by a sound wave propagating in the baryon photon fluid. When evaluated at recombination, $r_s(\eta_*) = 150$ Mpc and this scale is fundamental for BAO, making them **standard rulers**. Determining now $A(\eta)$, we can see that the above equations, together with the found solution for $B(\eta, k)$, can be cast as:

$$\frac{A'}{A} = -\frac{1}{4} \frac{R'}{1+R} \ , \tag{5.95}$$

which gives:

$$A(\eta) = (1+R)^{-1/4} \ . \tag{5.96}$$

The general, approximate, solution of the homogeneous equation is then:

$$(\Theta_0 + \Phi)(\eta, k) = \frac{1}{(1+R)^{1/4}} \left[C(k) \sin(k r_s) + D(k) \cos(k r_s) \right] \tag{5.97}$$

The condition $|A'|, R' \ll |B'|$, which was employed in order to find the above solution, can be checked as follows:

$$\frac{R'}{4(1+R)^{5/4}}, R' \ll \frac{k}{\sqrt{3(1+R)}} \ , \tag{5.98}$$

which essentially amounts to say that:

$$k \gg R' \ , \tag{5.99}$$

i.e. the solution found is good on sufficiently small scales. Since $R' = \mathcal{H} R \sim R/\eta$, we must have that $k\eta \gg R$. Since R is pretty small, being at most $R_* \approx 0.6$ at recombination, this condition means any scale at early times, but sub-horizon scales at recombination. Equation (5.97) gives us the general solution of the homogeneous part of Eq. (5.90). In order to find the general solution of the full equation we need to find a particular solution of Eq. (5.90). This can be obtained via Green's functions method. Let us define, in order

to keep a more compact notation, the independent solutions of the homogeneous equation that we have just found in Eq. (5.97) as follows:

$$S_1(\eta,k) \equiv \frac{1}{(1+R)^{1/4}}\sin(kr_s)\ , \qquad S_2(\eta,k) \equiv \frac{1}{(1+R)^{1/4}}\cos(kr_s)\ . \tag{5.100}$$

Taking into account the non-homogeneous term, the general solution of Eq. (5.90) is:

$$(\Theta_0+\Phi)(\eta,k) = C(k)S_1 + D(k)S_2 + \frac{k^2}{3}\int_0^\eta d\eta'\ \left[\frac{\Phi(\eta')}{1+R} - \Psi(\eta')\right] G(\eta,\eta')\ , \tag{5.101}$$

where $G(\eta,\eta')$ is the Green's function. We can determine the Green's function as:

$$G(\eta,\eta') = \frac{S_1(\eta')S_2(\eta) - S_1(\eta)S_2(\eta')}{W(\eta')}\ , \tag{5.102}$$

using the homogeneous solution, we obtain:

$$G(\eta,\eta') = \frac{1}{\sqrt{1+R)}}\frac{\sin[kr_s(\eta') - kr_s(\eta)]}{W(\eta')}\ , \tag{5.103}$$

and

$$W(\eta') = -\frac{1}{\sqrt{3}(1+R)}\ . \tag{5.104}$$

We are omitting the k-dependence for simplicity. With the above results we can write:

$$\begin{aligned}(\Theta_0+\Phi)(\eta,k) &= C(k)S_1 + D(k)S_2 \\ +\frac{k}{\sqrt{3}}\int_0^\eta d\eta'\ &\left[\frac{\Phi(\eta')}{1+R(\eta')} - \Psi(\eta')\right]\sqrt{1+R(\eta')}\sin[kr_s(\eta) - kr_s(\eta')]\ .\end{aligned} \tag{5.105}$$

For the primordial modes, in the limit $k\eta \to 0$, one gets at the dominant order:

$$(\Theta_0+\Phi)(0,k) = D(k)\ . \tag{5.106}$$

Hence, it is the adiabatic mode which multiplies the cosine. Since sine and cosine have a $\pi/2$ phase difference, the effect of different initial conditions is to change the scales for which the effective temperature fluctuations is maximum or minimum and hence the positions of the peaks in the $C_{TT,\ell}$'s. In the adiabatic case, we have:

$$(\Theta_0+\Phi)(\eta,k)=(\Theta_0+\Phi)(0,k)\frac{\cos[kr_s(\eta)]}{(1+R)^{1/4}}$$
$$+\frac{k}{\sqrt{3}}\int_0^\eta d\eta'\,\left[\frac{\Phi(\eta')}{1+R}-\Psi(\eta')\right]\sqrt{1+R}\sin[kr_s(\eta)-kr_s(\eta')] \tag{5.107}$$

This is the semi-analytic (semi because the integral has to be performed numerically) formula of [79]. The above solution (5.107) can also be used for baryons. Indeed, combining Eq. (5.56) with Eq. (5.85) and then with Eq. (5.54) we get:

$$\delta_{\rm b}'=3\Theta_0'+\frac{3R}{\tau'}\left[\Theta_0''+\Phi''+\mathcal{H}(\Theta_0'+\Phi')+\frac{k^2\Psi}{3}\right]\,. \tag{5.108}$$

Eliminating the second derivative by means of the differential equation (5.90), we have:

$$\delta_{\rm b}'=3\Theta_0'+\frac{R}{\tau'(1+R)}\left[-k^2\Theta_0+3\mathcal{H}(\Theta_0'+\Phi')\right]\,. \tag{5.109}$$

Just to make a rough estimative, let us neglect the second contribution (which is divided by τ' anyway which is much larger than $\mathcal{H}$ and also than k, for suitable scales) and use the homogeneous part of Eq. (5.107). It is straightforward then to integrate $\delta_{\rm b}'$ and obtain at recombination:

$$\delta_{\rm b}(\eta_*,k)\propto\cos[kr_s(\eta_*)]=\cos\left[2\pi\frac{r_s(\eta_*)}{\lambda}\right]\,. \tag{5.110}$$

So the scale $r_s(\eta_*)\approx 150$ Mpc is relevant for baryons, too. Indeed, at about this scale the matter power spectrum display the BAO feature.

5.4. Diffusion damping

In order to understand what happens to the $C_{TT,\ell}$'s when ℓ grows larger and larger we need to take into account smaller and smaller scales, because of the relation $\ell\approx k\eta_0$. As discussed earlier, for larger and larger k the ratio $-\tau'/k$ becomes smaller and smaller and so the TC approximation must be relaxed. In this section then we investigate what happens to the temperature fluctuations when the quadrupole moment Θ_2 is taken into account. Since this analysis accounts for the behavior of very small scales which entered the horizon deep into the radiation-dominated epoch, we can neglect the gravitational potentials since these rapidly decay. Moreover, being deep into the radiation-dominated epoch, we can also neglect R and thus take $3\Theta_1=V_{\rm b}$. Neglecting also polarisation, we have the following set of three equations for Θ_0, Θ_1 and Θ_2:

$$\Theta_0' + k\Theta_1 = 0 \,, \tag{5.111}$$

$$3\Theta_1' + 2k\Theta_2 - k\Theta_0 = 0 \,, \tag{5.112}$$

$$10\Theta_2' - 4k\Theta_1 = 9\tau'\Theta_2 \,. \tag{5.113}$$

In the last equation we can neglect Θ_2' with respect $\tau'\Theta_2$, as we already did earlier, and then find:

$$\Theta_2 = -\frac{4k}{9\tau'}\Theta_1 \,. \tag{5.114}$$

The minus sign might ring some alarm, but recall that τ' is always negative by definition. We can combine the above condition with the remaining equations in order to find a closed equation for Θ_0:

$$\boxed{\Theta_0'' + \left(-\frac{8k^2}{27\tau'}\right)\Theta_0' + \frac{k^2}{3}\Theta_0 = 0} \tag{5.115}$$

This is the equation for an harmonic oscillator that we have already found earlier in Eq. (5.64), only that now there appears a damping term which is relevant on small scales, i.e. when $k \sim -\tau'$. Baryons also provide a damping term, cf. Eq. (5.86), but they are irrelevant in the present case since we set $R = 0$. This damping term here depends on Θ_2 and is time-dependent. Let us consider it constant and assume a solution of the type $\Theta_0 \propto \exp(i\omega\eta)$. Substituting this ansatz in the equation, we find:

$$-\omega^2 + \left(-\frac{8k^2}{27\tau'}\right) i\omega + \frac{k^2}{3} = 0 \,. \tag{5.116}$$

The frequency must have an imaginary part, which accounts for the damping, thus let us stipulate:

$$\omega = \omega_R + i\omega_I \,, \tag{5.117}$$

Substituting this ansatz in the equation and find:

$$\omega_R = \frac{k}{\sqrt{3}} \,, \qquad \omega_I = -\frac{4k^2}{27\tau'} \,. \tag{5.118}$$

Hence, we can write the general solution for Θ_0 as:

$$\Theta_0 \propto e^{ik\eta/\sqrt{3}} e^{-k^2/k_{\rm Silk}^2} \,, \tag{5.119}$$

where we have introduced the comoving diffusion length, the **Silk length**, as

$$\lambda_{\rm Silk}^2 = \frac{1}{k_{\rm Silk}^2} \equiv -\frac{4\eta}{27\tau'} \ . \tag{5.120}$$

What does the diffusion length physically represent? It is the comoving distance travelled by a photon in a time η, but taking into account the collisions which it is suffering, i.e. its diffusion. Let us see this in some more detail. Since $-\tau'$ is the scattering rate, i.e. how many collisions take place per unit conformal time, then $-1/\tau'$ is the average conformal time between 2 consecutive collisions, which for a photon is also the average comoving distance between two collision, i.e. the mean free path. Now, we have:

$$\lambda_{\rm Silk}^2 \propto -\frac{\eta}{\tau'} \propto \lambda_{\rm MFP}\eta \ , \tag{5.121}$$

where we have used the comoving mean free path, $\lambda_{\rm MFP}$. Now, multiply and divide by $\lambda_{\rm MFP}$ and take the square root:

$$\lambda_{\rm Silk} \propto \lambda_{\rm MFP}\sqrt{\frac{\eta}{\lambda_{\rm MFP}}} \ , \tag{5.122}$$

Under the square root we have the comoving distance η divided by the photon comoving mean free path. This gives us the average number of collision N which the photons experience up to the time η and hence:

$$\lambda_{\rm Silk} \propto \sqrt{N}\lambda_{\rm MFP} \ , \tag{5.123}$$

which is the typical relation for diffusion. Below this scales $\lambda_{\rm Silk}$ all fluctuations are suppressed because photons cannot agglomerate since they escape away. This effect is known as **Silk damping** [167]. Therefore, the behaviour of the C_l's for large l's, as seen in Fig. 19, is also decaying, though not exactly as in the above solution since this has to be free-streamed first. We can do a more detailed calculation of the damping scale as follows. Let us neglect the gravitational potential and the $\ell \geq 3$ multipoles as before, but let us deal with more care of baryons and take into account polarisation. From Eq. (5.59) we have:

$$V_{\rm b} = 3\Theta_1 + \frac{R}{\tau'}\left(V_{\rm b}' + \mathcal{H}V_{\rm b}\right) \ , \tag{5.124}$$

and the six equations for the monopole, dipole and quadrupole of the temperature fluctuations and polarisation:

$$\Theta_0' + k\Theta_1 = 0 \,, \tag{5.125}$$

$$3\Theta_1' + 2k\Theta_2 - k\Theta_0 = \tau'(3\Theta_1 - V_{\rm b}) \,, \tag{5.126}$$

$$10\Theta_2' - 4k\Theta_1 = 9\tau'\Theta_2 - \tau'\Theta_{P0} - \tau'\Theta_{P2} \,, \tag{5.127}$$

$$2\Theta_{P0}' + 2k\Theta_{P1} = \tau'\Theta_{P0} - \tau'\Theta_{P2} - \tau'\Theta_2 \,, \tag{5.128}$$

$$3\Theta_{P1}' + 2k\Theta_{P2} - k\Theta_{P0} = 3\tau'\Theta_{P1} \,, \tag{5.129}$$

$$10\Theta_{P2}' - 4k\Theta_{P1} = 9\tau'\Theta_{P2} - \tau'\Theta_{P0} - \tau'\Theta_2 \,. \tag{5.130}$$

Now, assuming a solution of the type $\exp(i\int \omega d\eta)$ for all the above 7 variables and also assuming that $\omega \gg \mathcal{H}$, we have:

$$V_{\rm b} = \frac{3\Theta_1}{1 + Ri\omega\eta_c} \,, \tag{5.131}$$

where we have defined $\eta_c \equiv -1/\tau'$ as the the average conformal time between 2 consecutive collisions. We have thus a closed system for Θ_0, Θ_1, Θ_2, Θ_{P0}, Θ_{P1} and Θ_{P2}:

$$i\omega\Theta_0 + k\Theta_1 = 0 \,, \tag{5.132}$$

$$-k\Theta_0 + 3i\omega\Theta_1\left(1 + \frac{R}{1 + Ri\omega\eta_c}\right) + 2k\Theta_2 = 0 \,, \tag{5.133}$$

$$-4k\eta_c\Theta_1 + (10i\omega\eta_c + 9)\Theta_2 - \Theta_{P0} - \Theta_{P2} = 0 \,, \tag{5.134}$$

$$-\Theta_2 + (2i\omega\eta_c + 1)\Theta_{P0} + 2k\eta_c\Theta_{P1} - \Theta_{P2} = 0 \,, \tag{5.135}$$

$$-k\Theta_{P0} + 3(i\omega\eta_c + 1)\Theta_{P1} + 2k\eta_c\Theta_{P2} = 0 \,, \tag{5.136}$$

$$-\Theta_2 - \Theta_{P0} - 4k\eta_c\Theta_{P1} + (10i\omega\eta_c + 9)\Theta_{P2} = 0 \,. \tag{5.137}$$

We have already arranged the variables in order for the system matrix to appear clearly. The determinant of this matrix, in order to have a non trivial solution, must be zero. Considering the limit $\omega\eta_c \ll 1$, and keeping the first-order only in $\omega\eta_c$ we get:

$$\frac{k^2}{3} - \omega^2(1 + R) + \frac{2i}{30}\omega\eta_c\left[37k^2 - 285(1 + R)\omega^2 + 15\omega^2R^2\right] = 0 \,. \tag{5.138}$$

In order to solve for ω, let us again employ the smallness of $\omega\eta_c$ and stipulate that:

$$\omega = \omega_0 + \delta\omega \,, \tag{5.139}$$

where $\delta\omega$ is a small correction. From the above equation is then straightforward to obtain:

$$\frac{k^2}{3} - \omega_0^2(1+R) = 0 \,, \tag{5.140}$$

$$-2\omega_0\delta\omega(1+R) + \frac{2i}{30}\omega_0\eta_c\left[37k^2 - 285(1+R)\omega_0^2 + 15\omega_0^2R^2\right] = 0 \,. \tag{5.141}$$

The first equation gives the result that we have already encountered:

$$\boxed{\omega_0^2 = \frac{k^2}{3(1+R)} = k^2c_s^2} \tag{5.142}$$

which, substituted in the second equation, gives us:

$$\boxed{\delta\omega = \frac{i\eta_c k^2}{6(1+R)}\left[\frac{16}{15} + \frac{R^2}{1+R}\right]} \tag{5.143}$$

This result was obtained for the first time by [86]. See also the derivation of [200]. Therefore, the evolution of the multipoles is proportional to the following factor:

$$\exp\left(i\int \omega d\eta\right) = e^{ikr_s(\eta)}e^{-k^2/k_{\rm Silk}^2} \,, \tag{5.144}$$

where

$$\boxed{\frac{1}{k_{\rm Silk}^2} \equiv -\int_0^\eta d\eta' \frac{1}{6\tau'(1+R)}\left(\frac{16}{15} + \frac{R^2}{1+R}\right)} \tag{5.145}$$

From the best fit values of the parameter of the ΛCDM model we have:

$$\boxed{d_{\rm Silk} = 0.0066 \text{ Mpc}} \tag{5.146}$$

5.5. Line-of-sight integration

The approximate solutions found earlier are based on the TC limit, which allows us to take into account just the monopole and the dipole until recombination and then to better understand the physics behind the CMB anisotropies. On the other hand, observation demands more precise calculations to be compared with and therefore, at the end, numerical computation and codes such as CLASS are needed. Even so, there is a more efficient way of computing predictions on the CMB anisotropies than dealing directly with the hierarchy of Boltzmann equation and that is to formally integrate along the photon past light-cone according to a semi-analytic technique called **line-of-sight integration**,

due to Seljak and Zaldarriaga [166], and which was the basis for the CMBFAST code.[2] Recall the photon Boltzmann equations:

$$\Theta' + ik\mu\Theta = -\Phi' - ik\mu\Psi - \tau' \left[\Theta_0 - \Theta - i\mu V_{\rm b} - \frac{1}{2}\mathcal{P}_2(\mu)\Pi\right] , \tag{5.147}$$

$$\Theta'_P + ik\mu\Theta_P = -\tau' \left[-\Theta_P + \frac{1}{2}[1 - \mathcal{P}_2(\mu)]\Pi\right] , \tag{5.148}$$

where $\Pi = \Theta_2 + \Theta_{P2} + \Theta_{P0}$. Let us rewrite them as follows:

$$\Theta' + (ik\mu - \tau')\Theta = -\Phi' - ik\mu\Psi - \tau' \left[\Theta_0 - i\mu V_{\rm b} - \frac{1}{2}\mathcal{P}_2(\mu)\Pi\right] \equiv \mathcal{S}(\eta, k, \mu) , \tag{5.149}$$

$$\Theta'_P + (ik\mu - \tau')\Theta_P = -\frac{\tau'}{2}[1 - \mathcal{P}_2(\mu)]\Pi \equiv \mathcal{S}_P(\eta, k, \mu) , \tag{5.150}$$

where we have introduced two source functions on the right hand sides. Note that the dependence in on k and not on $\mathbf{k} = k\hat{z}$ because we are considering the equations for the transfer functions. Afterwards, before performing the anti-Fourier transform, we must rotate back $\hat{k}$ in a generic direction. Let us write the left hand sides as follows:

$$\Theta' + (ik\mu - \tau')\Theta = e^{-ik\mu\eta + \tau} \frac{d}{d\eta} \left(\Theta \, e^{ik\mu\eta - \tau}\right) , \tag{5.151}$$

with a similar expression for Θ_P. Substituting these into the Boltzmann equations and integrating formally from a certain initial $\eta_i \to 0$ to today η_0, we get:

$$\Theta(\eta_0)e^{-\tau(\eta_0)} = \Theta(\eta_i)e^{ik\mu(\eta_i - \eta_0) - \tau(\eta_i)} + \int_{\eta_i}^{\eta_0} d\eta \; e^{ik\mu(\eta - \eta_0) - \tau(\eta)} \mathcal{S}(\eta, k, \mu) , \tag{5.152}$$

$$\Theta_P(\eta_0)e^{-\tau(\eta_0)} = \Theta_P(\eta_i)e^{ik\mu(\eta_i - \eta_0) - \tau(\eta_i)} + \int_{\eta_i}^{\eta_0} d\eta \; e^{ik\mu(\eta - \eta_0) - \tau(\eta)} \mathcal{S}_P(\eta, k, \mu) , \tag{5.153}$$

Now recall the definition of the optical depth:

$$\tau \equiv \int_{\eta}^{\eta_0} d\eta' \; n_e \sigma_T a \; . \tag{5.154}$$

It is clear then that $\tau(\eta_0) = 0$ and, since $\eta_i \to 0$ is deep into the radiation-dominated epoch, then $\tau \propto 1/\eta$ is very large and we can neglect $\exp[-\tau(\eta_i)]$. Therefore, we are left with

$$\Theta(\eta_0, k, \mu) = \int_0^{\eta_0} d\eta \; e^{ik\mu(\eta - \eta_0) - \tau(\eta)} \mathcal{S}(\eta, k, \mu) , \tag{5.155}$$

$$\Theta_P(\eta_0, k, \mu) = \int_0^{\eta_0} d\eta \; e^{ik\mu(\eta - \eta_0) - \tau(\eta)} \mathcal{S}_P(\eta, k, \mu) \; . \tag{5.156}$$

[2] `https://lambda.gsfc.nasa.gov/toolbox/tb_cmbfast_ov.cfm`

where we have already implemented the limit $\eta_i \to 0$. Now we calculate the Θ_ℓ's inverting the Legendre expansion and obtain:

$$\Theta_\ell(\eta_0, k) = \frac{1}{(-i)^\ell} \int_{-1}^{1} \frac{d\mu}{2}\, \mathcal{P}_\ell(\mu) \int_0^{\eta_0} d\eta\, e^{ik\mu(\eta-\eta_0)-\tau(\eta)} \mathcal{S}(k,\eta,\mu)\ , \tag{5.157}$$

$$\Theta_{P\ell}(\eta_0, k) = \frac{1}{(-i)^\ell} \int_{-1}^{1} \frac{d\mu}{2}\, \mathcal{P}_\ell(\mu) \int_0^{\eta_0} d\eta\, e^{ik\mu(\eta-\eta_0)-\tau(\eta)} \mathcal{S}_P(k,\eta,\mu)\ , \tag{5.158}$$

The source terms have μ-dependent contributions (up to μ^2) that we can handle integrating by parts. Take for example the $-ik\mu\Psi$ contribution of $\mathcal{S}(k,\eta,\mu)$. Let I_Ψ be its integral, which can be rewritten as follows:

$$I_\Psi \equiv -\int_0^{\eta_0} d\eta\, ik\mu\Psi e^{ik\mu(\eta-\eta_0)-\tau(\eta)} = -\int_0^{\eta_0} d\eta\, \Psi e^{-\tau(\eta)} \frac{d}{d\eta}\left[e^{ik\mu(\eta-\eta_0)}\right]\ , \tag{5.159}$$

and now it is easy to integrate by parts and obtain:

$$I_\Psi = -\left.\Psi e^{-\tau(\eta)} e^{ik\mu(\eta-\eta_0)}\right|_0^{\eta_0} + \int_0^{\eta_0} d\eta\, e^{ik\mu(\eta-\eta_0)} \frac{d}{d\eta}\left[\Psi e^{-\tau(\eta)}\right]\ . \tag{5.160}$$

The first contribution gives $-\Psi(\eta_0)$, i.e. the gravitational potential evaluated at present time. This is just an undetectable offset that we incorporate into the definition of $\Theta_\ell(\eta_0, k)$, as the observed anisotropy, like we did at the beginning of this Chapter when dealing with the free-streaming solution. Taking care of the term containing μ^2, in $\mathcal{P}_2(\mu)$, we can see that:

$$\int_0^{\eta_0} d\eta\, \tau'\mu^2\Pi e^{ik\mu(\eta-\eta_0)-\tau(\eta)} = -\frac{1}{k^2}\int_0^{\eta_0} d\eta\, e^{ik\mu(\eta-\eta_0)} \frac{d^2}{d\eta^2}\left[\tau'\Pi e^{-\tau(\eta)}\right]\ . \tag{5.161}$$

care Combining all the terms treated with integration by parts, we get:

$$\Theta_\ell(k,\eta_0) = \frac{1}{(-i)^\ell} \int_{-1}^{1} \frac{d\mu}{2}\, \mathcal{P}_\ell(\mu) \int_0^{\eta_0} d\eta\, e^{ik\mu(\eta-\eta_0)}$$
$$\left[-\left(\Phi' + \tau'\Theta_0 + \frac{\tau'\Pi}{4}\right) e^{-\tau} + \left(\Psi e^{-\tau} - \frac{\tau' V_{\rm b} e^{-\tau}}{k}\right)' - \frac{3}{4k^2}\left(\tau'\Pi e^{-\tau}\right)''\right]\ , \tag{5.162}$$

$$\Theta_{P\ell}(k,\eta_0) = -\frac{3}{4(-i)^\ell} \int_{-1}^{1} \frac{d\mu}{2}\, \mathcal{P}_\ell(\mu) \int_0^{\eta_0} d\eta\, e^{ik\mu(\eta-\eta_0)} \left[\tau'\Pi e^{-\tau} + \frac{1}{k^2}\left(\tau'\Pi e^{-\tau}\right)''\right]\ . \tag{5.163}$$

Using now the relation of Eq. (5.15), we can cast the above equations as:

$$\Theta_\ell(\eta_0, k) = \int_0^{\eta_0} d\eta\, S(\eta, k) j_\ell\left[k(\eta_0 - \eta)\right]\ , \tag{5.164}$$

$$\Theta_{P\ell}(\eta_0, k) = \int_0^{\eta_0} d\eta\, S_P(\eta, k) j_\ell\left[k(\eta_0 - \eta)\right]\ . \tag{5.165}$$

with

$$S(\eta,k) \equiv (\Psi' - \Phi')e^{-\tau} + g\left(\Theta_0 + \frac{\Pi}{4} + \Psi\right) + \frac{1}{k}(gV_\mathrm{b})' + \frac{3}{4k^2}\left(g\Pi\right)'' \ , \tag{5.166}$$

$$S_P(\eta,k) \equiv \frac{3}{4}g\Pi + \frac{3}{4k^2}\left(g\Pi\right)'' \ , \tag{5.167}$$

where we have introduced the **visibility function**:

$$\boxed{g(\eta) \equiv -\tau' e^{-\tau}} \tag{5.168}$$

We can see that the visibility function is normalised to unity, i.e.

$$\int_0^{\eta_0} d\eta \; g(\eta) = 1 \ . \tag{5.169}$$

The visibility function represents the Poissonian probability that a photon is last scattered at a time η. It is very peaked at a time that we define as the one of recombination, i.e. at $\eta = \eta_*$, because for $\eta > \eta_*$ it is basically zero, since $\tau' = 0$. Before recombination, in the radiation-dominated epoch, we saw that $-\tau' \propto 1/\eta^2$ and thus $\tau \propto 1/\eta$ and $g \propto \exp(-1/\eta)/\eta^2$, i.e. it goes to zero exponentially fast. In Fig. 21 we plot the numerical calculation of the visibility function performed with CLASS for the standard model. Note the peak at about $z = 1000$, which has always been our reference for the recombination redshift. Note also another peak at about $z = 10$, representing the epoch of **reionisation**. Until now we have used the peakedness of the visibility function as if it were a Dirac delta $\delta(\eta - \eta_*)$, i.e. we have made the **sudden recombination approximation**. From Fig. 21 we can appreciate that it is a good approximation (mind the logarithmic scale there). As usual, in cosmology but not only, the calculations get more and more complicated and impossible to do analytically the more precision we demand.

Inserting the source terms (5.166) and (5.167) in the expressions for $\Theta_\ell(\eta_0,k)$ and $\Theta_{P\ell}(\eta_0,k)$ in the expression of Θ_ℓ and integrating by parts, we get:

$$\begin{aligned}\Theta_\ell(k,\eta_0) = &\int_0^{\eta_0} d\eta \; g\left(\Theta_0 + \Psi + \frac{\Pi}{4}\right) j_\ell\left[k(\eta_0 - \eta)\right] \\ &- \int_0^{\eta_0} d\eta \frac{gV_\mathrm{b}}{k}\frac{d}{d\eta} j_\ell\left[k(\eta_0 - \eta)\right] + \int_0^{\eta_0} d\eta \frac{3g\Pi}{4k^2}\frac{d^2}{d\eta^2} j_\ell\left[k(\eta_0 - \eta)\right] \\ &+ \int_0^{\eta_0} d\eta \; e^{-\tau}(\Psi' - \Phi') j_\ell\left[k(\eta_0 - \eta)\right] \ , \end{aligned} \tag{5.170}$$

$$\Theta_{P\ell}(k,\eta_0) = \int_0^{\eta_0} d\eta \; \frac{3g\Pi}{4} j_\ell\left[k(\eta_0 - \eta)\right] + \int_0^{\eta_0} d\eta \frac{3g\Pi}{4k^2}\frac{d^2}{d\eta^2} j_\ell\left[k(\eta_0 - \eta)\right] \ . \tag{5.171}$$

Assuming the visibility function to be a Dirac delta $\delta(\eta - \eta_*)$, i.e. the sudden recombination mentioned earlier, and neglecting Π, we recover formula (5.24). Note that neglecting

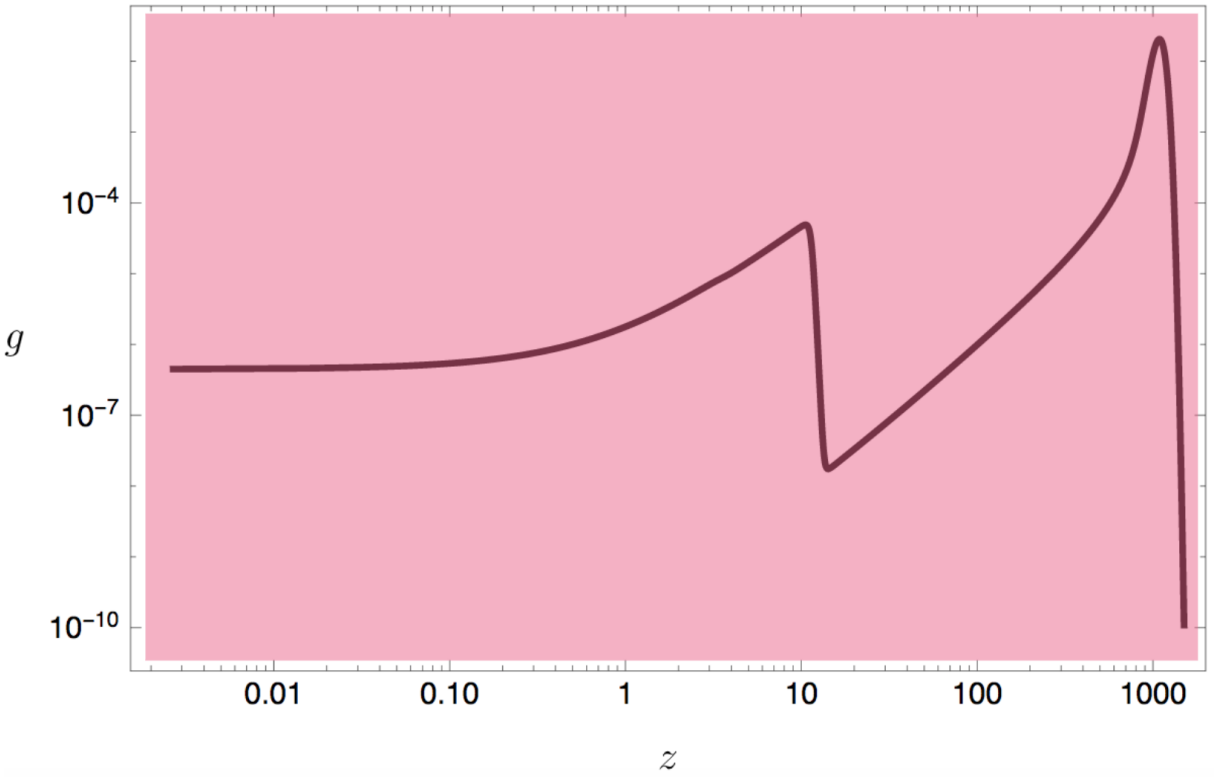

Figure 21 – Visibility function g as function of the redshift from the numerical calculation performed with CLASS for the standard model.

Π no polarisation is present. Indeed, from the above equation we see that a non-zero quadrupole moment of the photon distribution at recombination is essential in order to have polarisation. The above equations still need the Boltzmann hierarchy in order to be integrated, but just up to $\ell = 4$ (because Θ_2 and Θ_4 moments are contained in the equation for Θ_3') and hence are much more convenient from the computational point of view. The partial wave expansion of Θ given by:

$$\Theta(k, \mu) = \sum_{\ell} (-i)^{\ell} (2\ell + 1) \mathcal{P}_{\ell}(\mu) \Theta_{\ell}(k) \, , \tag{5.172}$$

and that we have used in the above calculations is valid as long as $\hat{k} = \hat{z}$. Now we have to rotate it in a general direction before performing the Fourier anti-transform. The task is simple because the temperature fluctuation is a scalar. Therefore:

$$\Theta(k, \hat{k} \cdot \hat{p}) = \sum_{\ell} (-i)^{\ell} (2\ell + 1) \mathcal{P}_{\ell}(\hat{k} \cdot \hat{p}) \Theta_{\ell}(k) \, . \tag{5.173}$$

The same is not true for Θ_P, since the Stokes parameters are not scalars. Using the

definition of $a_{T,\ell m}$, we can then write:

$$a^S_{T,\ell m} = \int d^2\hat{n}\; Y^{m*}_\ell(\hat{n}) \sum_l (-i)^\ell (2\ell+1) \int \frac{d^3\mathbf{k}}{(2\pi)^3} \mathcal{P}_\ell(\hat{k}\cdot\hat{p})\alpha(\mathbf{k})\Theta_\ell(k)\;. \tag{5.174}$$

The integration is over $d^2\hat{n}$, hence we must change $\hat{p} \to \hat{n} = -\hat{p}$ in the Legendre polynomial. This gives an extra $(-1)^\ell$ factor, due to the parity of the Legendre polynomials, and then using the addition theorem we obtain:

$$a^S_{T,\ell m} = \int d^2\hat{n}\; Y^{m*}_\ell(\hat{n}) \sum_l i^\ell (2\ell+1) \int \frac{d^3\mathbf{k}}{(2\pi)^3} \alpha(\mathbf{k}) \frac{4\pi}{2\ell'+1} \sum_{m'=-\ell'}^{\ell'} Y^{*m'}_{\ell'}(\hat{k}) Y^{m'}_{\ell'}(\hat{n})\Theta_\ell(k)\;. \tag{5.175}$$

Now the integration over the whole solid angle can be performed and the orthonormality of the spherical harmonics can be employed, obtaining thus:

$$\boxed{a^S_{T,\ell m} = 4\pi i^\ell \int \frac{d^3\mathbf{k}}{(2\pi)^3} Y^{m*}_\ell(\hat{k})\alpha(\mathbf{k})\Theta_\ell(k)} \tag{5.176}$$

This formula, together with Eq. (5.170) allows us to explicitly calculate the scalar contribution to the $a_{T,\ell m}$'s. Earlier, we have focused on the $C_{TT,\ell}$'s only, for which the calculations are simpler because there is no need of performing a spatial rotation, but we need to know the explicit form of the $a_{T,\ell m}$'s in order to compute the TE correlation spectrum.

5.6. Cosmological parameters determination

In this section we discuss how the CMB TT spectrum, i.e. the $C_{TT,\ell}$'s, are sensitive to the cosmological parameters. We have learned in this Chapter about many quantities which are of relevance in forming the shape of the spectrum but we have not actually derived an analytic, approximated formula in order to see this explicitly. These can be found in [131] and [200]. Here instead we plot with CLASS various spectra for varying parameters and discuss the physics behind the changes. Note that, for the standard Λ model, 6 of the overall parameters are usually left free and constrained by observation:

1. The amplitude of the primordial power spectrum: A_S;
2. The primordial tilt: n_S;
3. The baryonic abundance: $\Omega_{\mathrm{b}0}h^2$;

4. The CDM abundance: $\Omega_{c0}h^2$;

5. The reionization epoch: z_{reion};

6. The sound horizon at recombination: $r_s(\eta_*)$, which is related to the Hubble constant value H_0.

The other parameters can be derived by these ones. In particular, the amount of radiation is already well known by measuring the CMB temperature and so the amount of Λ and curvature is determined via the positions of the peaks, which depend on $r_s(\eta_*)$, which in turn depends on the baryon content. In Figs. 22 and 23 we start to show the numerical calculation of CMB TT power spectrum decomposed in the contributions discussed in this Chapter. See also [191]. We consider the ΛCDM as fiducial model.

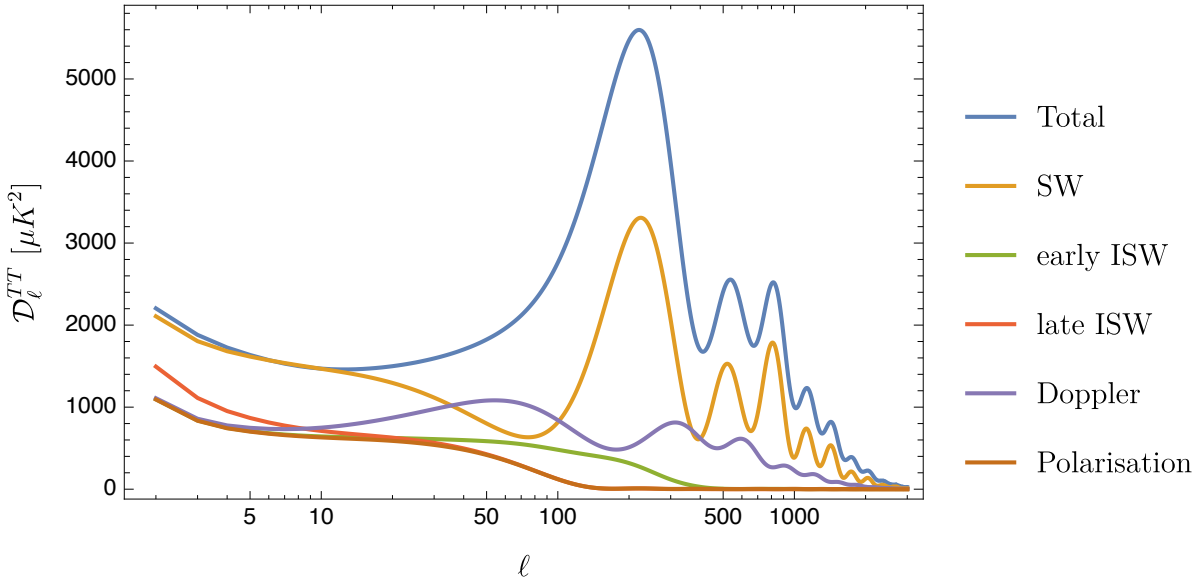

Figure 22 – Total CMB TT power spectrum (blue line) computed with CLASS and decomposed in the physically different contributions: Sachs-Wolfe effect (yellow line), early-times ISW effect (green line), late-times ISW effect (red line), Doppler effect (purple line), and polarisation (brown line).

In Fig. 24 we show what happens to CMB TT the spectrum for $\Omega_{b0}h^2$. Taking the first peak height as reference, the larger the value of $\Omega_{b0}h^2$ is, the higher the peak is. When we vary one of the density parameters, since their sum must be equal to one that means that also something else must vary. In this case we have chosen to vary Ω_Λ.

Why so? We have seen that baryons loading makes compression favoured over rarefaction and hence the first and the third peaks are higher for higher values of $\Omega_{b0}h^2$, but the second one is lower. In other words, the peaks relative height is very sensitive to the baryon content. The position of the first peak does not change much because it is most sensitive to the spatial curvature and this has been fixed to zero. Finally, the curves for

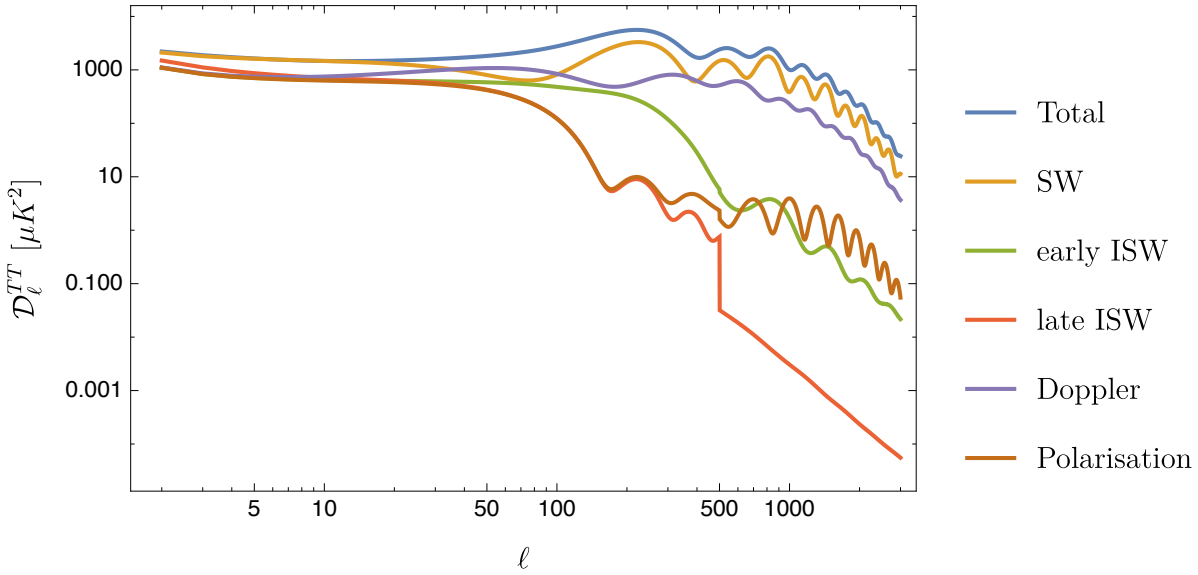

Figure 23 – Same as Fig. 22 but in logarithmic scale, in order to better distinguish the weakest contributions.

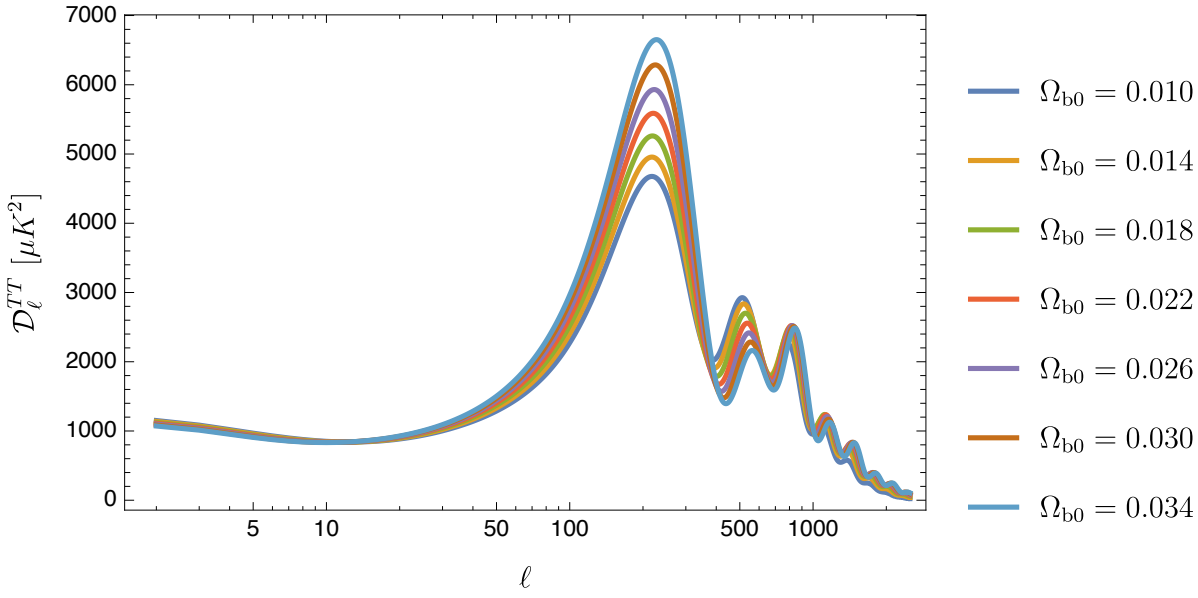

Figure 24 – CMB TT power spectrum computed with CLASS and varying $\Omega_{b0}h^2$. From the lowest first peak to the highest: $\Omega_{b0}h^2 = 0.010, 0.014, 0.018, 0.022, 0.026, 0.030, 0.034$.

larger $\Omega_{\rm b0}h^2$, as we commented, have less Ω_Λ and therefore less ISW effect. For these reason they are slightly lower for small ℓ.

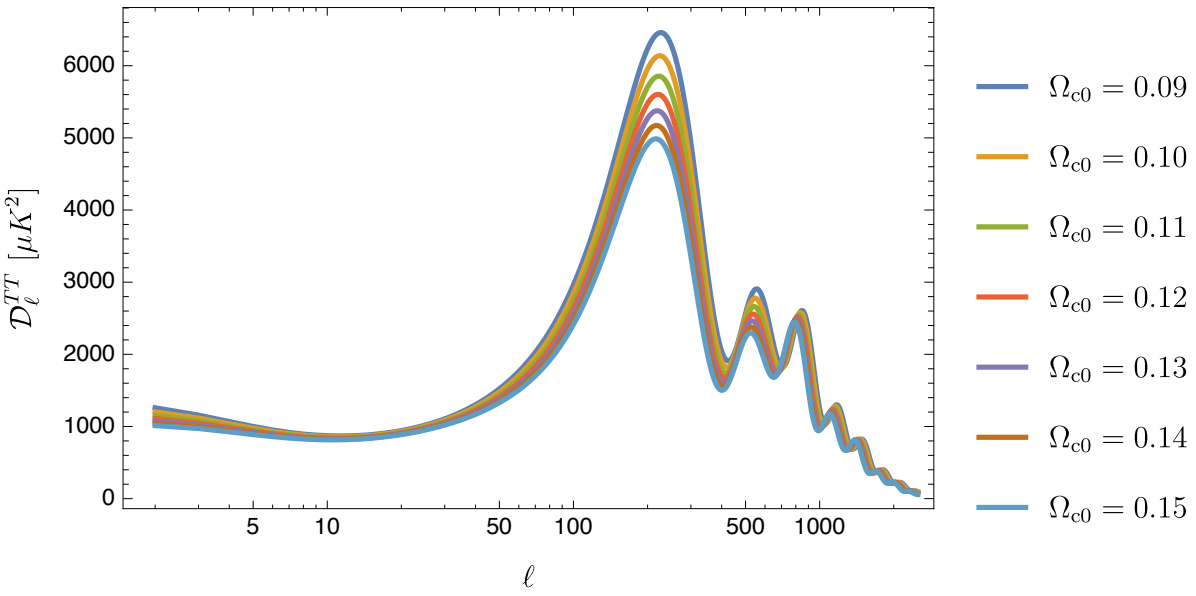

Figure 25 – CMB TT power spectrum computed with CLASS and varying $\Omega_{\rm c0}h^2$. From the highest first peak to the lowest: $\Omega_{\rm c0}h^2 = 0.09, 0.10, 0.11, 0.12, 0.13, 0.14, 0.15$.

In Fig. 25 we show what happens to CMB TT the spectrum for $\Omega_{\rm c0}h^2$. Taking the first peak height as reference, the larger the value of $\Omega_{\rm c0}h^2$ is, the lower the peak is. This behaviour is the opposite of the one that we found by varying $\Omega_{\rm b0}h^2$. Mostly CDM intervenes through the SW effect since it dominates the gravitational potential Ψ at recombination. The first peak is affected more because it corresponds to large scales, basically the horizon at recombination, and there the transfer function is approximately unit, meaning that $-\Psi$ is as large as possible. The subsequent peaks correspond to scales which entered the horizon much earlier and therefore the CDM influence there is weak. In this case also we have chosen to vary Ω_Λ in order to keep the total density budget. Indeed, the more CDM, the less Λ and the less ISW effect, as expected.

In Fig. 26 we show what happens to CMB TT the spectrum for $\tau_{\rm reion}$. As we have commented in the previous section, the overall effect of reionisation is simple because it happens very lately: a damping of the order $\exp(-2\tau_{\rm reion})$ for multipoles larger than a certain $\ell_{\rm reion}$ which we infer to be about 10 from the plots in Fig. 26.

From Fig. 27 we can appreciate how the CMB TT power spectrum is affected by the spatial geometry of the universe. From the leftmost spectrum to the rightmost one $\Omega_{\rm K0} = -0.2, -0.1, 0, 0.1, 0.2$. Hence, the position of the first peak is of great importance in order to determine whether our universe is closed or open. Note that the flat case is a limiting value which we cannot determine observationally, because of the experimental error; we can only conclude that observation is consistent with $\Omega_{\rm K0} = 0$, i.e. this value is

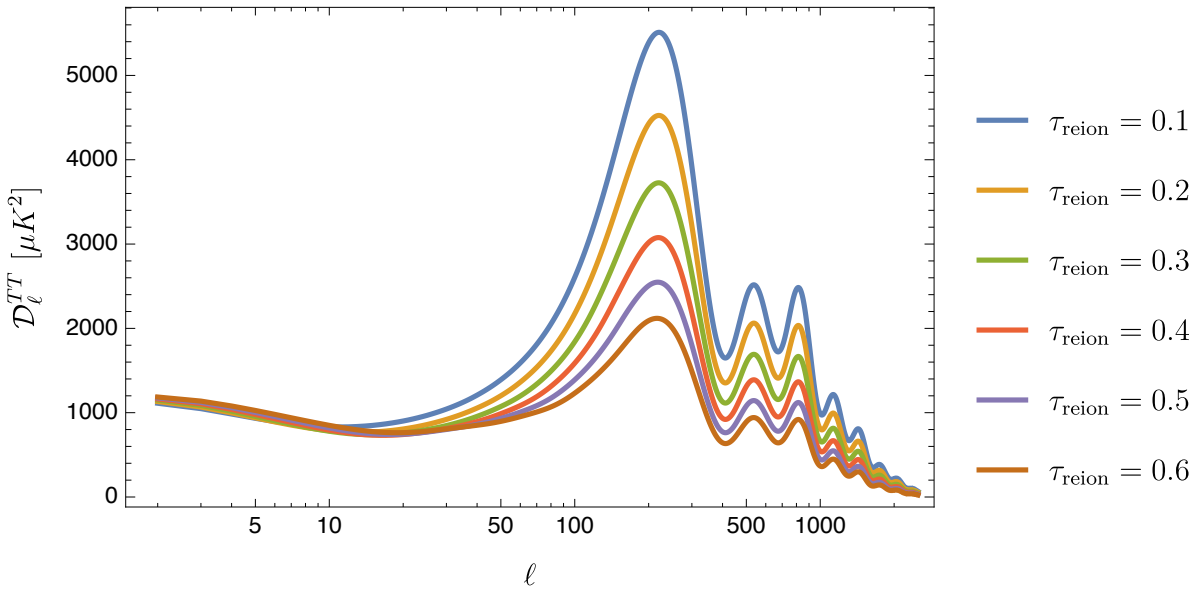

Figure 26 – CMB TT power spectrum computed with CLASS and varying $\tau_{\rm reion}$. From the highest first peak to the lowest: $\tau_{\rm reion} = 0.1, 0.2, 0.3, 0.4, 0.5, 0.6, 0.7$.

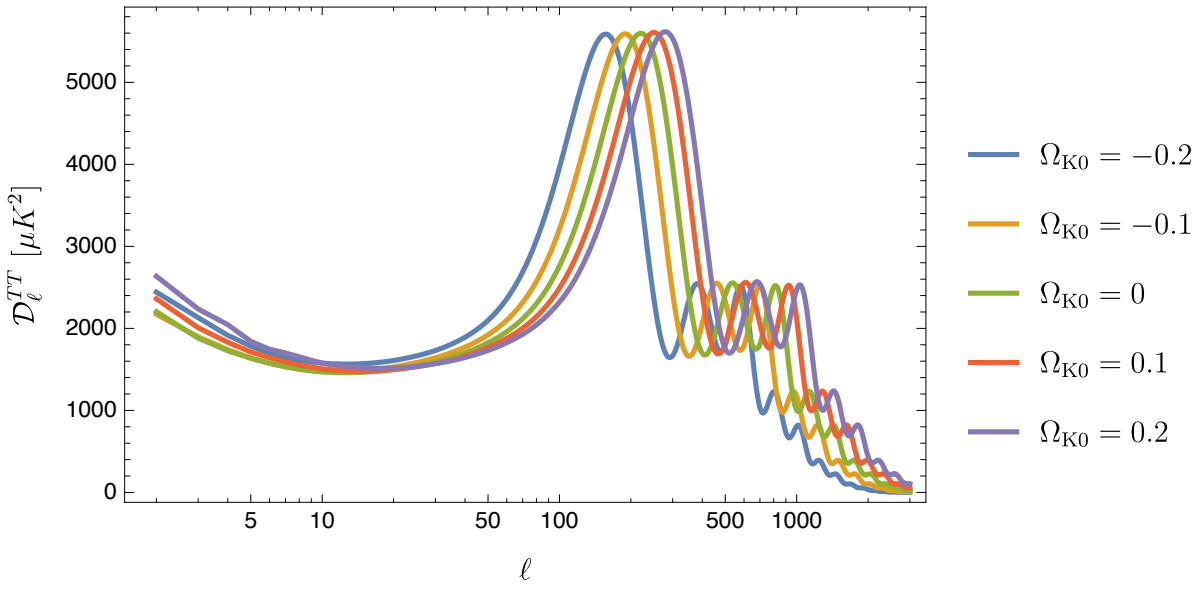

Figure 27 – CMB TT power spectrum computed with CLASS and varying $\Omega_{\rm K0}$. From the left to the right: $\Omega_{\rm K0} = -0.2, -0.1, 0, 0.1, 0.2$.

not ruled out. As we saw in Eq. (5.107), the length scale associated to the acoustic peaks is the sound horizon at recombination:

$$r_s(\eta_*) = \int_0^{\eta_*} c_s d\eta \ , \tag{5.177}$$

where the speed of sound of the baryon-photon plasma is given by Eq. (5.87):

$$c_s^2 = \frac{1}{3(1+R)} = \frac{4\Omega_{\gamma 0}}{3(4\Omega_{\gamma 0} + 3\Omega_{\rm b0} a)} \ . \tag{5.178}$$

The physical sound horizon is given by:

$$r_s^{\rm phys}(z_*) = \int_0^{t_*} c_s(t) dt = \int_{z_*}^{\infty} dz \frac{c_s(z)}{H(z)(1+z)} \ , \tag{5.179}$$

i.e. integrating the lookback time. We need the physical quantity in order to relate it with the angular-diameter distance to recombination:

$$d_{\rm A}(z_*) = \frac{1}{(1+z_*)} \int_0^{z_*} \frac{dz}{H(z)} \ , \tag{5.180}$$

and thus estimate the multipole corresponding to the first peak:

$$\ell_{\rm 1st} \approx \frac{1}{\theta_{\rm 1st}} = \frac{d_{\rm A}(z_*)}{r_s^{\rm phys}(z_*)} \ . \tag{5.181}$$

Let us approximate the physical sound horizon by assuming c_s constant and a matter-dominated universe. We have thus:

$$r_s^{\rm phys}(z_*) \approx \frac{c_s}{H_0\sqrt{\Omega_{\rm m0}}} \int_{z_*}^{\infty} \frac{dz}{(1+z)^{5/2}} = \frac{2c_s}{3H_0\sqrt{\Omega_{\rm m0}}} \frac{1}{(1+z_*)^{3/2}} \ , \tag{5.182}$$

and for the angular-diameter distance we also assume a matter plus Λ universe:

$$d_{\rm A}(z_*) = \frac{1}{H_0(1+z_*)} \int_0^{z_*} \frac{dz}{\sqrt{\Omega_{\rm m0}(1+z)^3 + (1-\Omega_{\rm m0})}} \ . \tag{5.183}$$

We can see that $d_{\rm A}(z_*)$ can be approximated as:

$$d_{\rm A}(z_*) \approx \frac{2}{7H_0(1+z_*)\sqrt{\Omega_{\rm m0}}} (9 - 2\Omega_{\rm m0}^3) \ . \tag{5.184}$$

Hence, we have:

$$\ell_{\rm 1st} \approx 0.74\sqrt{1+z_*}(9 - 2\Omega_{\rm m0}^3) \approx 220 \ , \tag{5.185}$$

which clearly shows how the position of the first peak changes as function of the total matter content.

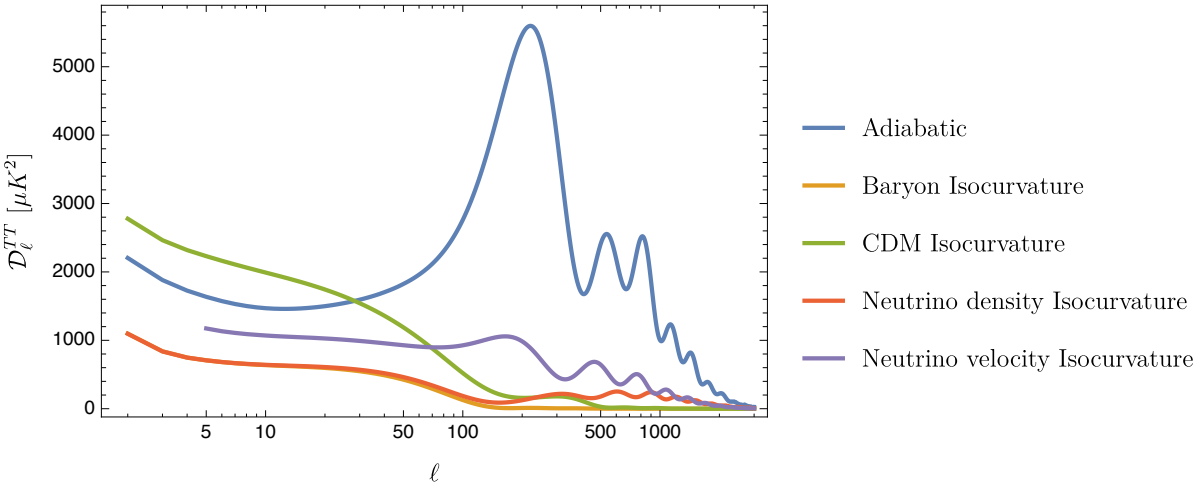

Figure 28 – CMB TT power spectrum computed with CLASS and varying initial conditions: adiabatic (blue line), baryon isocurvature (yellow line), CDM isocurvature (green line), neutrino density isocurvature (red line), neutrino velocity isocurvature (purple line).

In fig. 28 we show how the initial conditions dramatically affect the CMB TT power spectrum and how the adiabatic ones are favoured by observation (when comparing with the data points of Fig. 19).

5.7. Tensor contribution to the CMB TT correlation

Tensor perturbations also contribute to generate temperature anisotropies, which we report here after renormalising to the primordial mode $\beta(\mathbf{k}, \lambda)$,

$$\left(\frac{\partial}{\partial\eta} + ik\mu - \tau'\right)\Theta^{(T)}(\eta,k,\mu) + \frac{h'^T}{2} = -\tau'\left[\frac{3}{70}\Theta_4^{(T)} + \frac{1}{7}\Theta_2^{(T)} + \frac{1}{10}\Theta_0^{(T)} - \frac{3}{70}\Theta_{P4}^{(T)} + \frac{6}{7}\Theta_{P2}^{(T)} - \frac{3}{5}\Theta_{P0}^{(T)}\right] \equiv -\tau'\mathcal{S}^T(\eta,k)\ , \tag{5.186}$$

$$\left(\frac{\partial}{\partial\eta} + ik\mu - \tau'\right)\Theta_P^{(T)}(\eta,k,\mu) = \tau'\mathcal{S}^T(\eta,k)\ , \tag{5.187}$$

The label λ representing the two possible states of helicity is absent because of the renormalisation with $\beta(\mathbf{k}, \lambda)$. It represents the fact that the evolution of the two helicities is the same. The line-of-sight solutions of the above equations are the following:

$$\Theta^{(T)}(\eta_0,k,\mu)=\int_0^{\eta_0}d\eta\; e^{ik\mu(\eta-\eta_0)-\tau}\left[-h'^T/2-\tau'\mathcal{S}^T(\eta,k)\right]\;, \tag{5.188}$$

$$\Theta_P^{(T)}(\eta_0,k,\mu)=\int_0^{\eta_0}d\eta\; e^{ik\mu(\eta-\eta_0)-\tau}\tau'\mathcal{S}^T(\eta,k)\;. \tag{5.189}$$

We now focus on $\Theta^{(T)}(\eta_0,k,\mu)$. Defining:

$$S^T(\eta,k)\equiv e^{-\tau}\left[-h'^T/2-\tau'\mathcal{S}^T(\eta,k)\right]\;, \tag{5.190}$$

the tensor contribution to the temperature fluctuation is made up of the sum of the following two contributions:

$$f_\lambda(k\hat{z},\hat{p})\equiv 4\sqrt{\frac{\pi}{15}}Y_2^\lambda(\hat{p})\int_0^{\eta_0}d\eta\; S^T(\eta,k)e^{-i\mu kr(\eta)}\;, \tag{5.191}$$

where $r(\eta)\equiv\eta_0-\eta$ and where we stress that the result holds true for $\hat{k}=\hat{z}$ since this was the condition under which we derived the Boltzmann equation for photons. We cannot yet sum over λ because we have to include $\beta(\mathbf{k},\lambda)$ first. For this reason, we shall work on $f_\lambda(k\hat{z},\hat{p})$. In order to investigate temperature fluctuations in the sky, we need to anti-transform $\Theta^{(T)}(\mathbf{k},\hat{p})$ in order to employ the usual expansion:

$$\Theta^{(T)}(\hat{n})=\sum_{\ell m}a^T_{T,\ell m}Y^m_\ell(\hat{n})\;,\quad a^T_{T,\ell m}=\int d^2\hat{n}\; Y^{m*}_\ell(\hat{n})\Theta^{(T)}(\hat{n})\;. \tag{5.192}$$

So, let us proceed as follows. We trade $\hat{p}$ for the line-of-sight $\hat{n}=-\hat{p}$ and use the expansion of a plane wave in spherical harmonics:

$$e^{i\hat{k}\cdot\hat{n}kr}=\sum_{LM}i^L Y_L^{M*}(\hat{k})Y_L^M(\hat{n})j_L(kr)\;, \tag{5.193}$$

in Eq. (5.191). since $\hat{k}=\hat{z}$ then, we can see that:

$$Y_L^{M*}(\hat{k})=Y_L^{M*}(\hat{z})=\delta_{M0}\sqrt{\frac{2L+1}{4\pi}}\;, \tag{5.194}$$

i.e. for $\theta=0$ (representing the $\hat{z}$ direction) the spherical harmonics are non-vanishing only if $M=0$.

Therefore, we can write:

$$f_\lambda(k\hat{z},\hat{n})=\frac{2}{\sqrt{15}}Y_2^\lambda(\hat{n})\sum_L i^L\sqrt{2L+1}Y_L^0(\hat{n})\int_0^{\eta_0}d\eta\; S^T(\eta,k)j_L(kr)\;. \tag{5.195}$$

The idea is now to perform a rotation in order to put $\hat{k}$ in a generic direction. But then also $\hat{n}$ rotates and therefore we need to know how a spherical harmonics behaves under

rotations. In order to deal with just one spherical harmonic we take advantage of the following decomposition:

$$Y_2^{\pm 2}(\hat{n})Y_L^0(\hat{n}) = \sqrt{\frac{5(2L+1)}{4\pi}} \sum_{L'} \sqrt{2L'+1} \left(\begin{array}{ccc} L & 2 & L' \\ 0 & \pm 2 & \mp 2 \end{array} \right) \left(\begin{array}{ccc} L & 2 & L' \\ 0 & 0 & 0 \end{array} \right) Y_{L'}^{\pm 2}(\hat{n}) \; , \tag{5.196}$$

where we have employed the **Wigner 3j-symbols**, which are coefficients appearing in the quantum theory of angular momentum, when we combine two angular momenta and we want to write the state of total angular momentum as a linear combination on the basis of the tensor product of the two combined angular momenta. They are an alternative to the (perhaps more commonly used) Clebsch-Gordan coefficient See e.g. [96] and [202]. This expansion allows us to deal with just one spherical harmonics. Now we take advantage of the properties of the spherical harmonics under spatial rotation, i.e.

$$\boxed{Y_\ell^m(R\hat{n}) = \sum_{m'=-\ell}^{\ell} D^{(\ell)}_{m'm}(R^{-1}) Y_\ell^{m'}(\hat{n})} \tag{5.197}$$

where the $D^{(\ell)}_{m'm}$ are the elements of the **Wigner D-matrix**. See [96] for more detail. The above R is a generic rotation. Of course, we are interested in a $R(\hat{k})$ rotation which brings $\hat{k}$ in a generic direction. Hence, we can write:

$$f_\lambda(\mathbf{k}, \hat{n}) = \sum_L i^L \frac{2L+1}{\sqrt{3\pi}} \sum_{L'} \sqrt{2L'+1} \left(\begin{array}{ccc} L & 2 & L' \\ 0 & \lambda & -\lambda \end{array} \right) \left(\begin{array}{ccc} L & 2 & L' \\ 0 & 0 & 0 \end{array} \right) \sum_{m'} D^{(L')}_{m'\lambda}[R(\hat{k})] Y_{L'}^{m'}(\hat{n}) \int_0^{\eta_0} d\eta \; S^T(\eta, k) j_L(kr) \; . \tag{5.198}$$

Here we have dubbed $R\hat{n}$ the original line of sight and $\hat{n}$ the resulting one after the rotation. Now we can perform the Fourier anti-transform. Let us multiply $f_\lambda(\mathbf{k}, \hat{n})$ by $\beta(\mathbf{k}, \lambda)$ and $Y_\ell^{m*}(\hat{n})$ and integrate over $d^2\hat{n}$ in order to obtain the $a^T_{T,\ell m}$'s. We obtain:

$$a^T_{\ell m,\pm 2} = \sum_L i^L \frac{2L+1}{\sqrt{3\pi}} \sqrt{2\ell+1} \left(\begin{array}{ccc} L & 2 & \ell \\ 0 & \pm 2 & \mp 2 \end{array} \right) \left(\begin{array}{ccc} L & 2 & \ell \\ 0 & 0 & 0 \end{array} \right) \int \frac{d^3\mathbf{k}}{(2\pi)^3} D^{(\ell)}_{m\pm 2}[R(\hat{k})] \beta(\mathbf{k}, \pm 2) \int_0^{\eta_0} d\eta \; S^T(\eta, k) j_L(kr) \; . \tag{5.199}$$

We have used here the orthonormality relation of the spherical harmonics and distinguished the contributions from different helicities. Of course $a_{\ell m} = a_{\ell m,+2} + a_{\ell m,-2}$. It is now time

to compute the $3j$ symbols and to perform the summation over L. A general formula for those was obtained in [152], but we can read their expression from [96]. We then have the only following non-vanishing occurrences:

$$\begin{pmatrix} \ell & 2 & \ell \\ 0 & 0 & 0 \end{pmatrix} = (-1)^{\ell+1}\sqrt{\frac{\ell(\ell+1)}{(2\ell-1)(2\ell+1)(2\ell+3)}}\,, \tag{5.200}$$

$$\begin{pmatrix} \ell+2 & 2 & \ell \\ 0 & 0 & 0 \end{pmatrix} = (-1)^{\ell}\sqrt{\frac{3(\ell+1)(\ell+2)}{2(2\ell+1)(2\ell+3)(2\ell+5)}}\,, \tag{5.201}$$

$$\begin{pmatrix} \ell-2 & 2 & \ell \\ 0 & 0 & 0 \end{pmatrix} = (-1)^{\ell}\sqrt{\frac{3\ell(\ell-1)}{2(2\ell-3)(2\ell-1)(2\ell+1)}}\,. \tag{5.202}$$

In particular, there is no contribution coming from $L = \ell \pm 1$. The other three relevant (i.e. not considering those for $L = \ell \pm 1$ which are non-vanishing in this case) symbols are:

$$\begin{pmatrix} \ell & 2 & \ell \\ 0 & \pm 2 & \mp 2 \end{pmatrix} = (-1)^{\ell}\sqrt{\frac{3(\ell-1)(\ell+2)}{2(2\ell-1)(2\ell+1)(2\ell+3)}}\,, \tag{5.203}$$

$$\begin{pmatrix} \ell+2 & 2 & \ell \\ 0 & \pm 2 & \mp 2 \end{pmatrix} = (-1)^{\ell}\frac{1}{2}\sqrt{\frac{(\ell-1)\ell}{(2\ell+1)(2\ell+3)(2\ell+5)}}\,, \tag{5.204}$$

$$\begin{pmatrix} \ell-2 & 2 & \ell \\ 0 & \pm 2 & \mp 2 \end{pmatrix} = (-1)^{\ell}\frac{1}{2}\sqrt{\frac{(\ell+1)(\ell+2)}{(2\ell-3)(2\ell-1)(2\ell+1)}}\,, \tag{5.205}$$

We can derive the above expressions for the relevant Wigner $3j$ symbols given in [96] and put them in Eq. (5.199), such that:

$$a^T_{T,\ell m,\pm 2} = -i^{\ell}\sqrt{\frac{(2\ell+1)(\ell+2)!}{8\pi(\ell-2)!}}\int \frac{d^3\mathbf{k}}{(2\pi)^3} D^{(\ell)}_{m\pm 2}[R(\hat{k})]\beta(\mathbf{k},\pm 2)\int_0^{\eta_0} d\eta\; S^T(\eta,k) \left[\frac{j_{\ell-2}(kr)}{(2\ell-1)(2\ell+1)} + \frac{2j_{\ell}(kr)}{(2\ell-1)(2\ell+3)} + \frac{j_{\ell+2}(kr)}{(2\ell+1)(2\ell+3)}\right]\,. \tag{5.206}$$

Recall that $r = r(\eta) \equiv \eta_0 - \eta$. We can see that, using the recurrence relation [11]:

$$\frac{j_\ell(x)}{x} = \frac{j_{\ell-1}(x) + j_{\ell+1}(x)}{2\ell+1}\,, \tag{5.207}$$

we can write:

$$a^T_{T,\ell m} = -i^{\ell}\sqrt{\frac{(2\ell+1)(\ell+2)!}{8\pi(\ell-2)!}}\sum_{\lambda=\pm 2}\int \frac{d^3\mathbf{k}}{(2\pi)^3} D^{(\ell)}_{m,\lambda}[R(\hat{k})]\beta(\mathbf{k},\lambda) \int_0^{\eta_0} d\eta\; S^T(\eta,k)\frac{j_\ell(kr)}{(kr)^2}\,. \tag{5.208}$$

The Wigner D-matrix can be related to the spin-weighted spherical harmonics as follows:

$$D^{(\ell)}_{m,\pm 2}(\hat{k}) = \sqrt{\frac{4\pi}{2\ell+1}}\,{}_{\pm 2}Y^{-m}_{\ell}(\hat{k}) = \sqrt{\frac{4\pi}{2\ell+1}}\,{}_{\mp 2}Y^{m*}_{\ell}(\hat{k})\ , \tag{5.209}$$

so we have:

$$a^{T}_{T,\ell m} = -i^{\ell}\sqrt{\frac{(\ell+2)!}{2(\ell-2)!}}\sum_{\lambda=\pm 2}\int\frac{d^3\mathbf{k}}{(2\pi)^3}{}_{\lambda}Y^{m*}_{\ell}(\hat{k})\beta(\mathbf{k},\lambda)\int_0^{\eta_0}d\eta\ S^{T}(\eta,k)\frac{j_\ell(kr)}{(kr)^2} \tag{5.210}$$

This is our main result of this section. It is not surprising that $Y^{m*}_{\ell}(\hat{k})$ eventually appeared, being GW a spin-2 field. In order to compute the tensor contribution to the $C_{TT,\ell}$'s, we perform the ensemble average:

$$\langle a^{T}_{T,\ell m}a^{T*}_{T,\ell' m'}\rangle = C^{T}_{TT,\ell}\delta_{\ell\ell'}\delta_{mm'}\ . \tag{5.211}$$

Assuming Gaussian perturbations and the orthogonality property of the Wigner D-matrices or the spin-weighted spherical harmonics:

$$\int d^2\hat{k}\ D^{(\ell)}_{m,\pm 2}[R(\hat{k})]D^{(\ell')*}_{m',\pm 2}[R(\hat{k})] = \frac{4\pi}{2\ell+1}\delta_{\ell\ell'}\delta_{mm'}\ , \tag{5.212}$$

We can see that:

$$C^{T}_{TT,\ell} = \frac{(\ell+2)!}{4\pi(\ell-2)!}\int_0^{\infty}\frac{dk}{k}\Delta^2_h(k)\left|\int_0^{\eta_0}d\eta\ S^{T}(\eta,k)\frac{j_\ell(kr)}{(kr)^2}\right|^2 \tag{5.213}$$

Note that a factor 2 arises because of the two polarisation states. The above result was originally obtained in [9] (though not exactly in the same way and final form). The main difficulty we faced in computing the $a^{T}_{T,\ell m}$ was the spatial rotation which brought $\hat{k}$ in a generic direction. This can be avoided if we calculate straightaway $C^{T}_{TT,\ell}$ because it is rotationally invariant. Note that no correlation exists between scalar and tensor modes. In fact if we compute:

$$\langle a^{T}_{T,\ell m}a^{S*}_{T,\ell' m'}\rangle\ , \tag{5.214}$$

we would get zero, mathematically because of the integral:

$$\int d^2\hat{k}\ {}_2Y^{m}_{\ell}(\hat{k})Y^{m'}_{\ell'}(\hat{k}) = 0\ , \tag{5.215}$$

between a spin-2 spherical harmonic and a spin-0 one. Physically, because we know that at the linear order scalar and tensor perturbations do not couple. We can again approximate

this angular power spectrum for large values of ℓ as follows. First, $S^T(\eta, k)$ contains the derivative of h, which is maximum when a mode enters the horizon, for $k\eta \approx 1$, being almost zero elsewhere. Therefore, assuming instantaneous recombination, we can write:

$$C^T_{TT,\ell} = \frac{(\ell-1)\ell(\ell+1)(\ell+2)}{4\pi}\int_0^\infty \frac{dk}{k}\Delta^2_h(k)\frac{j^2_\ell(k\eta_0)}{(k\eta_0)^4}\ . \tag{5.216}$$

Defining the new variable $x \equiv k\eta_0$ and introducing the primordial tensor power spectrum we get:

$$C^T_{TT,\ell} \propto \frac{(\ell-1)\ell(\ell+1)(\ell+2)}{4\pi}\int_0^\infty dx\ x^{n_T-5}j^2_\ell(x)\ . \tag{5.217}$$

The integral can be performed exactly:

$$\int_0^\infty dx\ x^{n_T-5} = \frac{\sqrt{\pi}}{2}\frac{\Gamma[1-(n_T-4)/2]\Gamma[(n_T-4)/2+\ell]}{(4-n_T)\Gamma[1/2-(n_T-4)/2]\Gamma[\ell+2-(n_T-4)/2]}\ , \tag{5.218}$$

but in the case of $n_T = 0$, a scale-invariant primordial tensor spectrum, we get:

$$\frac{\ell(\ell+1)C^T_{TT,\ell}}{2\pi} \propto \frac{\ell(\ell+1)}{(\ell-2)(\ell+3)}\ . \tag{5.219}$$

The behaviour of the tensor contribution to the TT power spectrum is thus very different from the one coming from scalar perturbations. In Fig. 29 we display the numerical calculations done with CLASS of the total (solid line), scalar (dashed line) and tensor (dotted line) angular power spectra. The tensor contribution is practically irrelevant on very small angular scale (i.e. large ℓ) and on large angular scales they can be as large as 10% of the total. Typically then one can give upper limits on $C^T_{TT,\ell}/C^S_{TT,\ell}$ for small multipoles ($\ell = 2$ or $\ell = 10$) and this ratio is proportional to A_T/A_S and therefore on the parameter r, the tensor-to-scalar ratio, such that $r < 0.1$. In order to determine this constraint one has also to use polarisation data since with these we are able to disentangle the $A_S \exp(-2\tau_{\rm reion})$ dependence coming from the scalar contribution only to the temperature power spectrum.

5.8. Polarisation

In this section we address CMB polarisation. Recall that before recombination polarisation is also erased because of tight-coupling. Polarisation is generated thanks to the fact that recombination does not take place instantaneously, so the finite-thickness effect is indeed important. Moreover, since Thomson scattering is axially-symmetric, circular polarisation is not produced.

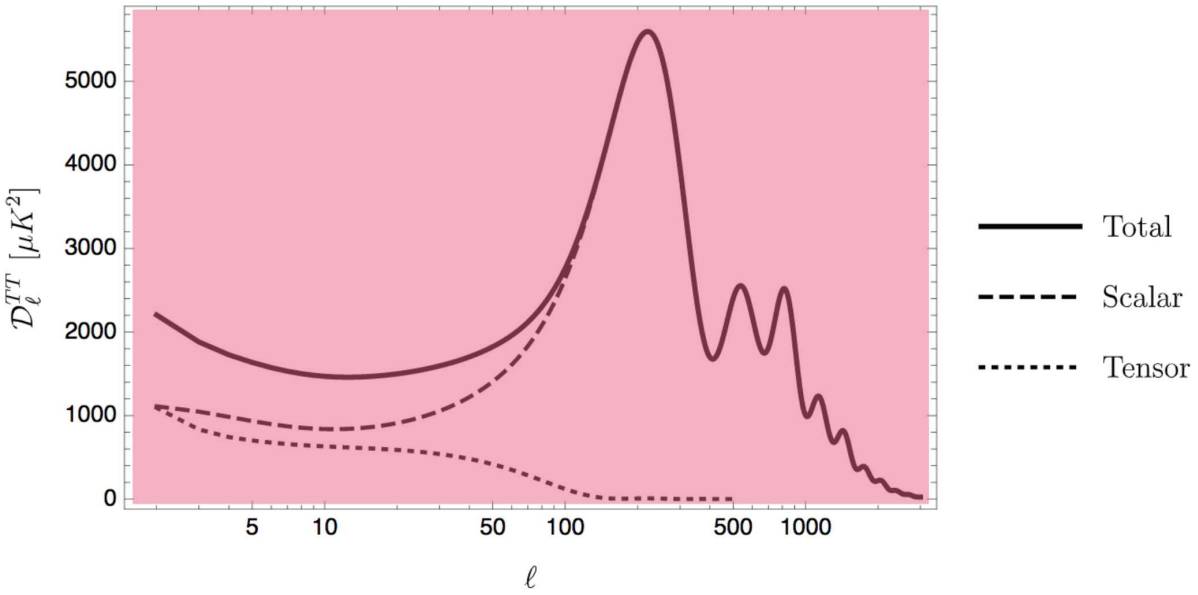

Figure 29 – Numerical calculations done with CLASS of the total (solid line), scalar (dashed line) and tensor (dotted line) angular power spectra

5.8.1 Scalar perturbations contribution to polarisation

Now, let us focus on scalar perturbations only and write down the line of sight solution for the combination $Q + iU$. Since we have chosen a reference frame in which $\hat{k} = \hat{z}$, there is no U polarisation. This can be also seen from the fact that $\mathcal{B}^0 = 0$. Hence, we shall again perform a rotation in order to compute the $a_{P,\ell m}$. We have called Θ_P the Stokes parameter Q in the $\hat{k} = \hat{z}$ frame. So, let us work on its line-of-sight solution, such that:

$$\Theta_P(k\hat{z}, \hat{n}) = \frac{3}{2}\sqrt{\frac{8\pi}{15}}{}_2Y_2^0(\hat{n}) \int_0^{\eta_0} d\eta \, e^{-i\mu kr} S_P^S(\eta, k) \, , \tag{5.220}$$

where we have defined a new source term:

$$S_P^S(\eta, k) \equiv g(\eta)\Pi(\eta, k) \, . \tag{5.221}$$

We could have written ${}_{-2}Y_2^0(\hat{n})$ instead of ${}_2Y_2^0(\hat{n})$, since they are equal. However, we are going to deal with $Q + iU$ first. The above equation can written as:

$$\Theta_P(k\hat{z}, \hat{n}) = \sqrt{\frac{9}{30}}{}_2Y_2^0(\hat{p}) \sum_L i^L \sqrt{2L+1} Y_L^0(\hat{n}) \int_0^{\eta_0} d\eta \, S_P^S(\eta, k) j_L(kr) \, , \tag{5.222}$$

where again $r \equiv \eta_0 - \eta$ and we have used the well-known-by-now expansion of a plane wave into spherical harmonics plus the fact that $\hat{k} = \hat{z}$. Now, as in Eq. (5.196) we can write the product of spherical harmonics as follows:

$$
{}_2Y^0_2(\hat{n})Y^0_L(\hat{n}) = \sqrt{\frac{5(2L+1)}{4\pi}}\sum_{L'}\sqrt{2L'+1}
\left(\begin{array}{ccc} L & 2 & L' \\ 0 & -2 & +2 \end{array}\right)\left(\begin{array}{ccc} L & 2 & L' \\ 0 & 0 & 0 \end{array}\right){}_2Y^0_{L'}(\hat{n}) \, , \tag{5.223}
$$

and thus obtain:

$$
(Q+iU)^S(\hat{n}) = \sqrt{\frac{3}{8\pi}}\sum_L i^L(2L+1)\sum_{L'}\sqrt{2L'+1}\left(\begin{array}{ccc} L & 2 & L' \\ 0 & -2 & 2 \end{array}\right)
\left(\begin{array}{ccc} L & 2 & L' \\ 0 & 0 & 0 \end{array}\right)\sum_{m'}{}_2Y^{m'}_{L'}(\hat{n})\int\frac{d^3\mathbf{k}}{(2\pi)^3}D^{(L')}_{m'0}(\hat{k})\alpha(\mathbf{k})\int_0^{\eta_0}d\eta\; S^S_P(\eta,k)j_L(kr) \, , \tag{5.224}
$$

where we have already considered the rotation which brings $\hat{k}$ in a generic direction. Now, from the expansion:

$$
(Q+iU)^S(\hat{n}) = \sum_{\ell m} a^S_{P,\ell m}\;{}_2Y^m_\ell(\hat{n}) \, , \tag{5.225}
$$

we are able to calculate the coefficients $a^S_{P,\ell m}$ by taking advantage of the orthonormality of the spin-2 spherical harmonics. We can therefore write:

$$
a^S_{P,\ell m} = \sqrt{\frac{3}{8\pi}}\sum_L i^L(2L+1)\sqrt{2\ell+1}\left(\begin{array}{ccc} L & 2 & \ell \\ 0 & -2 & 2 \end{array}\right)
\left(\begin{array}{ccc} L & 2 & \ell \\ 0 & 0 & 0 \end{array}\right)\int\frac{d^3\mathbf{k}}{(2\pi)^3}D^{(\ell)}_{m0}(\hat{k})\alpha(\mathbf{k})\int_0^{\eta_0}d\eta\; S^S_P(\eta,k)j_L(kr) \, . \tag{5.226}
$$

Remarkably, the sum over L can be performed in the very same way we did for the $a^T_{T,\ell m}$, since the $3j$ symbols are the same. Therefore, we have:

$$
a^S_{P,\ell m} = -\frac{3i^\ell}{8}\sqrt{\frac{(2\ell+1)(\ell+2)!}{\pi(\ell-2)!}}\int\frac{d^3\mathbf{k}}{(2\pi)^3}D^{(\ell)}_{m0}(\hat{k})\alpha(\mathbf{k})
\int_0^{\eta_0}d\eta\; S^S_P(\eta,k)\frac{j_\ell(kr)}{(kr)^2} \, , \tag{5.227}
$$

and using

$$
D^{(\ell)}_{m0}(\hat{k}) = \sqrt{\frac{4\pi}{2\ell+1}}Y^{-m}_\ell(\hat{k}) = \sqrt{\frac{4\pi}{2\ell+1}}Y^{m*}_\ell(\hat{k}) \, , \tag{5.228}
$$

we can write:

$$a^S_{P,\ell m} = -\frac{3i^\ell}{4}\sqrt{\frac{(\ell+2)!}{(\ell-2)!}}\int \frac{d^3\mathbf{k}}{(2\pi)^3} Y_\ell^{m*}(\hat{k})\alpha(\mathbf{k})\int_0^{\eta_0} d\eta\; S^S_P(\eta,k)\frac{j_\ell(kr)}{(kr)^2} \tag{5.229}$$

The expansion for $(Q-iU)^S(\hat{n})$ can be obtained by complex conjugation, i.e.

$$\begin{aligned}(Q-iU)(\hat{n}) = \sum_{\ell m} a^*_{P,\ell m}\; {}_2Y_\ell^{m*}(\hat{n}) &= \sum_{\ell m} a^*_{P,\ell m}\; {}_{-2}Y_\ell^{-m}(\hat{n}) \\ &= \sum_{\ell m} a^*_{P,\ell,-m}\; {}_{-2}Y_\ell^{m}(\hat{n})\;.\end{aligned} \tag{5.230}$$

There is no reality condition here holding true for the $a_{P,\ell m}$ as the one holding true for the $a_{T,\ell m}$, because $Q+iU$ is not real and is not a scalar. It is thus convenient to define the following combinations:

$$a_{E,\ell m} \equiv -(a_{P,\ell m} + a^*_{P,\ell,-m})/2\;, \quad a_{B,\ell m} \equiv i(a_{P,\ell m} - a^*_{P,\ell,-m})/2\;, \tag{5.231}$$

because the first has parity $(-1)^\ell$ whereas the second $(-1)^{\ell+1}$. Thus $Q \pm iU$ can be expanded as:

$$(Q \pm iU)(\hat{n}) = \sum_{\ell m}(-a_{E,\ell m} \mp i a_{B,\ell m})\; {}_2Y_\ell^m(\hat{n})\;. \tag{5.232}$$

Now, if we compute $a^{S*}_{P,\ell m}$, we obtain:

$$\begin{aligned}a^{S*}_{P,\ell m} = -\frac{3(-i)^\ell}{4}\sqrt{\frac{(\ell+2)!}{(\ell-2)!}}\int \frac{d^3\mathbf{k}}{(2\pi)^3} Y_\ell^{-m*}(\hat{k})\alpha(-\mathbf{k}) \\ \int_0^{\eta_0} d\eta\; S^S_P(\eta,k)\frac{j_\ell(kr)}{(kr)^2}\;,\end{aligned} \tag{5.233}$$

since $\alpha(\mathbf{k})^* = \alpha(-\mathbf{k})$ because of the reality condition of the power spectrum. Changing the integration variable to $\mathbf{k}$ and using the parity of the spherical harmonic:

$$Y_\ell^{-m*}(-\hat{k}) = (-1)^\ell Y_\ell^{-m*}(\hat{k})\;, \tag{5.234}$$

we can finally conclude that:

$$a^S_{P,\ell m} = a^{S*}_{P,\ell,-m}\;, \tag{5.235}$$

and therefore scalar perturbations only affect the E-mode, i.e.

$$a^S_{E,\ell m} = -a^S_{P,\ell m} \ , \qquad a^S_{B,\ell m} = 0 \ . \tag{5.236}$$

This means that, if the B-mode was detected, it would be a clear indication of the existence of primordial gravitational waves. From Eq. (5.229) we can then obtain the scalar contribution to the EE spectrum. Assuming adiabatic Gaussian perturbations:

$$C^S_{EE,\ell} = \frac{9}{64\pi}\frac{(\ell+2)!}{(\ell-2)!}\int \frac{dk}{k}\Delta^2_{\mathcal{R}}\left|\int_0^{\eta_0} d\eta \ S^S_P(\eta,k)\frac{j_\ell(kr)}{(kr)^2}\right|^2 \tag{5.237}$$

Using instead Eq. (5.176) we can compute the cross-correlation TE multipole coefficients:

$$C^S_{TE,\ell} = -\frac{3}{4}\sqrt{\frac{(\ell+2)!}{(\ell-2)!}}\int \frac{dk}{k}\Delta^2_{\mathcal{R}}\Theta_\ell(k)\int_0^{\eta_0} d\eta \ S^S_P(\eta,k)\frac{j_\ell(kr)}{(kr)^2} \tag{5.238}$$

Chapter 6

$C\nu B$ *and LSS*

On peut braver les lois humaines, mais non résister aux lois naturelles
(One can challenge human laws, but not the natural ones)

—Jules Verne, Vingt mille lieues sous le mers

In this Chapter I solve exactly some of the equations that we found in Appendix **??**, using some approximations. In particular, we can distinguish 4 cases of evolution:

1. On super-horizon scales,
2. In the matter-dominated epoch,
3. In the radiation-dominated epoch,
4. Deep inside the horizon,

for which it is possible to perform analytic calculations and thus gain a clearer physical insight. My scope is to understand the shape of the matter power spectrum, plotted in Fig. 30 from the analysis of the SDSS DR5 (Data Release 5) performed in [143]. Since we already know the form of the primordial power spectrum, the above task amounts to determine the matter, CDM plus baryons, transfer function. It must be noted that the data points in Fig. 30 are derived from the observation of the distribution of galaxies in the sky and hence provide information on the galaxy density contrast δ_g, which is in general a **biased tracer** of the underlying distribution of matter in the sense that the galaxy correlation function is not equal to the total matter correlation function [87]. At low redshift this bias is usually considered as a constant

$$\delta_g = b\delta_{\rm m} \ , \tag{6.1}$$

with $\delta_{\rm m}$ being the matter density contrast (baryonic plus CDM), but for larger redshift it might be a function of redshift and of the wavenumber, i.e. $b = b(k, z)$. Beyond the cosmic variance affecting in a relevant way any large-scale observation, the determination of the power spectrum is also afflicted by another noise, which is called *shot noise* and is due to the fact that δ_g is given by a discrete distribution (that of galaxies) tracing a continuous one (that of the underlying matter). Finally, spectra such as that in Fig. 30 are 3-d, in the sense that they are computed from the spatial distribution of galaxies. While determining the angular positions on the celestial sphere is not complicated, the only direct measure of distance that we have is the redshift. It is possible, of course, to transform the redshift into an actual distance (a proper distance, for example) through the cosmological model that we want to test, but determining redshift is time-consuming, especially if it is done via spectroscopy, and introduces extra errors due to peculiar motions and to photometry (if z is determined photometrically). Hence, it is perhaps more convenient to work with a 2-d power spectrum, the angular one $w(\theta)$, since angular positions on the celestial sphere are easily, precisely and rapidly determined.

6.1. Evolution on super-horizon scales

A given comoving wavenumber k is super-horizon at a certain conformal time η, if

$$k\eta \ll 1 \tag{6.2}$$

Since usually $\mathcal{H} \propto 1/\eta$, the above condition amounts to:

$$k \ll \mathcal{H} \tag{6.3}$$

which can be rewritten for the physical scale as follows:

$$\frac{k}{a} \ll H \tag{6.4}$$

The super-horizon regime is the same as that used in [113] and [38], where primordial modes are investigated. The main difference with what we are going to see here is that we do not limit ourselves to the radiation-dominated epoch, but investigate what happens through radiation-matter equality and also through matter-DE equality. Thus, the above conditions can be written as follows in the epochs of interest:

$$k \ll \mathcal{H} = \frac{1}{\eta} \quad \Rightarrow \quad k\eta \ll 1 \ , \tag{6.5}$$

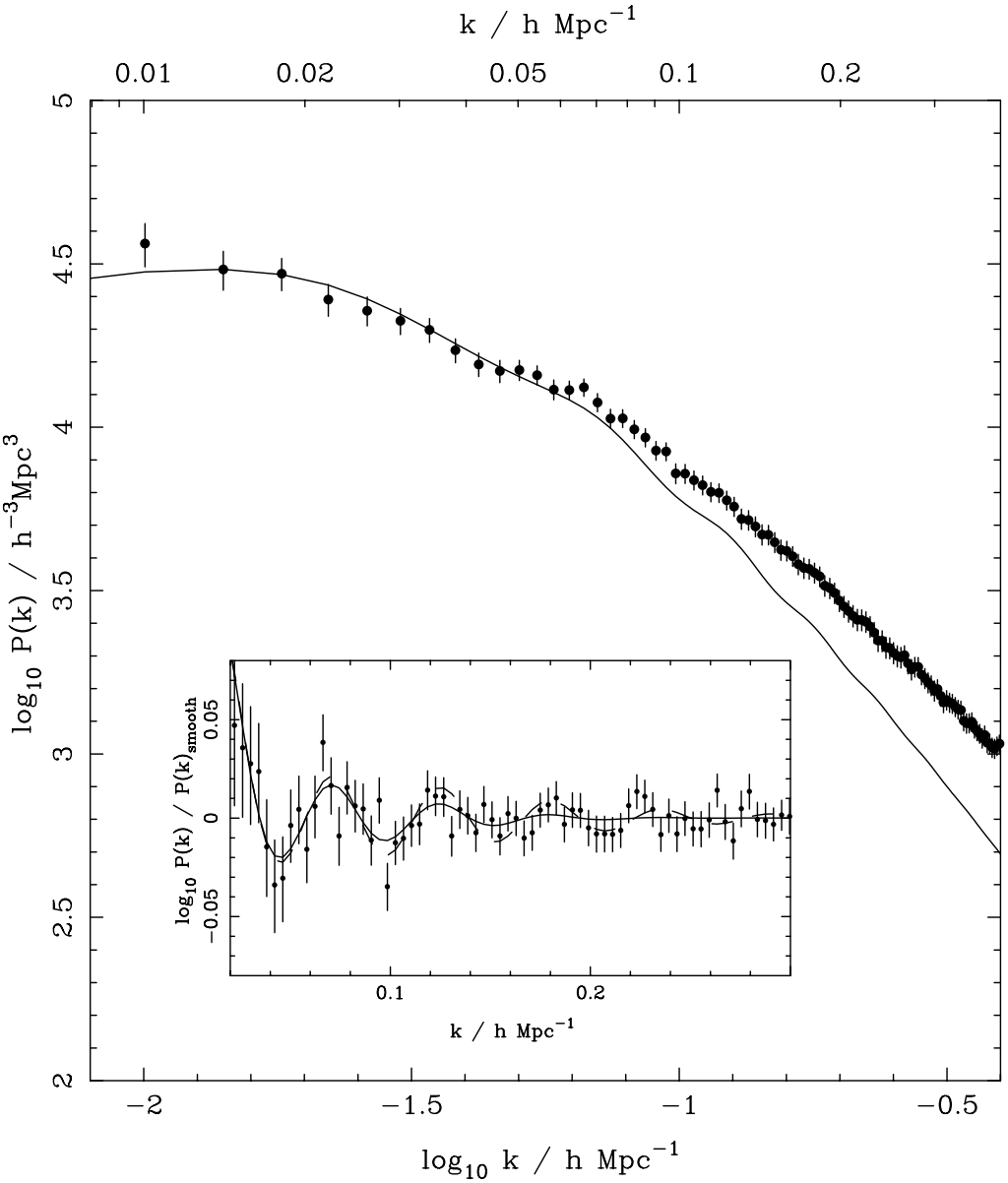

Figure 30 – Matter power spectrum, from [143].

during the radiation-dominated epoch (for which $a \propto \eta$),

$$k \ll \mathcal{H} = \frac{2}{\eta} \quad \Rightarrow \quad k\eta \ll 2 \,, \tag{6.6}$$

during the matter-dominated epoch (for which $a \propto \eta^2$) and

$$k \ll \mathcal{H} = \frac{H_\Lambda}{1 + H_\Lambda(\eta_0 - \eta)} \,, \tag{6.7}$$

for the Λ-dominated era. This is similar to the inflationary phase, but with $\eta > 0$, hence the above expression for the conformal Hubble factor is:

$$\delta'_\gamma = -4\Phi' \,, \quad \delta'_\nu = -4\Phi' \,, \quad \delta'_{\rm c} = -3\Phi' \,, \quad \delta'_{\rm b} = -3\Phi' \,, \tag{6.8}$$

the Poisson equation, It is as follows:

$$\frac{3}{\mathcal{H}}\left(\Phi' - \mathcal{H}\Psi\right) + \frac{k^2}{\mathcal{H}^2}\Phi = \frac{3}{2\rho_{\rm tot}}\left(\rho_{\rm c}\delta_{\rm c} + \rho_{\rm b}\delta_{\rm b} + \rho_\gamma\delta_\gamma + \rho_\nu\delta_\nu\right) \,, \tag{6.9}$$

where we put in evidence the $k^2/\mathcal{H}^2$ factor that we are going to neglect, and the anisotropic stress equation:

$$k^2(\Phi + \Psi) = -32\pi G a^2 \rho_\nu \mathcal{N}_2 \,. \tag{6.10}$$

Note that we have neglected the photon quadrupole contribution. It is an approximation motivated by the fact that before recombination the tight coupling with electrons washes out Θ_2, whereas after radiation-matter equality R_γ becomes rapidly ($\propto 1/a \propto 1/\eta^2$) negligible. When matter dominates, also R_ν is negligible, so we expect the potentials to become equal. Since our objective here is to perform an analytic calculation, we assume already $\Phi = -\Psi$. This is incorrect, strictly speaking, when considering the radiation-matter domination transition but it is fine when considering the matter-DE one. Therefore, let us rewrite Eq. (6.9) as follows:

$$3\mathcal{H}\left(\Phi' + \mathcal{H}\Phi\right) = \frac{3\mathcal{H}^2}{2\rho_{\rm tot}}\left(\rho_{\rm c}\delta_{\rm c} + \rho_{\rm b}\delta_{\rm b} + \rho_\gamma\delta_\gamma + \rho_\nu\delta_\nu\right) \,. \tag{6.11}$$

This equation holds true also in presence of DE, provided that the latter does not cluster (e.g. it is Λ).

6.1.1 Evolution through radiation-matter equality

In presence of radiation and matter only, Friedmann equation can be written as follows:

$$\mathcal{H}^2 = \frac{8\pi G a^2}{3}(\rho_{\rm m} + \rho_{\rm r}) = \frac{8\pi G}{3}\rho_{\rm m}\left(1 + \frac{1}{y}\right) \,, \tag{6.12}$$

where we have grouped together the species which evolve in the same way and indicated them with a subscript r, i.e. radiation (photons and neutrinos) and with a subscript m, i.e. matter (CDM and baryons). We have also employed the definition:

$$y \equiv \frac{\rho_{\rm m}}{\rho_{\rm r}} = \frac{a}{a_{\rm eq}} \, , \tag{6.13}$$

where $a_{\rm eq}$ is the equality scale factor. Assuming adiabaticity, i.e.

$$\delta_{\rm c} = \delta_{\rm b} = \frac{3}{4}\delta_\gamma = \frac{3}{4}\delta_\nu \equiv \delta_{\rm m} \, . \tag{6.14}$$

Rewriting Eq. (6.11) and using y as independent variable, we can see that:

$$y\frac{d\Phi}{dy} + \Phi = \frac{4+3y}{6(y+1)}\delta_{\rm m} \, . \tag{6.15}$$

We are looking now for a closed equation for Φ. Therefore, differentiate Eq. (6.15) with respect to y and use $\delta'_{\rm m} = -3\Phi'$ in order to find:

$$\frac{d^2\Phi}{dy^2} + \frac{(7y+8)(3y+4)+2y}{2y(y+1)(3y+4)}\frac{d\Phi}{dy} + \frac{1}{y(y+1)(3y+4)}\Phi = 0 \tag{6.16}$$

Quite unexpectedly, the above equation (6.16) can be solve exactly. Indeed, using the following transformation [91]:

$$u \equiv \frac{y^3\Phi}{\sqrt{1+y}} \, , \tag{6.17}$$

we can see that

$$\frac{d^2u}{dy^2} + \left[-\frac{2}{y} + \frac{3}{2(y+1)} - \frac{3}{3y+4}\right]\frac{du}{dy} = 0 \, . \tag{6.18}$$

Integrate once Eq. (6.18) and therefore:

$$\ln\frac{du}{dy} = C_1 + 2\ln y - \frac{3}{2}\ln(y+1) + \ln(3y+4) \, , \tag{6.19}$$

where C_1 is an integration constant. By exponentiating and integrating again show that:

$$\frac{y^3\Phi}{\sqrt{1+y}} = A\int_0^y dy\frac{y^2(3y+4)}{(1+y)^{3/2}} \, , \tag{6.20}$$

where A is an integration constant related to C_1 and assume that $y^3\Phi \to 0$ for $y \to 0$. Solving the above integration:

$$\Phi(y) = \frac{\Phi_{\rm P}}{10y^3}\left(16\sqrt{1+y} + 9y^3 + 2y^2 - 8y - 16\right) \ , \tag{6.21}$$

where $\Phi_{\rm P}$ is the primordial gravitational potential. From the above solution we see that for $y \to \infty$ (which here means deep into the matter-dominated epoch) the gravitational potential drops of 10%, i.e.

$$\Phi \to \frac{9}{10}\Phi_{\rm P} \ , \qquad \text{for } y \to \infty \ . \tag{6.22}$$

In Fig. 31 we display the evolution of $\Phi/\Phi_{\rm P}$ as function of y, as given by Eq. (6.22).

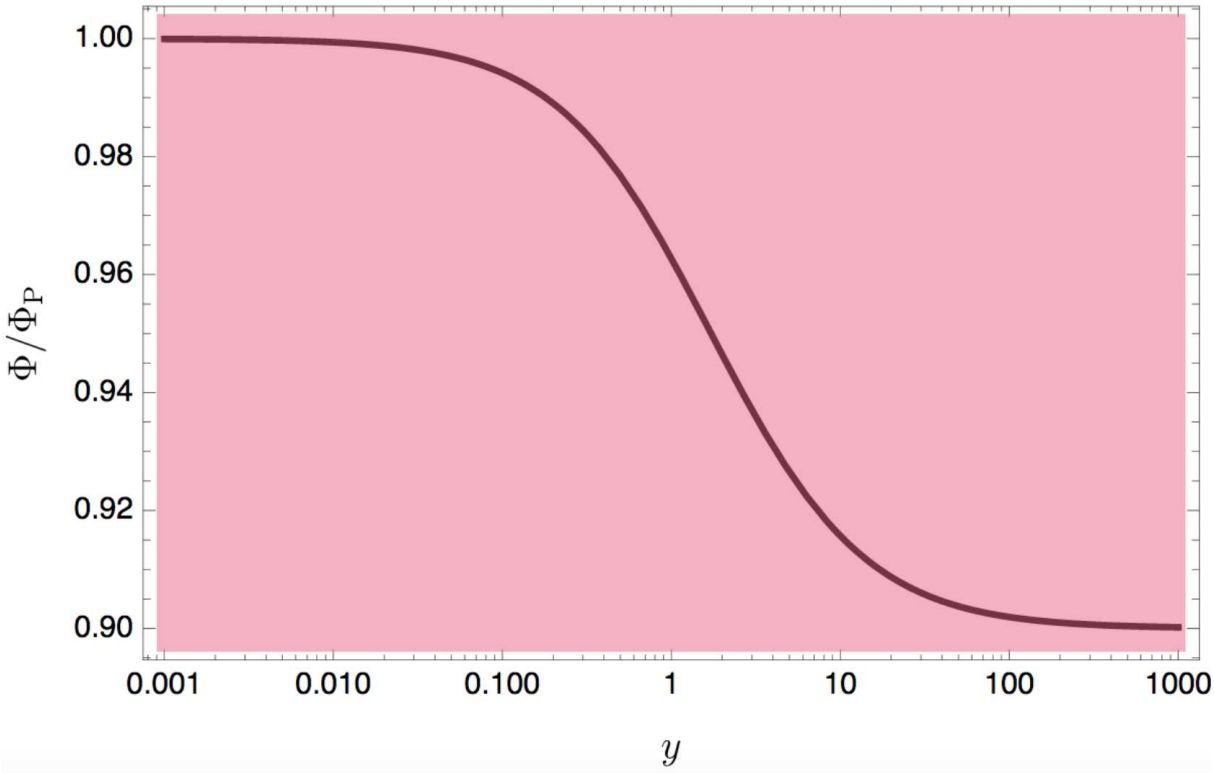

Figure 31 – Evolution of the gravitational potential Φ on super-horizon scales ($k = 0$) through radiation-matter equality. From Eq. (6.22).

It can be shown that Φ is constant on super-horizon scales for any background evolution with $w \neq -1$ constant and for adiabatic perturbations [134]. Setting $\Phi = -\Psi$, we can see that:

$$\Phi'' + 3\mathcal{H}\left(1 + c_{\rm ad}^2\right)\Phi' + \left[2\mathcal{H}' + \mathcal{H}^2\left(1 + 3c_{\rm ad}^2\right)\right]\Phi + k^2 c_{\rm ad}^2\Phi = -4\pi G a^2 \Gamma \ . \tag{6.23}$$

where we have defined $c_{\rm ad}^2 \equiv P'/\rho'$ as the **adiabatic speed of sound**. We can see that this equation can be cast as follows:

$$u'' + \left(k^2 c_{\rm a}^2 - \frac{\theta''}{\theta}\right) u = -a^2(\rho + P)^{-1/2}\Gamma \tag{6.24}$$

where

$$u \equiv \frac{\Phi}{4\pi G(\rho + P)^{1/2}} , \qquad \theta \equiv \frac{1}{a}\left(\frac{\rho}{\rho + P}\right)^{1/2} . \tag{6.25}$$

It is clear that the above transformation cannot treat the cosmological constant, for which $P = -\rho$. For $k = 0$ and $\Gamma = 0$ (adiabatic perturbations) its general solution is:

$$u = C_1\theta + C_2\theta \int \frac{d\eta}{\theta^2} . \tag{6.26}$$

Consider a single fluid model $P = w\rho$, with w constant and different from -1. Show, from solving the Friedmann equation, that:

$$a = (\eta/\eta_0)^{2/(1+3w)} , \tag{6.27}$$

where $w \neq -1/3$ (in this case the solution grows exponentially with the conformal time). Therefore:

$$\theta \int \frac{d\eta}{\theta^2} \propto \frac{a}{\mathcal{H}} , \tag{6.28}$$

and thus we can see that Φ is constant. Hence the 9/10 drop of Φ between the radiation-dominated era and the matter-dominated one can be extended to any kind of adiabatic fluid with $w \neq -1$ constant, using the constancy of $\mathcal{R}$ on large scales. See e.g. [131]. Indeed, we have

$$\mathcal{R} = \Phi + \mathcal{H}\frac{\Phi' - \mathcal{H}\Psi}{4\pi G a^2(\rho + P)} = \Phi + \frac{2}{3}\frac{\mathcal{H}^{-1}\Phi' + \Phi}{1 + w} . \tag{6.29}$$

Now, assume that w changes from a constant value w_i to another constant value w_f. For each of the two cases Φ is a constant, Φ_i and Φ_f, respectively. Then, taking advantage of the constancy of $\mathcal{R}$, we can say that:

$$\Phi_i + \frac{2}{3}\frac{\Phi_i}{1 + w_i} = \Phi_f + \frac{2}{3}\frac{\Phi_f}{1 + w_f} , \tag{6.30}$$

i.e

$$\Phi_f = \Phi_i \frac{5+3w_i}{5+3w_f}\frac{1+w_f}{1+w_i} \ , \tag{6.31}$$

with which we can easily check the result of Eq. (6.22).

6.1.2 Evolution in the Λ-dominated epoch

As already mentioned, we cannot use the above formulae for the case of greatest interest, which is for $w = -1$, i.e. the cosmological constant. In this case, we have to start directly from Eq. (6.23). Since $P = -\rho$ and constant, then $P' = 0$ and thus $c_{\rm ad} = 0$. Using Eq. (6.7) into Eq. (6.23) with $c_{\rm ad} = 0$ and $\Gamma = 0$, we can see that:

$$\Phi'' + \frac{3H_\Lambda}{1+H_\Lambda(\eta_0-\eta)}\Phi' + \frac{3H_\Lambda^2}{[1+H_\Lambda(\eta_0-\eta)]^2}\Phi = 0 \ . \tag{6.32}$$

Note that η does not go to infinity, but to a maximum value $\eta_\infty = \eta_0 - 1/H_\Lambda$ for which the scale factor diverges. Moreover, note that this equation, and its solution, are valid also for small scales because for $c_{\rm ad} = 0$ the k-dependence is suppressed. We can find the relation between the cosmic time t and the conformal time using Eq. (6.7) and show that $\eta_\infty = \eta_0 - 1/H_\Lambda$ corresponds to an infinite t. Change variable to the scale factor in Eq. (6.32), and show that:

$$\frac{d^2\Phi}{da^2} + \frac{5}{a}\frac{d\Phi}{da} + \frac{3}{a^2}\Phi = 0 \ . \tag{6.33}$$

Solve this equation, using a power-law ansatz, and show that:

$$\Phi = C_1 a^{-1} + C_2 a^{-3} \ . \tag{6.34}$$

Hence, when Λ dominates, Φ is not constant on super-horizon scales but vanishes rapidly, as $\Phi \propto 1/a$ or $\Phi \propto 1 + H_\Lambda(\eta_0 - \eta)$.

6.1.3 Evolution through matter-DE equality

In order to study the transition between the matter-dominated epoch and the DE-dominated one, we consider Eq. (6.11) neglecting radiation:

$$3\mathcal{H}\left(\Phi' + \mathcal{H}\Phi\right) = \frac{3\mathcal{H}^2\rho_{\rm m}}{2\rho_{\rm tot}}\delta_{\rm m} \ , \tag{6.35}$$

where we have already considered adiabatic perturbations. Now, let us introduce the following variable:

$$x \equiv \frac{\rho_x}{\rho_{\rm m}} = \frac{\tilde{\rho}(a/a_x)^{-3(1+w_x)}}{\tilde{\rho}(a/a_x)^{-3}} = \left(\frac{a}{a_x}\right)^{-3w_x} \ , \tag{6.36}$$

where ρ_x is a DE component with equation of state w_x, which we assume constant, and a_x is the scale factor at matter-DE equivalence, for which both the densities are equal to $\tilde{\rho}$. Note that $w_x < -1/3$, in order to have a useful DE (it has to produce an accelerated expansion) and recall that, in order for Eq. (6.35) to be valid, DE must not cluster. Following the same steps which brought us to Eq. (6.16), find a closed equation for Φ, using x as independent variable, we obtain:

$$\frac{d^2\Phi}{dx^2} + \frac{6w_x(x+1) - 2x - 5}{6w_x x(x+1)}\frac{d\Phi}{dx} - \frac{1}{3w_x x(x+1)}\Phi = 0 \ . \tag{6.37}$$

This equation can be cast as a hypergeometric equation and thus solved exactly [147]. Only one of the two independent solutions is well-behaved for $x \to 0$, i.e. is a constant:

$$\Phi \propto -2w_x + \frac{4w_x(1+x)}{5}{}_2F_1\left(1, 1 - \frac{1}{3w_x}, 1 - \frac{5}{6w_x}, -x\right) \to_{x\to 0} -\frac{6w_x}{5} \ . \tag{6.38}$$

The integration constant has to be picked in order to match with $9\Phi_{\rm P}/10$. In Fig. 32 we display the evolution of Φ, computed for $w_x = -1.5, -1, -0.5$ from Eq. (6.38). In Fig. 33 we display the evolution of the potentials Φ (solid line) and $-\Psi$ (dashed-line) for the ΛCDM model with adiabatic initial condition using CLASS. The wavenumber chosen here is $k = 10^{-4}$ Mpc^{-1}, which corresponds to a scale larger than the horizon today and hence which spent the whole evolution outside the horizon. Note how the two potentials display a difference at early times, due to the presence of neutrinos, which are of course taken into account in CLASS.

The investigation of the evolution of scales larger than the horizon today is not very useful because they are not observable. However, the scales that we do observe today were outside the horizon in the past. We shall see in the next section that in the matter-dominated regime the gravitational potential Φ is constant at all scales, even through horizon-crossing, and thus it is interesting to know the behaviour of super-horizon modes (the same behaviour is not shared by the density contrast). The same does not happen when radiation dominates, but instead the gravitational potential decays and oscillates rapidly for those scales which enter the horizon. Since the behaviour in the radiation-dominated and in the matter-dominated epoch is so dramatically different, it is useful to introduce the so-called **equivalence wave number**, i.e. the wavenumber

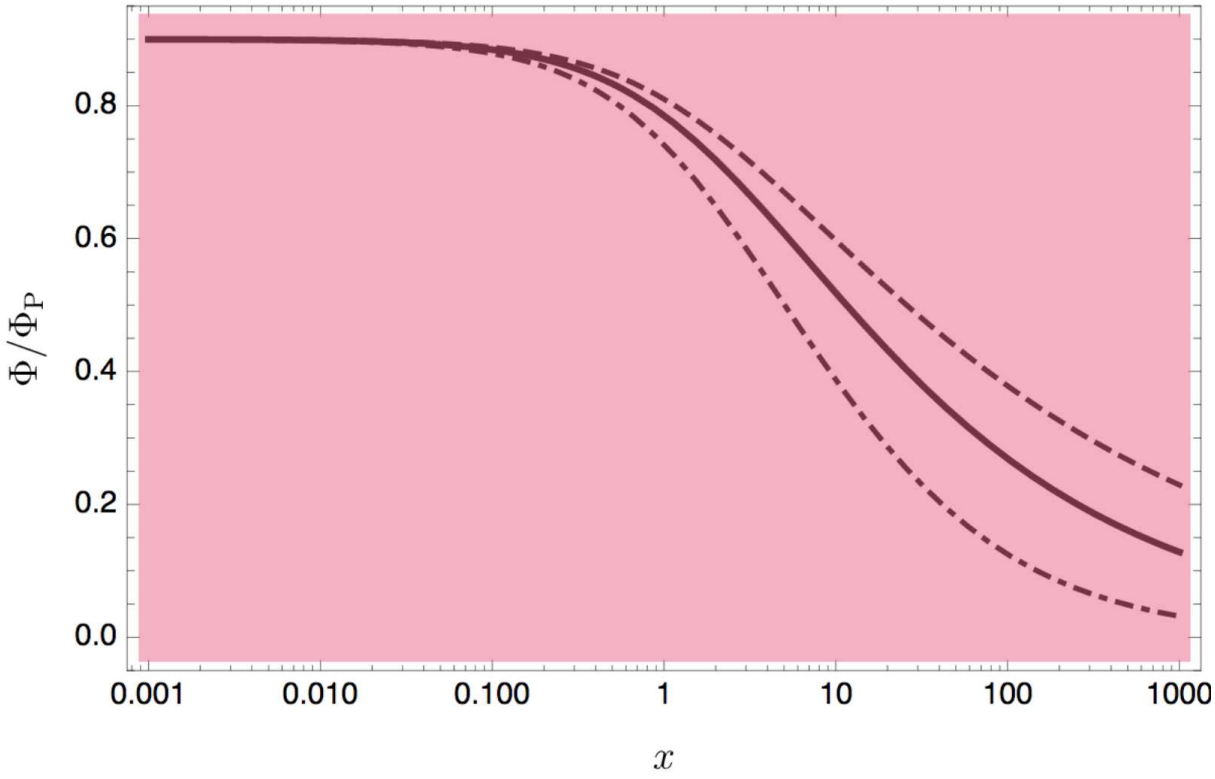

Figure 32 – Evolution of the gravitational potential Φ on super-horizon scales ($k = 0$) through matter-DE equality, from Eq. (6.38). The solid line represents the cosmological constant case $w_x = -1$, the dashed line $w_x = -1.5$ and the dash-dotted one $w_x = -0.5$.

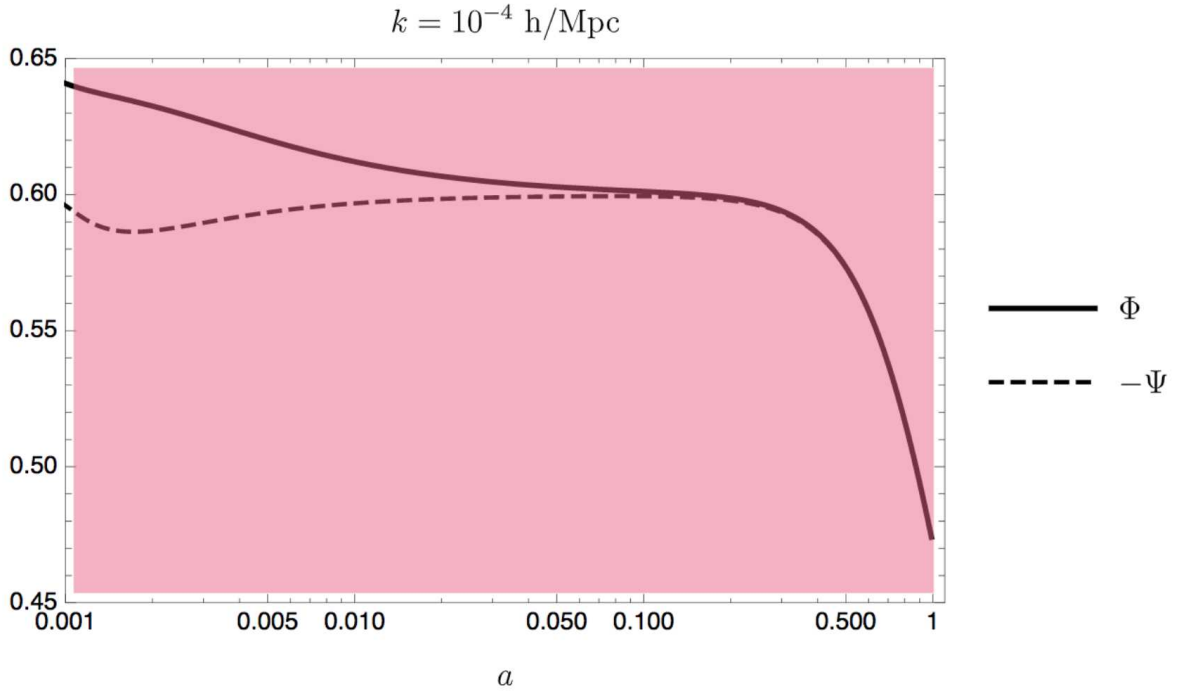

Figure 33 – Evolution of the potentials Φ (solid line) and $-\Psi$ (dashed-line) for the ΛCDM model with adiabatic initial condition using CLASS. The wavenumber chosen here is $k = 10^{-4}$ Mpc^{-1}.

corresponding to a scale which enters the horizon at the equivalence epoch, and thus defined as:

$$k_{\rm eq} \equiv \mathcal{H}_{\rm eq} \ . \tag{6.39}$$

Neglecting DE, Friedmann equation in presence of radiation and matter is written as follows:

$$\mathcal{H}^2 = \frac{8\pi G}{3}(\rho_{\rm m} + \rho_{\rm r})a^2 = H_0^2(\Omega_{\rm m0}a^{-1} + \Omega_{\rm r0}a^{-2}) \ , \tag{6.40}$$

and from this we can establish that, at equivalence, the conformal Hubble parameter has the following expression:

$$\mathcal{H}_{\rm eq}^2 = \frac{16\pi G}{3}\frac{\rho_{\rm R0}}{a_{\rm eq}^2} = 2H_0^2\Omega_{\rm r0}(1+z_{\rm eq})^2 = k_{\rm eq}^2 \ , \tag{6.41}$$

or, using the matter density parameter:

$$\mathcal{H}_{\rm eq}^2 = \frac{16\pi G}{3}\frac{\rho_{\rm M0}}{a_{\rm eq}} = 2H_0^2\Omega_{\rm m0}(1+z_{\rm eq}) = k_{\rm eq}^2 \ , \tag{6.42}$$

from which it is clear that:

$$1 + z_{\rm eq} = \frac{\Omega_{\rm m0}}{\Omega_{\rm r0}} \ . \tag{6.43}$$

Using the observed values for the density parameters, we have that:

$$k_{\rm eq} = \frac{\sqrt{2}H_0\Omega_{\rm m0}}{\sqrt{\Omega_{\rm r0}}} \approx 0.014 \ h \ {\rm Mpc}^{-1} \tag{6.44}$$

The behaviour of super-horizon modes is especially important in CMB physics. Indeed, for a given multipole ℓ the CMB temperature correlation spectrum C_ℓ is determined mostly by those wavenumbers which satisfy:

$$\ell \approx k(\eta_0 - \eta_*) = kr_* \approx k\eta_0 \ , \tag{6.45}$$

where η_0 is the present conformal time, η_* is the one corresponding to recombination and $r_* \equiv \eta_0 - \eta_*$ is the comoving distance to recombination. The last approximation is motivated by the fact that, using CLASS and the ΛCDM model, $\eta_* \approx 3 \times 10^2$ Mpc whereas $\eta_0 \approx 10^4$ Mpc. The above expression can be manipulated as follows:

$$\ell \approx k\eta\frac{\eta_0}{\eta} \approx k\eta\frac{1}{\sqrt{a}} \ , \tag{6.46}$$

where η is a generic past conformal time in the matter-dominated epoch and, for this reason, we have used $a \propto \eta^2$. So, e.g. at radiation-matter equality, i.e. $a \approx 10^{-4}$, the super-horizon scales $k\eta < 1$ contribute to the monopoles $\ell \lessapprox 100$ and at recombination $a_* \approx 10^{-3}$, $\ell \lessapprox 30$.

6.2. The matter-dominated epoch

Let us now neglect completely radiation. Being no photon and neutrino quadrupoles, then $\Phi = -\Psi$ and since matter dominates, $\delta P_{\rm tot} = 0$, such that, with a closed equation for Φ, we obtain:

$$\Phi'' + 3\mathcal{H}\Phi' + 2\mathcal{H}'\Phi + \mathcal{H}^2\Phi = -4\pi G a^2 \delta P_{\rm tot} = 0 \,, \tag{6.47}$$

which can be solved exactly since, being $a \propto \eta^2$, we have:

$$\Phi'' + \frac{6}{\eta}\Phi' = 0 \,. \tag{6.48}$$

The general solution is:

$$\Phi(k,\eta) = A(k) + B(k)(k\eta)^{-5} = A(k) + \hat{B}(k) a^{-5/2} \tag{6.49}$$

where $A(k)$, $B(k)$ and $\hat{B}(k)$ are functions of k, being the latter equal to B times the proportionality factor between the conformal time and the scale factor, which are related by $a \propto \eta^2$. We have kept a $k\eta$ dependence above because it is dimensionless, as Φ, A and B are. Now, let us neglect the decaying mode $(k\eta)^{-5}$ since it disappears very fast. The important result here is that the gravitational potential is constant at all scales, through horizon crossing, during matter domination. We shall see a very different behaviour when radiation dominates. Hence, provided that we are deep into the matter-dominated epoch, at large scales, when $k\eta < 1$, we can match the results for Φ of this section and the previous one and see that:

$$A(k < 1/\eta) = \frac{9}{10}\Phi_{\rm P}(k) \,, \qquad (\eta > \eta_{\rm eq}) \,. \tag{6.50}$$

So, the gravitational potential Φ, for those scales which enter the horizon during the matter dominated epoch, is a constant with value:

$$\Phi(k) = \frac{9}{10}\Phi_{\rm P}(k) \,, \qquad (k\eta_{\rm eq} < 1) \tag{6.51}$$

The condition $k\eta_{\rm eq} < 1$, which corresponds to $k < k_{\rm eq}$ guarantees that the mode was outside the horizon at equivalence and hence that it entered during matter domination. Considering the generalised Poisson equation with Φ constant, we have:

$$3\mathcal{H}^2\Phi + k^2\Phi = \frac{3\mathcal{H}^2}{2}\delta_{\rm m} \ , \tag{6.52}$$

where $\delta_{\rm m}$ is the density contrast of matter, which we define here as:

$$\delta_{\rm m} \equiv (1-\Omega_{\rm b0})\delta_{\rm c} + \Omega_{\rm b0}\delta_{\rm b} \ , \tag{6.53}$$

which comes from the fact that, being in the matter-dominated epoch, $\rho_{\rm tot} \propto a^{-3}$ and $\Omega_{\rm c0} + \Omega_{\rm b0} = 1$ (of course we keep on considering a spatially flat universe). We must be careful that even in the matter-dominated epoch, but before recombination, for those modes inside the horizon we can have that $\delta_{\rm c} \gg \delta_{\rm b}$ because baryons are tightly coupled to photons and thus $\delta_{\rm b}$ cannot grow, whereas CDM fluctuations can. For these modes, soon after recombination, $\delta_{\rm b}$ becomes equal to $\delta_{\rm c}$ or, in other words, baryons fall into the potential wells of CDM. We shall see this in more detail later. For large scales, those which enter the horizon after recombination, we have $\delta_{\rm c} = \delta_{\rm b} = \delta_{\rm m}$ (assuming, as usual, adiabaticity). For the moment, let us focus on the evolution for $\delta_{\rm m}$. It follows immediately that:

$$\delta_{\rm m}(k,\eta) = 2A(k)\left(1+\frac{k^2}{3\mathcal{H}^2}\right) = \frac{9\Phi_{\rm P}(k)}{5}\left(1+\frac{k^2\eta^2}{12}\right) \ , \qquad (k < k_{\rm eq}) \ . \tag{6.54}$$

Therefore, $\delta_{\rm m}$ is constant on super-horizon scales, but when a scale crosses the horizon it starts to grow as $\delta \propto \eta^2 \propto a$, as the plot in Fig. (34) shows. Note that the first equality holds true at any scales, but the second one only for $k < k_{\rm eq}$, because only in this regime we are allowed to use Eq. (6.50).

The power spectrum at any time during the matter dominated epoch can thus be put immediately in relation with the primordial one:

$$P_\delta(k,\eta) = \frac{81}{25}\left(1+\frac{k^2\eta^2}{12}\right)^2 P_\Phi(k) \ , \qquad (k < k_{\rm eq}) \ . \tag{6.55}$$

For $n_S = 1$ the primordial power spectrum goes as $P_\Phi \propto 1/k^3$, and thus the above matter one grows linearly with k (when $k\eta > 1$). From the above equation we can read off the matter transfer function, i.e.:

$$T_\delta(k,\eta) = \frac{9}{5}\frac{k^2\eta^2}{12} \ , \qquad (1/\eta < k < k_{\rm eq}) \ . \tag{6.56}$$

From this solution we can infer that the larger k is, i.e. the smaller the scale under consideration is, the more it grows. This scenario is called **bottom-up** because smaller

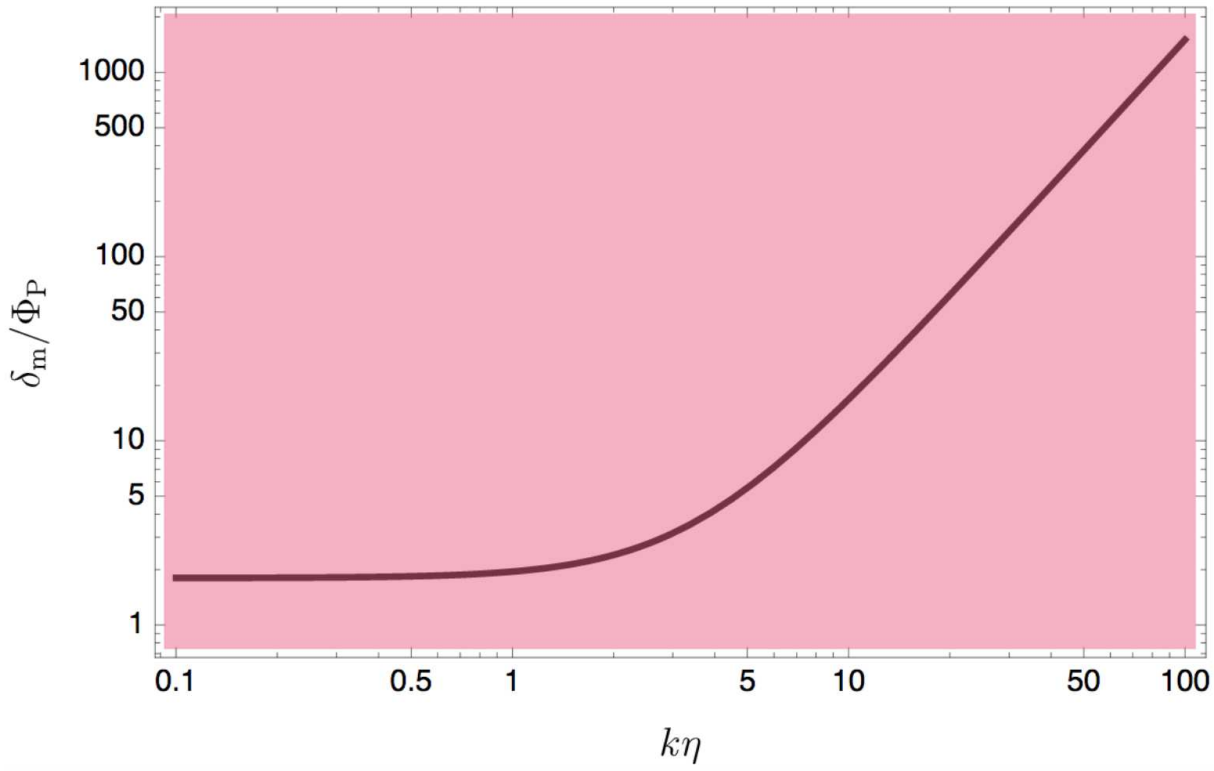

Figure 34 – Evolution of the matter density contrast $\delta_{\rm m}$ normalised to the primordial potential, in the matter-dominated era. From Eq. (6.54).

scales becomes non-linear before the larger ones. In other words, first small structures form and then these can merge in order to form larger structures. The bottom-up scenario is the contrary of the **top-down** scenario [207] by which first the largest structures form and then fragmentise in order to form the smaller ones. In Eq. (6.56) we can appreciate that the k-dependence and the η one are separate. The latter is proportional to $\eta^2 \propto a$ and is usually called **growth factor**. The separation of the k and η dependences takes place because matter has vanishing adiabatic speed of sound and the k-dependence of the equation governing $\delta_{\rm m}$ comes in multiplied by the gravitational potential, which is a constant (during matter domination). Putting to zero w, δP and the anisotropic stresses, which are indeed vanishing for CDM and also for baryons, after recombination. Show that:

$$\delta_{\rm m}'' + \mathcal{H}\delta_{\rm m}' = -k^2\Psi - 3\Phi'' - 3\mathcal{H}\Phi'. \tag{6.57}$$

In the above equation, the k-dependence enters only through $k^2\Psi$ and then, in the matter-dominated epoch we have that:

$$\delta_{\rm m}'' + \mathcal{H}\delta_{\rm m}' = k^2\Phi\ , \tag{6.58}$$

with Φ constant (if we neglect already the decaying mode). The transfer function that we have determined in this section is valid for small values of k, i.e. $k < k_{\rm eq} \approx 0.014\ h\ {\rm Mpc}^{-1}$,

which correspond to very large scales which we do not actually observe or for which the errors and the cosmic variance are too large. Indeed, in Fig. 30 there are data points only for scales larger than $k_{\rm eq}$. It is necessary therefore to understand how matter fluctuations behave during radiation-domination.

6.3. Baryons falling into the CDM potential wells

I offer here a simple calculation which should convey the idea of how important CDM is for structure formation. This is often stated otherwise as the fact that after recombination, baryons fall into the gravitational potential wells of CDM. As we anticipated earlier, before recombination baryons were tight-coupled to photons in the early-times plasma and, when they decouple and their over-densities are free to grow, in general we have $\delta_{\rm b} \ll \delta_{\rm c}$ for those modes which were well inside the horizon during recombination. Let us see this more quantitatively. In the same fashion by which we obtained Eq. (6.58), we can write the following coupled equations for CDM and baryons:

$$\delta_{\rm c}'' + \mathcal{H}\delta_{\rm c}' = k^2\Phi \ , \tag{6.59}$$

$$\delta_{\rm b}'' + \mathcal{H}\delta_{\rm b}' = k^2\Phi \ , \tag{6.60}$$

of which the baryonic one is valid only after recombination. These equations are coupled since Φ is determined by both the components. Indeed, from the Poisson equation we have that:

$$(3\mathcal{H}^2 + k^2)\Phi = \frac{3\mathcal{H}^2}{2\rho_{\rm tot}}(\rho_{\rm c}\delta_{\rm c} + \rho_{\rm b}\delta_{\rm b}) \equiv \frac{3\mathcal{H}^2}{2}\delta_{\rm m} \ , \tag{6.61}$$

Now, the two Eqs. (6.59) and (6.60) have solutions (neglecting the decaying mode):

$$\delta_{\rm c}(k,\eta) = C_1(k) + \frac{k^2\eta^2}{6}A(k) \ , \qquad \delta_{\rm b}(k,\eta) = C_2(k) + \frac{k^2\eta^2}{6}A(k) \ , \tag{6.62}$$

where we have used the constant potential solution for the potential, in Eq. (6.49) (also here neglecting the decaying mode). Using this solution in Eq. (6.53) and comparing with Eq. (6.54), we can conclude that:

$$C_1(k) + \Omega_{\rm b0}[C_2(k) - C_1(k)] = 2A(k) \ . \tag{6.63}$$

For large scales $k\eta \ll 1$ we already know that $\delta_{\rm c} = \delta_{\rm b} = \delta_{\rm m}$, because of adiabaticity, and hence $C_1 = C_2 = 2A$. For small scales, at recombination $\delta_{\rm c} \gg \delta_{\rm b}$ because baryons were

tightly coupled to photons and thus $\delta_{\rm b}$ could not grow. This, combined with the crucial fact that $\Omega_{\rm b0} = 0.04$ is small, makes $\delta_{\rm m}$ (and the gravitational potential) dominated by $\delta_{\rm c}$. Hence, again $\delta_{\rm c} = \delta_{\rm b}$ soon after recombination, the detailed transient coming from the decaying modes that we have neglected. In other words, baryons fall in the potential wells already created by CDM. Without CDM, $\delta_{\rm b}$ would grow proportionally to a, by a factor 10^3 by today, being of order 10^{-2}. This is way too small in order for account of the structures that we observe. In Fig. 35 we plot the evolution of $\delta_{\rm c}$ (solid line) and $\delta_{\rm b}$ (dashed line) for $k = 1$ Mpc^{-1} computed with CLASS. Note the oscillations in $\delta_{\rm b}$, which are related to the **baryon acoustic oscillations** (BAO) of the matter power spectrum, cf. the small box inside Fig. 30, but are not the same thing. The oscillations in the plot of Fig. 35 are function of the time (scale factor) evolution, whereas those in the matter power spectrum of Fig. 30 are function of the wavenumber k.

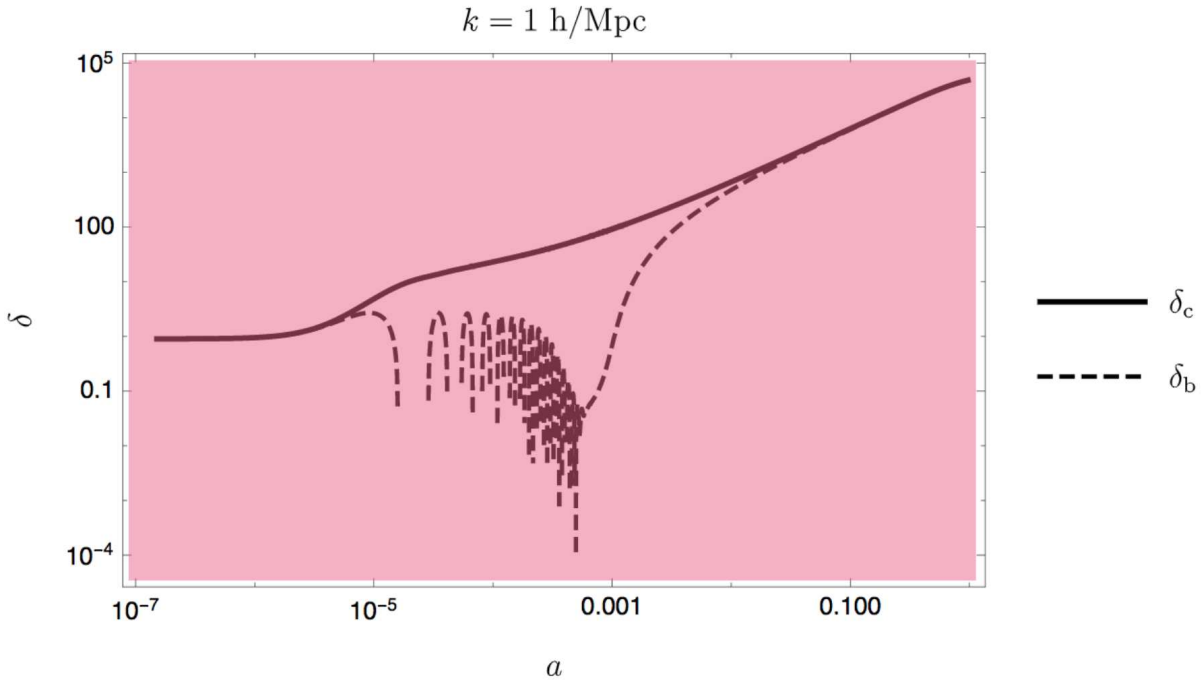

Figure 35 – Evolution of $\delta_{\rm c}$ (solid line) and $\delta_{\rm b}$ (dashed line) for $k = 1$ Mpc^{-1} computed with CLASS.

The oscillations of Fig. 35 are caused by the tight coupling of baryons with photons before recombination, when structure formation is impossible. On the other hand, CDM can grow even when radiation dominates and thus, for the chosen scale $k = 1$ Mpc^{-1}, the ratio $\delta_{\rm c}/\delta_{\rm b}$ is of about 3 orders of magnitude.

In Fig. 36 we plot again the evolution of $\delta_{\rm c}$ (solid line) and $\delta_{\rm b}$ (dashed line) for $k = 1$ Mpc^{-1} computed with CLASS, but this time with a negligible amount of CDM ($\Omega_{\rm c0}h^2 = 10^{-6}$). Note how $\delta_{\rm b}$ grows six orders of magnitude less today than in the standard case.

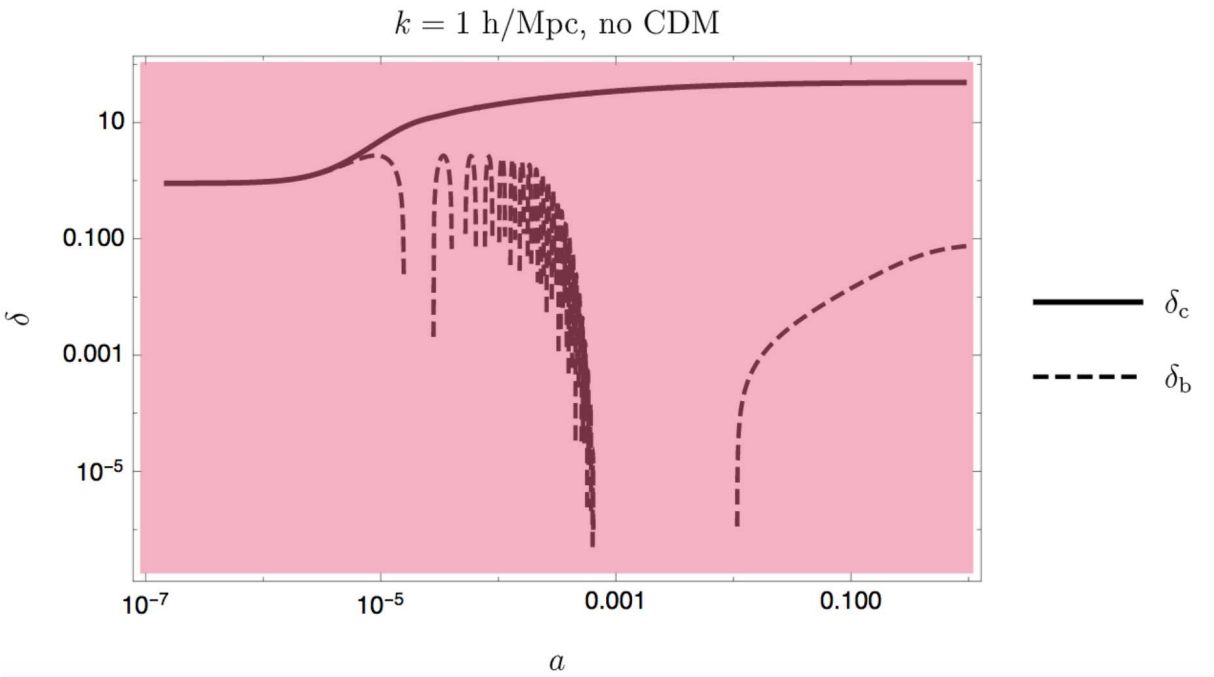

Figure 36 – Evolution of δ_c (solid line) and δ_b (dashed line) for $k = 1$ Mpc^{-1} computed with CLASS with a negligible amount of CDM ($\Omega_{c0}h^2 = 10^{-6}$).

6.4. The radiation-dominated epoch

Consider now the case of full radiation dominance and neglect δ_c and δ_b as source of the gravitational potentials. Moreover, assume adiabaticity, so that $\delta_\gamma = \delta_\nu = \delta_r$ and neglect the neutrino anisotropic stress, so that $\Phi = -\Psi$. Since we are deep into the radiation-dominated epoch, then $w = c_{ad}^2 = 1/3$ and thus from Eq. (6.23) we can immediately write:

$$\Phi'' + \frac{4}{\eta}\Phi' + \frac{k^2}{3}\Phi = 0 \,, \tag{6.64}$$

where we have used $a \propto \eta$. Defining

$$u \equiv \Phi\eta \,, \tag{6.65}$$

the above equation becomes

$$u'' + \frac{2}{\eta}u' + \left(\frac{k^2}{3} - \frac{2}{\eta^2}\right)u = 0 \,. \tag{6.66}$$

This is a Bessel equation with solutions $j_1(k\eta/\sqrt{3})$ and $n_1(k\eta/\sqrt{3})$, i.e. the spherical Bessel functions of order 1. Since n_1 diverges for $k\eta \to 0$, we discard it as unphysical.

Recovering the gravitational potential Φ and using the fact that [11]

$$j_1(x) = \frac{\sin x}{x^2} - \frac{\cos x}{x} \,, \tag{6.67}$$

and

$$\lim_{x\to 0} \frac{\sin x - x\cos x}{x^3} = \frac{1}{3} \,, \tag{6.68}$$

we can write

$$\Phi = 3\Phi_{\rm P} \frac{\sin\left(k\eta/\sqrt{3}\right) - (k\eta/\sqrt{3})\cos\left(k\eta/\sqrt{3}\right)}{(k\eta/\sqrt{3})^3} \,. \tag{6.69}$$

This solution shows that as soon as a mode k of the gravitational potential enters the horizon, it rapidly decays as $1/\eta^3$ or $1/a^3$ while oscillating.

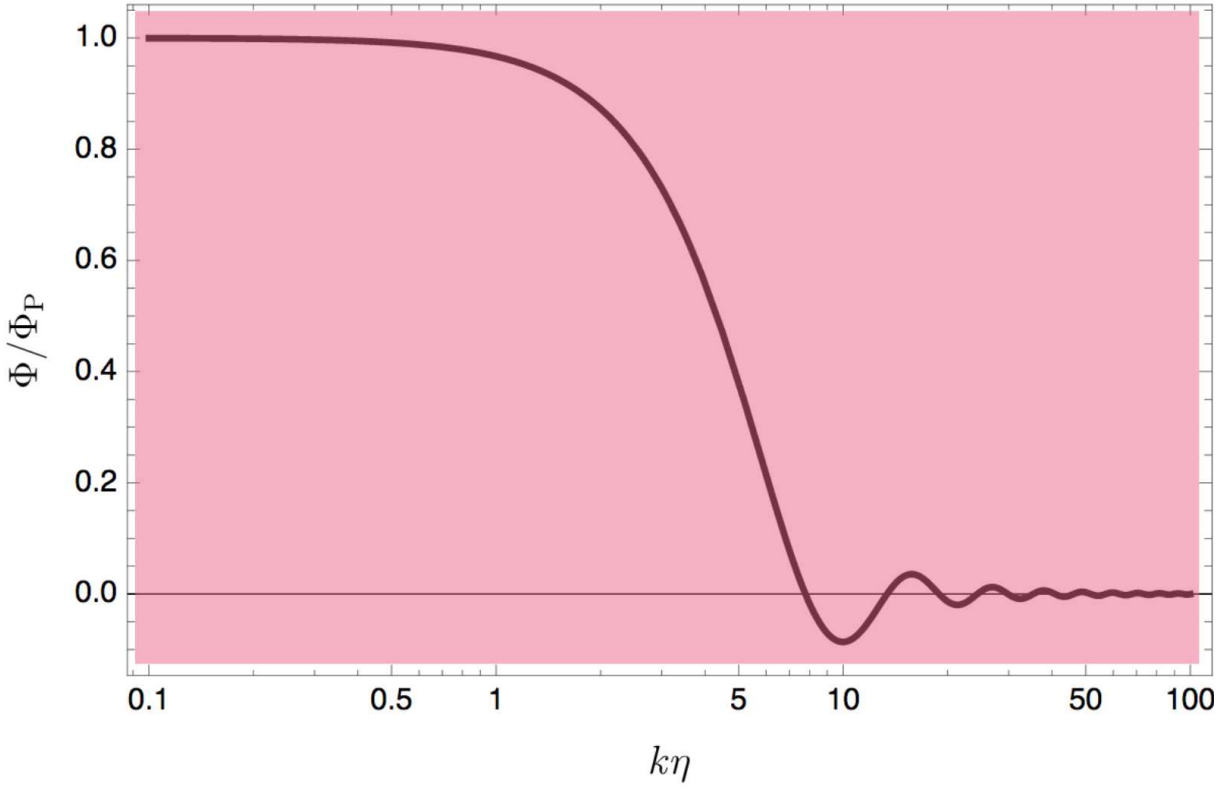

Figure 37 – Evolution of the gravitational potential Φ deep into the radiation-dominated era. From Eq. (6.69).

In Fig. 6.69 we plot the evolution of the gravitational potential, according to Eq. (6.69). Note how Φ starts to decay right after $k\eta > 1$, i.e. after horizon crossing.

The goodness of the solution (6.69) plotted in Fig. 37 can be appreciated in Fig. 38 where both Φ (solid line) and $-\Psi$ (dashed line) are plotted. Outside the horizon the two

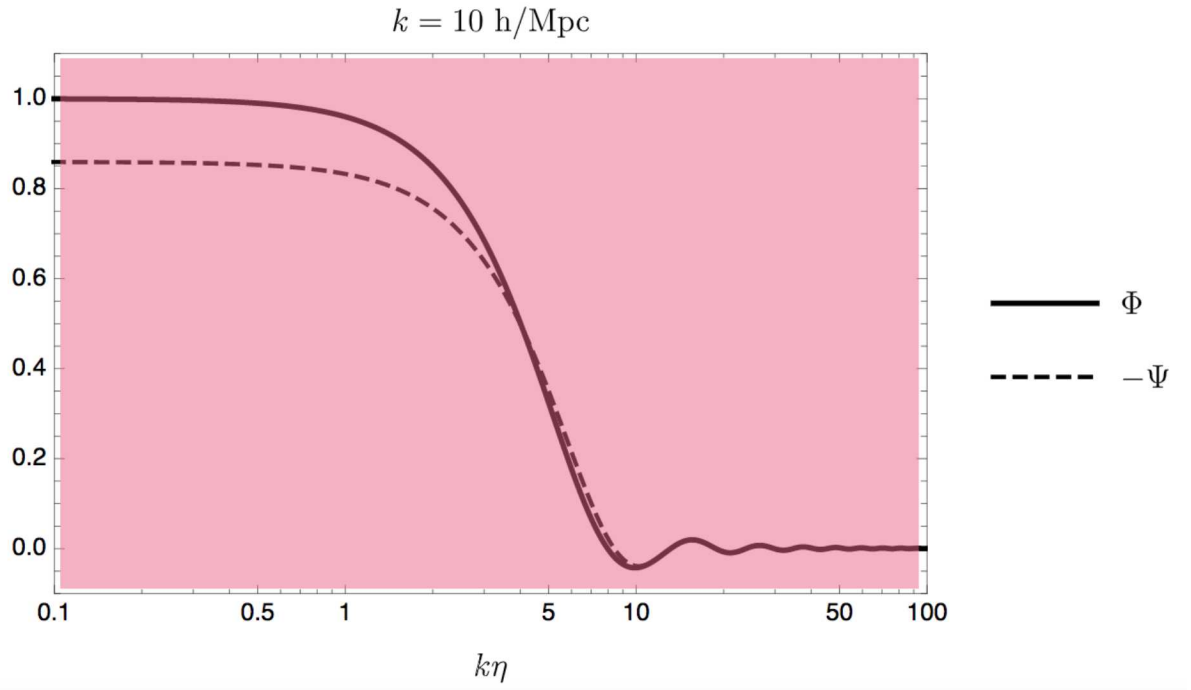

Figure 38 – Evolution of the gravitational potentials Φ (solid line) and $-\Psi$ (dashed line) deep into the radiation-dominated era computed with CLASS for the ΛCDM model and $k = 10$ Mpc^{-1}. Adiabatic perturbations have been used and the initial values have been normalised to that of Φ.

potentials are constant with a difference due to the neutrino fraction R_ν. As soon as they enter the horizon they rapidly decay to zero. Now, recall Eq. (6.57) that we derived for the matter density contrast. It can be used in the radiation-dominated epoch, but only for CDM:

$$\delta_{\rm c}'' + \frac{1}{\eta}\delta_{\rm c}' = k^2\Phi - 3\Phi'' - \frac{3}{\eta}\Phi' \,. \tag{6.70}$$

Using Eq. (6.64), we can write

$$\delta_{\rm c}'' + \frac{1}{\eta}\delta_{\rm c}' = 2k^2\Phi + \frac{9}{\eta}\Phi' \equiv S(k,\eta) \,. \tag{6.71}$$

As stated at the beginning of the section, we are so deep into the radiation-dominated epoch that the matter density contrast does not contribute to the gravitational potential but only feels it. Using Eq. (6.69) with $x \equiv k\eta$ as new independent variable, the function $S(x)$ has the following form:

$$\frac{S(x)}{k^2\Phi_{\rm P}} = \frac{9\left[(27x - 2x^3)\cos\left(x/\sqrt{3}\right) + \sqrt{3}\,(5x^2 - 27)\sin\left(x/\sqrt{3}\right)\right]}{x^5} \,, \tag{6.72}$$

and the equation for $\delta_{\rm c}$ becomes:

$$\frac{d}{dx}\left(x\frac{d\delta}{dx}\right) = 9\Phi_{\rm P}\frac{\left[(27x-2x^3)\cos\left(x/\sqrt{3}\right)+\sqrt{3}\,(5x^2-27)\sin\left(x/\sqrt{3}\right)\right]}{x^4}\,. \tag{6.73}$$

The homogeneous part of this equation has a simple solution:

$$\delta_{\rm hom} = C_1 + C_2\ln x\,, \tag{6.74}$$

i.e. a constant C_1 times a logarithmic contribution. A particular solution is obtained by integrating twice the right-hand side, thus obtaining:

$$\delta_{\rm part} = \frac{9\Phi_{\rm P}\left[-x^3{\rm Ci}\left(x/\sqrt{3}\right)+\sqrt{3}\,(x^2-3)\sin\left(x/\sqrt{3}\right)+3x\cos\left(x/\sqrt{3}\right)\right]}{x^3}\,, \tag{6.75}$$

where ${\rm Ci}(z)$ is the cosine integral function, defined as

$${\rm Ci}(z) \equiv -\int_z^\infty dt\frac{\cos t}{t}\,. \tag{6.76}$$

The above is a particular solution, therefore the integration constants which stem from the indefinite integration can be incorporated in C_1. The general solution for $\delta_{\rm c}$ is then:

$$\delta_{\rm c} = C_1 + C_2\ln x + \frac{9\Phi_{\rm P}\left[-x^3{\rm Ci}\left(x/\sqrt{3}\right)+\sqrt{3}\,(x^2-3)\sin\left(x/\sqrt{3}\right)+3x\cos\left(x/\sqrt{3}\right)\right]}{x^3}\,. \tag{6.77}$$

For $x\to 0$, we can expand the above solution as follows:

$$\delta(x\to 0) = C_1 + C_2\ln(x) + \Phi_{\rm P}\left[-9\ln(x) - 9\gamma + 6 + \frac{9\ln(3)}{2}\right] + \mathcal{O}\left(x^2\right)\,, \tag{6.78}$$

where γ is the Euler constant. Since $\ln x$ is divergent for $x\to 0$ and we do not want $\delta_{\rm c}$ to diverge, we have to ask:

$$C_2 = 9\Phi_{\rm P}\,. \tag{6.79}$$

Moreover, we know that $\delta_{\rm c}(x\to 0) = 3\Phi_{\rm P}/2$ when we choose adiabatic initial conditions (and neglect neutrinos), thus:

$$C_1 = -\frac{9}{2}\Phi_{\rm P}\left[-2\gamma + 1 + \ln(3)\right]\,. \tag{6.80}$$

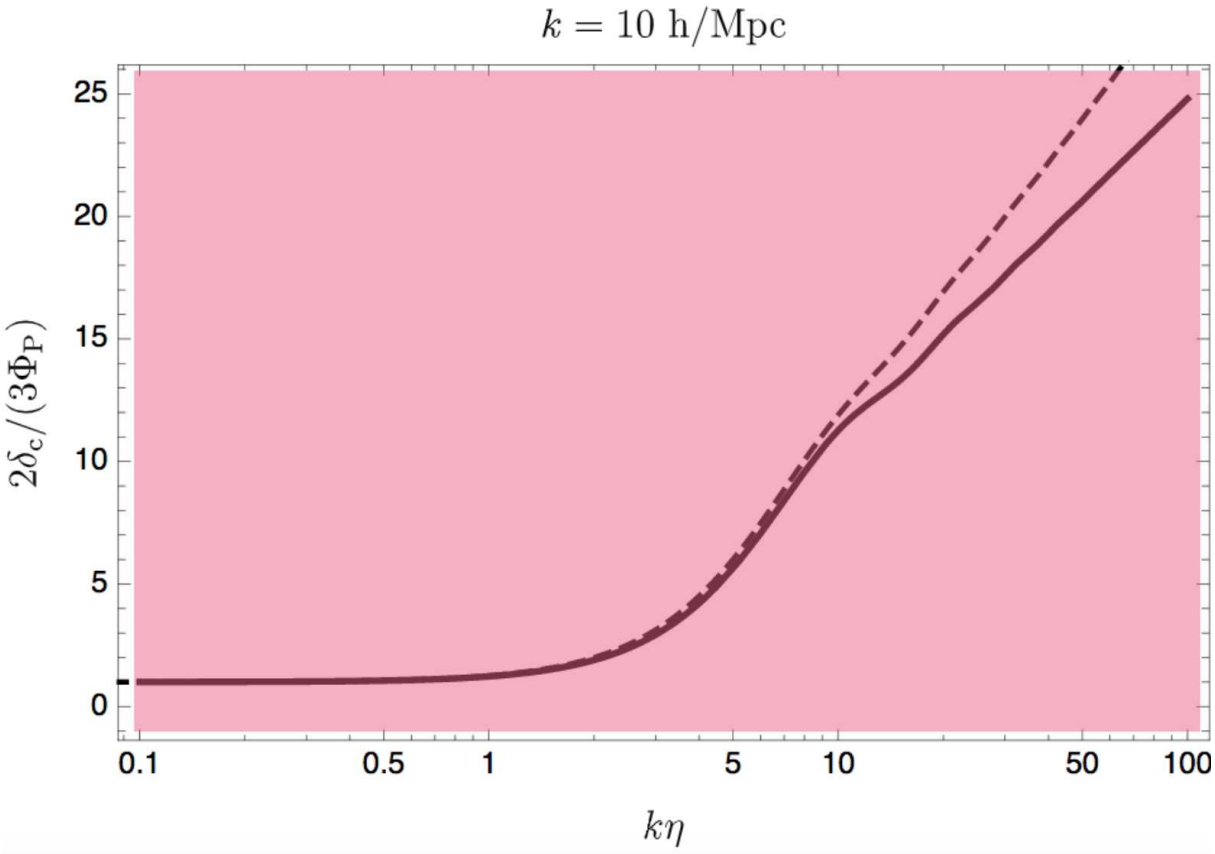

Figure 39 – Evolution of δ_c deep into the radiation-dominated era computed from Eqs. (6.77), (6.79) and (6.80) (solid line) compared with the numerical calculation performed with CLASS for $k = 10$ Mpc^{-1} (dashed line). Note the semi-logarithmic scale employed.

We plot the evolution of δ_c through horizon-crossing in Fig. 39.

For $x \gg 1$, deep inside the horizon, we can neglect the contribution $\delta_{\rm part}$ to the solution for δ_c since it decays rapidly. Thus, we can write the density contrast as follows:

$$\delta_c = -\frac{9}{2}\Phi_P\left[-2\gamma + 1 + \ln(3)\right] + 9\Phi_P \ln x = A\Phi_P \ln(Bk\eta) \,, \tag{6.81}$$

where

$$A = 9 \,, \qquad B = \exp\left[\gamma - \frac{1}{2} - \frac{\ln(3)}{2}\right] \approx 0.62 \,. \tag{6.82}$$

6.5. Deep inside the horizon

The last domain in which it is possible to analytically solve the equations for the perturbations is when $k \gg \mathcal{H}$, i.e. deep inside the horizon. We shall neglect baryons in this calculation (this is imprecise and we shall see why numerically) and assume $\Phi = -\Psi$

(which is a good approximation, on the basis of the results of the previous section). The relevant equations are thus the following ones:

$$\delta_{\rm c}' + kV_{\rm c} = -3\Phi' \ , \tag{6.83}$$

$$V_{\rm c}' + \mathcal{H}V_{\rm c} = -k\Phi \ , \tag{6.84}$$

$$k^2\Phi = 4\pi G a^2 \rho_{\rm c}\delta_{\rm c} \ . \tag{6.85}$$

In the latter equation we have neglected all the potential terms except for the one accompanied by k^2 and we have also neglected radiation perturbations. It is not evident why should we neglect $\rho_{\rm r}\delta_{\rm r}$ with respect $\rho_{\rm c}\delta_{\rm c}$ even when $\rho_{\rm r} \gg \rho_{\rm c}$ deep into the radiation-dominated epoch. Neglecting $\delta_{\rm b}$, at least, is justified by the fact that before recombination it behaves as the fluctuation in radiation and afterwards as that in CDM, while being $\Omega_{\rm b}$ always subdominant. An explanation of why we can neglect $\rho_{\rm r}\delta_{\rm r}$ is offered by Weinberg who shows that new modes appear (dubbed *fast*) which rapidly decay and oscillate [197]. He also takes into account baryons at first order in $\Omega_{\rm b0}$. Using again the variable $y \equiv a/a_{\rm eq}$ and manipulate the three equations above in order to obtain a single second-order equation for $\delta_{\rm c}$:

$$\frac{d^2\delta_{\rm c}}{dy^2} + \frac{2+3y}{2y(y+1)}\frac{d\delta_{\rm c}}{dy} - \frac{3}{2y(y+1)}\delta_{\rm c} = 0 \ . \tag{6.86}$$

This equation is known as **Mészáros equation** [125]. A solution can be found at once, multiplying by $2y(y+1)$:

$$2y(y+1)\frac{d^2\delta_{\rm c}}{dy^2} + 2\frac{d\delta_{\rm c}}{dy} + 3y\frac{d\delta_{\rm c}}{dy} - 3\delta_{\rm c} = 0 \ . \tag{6.87}$$

A linear ansatz $\delta_{\rm c} \propto y$ kills the second derivative and the last two terms on the left hand side. Therefore, the simple solution we looked for is:

$$D_1(y) \equiv y + \frac{2}{3} \tag{6.88}$$

This is also the growing mode. For $y \ll 1$, i.e. before matter-radiation equality, δ is practically constant, whereas for $y \gg 1$ we have the known growth linear with respect to the scale factor. In order to find the other independent solution say D_2, we can use the Wronskian:

$$W(y) = D_1\frac{dD_2}{dy} - \frac{dD_1}{dy}D_2 \ . \tag{6.89}$$

The Wronskian satisfies the simple first-order differential equation:

$$\frac{dW}{dy} = -\frac{2+3y}{2y(y+1)}W \ , \tag{6.90}$$

from which one gets

$$W = \frac{1}{y\sqrt{1+y}} \ . \tag{6.91}$$

From the very definition of the Wronskian in Eq. (6.89), we can write a first-order equation also for D_2, which is the following:

$$(y+2/3)^2 \, \frac{d}{dy}\left(\frac{D_2}{y+2/3}\right) = \frac{1}{y\sqrt{1+y}} \ . \tag{6.92}$$

Integrate it the result is:

$$D_2 = \frac{9}{2}\sqrt{1+y} - \frac{9}{4}\,(y+2/3)\ln\left(\frac{\sqrt{y+1}+1}{\sqrt{y+1}-1}\right) . \tag{6.93}$$

This mode grows logarithmically when $y \ll 1$, recovering the logarithmic solution of the previous section. It decays as $1/y^{3/2}$ for $y \gg 1$. The complete solution for $\delta_{\rm c}$ on small scales $k \gg \mathcal{H}$ and through radiation-matter equality is then:

$$\delta_{\rm c}(k,a) = C_1(k)D_1(a) + C_2(k)D_2(a) \ . \tag{6.94}$$

The dependence of C_1 and C_2 from k can be established by matching this solution with the one of the previous section in Eq. (6.81).

6.5.1 CDM transfer function and power spectrum

As we discussed earlier and as it is clear from Fig. 30 the today observed scales in the matter power spectrum are those for which $k > k_{\rm eq}$, i.e. those which entered the horizon before matter equality. In the last two section we have obtained exact solution for $\delta_{\rm c}$ deep into the radiation-dominated epoch for all scales and through radiation-matter equality at very small scales. There is then the possibility of matching the two solutions on very small scales and thus obtain in this regime the CDM transfer function until today. Considering the following two solutions found in the previous sections, i.e.

$$\delta_{\rm c}(k,\eta) = A\Phi_{\rm P}(k)\ln(Bk\eta) \ , \tag{6.95}$$

$$\delta_{\rm c}(k,a) = C_1(k)D_1(a) + C_2(k)D_2(a) \ , \tag{6.96}$$

which are valid on very small scales, i.e. $k\eta \gg 1$. The purpose is to find the functional forms of $C_1(k)$ and $C_2(k)$. Using Eqs. (6.40) and (6.41), one can approximate the Hubble parameter deep into the radiation era as follows:

$$\mathcal{H} \approx \frac{\mathcal{H}_{\rm eq} a_{\rm eq}}{\sqrt{2} a} \,, \tag{6.97}$$

and solving using the conformal time, one has:

$$a = \frac{\mathcal{H}_{\rm eq} a_{\rm eq}}{\sqrt{2}} \eta \,. \tag{6.98}$$

The proportionality constant is the correct one which gives $\mathcal{H} = 1/\eta$ when substituted in the approximated formula for $\mathcal{H}$. We can thus write the logarithmic solution for $\delta_{\rm c}$, deep into the radiation-dominated era, as follows:

$$\delta_{\rm c}(k, a) = A \Phi_{\rm P}(k) \ln \left(B k \frac{\sqrt{2} a}{\mathcal{H}_{\rm eq} a_{\rm eq}} \right) \,. \tag{6.99}$$

Introducing $y \equiv a/a_{\rm eq}$, the equivalence wavenumber $k_{\rm eq} = \mathcal{H}_{\rm eq}$ and the rescaled wavenumber:

$$\boxed{\kappa \equiv \frac{\sqrt{2} k}{k_{\rm eq}} = \frac{k \sqrt{\Omega_{\rm r0}}}{H_0 \Omega_{\rm m0}} = \frac{k}{0.052 \; \Omega_{\rm m0} \; h^2 \; {\rm Mpc}^{-1}}} \tag{6.100}$$

one has:

$$\delta_{\rm c}(k, a) = A \Phi_{\rm P}(k) \ln \left(B \kappa y \right) \,. \tag{6.101}$$

Recall that this solution is valid deep into the radiation-dominated epoch, thus $y \ll 1$. At the same time, it holds true only on very small scales, i.e. $k\eta \gg 1$. Using the above formulae, this means:

$$k\eta = k \frac{\sqrt{2} a}{\mathcal{H}_{\rm eq} a_{\rm eq}} = k \frac{\sqrt{2} a}{k_{\rm eq} a_{\rm eq}} = \kappa y \gg 1 \,. \tag{6.102}$$

Therefore, if we want to match radiation-domination solution with the solution of the Mészáros equation, we need to choose a suitable y_m at which performing the junction of the two solutions such that $1/\kappa \ll y_m \ll 1$. Asking the equality of the two solutions and their derivatives at y_m implies to solve the following system:

$$A \Phi_{\rm P} \ln(B \kappa y_m) = C_1 \left(y_m + 2/3 \right) + C_2 D_2(y_m) \,, \tag{6.103}$$

$$\frac{A \Phi_{\rm P}}{y_m} = C_1 + C_2 \left. \frac{dD_2}{dy} \right|_{y = y_m} \,. \tag{6.104}$$

Solving the above system and take the dominant contribution for $y_m \to 0$ (because the junction condition has to be imposed for $y_m \ll 1$), we obtain:

$$C_1 = \frac{3}{2} A\Phi_{\rm P} \ln\left(4B\kappa e^{-3}\right) \ , \qquad C_2 = \frac{2}{3} A\Phi_{\rm P} \ . \tag{6.105}$$

Therefore, the solution for $\delta_{\rm c}$ valid at all time and at small scales is the following:

$$\delta_{\rm c}(k,y) = \frac{3}{2} A\Phi_{\rm P} \ln\left(4\sqrt{2}B\kappa e^{-3}\right)(y+2/3) + \frac{2}{3} A\Phi_{\rm P} D_2(y) \ , \quad (\kappa \gg 1) \ . \tag{6.106}$$

We can project this solution at late times, when matter dominates and thus neglect the decaying mode D_2 and write:

$$\delta_{\rm c}(k,a) = \frac{3}{2} A\Phi_{\rm P} \ln\left(\frac{4\sqrt{2}Be^{-3}k}{k_{\rm eq}}\right)\frac{a}{a_{\rm eq}} \ , \quad (a \gg a_{\rm eq}, k \gg k_{\rm eq}) \tag{6.107}$$

Note again the separated dependence from k and from the scale factor, being the growth function $D(a) = a$. This allows us to write the transfer function for CDM as follows, using Eq. (6.42) in order to eliminate $a_{\rm eq}$:

$$T_\delta(k) = \frac{Ak_{\rm eq}^2}{2H_0^2\Omega_{\rm m0}} \ln\left(\frac{4\sqrt{2}Be^{-3}k}{k_{\rm eq}}\right) D(a) \ , \quad (a \gg a_{\rm eq}, k \gg k_{\rm eq}) \tag{6.108}$$

Recall that the factor $3\Phi_{\rm P}/2$ is the adiabatic initial condition on $\delta_{\rm c}$ and thus enters the primordial power spectrum. The above transfer function can be generalised including DE, if the latter does not cluster. If it is the case, as for the cosmological constant, its effect enters only the growth factor and in $k_{\rm eq}$ since, being another component and having the fixed total $\Omega_{\rm r0} + \Omega_{\rm m0} + \Omega_\Lambda = 1$, the relative amount of radiation and matter has to change (usually the amount of radiation is fixed) and thus $k_{\rm eq}$ changes. We can also determine the transfer function for the gravitational potential Φ at late times. From Eq. (6.85) we have that:

$$k^2\Phi = 4\pi G a^2 \rho_{\rm m}\delta_{\rm m} = \frac{3H_0^2\Omega_{\rm m0}}{2a}\delta_{\rm m} \ , \tag{6.109}$$

where we have included baryons, since we are considering late times and we have seen that after recombination $\delta_{\rm b} = \delta_{\rm c}$. We are neglecting any DE contribution in the expansion of the universe and considering a radiation plus matter model. Hence, $\Omega_0 \approx 1$. We thus have for the gravitational potential, combining Eqs. (6.107) and (6.109):

$$\Phi(k) = \frac{9Ak_{\rm eq}^2}{8k^2}\Phi_{\rm P}(k) \ln\left(\frac{4\sqrt{2}Be^{-3}k}{k_{\rm eq}}\right) \ , \qquad k \gg k_{\rm eq} \tag{6.110}$$

The transfer function for the gravitational potential is usually normalised to $9\Phi_{\rm P}/10$ and therefore:

$$T_\Phi(k) = \frac{5Ak_{\rm eq}^2}{4k^2}\ln\left(\frac{4\sqrt{2}Be^{-3}k}{k_{\rm eq}}\right) , \qquad k \gg k_{\rm eq} \tag{6.111}$$

Using $\Omega_{\rm r0}h^2 = 4.15\times10^{-5}$ in Eq. (6.44) and defining

$$q \equiv k \times \frac{\rm Mpc}{\Omega_{\rm m0}h^2} , \tag{6.112}$$

we can cast the above transfer function in the following form:

$$\boxed{T_\Phi(k) = \frac{\ln(2.40q)}{(4.07q)^2}} \tag{6.113}$$

See also [200, pag. 310]. We have written the transfer function as in Eq. (6.113) because it is simpler to compare it with the numerical fit of Bardeen, Bond, Kaiser and Szalay (BBKS) of the exact transfer function [22], which is the following:

$$T_{\rm BBKS}(k) = \frac{\ln(1+2.34q)}{2.34q}\left[1+3.89q+(16.2q)^2+(5.47q)^3+(6.71q)^4\right]^{-1/4} , \tag{6.114}$$

and see that for large q it goes as $\ln(2.34q)/(3.96q)^2$, which is in good agreement with our analytic estimate (6.113). Given the transfer function T_Φ, $\delta_{\rm m}$ can be written, from Eq. (6.109), as:

$$\delta_{\rm m}(k,a) = \frac{2a}{3H_0^2\Omega_{\rm m0}}k^2\Phi = \frac{3k^2}{5H_0^2\Omega_{\rm m0}}\Phi_{\rm P}(k)T_\Phi(k)a = \frac{3k^2}{5H_0^2\Omega_{\rm m0}}\Phi_{\rm P}(k)T_\Phi(k)D(a) . \tag{6.115}$$

In the last equality we have recovered the growth factor $D(a)$ in order to provide a more general formula. From this solution we can obtain the power spectrum for $\delta_{\rm m}$ starting from the primordial one for Φ, i.e.

$$P_\delta(k,a) = \frac{9k^4}{25H_0^4\Omega_{\rm m0}^2}P_\Phi(k)T_\Phi^2(k)D^2(a) . \tag{6.116}$$

Using $\Phi = -\Psi$, since we are neglecting neutrinos, $\Phi_{\rm P} = 2\mathcal{R}/3$ and thus the primordial power spectrum of Φ can be traded with the $\mathcal{R}$ one, and we get:

$$P_\delta(k,a) = \frac{4k^4}{25H_0^4\Omega_{\rm m0}^2}P_\mathcal{R}(k)T_\Phi^2(k)D^2(a) . \tag{6.117}$$

We can write the explicit dependence of the primordial power spectrum of k as follows:

$$P_\delta(k,a) = \frac{8\pi^2 k}{25 H_0^4 \Omega_{\rm m0}^2} A_S \left(\frac{k}{k_*}\right)^{n_S-1} T_\Phi^2(k) D^2(a) \tag{6.118}$$

The power spectrum $P_\delta(k,a)$ can be determined through the observation of the distribution of galaxies in the sky. Therefore, through the above formula we can probe many quantities of great interest such as the primordial tilt of the power spectrum. Now, let us make a plot of the power spectrum today ($z = 0$) using CLASS and fixing all the parameters to the ΛCDM best fit values except for $\Omega_{\rm m0}$, which we let free. We show in Fig. 40 the shape of the matter power spectrum for $\Omega_{\rm m0} = 0.1$ (blue) and $\Omega_{\rm m0} = 0.3$ (yellow), $\Omega_{\rm m0} = 0.7$ (green) and $\Omega_{\rm m0} = 0.99$ (red).

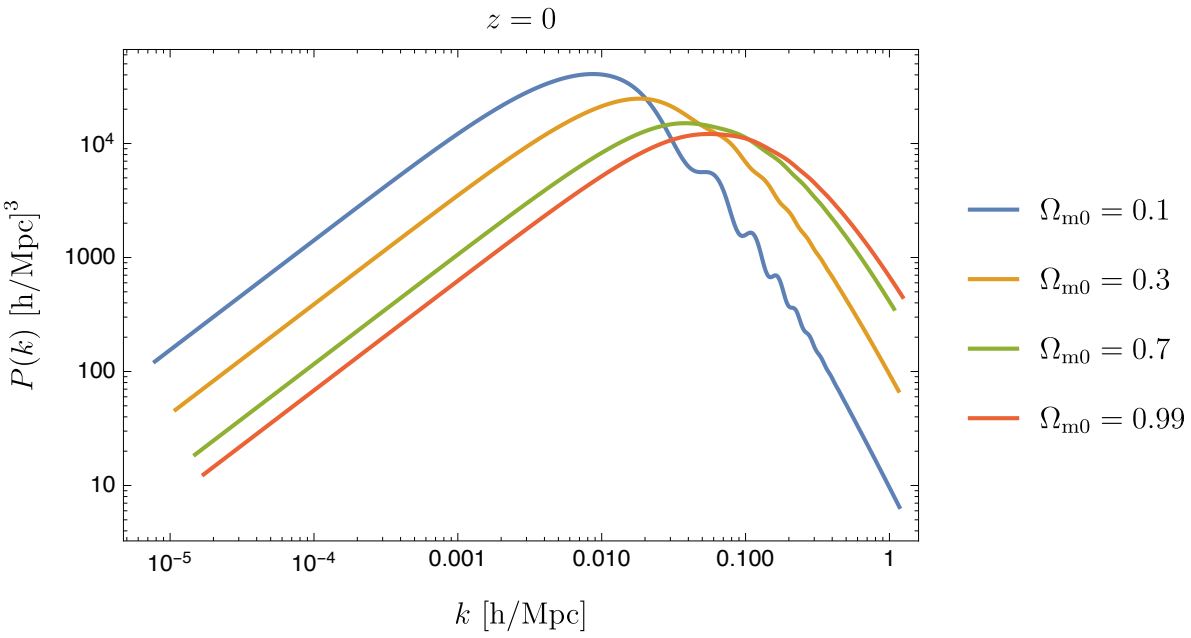

Figure 40 – Matter power spectra for (left to right, in case no colours are available) $\Omega_{\rm m0} = 0.1$ (blue), $\Omega_{\rm m0} = 0.3$ (yellow), $\Omega_{\rm m0} = 0.7$ (green) and $\Omega_{\rm m0} = 0.99$ (red).

The first interesting feature of the power spectrum is that it has a maximum. This maximum takes place roughly at $k_{\rm eq}$ for the following reason: entering the horizon at equivalence is the best time to do that in order for a matter fluctuation to grow more. In fact, as we have seen, scales that entered the horizon earlier (i.e. $k > k_{\rm eq}$) are suppressed because radiation is dominating and that δ grows logarithmically during this epoch, cf. Eq. (6.77). These are the scales of great observational interest, as can be appreciated from Fig. 30. On the other hand, the scales that entered after the equivalence grow proportionally to a, cf. Eq. (6.54). Evidently, the scale which entered at equivalence has had more time to grow than all the others, hence the the maximum or **turnover** in the power spectrum. The second interesting feature of the power spectrum is that its maximum is shifted to the left when we reduce $\Omega_{\rm m0}$. This means that the equivalence

wavenumber $k_{\rm eq}$ is smaller when $\Omega_{\rm m0}$ is smaller and this can be immediately seen from Eq. (6.44) if we fix $\Omega_{\rm r0}$. Remarkably, observation favours the line for $\Omega_{\rm m0} = 0.3$ of Fig. 40, as can also be seen from Fig. 30. Since the radiation content is very well established from CMB observation (and our knowledge of neutrinos) as well as the spatial flatness of the universe and H_0 are also well-determined, the only way to make the total is to add a further component, which clearly is DE. The important point here is that the necessity for DE can already be seen by analysing the large scale structure of the universe (together with CMB) and this was realised well before type Ia supernovae started to be used as standard candles [117], [60]. For completeness, in Fig. 41 we plot with CLASS the matter power spectrum at $z = 0$ for the ΛCDM model, with different choices of the initial conditions.

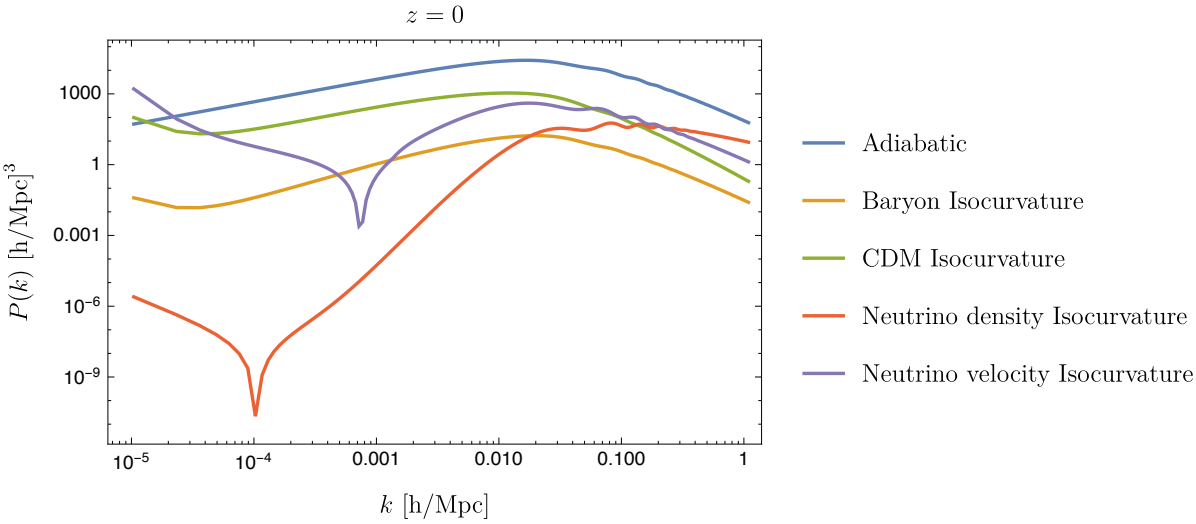

Figure 41 – Matter power spectra for different initial conditions: Adiabatic (blue), Baryon Isocurvature (yellow), CDM Isocurvature (green), Neutrino density Isocurvature (red), and Neutrino velocity Isocurvature (purple).

The transfer function thus tells us how the shape of the primordial power spectrum is changed through the cosmological evolution and through the analytic estimates that we have done in this Chapter we understood that the k-dependence is set up during radiation-domination. However, we have made two important assumptions in our calculations: we have neglected baryons and neutrino anisotropic stress (we have taken into account neutrinos from the point of view of the background expansion). If we aim to precise predictions, and we have to in order to keep the pace with the increasing sophistication of the observational techniques, we must take into account them. A more precise fitting formula (to numerical calculations performed with CMBFAST) taking into account baryons and neutrino anisotropic stress is given by [62].

In Fig. 42 we compare the BBKS transfer function with the numerical calculation of CLASS, adopting $\Omega_{\rm m0} = 0.95$ while leaving all the remaining cosmological parameters as in the ΛCDM model, except for Ω_Λ which is adjusted to the value $\Omega_\Lambda = 1.632908 \times 10^{-3}$

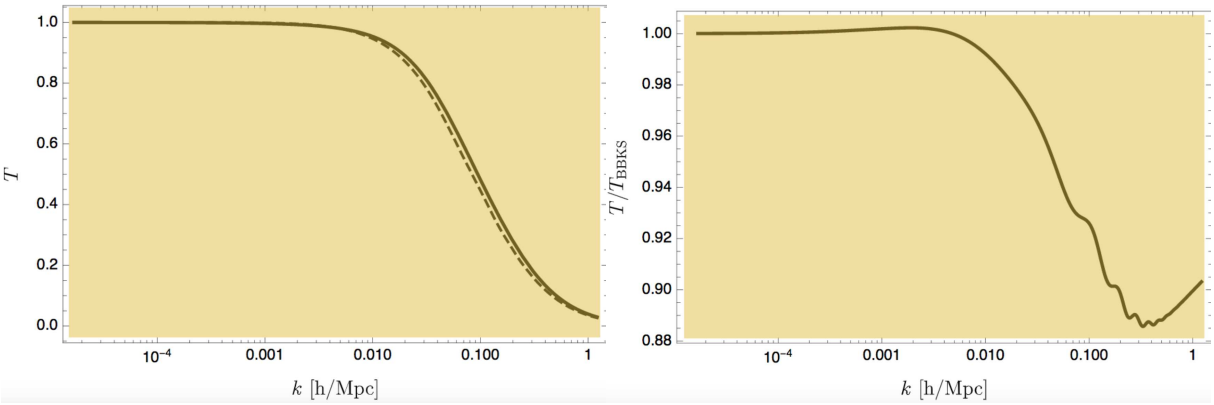

Figure 42 – *Left Panel.* Evolution of BBKS transfer function of Eq. (6.114) (solid line) compared with the numerical computation of CLASS, using $\Omega_{\mathrm{m0}} = 0.95$ (which means negligible DE). *Right Panel.* Ratio between the numerical result and the BBKS transfer function.

in order to match the correct budget of energy density. So, in practice, we are neglecting DE. As can be appreciated from the plots, the BBKS transfer function overestimates of about 5% the correct transfer function for scales $k \gtrsim 0.1$ h Mpc^{-1}, see also [57, pag. 208]. The reason is that baryons behave like radiation before decoupling, because of their tight coupling due to Thomson scattering. Therefore, they contribute further to thwart scales entering the horizon before the equivalence.

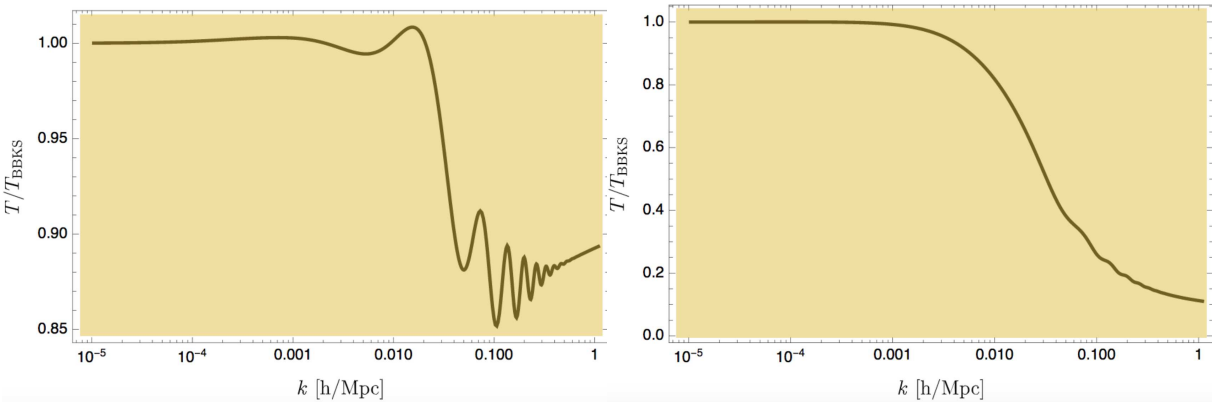

Figure 43 – *Left Panel.* Ratio between the numerical result computed with CLASS assuming the ΛCDM model, and the BBKS transfer function with $\Omega_{\mathrm{m0}}h^2 = 0.12038$. *Right Panel.* Ratio between the numerical result computed with CLASS assuming the ΛCDM model, and the BBKS transfer function with $\Omega_{\mathrm{m0}} = 1$.

In Fig. 43 we display the ratio between the numerical transfer function computed with CLASS for the ΛCDM model and the BBKS transfer function in two cases. In the left panel, the same matter density parameter of the ΛCDM model is used for both the transfer functions. In the right panel, we used the BBKS transfer function with $\Omega_{\mathrm{m0}} = 1$. The latter choice was made in order to reproduce the plot of [57, pag. 208] and thus to show the very large correction due to the cosmological constant which, if not taken into account,

leads to a 80% error at the scale $k = 0.1\ h\ \mathrm{Mpc}^{-1}$. When Λ is taken into account properly, the BBKS transfer function still overestimates the correct transfer function of at least a 10% on small scales, which implies an imprecision of 1% in the power spectrum (since this depends on the squared transfer function). Moreover, as it is obvious since it does not include baryons, the BBKS cannot describe the BAO, which appear as oscillations in the transfer function at about $k = 0.1\ h\ \mathrm{Mpc}^{-1}$ in Fig. 43.

6.5.2 The initial power spectrum

The Harrison–Zeldovich spectrum. Initially it may seem as if $P(k)$ is a function that can be chosen arbitrarily, but one objective of cosmology is to calculate this power spectrum and to compare it to observations. More than 30 years ago, arguments were already developed to specify the functional form of the initial power spectrum. At early times, the expansion of the Universe follows a power law, $a(a) \propto t^{1/2}$ in the radiation-dominated era. At that time, no natural length-scale existed in the Universe to which one might compare a wavelength. The only mathemat- ical function that depends on a length but does not contain any characteristic scale is a power law; hence for very early times one should expect:

$$P(k) \propto k^{n_s}. \tag{6.119}$$

Many years ago, Harrison, Zeldovich, Peebles and others argued that $n_s = 1$, as for this slope, the amplitude of the fluctuations of the gravitational potential are constant, i.e., preferring neither small nor large scales. For this reason, the spectrum (6.5.2) with $n_s = 1$ is called a scale-invariant spectrum, or Harrison–Zeldovich spectrum (see Fig. 44). With such a spectrum, we may choose a time ti after the inflationary epoch and write:

$$P(k, t) = D^2(t) A k^{n_s} \tag{6.120}$$

where A is a normalization constant that cannot be determined from theory but has to be fixed by observations, as we will see in the following sections of this chapter.

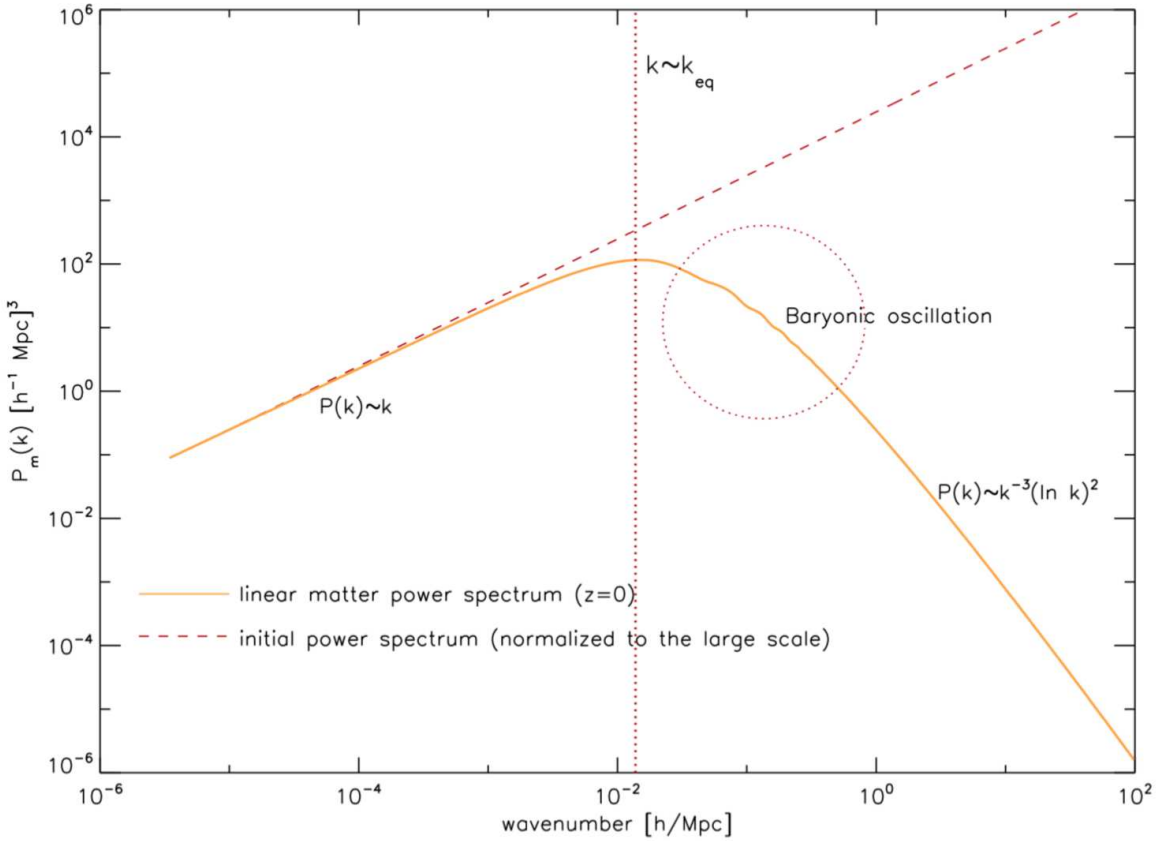

Figure 44 – Scale-invariant power spectrum spectrum and its suppression due to the matter content.

6.5.3 The mass variance of the matter clustering and σ_8 tension

The root mean square (rms) amplitude of mass fluctuations inside a particular spherically-symmetric window is:

$$\sigma_R^2(z) = \frac{1}{2\pi^2}\int_0^\infty P(k,z)W_R^2(k)dk, \tag{6.121}$$

where P(k,z) is the power spectrum and $W_R(k)$ is the window function with R symbolizing a physical scale. The two most popular choices for window functions are the real-space spherical top-hat of radius R:

$$W_R(k) = \frac{3}{(kR)^3}\left[\sin(kR) - kR\cos(kR)\right] \tag{6.122}$$

$$M_R = \frac{4\pi}{3}\rho_c\Omega_0 R^3 \tag{6.123}$$

and the Gaussian window of scale length R:

$$W_R(k) = \exp\left(-\frac{(kR)^2}{2}\right) \tag{6.124}$$

$$M_R = (2\pi)^{3/2}\,\rho_c \Omega_0 R^3 \tag{6.125}$$

where M_R is the mass included in the window. One can write the equation (6.126) as:

$$\sigma_R^2(z) = D^2(z)\sigma_R^2(z=0) \tag{6.126}$$

assuming the normalization $D(z=0)=1$ for the linear growth function $D(z)$ [345]. From the analyses of diverse cosmological tracers it is common to perform the measurements at scales of $R = 8Mpc/h$, that is, $\sigma_{8,0} \equiv \sigma_8(z=0)$.

The standard Λ Cold Dark Matter cosmological model provides an amazing fit to current cosmological data. However, some statistically-significant tensions in cosmological parameter estimations emerged between the Planck experiment, measuring the Cosmic Microwave Background (CMB) anisotropies, and other low-redshift cosmological probes. In addition to the long standing Hubble constant H_0 disagreement, which we analyze in the chapter 2, a tension of the Planck data with weak lensing measurements and redshift surveys has been reported, about the value of the matter energy density Ω_m, and the amplitude or rate of growth of structure $(\sigma_8, f\sigma_8)$, where is the growth rate, which represents a measure of the matter clustering evolution from the primordial density fluctuations to the large-scale structures observed today. Although this tension could be due to systematic errors, it is worthwhile to investigate the possibility of new physics beyond the standard model. The tension can be visualized in the σ_8 vs Ω_m plane (see Fig. 45), and is often quantified using the following parameter:

$$S_8 \equiv \sigma_8\sqrt{\frac{\Omega_m}{0.3}}, \tag{6.127}$$

along the main degeneracy direction of weak lensing measurements. This can be also related to $f\sigma_8(z=0)$, measured by galaxy redshift space distortions (RSD) [346, 347], where $f = [\Omega_m(z)]^{0.55}$ approximates the growth rate.

The mismatch between the high S_8 value estimated by Planck assuming ΛCDM (grey contour in Fig. 45), $S_8 = 0.834 \pm 0.016$, and the lower value preferred by cosmic shear measurements, it is known as the S_8 tension. This tension is above the 2σ level with KiDS-450 [349–352] ($S_8 = 0.745 \pm 0.039$) and KiDS-450+2dFLenS [353] ($S_8 = 0.742 \pm 0.035$),

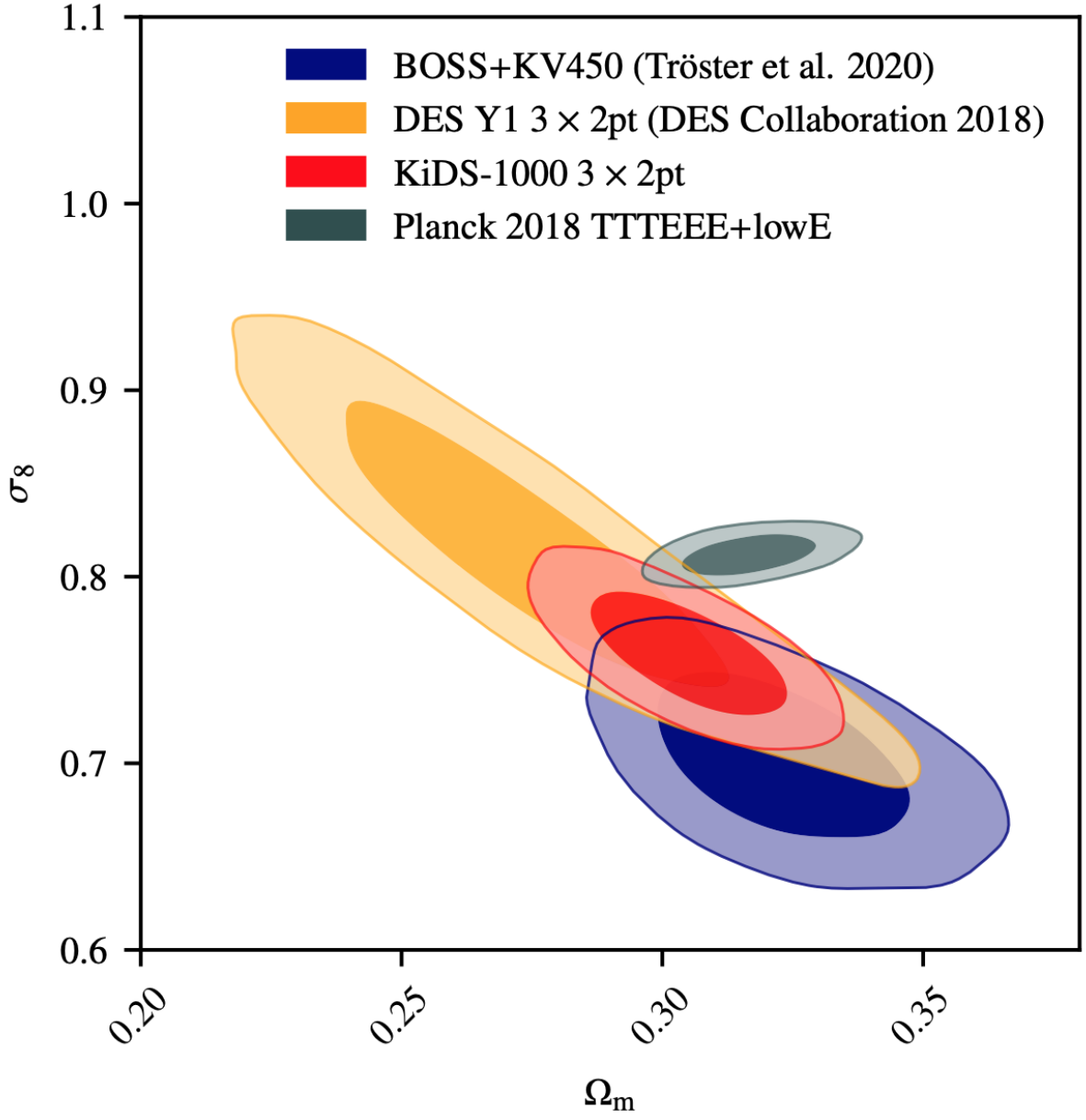

Figure 45 – 68% CL and 95% CL contour plots for σ_8 and Ω_m(from Ref. [348]).

with KiDS+VIKING-450 (KV450) [354] ($S_8 = 0.737^{+0.040}_{-0.036}$), with DES [355, 356] ($S_8 = 0.783^{+0.021}_{-0.025}$), and with CFHTLenS [357–359]. Recently, KiDS-1000 [348] reported a $\sim 3\sigma$ tension ($S_8 = 0.766^{+0.020}_{-0.014}$, red contour in Fig. 45) with Planck. This is already obvious from cosmic shear alone [360], but when combined with galaxy clustering, the degeneracy breaking between σ_8 and Ω_m does not change the tension level. Therefore, the combined analysis helps in pointing out that the tension, at 3.1σ in this case, is driven by σ_8 rather than Ω_m. In addition, there is the Lyman-α result [361], a late time probe probing scales similar to weak lensing, completely in agreement with a lower S_8 value and in tension at $\sim 2.6\sigma$ with Planck. The tension becomes 3.2σ if we consider the combination of KV450 and DES-Y1 [362, 363] or 3.4σ for BOSS+KV450 [364] ($S_8 = 0.728 \pm 0.026$, blue contour in Fig. 45). Preferring a higher value for the S_8 parameter there is also the measurement from the first-year data of HSC SSP [365], for which $S_8 = 0.804^{+0.032}_{-0.029}$ (see Fig. 46), but also KiDS-450+GAMA [366] finding $S_8 = 0.800^{+0.029}_{-0.027}$. Finally, in agreement with a lower value $S_8 = 0.703 \pm 0.045$ there is an estimate from the BOSS Galaxy Power Spectrum [367]. It has been pointed out in [368] that this tension could be related to the excess of lensing measured by Planck, mimicking a larger S_8. However, also ACT+WMAP [369] find a large $S_8 = 0.840 \pm 0.030$ even if it does not see a peculiar value for the lensing amplitude, while SPTpol [370] and the Planck CMB lensing [371] measurements prefer a lower value. Another possibility is the misuse of the units h^{-1}Mpc in observational cosmology in [372]. It might be worth mentioning that, while weak lensing analyses are carried out with a blinding procedure for KiDS, DES and HSC, the CMB analyses are either not blind or only partially blind. The H_0 disagreement is correlated to the σ_8 problem, indeed the solutions proposed to alleviate the first one, are exacerbating the CMB tension with the lower σ_8 values obtained from more direct measurements, such as galaxy clusters using the Sunyaev-Zel'dovich effect [373–375], i.e. measuring the number of clusters of a certain mass M over a range of redshift.

For example, late time transitions preferring a higher H_0 value, if they match the CMB data, prefer a lower Ω_m as well, to preserve the well measured value of $\Omega_m h^2$, known as geometric degeneracy. This effect produces a modification of distances to sources, the growth of structure, and of the sound horizon and CMB anisotropies [376], and usually results in higher σ_8 than for ΛCDM because of an extended era of matter domination. However, also early-time dark energy solutions of the H_0 tension increase σ_8 because they need a higher primordial curvature perturbation amplitude to offset the damping effect of the unclustered component. Therefore, because of the mutual effects and correlations, it is important to perform a conjoined analysis, fitting with a single model a full array of data [377–380], and not just one parameter alone. At the same time, if a model solves the S_8 tension (the $z = 0$ value), the growth history at different redshift, by plotting $f\sigma_8(z)$ directly against $H(z)$, should be checked [381, 382], because conjoint history can deviate significantly at intermediate scales. Hence, any solution to the S_8 tension should

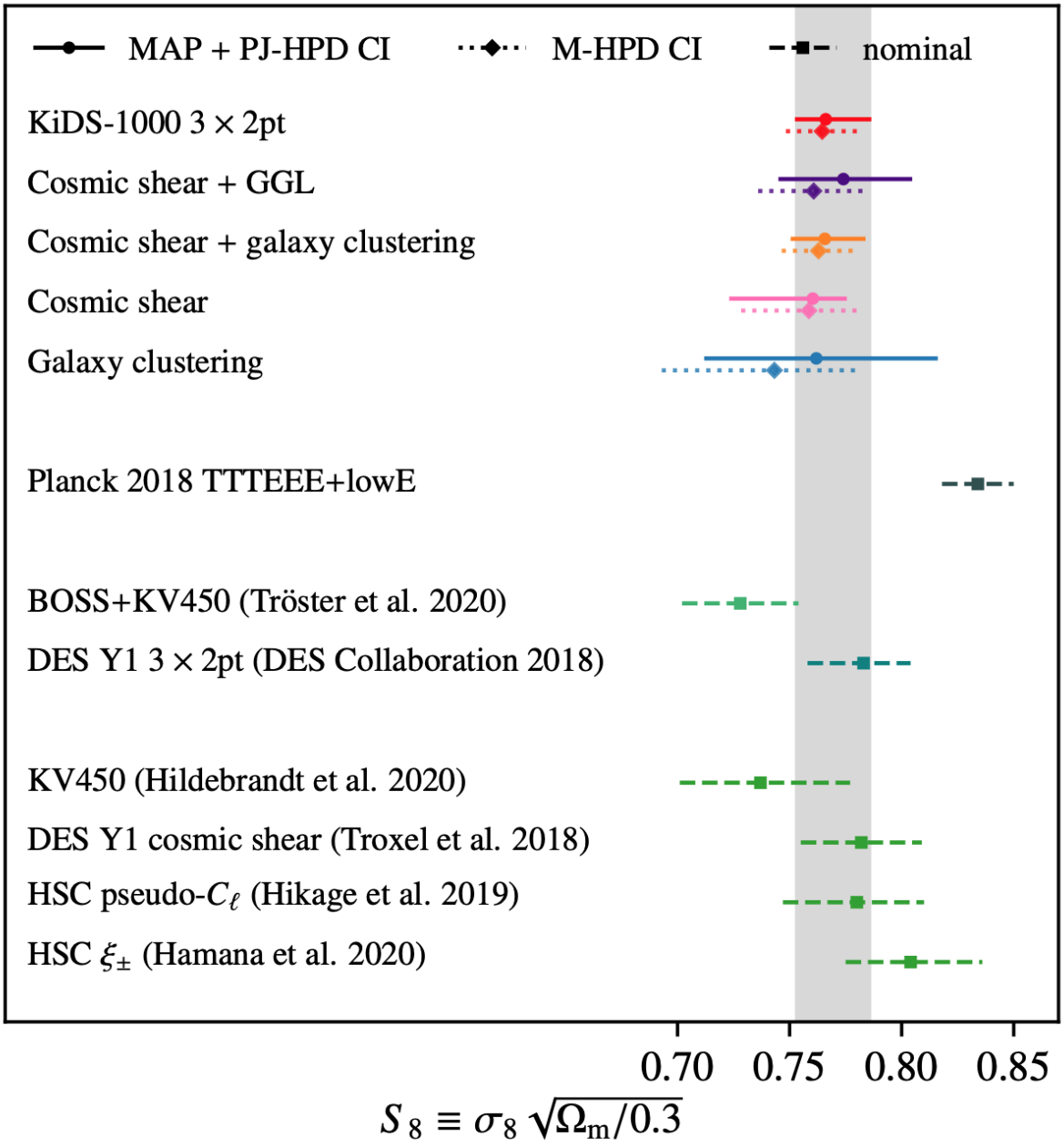

Figure 46 – Whisker plot showing the 68% error bars on S_8 (from Ref. [348]).

pass other cosmological tests, i.e. it should simultaneously fit the expansion and growth histories probed by Baryon Acoustic Oscillations (BAO), RSD-lensing cross correlations, galaxy power spectrum shape and void measurements [383].

There are many papers investigating this tension [368, 372, 384–414], but the solutions proposed are not enough to put in agreement all the cosmological available data [415–417]. We can distinguish the following categories:

- Axion monodromy inflation [404].
- Extended parameter spaces [368, 385, 386, 388, 389] with $A_L > 1$ [418], i.e. using the phenomenological lensing parameter as a consistency check and determining whether it is different from unity [453].
- Active and Sterile Neutrinos [402, 403].
- Interacting dark energy models, where the energy flows from the dark matter to the dark energy [390, 391].
- Decaying dark matter [410, 411, 420, 421], or Cannibal dark matter [412].
- Minimally and non-minimally coupled scalar field models as possible alternatives for dark energy [398].
- Modified Gravity models [399, 400, 422, 423].
- Running vacuum models in which $\Lambda = \Lambda(H)$ is an affine power-law function of the Hubble rate [392, 393, 424–429].
- Quartessence, a single dark component mimicking both dark matter and dark energy [395].

Along with the above possibilities to resolve this tension, I will present the possibility of using lepton asymmetry in order to resolve it, since this introduces new relativistic degrees of freedom, which increases the radiation energy density in the early universe. So in this way I will show in the Chapter 7, that we can alleviate the tension of σ_8 and H_0.

6.6. Massive neutrino impact on the power spectrum

Standard Model neutrinos are initially relativistic, following a thermal distribution after decoupling from the primordial plasma when the Universe had a temperature of around $k_B T \approx 1 MeV$. The neutrino temperature decreases as the scale factor grows, until their rest-mass energy dominates and they become indistinguishable from cold dark matter. For a neutrino of mass m_ν the transition occurs at:

$$1 + z \approx 1987 \left(\frac{m_\nu}{1eV} \right), \tag{6.128}$$

so current limits indicate a transition epoch of $120 \leq z \leq 460$ for a normal mass hierarchy.

This limit implies that the neutrinos were still relativistic when the CMB decoupled, so they would be indistinguishable from massless neutrinos in the primary anisotropies. However, higher mass neutrinos become non-relativistic sooner, which reduces the early-time Integrated Sachs-Wolfe (ISW) effect. This gravitational redshift of the CMB photons arises while the non-negligible radiation component causes the potentials of the density fluctuations to evolve and affects the anisotropies on scales around the first acoustic peak. This effect is not sensitive to masses which remain relativistic until well after decoupling, but further information comes from probes of later-time large scale structure (LSS) measurements. Massive neutrinos interact weakly, allowing them to free-stream out of overdensities while relativistic, so the growth rate of matter perturbations inside the horizon is suppressed compared to a universe with only cold dark matter. For comoving wavenumbers $k \gg k_{fs}$, Hu et al. [430] show that the suppression of the matter power spectrum today, $P(k)$, is proportional to the sum of the neutrino masses:

$$\frac{P_{\sum m_\nu}(k) - P_{\sum m_\nu=0}(k)}{P_{\sum m_\nu=0}(k)} \approx -0.07 \left(\frac{\sum m_\nu}{0.1eV}\right) \left(\frac{\Omega_m h^2}{0.136}\right)^{-1}, \tag{6.129}$$

where the comoving free-streaming scale is given by

$$k_{fs} = 0.0072 \left(\frac{\sum m_\nu}{0.1eV}\right)^{1/2} \left(\frac{\Omega_m}{0.135}\right)^{1/2} h \quad Mpc^{-1}, \tag{6.130}$$

as illustrated in Fig. 47. For current limits this scale is estimated to lie in the range $0.005 \lesssim k_{fs} \lesssim 0.011$. The suppression of small-scale power can be probed using galaxy clustering and the gravitational lensing of galaxies. These are promising avenues for neutrino mass measurements, although these observables are sensitive to non-linearities in the matter power spectrum and scale-dependent galaxy and shape biases. An alternative route is through the gravitational lensing of the CMB. Here the CMB photons are deflected by the large-scale structure, integrated over the photon path since decoupling.

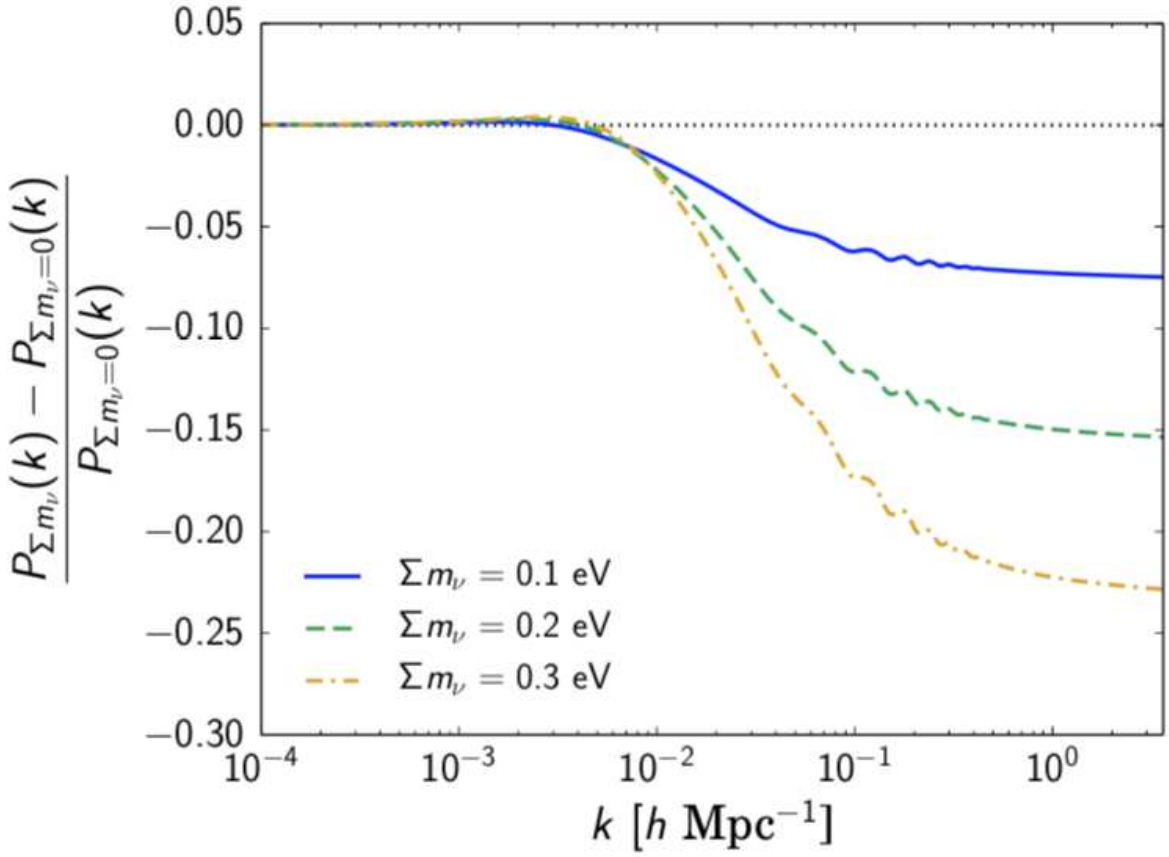

Figure 47 – Effect of neutrino mass on matter power spectra. Fractional change of the matter power spectrum today $P(k)$ for different mass values of the neutrinos: $\sum m_\nu = 0$ eV (black dotted line), $\sum m_\nu = 0.1$ eV (blue continuous line), $\sum m_\nu = 0.2$ eV (green dashed line), $\sum m_\nu = 0.3$ eV (dashed and dotted yellow line).

Chapter 7

Testing the properties of $C\nu B$ from current cosmological data

Based on: "**Probing the properties of relic neutrinos using the cosmic microwave background, the Hubble Space Telescope and galaxy clusters**", on.Not.Roy.Astron.Soc. 473 (2018) 4, 4404-4409.[1]

7.1. Main physical properties of $C\nu B$ from de current data

The total radiation density energy can be parametrized (when the neutrinos are relativistic) by

$$\rho_r = \left[1 + \frac{7}{8}\left(\frac{4}{11}\right)^{4/3} N_{\rm eff}\right]\rho_\gamma, \tag{7.1}$$

where the factor 7/8 appears because neutrinos are fermions. Neutrinos become non-relativistic when their average momentum falls below their mass. In section 4.4.2, I presented a brief description of the massive degenerate neutrinos. Some approximations for massive neutrino have been discussed in the literature [223, 227–229]. Here, let us follow the methodology and notation of [230], where an extension of the ultrarelativistic fluid approximation is presented. Within the fluid approximation, the continuity, Euler, and shear equations, in the synchronous gauge, are given by

$$\dot{\delta}_\nu = -(1+w_\nu)\left(\theta_\nu + \frac{\dot{h}}{2}\right) - 3\frac{\dot{a}}{a}(c^2_{\rm eff} - w_\nu)\delta_\nu + 9\left(\frac{\dot{a}}{a}\right)^2(1+w_\nu)(c^2_{\rm eff} - c^2_g)\frac{\theta_\nu}{k^2}, \tag{7.2}$$

[1] https://academic.oup.com/mnras/article/473/4/4404/4643131

$$\dot{\theta}_\nu = -\frac{\dot{a}}{a}(1-3c^2_{\rm eff})\theta_\nu + \frac{c^2_{\rm eff}}{1+w_\nu}k^2\delta - k^2\sigma_\nu, \tag{7.3}$$

and

$$\dot{\sigma}_\nu = -3\Big(\frac{1}{\tau} + \frac{\dot{a}}{a}\Big[\frac{2}{3} - c_g^2 - \frac{p_{pseudo}}{3p}\Big]\Big)\sigma_\nu + \frac{8}{3}\frac{c^2_{\rm vis}}{1+w_\nu}\Big[\theta_\nu + \dot{h}\Big]. \tag{7.4}$$

In equations (7.2)-(7.4), $w_\nu = p_\nu/\rho_\nu$ (which starts with $w_\nu = 1/3$ at early times and drops to $w_\nu \simeq 0$ when neutrinos become nonrelativistic), $c^2_{\rm vis} = 3w_\nu c_g^2$ and

$$c_g^2 = \frac{w_\nu}{3+3w_\nu}\Big(5 - \frac{p_{pseudo}}{p}\Big), \tag{7.5}$$

where the quantity p_{pseudo} is the so-called the pseudo-pressure. See [230] and [222] for details of the Boltzmann hierarchy. In the application of the eqs. (7.2)-(7.4), we consider three active neutrinos: one massive neutrino ν_1 and two massless neutrinos ν_2 and ν_3, which is standard practice in the literature. Because here we have the standard ΛCDM scenario, the baryons, cold dark matter, and photons follow the standard evolution (both at the background and perturbation levels).

7.2. Models and data analysis

We consider two different models. First, let us take ΛCDM + $N_{\rm eff}$ + $\sum m_\nu$ + $c^2_{\rm eff}$ + $c^2_{\rm vis}$ + ξ (**Model I**). Then, we take a particular case of the Model I when $c^2_{\rm eff} = c^2_{\rm vis} = 1/3$, i.e., ΛCDM + $N_{\rm eff}$ + $\sum m_\nu$ + ξ (**Model II**). Following the *Planck* collaboration, we fix the mass ordering of the active neutrinos to the normal hierarchy with the minimum masses allowed by oscillation experiments, i.e., $\sum m_\nu = 0.06$ eV. In this work, we consider one massive neutrino flavour ν_1 and two massless flavours ν_2, ν_3 with degeneracy parameter $\xi_\nu = \xi_{\nu 1} = \xi_{\nu 2} = \xi_{\nu 3}$. In order to constrain the free parameters of the models, we consider the following data sets:

CMB: We consider a conservative data set from *Planck* 2015 comprised of the likelihoods of temperature power spectrum (TT), low-polarisation and lensing reconstruction.

BAO: The BAO measurements from the Six Degree Field Galaxy Survey (6dF) [231], the Main Galaxy Sample of Data Release 7 of Sloan Digital Sky Survey (SDSS-MGS) [232], the LOWZ and CMASS galaxy samples of the Baryon Oscillation Spectroscopic Survey (BOSS-LOWZ and BOSS-CMASS, respectively) [233], and the distribution of the

Table 6 – Cluster abundance measurements given in terms of S_8 included in our analysis.

Type	α	β	Measurement	Reference
Number counts	1.0	0.5	0.465 ± 0.03	[238]
Number counts	0.25	0.41	0.832 ± 0.03	[239]
X-ray counts	0.32	0.30	0.86 ± 0.04	[240]
Sunyaev-Zeldovich effect	0.25	0.298	0.785 ± 0.037	[241]
X-ray cross CMB	0.30	0.26	0.80 ± 0.02	[242]
X-ray luminosities	0.30	0.25	0.80 ± 0.04	[243]
Sunyaev-Zeldovich effect	0.27	0.301	0.782 ± 0.01	[244]
X-ray masses	0.25	0.47	0.813 ± 0.013	[245]
Tomographic weak lensing	0.27	0.46	0.774 ± 0.040	[246]

LymanForest in BOSS (BOSS-Ly) [234]. These data points are summarized in table I of [235].

HST: We include the new local value of Hubble constant, $H_0 = 73.02 \pm 1.79$ km/s/Mpc as measured by [305] with a 2.4 per cent determination.

GC: The measurements from the abundance of GCs are a powerful probe of the growth of cosmic structures. However, this cosmological test depends on the calibration of the mass-observable relation, which can represents uncertainty in the measure of clusters samples properties. It is well known that cluster data are in tension with CMB data up to 95 per cent CL, especially when taking into account contributions due to non-linear scales. In orden to explore the full GC counts as a cosmological probe, it is necessary to take into account the modelling the number of haloes within a redshift and mass bin, for example. This modelling is hard and expensive to perform. However, the cosmological information enclosed in the cluster abundance is efficiently parametrized by $S_8 = \sigma_8(\Omega_m/\alpha)^\beta$, where σ_8 is the linear amplitude of fluctuations on 8 Mpc/h scale and α and β are the fiducial value adopted in each survey analysis. It can be an exhausting task to analyze different clusters samples in order to verify possible systematic effects that might exist in each survey. [237] show that cluster abundance (from the full expression) carries less information about geometry parameters than about growth of structures (to constrain the growth parameters). This consideration justifies the choice of using CG data in the plan S_8, which also minimizes the computational cost. This methodology was also recently adopted by [236]. Table 6 summarizes the measures of S_8 used in this work.

We use the publicly available CLASS [269] and Monte Python [266] codes for constraining parameters of the models considered in the present work. We use Metropolis Hastings algorithm with uniform priors on the model parameters to obtain correlated Markov Chain Monte Carlo samples by considering two combinations of data sets: CMB + BAO + *HST* and CMB + BAO + *HST* + GC. All the parameter chains in our analysis converge according to the Gelman-Rubin criteria $1 - R < 0.01$ [247].

Table 7 – Constraints at 68 and 95 per cent CLs on some parameters of the Model I. The parameter H_0 is in the units of km s^{-1} Mpc^{-1} and $\sum m_\nu$ is in units of eV.

Parameter	CMB + BAO + H_0	CMB + BAO + H_0 + GC
$\sum m_\nu$	$< 0.24\,(< 0.36)$	$< 0.64\,(< 0.81)$
$c^2_{\rm vis}$	$0.63^{+0.17+0.32}_{-0.17-0.32}$	$0.58^{+0.22+0.40}_{-0.25-0.40}$
$c^2_{\rm eff}$	$0.311^{+0.012+0.028}_{-0.015-0.027}$	$0.319^{+0.013+0.024}_{-0.013-0.027}$
ξ_ν	$0.1^{+0.54+1.0}_{-0.54-1.0}$	$0.02^{+0.50+0.90}_{-0.50-0.85}$
$N_{\rm eff}$	$3.41^{+0.23\,+0.43}_{-0.23\,-0.42}$	$3.66^{+0.26\,+0.48}_{+0.26\,-0.49}$
Ω_Λ	$0.706^{+0.008+0.016}_{-0.008-0.016}$	$0.706^{+0.008+0.015}_{-0.008-0.015}$
Y_{He}	$0.2523^{+0.0029+0.0054}_{-0.0029-0.0056}$	$0.2557^{+0.0032+0.0059}_{-0.0032-0.0063}$
H_0	$69.8^{1.3+2.5}_{1.3-2.5}$	$70.7^{+1.2+2.4}_{-1.2-2.2}$
σ_8	$0.839^{+0.018+0.036}_{-0.018-0.037}$	$0.776^{+0.010+0.019}_{-0.010-0.019}$

Table 8 – Constraints at 68 and 95 per cent CLs on some parameters of the Model II. The parameter H_0 is in the units of km s^{-1} Mpc^{-1} and $\sum m_\nu$ is in units of eV.

Parameter	CMB + BAO + H_0	CMB + BAO + H_0 + GC
$\sum m_\nu$	$< 0.18\,(< 0.30)$	$< 0.52\,(< 0.64)$
ξ_ν	$0.05^{+0.56+0.97}_{-0.56-0.99}$	$-0.02^{+0.51+0.92}_{-0.51-0.89}$
$N_{\rm eff}$	$3.49^{+0.21\,+0.44}_{-0.23\,-0.42}$	$3.65^{+0.28\,+0.57}_{-0.28\,-0.60}$
Ω_Λ	$0.703^{+0.009+0.015}_{-0.008-0.016}$	$0.706^{+0.008+0.015}_{-0.008-0.016}$
Y_{He}	$0.2537^{+0.0028+0.0056}_{-0.0028-0.0056}$	$0.2557^{+0.0038+0.0071}_{-0.0032-0.0077}$
H_0	$70.5^{+1.3+2.7}_{-1.3-2.6}$	$71.2^{+1.4+2.6}_{-1.4-2.7}$
σ_8	$0.823^{+0.016+0.030}_{+0.014-0.032}$	$0.777^{+0.010+0.020}_{-0.010-0.019}$

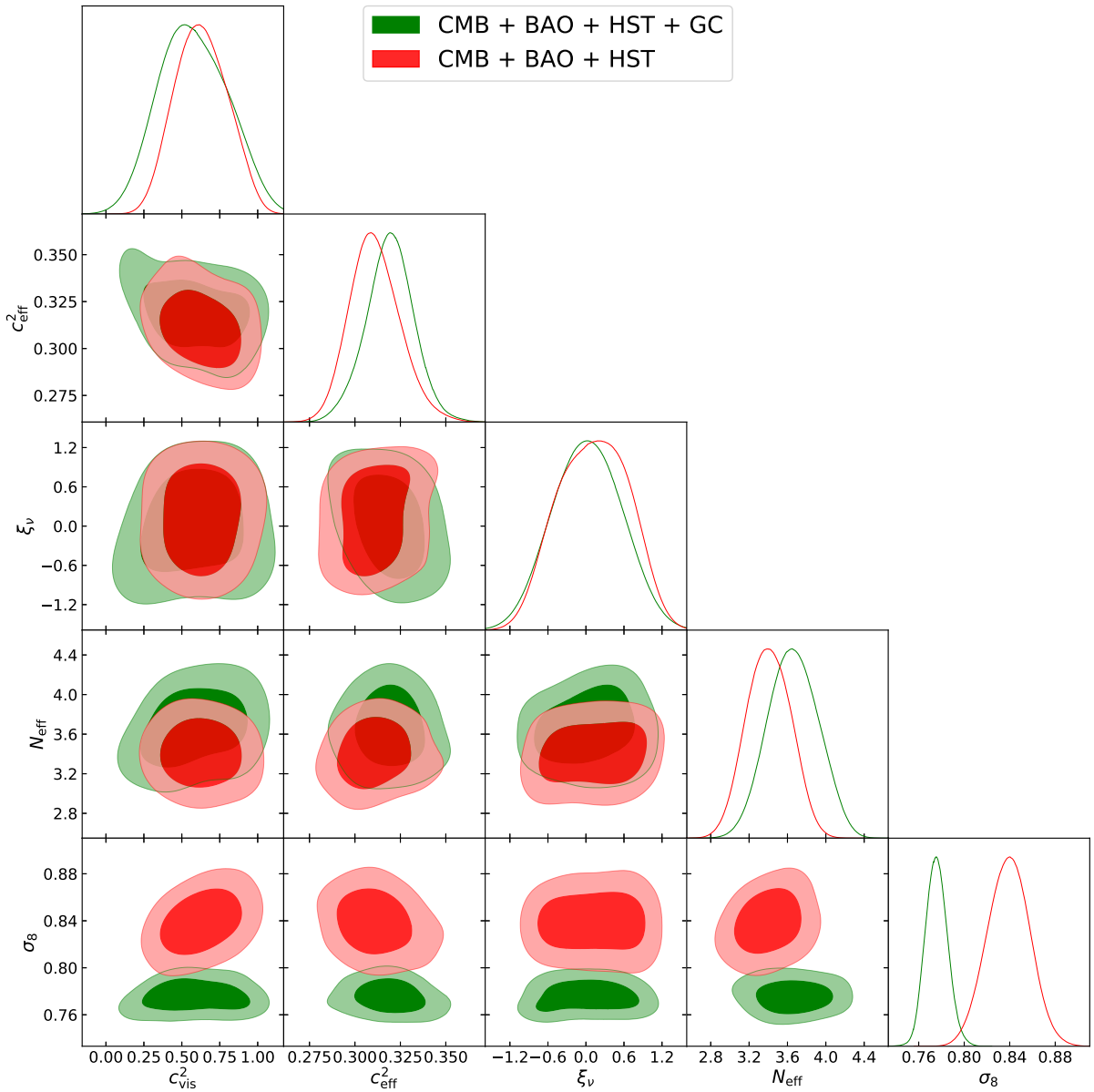

Figure 48 – One-dimensional marginalized distribution and 68 and 95 per cent CLs regions for some selected parameters of the Model I.

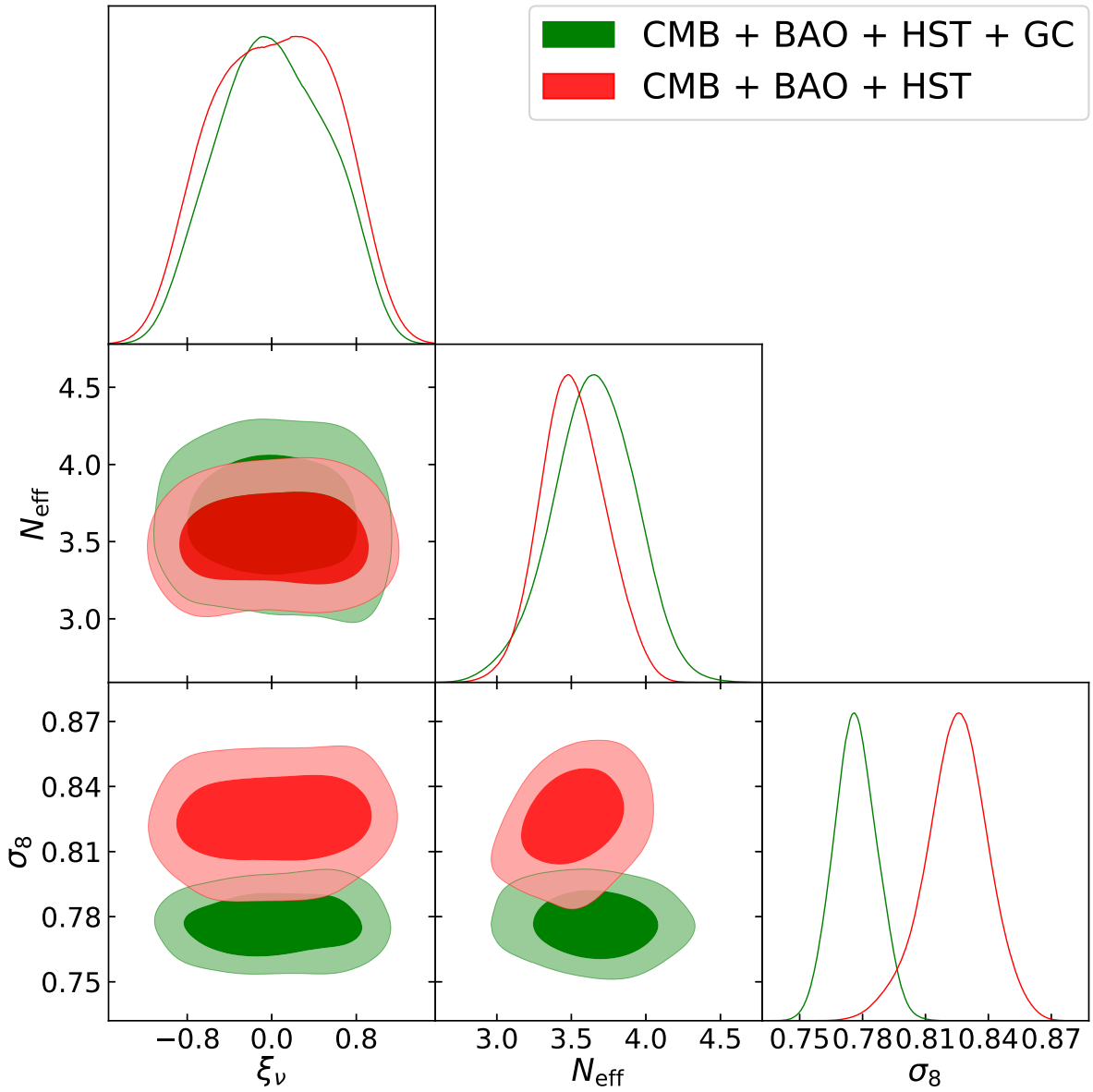

Figure 49 – One-dimensional marginalized distribution and 68 per cent CL and 95 per cent CL regions for some selected parameters of the Model II.

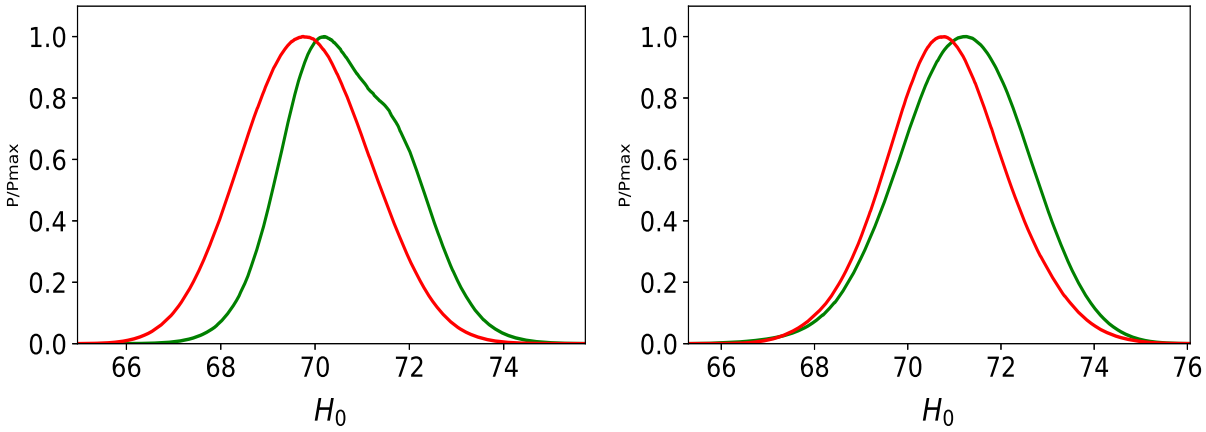

Figure 50 – The likelihoods of the parameter H_0 for Model I (left panel) and Model II (right panel), in red (CMB + BAO + *HST*) and green (CMB + BAO + *HST* + GC).

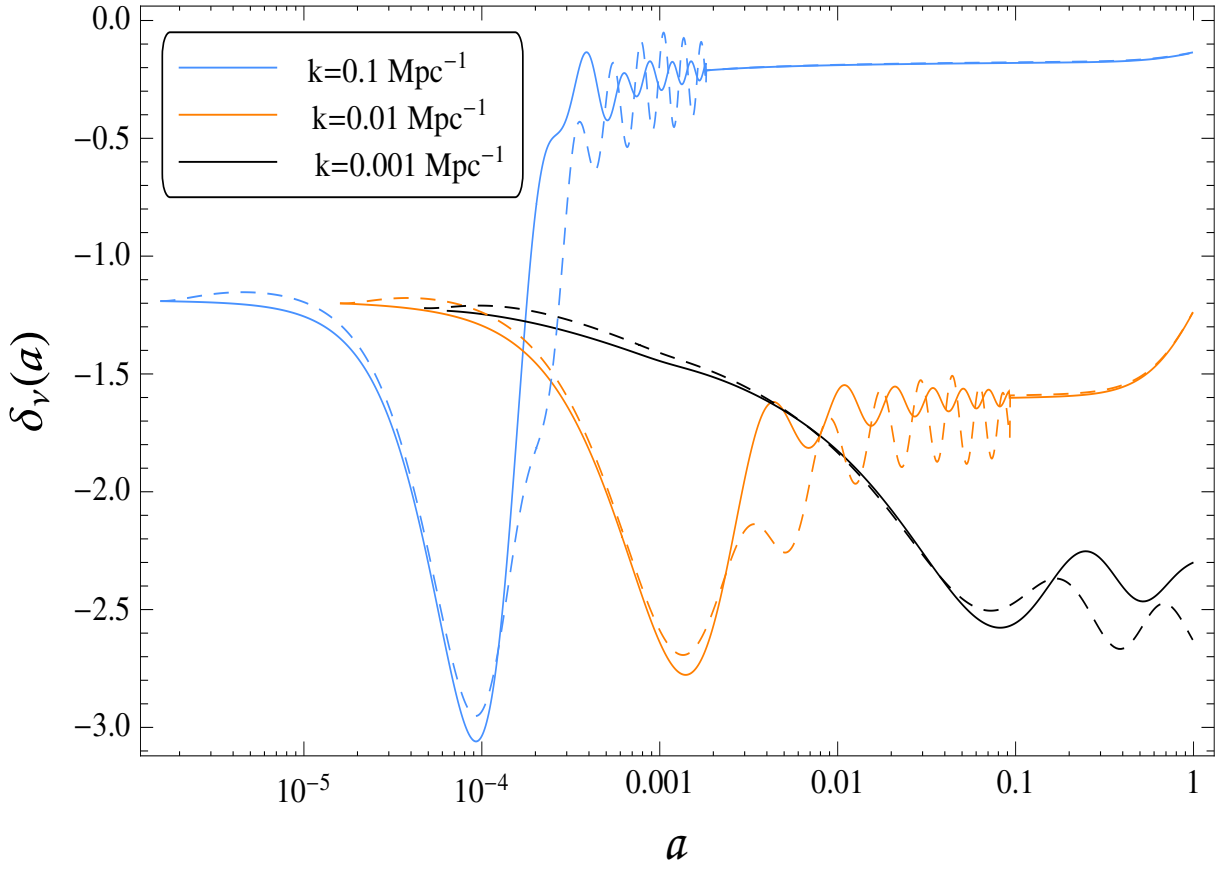

Figure 51 – Neutrino density perturbations as a function of scale factor for three fixed scales, $k = 0.001$ Mpc^{-1}, 0.01 Mpc^{-1} and 0.1 Mpc^{-1}. In drawing the graphs we have taken the best fit values from our analysis. The continuous and dashed line represent the models I and II from CMB + BAO + *HST* + GC, respectively.

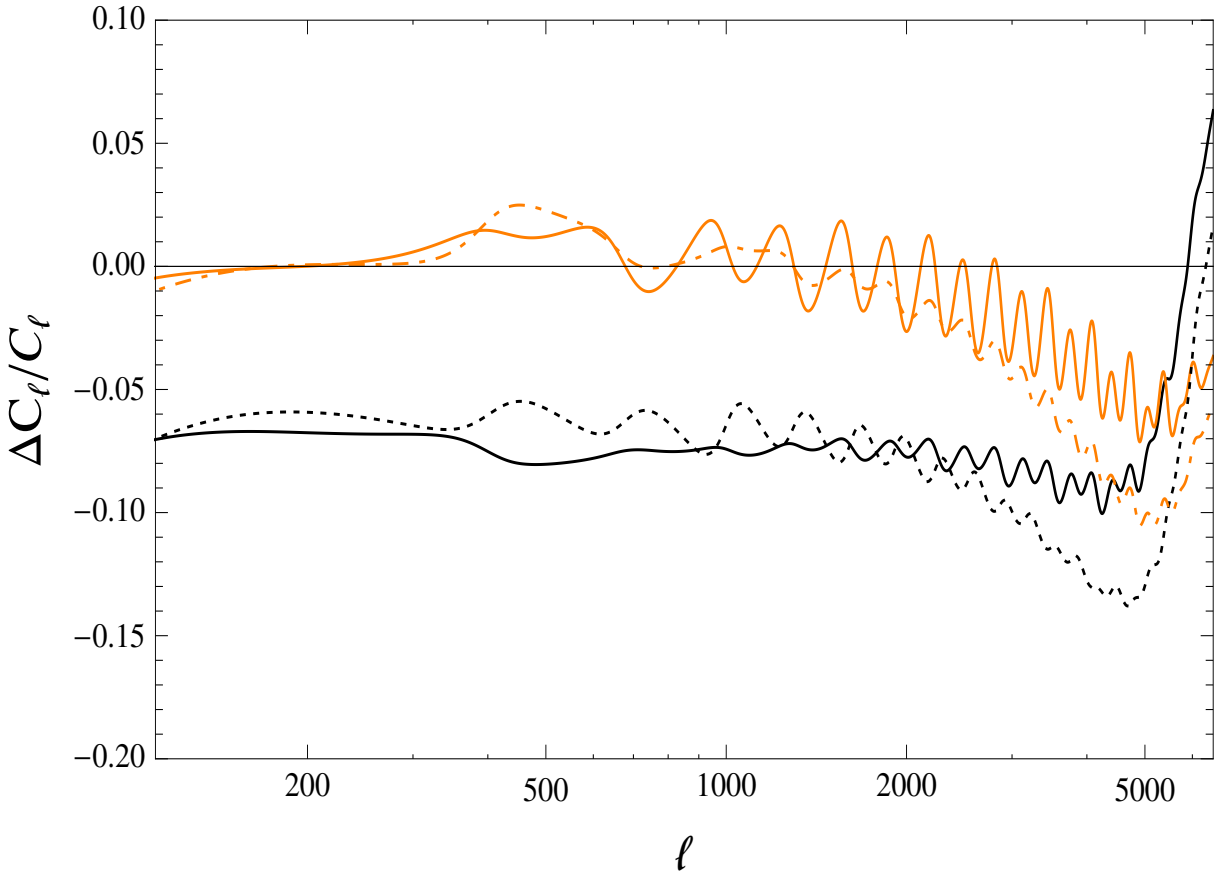

Figure 52 – CMB temperature power spectrum difference among the models investigated here and the six parameter ΛCDM model, i.e., $\Delta C_l/C_l = (C_l^{\Lambda CDM\ extended} - C_l^{\Lambda CDM\ Planck\ 2015})/C_l^{\Lambda CDM\ Planck\ 2015}$. The black continuous and dotted lines represent the Model II from CMB + BAO + *HST* and CMB + BAO + *HST* + GC, respectively. The orange continuous and dotted lines represent the Model I from CMB + BAO + *HST*and CMB + BAO + *HST* + GC, respectively. In drawing the graphs we have taken the best fit values from our analysis and Planck collaboration paper.

7.3. Probing the properties of relic neutrinos

Table 7 summarizes the main results of the statistical analysis carried out using two different combinations for the Model I, CMB + BAO + *HST* and CMB + BAO + *HST* + GC. Fig. 48 shows the parametric space for some parameters of the Model I and its correlations. In both cases, we do not notice significant changes in the parameters ξ_ν and $c^2_{\rm eff}$ from standard prevision, i.e., $(\xi_\nu, c^2_{\rm eff}) = (0, 1/3)$. We note a small deviation on the viscosity parameter, $c^2_{\rm eff} \neq 1/3$, at 68 per cent CL in both analysis. Any value besides $c^2_{\rm eff} = 1/3$ can be interpreted as an explicit coupling of the relativistic neutrino (or some dark radiation) to a nonrelativistic particle species, e.g, cold dark matter [216, 248–250]. In general terms, the presence of a dark radiation-dark matter interaction, the clustering properties of the dark radiation can be modified (see [216, 248–250] and references therein). That is, if dark radiation is composed of interacting particles, the values of the parameters

$c^2_{\rm eff}$ and $c^2_{\rm vis}$ can differ from the usual ones. In this present work, we report that sound speed in the CνB rest frame is closed in the standard value, that is, $c^2_{\rm eff} = 1/3$ and $c^2_{\rm vis} \neq 1/3$ at 68 per cent CL, in both analysis. In the standard scenario (three active neutrinos and considering effects related to non-instantaneous neutrino decoupling), we have $N_{\rm eff} \simeq 3.046$. As previously introduced, the presence of a dark radiation is usually parametrized in the literature by $\Delta N_{\rm eff} \simeq N_{\rm eff} - 3.046$. From our results, we can note a small excess over $N_{\rm eff}$. More specifically, we have $\Delta N_{\rm eff} \simeq 0.364\,(0.614)$ from the best-fitting values for CMB + BAO + *HST* (CMB + BAO + *HST* + GC). When evaluated the border at 95 per cent CL, we note $\Delta N_{\rm eff} < 0.794\,(1.09)$ from CMB + BAO + *HST* (CMB + BAO + *HST* + GC. There are many candidates for dark radiation, for instance, sterile neutrinos [251], thermal axions [252] and Goldstone bosons [253]. We can note that the constraints for $\Delta N_{\rm eff}$ is consistent with a partly thermalized sterile neutrino or a Goldstone boson from CMB + BAO + *HST*+ GC (best fit) and CMB + BAO + *HST* (border 95 per cent CL). A fully thermalized sterile neutrino is consistent at 95 per cent CL from CMB + BAO + *HST* + GC. About the neutrino mass scale, we have $\sum m_\nu < 0.36$ eV (< 0.81 eV) at 95 per cent CL from CMB + BAO + *HST* (CMB + BAO + *HST* + GC). We see a variation around 0.45 eV when the GC data are added.

Table 12 summarizes the main results of the statistical analysis carried out using two different combinations for the Model II, CMB + BAO + *HST* and CMB + BAO + *HST* + GC. Fig. 49 shows the parametric space for some parameters of the Model II. In both analysis, we do not observe significant deviation of the degeneracy parameter ξ_ν from the null value. However, in Model II, a small variation on $\Delta N_{\rm eff}$ can be noticed compared to the Model I. We have $\Delta N_{\rm eff} \simeq 0.454\,(0.604)$ from CMB + BAO + *HST* (CMB + BAO + *HST* + GC), respectively. A border at 95 per cent CL reads $\Delta N_{\rm eff} < 0.884\,(< 1.17)$ for CMB + BAO + *HST* (CMB + BAO + *HST* + GC). Here, a partly thermalized sterile neutrino or a Goldstone boson can be accommodated in both analyzes. Within the context of the Model II, when the GC data is added to CMB + BAO + *HST*, we have a variation of around 0.34 eV on the neutrino mass scale. The correlation between the extra relativistic degrees of freedom and the Hubble constant H_0 is well known. Within the standard ΛCDM baseline, the *Planck* collaboration [213] measured $H_0 = 67.27 \pm 0.66$ km s^{-1} Mpc^{-1}, that is about 99 per cent CL deviations away from the locally measured value $H_0 = 73.24 \pm 1.74$ km s^{-1} Mpc^{-1}, reported in [305]. The left panel of Fig. 50 showsl the likelihoods for H_0 resulting from the two cases analysed here. Changes in the central value of H_0 are not observed, and both cases return very similar fits with $H_0 \simeq 70$ km s^{-1} Mpc^{-1}. That intermediate value in comparison with the local and global constraints can assuage the current tension on the Hubble constant. In our analysis, we are take ξ_ν as a free parameter (see i.e. Fig. 53). In addition to interpreting $\Delta N_{\rm eff}$ only as a contribution due a some dark radiation, it is well known that the impact of the leptonic asymmetry increases the radiation energy density. Assuming three neutrino species with degenerated

chemical potential ξ_ν, we can write

$$\Delta N_{\rm eff} = \Delta N^{\xi}_{\rm eff} + \Delta N^{\rm dr}_{\rm eff}, \tag{7.6}$$

where $\Delta N^{\xi}_{\rm eff}$, $\Delta N^{\rm dr}_{\rm eff}$ represents the contribution from the cosmological lepton asymmetry and dark radiation, respectively. The increase via the leptonic asymmetry can be parametrized by

$$\Delta N^{\xi}_{\rm eff} = \frac{90}{7}\left(\frac{\xi_\nu}{\pi}\right)^2 + \frac{45}{7}\left(\frac{\xi_\nu}{\pi}\right)^4. \tag{7.7}$$

It is important to make clear that in all analyses, we are taking $N_{\rm eff}$ as free parameter, and we do not directly evaluating $\Delta N_{\rm eff}$ in our chains. Without loss of generality, we can evaluate the contribution in equation (7.7) via the standard error propagation theory. We note, $\Delta N^{\xi}_{\rm eff} = 0.013 \pm 0.261\,(0.0005 \pm 0.044)$ for the Model I from CMB + BAO + *HST* (CMB + BAO + *HST*+ GC). For the Model II, we have $\Delta N^{\xi}_{\rm eff} = 0.0032 \pm 0.127\,(0.00052 \pm 0.046)$ for CMB + BAO + *HST* (CMB + BAO + *HST* + GC). Therefore, in general, from our analysis we can claim that the contribution from $\Delta N^{\xi}_{\rm eff}$ is very small, i.e., $\Delta N^{\xi}_{\rm eff} \ll \Delta N^{\rm dr}_{\rm eff}$ and $\Delta N_{\rm eff} \simeq \Delta N^{\rm dr}_{\rm eff}$. Fig. 51 (left panel) shows the linear neutrino perturbations as a function of the scale factor for three different scales. The solid and dashed lines represent models I, II, respectively, using the best fit from CMB + BAO + *HST* + GC. Having an account of the physical variation of Model I ($c^2_{\rm eff}$ and $c^2_{\rm vis}$ from the best fit in table II) to Model II ($c^2_{\rm eff} = c^2_{\rm vis} = 1/3$), this causes a very small change in the amplitude and phase of the density perturbations. Variation in the degeneracy parameter does not significantly affect the perturbations. In the right panel (Fig. 52), we have a comparison of the effects on CMB TT of the extended models investigated here and the six parameter ΛCDM model from *Planck* team [213]. We can see that the theoretical prediction of the Model II up to $l \lesssim 3000$ is very similar to the six parameter ΛCDM model. The Model I shows variations around 7 per cent up to the range of the *Planck* CMB TT data.

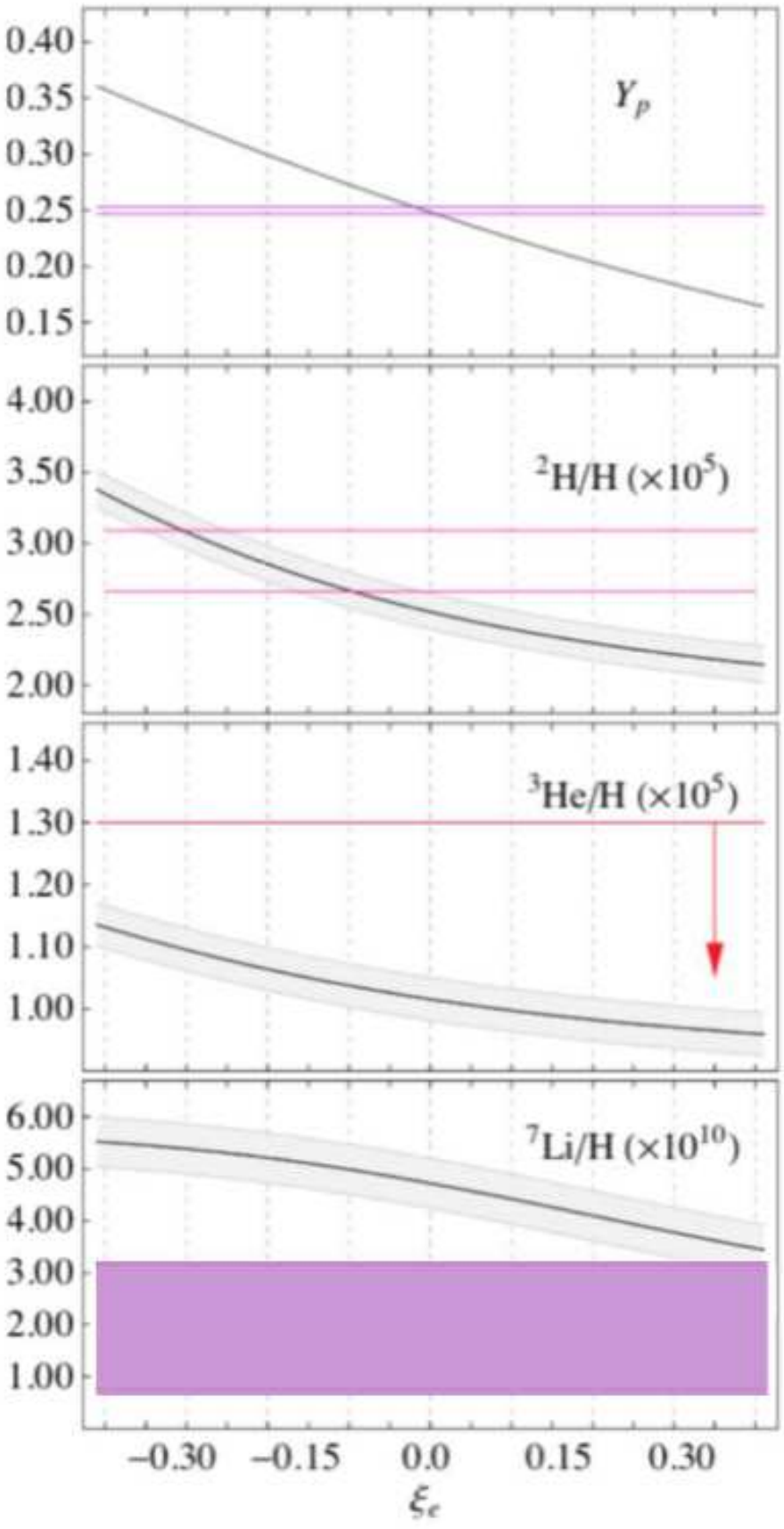

Figure 53 – Lepton asymmetry parameter vs BBN: Here we show how the lepton asymmetry parameter varies with respect to different species of baryons, linked through the Eq. (7.7)

Chapter 8

Forecast on lepton asymmetry from future CMB experiments

Based on: "**Forecast on lepton asymmetry from future CMB experiments**", Mon.Not.Roy.Astron.Soc. 485 (2019) 2, 2486-2491.[1]

8.1. Cosmological lepton asymmetry and Sakharov conditions

It is normally assumed that cosmological lepton charge asymmetry, i.e the difference between the number densities of neutrinos and antineutrinos, is vanishingly small. Of course relic neutrinos are not observed directly but the asymmetries that can be observed are very small; baryon asymmetry is $\beta_B = (n_B - n_{\bar{B}})/n_\gamma = (\text{a few}) \times 10^{-10}$ and electric asymmetry is probably exactly zero. So by analogy, the asymmetry between leptons and antileptons $\beta_L = (n_L - n_{\bar{L}})/n_\gamma$ is assumed to be also small. Moreover, there are some theoretical grounds for a small lepton asymmetry (for a review see e.g. [435]). In $SU(5)$ grand unification models the difference of leptonic and baryonic charges, $(B - L)$, is conserved, so lepton and baryon asymmetry must be the same. Even in $SO(10)$, where this conservation law is not valid, the asymmetries have similar magnitude in simple versions of the theory. Despite that, it was suggested in ref. [436] that a large lepton asymmetry together with a small baryonic one might be generated in grand unified theories. A model which permitted to realize generation of a small β_B and a much larger β_L in the frameworks of $SO(10)$-symmetry was proposed in ref. [437]. On the other hand $(B - L)$ is conserved in electroweak theory, and thus if electroweak baryogenesis is operative, then after electroweak phase transition any preexisting baryon or lepton asymmetry would be redistributed in more or less equal shares between baryons and leptons.

[1] `https://academic.oup.com/mnras/article/485/2/2486/5365435?login=false`.

Nevertheless, a few theoretical models predicting a large difference between β_B and β_L have been proposed during the past decade. To avoid electroweak "equalization" one has to assume that either generation of lepton asymmetry took place after electroweak phase transition or that the electroweak washing-out of preexisting asymmetries is not effective. A possible mechanism to suppress electroweak non-conservation of baryons and leptons is triggered by lepton asymmetry itself. As was pointed out in ref. [438] a large charge asymmetry suppresses symmetry restoration at high temperatures. The suppression of symmetry restoration or even symmetry breaking at high T, induced by large chemical potentials, was found in several papers in different theories [439,440]. It means in particular that due to this effect electroweak non-conservation of baryonic and leptonic charges in strongly asymmetric background would always be exponentially small [441]. As was shown in ref. [442] electroweak symmetry in the minimal standard model is not restored at high temperatures if $\xi_\nu = 2.5 - 5.3$ and the masses of the Higgs bosons lie in the range 100-800 GeV. Another logically possible, though rather unnatural, way to avoid contradiction with electroweak baryogenesis is to assume that the total lepton asymmetry is small,

$$\beta_L = \beta_e + \beta_\mu + \beta_\tau \sim \beta_B \approx (\text{a few} \times 10^{-10}) \tag{8.1}$$

while individual β_j could be much larger, even of the order of unity. A rather interesting argument in favor of this was found recently in ref. [443]: if electron number and lepton number are equal and opposite, then baryon asymmetry produced by electro-weak processes in the standard model is equal to the observed one within a factor of 2 and has the correct sign. A model predicting a large (even of order unity) lepton asymmetry together with a small baryonic one was proposed in refs. [435, 444] in the frameworks of Affleck and Dine baryogenesis scenario [445]. Other models in the same frameworks were suggested recently in [446, 447]. A possible way to create an overpopulated, though not necessarily asymmetric, cosmological neutrino density through decays of a heavier particle was considered in ref. [448]. A possibility of generation of a large asymmetry by active/sterile neutrino oscillations was advocated in ref. [449] and in many subsequent papers. Thus, there are plenty of mechanisms of efficient leptogenesis and it is not excluded that cosmological lepton asymmetry is large, and it is worthwhile to discuss its observational manifestations. The earlier papers on the subject are reviewed e.g. in [436].

In 1967, Andrei Sakharov proposed [450] a set of three necessary conditions that a baryon-generating interaction must satisfy to produce matter and antimatter at different rates. These conditions were inspired by the recent discoveries of the CMB and CP-violation in the neutral kaon system [451]. The three necessary "Sakharov conditions" are:

- Baryon number β violation.
- C-symmetry and CP-symmetry violation.
- Interactions out of thermal equilibrium.

Baryon number violation is a necessary condition to produce an excess of baryons over anti-baryons. But C-symmetry violation is also needed so that the interactions which produce more baryons than anti-baryons will not be counterbalanced by interactions which produce more anti-baryons than baryons. CP-symmetry violation is similarly required because otherwise equal numbers of left-handed baryons and right-handed anti-baryons would be produced, as well as equal numbers of left-handed anti-baryons and right-handed baryons. Finally, the interactions must be out of thermal equilibrium, since otherwise CPT symmetry would assure compensation between processes increasing and decreasing the baryon number. Currently, there is no experimental evidence of particle interactions where the conservation of baryon number is broken perturbatively: this would appear to suggest that all observed particle reactions have equal baryon number before and after. Mathematically, the commutator of the baryon number quantum operator with the (perturbative) Standard Model hamiltonian is zero: $[B, H] = BH - HB = 0$. However, the Standard Model is known to violate the conservation of baryon number only non-perturbatively: a global U(1) anomaly. To account for baryon violation in baryogenesis, such events (including proton decay) can occur in Grand Unification Theories (GUTs) and supersymmetric (SUSY) models via hypothetical massive bosons such as the X boson. The second condition – violation of CP-symmetry – was discovered in 1964 (direct CP-violation, that is violation of CP-symmetry in a decay process, was discovered later, in 1999). Due to CPT symmetry, violation of CP-symmetry demands violation of time inversion symmetry, or T-symmetry. In the out-of-equilibrium decay scenario, the last condition states that the rate of a reaction which generates baryon-asymmetry must be less than the rate of expansion of the universe. In this situation the particles and their corresponding antiparticles do not achieve thermal equilibrium due to rapid expansion decreasing the occurrence of pair-annihilation.

8.2. $C\nu B$ and lepton asymmetry

The current contribution of neutrinos to the energy density of the Universe is given by,

$$\rho_\nu = 10^4 h^2 \Omega_\nu \text{ eVcm}^{-3}, \tag{8.2}$$

where $\Omega_{\nu 0}$ is the neutrino energy density in units of critical density. As usual, relativistic neutrinos contribute to the total energy density of radiation ρ_r, typically parametrized as

$$\rho_r = \left[1 + \frac{7}{8}\left(\frac{4}{11}\right)^{4/3} N_{\rm eff}\right]\rho_\gamma, \tag{8.3}$$

where ρ_γ is the energy density of photons; the factor 7/8 is due to the neutrinos that are fermions, and $N_{\rm eff} = 3.046$ is the value of the effective number of neutrinos species in the standard case, with zero asymmetries and no extra relativistic degrees of freedom. Neutrinos become nonrelativistic when their average momentum falls below their mass. In the very early Universe, neutrinos and anti-neutrinos of each flavor ν_i $(i = e, \mu, \tau)$ behave like relativistic particles. Both the energy density and pressure of one species of massive degenerate neutrinos and anti-neutrinos are described by (here we adopt the geometrical unit system where $\hbar = c = k_B = 1$)

$$\rho_{\nu_i} + \rho_{\bar{\nu}_i} = T_\nu^4 \int \frac{d^3q}{2(\pi)^3} q^2 E_{\nu_i} (f_{\nu_i}(q) + f_{\bar{\nu}_i})) \tag{8.4}$$

and

$$3(p_{\nu_i} + p_{\bar{\nu}_i}) = T_\nu^4 \int \frac{d^3q}{2(\pi)^3} \frac{q^2}{E_{\nu_i}} (f_{\nu_i}(q) + f_{\bar{\nu}_i})), \tag{8.5}$$

where $E_{\nu_i}^2 = q^2 + a^2 m_{\nu_i}$ is one flavor neutrino/anti-neutrino energy and $q = ap$ is the comoving momentum. The functions f_{ν_i}, $f_{\bar{\nu}_i}$ are the Fermi-Dirac phase space distributions given by

$$f_{\nu_i}(q) = \frac{1}{e^{E_{\nu_i}/T_\nu - \xi_\nu} + 1}, f_{\bar{\nu}_i}(q) = \frac{1}{e^{E_{\bar{\nu}_i}/T_\nu - \xi_{\bar{\nu}}} + 1}, \tag{8.6}$$

where $\xi_\nu = u_\nu / T_{\nu 0}$ is the neutrino degeneracy parameter and μ is the neutrino chemical potential. In the early Universe, we assumed that neutrinos-anti-neutrinos are produced in thermal and chemical equilibrium. Their equilibrium distribution functions have been frozen from the time of decoupling to the present. Then, as the chemical potential u_ν scales as T_ν, the degeneracy parameter ξ_ν remains constant and it is different from zero if a neutrino-anti-neutrino asymmetry has been produced before the decoupling. The energy of neutrinos changes according to cosmological redshift after decoupling, which is a moment when they are still relativistic. The neutrino degeneracy parameter ξ_ν is conserved, and its significant and non-null values may have imprints on the some important physical processes through the evolution of the Universe, such as BBN, photon decoupling and LSS, among others (see [260, 273, 288, 289, 291–293, 304, 310, 311, 319]). If ξ_ν remains constant,

finite and non-zero after decoupling, then it could lead to an asymmetry on the neutrinos and anti-neutrinos given by

$$\eta_\nu \equiv \frac{n_{\nu_i} - n_{\bar{\nu}_i}}{n_\gamma} = \frac{1}{12\zeta(3)} \sum_i y_\nu \left(\pi^2 \xi_i + \xi_i^3\right), \tag{8.7}$$

where $n_{\nu_i}(n_{\bar{\nu}_i})$ is the neutrino (anti-neutrino) number density, n_γ is the photon number density, $\zeta(3) \approx 1.20206$, and $y_\nu^{1/3} = T_{\nu_i}/T_\gamma$ is the ratio of neutrino and photons temperatures to the present, where T_γ is the temperature of the CMB ($T_0 = 2.726K$). Neutrino asymmetry it is a quantity that varies with time and the value of the factor $(T_{\nu_i}/T_\gamma)^3$ before of the electron-positron annihilation ($(T_{\nu_i}/T_\gamma)^3 = 1$) differs from its standard value after electron-positron pair annihilation to photons by $(T_{\nu_i}/T_\gamma) = 4/11$. As we have mentioned above, the neutrino asymmetry can produce changes in the expansion rate of the Universe at early times, which can be expressed as an excess in $N_{\rm eff}$ in the form

$$\Delta N_{\rm eff} = \frac{15}{7} \sum_i \left[2\left(\frac{\xi_i}{\pi}\right)^2 + \left(\frac{\xi_i}{\pi}\right)^4\right]. \tag{8.8}$$

The evidence of any positive deviation from the standard theoretical value of $N_{\rm eff}$ can also be a signal that the radiation content of the Universe is not only due to photons or relativistic neutrinos, but also some extra relativistic relics, known in the literature as "dark radiation". Nowadays, Plank team, has constrained this value $N_{\rm eff} = 3.04 \pm 0.33$ at 95% of confidence level (CL) within the $\Lambda CDM + \Sigma m_\nu$ model, with $\Sigma m_\nu < 0.194$ eV (from CMB alone).

In what follows, let us impose new observational limits on ξ by taking predictions from some future CMB experiments.

8.3. Models and data analysis

Here we intend to predict the ability of future CMB experiments to constrain the neutrino lepton asymmetry as well as the neutrino mass scale. We follow the common approach already used (see for example [281, 284]), on mock data for some possible future experimental configurations, assuming a fiducial flat ΛCDM model compatible with the Planck 2018 results. We use the publicly available Boltzmann code class [269] to compute the theoretical CMB angular power spectra C_l^{TT}, C_l^{TE}, C_l^{EE} for temperature, cross temperature-polarization and polarization. Together with the primary anisotropy signal, we also take into account the information from CMB weak lensing, considering the

power spectrum of the CMB lensing potential C_l^{PP}. The BB missions are clearly sensitive also to the BB lensing polarization signal, but here we adopt a bit conservative approach to not include it in the forecasts. In our simulations, we have used an instrumental noise given by the usual expression

$$N_l = w^{-1} \exp\Big(l(l+1)\theta^2/8\ln(2)\Big), \tag{8.9}$$

where θ is the experimental FWHM angular resolution, w^{-1} is the experimental power noise expressed in μK-arcmin. The total variance of the multipoles a_{lm} is therefore given by the sum of the fiducial C_l's with the instrumental noise N_l. The simulated experimental data are then compared with a theoretical model assuming a Gaussian likelihood $\mathcal{L}$ given by

$$-2\ln\mathcal{L} = \sum_l (2l+1) f_{sky}\Big(\frac{D}{|\bar{C}|} + \ln\frac{|\bar{C}|}{|\hat{C}|} - 3\Big), \tag{8.10}$$

where $\bar{C}_l$ and $\hat{C}_l$ are the assumed fiducial and theoretical spectra plus noise, and $|\bar{C}|$ and $|\hat{C}|$ are the determinants of the theoretical and observed data covariance matrices given by

$$|\bar{C}| = \bar{C}_l^{\,TT}\bar{C}_l^{\,EE}\bar{C}_l^{\,PP} - (\bar{C}_l^{\,TE})^2\bar{C}_l^{\,PP} - (\bar{C}_l^{\,TP})^2\bar{C}_l^{\,EE}, \tag{8.11}$$

$$|\hat{C}| = \hat{C}^{TT}\hat{C}^{EE}\hat{C}^{PP} - (\hat{C}^{TE})^2\hat{C}^{PP} - (\hat{C}^{TP})^2\hat{C}^{EE}, \tag{8.12}$$

D is defined as

$$\begin{aligned} D = \hat{C}^{TT}\bar{C}_l^{\,EE}\bar{C}_l^{\,PP} + \bar{C}_l^{\,TT}\hat{C}^{EE}\bar{C}_l^{\,PP} + \bar{C}_l^{\,TT}\bar{C}_l^{\,EE}\hat{C}^{PP} \\ -\bar{C}_l^{\,TE}(\bar{C}_l^{\,TE}\hat{C}^{PP} + 2\hat{C}^{TE}\bar{C}_l^{\,PP}) \\ -\bar{C}_l^{\,TP}(\bar{C}_l^{\,TP}\hat{C}^{EE} + 2\hat{C}^{TP}\bar{C}_l^{\,EE}), \end{aligned} \tag{8.13}$$

and finally f_{sky} is the sky fraction sampled by the experiment after foregrounds removal. In Table 9, we have summarized the experimental specifications for CORE and CMB-S4 data. Forecasting is based on future CMB experiments to probe neutrinos properties, also investigated in [270, 272, 299].

Table 9 – Experimental specifications for CORE and CMB-S4 with beam width, power noise sensitivities of the temperature and polarization.

Experiment	Beam	Power noise [μK-arcmin]	$l_{\rm min}$	$l_{\rm max}$	$f_{\rm sky}$
Core	6.0	2.5	2	3000	0.7
S4	3.0	1.0	50	3000	0.4

Table 10 – Summary of the observational constraints from both CORE and CMB-S4 experiments. The notations σ(Core) and σ(S4), represent the 68% CL estimation on the fiducial values from CORE and CMB-S4, respectively. The parameter H_0 is in km s^{-1} Mpc^{-1} units and $\sum m_\nu$ is in eV units.

Parameter	Fiducial value	σ(Core)	σ(S4)
$10^2\omega_b$	2.22	0.000057	0.00012
ω_{cdm}	0.11919	0.00037	0.0000093
H_0	68.0	0.32	0.0088
$\ln 10^{10} A_s$	3.0753	0.0056	0.0035
n_s	0.96229	0.0022	0.0054
$\tau_{\rm reio}$	0.055	0.0028	0.00025
$\sum m_\nu$	0.06	0.024	0.00053
ξ_ν	0.05	0.071	0.027

8.4. Forecast on lepton asymmetry

We have used the publicly available CLASS [269] and Monte Python [266] codes for the model considered in the present work, where we have introduced the ξ corrections on $N_{\rm eff}$ defined in Eq. (8.8) in CLASS code. We have considered one massive and two massless neutrino states, as standard in the literature, and we fixed the mass ordering to the normal hierarchy with the minimum mass $\sum m_\nu = 0.06$ eV. In our forecasts, we have assumed the following set of the cosmological parameters:

$$\{100\omega_{\rm b},\, \omega_{\rm cdm},\, \ln 10^{10} A_s,\, n_s,\, \tau_{\rm reio},\, H_0,\, \sum m_\nu,\, \xi\}.$$

where the parameters are: baryon density, CDM density, amplitude and slope of the primordial spectrum of metric fluctuations, optical depth to reionization, Hubble constant, neutrino mass scale, and the degeneracy parameter characterizing the degree of leptonic asymmetry, respectively, with the fiducial values {2.22, 0.119, 3.07, 0.962, 0.05, 68.0, 0.06, 0.05 }. The details of the methodology used in the probability can be seen in [281, 284].

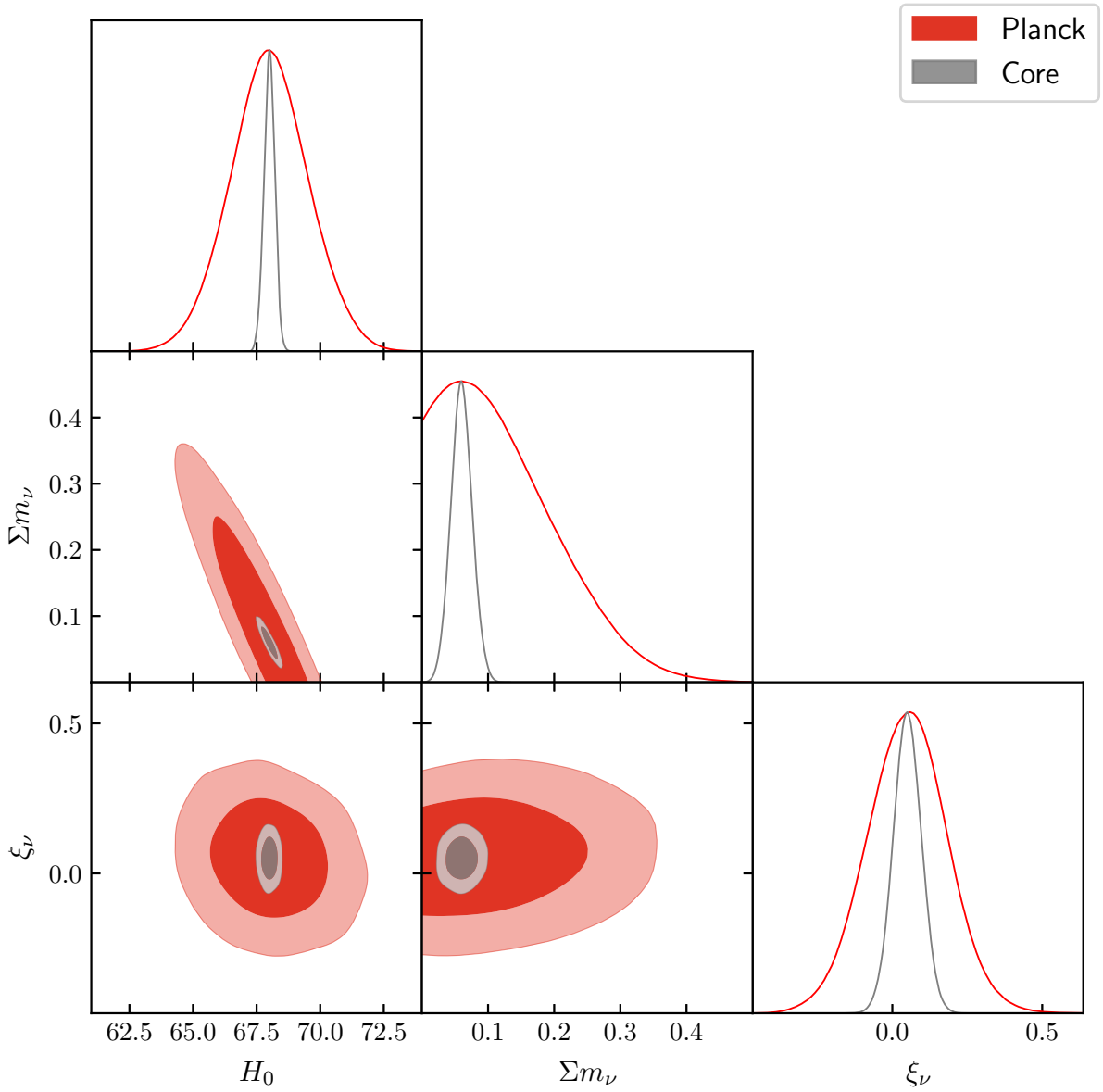

Figure 54 – One-dimensional marginalized distribution and 68% CL and 95% CL regions for some selected parameters taking into account Planck and CORE experiments.

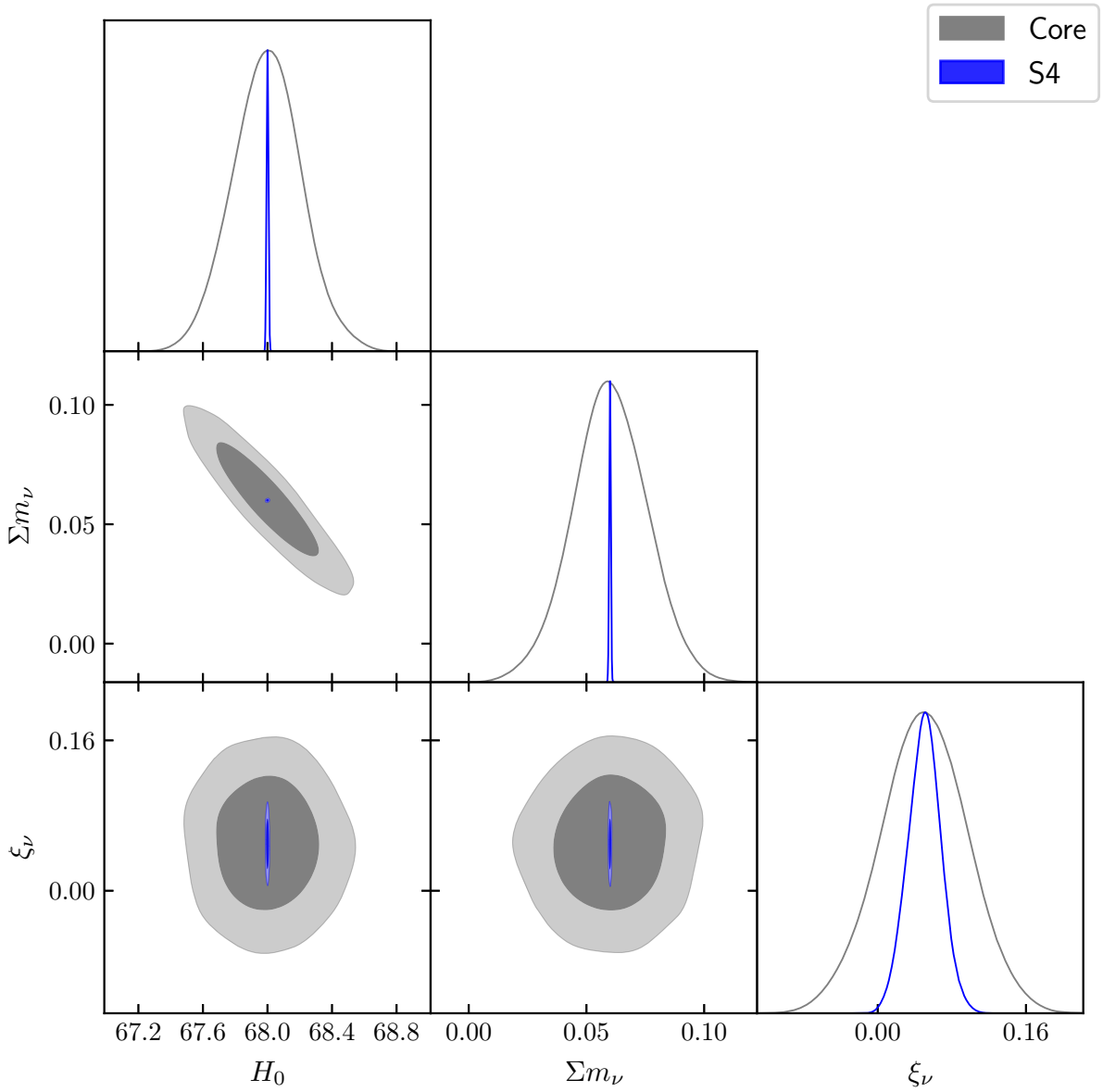

Figure 55 – One-dimensional marginalized distribution and 68% CL and 95% CL regions for some selected parameters taking into account CORE and S4 experiments.

Table 10 shows the constraints on the model baseline imposed by the CORE and S4 experiments. Figures 54 and 55 show the parametric space for some parameters of interest in our work, from Planck/CORE and CORE/S4 constraints, respectively. From Planck data, we can note that the degeneracy parameter is constrained to $\xi_\nu = 0.05 \pm 0.20$ (± 0.33) at 68% CL and 95% CL., which is a result compatible with the null hypothesis even to 1σ CL. In [301], the authors obtain $\xi = -0.002^{+0.114}_{-0.11}$ at 95% CL from Planck data. Evidence for cosmological lepton asymmetry from CMB data have been found in [273].

On the other hand, the constraints on the degeneracy parameter are close to the null value also within the accuracy achieved by CORE data, $\xi_\nu = 0.05 \pm 0.071$ (± 0.11) at 68% CL and 95% CL, being compatible with the null hypothesis even to 1σ CL, as in the case of Planck data, used in the present work. However, with respect to the accuracy obtained by CMB-S4, we find $\xi_\nu = 0.05 \pm 0.027$ (± 0.043) at 68% CL (95% CL), respectively. These constraints can rule out the null hypothesis up to 2σ CL on ξ_ν. In principle this last result can open the door to the possibility to unveil the physical nature of neutrinos, that is, the neutrinos can be Dirac particles against the null hypothesis of Majorana particles. However, these results must be firmly established from the point of view of particle physics, for example, from ground-based experiments such as PandaX-III (Particle And Astrophysical Xenon Experiment III), which are supposed to explore the nature of neutrinos, including physical properties such as the absolute scale of the neutrino masses and the aforementioned violation of leptonic number conservation through Neutrinoless Double Beta Decay (NLDBD), and whose observation will be a clear signal that the neutrinos are their own antiparticles (for more details see [276]). These results could be available within the next decade.

In Figure 54, we can note that there is a high anti-correlation between the neutrinos' masses and H_0, that will increase the tension between the local and global measures of H_0, if the masses of the neutrinos increase (therefore they will decrease the value of H_0), such that, constraints on those parameters must be cautiously interpreted until such tension can be better understood. Within the standard base-ΛCDM cosmology, the Planck Collaboration [303] reports $H_0 = 67.36 \pm 0.54\, km\, s^{-1} Mpc^{-1}$, which is about 99% away from the locally measured value $H_0 = 72.24 \pm 1.74\, km\, s^{-1} Mpc^{-1}$ reported in [305]. We obtain, $H_0 = 68.00 \pm 2.32$ (± 3.78) $km\, s^{-1} Mpc^{-1}$ at 68% CL and 95% CL, for our model with Planck data, which can reduce the tension between the global and local value of H_0 at least 2σ. The difference of our results from Planck 2018 is due to our extended parameter space. On the other hand, from the Planck data analysis we can note that the neutrino mass scale is constrained to $\sum m_\nu < 0.36$ eV at 95% CL, which is in good agreement with the one obtained by Planck Collaboration, i.e., $\sum m_\nu < 0.24$ eV [303]. From the $\sum m_\nu - H_0$ plane, we note that no relevant changes are obtained with respect to the mass splitting, which requires that $\sum m_\nu < 0.1$ eV to rule out the inverted mass hierarchy ($m_2 \gtrsim m_1 \ggg m_3$). However, these results start to favor the scheme of normal hierarchy

($m_1 \ll m_2 < m_3$). The results from CORE and S4 present considerable improvements with respect to Planck data, see Figures 54 and 55. With respect to neutrino mass scale bounds imposed from CORE and S4 data, we find the limits $0.021 < \sum m_\nu \lesssim 0.1$ eV and $0.05913 < \sum m_\nu \lesssim 0.061$ eV at 95% CL, for CORE and S4, respectively. Thus, these are unfavorable to the inverted hierarchy scheme mass at least at 95% CL in both cases.

In the standard scenario of three active neutrinos, if we consider effects of non-instantaneous decoupling, we have $N_{\rm eff} = 3.046$. We emphasize that this value is fixed in our analysis. It is well known that the impact of the leptonic asymmetry increase the radiation energy density with the form, $N_{\rm eff} = 3.046 + \Delta N_{\rm eff}^{\xi_\nu}$, where $\Delta N_{\rm eff}^{\xi_\nu}$ is due to the leptonic asymmetry induced via Eq. (8.8). Without losing of generality, we can evaluate the contribution $\Delta N_{\rm eff}^{\xi_\nu}$ via the standard error propagation theory. We note that, $\Delta N_{\rm eff}^{\xi_\nu} = 0.002 \pm 0.019$ (± 0.030) for Planck data, $\Delta N_{\rm eff}^{\xi_\nu} = 0.0022 \pm 0.0083$ (± 0.013) for CORE data and $\Delta N_{\rm eff}^{\xi_\nu} = 0.0022 \pm 0.0045$ (± 0.0059) for S4 data, all limits being at 68% and 95% CL. Therefore, we can assert that the contributions from ξ_ν on $N_{\rm eff}$ are very small. But in the case of CMB-S4, even this contribution is very small, it can be non-null.

Chapter 9

Observing Dirac neutrinos with CMB and other cosmological tests

Based on: "**Unveiling the nature of Dirac's neutrinos in light of the latest cosmological evidence: The case for dark radiation and PBH.**" Send to Symmetry MDPI, Special Issue "Neutrino Physics and Symmetry".

9.1. The case for dark radiation

Future cosmological observations will measure the radiation density of the early universe at the percent level. These observations will probe the physics of neutrinos, as well as the possible existence of extra light particles that are more weakly coupled to the SM than neutrinos. Examples of light relics that can be constrained in this way are the QCD axion [337–339], axion-like particles (ALPs) [340], dark photons [534] and light sterile neutrinos [342]. These particles may be so weakly coupled that they are hard to detect in terrestrial experiments, but the large number densities in the early universe make their gravitational imprints observable. Let us assume that some physics beyond the Standard Model adds an extra radiation density ρ_X to the early universe. It is conventional to measure this density relative to the density of a SM neutrino species:

$$\Delta N_{\text{eff}} \equiv \frac{\rho_X}{\rho_\nu} = \frac{1}{a_\nu}\frac{\rho_X}{\rho_\gamma}, \tag{9.1}$$

and define $N_{\text{eff}} = N_\nu + \Delta N_{\text{eff}}$ as the *effective number of neutrinos*, although ρ_X may have nothing to do with neutrinos. Current measurements of the CMB anisotropies and the light element abundances find

$$N_{\text{eff}}^{\text{CMB}} = 3.04 \pm 0.18\,, \tag{9.2}$$

$$N_{\text{eff}}^{\text{BBN}} = 2.85 \pm 0.28\,, \tag{9.3}$$

which is consistent with the SM prediction,[1] $N_{\text{eff}} = 3.046$. Future CMB observations have the potential to improve these constraints by an order of magnitude [343]. A natural source for $\Delta N_{\text{eff}} \neq 0$ are extra relativistic particles. Let us therefore consider a light species X as the only additional particle in some BSM theory. Assuming that this species was in thermal equilibrium with the SM at some point in the history of the universe, we can compute its contribution to N_{eff} in the same way as we derived the relic density of neutrinos in section 4.4. For concreteness, let us assume that the particles of the species X decouple before neutrino decoupling, $T_{\text{dec},X} > 10$ MeV. Particle-antiparticle annihilations until neutrino decoupling will lead to a difference between the temperature associated with the species X and that of neutrinos:

$$\begin{aligned} T_X = \left(\frac{g_*(T_{\text{dec},\nu})}{g_*(T_{\text{dec},X})}\right)^{1/3} T_\nu &= \left(\frac{10.75}{106.75}\right)^{1/3} \left(\frac{106.75}{g_*(T_{\text{dec},X})}\right)^{1/3} T_\nu \\ &= 0.465 \left(\frac{106.75}{g_*(T_{\text{dec},X})}\right)^{1/3} T_\nu\,. \end{aligned} \tag{9.4}$$

After neutrino decoupling, T_X and T_ν evolve in the same way, with both receiving the same suppression relative to T_γ from e^+e^- annihilation. As long as both X and ν are relativistic, they therefore maintain a constant energy ratio

$$\Delta N_{\text{eff}} \equiv \frac{\rho_X}{\rho_\nu} = \frac{g_{*,X}}{g_{*,\nu}} \left(\frac{T_X}{T_\nu}\right)^4 = 0.027\, g_{*,X} \left(\frac{106.75}{g_*(T_{\text{dec},X})}\right)^{4/3}\,, \tag{9.5}$$

where $g_{*,\nu} = \frac{7}{4}$ and $g_{*,X} = \{1, \frac{7}{4}, 2, \ldots\}$ are the internal degrees of freedom for spin $\{0, \frac{1}{2}, 1, \ldots\}$ particles. Figure 56 shows the contribution of a single decoupled species as a function of its decoupling temperature. We see that the contributions asymptote to fixed values for decoupling temperatures above the mass of the top quark (the heaviest particle of the SM). Using $g_*(T_{\text{dec},X}) \leq 106.75$ in expression (9.5), we find that the extra species

[1] The predicted value of $N_{\text{eff}} = 3.046$ accounts for plasma corrections of quantum electrodynamics, flavour oscillations and, in particular, the fact that neutrinos have not fully decoupled when electrons and positrons annihilated.

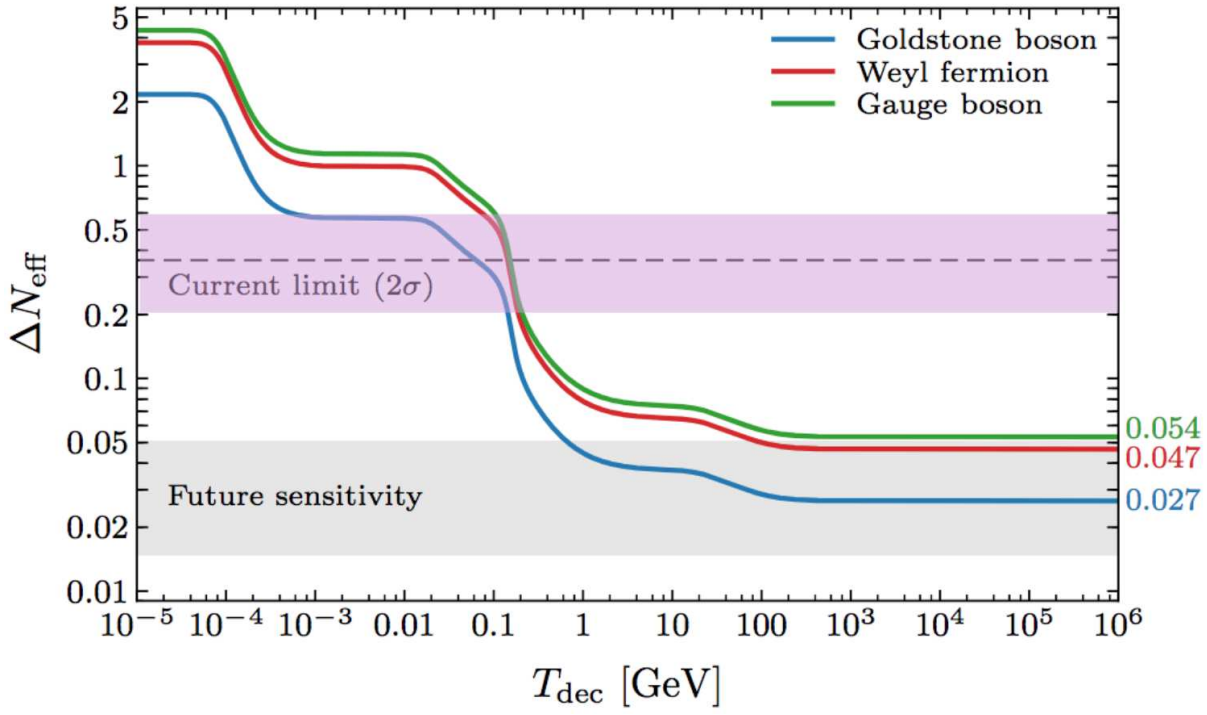

Figure 56 – Contributions of a single thermally-decoupled Goldstone boson, Weyl fermion or massless gauge boson to the effective number of neutrinos, $\Delta N_{\rm eff}$, as a function of its decoupling temperature $T_{\rm dec}$.

X contributes the following minimal amount[2]

$$\boxed{\Delta N_{\rm eff} > 0.027\, g_{*,X}} = \begin{cases} 0.054 & \text{gauge boson} \\ 0.047 & \text{Weyl fermion} \\ 0.027 & \text{Goldstone boson} \end{cases} \tag{9.6}$$

As we will see, this is an interesting target for future CMB experiments as CMB-S4 or CORE.

[2] In deriving this bound, we assumed an extension of the SM in which there is no significant entropy production after decoupling and that the species X is the only addition to the SM particle content. Additional particles may both increase $\Delta N_{\rm eff}$ is there are light enough, or decrease it if they are relativistic at the decoupling of X, but become non-relativistic before neutrino decoupling. While entropy production typically dilutes the effects of extra relativistic species, it can also lead to additional effects that can be looked for in cosmological observations. For a more detailed discussion of these issues, see [344].

9.2. Dirac neutrinos

Any extra non-photon radiation energy density $\rho_{\rm rad}$ is usually normalized to the number density of one active neutrino flavor, $N_{\rm eff} \equiv (8/7)\,(11/4)^{4/3}\,\rho_{\rm rad}/\rho_\gamma$. The current Planck measurement is $N_{\rm eff} = 2.99 \pm 0.17$ (including baryon acoustic oscillation (BAO) data) [453], perfectly consistent with the Standard Model (SM) expectation $N_{\rm eff}^{\rm SM} = 3.045$ [454–456]. CMB Stage IV (CMB-S4) experiments have the potential to constrain $\Delta N_{\rm eff} \equiv N_{\rm eff} - N_{\rm eff}^{\rm SM} = 0.060$ (at 95% C.L.) [457, 458], which is very sensitive to new *light* degrees of freedom that were in equilibrium with the SM at some point, even if it decoupled at multi-TeV temperatures. Indeed, a relativistic particle ϕ that decouples from the SM plasma at temperature $T_{\rm dec}$ contributes

$$\Delta N_{\rm eff} \simeq 0.027 \left(\frac{106.75}{g_\star(T_{\rm dec})}\right)^{4/3} g_s\,, \tag{9.7}$$

where g_s is the number of spin degrees of freedom of ϕ (multiplied by 7/8 for fermions) and $g_\star(T_{\rm dec})$ is the sum of all relativistic degrees of freedom except ϕ at $T = T_{\rm dec}$. At temperatures above the electroweak scale, $g_\star$ saturates to 106.75, the maximum amount of entropy available from SM particles (see Appendix B). Reference [459] has recently studied the impact of CMB-S4 on axions and axion-like particles ($g_s = 1$), which are reasonably well motivated but could easily lead to an entropy-suppressed contribution $\Delta N_{\rm eff} \simeq 0.027$ that is below the CMB-S4 reach. It should be kept in mind, however, that an even better motivation for light degrees of freedom comes from the discovery of non-zero neutrino masses: if neutrinos are *Dirac* particles then we necessarily need two or three effectively massless chirality partners ν_R in our world, which would contribute a whooping $\Delta N_{\rm eff} \geq 2 \times 0.047 = 0.09$ (two ν_R) or even $\Delta N_{\rm eff} \geq 0.14$ (three ν_R) if thermalized with the SM, easily falsifiable or detectable! While it is well known that just SM + Dirac ν does not put ν_R in equilibrium due to the tiny Yukawa couplings $m_\nu/\langle H\rangle \lesssim 10^{-11}$ [460, 461], one often expects additional interactions for ν_R in order to explain the smallness of neutrino masses, to generate the observed matter–anti-matter asymmetry of our Universe, and to protect the Dirac nature from quantum gravity, as we will highlight below. All of these new ν_R interactions will then face strong constraints from CMB-S4 that will make it difficult to see the mediator particles in any other experiment, in particular at the LHC. The basic idea to measure new interactions via $N_{\rm eff}$ in Big Bang nucleosynthesis (BBN) or the CMB is of course old [573, 574], see for example the reviews [464–466]. It is timely to revisit these limits though since we are on the verge of reaching an important milestone: sensitivity to Dirac-neutrino induced $\Delta N_{\rm eff}$ even if the ν_R decoupled above the *electroweak* phase transition! As we will outline in this article, the non-observation of any $\Delta N_{\rm eff}$ in CMB-S4 will then have serious consequences for almost all Dirac-neutrino models, in particular those addressing the origin of the small neutrino mass.

Observing $N_{\rm eff}$

The CMB is sensitive to the radiation energy density of the Universe via the variant effects of radiation on the features of the acoustic peaks of the CMB and its damping tail. The acoustic scale of the CMB is altered inversely proportionally to the Hubble rate at the time of last scattering, $\theta_{\rm sound} \propto H^{-1}$, while the scattering causing the exponentially suppressed damping tail of the CMB anisotropies goes as $\theta_{\rm damping} \propto H^{-1/2}$. These differential effects provide the primary signatures of extra $\Delta N_{\rm eff}$ in the CMB power spectrum. The primordial helium abundance, Y_p, also changes the scales of $\theta_{\rm sound}$ to $\theta_{\rm damping}$ similarly, however the near degeneracy between $N_{\rm eff}$ and Y_p is broken by other physical effects, including the early integrated Sachs–Wolfe effect, effects of a high baryon fraction, as well as the acoustic phase shift of the acoustic oscillations [467, 468]. The limit from Planck plus BAO data is $N_{\rm eff} = 2.99 \pm 0.17$ [453], where the limit is from a single parameter extension of the standard ΛCDM 6-parameter cosmological model. We translate this into a 2σ constraint $\Delta N_{\rm eff} < 0.28$. Currently underway and future experiments are forecast to have even greater sensitivity, even with more conservative assumptions about the possible presence of new physics. The South Pole Telescope SPT-3G is a ground-based telescope currently in operation, with a factor of ~ 20 improvement over its predecessor. SPT-3G is forecast to have a sensitivity of $\sigma(\Delta N_{\rm eff}) = 0.058$, given here as the single standard deviation (1σ) sensitivity [469]. This sensitivity is conservative in that it includes the variation of a nine-parameter model for all of the new physics which SPT-3G will be tackling: ΛCDM (six parameters), $N_{\rm eff}$, active neutrino mass (Σm_ν), plus tensors. We estimate the 2σ sensitivity of SPT-3G as $\Delta N_{\rm eff} < 0.12$. The CMB Simons Observatory (SO), which will see first light in 2021, is forecast to have 1σ sensitivity in the range of $\sigma(\Delta N_{\rm eff}) = 0.05$ to 0.07 [470]. For the noise level and resolution of CMB-S4, the differential effects on the acoustic peaks and damping tail are predominately measured through the TE spectrum at multipoles $\ell > 2500$ [458]. The sensitivity of CMB-S4 is forecast to be $\Delta N_{\rm eff} = 0.060$ at 95% C.L., as a single parameter extension to ΛCDM. In Fig. 57 we show the current 2σ limit on $N_{\rm eff}$ as well as the SPT-3G, SO, and CMB-S4 forecast as a function of the decoupling temperature $T_{\rm dec}$ using Eq. (9.7). The current Planck limit requires $T_{\rm dec} \gtrsim 0.55 GeV$ for three right-handed neutrinos, whereas SPT-3G, SO, and CMB-S4 can conclusively probe this scenario for arbitrary decoupling temperatures. If only *two* ν_R are in equilibrium, then SPT-3G/SO can probe $T_{\rm dec} \sim 30 GeV$ and CMB-S4 is required to reach arbitrary decoupling temperatures. It is then clear that SPT-3G, SO, and CMB-S4 provide a significant sensitivity to the new physics of Dirac-neutrino models.

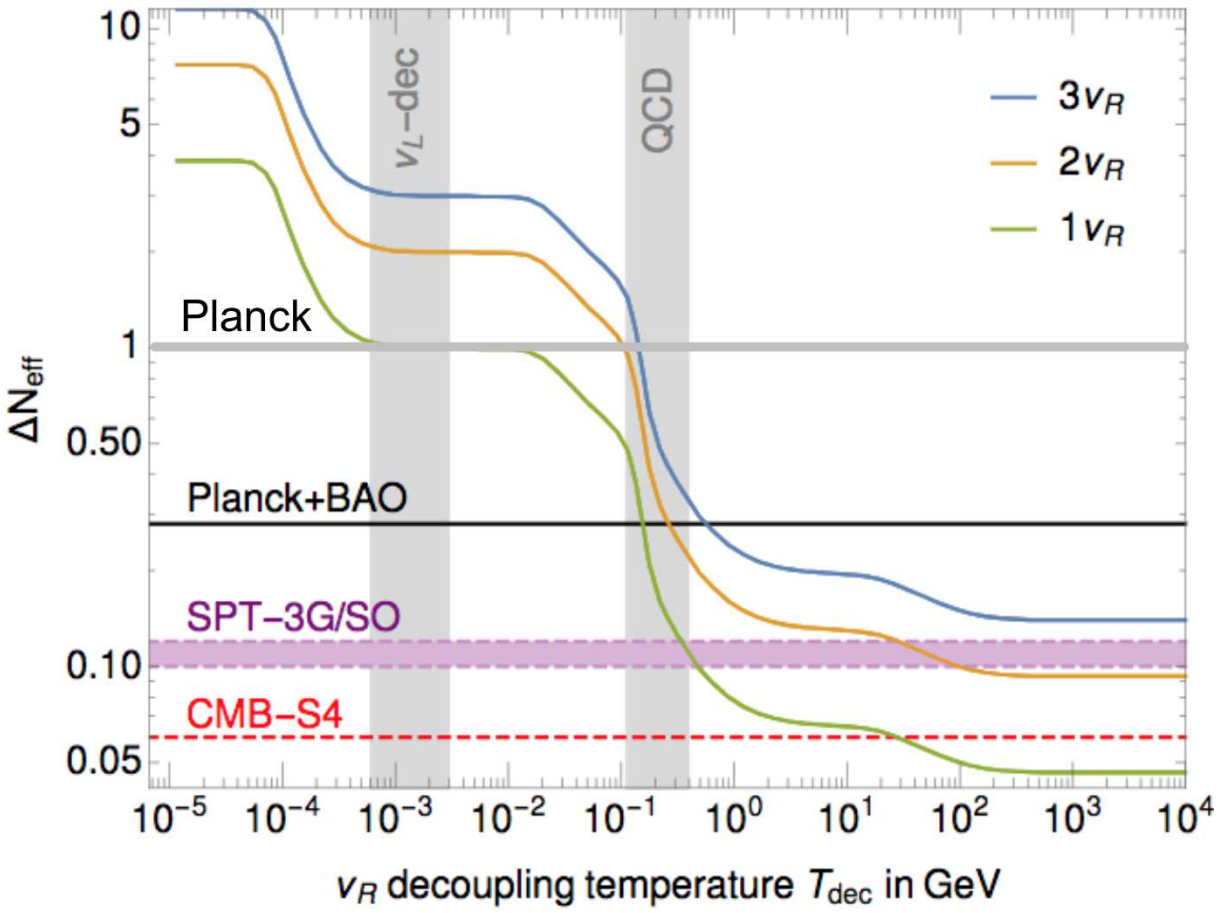

Figure 57 – Contribution of one, two or three right-handed neutrinos ν_R to $\Delta N_{\rm eff}$ as a function of their common decoupling temperature $T_{\rm dec}$. The horizontal lines indicate the current 2σ limit from Planck+BAO as well as the projected reach of SPT-3G, SO, and CMB-S4.

Impact on Dirac neutrino models

In the following we will discuss the impact a near-future constraint $\Delta N_{\rm eff} < 0.06$ would have on models involving *Dirac* neutrinos, which automatically bring two to three relativistic states ν_R that could be in equilibrium and contribute to $N_{\rm eff}$. As with all constraints from cosmology, our conclusions rest on additional assumptions regarding the cosmological evolution, namely:

1. We assume general relativity and the cosmological standard model ΛCDM.

2. We assume that the (reheating) temperature of the Universe reached at least the mass of the particles that couple to ν_R. This is a strong assumption since we technically only know that the Universe was at least $\sim 5MeV$ hot [471], everything beyond being speculation. Note however that most solutions to the matter–anti-matter asymmetry require at least electroweak temperatures in order to thermalize sphalerons. Dark matter production also typically requires TeV-scale temperatures, at least for weakly

interacting massive particles.

3. No significant entropy dilution. To dilute three ν_R down to $\Delta N_{\rm eff} < 0.06$ via Eq. (9.7) one would need to roughly double the SM particle content. This means that Dirac neutrinos would evade $N_{\rm eff}$ constraints if they decoupled at temperatures above the hypothetical supersymmetry or grand-unified-theory breaking scales, as both of these SM extensions bring a large number of new particles with them. A different way to generate entropy comes from an early phase of matter domination, which requires a heavy particle that goes out of equilibrium while relativistic and then decays sufficiently late so it has time to dominate the energy density of the Universe [472, 473].

Note that even if the ν_R never reached thermal equilibrium, it is possible that they were created non-thermally and still leave an imprint in $N_{\rm eff}$ [474]. Following Refs. [474–476] it might even be possible to distinguish this ν_R origin of $\Delta N_{\rm eff}$ by observation of the cosmic neutrino background, e.g. with PTOLEMY [477]. This will not be discussed here. We will further restrict our discussion to renormalizable UV-complete quantum field theories. An alternative approach would be to study higher-dimensional operators of an effective field theory with SM fields + Dirac-ν and put constraints on the Wilson coefficients, e.g. on the Dirac-ν magnetic moments [478–483]. However, higher-dimensional operators will give ν_R production rates that are dominated by the highest available temperature and thus depend explicitly on it [459]. In any renormalizable realization of such operators this growing rate would be cured once the underlying mediators go into equilibrium, which then brings us back to the approach pursued here. Before moving on to the impact of $N_{\rm eff}$ measurements on Dirac neutrino models, let us briefly comment on associated cosmological signatures that arise in our Dirac-neutrino setup. At high temperatures, three ν_R simply contribute to $N_{\rm eff}$ as relativistic particles, as discussed above. However, since they have the same mass as the active neutrinos but a lower temperature, $T_{\nu_R} = (\Delta N_{\rm eff}/3)^{1/4} T_{\nu_L}$, they will become non-relativistic slightly *before* the active neutrinos and thus modify the usual neutrino free-streaming behavior by introducing an additional scale. Once the ν_L also turn non-relativistic we find the total neutrino energy density

$$\Omega_\nu h^2 \simeq \left[1 + \left(\frac{\Delta N_{\rm eff}}{3}\right)^{3/4}\right] \frac{\sum_{j=1}^{3} m_{\nu_j}}{94 \quad eV}, \tag{9.8}$$

which is at least 10% larger compared to the case of non-thermalized ν_R. Equation (9.2) would provide an excellent test of the Dirac-neutrino origin of a measured $\Delta N_{\rm eff}$ if the sum of neutrino masses could be determined independently, for example by measuring the absolute neutrino mass scale in KATRIN [484] and the mass hierarchy in

oscillation experiments. The contribution of the ν_R can be matched to a small effective sterile neutrino mass

$$m^{\text{eff}}_{\nu,\text{sterile}} = (\Delta N_{\text{eff}}/3)^{3/4} \sum_{j=1}^{3} m_{\nu_j}, \tag{9.9}$$

as defined and constrained in combination with N_{eff} by Planck [453]. As of now, the cosmological neutrino mass measurements obtained via Ω_ν are less helpful to constrain Dirac neutrinos than ΔN_{eff}, although the increased precision on Ω_ν in CMB-S4 [458] and DESI [485] will still provide useful information.

$U(1)_{B-L}$ and other gauge bosons

One important task of Dirac-neutrino model building is to protect the Dirac nature, i.e. to forbid any and all $\Delta L = 2$ Majorana mass terms for the neutrinos. While this can easily be achieved by imposing a global lepton number symmetry $U(1)_L$ on the Lagrangian, there is the looming danger that quantum gravity might break such global symmetries [486]. To protect the Dirac nature from quantum gravity it might then be preferable to use a *gauge symmetry* to distinguish neutrino from anti-neutrino. The simplest choice is $U(1)_{B-L}$, which is already anomaly-free upon introduction of the three ν_R that we need for Dirac neutrino masses. For unbroken $U(1)_{B-L}$ the Z' gauge boson can still have a Stückelberg mass, a scenario discussed in Refs. [488, 524].[3] In a more extended scenario one can even break $U(1)_{B-L}$ spontaneously, as long as it is by more than two units in order to forbid Majorana mass terms [493]. The simplest example given in Ref. [542] has a spontaneous symmetry breaking $U(1)_{B-L} \to \mathbb{Z}_4$, where the remaining discrete gauge symmetry protects the Dirac nature of the neutrinos and the $\Delta(B-L) = 4$ interactions allow for leptogenesis [543], as discussed below. This *broken* $U(1)_{B-L}$ scenario also allows an embedding into larger gauge groups such as left–right, Pati–Salam or $SO(10)$ [493]. Protecting the Dirac nature of neutrinos in its strongest form thus requires ν_R couplings to new gauge bosons, the most minimal example being a Z' from $U(1)_{B-L}$. These new gauge bosons can then lead to a thermalization of ν_R with the rest of the SM plasma in the early Universe, e.g. via s-channel processes $\bar{f}f \leftrightarrow \bar{\nu}_R\nu_R$ [497, 499, 575, 577], which then increases N_{eff}. Equilibrium is attained when this rate Γ exceeds the Hubble rate $H(T) \sim T^2/M_{\text{Pl}}$ at a certain temperature. The behavior of $\Gamma/H(T)$ is shown in Fig. 58, using Eq. (12) from Ref. [488]. As can be seen, the ratio $\Gamma/H(T)$ is largest at the temperature $T \sim M_{Z'}/3$, where inverse decays of Z' are highly efficient, so the most aggressive assumption is that the Universe reached this temperature. Notice that a light Z' will itself start to contribute to N_{eff} [576, 578].

[3] Constraints on a $U(1)_{B-L}$ with *Majorana* neutrinos have been discussed extensively in the literature, e.g. in Refs. [491, 492, 528, 539].

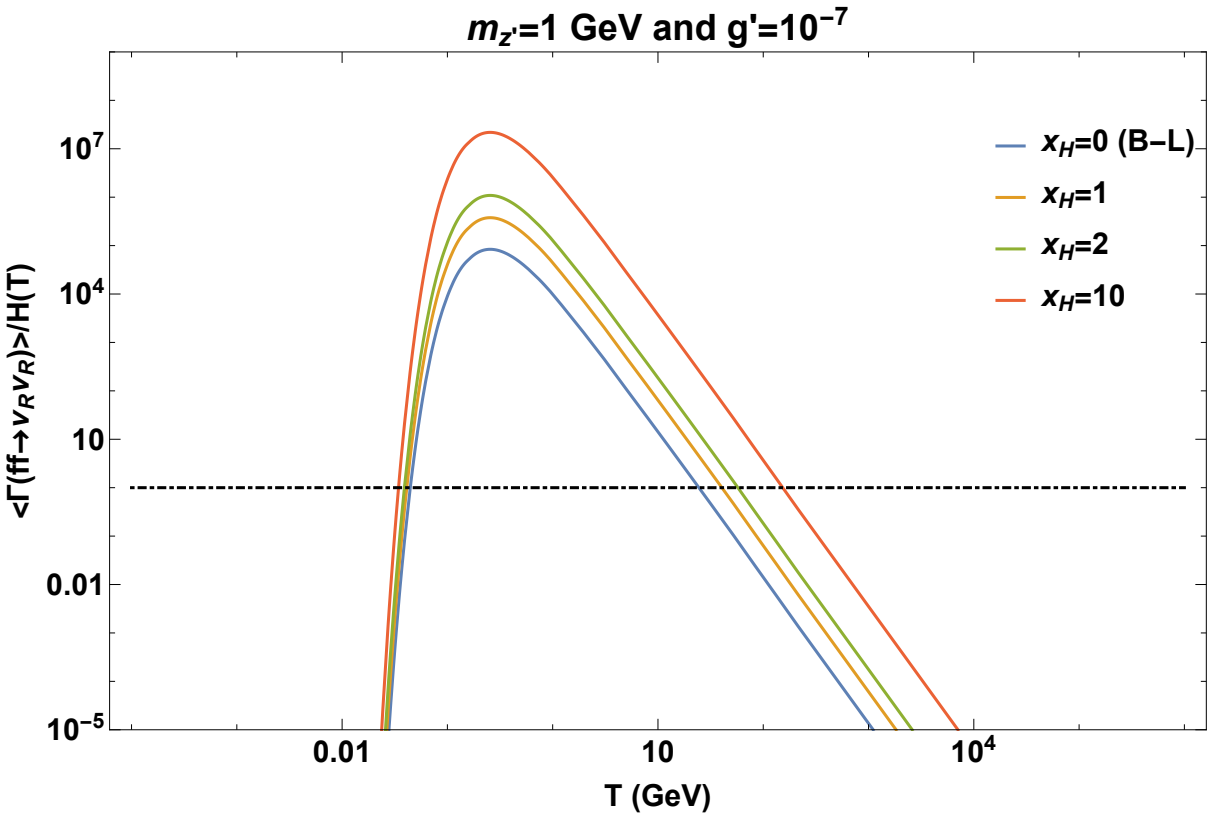

Figure 58 – Thermally averaged rate $\langle\Gamma(\bar{f}f \leftrightarrow \bar{\nu}_R\nu_R)\rangle$ [488] divided by the Hubble rate $H(T)$ as a function of temperature for some values of $U(1)_{B-L}$ gauge and coupling $g' = 10^{-7}$ and Z' mass $M_{Z'} = 1$ GeV. The ν_R are thermalized in the region above the horizontal black line.

For heavy Z' masses above 20 GeV, we demand that the ν_R go out of equilibrium before $T \sim 0.5$ GeV (Fig. 57), which corresponds to the constraint $M_{Z'}/g' > 14$ TeV, far better than pre-Planck limits [488,497,499,575,577]. A similar limit was recently derived in Ref. [502]. For masses $MeV < M_{Z'} \lesssim 10$ GeV the limit becomes much stronger due to the s-channel resonance of the rate, or equivalently the efficient inverse decay of Z'. Here we demand that the ν_R are out of equilibrium for all temperatures between MeV and $T \sim 0.5$ GeV. For Z' masses below MeV it becomes possible for the ν_R to go into equilibrium *below* $T \sim$ MeV, leaving BBN unaffected. However, even in this case the thermalization of ν_L, ν_R, and Z' after ν_L decoupling would leave an impact on $N_{\rm eff}$ [503, 504], already excluded by CMB data. As a result, we have to forbid ν_R/Z' thermalization for all temperatures between eV (CMB formation) and $T \sim 0.5$ GeV, updating Ref. [488]. which gives the black exclusion line in Fig. **??**. This existing $N_{\rm eff}$ constraint is stronger than most laboratory experiments, except for dilepton searches at the LHC. If future measurements in SPT-3G, SO, and CMB-S4 push the $\Delta N_{\rm eff}$ bound below 0.14, the limits on Z' will change dramatically to

$$g' < 2 \times 10^{-7}\sqrt{M_{Z'}/TeV}, \tag{9.10}$$

shown as a red dashed line in Fig. **??**, because we have to demand that the ν_R were *never* in equilibrium with the SM. Once again, this limit assumes that the Universe reached a temperature of at least $T \sim M_{Z'}/3$, otherwise the bound weakens. Keeping these assumptions in mind it is clear from Fig. **??** that the non-observation of $\Delta N_{\rm eff}$ in future CMB experiments will make it impossible to find a Z' coupled to Dirac neutrinos in any laboratory experiment. Turning this around, the observation of a $U(1)_{B-L}$ gauge boson in a collider or scattering experiment would then prove that neutrinos are Majorana particles. This conclusion is not limited to $B-L$ but extends to other Z' [497, 499, 502, 516, 575, 577] or W' [517, 573, 574] models. In general, new gauge interactions of ν_R will face strong constraints from CMB-S4 that will make it difficult to see the gauge bosons, say Z' or W_R, in any other experiment, in particular at the LHC. The particle content and the respective quantum numbers of the model $U(1)_X$ ($X = \beta Y + B - L$, $\beta \in$ Re) is listed in Table 11. The presence of three RHNs (one per generation) cancels gravitational and mixed chiral anomalies of both gauge symmetries.

	$SU(3)_C$	$SU(2)_L$	$U(1)_Y$	$U(1)_X$
Q_L	**3**	**2**	$\frac{1}{6}$	$\frac{\beta}{6}+\frac{1}{3}$
u_R	**3**	**1**	$\frac{2}{3}$	$\frac{2\beta}{3}+\frac{1}{3}$
d_R	**3**	**1**	$-\frac{1}{3}$	$-\frac{\beta}{3}+\frac{1}{3}$
L_L	**1**	**2**	$-\frac{1}{2}$	$-\frac{\beta}{2}-1$
e_R	**1**	**1**	-1	$-\beta-1$
N_R	**1**	**1**	0	-1
H	**1**	**2**	0	$-\frac{\beta}{2}$

Table 11 – The charges assigment to the particle content of the minimal $U(1)_X$ model symmetry. Three RHNs (N_R, $j = 1, .., 3$) are necessary to cancel, generation per generation, the superposition of chiral anomalies. The minimal $B-L$ model is the limit of $\beta \to 0$. The $U(1)_X$ gauge interaction becomes similar (up to a sign) to the SM hypercharge interaction for $\beta > 1$ ("hyper-charge oriented" $U(1)_X$)

9.3. Thermalization in the early Universe

Big Bang nucleosynthesis (BBN) describes successfully our Universe at temperatures around MeV, and places strong bounds on the number of relativistic degrees of freedom. The latter are typically parameterized via $N_{\rm eff}$, the effective number of neutrinos, predicted to be 3 by the SM. We take $N_{\rm eff} < 4$ as a conservative 95% C.L. limit from BBN [572], which in particular forbids the thermalization of our three light right-handed neutrinos ν_R, and thus constrains the strength of the $B-L$ gauge interactions that would put them in equilibrium. The interaction rate of ν_R therefore has to be smaller than the Hubble expansion rate $H(T) \sim T^2/M_{\rm Pl}$ around $T \sim 1\,\text{MeV}$. Such reasoning has long since been used to constrain right-handed neutrino interactions [573, 574]. To calculate the thermally

averaged interaction rate for $\overline{f}f \leftrightarrow \overline{\nu}_R\nu_R$ induced by Z' exchange we follow Ref. [575]:

$$\begin{aligned}\langle\Gamma(\overline{f}f \leftrightarrow \overline{\nu}_R\nu_R)\rangle = \frac{2}{n_{\nu_R}(T)}\int \frac{\mathrm{d}^3\vec{p}}{(2\pi)^3}\frac{\mathrm{d}^3\vec{k}}{(2\pi)^3}\, f_\nu(p) f_\nu(k) \\ \times\, v_{\mathrm{M}}\sigma_{\overline{\nu}_R\nu_R\to\overline{f}f}(s)\,,\end{aligned} \tag{9.11}$$

with the Fermi–Dirac distribution $f_\nu(k) = (e^{k/T}+1)^{-1}$, the ν_R number density $n_{\nu_R} = 3\zeta(3)T^3/2\pi^2$, and the Møller velocity v_{M}. The interaction cross section σ is to be evaluated at the center-of-mass energy $s = 2pk(1-\cos\theta)$, θ being the angle between the two colliding ν_R particles. Unlike Ref. [575], we do not restrict ourselves to the limiting case $M_{Z'} \gg T$, but rather use the full Z' propagator. For $M_{Z'} \sim T$, on-shell production of Z' becomes possible and the interaction rate is resonantly enhanced, calculated most easily in the narrow-width approximation for the Z' propagator

$$\frac{1}{(s-M_{Z'}^2)^2 + M_{Z'}^2\Gamma_{Z'}^2} \qquad \to \qquad \frac{\pi}{M_{Z'}\Gamma_{Z'}}\delta(s-M_{Z'}^2)\,. \tag{9.12}$$

This step is equivalent to simply studying the inverse decay $\overline{f}f \to Z'$, as has been done recently in Ref. [576] in a similar context. The thermally averaged interaction rate between right-handed neutrinos and massless fermions f via s-channel Z' exchange then takes the form

$$\langle\Gamma(\overline{f}f \leftrightarrow \overline{\nu}_R\nu_R)\rangle = N_C(f)[Q_{B-L}(f)]^2\frac{g'^4}{36\pi^3\zeta(3)}T \tag{9.13}$$

$$\times \begin{cases} \frac{\pi^4}{144}\,, & x \lesssim \sqrt{\epsilon}\,, \\ 1.15\frac{\pi}{8}\frac{M_{Z'}}{\Gamma_{Z'}}\frac{x^3}{e^x-1}\,, & \sqrt{\epsilon} \lesssim x \lesssim 14\sqrt{\log\epsilon^{-1}}\,, \\ \frac{49\pi^8}{2700}x^{-4}\,, & x \gtrsim 14\sqrt{\log\epsilon^{-1}}\,, \end{cases} \tag{9.14}$$

with $x \equiv M_{Z'}/T$ and $\epsilon \equiv \Gamma_{Z'}/M_{Z'} \ll 1$. Here, $N_C(f)$ $[Q_{B-L}(f)]$ denotes the color multiplicity [$B-L$ charge] of fermion f. The rate reduces to the well-known limits for off-shell Z' exchange $\langle\Gamma\rangle \propto (g'/M_{Z'})^4T^5$ for $M_{Z'} \gg T$ and $\langle\Gamma\rangle \propto g'^4T$ for $M_{Z'} \ll T$, but is also applicable in the resonant region $M_{Z'} \sim T$. Due to the thermal distribution of plasma particles, the on-shell production (inverse decay) is feasible over a wide range of temperatures, dominating the ν_R interaction rate roughly in the range $\sqrt{\epsilon} \lesssim x \lesssim 14\sqrt{\log\epsilon^{-1}}$. In this intermediate regime we find the function given in Eq. (9.14) that fits well to the numerical results of the narrow-width approximation;[4] in particular, it yields the characteristic $\langle\Gamma\rangle \propto g'^2M_{Z'}^2/T$ behavior for inverse decays for $x < 1$ (Recall the calculations with the Z boson Eq. (3.6)) [576]. For $x \gtrsim 1$, the rate is suppressed by a Boltzmann factor e^{-x} as expected. For the total rate one has to sum over all fermions f that are in equilibrium at temperature T. Following our discussion of Z' branching ratios to light hadrons, we only consider the coupling to leptons. We also reintroduce the lepton mass

[4] Assuming Maxwell–Boltzmann statistics for the ν_R allows for an analytic evaluation of the narrow-width integral and replaces the intermediate function in Eq. (9.14) by $\pi x^3K_1(x)/4\epsilon$.

thresholds in our numerical calculations to improve our accuracy. With the interaction rate at our disposal, we can study ν_R thermalization; it is evident that the right-handed neutrinos are either out of equilibrium during radiation domination ($\langle\Gamma\rangle < H(T)$), or go in *and out* of equilibrium during some epoch. If the ν_R are in equilibrium and go out before the Universe cools down to about $T(\nu_R) \sim 150$–$200\,\mathrm{MeV}$ [577], they will contribute to N_{eff} in an entropy-suppressed fashion [573, 574], namely $\Delta N_{\mathrm{eff}} < 1$, compatible with current data. For masses $M_{Z'} > 10\,\mathrm{GeV}$, the ν_R decoupling before $T(\nu_R) \sim 150\,\mathrm{MeV}$ then gives the well-known limits of the form $M_{Z'}/g' > 6.7\,\mathrm{TeV}$ [575]. For $1\,\mathrm{GeV} < M_{Z'} < 10\,\mathrm{GeV}$, the limits on g' strengthen considerably due to resonant Z' production, down to $g' < 6\times10^{-9}$ at $M_{Z'} = 1\,\mathrm{GeV}$. For lower masses, it becomes impossible to decouple at $T(\nu_R)$, and we have to demand that the (resonant) interaction rate is smaller than $H(T)$ for all temperatures $1\,\mathrm{MeV} < T < 150\,\mathrm{MeV}$.[5] Brushing the resonance peak—sitting at $x \simeq 2.8$—against $H(T)$ then yields the limit $g' \lesssim 10^{-9}\sqrt{M_{Z'}/100\,\mathrm{MeV}}$ for $1\,\mathrm{MeV} \lesssim M_{Z'} < 1\,\mathrm{GeV}$. For Z' masses below MeV, we demand that the ν_R come in to thermal equilibrium *after* $T \sim 1\,\mathrm{MeV}$, so $\langle\Gamma\rangle(1\,\mathrm{MeV}) < H(1\,\mathrm{MeV})$. Since the rate goes with $\langle\Gamma\rangle \propto g'^2 M_{Z'}^2/T$ initially, the limits are of the form $g' \lesssim 3\times10^{-7}\,\mathrm{keV}/M_{Z'}$, as expected from inverse decay [576]. (Note that such a light Z' starts to contribute to N_{eff} itself, in addition to the ν_R.) Finally, for $M_{Z'} < 10\,\mathrm{eV}$, on-shell Z' production at BBN temperatures becomes sub-dominant to the off-shell rate $\langle\Gamma\rangle \propto T$ and the limit becomes independent of $M_{Z'}$: $g' < 2.5\times10^{-5}$ [578]. Overall, we find that BBN gives the strongest constraints on unbroken $B-L$ for Z' masses between 100 MeV and 100 GeV, only briefly surpassed by BaBar. From keV to 100 MeV they are however less stringent than stellar evolution bounds. Resonant Z' production dominates over the previously used approximations for masses spanning nine orders of magnitude ($10\,\mathrm{eV} < M_{Z'} \lesssim 10\,\mathrm{GeV}$), and is surely of interest for other models with mediator particles in this range. We stress again that a thermalization of ν_R via Z' is not problematic for the baryon-asymmetry mechanism neutrinogenesis [523], because the Z' interactions conserve individual particle number and hence would not erase an existing ν_R asymmetry.

9.4. Cosmological phenomenology

To put observational constraints we use the Friedmann equation in the standard FLRW cosmology. The comoving sound horizon r_s and the angular diameter distance to the surface of the last scattering D_A are defined to be

$$r_s = \int_0^{a_{rec}} \frac{c_s(a)}{a^2 H(a)} da, \quad D_A = \int_{a_{rec}}^1 \frac{da}{a^2 H(a)}, \tag{9.15}$$

where $a = 1/(1+z)$ is the scale factor, $c_s(a)$ is the sound speed of hte photon-baryon

[5] Because of this, only the limits for $M_{Z'} \gtrsim 1\,\mathrm{GeV}$ are sensitive to the precise bound we use for N_{eff}.

plasma and a_{rec} is the scale factor at recombination epoch. As we can see in equation (9.15), the limits on the integral show the evolution of the expansion rate of the universe, before, during and after the recombination epoch, which occurs at a redshift of $z_* = 1089.92 \pm 0.25$ at 68 percent CL from Planck 2018 (TT,TE,EE+lowE+lensing). The existence of an extra radiation energy source during CMB epoch, where $\Delta N_{eff} \neq 0$, in general it reduces the comoving sound horizon r_s and thus can induce an increase in the current value of the expansion rate of the universe, H_0. On the other hand, The angle subtended by the sound horizon at the recombination time is given by $\theta_s(z_*) = r_s(z_*)/D_A(z_*)$, which is a very precise measure determined by final full-mission Planck 2018 measurements of the CMB anisotropies as $100\theta_s(z_*) = 1.04109 \pm 0.00030$ at 68 percent CL (TT,TE,EE+lowE+lensing). Thus, if $r_s(z_*)$ decreases, it is necessary to compensate with a decrease in $D_A(z_*)$, which implies an increase in H_0. This is the reason why to introduce extra radiation in the form of ΔN_{eff}, makes the H_0 measure inferred from CMB experiments this closer to the local measurements. As ΔN_{eff} increases, additional suppression of CMB temperature anisotropy power spectrum at small scales is generated, specifically in the range of the so-called Silk damping, and therefore certain physical quantities have to be compensated in order that these scales, which are very well determined, do not vary substantially.

Our model is: ΛCDM + Σm_ν + $M_z^{'}$, in a flat Universe. Following the Planck collaboration, we fix the mass ordering of the active neutrinos to the normal hierarchy with the minimum masses allowed by oscillation experiments, i.e., $\Sigma m_\nu = 0.06$ eV. In this work, we consider two massive neutrino flavour ν_1 and ν_2, and one massless flavour. We summarize below the data sets used in our analysis:

Cosmic Microwave Background (CMB): We consider a conservative data set from Planck 2018 comprised of the likelihoods of temperature power spectrum TT, TE, EE, low-polarisation and lensing reconstruction.

Baryon Acoustic Oscillations (BAO): The BAO is another important cosmological probe, which can trace expanding spherical wave of baryonic perturbations from acoustic oscillations at recombination time through the large-scale structure correlation function, which displays a peak around $150h^{-1}$Mpc. We use BAO measurements from Sloan Digital Sky Survey (SDSS) III DR-12 at three effective binned redshifts $z =$ 0.38, 0.51 and 0.61, reported in [587], the clustering of the SDSS-IV extended Baryon Oscillation Spectroscopic Survey DR14 quasar sample at four effective binned redshifts $z = 0.98$, 1.23, 1,52 and 1.94, reported in [588], and the high-redshift Lyman-α measurements at $z = 2.33$ and $z = 2.4$ reported in [589] and [590], respectively. Note that the observations are presented in terms of $H(z) \times (r_d/r_{d,fid})$ km s^{-1}Mpc^{-1}, where r_d is co-

moving sound horizon and $r_{d,fid}$ is the fiducial input value provided in the above references.

Supernovae Type Ia (SN): The SN traditionally have been one of the most important astrophysical tools in establishing the so-called standard cosmological model. For the present analysis, we use the Pantheon compilation, which consists of 1048 SNIa distributed in a redshift range $0.01 < z < 2.3$ [591]. Under the consideration of a spatially flat Universe, the full sample of Pantheon can be summarized into six model independent $E(z)^{-1}$ data points [592]. We consider the six data points reported by [593] in the form of $E(z)$, including theoretical and statistical considerations made by the authors there for its implementation.

Cosmic Chronometers (CC): The CC approach is a powerful method to trace the history of cosmic expansion through the measurement of $H(z)$. We consider the compilation of Hubble parameter measurements provided by [586]. This compilation consists of 30 measurements distributed over a redshift range $0 < z < 2$.

Galaxy Clusters (GC): The measurements from the abundance of GCs are a powerful probe of the growth of cosmic structures. the cosmological information enclosed in the cluster abundance is efficiently parametrized by $S_8 = \sigma_8(\Omega_m/\alpha)^\beta$, where σ_8 is the linear amplitude of fluctuations on 8 Mpc/h scale, and α, β are the fiducial value adopted in each survey analysis.

Big Bang Nucleosynthesis (BBN): Under assumption that BBN proceeded in the standard way, and that N_{eff} remains constant between BBN and last scattering, we exploit the fact that $Y_p = 0.2449 \pm 0.0040$, $^3He/H = (1.90 \pm 0.06) \times 10^{-5}$ and $D/H = (2.27 \pm 0.04) \times 10^{-5}$, is related to $\eta_{10}(\Omega_b h^2)$ and ΔN_{eff} [594].

We use the publicly available CLASS [269] and Monte Python [266] codes for constraining parameters of the models considered in the present work. We use Metropolis Hastings algorithm with uniform priors on the model parameters to obtain correlated Markov Chain Monte Carlo samples by considering two combinations of data sets: SN + BAO + GC + H(z) + BBN and SN + BAO + GC + H(z) + BBN + CMB. All the parameter chains in our analysis converge according to the Gelman-Rubin criteria $1 - R < 0.01$ [247].

Table 12 summarizes the main results of the statistical analysis carried out using two different combinations for our model, SN + BAO + GC + H(z) + BBN and SN +

Table 12 – Constraints at 95 per cent CL on parameters of the Model. The parameter h is dimensionless, $\sum m_\nu$ is in units of eV and $M_{z'}$ is in units of GeV.

Parameter	SN + BAO + GC + H(z) + BBN	SN + BAO + GC + H(z) + BBN + CMB
h	0.709 ± 0.012	0.70 ± 0.11
Ω_m	0.245 ± 0.012	0.241 ± 0.010
$\sum m_\nu$	< 0.32	< 0.28
$M_{z'}$	< 17.2	< 12.8
σ_8	0.814 ± 0.0181	0.828 ± 0.0172

BAO + GC + H(z) + BBN + CMB. Fig. 59 shows the parametric space for all parameters of the Model and its correlations. In the standard scenario (three active neutrinos and considering effects related to non-instantaneous neutrino decoupling), we have $N_{\rm eff} \simeq 3.046$. As previously introduced, the presence of a dark radiation is usually parametrized in the literature by $\Delta N_{\rm eff} \simeq N_{\rm eff} - 3.046$. From our results, we can note that the upper limits on $M_{z'}$, exclude values above of 17.2 GeV with SN + BAO + GC + H(z) + BBN and 12.8 GeV with SN + BAO + GC + H(z) + BBN + CMB, which is consistent with previous studies (see for example [595]) and their average values are within the range of thermalization that we demand (0.0018 GeV and 0.0019 for SN + BAO + GC + H(z) + BBN and with SN + BAO + GC + H(z) + BBN + CMB, respectively).

Regarding the mass scale of neutrinos we can notice that is constrained to $\sum m_\nu < 0.32$ with SN + BAO + GC + H(z) + BBN and $\sum m_\nu < 0.28$ with SN + BAO + GC + H(z) + BBN + CMB, at 95 percent CL, which is in good agreement with the one obtained by Planck Collaboration [602]. From the plane $h - \sum m_\nu$ (Fig. 59), we can note that no relevant changes are obtained with respect to the mass splitting, which requires that $\sum m_\nu < 0.1$ to rule out the inverted mass hierarchy. However, these results starts to favor the scheme of normal hierarchy. On the other hand, a fully thermalized sterile neutrino is consistent at 95 per cent CL with *planck* TT,TE,EE+lowE+lensing+BAO (i.e. $m^{\rm eff}_{\nu,{\rm sterile}} < 0.23$ eV [595]) from SN + BAO + GC + H(z) + BBN ($m^{\rm eff}_{\nu,{\rm sterile}} < 0.47$ eV) and SN + BAO + GC + H(z) + BBN + CMB ($m^{\rm eff}_{\nu,{\rm sterile}} < 0.41$ eV), results that have been obtained from Eq. (9.9).

Finally, Fig. 59 shows us the likelihoods for h resulting from the two cases analysed here (with and without CMB data), namely 0.709 ± 0.012 for SN + BAO + GC + H(z) + BBN and 0.70 ± 0.11 for SN + BAO + GC + H(z) + BBN + CMB. Changes in the central value of H0 are not observed, and both cases return very similar fits with $h \simeq 0.70$.

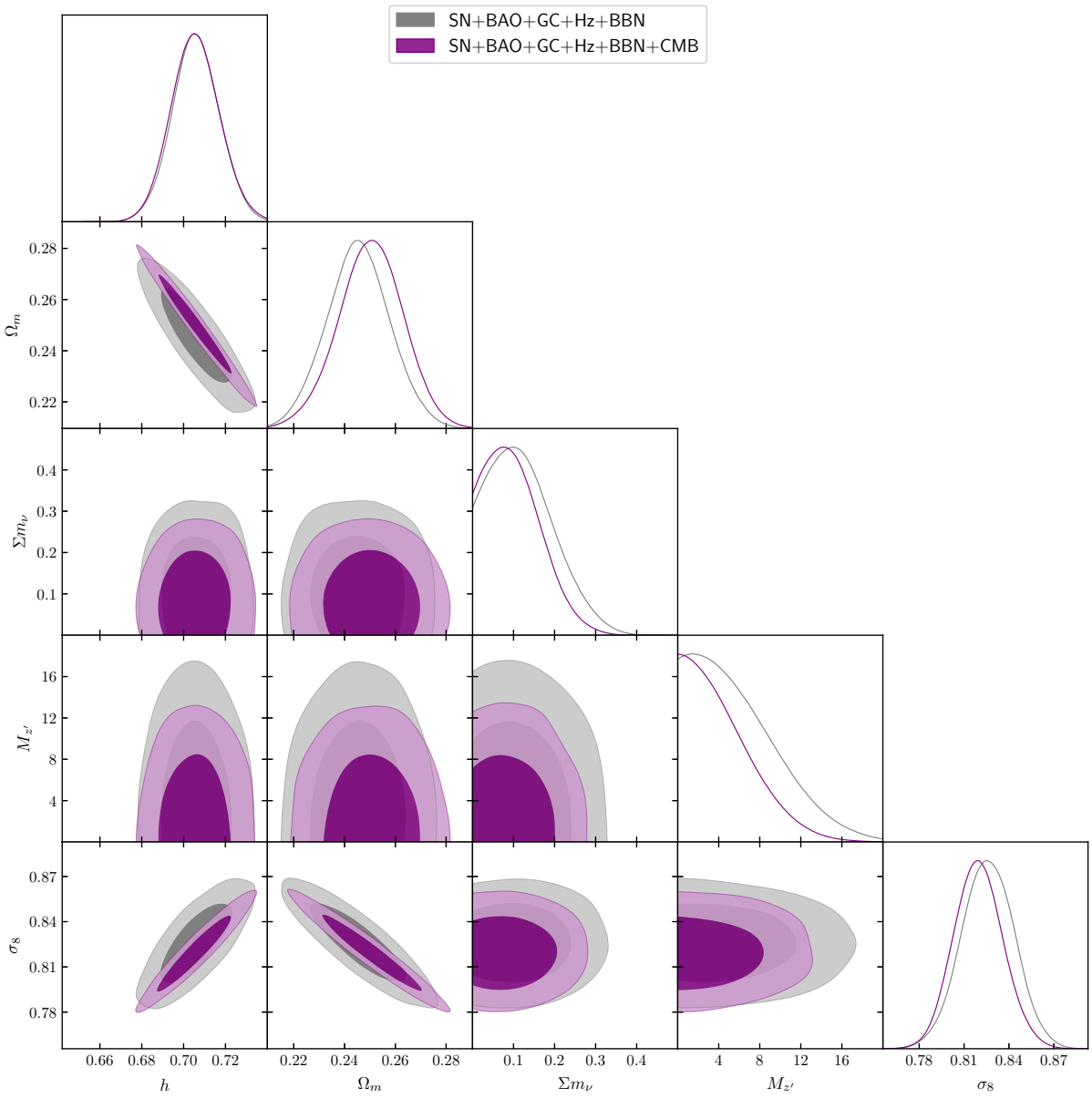

Figure 59 – Parametric space at 68% and 95% CL and one-dimensional marginalized distribution of h, Ω_m, $M_z^{'}$ and σ_8 for our model, resulting from SN+BAO+GC+Hz+BBN (Gray) and SN+BAO+GC+Hz+BBN+CMB (Purple) analysis.

That intermediate value in comparison with the local and global constraints can alleviate the current tension on the Hubble constant. On the other hand, We find that the tension in σ_8 can be partially relieved, since, although the statistical confidence limits are wide, there is a tendency towards high values of S8 and low values of Ω_m (see $\Omega_m - \sigma_8$ plane in Fig. 59 and central vlues in Tab. 12).

Chapter 10

Conclusions and perspectives

In this work, we have derived new constraints relative to the lepton asymmetry through the degeneracy parameter by using the CMB angular power spectrum from the Planck data and future CMB experiments like CORE and CMB-S4. We have analyzed the impact of a lepton asymmetry on $N_{\rm eff}$ where, as expected, we noticed very small corrections on $\Delta N_{\rm eff}$, but non-negligible corrections at the level of CMB-S4 experiments. Within this cosmological scenario, we have also investigated the neutrino mass scale in combination with the cosmological lepton asymmetry. We have found strong limits on $\sum m_\nu$, where the mass scale for both, CORE and CMB-S4 configurations, are well bound to be $\sum m_\nu < 0.1$ eV at 95% CL, therefore, favoring a normal hierarchy scheme within the perspective adopted here. As future perspective, it can be interesting to consider a neutrino asymmetry interaction with the dark sector of the Universe, and to see how this coupling can affect the neutrino and dark matter/dark energy properties, as well as to bring possible new corrections on $\Delta N_{\rm eff}$ due to such interaction.

We have updated and improved the constraints on the neutrino properties within an extended ΛCDM $+N_{\rm eff}+\sum m_\nu + c^2_{\rm eff} + c^2_{\rm vis} + \xi_\nu$ scenario using *HST* and GC data as well as CMB measurements. We find that $c^2_{\rm vis}$ can minimally deviate from its standard value at 68 per cent CL. A significant increase on $N_{\rm eff}$ can be seen, showing the possibility of presence of some dark radiation such as a partly thermalized sterile neutrino or a Goldstone boson when the GC data are added. The presence the GC data practically doubles the value of the neutrino mass scale (see table 7). Cosmological constraints from GC can be affected from several systematics, such as the biased mass-observable relation, multiplicative shear bias, mean redshift bias, baryon feedback, and intrinsic alignment. Therefore, these small increases on $N_{\rm eff}$ that we noticed here could certainly due to systematic effects in GC data compilation. The constrains on σ_8 with and without GC are not really consistent, where

we can easily see there a tension of approximately 2σ CL on σ_8 (see Figures 48 and 49). For a discussion aof this (new physics or systematic effects), we refer to [254] and references therein. We do not find significant deviation for $c^2_{\rm eff}$ and ξ_ν. In the particular case of ΛCDM $+N_{\rm eff} + \sum m_\nu + \xi_\nu$, no significant changes are observed in relation to the general case, and therefore the conclusions about the properties of the free parameters are the same. In both models, no mean deviations are found for the degeneracy parameter and $\xi_\nu \simeq 0$. It is known that the neutrino properties can correlate in different ways with other cosmological parameters. In the present work, we have considered the ΛCDM model to investigate the constraints on the properties of the relic neutrinos. Recently, it has been discovered that the presence of massive neutrinos in cosmic dynamics can lead to small deviations of the ΛCDM scenario [255–259]. Therefore, it is plausible to consider a parametric space extension by including neutrinos properties to models beyond the ΛCDM model (phenomenology of dark energy and modified gravity models). It can bring new perspectives in this direction.

Measurements of the radiation density in the early Universe, usually parametrized via the effective number of neutrino species, have achieved incredible precision within the last decade, thanks to experiments such as Planck. The ongoing SPT-3G experiment and the future Simons Observatory and CMB-S4 experiment will further increase our knowledge and reach sensitivities down to $\Delta N_{eff} \simeq 0.06$ (95% C.L.). This makes it possible to detect or exclude new ultralight particles even if they decoupled very early in the Universe. Here we show that one of the best motivations for such light particles comes from the observation of neutrino oscillations. Indeed, if neutrinos are Dirac particles like all other known fermions, we must extend the Standard Model by two or three practically massless chirality partners ν_R. Models that address the Dirac stability, the smallness of neutrino masses, or the matter–anti-matter asymmetry of our Universe typically endow the ν_R with additional interactions that could lead to thermalization in the early Universe and hence a measurable contribution to N_{eff}. On the other hand, fostering the only ungauged anomaly-free symmetry of the standard Model, $U(1)_{B-L}$, to a local symmetry requires the introduction of three RHN, which make neutrinos massive. It is, therefore, essential to point out that there is currently no theoretical or phenomenological argument against an unbroken $U(1)_{B-L}$ gauge symmetry featuring Dirac neutrinonos and neutrinogenesis to explain the baryon asymmetry of the Universe. We can even give the new gauge boson Z' mass $M_{Z'}$, a new dimensionful parameter disconnected from other scales. We have shown, in particular, that a successful cosmological test provides strong constraints in the mass of Z' boson due to the resonant enhancement of the thermalization rate, previously unexplored.

Finally I would like to mention that several methods have been proposed in order to detect this cosmic neutrino background, which would be a milestone in the history of physics, since we would be observing the universe approximately 1 second after the big bang, thus leading us to a totally unexplored physics (For some references about it, please check [596], [597] and [598]). However, being a purely experimental work, it is outside the scope of this thesis, which also leaves new avenues for future projects. On the other hand, from the theoretical-observational point of view, we also find new perspectives and projections to explore, which means that new graduate theses can be proposed for the future, not only from the UFJF physics department but not from other parts of Brazil and this thesis lays the foundations for this new line of research that combines both particle physics and cosmology.

Chapter A

Appendix to chapter 5

"Without effort, you can't pull a fish out of the pond." – Russian proverb.

Perturbations in cosmology

As we have seen in Chapter 2, the assumption of homogeneous and isotropic universe is very useful and productive, but it is reliable only on very large scales (above 200 Mpc). Its shortcomings become evident when we start to investigate how structures, such as galaxies and their clusters, form, since these are huge deviations from the cosmological principle. In this Chapter we address small deviations from the cosmological principle, considering perturbations in the FLRW metric. This is the starting point of the incredibly difficult task of understanding how structures form in an expanding universe, which ultimately needs powerful machines and numerical simulations. The material for this Chapter is mainly drawn from the textbooks [57], [131], [200] and from the papers/reviews [21], [91], [134], [113]. We assume hereafter $K = 0$, both for simplicity and because we have seen that there is strong observational evidence of a spatially flat universe. From this Chapter on, we also start to adopt natural $\hbar = c = 1$ units.

From the perturbations of the FLRW metric to the linearised Einstein tensor

Let $\bar{g}_{\mu\nu}$ be the FLRW metric, and write it using the conformal time:

$$\bar{g}_{\mu\nu} = a^2(\eta)(-d\eta^2 + \delta_{ij}dx^i dx^j) \ . \tag{A.1}$$

This metric describes the **background spacetime**, or manifold. However, the background spacetime is fictitious, in the sense that we are now considering deviations from homogeneity and isotropy and therefore the actual **physical spacetime** is a different manifold described by the metric $g_{\mu\nu}$. Defining the difference:

$$\delta g_{\mu\nu}(x) = g_{\mu\nu}(x) - \bar{g}_{\mu\nu}(x) \ , \tag{A.2}$$

at a certain spacetime coordinate x is an ill-posed statement because $g_{\mu\nu}$ and $\bar{g}_{\mu\nu}$ are tensors defined on different manifolds and x is a coordinate defined through different charts. Even if we embed the two manifolds in a single one, still the difference between two tensors evaluated at different points is an ill-defined operation. Therefore, in order to make Eq. (A.2) meaningful, we need an extra ingredient: a map which identifies points of the background manifold with those of the physical manifold. This map is called **gauge**, is arbitrary and allows us to use a fixed coordinate system (a chart) in the background manifold also for the points in the physical manifold. In other words, we shall still use conformal or cosmic time plus comoving spatial coordinates even when describing perturbative quantities. This property leads to the so-called **problem of the gauge**, which we will briefly discuss later. For more details on these topics, see [176] and [118]. Metric $g_{\mu\nu}$ has in general 10 independent components that, in a generic gauge, we write down in the following form:

$$g_{\mu\nu} = a^2(\eta) \left\{ \begin{array}{cc} -[1+2\psi(\eta,\mathbf{x})] & w_i(\eta,\mathbf{x}) \\ \\ w_i(\eta,\mathbf{x}) & \delta_{ij}[1+2\phi(\eta,\mathbf{x})] + \chi_{ij}(\eta,\mathbf{x}) \end{array} \right\} \ , \qquad \delta^{ij}\chi_{ij} = 0 \ , \tag{A.3}$$

where $\psi,\ \phi,\ w_i,\ \chi_{ij}$ $(i,j=1,2,3)$ are functions of the background spacetime coordinates x^μ, in our case conformal time and comoving spatial coordinates.[1] From now on we omit their explicit functional dependence wherever possible, in order to keep a lighter notation. As we mentioned above, the liberty of choosing a gauge allows us to fix a coordinate system in the background manifold. The latter shall be one in which homogeneity and isotropy are manifest, of course. Therefore, we could use any time parametrisation, though we will employ conformal time the most because it has the important physical meaning of the comoving particle horizon, and as for the spatial coordinates we shall always choose the comoving ones for which at any given and fixed time the background spatial metric is Euclidean, i.e. $\delta_{ij}dx^i dx^j$. For this reason, the perturbations in Eq. (A.3) can be regarded

[1] The reason why ψ and ϕ are multiplied by 2 in the perturbed metric is just for pure future convenience of calculation.

as usual 3-vectors, defined from the rotation group SO(3). Let us elaborate more on this point. Consider the coordinate transformation:

$$\frac{\partial x^{\mu}}{\partial x^{\nu'}} = \begin{pmatrix} 1 & 0 \\ 0 & R^{i}{}_{j} \end{pmatrix} , \tag{A.4}$$

where $R^{i}{}_{j}$ is a rotation. By definition, a rotation is characterised by $R^{T}R = I$, i.e. the transposed matrix is also the inverse, hence $\delta_{kl}R^{k}{}_{i}R^{l}{}_{j} = \delta_{ij}$. Applying this transformation to metric (A.3) we get:

$$g'_{00} = g_{00} , \quad g'_{0i} = R^{k}{}_{i}g_{0k} , \quad g'_{ij} = R^{k}{}_{i}R^{l}{}_{j}g_{kl} , \tag{A.5}$$

and hence, recalling that $R^{k}{}_{i}R^{l}{}_{j}\delta_{kl} = \delta_{ij}$, we finally find:

$$\psi' = \psi , \quad w'_{i} = R^{k}{}_{i}w_{k} , \quad \phi' = \phi , \quad \chi'_{ij} = R^{k}{}_{i}R^{l}{}_{j}\chi_{kl} . \tag{A.6}$$

Therefore, ψ and ϕ are two 3-scalars, w_i $(i = 1, 2, 3)$ is a 3-vector, χ_{ij} is a 3-tensor $(i, j = 1, 2, 3)$ and the indices of w_i and χ_{ij} are raised and lowered by δ_{ij}. Note that the 6 components of χ_{ij} are not independent because $\delta^{ij}\chi_{ij} = 0$. In other words, χ_{ij} is traceless and we have already put in evidence the spatial trace of the metric through ϕ. One does this also because the spatial intrinsic curvature depends only on ϕ, not on χ_{ij}.[2] Now, if the gauge chosen in Eq. (A.3) is such that:

$$|\bar{g}_{\mu\nu}| \gg |\delta g_{\mu\nu}| , \tag{A.7}$$

then we are dealing with *perturbations*. They are considered small, or linear, or at first-order if we neglect powers with exponent larger than one in the quantities themselves and in their derivatives. Not only, also combinations among different perturbations are neglected. For example, ψ^2, ϕw_i, $w^i\chi_{ij}$, $\phi'\phi$ and so on are all second order perturbations, and therefore negligible. Let us see how this works when computing the Christoffel symbols for metric (A.3). Substituting the decomposition (A.2) into the definition of Christoffel symbol we have:

$$\begin{aligned} \Gamma^{\mu}_{\nu\rho} = \frac{1}{2}g^{\mu\sigma}\left(g_{\sigma\nu,\rho} + g_{\sigma\rho,\nu} - g_{\nu\rho,\sigma}\right) = \frac{1}{2}\bar{g}^{\mu\sigma}\left(\bar{g}_{\sigma\nu,\rho} + \bar{g}_{\sigma\rho,\nu} - \bar{g}_{\nu\rho,\sigma}\right) \\ \frac{1}{2}\bar{g}^{\mu\sigma}\left(\delta g_{\sigma\nu,\rho} + \delta g_{\sigma\rho,\nu} - \delta g_{\nu\rho,\sigma}\right) + \frac{1}{2}\delta g^{\mu\sigma}\left(\bar{g}_{\sigma\nu,\rho} + \bar{g}_{\sigma\rho,\nu} - \bar{g}_{\nu\rho,\sigma}\right) , \end{aligned} \tag{A.8}$$

[2] One can guess this by simply noting that the spatial curvature is a 3-scalar and one cannot form any 3-scalar at first-order from χ_{ij} since it is traceless.

where the comma denotes the usual partial derivative. Note that we have assumed the same decomposition of Eq. (A.2) also for the covariant components of the metric and neglected terms such as $\delta g^{\mu\sigma}\delta g_{\sigma\nu,\rho}$, i.e. perturbative quantities multiplied by their derivatives. It is important to realise that $\delta g^{\mu\sigma}$ is not simply $\delta g_{\mu\sigma}$ with indices raised by $\bar{g}^{\mu\sigma}$. Since

$$g^{\mu\rho}g_{\rho\nu} = \delta^{\mu}{}_{\nu} \ , \qquad \bar{g}^{\mu\rho}\bar{g}_{\rho\nu} = \delta^{\mu}{}_{\nu} \ , \tag{A.9}$$

because both are metrics, using Eq. (A.2), we can see that

$$\boxed{\delta g^{\mu\nu} = -\bar{g}^{\mu\rho}\delta g_{\rho\sigma}\bar{g}^{\nu\sigma}} \tag{A.10}$$

In particular, in our scenario of cosmological perturbations, we shall write the total metric, using the conformal time, as follows:

$$g_{\mu\nu} = a^2(\eta_{\mu\nu} + h_{\mu\nu}) \ . \tag{A.11}$$

Hence, the perturbed contravariant metric is the following:

$$\delta g^{00} = -\frac{1}{a^2}h_{00} \quad \delta g^{0i} = \frac{1}{a^2}\delta^{il}h_{0l} = \frac{1}{a^2}h_{0i} \ , \quad \delta g^{ij} = -\frac{1}{a^2}\delta^{il}h_{lm}\delta^{mj} = -\frac{1}{a^2}h_{ij} \ , \tag{A.12}$$

where we have used our hypothesis that the indices of h_{ij} are raised by δ^{ij} and the property $h^{ij} = h_{ij}$. Do not be confused by the fact that $\delta g_{\mu\nu}$ is the perturbed covariant metric but $\delta g^{\mu\nu}$ *is not* the contravariant perturbed metric. One does raise the indices of the contravariant perturbed metric with the background one, but a minus sign must be taken into account. This fact is not dissimilar from considering the Taylor expansion

$$\frac{1}{1+x} = 1 - x + \mathcal{O}(x^2) \ . \tag{A.13}$$

The perturbed Christoffel symbols

It is clear from Eq. (A.8) that we can decompose the affine connection as follows:

$$\Gamma^{\mu}_{\nu\rho} = \bar{\Gamma}^{\mu}_{\nu\rho} + \delta\Gamma^{\mu}_{\nu\rho} \ , \tag{A.14}$$

where the barred one is computed from the background metric only. Therefore, we can see that

$$\boxed{\delta\Gamma^{\mu}_{\nu\rho} = \frac{1}{2}\bar{g}^{\mu\sigma}\left(\delta g_{\sigma\nu,\rho} + \delta g_{\sigma\rho,\nu} - \delta g_{\nu\rho,\sigma} - 2\delta g_{\sigma\alpha}\bar{\Gamma}^{\alpha}_{\nu\rho}\right)} \tag{A.15}$$

The background Christoffel symbols were calculated already in Chapter 2 but for the FLRW metric written in the cosmic time. Then, the only non-vanishing background Christoffel symbols are:

$$\bar{\Gamma}^{0}_{00} = \frac{a'}{a}\,, \quad \bar{\Gamma}^{0}_{ij} = \frac{a'}{a}\delta_{ij}\,, \quad \bar{\Gamma}^{i}_{0j} = \frac{a'}{a}\delta^{i}{}_{j}\,, \tag{A.16}$$

where the prime denotes derivation with respect to the conformal time. One can make the calculation directly from the FLRW metric written in the conformal time or use the results already found in Eq. (2.35) for the FLRW metric written in the cosmic time and use the transformation relation for the Christoffel symbol:

$$\bar{\Gamma}'^{\mu}_{\nu\rho} = \bar{\Gamma}^{\alpha}_{\beta\gamma}\frac{\partial x^{\beta}}{\partial x'^{\nu}}\frac{\partial x^{\gamma}}{\partial x'^{\rho}}\frac{\partial x'^{\mu}}{\partial x^{\alpha}} + \frac{\partial x'^{\mu}}{\partial x^{\sigma}}\frac{\partial^2 x^{\sigma}}{\partial x'^{\nu}\partial x'^{\rho}}\,, \tag{A.17}$$

where the primed coordinates are in the conformal time and hence:

$$\frac{\partial x'^{0}}{\partial x^{0}} = \frac{1}{a}\,, \qquad \frac{\partial x'^{l}}{\partial x^{m}} = \delta^{l}{}_{m}\,, \tag{A.18}$$

being the other cases vanishing. It is a good and reassuring exercise to do in both ways and check that the result is the same. First of all, we shall use mostly the conformal time throughout these notes since, as we saw earlier, it represents the comoving particle horizon and it will allow us to clearly distinguish the evolution of super-horizon (hence causally disconnected) scales from sub-horizon ones. On the other hand, the most economic way to compute the linearised Einstein equations is using the cosmic time and stopping to the calculation of the Ricci tensor by considering the Einstein equations in the form

$$R_{\mu\nu} = 8\pi G\left(T_{\mu\nu} - \frac{1}{2}g_{\mu\nu}T\right)\,, \tag{A.19}$$

as done e.g. in [200]. It is the most economic way because in the cosmic time we have only 2 non-vanishing Christoffel symbols, whereas in the conformal time we have three, and because we are spared to compute the perturbed Ricci scalar. Once done this calculation, it is straightforward to come back to the conformal time. In the following we shall anyway

go on using the conformal time, because it is a good workout. Compare the results found here with those in [200, Chapter 5] using the tensorial properties:

$$R_{\mu\nu} = \tilde{R}_{\rho\sigma}\frac{\partial\tilde{x}^\rho}{\partial x^\mu}\frac{\partial\tilde{x}^\sigma}{\partial x^\nu} \ , \quad h_{\mu\nu} = \tilde{h}_{\rho\sigma}\frac{\partial\tilde{x}^\rho}{\partial x^\mu}\frac{\partial\tilde{x}^\sigma}{\partial x^\nu} \ , \tag{A.20}$$

where the quantities with tilde are in the cosmic time. Since the change from cosmic to conformal time does not affect the spatial coordinates, we have that:

$$R_{00} = \tilde{R}_{00}a^2 \ , \quad R_{0i} = \tilde{R}_{0i}a \ , \quad R_{ij} = \tilde{R}_{ij} \ , \tag{A.21}$$

and similarly for $h_{\mu\nu}$. With this map, we can check the results that we are going to find here with those in [200]. Mind that in [200] the Ricci tensor is defined with the opposite sign with respect to ours here. We are now in the position of writing the perturbed Christoffel symbols. We do so without leaving $h_{\mu\nu}$ explicit from Eq. (A.3). Find that:

$$\delta\Gamma^0_{00} = -\frac{1}{2}h'_{00} \ , \quad \delta\Gamma^0_{i0} = -\frac{1}{2}\left(h_{00,i} - 2\mathcal{H}h_{0i}\right) \ , \tag{A.22}$$

$$\delta\Gamma^i_{00} = h'_{i0} + \mathcal{H}h_{i0} - \frac{1}{2}h_{00,i} \ , \tag{A.23}$$

$$\delta\Gamma^0_{ij} = -\frac{1}{2}\left(h_{0i,j} + h_{0j,i} - h'_{ij} - 2\mathcal{H}h_{ij} - 2\mathcal{H}\delta_{ij}h_{00}\right) \ , \tag{A.24}$$

$$\delta\Gamma^i_{j0} = \frac{1}{2}h'_{ij} + \frac{1}{2}\left(h_{i0,j} - h_{0j,i}\right) \ , \tag{A.25}$$

$$\delta\Gamma^i_{jk} = \frac{1}{2}\left(h_{ij,k} + h_{ik,j} - h_{jk,i} - 2\mathcal{H}\delta_{jk}h_{i0}\right) \ . \tag{A.26}$$

The prime denotes derivative with respect to the conformal time. The indices might seem unbalanced, but we have used the fact that h_{i0} and h_{ij} are 3-tensors with respect to the metric δ_{ij} and hence, for example, $h^i{}_0 = h_{i0}$. Recall that

$$\mathcal{H} \equiv \frac{a'}{a} \ , \tag{A.27}$$

i.e. $\mathcal{H}$ is the Hubble factor written in conformal time.

The perturbed Ricci tensor and Einstein tensor

With this result we are going to compute the components of the perturbed Ricci tensor. Recall that this is defined as:

$$R_{\mu\nu} = \Gamma^\rho_{\mu\nu,\rho} - \Gamma^\rho_{\mu\rho,\nu} + \Gamma^\rho_{\mu\nu}\Gamma^\sigma_{\rho\sigma} - \Gamma^\rho_{\mu\sigma}\Gamma^\sigma_{\nu\rho} \ , \tag{A.28}$$

and hence, when substituting Eq. (A.14), we get

$$R_{\mu\nu} = \bar{\Gamma}^{\rho}_{\mu\nu,\rho} - \bar{\Gamma}^{\rho}_{\mu\rho,\nu} + \bar{\Gamma}^{\rho}_{\mu\nu}\bar{\Gamma}^{\sigma}_{\rho\sigma} - \bar{\Gamma}^{\rho}_{\mu\sigma}\bar{\Gamma}^{\sigma}_{\nu\rho}$$
$$+\delta\Gamma^{\rho}_{\mu\nu,\rho} - \delta\Gamma^{\rho}_{\mu\rho,\nu} + \bar{\Gamma}^{\rho}_{\mu\nu}\delta\Gamma^{\sigma}_{\rho\sigma} + \delta\Gamma^{\rho}_{\mu\nu}\bar{\Gamma}^{\sigma}_{\rho\sigma} - \bar{\Gamma}^{\rho}_{\mu\sigma}\delta\Gamma^{\sigma}_{\nu\rho} - \delta\Gamma^{\rho}_{\mu\sigma}\bar{\Gamma}^{\sigma}_{\nu\rho} \ , \tag{A.29}$$

by neglecting second order terms in the connection. It is clear that we can expand also the Ricci tensor as:

$$R_{\mu\nu} = \bar{R}_{\mu\nu} + \delta R_{\mu\nu} \ , \tag{A.30}$$

and we compute now its perturbed components. After opening up all the sums, we can see that:

$$\delta R_{00} = \delta\Gamma^{l}_{00,l} - \delta\Gamma^{l}_{0l,0} - \mathcal{H}\delta\Gamma^{l}_{0l} + 3\mathcal{H}\delta\Gamma^{0}_{00} \ , \tag{A.31}$$

and substituting the previous results, one gets:

$$\delta R_{00} = -\frac{1}{2}\nabla^2 h_{00} - \frac{3}{2}\mathcal{H}h'_{00} + h'_{k0,k} + \mathcal{H}h_{k0,k} - \frac{1}{2}\left(h''_{kk} + \mathcal{H}h'_{kk}\right) \ . \tag{A.32}$$

Here we have defined $\delta^{ij}\partial_i\partial_j \equiv \nabla^2$ as the Laplacian in comoving coordinates. Note that $h_{kk} = \delta^{lm}h_{lm}$, i.e. in the present instance repeated indices are summed even if both covariant or contravariant. Of course, we can repeat the above procedure also for the other components. Find that:

$$\delta R_{0i} = -\mathcal{H}h_{00,i} - \frac{1}{2}\left(\nabla^2 h_{0i} - h_{k0,ik}\right) + \left(\frac{a''}{a} + \mathcal{H}^2\right)h_{0i} - \frac{1}{2}\left(h'_{kk,i} - h'_{ki,k}\right) \ , \tag{A.33}$$

and

$$\delta R_{ij} = \frac{1}{2}h_{00,ij} + \frac{\mathcal{H}}{2}h'_{00}\delta_{ij} + \left(\mathcal{H}^2 + \frac{a''}{a}\right)h_{00}\delta_{ij}$$
$$-\frac{1}{2}\left(\nabla^2 h_{ij} - h_{ki,kj} - h_{kj,ki} + h_{kk,ij}\right) + \frac{1}{2}h''_{ij} + \mathcal{H}h'_{ij} + \left(\mathcal{H}^2 + \frac{a''}{a}\right)h_{ij}$$
$$+\frac{\mathcal{H}}{2}h'_{kk}\delta_{ij} - \mathcal{H}h_{k0,k}\delta_{ij} - \frac{1}{2}(h'_{0i,j} + h'_{0j,i}) - \mathcal{H}(h_{0i,j} + h_{0j,i}) \ . \tag{A.34}$$

In the same way we decomposed metric (A.2), we decompose the Einstein tensor. We shall work with mixed indices:

$$G^{\mu}{}_{\nu} = g^{\mu\rho}R_{\rho\nu} - \frac{1}{2}\delta^{\mu}{}_{\nu}R = \bar{g}^{\mu\rho}\bar{R}_{\rho\nu} - \frac{1}{2}\delta^{\mu}{}_{\nu}\bar{R} + \bar{g}^{\mu\rho}\delta R_{\rho\nu} + \delta g^{\mu\rho}\bar{R}_{\rho\nu} - \frac{1}{2}\delta^{\mu}{}_{\nu}\delta R \,, \tag{A.35}$$

where $\bar{G}^{\mu}{}_{\nu} = \bar{R}^{\mu}{}_{\nu} - \frac{1}{2}\delta^{\mu}{}_{\nu}\bar{R}$ is the background Einstein tensor and depends purely from the background metric $\bar{g}_{\mu\nu}$ whereas

$$\delta G^{\mu}{}_{\nu} = \bar{g}^{\mu\rho}\delta R_{\rho\nu} + \delta g^{\mu\rho}\bar{R}_{\rho\nu} - \frac{1}{2}\delta^{\mu}{}_{\nu}\delta R \,, \tag{A.36}$$

is the linearly perturbed Einstein tensor, which depends from both $\bar{g}_{\mu\nu}$ and $h_{\mu\nu}$. Compute the perturbed Ricci scalar:

$$\delta R = g^{\mu\nu}R_{\mu\nu} = \bar{g}^{\mu\nu}\delta R_{\mu\nu} + \delta g^{\mu\nu}\bar{R}_{\mu\nu} \,. \tag{A.37}$$

Expand the above expression and use formula (A.10) in order to find:

$$\delta R = -\frac{1}{a^2}\delta R_{00} + \frac{1}{a^2}\delta^{ij}\delta R_{ij} - a^2 h_{\rho\sigma}\bar{g}^{\rho\mu}\bar{g}^{\sigma\nu}\bar{R}_{\mu\nu} \,, \tag{A.38}$$

and then, recalling that the background Ricci tensor is:

$$\bar{R}_{00} = 3\left(\mathcal{H}^2 - \frac{a''}{a}\right) \,, \quad \bar{R}_{ij} = \delta_{ij}\left(\mathcal{H}^2 + \frac{a''}{a}\right) \,, \tag{A.39}$$

one can write:

$$\delta R = -\frac{1}{a^2}\delta R_{00} - \frac{3}{a^2}h_{00}\left(\mathcal{H}^2 - \frac{a''}{a}\right) + \frac{1}{a^2}\delta^{ij}\delta R_{ij} - \frac{1}{a^2}h_{kk}\left(\mathcal{H}^2 + \frac{a''}{a}\right) \,, \tag{A.40}$$

Substituting the formulae for the perturbed Ricci tensor, one finds:

$$\begin{aligned} a^2\delta R = {} & \nabla^2 h_{00} + 3\mathcal{H}h'_{00} + 6\frac{a''}{a}h_{00} - 2h'_{k0,k} - 6\mathcal{H}h_{k0,k} \\ & + h''_{kk} + 3\mathcal{H}h'_{kk} - \nabla^2 h_{kk} + h_{kl,kl} \,. \end{aligned} \tag{A.41}$$

The second line represents $a^2\delta R^{(3)}$, i.e. the intrinsic spatial perturbed curvature scalar. Now, let us calculate the mixed components of the perturbed Einstein tensor. We can see that:

$$\boxed{2a^2\delta G^0{}_0 = -6\mathcal{H}^2 h_{00} + 4\mathcal{H}h_{k0,k} - 2\mathcal{H}h'_{kk} + \nabla^2 h_{kk} - h_{kl,kl}} \tag{A.42}$$

and

$$\boxed{2a^2\delta G^0{}_i = 2\mathcal{H}h_{00,i} + \nabla^2 h_{0i} - h_{k0,ki} + h'_{kk,i} - h'_{ki,k}} \tag{A.43}$$

and

$$\begin{aligned} 2a^2\delta G^i{}_j = \Big[& -4\frac{a''}{a}h_{00} - 2\mathcal{H}h'_{00} - \nabla^2 h_{00} + 2\mathcal{H}^2 h_{00} - 2\mathcal{H}h'_{kk} \\ & + \nabla^2 h_{kk} - h_{kl,kl} + 2h'_{k0,k} + 4\mathcal{H}h_{k0,k} - h''_{kk}\Big]\delta^i{}_j + h_{00,ij} - \nabla^2 h_{ij} \\ & + h_{ki,kj} + h_{kj,ki} - h_{kk,ij} + h''_{ij} + 2\mathcal{H}h'_{ij} - (h'_{0i,j} + h'_{0j,i}) - 2\mathcal{H}(h_{0i,j} + h_{0j,i}) \ . \end{aligned} \tag{A.44}$$

Now we turn to the right hand side of the Einstein equations, i.e. the energy-momentum tensor.

Perturbation of the energy-momentum tensor

In the following we shall use mostly the energy-momentum tensor defined through the distribution function and its perturbation. However, let us see how to perturb the background, perfect fluid energy-momentum tensor. This was introduced as:

$$\bar{T}_{\mu\nu} = (\bar{\rho} + \bar{P})\bar{u}_\mu \bar{u}_\nu + \bar{P}\bar{g}_{\mu\nu} \ , \tag{A.45}$$

as the tensor describing a fluid with no dissipation, i.e. constant entropy along the flow[3]. Let us rewrite $\bar{T}_{\mu\nu}$ as follows:

$$\bar{T}_{\mu\nu} = \bar{\rho}\bar{u}_\mu \bar{u}_\nu + \bar{P}\bar{\theta}_{\mu\nu} \ , \qquad \bar{\theta}_{\mu\nu} \equiv \bar{g}_{\mu\nu} + \bar{u}_\mu \bar{u}_\nu \ . \tag{A.46}$$

[3] We can compute $\bar{u}^\nu \nabla_\nu \bar{u}^\mu$, demand its vanishing and check via the second law of thermodynamics that this corresponds to a constant entropy.

The tensor $\bar{\theta}_{\mu\nu}$ acts as a projector on the hypersurface orthogonal to the four-velocity (We know that $\bar{\theta}_{\mu\nu}\bar{u}^{\mu} = 0$.). This is an example of 3+1 decomposition, which is particularly useful when we study a fluid flow, such that:

$$\bar{\rho} = \bar{T}_{\mu\nu}\bar{u}^{\mu}\bar{u}^{\nu} \ , \quad 3\bar{P} = \bar{T}_{\mu\nu}\bar{\theta}^{\mu\nu} \ , \quad T \equiv \bar{g}^{\mu\nu}\bar{T}_{\mu\nu} = -\rho + 3P \ , \tag{A.47}$$

i.e. the fluid density is the projection of the energy-momentum tensor along the 4-velocity of the fluid element and the pressure is the projection of the energy-momentum tensor on the 3-hypersurface orthogonal to the four-velocity. The most general energy-momentum tensor, which also includes the possibility of dissipation, can be then written by straightforwardly generalising Eq. (A.46), i.e.

$$\boxed{T_{\mu\nu} = \rho u_{\mu}u_{\nu} + q_{\mu}u_{\nu} + q_{\nu}u_{\mu} + (P+\pi)\theta_{\mu\nu} + \pi_{\mu\nu}} \tag{A.48}$$

where q_{μ} is the *heat transfer* contribution, satisfying $q_{\mu}u^{\mu} = 0$ and thus contributing with 3 independent components; $\pi_{\mu\nu}$ is the *anisotropic stress*, it is traceless and satisfies $\pi_{\mu\nu}u^{\mu} = 0$, hence providing 5 independent components. The trace of $\pi_{\mu\nu}$ is π, it is called *bulk viscosity* and has been put in evidence together with the pressure. For more detail about dissipative processes in cosmology and the above decomposition of the energy-momentum tensor, see the review [114]. The anisotropic stress $\pi_{\mu\nu}$ is not necessarily related to viscosity, but can exist for relativistic species such as photons and neutrinos because of the quadrupole moments of their distributions, as we shall see later. On the other hand, heat fluxes and bulk viscosity are related to dissipative processes, and we neglect them in these notes starting from the next section. Now we consider the energy-momentum tensor of Eq. (A.48) as made up of a background contribution plus a linear perturbation, i.e. we expand

$$\rho = \bar{\rho} + \delta\rho(\eta, \mathbf{x}) \ , \quad P = \bar{P} + \delta P(\eta, \mathbf{x}) \ , \quad u^{\mu} = \bar{u}^{\mu} + \delta u^{\mu}(\eta, \mathbf{x}) \ , \tag{A.49}$$

which are the physical density, pressure and four-velocity, which, remember, depend on the background quantities because of our choice of a gauge. The barred quantities depend only on η, since they are defined on the FLRW background. Heat fluxes, bulk viscosity and anisotropic stresses are purely perturbed quantities.[4] Therefore, we have:

$$T_{\mu\nu} = \bar{T}_{\mu\nu} + \delta\rho\bar{u}_{\mu}\bar{u}_{\nu} + \bar{\rho}\delta u_{\mu}\bar{u}_{\nu} + \bar{\rho}\bar{u}_{\mu}\delta u_{\nu} + q_{\mu}\bar{u}_{\nu} + q_{\nu}\bar{u}_{\mu} + \bar{\theta}_{\mu\nu}(\delta P + \pi) + \bar{P}\delta\theta_{\mu\nu} + \pi_{\mu\nu} \ , \tag{A.50}$$

[4] Bulk viscosity is compatible with the cosmological principle and can be contemplated also at background level. It plays a central role in the so-called **bulk viscous cosmology**, see [208].

where one can straightforwardly identify the perturbed energy-momentum tensor and where

$$\delta\theta_{\mu\nu} = h_{\mu\nu} + \delta u_\mu \bar{u}_\nu + \bar{u}_\mu \delta u_\nu \ . \tag{A.51}$$

Now, recall that the background four-velocity satisfies the normalisation:

$$\bar{g}_{\mu\nu}\bar{u}^\mu\bar{u}^\nu = -1 \ . \tag{A.52}$$

Let us choose a frame in which to make explicit the components of the energy-momentum tensor. Of course, we use comoving coordinates, for which one has $\bar{u}^i = 0$. From Eq. (A.52) we have then

$$a^2(\bar{u}^0)^2 = 1 \ , \tag{A.53}$$

and we choose the positive solution $\bar{u}^0 = 1/a$, which implies $u_0 = -a$.[5] When we choose these coordinates, the relations $q_\mu u^\mu = \pi_{\mu\nu}u^\mu = 0$ imply that $q_0 = \pi_{\mu 0} = 0$, i.e. the heat flux and the anisotropic stress have only spatial components. We can calculate the components of the energy-momentum tensor (A.50), such that:

$$T_{00} = \bar{\rho}(1+\delta)a^2 - 2a(\bar{\rho}+\bar{P})\delta u_0 + \bar{P}h_{00} \ , \tag{A.54}$$

$$T_{0i} = -a(\bar{\rho}+\bar{P})\delta u_i - aq_i + \bar{P}h_{0i} \ , \tag{A.55}$$

$$T_{ij} = (\bar{P} + \delta P + \pi)a^2\delta_{ij} + \bar{P}h_{ij} + \pi_{ij} \ , \tag{A.56}$$

where we have introduced one of the main characters of these notes, the **density contrast**:

$$\boxed{\delta \equiv \frac{\delta\rho}{\bar{\rho}}} \tag{A.57}$$

The density contrast is very important because describes how structure formation begins. Note how the presence of perturbations in the four-velocity gives rise to mixed time-space components in the energy-momentum tensor, i.e. the breaking of homogeneity and isotropy allows for extra fluxes beyond the Hubble one. Note that the total four-velocity also satisfies a normalisation relation, with respect to the total metric, i.e.

$$g_{\mu\nu}u^\mu u^\nu = -1 \ . \tag{A.58}$$

[5] It amounts to choose that the conformal time and the fluid element proper time flow in the same direction.

If we expand this relation up to the first order we find:

$$\bar{g}_{\mu\nu}\bar{u}^{\mu}\bar{u}^{\nu} + h_{\mu\nu}\bar{u}^{\mu}\bar{u}^{\nu} + 2\bar{g}_{\mu\nu}\delta u^{\mu}\bar{u}^{\nu} = -1 \ . \tag{A.59}$$

Using Eq. (A.52) and $\bar{u}^i = 0$, we find that:

$$h_{00} + 2\bar{g}_{00}a\delta u^0 = 0 \ , \tag{A.60}$$

and thus we can relate the metric perturbation h_{00} to δu^0 as follows:

$$\boxed{\delta u^0 = \frac{h_{00}}{2a^3}} \tag{A.61}$$

Care is needed when we want to compute the covariant components of the perturbed four-velocity δu_μ. These are not simply $\delta u_\mu = \bar{g}_{\mu\nu}\delta u^\nu$. It is the same care we had to apply when considering the relation between $\delta g^{\mu\nu}$ and $h_{\mu\nu}$. So, let us define:

$$\boxed{\delta u_i = a v_i} \tag{A.62}$$

with v_i components of a 3-vector, i.e. its index is raised by δ^{ij} so that $v^i = v_i$. Let us compute now the components δu^i. We must start from the covariant expression for the total four velocity, i.e.

$$\bar{u}_\mu + \delta u_\mu = u_\mu = g_{\mu\nu}u^\nu = g_{\mu\nu}(\bar{u}^\nu + \delta u^\nu) \ , \tag{A.63}$$

and expanding up to first order, we get

$$\bar{u}_\mu + \delta u_\mu = \bar{g}_{\mu\nu}\bar{u}^\nu + \bar{g}_{\mu\nu}\delta u^\nu + h_{\mu\nu}\bar{u}^\nu \ . \tag{A.64}$$

Equating order by order we obtain $\bar{u}_\mu = \bar{g}_{\mu\nu}\bar{u}^\nu$, as expected, and

$$\boxed{\delta u_\mu = \bar{g}_{\mu\nu}\delta u^\nu + h_{\mu\nu}\bar{u}^\nu} \tag{A.65}$$

so that

$$\boxed{\delta u^\mu = \bar{g}^{\mu\nu}\delta u_\nu - \bar{g}^{\mu\rho}h_{\rho\nu}\bar{u}^\nu} \tag{A.66}$$

So, there is an extra term $h_{\mu\nu}\bar{u}^{\nu}$. This comes from the fact that $\bar{g}_{\mu\nu}$ raises or lowers indices for the background quantities only whereas $g_{\mu\nu}$ raises or lowers indexes for the full quantities only, and δu^{μ} is neither. From Eq. (A.65) and (A.66) we have that

$$\boxed{\delta u_0 = \frac{h_{00}}{2a} \,, \qquad a\delta u^i = v_i - \frac{1}{a^2}h_{i0}} \tag{A.67}$$

We can rewrite the components of the energy-momentum tensor as:

$$T_{00} = \bar{\rho}(1+\delta)a^2 - \bar{\rho}h_{00} \,, \tag{A.68}$$

$$T_{0i} = -a^2(\bar{\rho}+\bar{P})v_i - aq_i + \bar{P}h_{0i} \,, \tag{A.69}$$

$$T_{ij} = (\bar{P}+\delta P+\pi)a^2\delta_{ij} + \bar{P}h_{ij} + \pi_{ij} \,, \tag{A.70}$$

In order to calculate the mixed components we use the standard relation:

$$T^{\mu}{}_{\nu} = g^{\mu\rho}T_{\rho\nu} = \bar{g}^{\mu\rho}\bar{T}_{\rho\nu} + \bar{g}^{\mu\rho}\delta T_{\rho\nu} + \delta g^{\mu\rho}\bar{T}_{\rho\nu} \,. \tag{A.71}$$

Also we can compute the mixed components of the energy-momentum tensor, such that:

$$T^{0}{}_{0} = -\bar{\rho}(1+\delta) \,, \tag{A.72}$$

$$T^{0}{}_{i} = \left(\bar{\rho}+\bar{P}\right)v_i + a^{-1}q_i \,, \tag{A.73}$$

$$T^{i}{}_{0} = -\left(\bar{\rho}+\bar{P}\right)(v_i - h_{0i}a^{-2}) - a^{-1}q_i \,, \tag{A.74}$$

$$T^{i}{}_{j} = \delta^{i}{}_{j}(\bar{P}+\delta P+\pi) + \pi^{i}{}_{j} \,, \tag{A.75}$$

where we have stipulated that $\delta^{il}\pi_{lj}a^{-2} = \pi^{i}{}_{j}$. In the following we shall mainly use, especially for photons and neutrinos, the energy-momentum tensor computed from kinetic theory, i.e. Eq. (**??**):

$$T^{\mu}{}_{\nu} = \int \frac{d^3\mathbf{p}}{(2\pi)^3}\frac{p^{\mu}p_{\nu}}{p^0}f \,, \tag{A.76}$$

in which the distribution function is also perturbed:

$$\boxed{f = \bar{f} + \mathcal{F}} \tag{A.77}$$

thus allowing to define a perturbed energy-momentum tensor as follows:

$$\delta T^{\mu}{}_{\nu} = \int \frac{d^3\mathbf{p}}{(2\pi)^3}\frac{p^{\mu}p_{\nu}}{p^0}\mathcal{F} \,, \tag{A.78}$$

The momentum used here is the proper one which, recall, has the metric embedded in its definition so that:

$$p^i = p_i \ , \quad p^2 = \delta_{ij} p^i p^j \ , \quad E = p^0 \ , \quad p_0 = -E \ . \tag{A.79}$$

These relations provide directly the mass-shell one $E^2 = p^2 + m^2$ from $g_{\mu\nu} P^\mu P^\nu = -m^2$. Note that we are assuming $g_{0i} = 0$, also at perturbative level thanks to gauge freedom, otherwise the relations above would be incorrect since the spatial metric would not be g_{ij} but $g_{ij} - g_{0i} g_{0j} / g_{00}$. See [95] for a nice explanation of this fact. Then, from the above definition of perturbed energy-momentum, we have:

$$\delta T^0{}_0 = -\int \frac{d^3\mathbf{p}}{(2\pi)^3} E(p) \mathcal{F} = -\delta\rho \ , \tag{A.80}$$

which makes sense, and is consistent with Eq. (A.72), because we are weighting the particle energy with the perturbed distribution function. The mixed components are:

$$\delta T^0{}_i = \int \frac{d^3\mathbf{p}}{(2\pi)^3} p_i \mathcal{F} = (\bar{\rho} + \bar{P}) v_i \ , \quad \delta T^i{}_0 = -\int \frac{d^3\mathbf{p}}{(2\pi)^3} p^i \mathcal{F} = -(\bar{\rho} + \bar{P}) v_i \ , \tag{A.81}$$

compatible with Eqs. (A.73) and (A.74) since we are assuming $h_{0i} = 0$ (and neglecting already the heat fluxes). Note the multiplication by $\bar{\rho} + \bar{P}$. Physically the integral gives the perturbed spatial momentum density, which can be decomposed in the velocity flow times the inertial mass density, which is $\bar{\rho} + \bar{P}$ in GR. Finally:

$$\delta T^i{}_j = \int \frac{d^3\mathbf{p}}{(2\pi)^3} \frac{p^i p_j}{E} \mathcal{F} = \delta^i{}_j \delta P + \pi^i{}_j \ , \tag{A.82}$$

from which we can define the perturbed pressure as the trace part:

$$\delta P = \frac{1}{3} \delta^{ij} \delta T_{ij} = \int \frac{d^3\mathbf{p}}{(2\pi)^3} \frac{p^2}{3E} \mathcal{F} \ , \tag{A.83}$$

and the anisotropic stress as the traceless part:

$$\pi^i{}_j = \delta T^i{}_j - \frac{1}{3} \delta^i{}_j \delta^{lm} \delta T_{lm} = \int \frac{d^3\mathbf{p}}{(2\pi)^3} \frac{1}{E} \left(p^i p_j - \frac{1}{3} \delta^i{}_j p^2 \right) \mathcal{F} \ . \tag{A.84}$$

The evolution equations for the perturbations are given by the **linearised Einstein equations**:

$$\delta G^{\mu}{}_{\nu} = 8\pi G \delta T^{\mu}{}_{\nu} \ . \tag{A.85}$$

Unfortunately, Eq. (A.85) is not sufficient to completely describe the behaviour of both matter and metric quantities if the fluid components are more than one. See e.g. [71]. We shall make use of the perturbed Boltzmann equations for each component of our cosmological model.

The problem of the gauge and gauge transformations

As we have mentioned in the previous section, a gauge is a map between the points of the physical manifold and those of the background one which allows us to define the difference between tensors defined on the two manifolds. Suppose we change gauge from a $\mathcal{G}$ to a $\hat{\mathcal{G}}$. Metric (A.3) then becomes:

$$g_{\mu\nu} = a^2(\eta) \left\{ \begin{array}{cc} -[1+2\hat{\psi}(\eta,\mathbf{x})] & \hat{w}_i(\eta,\mathbf{x}) \\ \\ \hat{w}_i(\eta,\mathbf{x}) & \delta_{ij}[1+2\hat{\phi}(\eta,\mathbf{x})] + \hat{\chi}_{ij}(\eta,\mathbf{x}) \end{array} \right\} \ , \qquad \delta^{ij}\hat{\chi}_{ij} = 0 \ . \tag{A.86}$$

We have new hatted functions representing perturbations depending again on the background coordinates, which we have fixed. A similar map can be defined also on the single background manifold, so in absence of perturbations, and it can be deceiving, in the sense that quantities similar to perturbations might appear even if we are in the background manifold. Let us rephrase this. The problem when considering fluctuations in GR is that we cannot be sure, by only looking at a metric, that there are real fluctuations about a known background or it is the metric which is written in a not very appropriate coordinate system. For example, consider the following time transformation for the FLRW metric:

$$d\eta = g(t,\mathbf{x})dt \ . \tag{A.87}$$

Then, the FLRW metric becomes:

$$ds^2 = -a(t,\mathbf{x})^2 g(t,\mathbf{x})^2 dt^2 + a(t,\mathbf{x})^2 \delta_{ij} dx^i dx^j \ , \tag{A.88}$$

and recalling back $t \to \eta$ we get:

$$ds^2 = -a(\eta,\mathbf{x})^2 g(\eta,\mathbf{x})^2 d\eta^2 + a(\eta,\mathbf{x})^2 \delta_{ij} dx^i dx^j \ . \tag{A.89}$$

Now the metric coefficients depend on the position so we may think that homogeneity and isotropy are lost, but it was just a coordinate transformation. This *is not* the problem of the gauge, but is the general covariance typical of GR. As we show above, it is not even necessarily related to perturbations but it is just a coordinate transformation masking the metric in the form that we are used to see it. Computing relativistic invariants or Killing vectors allows to determine if the above is the FLRW metric or not. *The problem of the gauge* is the dependence of the perturbations on the gauge. In the following we will see how a gauge transformation manifests itself through a change of coordinates and deal with the problem of the gauge by introducing *gauge-invariant variables*. Loosely speaking, we will see that the gauge is the *functional dependence* of the perturbative quantities on the coordinates, whereas the background quantities maintain their functional form. For a more complete treatment of the gauge problem, see for example [176], [134] and [118].

Coordinates and gauge transformations

In order to understand how a gauge transformation changes the functional dependence of the perturbative quantities we express the change from a gauge $\mathcal{G}$ to a gauge $\hat{\mathcal{G}}$ as the following infinitesimal coordinate transformation:

$$x^\mu \to \hat{x}^\mu = x^\mu + \xi^\mu(x) \ , \tag{A.90}$$

where x^μ are the background coordinates and ξ^μ is a generic vector field, *the gauge generator*, which must be $|\xi^\mu| \ll 1$ in order to preserve the smallness of the perturbation. From a geometric point of view, we fix a point on the background manifold and by changing gauge we change the corresponding point on the physical manifold. This point has coordinates different from the first one and given by Eq. (A.90). The gauge generator can be seen then as a vector field on the physical manifold and the Lie derivative of the metric along ξ tells us how the perturbative quantities change their functional form. Under a coordinate transformation, the metric tensor $g_{\mu\nu}$, as well as any other tensor of the same rank, transforms in the following way:

$$g_{\mu\nu}(x) = \frac{\partial \hat{x}^\rho}{\partial x^\mu}\frac{\partial \hat{x}^\sigma}{\partial x^\mu}\hat{g}_{\rho\sigma}(\hat{x}) \ , \tag{A.91}$$

which, using Eq. (A.90), can be cast as follows:

$$g_{\mu\nu}(x) = \left(\delta^\rho{}_\mu + \partial_\mu \xi^\rho\right)\left(\delta^\sigma{}_\nu + \partial_\nu \xi^\sigma\right)\hat{g}_{\rho\sigma}(\hat{x}) \ . \tag{A.92}$$

Writing down Eq. (A.92) up to first order, one obtains:

$$g_{\mu\nu}(x) = \hat{g}_{\mu\nu}(x) + \partial_\alpha \hat{g}_{\mu\nu}(x)\xi^\alpha + \partial_\mu \xi^\rho \hat{g}_{\rho\nu}(x) + \partial_\nu \xi^\rho \hat{g}_{\rho\mu}(x) \ , \tag{A.93}$$

where we have also expanded $\hat{g}_{\rho\sigma}(\hat{x})$ about x using Eq. (A.90). We can see that Eq. (A.93) can be cast in the following form:

$$g_{\mu\nu}(x) = \hat{g}_{\mu\nu}(x) + \partial_\alpha g_{\mu\nu}(x)\xi^\alpha + \partial_\mu \xi^\rho g_{\rho\nu}(x) + \partial_\nu \xi^\rho g_{\rho\mu}(x) \ , \tag{A.94}$$

i.e. prove that we can remove the hat from the metric when it is multiplied by ξ. Then, cast the above equation as follows:

$$g_{\mu\nu}(x) = \hat{g}_{\mu\nu}(x) + \nabla_\nu \xi_\mu + \nabla_\mu \xi_\nu \ . \tag{A.95}$$

This equation shows how the functional form of the metric components, i.e. the gauge, changes upon a coordinate transformation. If Eq. (A.90) is an isometry, i.e. $g_{\mu\nu}(x) = \hat{g}_{\mu\nu}(x)$, one gets the *Killing equation*:

$$\nabla_\nu \xi_\mu + \nabla_\mu \xi_\nu = 0 \ . \tag{A.96}$$

Now we use the perturbed FLRW metric (A.3) in Eq. (A.93), and we can see that at the order zero:

$$\hat{a}(\eta) = a(\eta) \tag{A.97}$$

i.e. the scale factor maintains its functional form, confirming the property of the gauge, which maintains the functional form of the background quantities. Then, show that at first-order the following transformation relations hold:

$$\hat{\psi} = \psi - \mathcal{H}\xi^0 - \xi^{0\prime} \qquad \hat{w}_i = w_i - \zeta_i' + \partial_i \xi^0 \tag{A.98}$$

$$\hat{\phi} = \phi - \mathcal{H}\xi^0 - \frac{1}{3}\partial_l \xi^l \qquad \hat{\chi}_{ij} = \chi_{ij} - \partial_j \zeta_i - \partial_i \zeta_j + \frac{2}{3}\delta_{ij}\partial_l \xi^l \tag{A.99}$$

where $\zeta_i \equiv \delta_{il}\xi^l$. We have introduced ζ_i in order not to make confusion with the spatial part of ξ_μ, which is $\xi_i = a^2 \delta_{il}\xi^l = a^2 \zeta_i$. In the very same fashion we adopted for the metric, we can also find the transformation rules for the components of the energy-momentum

tensor. That is, through the same steps that we have just used for the metric, we can write:

$$\hat{T}_{\mu\nu}(x) = T_{\mu\nu}(x) - \partial_\alpha T_{\mu\nu}(x)\xi^\alpha - \partial_\mu \xi^\rho T_{\rho\nu}(x) - \partial_\nu \xi^\rho T_{\rho\mu}(x) \ . \tag{A.100}$$

Using the above transformation with $T_{\mu\nu}$ given by Eq. (A.68)-(A.70), we find that at zeroth order one has:

$$\hat{\bar{\rho}}(\eta) = \bar{\rho}(\eta) \qquad \hat{\bar{P}}(\eta) = \bar{P}(\eta) \tag{A.101}$$

i.e. the background density and pressure maintain their functional forms. Then, show that at first order the following transformation relations hold:

$$\hat{\delta\rho} = \delta\rho - \bar{\rho}'\xi^0 \qquad \hat{v}_i = v_i + \partial_i \xi^0 \qquad \hat{q}_i = q_i \tag{A.102}$$

$$\hat{\pi} = \pi \qquad \hat{\delta P} = \delta P - \bar{P}'\xi^0 \qquad \hat{\pi}_{ij} = \pi_{ij} \tag{A.103}$$

In order to find these relations you have to use those for the metric quantities. Moreover, one obtains $\hat{q}_i = q_i$ noticing that $\bar{\rho} + \bar{P}$ is arbitrary. One the other hand, we do not have a mathematical way to separate the transformations for δP and π. We do that by giving the physical argument by which π is related to dissipative processes whereas δP is not. In general, perturbations of quantities which are vanishing or constant in the background are automatically gauge-invariant and one can see this explicitly above for the heat flux, the bulk viscosity and the anisotropic stress. This property is formalised in the *Stewart-Walker lemma* [177]. It stimulates for example the use of the perturbed Weyl tensor (which is vanishing in FLRW metric) and the quasi-Maxwellian equations [77], [85].

The Scalar-Vector-Tensor decomposition

The scalar-vector-tensor (SVT) decomposition was introduced by Lifshitz in 1946 [103], who was the first to address cosmological perturbations. See also [104] and [113], for a particularly detailed account. It consists of the following procedure. We have already seen that the perturbed metric can be written in terms of two scalars ψ and ϕ, a 3-vector w_i and a 3-tensor χ_{ij}. However, we can "squeeze out" two more scalars from w_i and χ_{ij} and one more vector from χ_{ij}. Helmholtz theorem for a brief reminder) states that, under

certain conditions of regularity, any spatial vector w_i can be uniquely decomposed in its longitudinal part plus its orthogonal contribution:

$$w_i = w_i^{\parallel} + w_i^{\perp} \ , \tag{A.104}$$

which are respectively irrotational and solenoidal (divergenceless), namely:

$$\epsilon^{ijk}\partial_j w_k^{\parallel} = 0 \ , \qquad \partial^k w_k^{\perp} = 0 \ , \tag{A.105}$$

where ϵ^{ijk} is the Levi-Civita symbol.[6] By Stokes theorem, the irrotational part can be written as the gradient of a scalar say w so that, finally, we can write w_i as follows:

$$w_i = \partial_i w + S_i \tag{A.106}$$

where we have defined $S_i \equiv w_i^{\perp}$, because it is simpler to write. Therefore, w is the *scalar* part of w_i and S_i is the *vector* part of w_i. Usually, when in cosmology one talks about a *vector perturbation* one is referring to S_i, i.e. to a vector which cannot be written as a gradient of a scalar. Similarly to the vector case, any spatial rank-2 tensor say χ_{ij} can be decomposed in its longitudinal part $\chi_{ij}^{\parallel}$ plus its orthogonal part $\chi_{ij}^{\perp}$ plus the transverse contribution χ_{ij}^{T}:

$$\chi_{ij} = \chi_{ij}^{\parallel} + \chi_{ij}^{\perp} + \chi_{ij}^{T} \ , \tag{A.107}$$

defined as follows:

$$\epsilon^{ijk}\partial^l\partial_j\chi_{lk}^{\parallel} = 0 \ , \qquad \partial^i\partial^j\chi_{ij}^{\perp} = 0 \ , \qquad \partial^j\chi_{ij}^{T} = 0 \ . \tag{A.108}$$

Basically, one builds a vector by taking the divergence of χ_{ij} and then applies Helmholtz theorem to it. This implies that the longitudinal and the orthogonal parts can be further decomposed in the same spirit of Eq. (A.105) in the following way:

$$\chi_{ij}^{\parallel} = \left(\partial_i\partial_j - \frac{1}{3}\delta_{ij}\nabla^2\right)2\mu \ , \qquad \chi_{ij}^{\perp} = \partial_j A_i + \partial_i A_j \ , \qquad \partial^i A_i = 0 \ , \tag{A.109}$$

where μ is a scalar, A_i is a divergenceless vector and recall that $\nabla^2 \equiv \delta^{lm}\partial_l\partial_m$. We can thus write χ_{ij} in the following form:

$$\chi_{ij} = \left(\partial_i\partial_j - \frac{1}{3}\delta_{ij}\nabla^2\right)2\mu + \partial_j A_i + \partial_i A_j + \chi_{ij}^{T} \tag{A.110}$$

[6] Reminder: $\epsilon^{123} = 1$ and it changes sign upon any odd permutation of its indices. It follows that $\epsilon^{ijk} = 0$ if two or more indices are equal.

The transverse part χ_{ij}^T cannot be decomposed in any scalar or divergenceless vector. Therefore, it constitutes a *tensor perturbation*. The SVT decomposition is a fundamental tool for the investigation of first order perturbations because the three classes do not mix up and therefore they can be independently analysed. The absence of mixing is due to the fact that any kind of interaction term among the three categories would be of second order and therefore negligible. Let us see how each class of perturbations transforms. Apply Helmholtz theorem also to the spatial part of ξ^μ as follows:

$$\xi^0 \equiv \alpha \ , \qquad \zeta_i = \partial_i \beta + \epsilon_i \ , \qquad (\partial^l \epsilon_l = 0) \ , \tag{A.111}$$

where α and β are scalars and ϵ^i is a divergenceless vector. Now let us write the transformations found in Eqs. (A.98) and (A.99) using the SVT decomposition:

$$\hat{\psi} = \psi - \mathcal{H}\alpha - \alpha' \ , \tag{A.112}$$

$$\partial_i \hat{w} + \hat{S}_i = \partial_i w + S_i - \partial_i \beta' - \epsilon_i' + \partial_i \alpha \ , \tag{A.113}$$

$$\hat{\phi} = \phi - \mathcal{H}\alpha - \frac{1}{3}\nabla^2 \beta \ , \tag{A.114}$$

$$\left(\partial_i \partial_j - \frac{1}{3}\delta_{ij}\nabla^2\right) 2\hat{\mu} + \partial_j \hat{A}_i + \partial_i \hat{A}_j + \hat{\chi}_{ij}^T = \left(\partial_i \partial_j - \frac{1}{3}\delta_{ij}\nabla^2\right) 2\mu$$
$$+\partial_j A_i + \partial_i A_j + \chi_{ij}^T - 2\partial_j \partial_i \beta - \partial_j \epsilon_i - \partial_i \epsilon_j + \frac{2}{3}\delta_{ij}\nabla^2 \beta \ . \tag{A.115}$$

We are now in the position of writing explicitly the transformation rules for each class of perturbation.

Scalar perturbations and their gauge-invariant combinations

By taking the divergence ∂^i of Eq. (A.113) and twice the divergence $\partial^i \partial^j$ of Eq. (A.115), we eliminate all the vector and tensor contributions and are left with the transformation equations for the scalar perturbations only:

$$\hat{\psi} = \psi - \mathcal{H}\alpha - \alpha' \ , \tag{A.116}$$

$$\nabla^2 \hat{w} = \nabla^2 \left(w - \beta' + \alpha\right) \ , \tag{A.117}$$

$$\hat{\phi} = \phi - \mathcal{H}\alpha - \frac{1}{3}\nabla^2 \beta \ , \tag{A.118}$$

$$\nabla^2 \nabla^2 \hat{\mu} = \nabla^2 \nabla^2 (\mu - \beta) \ . \tag{A.119}$$

From the above transformations we obtain:

$$\hat{\psi} = \psi - \mathcal{H}\alpha - \alpha' \tag{A.120}$$

$$\hat{w} = w - \beta' + \alpha \tag{A.121}$$

$$\hat{\phi} = \phi - \mathcal{H}\alpha - \frac{1}{3}\nabla^2\beta \tag{A.122}$$

$$\hat{\mu} = \mu - \beta \tag{A.123}$$

In principle, we should have extra functions in the second and fourth equations, coming from the integration of ∇^2 and $\nabla^2\nabla^2$, but these are *spurious gauge modes* which can be set to zero without losing of generality. The following combinations of scalar perturbations are gauge-invariant:

$$\Psi = \psi + \frac{1}{a}\left[(w - \mu')\, a\right]' \qquad \Phi = \phi + \mathcal{H}\,(w - \mu') - \frac{1}{3}\nabla^2\mu \tag{A.124}$$

They are the famous *Bardeen's potentials* [21]. In general, the Bardeen potentials are gauge-invariant and there are only two of them. The same technique that we have just used for the metric perturbations can be applied to the matter quantities in Eqs. (A.102) and (A.103). Applying the SVT decomposition to v_i:

$$v_i = \partial_i v + U_i\ , \qquad (\partial^l U_l = 0)\ , \tag{A.125}$$

we can see that, for scalar perturbations, one gets:

$$\hat{\delta\rho} = \delta\rho - \bar{\rho}'\alpha \quad \Rightarrow \quad \hat{\delta} = \delta + 3\mathcal{H}(1 + \bar{P}/\bar{\rho})\alpha \tag{A.126}$$

$$\hat{v} = v + \alpha \tag{A.127}$$

$$\hat{\delta P} = \delta P - \bar{P}'\alpha \tag{A.128}$$

Note how a cosmological constant has gauge invariant perturbations. As we did earlier for the geometric quantities, we can combine the above transformations for matter in order to obtain gauge-invariant variables. The strategy is, in general, to combine the transformations in order to eliminate α and β. The result is then manifestly gauge-invariant. Using matter quantities only, we can eliminate α from Eqs. (A.126) and (A.128), thus obtaining the following gauge-invariant perturbation:

$$\Gamma \equiv \delta P - \frac{\bar{P}'}{\bar{\rho}'}\delta\rho \tag{A.129}$$

This is the *entropy perturbation*. The ratio $\delta P/\delta\rho$ is called *effective speed of sound*, whereas the ratio $\bar{P}'/\bar{\rho}'$ is called *adiabatic speed of sound*. When the two are equal, i.e. $\Gamma = 0$ one finds $dS = 0$, i.e. one has adiabaticity. The other gauge-invariant combinations are:

$$\delta\rho_m^{(\mathrm{gi})} \equiv \bar{\rho}\Delta \equiv \delta\rho + \bar{\rho}'v \qquad \delta P_m^{(\mathrm{gi})} \equiv \delta P + \bar{P}'v \tag{A.130}$$

i.e. the gauge-invariant density, also called *comoving-gauge density perturbation*, and pressure perturbations. The subscript m refers to "matter", since it is also possible to build gauge-invariant perturbations of the density and pressure using metric quantities. We are borrowing this notation from [21]. We can now think of combining the geometric and matter transformations, a total of 7 relations, trying to eliminate α and β in order to create new gauge-invariant variables. Indeed, we can form the so-called *comoving curvature perturbation*

$$\mathcal{R} \equiv \phi + \mathcal{H}v - \frac{1}{3}\nabla^2\mu \tag{A.131}$$

also known as *Lukash variable* [110], and we can form the quantity:

$$\zeta \equiv \phi + \frac{\delta\rho}{3(\bar{\rho} + \bar{P})} - \frac{1}{3}\nabla^2\mu \tag{A.132}$$

which was introduced first in [23] but started to be exploited in [190]. These $\mathcal{R}$ and ζ are especially important in the framework of inflation because they are conserved on large scales and for adiabatic perturbations, as noticed in [21] (at least for $\mathcal{R}$). Again, we can form gauge-invariant density, velocity and pressure perturbations:

$$\delta\rho_g^{(\mathrm{gi})} \equiv \delta\rho + \bar{\rho}'\,(w - \mu') \quad v^{(\mathrm{gi})} \equiv v - (w - \mu') \quad \delta P_g^{(\mathrm{gi})} \equiv \delta P + \bar{P}'\,(w - \mu') \tag{A.133}$$

In general, having 2 gauge variables α and β and 7 transformations, we can build 5 independent scalar gauge-invariant perturbations.

Vector perturbations and their gauge-invariant combinations

We can now eliminate the scalar contribution from Eq. (A.113) and consider the divergence ∂^j of Eq. (A.115). In this way we shall find the transformations for vector perturbations:

$$\hat{S}_i = S_i - \epsilon_i' \tag{A.134}$$

$$\nabla^2\hat{A}_i = \nabla^2(A_i - \epsilon_i)\ . \tag{A.135}$$

From the second equation, we can find the following transformation:

$$\hat{A}_i = A_i - \epsilon_i \tag{A.136}$$

It is possible to define a new gauge-invariant vector potential, which has the following form:

$$W_i \equiv S_i - A_i' \tag{A.137}$$

In general, W_i is gauge-invariant and there are only one gauge-invariant vector perturbation. Using the SVT decomposition of Eq. (A.125), show that from the matter sector we just have:

$$\hat{U}_l = U_l \ , \tag{A.138}$$

i.e. the vector contribution of v_i is already gauge-invariant.

Tensor perturbations

Since an infinitesimal gauge transformation, cf. Eq. (A.90), cannot be realised by any rank-2 tensor, the following result is not unexpected:

$$\hat{\chi}_{ij}^T = \chi_{ij}^T \tag{A.139}$$

i.e. that the transverse part of χ_{ij} is already gauge-invariant.

Summary

We have thus seen that a generic perturbation of the metric can be split in:

- 4 scalar functions;
- 2 divergenceless 3-vectors, for a total of 4 independent components (2 each);
- A transverse, traceless spatial tensor of rank 2, χ_{ij}^T. It has 2 independent components.

The total number of independent components sums up to 10, as it should be. The above decomposition holds true not only for the metric but for any rank-2 symmetric tensor.

Gauges

Thanks to gauge freedom we can set any 4 components of the metric to zero. There are two particularly useful choices: the synchronous gauge and the Newtonian gauge.

Synchronous gauge.

This is realised by the choice:

$$\hat{\psi} = 0 \ , \qquad \hat{w}_i = 0 \ . \tag{A.140}$$

Note that $\hat{w}_i = 0$ means that both the scalar and the vector part of w_i are being set to zero. Using the transformations found in the previous subsection, we find:

$$\begin{cases} \psi - \mathcal{H}\alpha - \alpha' = 0 \\ \\ w - \beta' + \alpha = 0 \\ \\ S_i - \epsilon_i' = 0 \end{cases} \ . \tag{A.141}$$

This must be interpreted as a system of equations for the unknowns α, β and ϵ_i, i.e. from a generic gauge we want to know which transformations we have to perform in order to go to the synchronous gauge. We have 4 equation for 4 unknowns, so we expect to determine a single solution. However, the above equations are differential and this implies the following:

$$\begin{cases} \alpha = \frac{1}{a} \int d\eta \ a\psi + f(\mathbf{x}) \\ \\ \beta = \int d\eta \ (w + \alpha) + g(\mathbf{x}) \\ \\ \epsilon_i' = \int d\eta \ S_i + h(\mathbf{x}) \end{cases} \ . \tag{A.142}$$

Since we have only time derivatives, the integrations give rise to purely space-dependent functions, which we have called f, g and h here, and which are *spurious gauge modes*.

Newtonian gauge.

This is realised by the choice:

$$\hat{w} = 0 \ , \qquad \hat{\mu} = 0 \ , \qquad \hat{\chi}_{ij}^{\perp} = 0 \ . \tag{A.143}$$

Using the transformations found in the previous subsection, we find:

$$\begin{cases} w - \beta' + \alpha = 0 \\ \\ \mu - \beta = 0 \\ \\ A_i - \epsilon_i = 0 \end{cases} . \tag{A.144}$$

It easy to see that the second and the third equation are algebraic and determine β and ϵ_i. Substituting the solution for β into the first equation, we then find α. There is no integration to perform, therefore no spurious gauge mode appears. An important fact that makes the conformal Newtonian gauge somewhat special is that $\hat{\psi} = \Psi$ and $\hat{\phi} = \Phi$, i.e. the metric perturbations become identical to the Bardeen potentials. These lecture notes are based on the use of the Newtonian gauge.

Transformations between the two gauges

It is useful to provide the transformation rules among the metric perturbations in the two gauges, for those readers who might want to translate into the synchronous gauge the results of these notes and comparing them with the huge literature in which this gauge is employed. For the scalar case, using Eqs. (A.120)-(A.123) and assuming that the hatted quantities are the synchronous ones whereas the non-hatted perturbations are the conformal Newtonian ones, we get:

$$0 = \psi_N - \mathcal{H}\alpha - \alpha' , \tag{A.145}$$

$$0 = 0 - \beta' + \alpha , \tag{A.146}$$

$$\phi_S = \phi_N - \mathcal{H}\alpha - \frac{1}{3}\nabla^2\beta , \tag{A.147}$$

$$\mu_S = -\beta . \tag{A.148}$$

The second and the fourth equation completely specify the transformation in terms of μ_S, i.e. we have:

$$\alpha = \beta' = -\mu_S' \tag{A.149}$$

and the metric potentials are related by:

$$\psi_N = -\mathcal{H}\mu_S' - \mu_S'' \qquad \phi_N = \phi_S - \mathcal{H}\mu_S' - \frac{1}{3}\nabla^2\mu_S \tag{A.150}$$

In the literature, see e.g. [113], the Fourier transforms of ϕ_S and μ_S are usually named h and 6η, respectively. For vector perturbations we have:

$$0 = S_N^i - \epsilon^{i'} \ , \tag{A.151}$$

$$A_S^i = 0 - \epsilon^i \ , \tag{A.152}$$

from which it is straightforward to obtain:

$$S_N^i = -A_S^{i'} \ . \tag{A.153}$$

Of course, tensor perturbations are naturally gauge-invariant and thus have the same functional form in the two gauges. This is also true for any tensor of rank equal or higher than 2.

Normal mode decomposition

We are now in the position of writing down explicitly the Einstein equations, fixing a gauge of our choice, which will be the Newtonian one. We expect these equations to be linear second order partial differential equations, given the perturbation scheme employed. Because of this, it is very convenient to express the perturbations as superpositions of normal modes, i.e. the eigenmodes $Q(\mathbf{k}, \mathbf{x})$ of the Laplacian operator, defined via the Helmholtz equation:

$$\nabla^2 Q(\mathbf{k}, \mathbf{x}) = -k^2 Q(\mathbf{k}, \mathbf{x}) \ . \tag{A.154}$$

For flat spatial slicing, which is considered here, this normal mode decomposition of course amounts to a Fourier transform, i.e.

$$Q(\mathbf{k}, \mathbf{x}) = e^{i\mathbf{k}\cdot\mathbf{x}} \ , \tag{A.155}$$

and a given quantity $X(\eta, \mathbf{x})$ is expressed as:

$$\tilde{X}(\eta, \mathbf{k}) = \int d^3\mathbf{x} \ X(\eta, \mathbf{x}) e^{-i\mathbf{k}\cdot\mathbf{x}} \ , \qquad X(\eta, \mathbf{x}) = \int \frac{d^3\mathbf{k}}{(2\pi)^3} \ \tilde{X}(\eta, \mathbf{k}) e^{i\mathbf{k}\cdot\mathbf{x}} \ . \tag{A.156}$$

Consider for example the metric perturbations ψ, ϕ, w_i and χ_{ij}. For ψ and ϕ we simply have that:

$$\psi(\eta,\mathbf{x}) = \int \frac{d^3\mathbf{k}}{(2\pi)^3}\,\tilde{\psi}(\eta,\mathbf{k})e^{i\mathbf{k}\cdot\mathbf{x}}\,, \quad \phi(\eta,\mathbf{x}) = \int \frac{d^3\mathbf{k}}{(2\pi)^3}\,\tilde{\phi}(\eta,\mathbf{k})e^{i\mathbf{k}\cdot\mathbf{x}}\,, \tag{A.157}$$

and similar expressions also apply for $\delta\rho$ and δP. Using its SVT decomposition in Eq. (A.106), we have for w_i the following Fourier transformation:

$$w_i(\eta,\mathbf{x}) = \int \frac{d^3\mathbf{k}}{(2\pi)^3}\,\tilde{w}_i(\eta,\mathbf{k})e^{i\mathbf{k}\cdot\mathbf{x}} = \int \frac{d^3\mathbf{k}}{(2\pi)^3}\,[\tilde{\partial_i w}(\eta,\mathbf{k}) + \tilde{S}_i(\eta,\mathbf{k})]e^{i\mathbf{k}\cdot\mathbf{x}}\,. \tag{A.158}$$

The Fourier transform of a partial spatial derivative is

$$\tilde{\partial_i w}(\eta,\mathbf{k}) = ik_i\tilde{w}(\eta,\mathbf{k})\,, \tag{A.159}$$

and therefore we have:

$$w_i(\eta,\mathbf{x}) = i\int \frac{d^3\mathbf{k}}{(2\pi)^3}\,k_i\tilde{w}(\eta,\mathbf{k})e^{i\mathbf{k}\cdot\mathbf{x}} + \int \frac{d^3\mathbf{k}}{(2\pi)^3}\,\tilde{S}_i(\eta,\mathbf{k})e^{i\mathbf{k}\cdot\mathbf{x}}\,. \tag{A.160}$$

So we see that the Fourier transforms of ψ or ϕ and w are not treated on an equal footing, because $\tilde{w}$ is multiplied by a k_i. A similar argument goes also for v_i. Finally, doing the same for χ_{ij} in Eq. (A.110), one gets:

$$\begin{aligned}\chi_{ij}(\eta,\mathbf{x}) &= \int \frac{d^3\mathbf{k}}{(2\pi)^3}\,\left(-k_ik_j + \frac{1}{3}\delta_{ij}k^2\right)2\tilde{\mu}(\eta,\mathbf{k})e^{i\mathbf{k}\cdot\mathbf{x}} \\ +i\int \frac{d^3\mathbf{k}}{(2\pi)^3}\,[k_j\tilde{A}_i(\eta,\mathbf{k}) + k_i\tilde{A}_j(\eta,\mathbf{k})]e^{i\mathbf{k}\cdot\mathbf{x}} &+ \int \frac{d^3\mathbf{k}}{(2\pi)^3}\,\tilde{\chi}^T_{ij}(\eta,\mathbf{k})e^{i\mathbf{k}\cdot\mathbf{x}}\,,\end{aligned} \tag{A.161}$$

with a similar expansion holding true for $\pi^i{}_j$. We see that $\tilde{\mu}$ is multiplied by a factor k^2 and $\tilde{A}_i$ is multiplied by a factor k. Therefore, in order to properly compare perturbations, *par condicio* is restored by "correcting" as follows:

$$\tilde{w} \equiv -\frac{1}{k}\tilde{B}\,, \quad \tilde{v} \equiv -\frac{1}{k}\tilde{V}\,, \quad \tilde{\mu} \equiv \frac{1}{k^2}\tilde{E}\,, \quad \tilde{A}_i \equiv -\frac{1}{2k}\tilde{F}_i\,. \tag{A.162}$$

In this way, all scalar quantities are treated on the same footing. Let us see what happens to the comoving gauge density perturbation:

$$\boxed{\tilde{\Delta} = \tilde{\delta} + 3(1+\bar{P}/\bar{\rho})\frac{\mathcal{H}}{k}\tilde{V}} \tag{A.163}$$

Since $\mathcal{H} \propto 1/\eta$, on sub-horizon scales, i.e. for $k\eta \gg 1$, the density contrast becomes gauge-invariant. We present this fact in Fig. 60, where we plot the evolution of the modulus of the CDM density contrast $\delta_{\rm c}$ as function of k and for $z = 0$, computed with CLASS [100] in the synchronous (solid line) and Newtonian (dashed line) gauges.

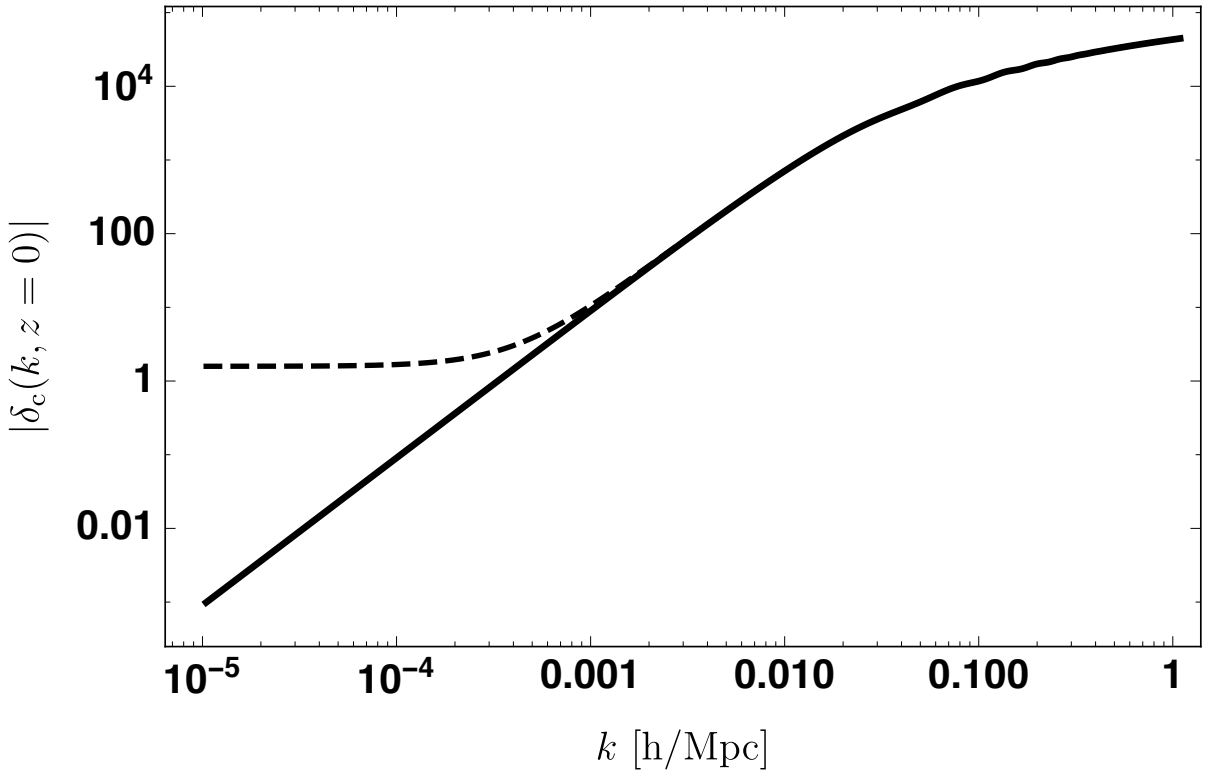

Figure 60 – Plot of the modulus of the CDM density contrast at $z = 0$ (today) as function of k, using CLASS. The solid line is the result obtained using the synchronous gauge whereas the dashed one is obtained using the Newtonian one. The initial conditions are adiabatic and normalised in order to have $\mathcal{R} = 1$. All the cosmological parameters have been set, as default, corresponding to the Planck best fit of the ΛCDM model [13].

The plots in Fig. 60 are drawn for $z = 0$, hence the value of the Hubble parameter is the Hubble constant, $H_0 = 3 \times 10^{-4}\ h\ \mathrm{Mpc}^{-1}$. Indeed, when $k > H_0$ the two evolutions coincide. Now we have to understand how to extract the scalar and vector part from a full 3-vector quantity. Let us reformulate the FT of w_i as follows:

$$\tilde{w}_i(\eta, \mathbf{k}) = -i\hat{k}_i \tilde{B}(\eta, \mathbf{k}) + \tilde{S}_i(\eta, \mathbf{k}) \ . \tag{A.164}$$

We see that we can isolate the scalar part of the FT transform of a 3-vector perturbation by contracting it with $i\hat{k}^i$. Indeed:

$$i\hat{k}^i \tilde{w}_i(\eta, \mathbf{k}) = \tilde{B}(\eta, \mathbf{k}) \ , \tag{A.165}$$

because $\hat{k}^i \tilde{S}_i = 0$, since $\partial^i S_i = 0$. The vector part is therefore obtained by subtracting the scalar part:

$$\tilde{S}_i = \left(\delta^j{}_i - \hat{k}^j \hat{k}_i\right) \tilde{w}_j \ . \tag{A.166}$$

We can easily check that this formula satisfies $\hat{k}^i \tilde{S}_i = 0$. For the traceless spatial metric perturbation in Eq. (A.110), we can write:

$$\tilde{\chi}_{ij} = -\left(\hat{k}_i \hat{k}_j - \frac{1}{3}\delta_{ij}\right) 2\tilde{E} - \frac{i}{2}\hat{k}_j \tilde{F}_i - \frac{i}{2}\hat{k}_i \tilde{F}_j + \tilde{\chi}^T_{ij} \ . \tag{A.167}$$

Here the scalar contribution can be isolated by contracting with $-3\hat{k}^i\hat{k}^j/2$. In fact:

$$-\frac{3}{2}\hat{k}^i \hat{k}^j \tilde{\chi}_{ij} = 2\tilde{E} \ . \tag{A.168}$$

The vector contribution is obtained contracting once with $2i\hat{k}^i$ and using Eq. (A.168), i.e.

$$\tilde{F}_i = 2i \left(\delta^j{}_i - \hat{k}^j \hat{k}_i\right) \hat{k}^l \tilde{\chi}_{jl} \ . \tag{A.169}$$

For the tensor part, we have:

$$\tilde{\chi}^T_{ij} = \left(\delta^l{}_i - \hat{k}^l \hat{k}_i\right) \left(\delta^m{}_j - \hat{k}^m \hat{k}_j\right) \tilde{\chi}_{lm} + \frac{1}{2}(\delta_{ij} - \hat{k}_i \hat{k}_j)\hat{k}^l \hat{k}^m \tilde{\chi}_{lm} \ . \tag{A.170}$$

and we can verify that $\hat{k}^i \tilde{\chi}^T_{ij} = \hat{k}^j \tilde{\chi}^T_{ij} = 0$ and $\delta^{ij}\tilde{\chi}^T_{ij} = 0$. Recall that $\tilde{\chi}_{ij}$ is already traceless.

Einstein equations for scalar perturbations

In this section we focus on scalar perturbations and employ the Newtonian gauge. Our perturbed metric is then:

$$g_{00} = -a(\eta)^2[1 + 2\Psi(\eta, \mathbf{x})] \ , \quad g_{0i} = 0 \ , \quad g_{ij} = a(\eta)^2 \delta_{ij} \left[1 + 2\Phi(\eta, \mathbf{x})\right] \ , \tag{A.171}$$

where we are employing the Bardeen potentials, exploiting the fact that $w = \mu = 0$. In metric (A.171) Ψ plays the role of the Newtonian potential and Φ is the spatial curvature perturbation. If we calculate from scratch the perturbed Einstein tensor $\delta G^\mu{}_\nu$ from metric (A.171), and do it again using also Eqs. (A.42)-(A.44), we obtain:

$$a^2\delta G^0{}_0 = -6\mathcal{H}\Phi' + 6\mathcal{H}^2\Psi + 2\nabla^2\Phi \ , \tag{A.172}$$

$$a^2\delta G^0{}_i = 2\partial_i(\Phi' - \mathcal{H}\Psi) \ , \tag{A.173}$$

$$a^2\delta G^i{}_j = \left[-2\Phi'' - 4\mathcal{H}\Phi' + 2\mathcal{H}\Psi' + 4\frac{a''}{a}\Psi - 2\mathcal{H}^2\Psi + \nabla^2(\Phi+\Psi)\right]\delta^i{}_j$$
$$-\partial^i\partial_j(\Phi+\Psi) \ . \tag{A.174}$$

Note again that $\partial^i = \partial_i$ since it is the partial derivative with respect to comoving coordinates and $\nabla^2 = \delta^{lm}\partial_l\partial_m$ is the comoving Laplacian. Being comoving, it is always accompanied by a factor $1/a^2$, since together they form the physical Laplacian.

The relativistic Poisson equation

The $0-0$ Einstein equation is the following:

$$-3\mathcal{H}\Phi' + 3\mathcal{H}^2\Psi + \nabla^2\Phi = 4\pi G a^2 \delta T^0{}_0 \ . \tag{A.175}$$

Using the perturbed energy momentum tensor component $\delta T^0{}_0$, as we can read from Eq. (A.72), we have:

$$3\mathcal{H}\Phi' - 3\mathcal{H}^2\Psi - \nabla^2\Phi = 4\pi G a^2 \delta\rho_{\rm tot} \tag{A.176}$$

where the total perturbed density is

$$\delta\rho_{\rm tot} = \sum_i \delta\rho_i = \sum_i \rho_i\delta_i \ , \tag{A.177}$$

i.e. it is the sum of the perturbed densities of all the material components that constitute our cosmological model, in the same way that we did for the background. We start here to eliminate the bar over the background quantities. We shall consider the ΛCDM as our standard cosmological model. Thus, we have to deal with 4 contributions:

1. Photons;
2. Neutrinos;
3. CDM;
4. Baryons.

Each of these has its own energy-momentum tensor and the total one, which enters the right hand side of the Einstein equations, is their sum. The cosmological constant only contributes at background level. We have found above the *relativistic Poisson equation*. Indeed, if we consider $a = 1$, and hence $\mathcal{H} = 0$, we recover the usual Newtonian Poisson equation (or almost, since we have two potentials in GR). Written in terms of the density contrast, using Eq. (A.72), the relativistic Poisson equation is the following:

$$3\mathcal{H}\Phi' - 3\mathcal{H}^2\Psi - \nabla^2\Phi = 4\pi G a^2 \left(\rho_{\rm c}\delta_{\rm c} + \rho_{\rm b}\delta_{\rm b} + \rho_\gamma\delta_\gamma + \rho_\nu\delta_\nu\right) \tag{A.178}$$

As one can see, Eq. (A.178) is a second order partial differential equation (PDE) which is *linear*, because we are doing first-order perturbation theory and thus all the perturbative variables appear with power 1. Because of this, as we anticipated, it is very convenient to introduce the Fourier transform of the latter, thus transforming Eq. (A.178) in a linear ordinary differential equation (ODE). Hereafter, we shall constantly employ the Fourier transform, but drop the tilde above the transformed quantities as it customary in cosmology because almost always one deals directly with the Fourier modes rather than with the configuration space. Therefore, Eq. (A.178) Fourier-transformed and written in the conformal time is the following:

$$3\mathcal{H}\Phi' - 3\mathcal{H}^2\Psi + k^2\Phi = 4\pi G a^2 \left(\rho_{\rm c}\delta_{\rm c} + \rho_{\rm b}\delta_{\rm b} + \rho_\gamma\delta_\gamma + \rho_\nu\delta_\nu\right) \tag{A.179}$$

The equation for the anisotropic stress

The next Einstein equation that we present is the traceless part of $\delta G^i{}_j$, which we know from Eq. (A.75) to be related to the anisotropic stress π_{ij}. From Eq. (A.174), we can calculate the trace and the traceless part of $\delta G^i{}_j$, such that:

$$a^2\delta G^l{}_l = -6\Phi'' - 12\mathcal{H}\Phi' + 6\mathcal{H}\Psi' + 12\frac{a''}{a}\Psi - 6\mathcal{H}^2\Psi + 2\nabla^2(\Phi + \Psi)\,, \tag{A.180}$$

and then

$$a^2\delta G^i{}_j - \frac{1}{3}\delta^i{}_j a^2\delta G^l{}_l = -\left(\partial^i\partial_j - \frac{1}{3}\delta^i{}_j\nabla^2\right)(\Phi + \Psi)\,. \tag{A.181}$$

The Fourier transform of the latter can be written in the following form:

$$a^2\delta G^i{}_j - \frac{1}{3}\delta^i{}_j a^2\delta G^l{}_l = k^2\left(\hat{k}^i\hat{k}_j - \frac{1}{3}\delta^i{}_j\right)(\Phi + \Psi)\,, \tag{A.182}$$

where we have used $k^i = k\hat{k}^i$ and $\hat{k}^i$ is the unit vector denoting the direction of $\mathbf{k}$. The spatial traceless Einstein equation can thus be written as:

$$k^2 \left(\hat{k}^i \hat{k}_j - \frac{1}{3} \delta^i{}_j \right) (\Phi + \Psi) = 8\pi G a^2 \pi^i{}_j, \tag{A.183}$$

since $\pi^i{}_j$ is the spatial traceless part of the energy-momentum tensor, as we know from Eq. (A.75). On the left hand side, we notice the same operator multiplying the scalar contribution of χ_{ij} in Eq. (A.167). Hence, only the scalar contribution of $\pi^i{}_j$ would contribute on the right hand side. Indeed, contracting the above equation with $\hat{k}_i \hat{k}^j$, as in Eq. (A.168), we obtain:

$$k^2(\Phi + \Psi) = 12\pi G a^2 \hat{k}_i \hat{k}^j \pi^i{}_j. \tag{A.184}$$

Our $\hat{k}_i \hat{k}^j \pi^i{}_j$ corresponds to the $-(\rho + P)\sigma$ used in [113]. We leave this equation as it is for the moment. We shall see that $\hat{k}_i \hat{k}^j \pi^i{}_j$ is sourced by the quadrupole moments of the photon and neutrino distributions. This equation tells us that $\Phi = -\Psi$, i.e. there exists only one gravitational potential, unless a quadrupole moment of the energy content distribution is present. For example, when CDM dominated the universe then $\Phi = -\Psi$ but this is not the case in the early universe, because of neutrinos. Even when CDM or DE dominates but the underlying theory of gravity is not GR one might have $\Phi \neq -\Psi$.[7]

The equation for the velocity

The $0-i$ Einstein equation can be written using Eqs. (A.173) and (A.73) as follows:

$$\partial_i(\Phi' - \mathcal{H}\Psi) = 4\pi G a^2 (\rho + P) v_i \, . \tag{A.185}$$

Upon Fourier Transform we get:

$$ik_i(\Phi' - \mathcal{H}\Psi) = 4\pi G a^2 (\rho + P) v_i \, , \tag{A.186}$$

and now we must get the scalar part of this vectorial equation, contracting by $i\hat{k}^i$, as we showed in Eq. (A.165). Hence, we get:

$$k(-\Phi' + \mathcal{H}\Psi) = 4\pi G a^2 (\rho + P) V \tag{A.187}$$

[7] One can probe the value of $\Phi + \Psi$ via weak lensing, which we do not address in these notes. See e.g. [58] for a treatise on gravitational lensing.

Comparing with the notation employed in [113], one has $\theta = kV$. Note that the $(\rho + P)\, V$ in the above equation is the total one, hence making explicit the various contributions one has:

$$k(-\Phi' + \mathcal{H}\Psi) = 4\pi G a^2 \left(\rho_{\rm c} V_{\rm c} + \rho_{\rm b} V_{\rm b} + \frac{4}{3}\rho_\gamma V_\gamma + \frac{4}{3}\rho_\nu V_\nu\right) \tag{A.188}$$

where we have considered the usual equations of state for the various components, i.e. $P_{\rm c} = P_{\rm b} = 0$ and $P_\gamma = \rho_\gamma/3$ and $P_\nu = \rho_\nu/3$.

The equation for the pressure perturbation

Using Eq. (A.180), we can immediately write down the last Einstein equation for scalar perturbations:

$$\boxed{\Phi'' + 2\mathcal{H}\Phi' - \mathcal{H}\Psi' - (2\mathcal{H}' + \mathcal{H}^2)\Psi + \frac{k^2}{3}(\Phi + \Psi) = -4\pi G a^2 \delta P} \tag{A.189}$$

We will use the previously derived transformations (A.150) from the Newtonian to the synchronous gauge and write there the Einstein equations.

Einstein equations for tensor perturbations

Our perturbed FLRW metric, with tensor perturbations only, can be cast as follows:

$$g_{00} = -a^2\ , \qquad g_{0i} = 0\ , \qquad g_{ij} = a^2(\delta_{ij} + h^T_{ij})\ , \tag{A.190}$$

where h^T_{ij} is divergenceless and traceless. Starting from metric (A.190) and calculating the perturbed Einstein tensor $\delta G^\mu{}_\nu$, and verify the calculations also using Eqs. (A.42)-(A.44), we can see that the only non vanishing components are:

$$2a^2 \delta G^i{}_j = h^{T\prime\prime}_{ij} + 2\mathcal{H} h^{T\prime}_{ij} - \nabla^2 h^T_{ij}. \tag{A.191}$$

Notice that the wave operator has appeared. The calculation of the above exercise is pretty straightforward because the tensor nature of the perturbation h^T_{ij} already suggests that it cannot contribute to R_{00}, R_{0i} and the Ricci scalar R (at first-order). The tensor part of the Einstein equations is thus:

$$h^{T\prime\prime}_{ij} + 2\mathcal{H} h^{T\prime}_{ij} + k^2 h^T_{ij} = 16\pi G a^2 \pi^T_{ij}, \tag{A.192}$$

where π_{ij}^T is the tensorial part of the anisotropic stress, which can be computed from the total as in Eq. (A.170):

$$\pi_{ij}^T = \left(\delta^l{}_i - \hat{k}^l\hat{k}_i\right)\left(\delta^m{}_j - \hat{k}^m\hat{k}_j\right)\pi_{lm} + \frac{1}{2}\hat{k}^l\hat{k}^m\pi_{lm}\left(\delta_{ij} - \hat{k}_i\hat{k}_j\right) \ . \tag{A.193}$$

In Fourier space, the divergenceless condition can be written down as:

$$\hat{k}^i h_{ij}^T = 0 \ . \tag{A.194}$$

Therefore, h_{ij}^T can be expanded with respect to a 2-dimensional basis $\{\hat{e}_1, \hat{e}_2\}$ defined on the 2-dimensional subspace orthogonal to $\hat{k}$. The basis satisfies thus the condition:

$$\gamma^{ij}e_{a,i}\hat{k}_j = 0 \ , \qquad \gamma^{ij}e_{a,i}e_{b,j} = \delta_{ab} \ , \tag{A.195}$$

where γ_{ij} is the metric on the 2-dimensional subspace and $a, b \in \{1, 2\}$. We can write then h_{ij}^T as follows:

$$h_{ij}^T(\mathbf{k}) = (e_{1,i}e_{1,j} - e_{2,i}e_{2,j})(\hat{k})h_+(\mathbf{k}) + (e_{1,i}e_{2,j} + e_{2,i}e_{1,j})(\hat{k})h_\times(\mathbf{k}) \ . \tag{A.196}$$

Note the dependence on $\hat{k}$ of the combinations of the 2-dimensional basis vectors. In fact these depend on the orientation of $\hat{k}$. Substituting the above expansion into Eq. (A.192) and in absence of quadrupole moments, $h_{+,\times}$ satisfy then the equation:

$$h''_{+,\times} + 2\mathcal{H}h'_{+,\times} + k^2 h_{+,\times} = 0, \tag{A.197}$$

which we will employ in order to investigate the GW production during inflation. If we choose a Cartesian reference frame and $\hat{k} = \hat{z}$, i.e. a propagation direction of a gravitational wave along $\hat{z}$, then a natural choice is $\hat{e}_1 = \hat{x}$ and $\hat{e}_2 = \hat{y}$ and the perturbed metric can be written as:

$$h_{ij}^T(k\hat{z}) = \begin{pmatrix} h_+ & h_\times & 0 \\ h_\times & -h_+ & 0 \\ 0 & 0 & 0 \end{pmatrix} \ . \tag{A.198}$$

Though this a convenient way of expressing $h_{ij}^T(k\hat{z})$, one usually prefers to use the combinations:

$$h_+ \mp i h_\times \ , \tag{A.199}$$

since these have helicity ± 2, see e.g. [194]. In order to see this, we apply a rotation about $\hat{z}$ and calculate how $h_{ij}^T(k\hat{z})$ transforms. We can apply the rotation:

$$R^i{}_j(\theta) = \begin{pmatrix} \cos\theta & -\sin\theta & 0 \\ \sin\theta & \cos\theta & 0 \\ 0 & 0 & 1 \end{pmatrix} , \tag{A.200}$$

about the $\hat{z}$ axis to h_{ij}^T, and compute the components:

$$\bar{h}_{lm}^T = R^i{}_l R^j{}_m h_{ij}^T , \tag{A.201}$$

and therefore we can see that:

$$\bar{h}_+ = \cos^2\theta h_+ + 2\sin\theta\cos\theta h_\times - \sin^2\theta h_+ = \cos 2\theta h_+ + \sin 2\theta h_\times , \tag{A.202}$$

$$\bar{h}_\times = \cos^2\theta h_\times - 2\sin\theta\cos\theta h_+ - \sin^2\theta h_\times = \cos 2\theta h_\times - \sin 2\theta h_+ . \tag{A.203}$$

Hence, the aforementioned combinations $h_+ \pm i h_\times$ transform as:

$$\boxed{\bar{h}_+ \pm i\bar{h}_\times = e^{\mp 2i\theta}(h_+ \pm i h_\times)} \tag{A.204}$$

and have thus helicity ∓ 2. Sometimes the sign could be a bit confusing depending in which sense the rotation is performed. By convention, $\theta > 0$ denotes an anti-clockwise rotation so a rotation of θ about the $\hat{z}$ axis corresponds to a $-\theta$ rotation about the $-\hat{z}$ axis, which is the line of sight and therefore the relevant direction for the observer. So, the observed helicities have opposite sign with respect to the propagating ones. So, we write the total tensor perturbation as a sum over the helicities:

$$h_{ij}^T(\eta, k\hat{z}) = \sum_{\lambda=\pm 2} e_{ij}(\hat{z}, \lambda) h(\eta, k\hat{z}, \lambda) , \tag{A.205}$$

where:

$$e_{11}(\hat{z}, \pm 2) = -e_{22}(\hat{z}, \pm 2) = \mp i e_{12}(\hat{z}, \pm 2) = \mp i e_{21}(\hat{z}, \pm 2) = \frac{1}{\sqrt{2}} , \tag{A.206}$$

and of course $e_{3i} = e_{i3} = 0$. Therefore, from Eq. (A.205) we get:

$$h_+(\eta, k\hat{z}) = \frac{1}{\sqrt{2}} h(\eta, k\hat{z}, +2) + \frac{1}{\sqrt{2}} h(\eta, k\hat{z}, -2) , \tag{A.207}$$

$$h_\times(\eta, k\hat{z}) = \frac{i}{\sqrt{2}} h(\eta, k\hat{z}, +2) - \frac{i}{\sqrt{2}} h(\eta, k\hat{z}, -2) , \tag{A.208}$$

and inverting:

$$\sqrt{2}h(\eta, k\hat{z}, +2) = h_+(\eta, k\hat{z}) - ih_\times(\eta, k\hat{z}) \ , \tag{A.209}$$

$$\sqrt{2}h(\eta, k\hat{z}, -2) = h_+(\eta, k\hat{z}) + ih_\times(\eta, k\hat{z}) \ . \tag{A.210}$$

For $\mathbf{k}$ in a generic direction, we have that:

$$h_{ij}^T(\eta, \mathbf{k}) = \sum_{\lambda=\pm 2} e_{ij}(\hat{k}, \lambda) h(\eta, \mathbf{k}, \lambda) \ , \tag{A.211}$$

where the polarisation tensor is defined as:

$$e_{ij}(\hat{k}, \pm 2) = \sqrt{2} e_{\pm,i} e_{\pm,j} \ , \tag{A.212}$$

where the *polarisation vectors* are:

$$e_{\pm,i}(\hat{k}) \equiv \frac{(e_1 \pm i e_2)_i}{\sqrt{2}} \ . \tag{A.213}$$

Of course $e_{ij}(\hat{k}, \lambda)$ has the same symmetry of $h_{ij}^T(\eta, \mathbf{k})$ and thus is traceless and transverse, i.e.

$$\hat{k}^l e_{lm}(\hat{k}, \lambda) = 0 \ , \tag{A.214}$$

Again, the two $h(\eta, \mathbf{k}, \pm 2)$ satisfy the same Eq. (A.197) as for $h_{+,\times}$. When we will discuss about the effect of GW on photon propagation and CMB we shall have then to deal with two directions: one is the GW direction $\hat{k}$ and the other is the photon direction of propagation, $\hat{p}$. In general a frame $\hat{k} = \hat{z}$ is chosen in order to simplify the calculations. But then, before taking the anti-Fourier transform and obtaining the physical quantities in the real space one has to remember of performing a rotation which brings $\hat{k}$ back in a generic direction.

Einstein equations for vector perturbations

Finally, we address vector perturbations. The vector-perturbed FLRW metric, in the Newtonian gauge, has the following form:

$$g_{00} = -a^2 \ , \qquad g_{0i} = 0 \ , \qquad g_{ij} = a^2(\delta_{ij} + h_{ij}^V) \ , \tag{A.215}$$

where

$$h_{ij}^V = \partial_i A_j + \partial_j A_i \ , \tag{A.216}$$

and A_i is a divergenceless vector, i.e. $\partial_i A^i = 0$. We can repeat the same calculations performed in the tensor case but now for h_{ij}^V. Notice a very important difference: h_{ij}^V is traceless but not divergenceless. We can compare the results with those found using Eqs. (A.42)-(A.44). Show that the non-vanishing components of the perturbed Einstein tensor are:

$$\begin{aligned} 2a^2\delta G^0{}_i &= -\partial_l h_{li}^{V\prime} = -\nabla^2 A_i' \ , & \text{(A.217)} \\ 2a^2\delta G^i{}_j &= h_{ij}^{V\prime\prime} + 2\mathcal{H}h_{ij}^{V\prime} = (\partial_i A_j + \partial_j A_i)'' + 2\mathcal{H}(\partial_i A_j + \partial_j A_i)' \ . & \text{(A.218)} \end{aligned}$$

With the Laplacian missing, the last equation has no more the wave behaviour that the corresponding tensor equation has. With no vector sources, show then that in the early, radiation-dominated universe, for which $\mathcal{H} = 1/\eta$, one has:

$$h_{ij}^V \propto 1/\eta^2 \ , \tag{A.219}$$

and hence vector perturbations vanish, if not sourced. Einstein equations are thus:

$$\begin{aligned} kF_i' &= -32\pi G a^2(\rho + P)U_i \ , & \text{(A.220)} \\ (i\hat{k}_i F_j + i\hat{k}_j F_i)'' + 2\mathcal{H}(i\hat{k}_i F_j + i\hat{k}_j F_i)' &= -32\pi G a^2 \pi_{ij}^V \ , & \text{(A.221)} \end{aligned}$$

where U_i is the vector part of v_i, defined in Eq. (A.125), F_i is defined in Eq. (A.162) and π_{ij}^V is the vector part of the anisotropic stress, defined as from Eq. (A.169):

$$\pi_{ij}^V = 2i\left(\delta^m{}_i - \hat{k}^m\hat{k}_i\right)\hat{k}^l\pi_{lm}\hat{k}_j + 2i\left(\delta^m{}_j - \hat{k}^m\hat{k}_j\right)\hat{k}^l\pi_{lm}\hat{k}_i \ , \tag{A.222}$$

Of course, we have that:

$$\hat{k}^i F_i = 0 \ , \qquad \hat{k}^i U_i = 0 \ , \qquad \hat{k}^i\hat{k}^j\pi_{ij}^V = 0 \ . \tag{A.223}$$

Contracting the second Einstein equation with $i\hat{k}^j$ leaves us with:

$$\boxed{F_i'' + 2\mathcal{H}F_i' = 32\pi G a^2 i\hat{k}^j\pi_{ij}^V} \tag{A.224}$$

We choose, as in the tensor case, to align $\hat{k}$ to $\hat{z}$. Therefore, the divergenceless of A_i implies that

$$ik^i A_i = 0 \quad \Rightarrow \quad A_3 = 0 \,, \tag{A.225}$$

and from Eq. (A.216) we have:

$$h_{ij}^V = ik_i A_j + ik_j A_i = -\frac{i}{2}\hat{k}_i F_j - \frac{i}{2}\hat{k}_j F_i \,. \tag{A.226}$$

So, h_{ij}^V can be written as follows:

$$h_{ij}^V = \begin{pmatrix} 0 & 0 & -iF_1/2 \\ 0 & 0 & -iF_2/2 \\ -iF_1/2 & -iF_2/2 & 0 \end{pmatrix} \,. \tag{A.227}$$

Applying the same rotation about $\hat{z}$ as we did for tensor perturbations, we obtain:

$$\bar{F}_1 = F_1 \cos\theta - F_2 \sin\theta \,, \tag{A.228}$$

$$\bar{F}_2 = F_1 \sin\theta + F_2 \cos\theta \,. \tag{A.229}$$

Hence we have:

$$\bar{F}_1 + i\bar{F}_2 = (F_1 + iF_2)e^{i\theta} \,, \tag{A.230}$$

$$\bar{F}_1 - i\bar{F}_2 = (F_1 - iF_2)e^{-i\theta} \,, \tag{A.231}$$

and therefore the quantities:

$$F_\pm \equiv F_1 \pm iF_2 \,, \tag{A.232}$$

are fields with helicity ± 1.

Overview of cosmological perturbations including $C\nu B$

In this last section I will present a general summary of the basic equations for linear perturbations that will be used in subsequent chapters, for the different species that constitute the inventory of the universe.

- **Dark matter**:

$$\delta' + ikv = -3\Phi' \qquad Continuity \tag{A.233}$$

$$v' + \frac{a'}{a}v = -ik\Psi \qquad Euler \tag{A.234}$$

- **Baryons with photons interactions**:

$$\delta_b' + ikv_b = -3\Phi' \qquad Continuity \tag{A.235}$$

$$v_b' + \frac{a'}{a}v_b = -ik\Psi + \frac{\tau'}{R}\left(v_b + 3i\Theta_1\right) \qquad Euler \tag{A.236}$$

- **Photon temperature**:

$$\Theta = \frac{\Delta T}{T} \tag{A.237}$$

$$\Theta' + ik\mu\Theta = -\Phi' - ik\mu\Psi - \tau'\left(\Theta_0 - \Theta + \mu v_b - \frac{1}{2}P_2\left(\mu\right)\Theta_2\right) \tag{A.238}$$

- **Gravity**:

$$k^2\Phi + 3\frac{a'}{a}\left(\Phi' - \Psi\frac{a'}{a}\right) = 4\pi G a^2\left(\rho_m\delta_m + 4\rho_r\Theta_{r,0}\right) \tag{A.239}$$

$$k^2\left(\Phi + \Psi\right) = -32\pi G a^2\rho_r\Theta_{r,2} \tag{A.240}$$

- **Neutrinos equations for continuity, Euler and shear**:

$$\delta_\nu' + 3\frac{a'}{a}\left(c_{eff}^2 - w_\nu\right)\delta = -\left(1 + w_\nu\right)\left(\Theta_\nu + \frac{h'}{2}\right) + 9\frac{a'^2}{a}\left(1 + w_\nu\right)\left(c_{eff}^2 - c_g^2\right)\frac{\Theta_\nu}{k^2} \tag{A.241}$$

$$\Theta_\nu' + \frac{a'}{a}\left(1 - 3c_{eff}^2\right)\Theta = \frac{c_{eff}^2}{1 + w_\nu}k^2 - k^2\sigma_\nu \tag{A.242}$$

$$\sigma_\nu' + 3\left(\frac{1}{\tau} + \frac{a'}{a}\left[\frac{2}{3} - c_g^2 - \frac{P_{pseudo}}{3P}\right]\right)\sigma_\nu = \frac{8}{3}\frac{c_{vis}^2}{1 + w_\nu}\left(\Theta_\nu + h'\right) \tag{A.243}$$

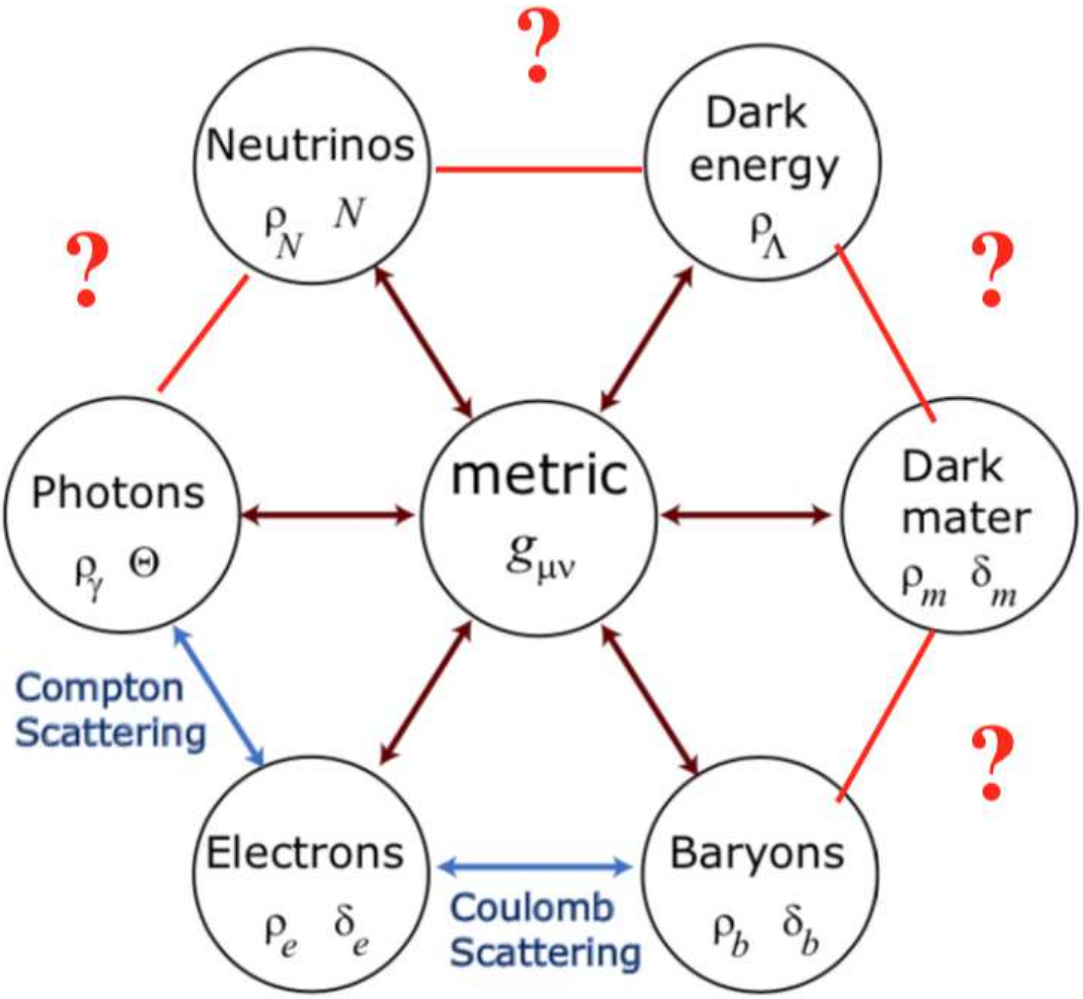

Figure 61 – Interactions between the different forms of matter in the universe.

We derived the evolution equations for all matter and metric perturbations. In principle, we could now solve these equations. The complex interactions between the different species (see Fig. 61) means that we get a large number of coupled differential equations. This set of equations is easy to solve numerically and this is what is usually done. However, our goal in next chapters is to obtain some analytical insights into the basic qualitative features of the solutions.

Chapter B

Appendix to chapter 7, 8 & 9

In this section we investigate in some detail the freeze-out and relic abundance of CDM. In general, with **thermal relic** one refers to the abundance of a certain species left over from the annihilation suffered in thermal bath and, after its decoupling, from the dilution caused by the expansion of the universe. To this purpose, consider the following process:

$$X + \bar{X} \leftrightarrow l + \bar{l}\,, \tag{B.1}$$

where X represents the DM particle and l a lepton. Due to the expansion of the universe, at a certain point the annihilation of DM is no more efficient and thus its abundance is fixed. This is precisely what we want to calculate. We could then put constraints on the cross-section of the above process and on the mass of the DM particle by measuring the abundance of DM necessary today in order to be in agreement with the cosmological observations. We are assuming here that DM is made up of massive particles which were in thermal equilibrium with the rest of the standard model particles in the primordial universe, hence the name **thermal relics**. Moreover, since we are considering CDM, or more in general particle which decouple from the primordial plasma when nonrelativistic, ours is a calculation of **cold relics abundance**. The Boltzmann equation for the above process has the following form:

$$\frac{1}{a^3}\frac{d(n_X a^3)}{dt} = \langle \sigma v \rangle \left(n_X^{(0)2} - n_X^2 \right)\,, \tag{B.2}$$

where we have assumed $n_l^{(0)} = n_l$, because we are in thermal bath with very high temperature (e.g. larger than 100 GeV for WIMPs). Now we take advantage of the scaling

$T \propto 1/a$ and define the following dimensionless quantities:

$$Y \equiv \frac{n_X \hbar^3}{(k_{\rm B}T)^3} \,, \qquad Y_{\rm eq} \equiv \frac{n_X^{(0)} \hbar^3}{(k_{\rm B}T)^3} \,, \qquad x \equiv \frac{mc^2}{k_{\rm B}T} \,, \qquad \lambda \equiv \frac{(mc^2)^3 \langle \sigma v \rangle}{H(m)\hbar^3} \,, \tag{B.3}$$

where $H(m) = H(x = 1)$ is the Hubble parameter corresponding to a thermal energy $k_{\rm B}T = mc^2$, with m being the mass of the DM particle. Note that, being deep in the radiation-dominated era, the Hubble parameter scales as follows:

$$H = \frac{H(x=1)}{x^2} \,. \tag{B.4}$$

The Boltzmann equation thus becomes:

$$\frac{(k_{\rm B}T)^3}{\hbar^3} \frac{dY}{dx} \frac{H(x=1)}{x} = \langle \sigma v \rangle \frac{(k_{\rm B}T)^6}{\hbar^6} \left(Y_{\rm eq}^2 - Y^2 \right) \,, \tag{B.5}$$

and finally

$$\boxed{\frac{dY}{dx} = -\frac{\lambda}{x^2} \left(Y^2 - Y_{\rm eq}^2 \right)} \tag{B.6}$$

In this case Saha equation is simply $Y = Y_{\rm eq}$ and from Eq. (4.71) we know that $Y_{\rm eq} \to 0$ for $x \to \infty$, because of the dilution due to the cosmological expansion. On the other hand, we also expect, as we saw for recombination, that Y attains an asymptotic value which we call Y_∞ and with which we shall calculate the present abundance of DM. The departure between the Saha equation solution and the Boltzmann equation solution is the **freeze-out** and, as we know, it takes place approximately when $\Gamma \sim H$. Using Eq. (4.71) in order to express $Y_{\rm eq}$, we can numerically solve Eq. (B.6). In order to do this, we set a small initial value $x = x_i$ such that $Y(x_i) = Y_{\rm eq}(x_i)$ and fix λ to be a constant. In Figs. 62 and 63 we choose $x_i = 0.01$ and $\lambda = 1, 10, 100$ for a fermionic DM species.

From Fig. 62 one can appreciate that Y attains a residual abundance and that, as expected, the latter is smaller the larger λ is. This happens because for larger values of λ the interaction is more efficient. In Fig. 63 we show the behaviour of the relative difference $Y/Y_{\rm eq} - 1$ in order to understand when the freeze-out approximately takes place. Of course, the freeze-out is not a specific instant, but depends on a criterion that we choose. For example, from inspection of Fig. 63, we see that $Y/Y_{\rm eq} - 1$ at $x \approx 10$ starts to increase with more steepness and therefore we might establish that $x_{\rm f} \approx 10$. Moreover, this value is very weakly dependent on λ.

Now, what is the difference between fermionic and bosonic DM? In Fig. 64 we plot Y in the bosonic DM (solid lines) and fermionic DM (dashed lines) for $\lambda = 10, 100$. As one can see, there are two differences: *i*) When x is small the baryonic abundance is larger than

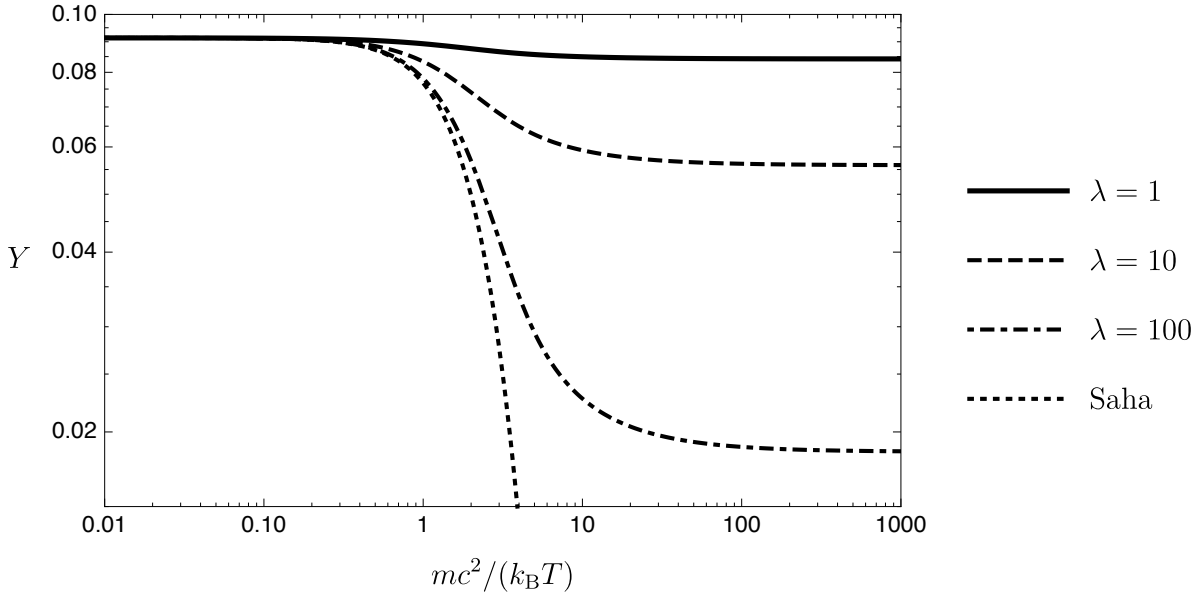

Figure 62 – Numerical solution of Eq. (B.6) for the case of fermionic DM.

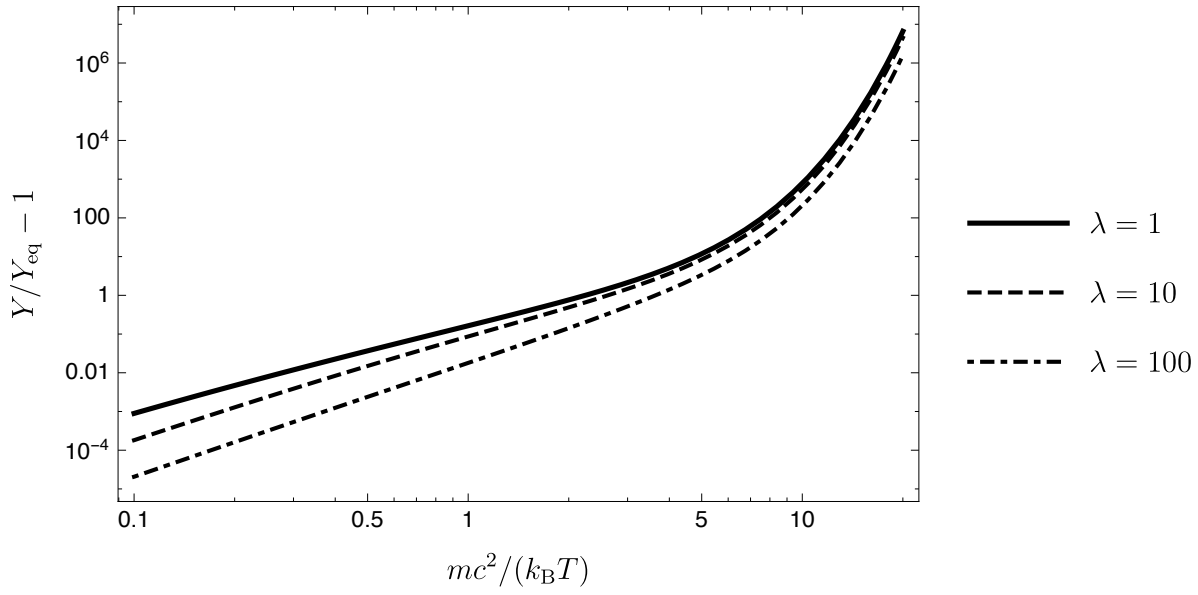

Figure 63 – Relative difference $Y/Y_\mathrm{eq} - 1$.

the fermionic one (because of the ± 1 at the denominator of the distribution function) of a factor 4/3; *ii*) for large x, the larger λ is, the smaller becomes the difference between the fermionic and bosonic relic abundances.

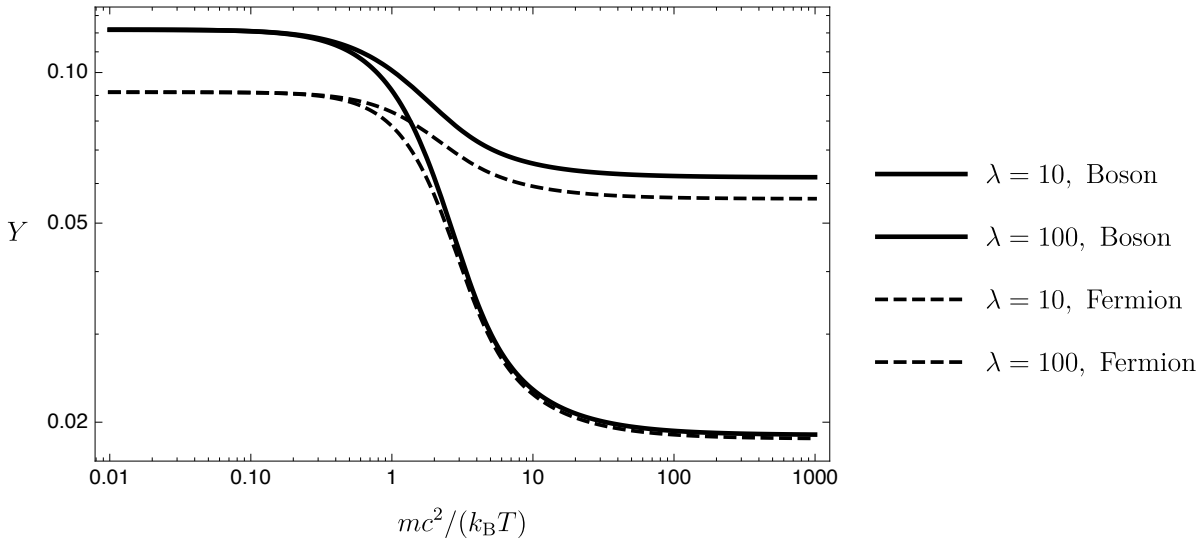

Figure 64 – Comparison of the numerical solutions of Eq. (B.6) for the cases of bosonic DM (solid lines) and fermionic DM (dashed lines) and $\lambda = 10$ (top two lines) and $\lambda = 100$ (bottom two lines, almost superposed).

We now relate the relic abundance to the DM annihilation cross-section. For $x \gg 1$ we know that $Y_{\rm eq}$ is vanishing, and the Boltzmann equation can be written as:

$$\frac{dY}{dx} \approx -\frac{\lambda}{x^2} Y^2 \,, \tag{B.7}$$

whose solution is:

$$\frac{1}{Y_\infty} - \frac{1}{Y_f} \approx \frac{\lambda}{x_{\rm f}} \,. \tag{B.8}$$

We have again considered here a constant λ, for simplicity. As we can see from Fig. 62, $Y_{\rm f} - Y_\infty > 0$ and the difference gets larger the larger λ is. Moreover, $x_{\rm f} \approx 10$, so that we can simplify

$$Y_\infty \approx \frac{10}{\lambda} \,. \tag{B.9}$$

When Y has attained Y_∞, the abundance of particle is fixed and their number density starts to be diluted as $n_X \propto a^{-3}$. Therefore, we can can write down the present-time energy density as follows:

$$\rho_{X0} = n_1 m \frac{a_1^3}{a_0^3} = m Y_\infty \frac{(k_{\rm B}T_1)^3}{\hbar^3} \frac{a_1^3}{a_0^3} = \frac{10m}{\lambda} \frac{(k_{\rm B}T_0)^3}{\hbar^3} \left(\frac{a_1^3 T_1^3}{a_0^3 T_0^3} \right) \,. \tag{B.10}$$

We have introduced here the photon temperature (the only one we can measure). The ratio between parenthesis is not just equal to 1. We have seen an example of this discrepancy when we calculated the photon-neutrinos temperatures ratio. The reason is that not all along the cosmological evolution T decays as the inverse scale factor. When there are processes such as electron-positron annihilation, more photons are injected in the thermal bath and the temperature scales in a milder way than $1/a$. It is now time to tackle more seriously the issue of the effective numbers of relativistic degrees of freedom.

The effective numbers of relativistic degrees of freedom

Let T be the photon temperature, which we always use as reference since it is the only one we can measure, from CMB. In Eq. (B.13), we wrote the energy density of all the relativistic species in the following way:

$$\varepsilon = \frac{\pi^2 (k_{\rm B} T)^4}{30(\hbar c)^3} g_* \ , \tag{B.11}$$

where, actually $g_* = g_*(T)$ because when $k_{\rm B}T$ drops below the mc^2 of a species, this becomes non-relativistic and is removed from the above equation. Thus g_* varies, but very rapidly close to the thresholds of the mass energies. Far from those, g_* it is practically constant.

In Fig. 65 we plot g_* calculated from Eq. (B.12) and Eq. (B.13) for the species of Table 13. The residual non-vanishing value of $g_*(T)$ for low temperatures is due to the massless species, i.e. photons and neutrinos. Note that this plot is just an illustrative example, because it employs Eq. (B.12) during the entire evolution, i.e. it assumes thermal equilibrium all the time, and, moreover, the QCD phase transition at 200 MeV and the difference between photon and neutrino temperature after electron-positron annihilation at 0.5 MeV have been put "by hand". The correct calculation should employ the energy density obtained from the solutions of the Boltzmann equations of the various species, which correctly track the evolutions when $\Gamma \sim H$, i.e. out of equilibrium. The effective numbers of relativistic degrees of freedom gets two contributions. One from the relativistic particles that are in thermal equilibrium with the photons:

$$g_*^{\rm therm} \equiv \sum_{i={\rm bosons}} g_i + \frac{7}{8} \sum_{i={\rm fermions}} g_i \ , \tag{B.12}$$

and another from the relativistic particles that are no more in thermal equilibrium with

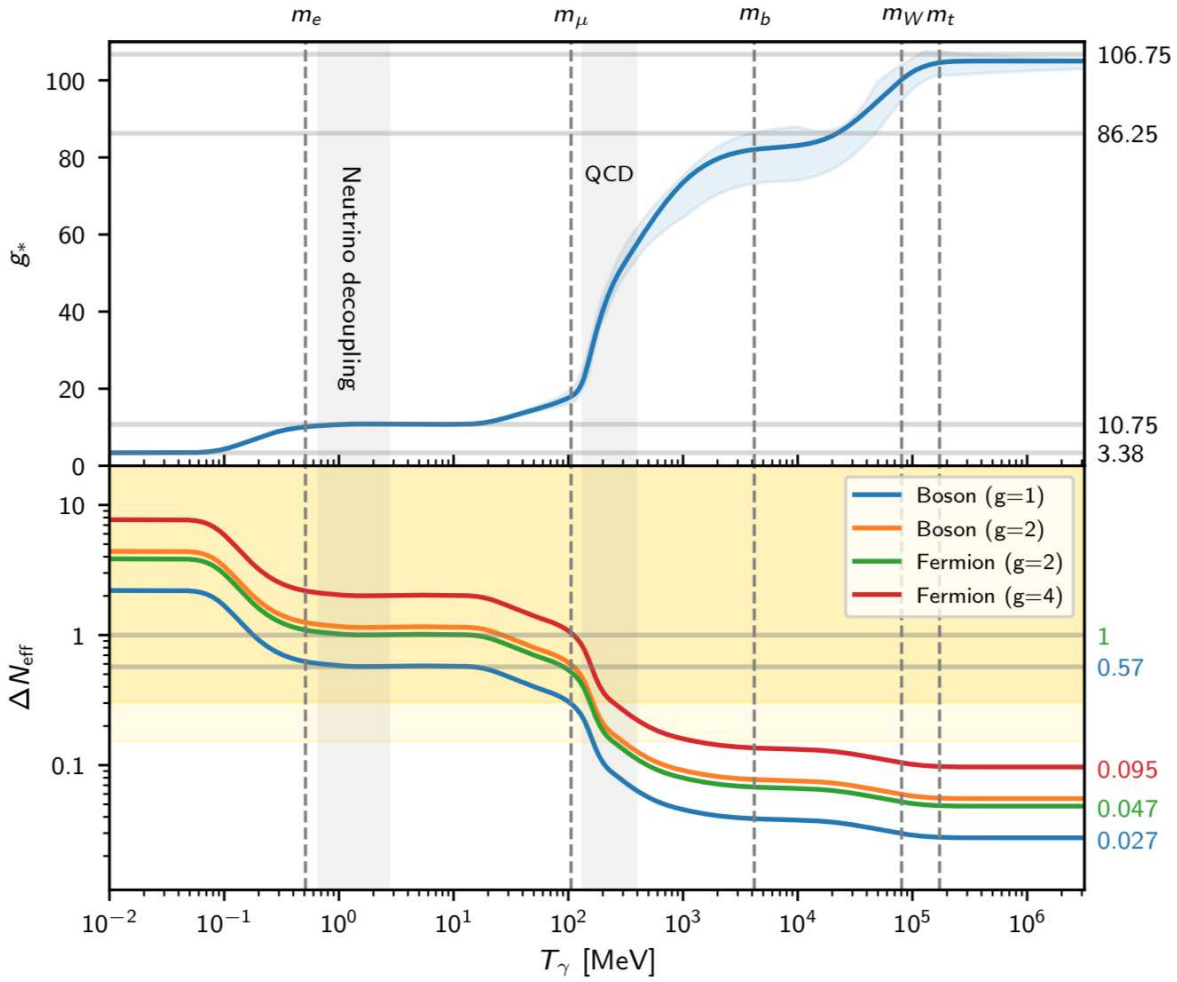

Figure 65 – Evolution of g_* calculated from Eq. (B.12) and Eq. (B.13) for the species of Table 13 and constraints on additional relativistic particles. *Top*:Evolution of the effective degrees of freedom for Standard Model particle density, g_*, as a function of photon temperature in the early Universe. Vertical bands show the approximate temperature of neutrino decoupling and the QCD phase transition, and dashed vertical lines denote some mass scales at which corresponding particles annihilate with their antiparticles, reducing g_*. Note the QCD phase transition at 200 MeV and the difference between photon and neutrino temperature after electron-positron annihilation at 0.5 MeV. The solid line shows the fit of [599] plus standard evolution at $T_\gamma < 1$ MeV, and the pale blue bands the estimated $\pm 1\sigma$ error region from [600]. Numbers on the right indicate specific values of g_* expected from simple degrees of freedom counting. *Bottom*: Expected $\Delta N_{\rm eff}$ today for species decoupling from thermal equilibrium as a function of the decoupling temperature, where lines show the prediction from the [599] fit assuming a single scalar boson ($g = 1$, blue), bosons with $g = 2$ (e.g., a massless gauge vector boson, orange), a Weyl fermion with $g = 2$ (green), or fermions with $g = 4$ (red). One-tailed 68% and 95% regions excluded by *planck* TT,TE,EE+lowE+lensing+BAO are shown in gold; this rules out at 95% significance light thermal relics decoupling after the QCD phase transition (where the theoretical uncertainty on g_* is negligible), including specific values indicated on the right axis of $\Delta N_{\rm eff} = 0.57$ and 1 for particles decoupling between muon and positron annihilation. At temperatures well above the top quark mass and electroweak phase transition, g_* remains somewhat below the naive 106.75 value expected for all the particles in the Standard Model, giving interesting targets for $\Delta N_{\rm eff}$ that may be detectable in future CMB experiments (see e.g. [601]). You can find this plot at [602] and an extensive discussion of its content right there.

the photons:

$$g_*^{\rm dec} \equiv \sum_{i={\rm bosons}} g_i \frac{T_i^4}{T^4} + \frac{7}{8} \sum_{i={\rm fermions}} g_i \frac{T_i^4}{T^4} \ . \tag{B.13}$$

The latter are basically neutrinos only. Why do we insist on relativistic species? Because, as we showed, these are the only one which contribute to the entropy density s:

$$\boxed{s = \frac{2\pi^2 k_{\rm B}^4 T^3}{45(\hbar c)^3} g_{*S}} \tag{B.14}$$

where g_{*S} is the effective number of degrees of freedom for the entropy. Now, also to g_{*S} contribute species which are in thermal equilibrium with the photons and for which:

$$g_{*S}^{\rm therm} = g_*^{\rm therm} = \sum_{i={\rm bosons}} g_i + \frac{7}{8} \sum_{i={\rm fermions}} g_i \ , \tag{B.15}$$

and species that are no more in thermal equilibrium with the photons and for which:

$$g_{*S}^{\rm dec} = \sum_{i={\rm bosons}} g_i \frac{T_i^3}{T^3} + \frac{7}{8} \sum_{i={\rm fermions}} g_i \frac{T_i^3}{T^3} \neq g_*^{\rm dec} \ . \tag{B.16}$$

Because of the last inequality, due to the different scaling of s and ε with the temperature, we expect $g_* \neq g_{*S}$. Now, sa^3 is a very useful quantity since it is conserved, as we showed earlier. When a species becomes non-relativistic, its contribution to s is exponentially suppressed as $\exp(-mc^2/k_{\rm B}T)$. Therefore, the non-relativistic species passes its entropy to rest of the thermal bath such that sa^3 does not change. What is the value of g_* and of g_{*S}? We need to recover our knowledge of particle physics in Table 13. Summing up all the contributions we have from bosons and fermions:

$$g_{\rm bosons} = 28 \ , \qquad g_{\rm fermions} = 90 \ , \tag{B.17}$$

so that

$$g_* = 28 + \frac{7}{8} \cdot 90 = 106.75 \ . \tag{B.18}$$

When the temperature drops below one species mass, this becomes non-relativistic and then its $g_{\rm s}$ does not contribute anymore to the above sum. Note that before neutrino decoupling $g_* = g_{*S}$.

Particle		mass	spin	g_s
Quarks	$t, \bar{t}$	173 GeV	$\frac{1}{2}$	$2 \cdot 2 \cdot 3 = 12$
	$b, \bar{b}$	4 GeV		
	$c, \bar{c}$	1 GeV		
	$s, \bar{s}$	100 MeV		
	$d, \bar{d}$	5 MeV		
	$u, \bar{u}$	2 MeV		
Gluons	g_i	0 GeV	1	$8 \cdot 2 = 16$
Leptons	$\tau^{\pm}$	1777 MeV	$\frac{1}{2}$	$2 \cdot 2 = 4$
	$\mu^{\pm}$	106 MeV		
	$e^{\pm}$	511 keV		
	$\nu_\tau, \bar{\nu}_\tau$	< 0.6 eV	$\frac{1}{2}$	$2 \cdot 1 = 2$
	$\nu_\mu, \bar{\nu}_\mu$	< 0.6 eV		
	$\nu_e, \bar{\nu}_e$	< 0.6 eV		
Gauge Bosons	W^+	80 GeV	1	3
	W^-	80 GeV		
	Z^0	91 GeV		
	γ	0		2
Higgs Bosons	H^0	125 GeV	0	1

Table 13 – The standard model particles, with their mass, spin and degeneracies g_s.

Relic abundance of DM and the WIMP possibility

On the basis of the discussion of the previous subsection, we can therefore write Eq. (B.10) as follows:

$$\Omega_{X0} = \frac{\rho_{X0}}{\rho_{\mathrm{cr},0}} = \frac{10m}{\lambda \rho_{\mathrm{cr},0}} \frac{(k_{\mathrm{B}} T_0)^3}{\hbar^3} \frac{g_{*S}(T_0)}{g_{*S}(m)} \,, \tag{B.19}$$

where $g_{*S}(m)$ is the number of effective degrees of freedom in entropy for a thermal energy equal to the DM particle mass. This must be certainly larger than 1 MeV, roughly when neutrino decoupling takes place, therefore $g_* = g_{*S}$. Moreover,

$$g_{*S}(T_0) = 2 + \frac{7}{8} \cdot 6 \cdot \left(\frac{T_\nu}{T_0} \right)^3 = 2 + \frac{7}{8} \cdot 6 \cdot \frac{4}{11} = 3.91 \,, \tag{B.20}$$

and so we can rewrite Eq. (B.19) as follows:

$$\Omega_{X0} = \frac{8\pi G H(m) x_{\mathrm{f}} (k_{\mathrm{B}} T_0)^3}{3 H_0^2 m^2 c^6 \langle \sigma v \rangle} \frac{g_{*S}(T_0)}{g_*(m)} \,, \tag{B.21}$$

where we have also made λ explicit. The Hubble parameter $H(m)$ can be written as:

$$H^2(m) = \frac{8\pi G}{3c^2} g_*(m) \frac{\pi^2}{30} \frac{(mc^2)^4}{(\hbar c)^3} \,, \tag{B.22}$$

so that we have finally:

$$\Omega_{X0}h^2 \approx 0.331\frac{x_\mathrm{f}}{\sqrt{g_*(m)}}\frac{10^{-37}\ \mathrm{cm}^2}{\langle\sigma v/c\rangle} \approx 0.331\frac{x_\mathrm{f}}{\sqrt{g_*(m)}}\frac{2.57\times10^{-10}\ \mathrm{GeV}^{-2}}{\langle\sigma v/c\rangle}\ . \tag{B.23}$$

As we saw, reasonable values are $x_\mathrm{f} \approx 10$ and $g_* \approx 100$. A cross-section of the order of $G_\mathrm{F}^2 \sim 10^{-10}\ \mathrm{GeV}^{-2}$ gives the right order of magnitude of the present abundance of CDM. This coincidence is known as **WIMP miracle**.[1]

Relic abundance of baryons

The very same result of Eq. (B.23) can be used for the annihilation of baryons:

$$\mathrm{b} + \bar{\mathrm{b}} \leftrightarrow \gamma + \gamma\ . \tag{B.24}$$

Let us consider only nucleons, i.e. protons and neutrons, since their mass is the dominant one for the baryonic energy density. The annihilation cross-section is of the order of:

$$\langle\sigma v/c\rangle \approx \frac{(\hbar c)^2}{(m_\pi c^2)^2}\ , \tag{B.25}$$

where $m_\pi c^2 \approx 140$ MeV is the mass of the meson π, which can be thought as the mediator of the strong interaction among nucleons. Substituting into Eq. (B.23) we get:

$$\Omega_{\mathrm{b}0}h^2 \approx 10^{-11}\ , \tag{B.26}$$

i.e. a value many orders of magnitude below the observed one and that thus constitutes a compelling argument for the necessity of baryogenesis. Focusing on electrons and positrons, the annihilation cross section is of the order

$$\langle\sigma v/c\rangle \approx \frac{\alpha^2(\hbar c)^2}{(m_e c^2)^2} \approx 204\ \mathrm{GeV}^{-2}\ , \tag{B.27}$$

and from Eq. (B.23) we get:

$$\Omega_{e0}h^2 \approx 10^{-12}\ . \tag{B.28}$$

[1] One can think of different cross sections and thus find CDM candidates lighter than WIMPs. See e.g. [150]. This possibility is also called *WIMPless miracle*.

Bibliography

[1] Sloan Digital Sky survey (SDSS).

[2] The 2dF Galaxy Redshift Survey (2dFGRS).

[3] The Millennium Simulation Project.

[4] Abbott, B. et al. (2017a). GW170817: Observation of Gravitational Waves from a Binary Neutron Star Inspiral. *Phys. Rev. Lett.*, 119(16):161101.

[5] Abbott, B. P. et al. (2016a). GW151226: Observation of Gravitational Waves from a 22-Solar-Mass Binary Black Hole Coalescence. *Phys. Rev. Lett.*, 116(24):241103.

[6] Abbott, B. P. et al. (2016b). Observation of Gravitational Waves from a Binary Black Hole Merger. *Phys. Rev. Lett.*, 116(6):061102.

[7] Abbott, B. P. et al. (2017b). A gravitational-wave standard siren measurement of the Hubble constant. *Nature*, 551(7678):85–88.

[8] Abbott, B. P. et al. (2017c). Multi-messenger Observations of a Binary Neutron Star Merger. *Astrophys. J.*, 848(2):L12.

[9] Abbott, L. F. and Wise, M. B. (1984). Constraints on Generalized Inflationary Cosmologies. *Nucl. Phys.*, B244:541–548.

[10] Abbott, T. M. C. et al. (2017d). Dark Energy Survey Year 1 Results: Cosmological Constraints from Galaxy Clustering and Weak Lensing.

[11] Abramowitz, M. and Stegun, I. A. (1972). *Handbook of Mathematical Functions With Formulas, Graphs, and Mathematical Tables*. Dover.

[12] Adam, R. et al. (2016). Planck 2015 results. I. Overview of products and scientific results. *Astron. Astrophys.*, 594:A1.

[13] Ade, P. A. R. et al. (2016a). Planck 2015 results. XIII. Cosmological parameters. *Astron. Astrophys.*, 594:A13.

[14] Ade, P. A. R. et al. (2016b). Planck 2015 results. XVII. Constraints on primordial non-Gaussianity. *Astron. Astrophys.*, 594:A17.

[15] Ade, P. A. R. et al. (2016c). Planck 2015 results. XX. Constraints on inflation. *Astron. Astrophys.*, 594:A20.

[16] Albrecht, A. and Steinhardt, P. J. (1982). Cosmology for Grand Unified Theories with Radiatively Induced Symmetry Breaking. *Phys. Rev. Lett.*, 48:1220–1223.

[17] Alpher, R. A., Bethe, H., and Gamow, G. (1948). The origin of chemical elements. *Phys. Rev.*, 73:803–804.

[18] Amendola, L. and Tsujikawa, S. (2010). *Dark energy: theory and observations*. Cambridge University Press.

[19] Avelino, A. and Kirshner, R. P. (2016). The dimensionless age of the Universe: a riddle for our time. *Astrophys. J.*, 828(1):35.

[20] Baqui, P. O., Fabris, J. C., and Piattella, O. F. (2016). Cosmology and stellar equilibrium using Newtonian hydrodynamics with general relativistic pressure. *JCAP*, 1604(04):034.

[21] Bardeen, J. M. (1980). Gauge Invariant Cosmological Perturbations. *Phys. Rev.*, D22:1882–1905.

[22] Bardeen, J. M., Bond, J. R., Kaiser, N., and Szalay, A. S. (1986). The Statistics of Peaks of Gaussian Random Fields. *Astrophys. J.*, 304:15–61.

[23] Bardeen, J. M., Steinhardt, P. J., and Turner, M. S. (1983). Spontaneous Creation of Almost Scale - Free Density Perturbations in an Inflationary Universe. *Phys. Rev.*, D28:679.

[24] Battye, R. A., Charnock, T., and Moss, A. (2015). Tension between the power spectrum of density perturbations measured on large and small scales. *Phys. Rev.*, D91(10):103508.

[25] Berestetskii, V. B., Lifshitz, E. M., and Pitaevskii, L. P. (1982). *Quantum Electrodynamics*, volume 4 of *Course of Theoretical Physics*. Pergamon Press, Oxford.

[26] Bernstein, J. (1988). *Kinetic theory in the expanding universe*.

[27] Bertone, G. and Hooper, D. (2016). A History of Dark Matter.

[28] Betoule, M. et al. (2014). Improved cosmological constraints from a joint analysis of the SDSS-II and SNLS supernova samples. *Astron. Astrophys.*, 568:A22.

[29] Bolliet, B., Barrau, A., Martineau, K., and Moulin, F. (2017). Some Clarifications on the Duration of Inflation in Loop Quantum Cosmology. *Class. Quant. Grav.*, 34(14):145003.

[30] Bond, J. R. and Efstathiou, G. (1984). Cosmic background radiation anisotropies in universes dominated by nonbaryonic dark matter. *Astrophys. J.*, 285:L45–L48.

[31] Bonometto, S. (2008). *Cosmologia & cosmologie*. Zanichelli.

[32] Bonvin, V. et al. (2017). H0LiCOW - V. New COSMOGRAIL time delays of HE 0435-1223: H_0 to 3.8 per cent precision from strong lensing in a flat ΛCDM model. *Mon. Not. Roy. Astron. Soc.*, 465(4):4914–4930.

[33] Bouchet, F. R. et al. (2011). COrE (Cosmic Origins Explorer) A White Paper.

[34] Boylan-Kolchin, M., Bullock, J. S., and Kaplinghat, M. (2011). Too big to fail? The puzzling darkness of massive Milky Way subhaloes. *Mon. Not. Roy. Astron. Soc.*, 415:L40.

[35] Brandenberger, R. and Peter, P. (2017). Bouncing Cosmologies: Progress and Problems. *Found. Phys.*, 47(6):797–850.

[36] Brandenberger, R. H. and Martin, J. (2013). Trans-Planckian Issues for Inflationary Cosmology. *Class. Quant. Grav.*, 30:113001.

[37] Brans, C. and Dicke, R. H. (1961). Mach's principle and a relativistic theory of gravitation. *Phys. Rev.*, 124:925–935.

[38] Bucher, M., Moodley, K., and Turok, N. (2000). The General primordial cosmic perturbation. *Phys. Rev.*, D62:083508.

[39] Bullock, J. S. and Boylan-Kolchin, M. (2017). Small-Scale Challenges to the ΛCDM Paradigm. *Ann. Rev. Astron. Astrophys.*, 55:343–387.

[40] Butkov, E. (1968). *Mathematical Physics*. Addison-Wesley Publishing Company, Incorporated.

[41] Camarena, D. and Marra, V. (2016). Cosmological constraints on the radiation released during structure formation. *Eur. Phys. J.*, C76(11):644.

[42] Chandrasekhar, S. (1960). *Radiative transfer*. New York: Dover.

[43] Chluba, J. (2014). Science with CMB spectral distortions. In *Proceedings, 49th Rencontres de Moriond on Cosmology: La Thuile, Italy, March 15-22, 2014*, pages 327–334.

[44] Chluba, J. and Sunyaev, R. A. (2012). The evolution of CMB spectral distortions in the early Universe. *Mon. Not. Roy. Astron. Soc.*, 419:1294–1314.

[45] Clowe, D., Bradac, M., Gonzalez, A. H., Markevitch, M., Randall, S. W., Jones, C., and Zaritsky, D. (2006). A direct empirical proof of the existence of dark matter. *Astrophys. J.*, 648:L109–L113.

[46] Coc, A. (2016). Primordial Nucleosynthesis. *J. Phys. Conf. Ser.*, 665(1):012001.

[47] Coleman, S. R. and Weinberg, E. J. (1973). Radiative Corrections as the Origin of Spontaneous Symmetry Breaking. *Phys. Rev.*, D7:1888–1910.

[48] Crittenden, R., Bond, J. R., Davis, R. L., Efstathiou, G., and Steinhardt, P. J. (1993). The Imprint of gravitational waves on the cosmic microwave background. *Phys. Rev. Lett.*, 71:324–327.

[49] de Bernardis, P. et al. (2000). A Flat universe from high resolution maps of the cosmic microwave background radiation. *Nature*, 404:955–959.

[50] De Felice, A. and Tsujikawa, S. (2010). f(R) theories. *Living Rev. Rel.*, 13:3.

[51] de Sitter, W. (1917). On the relativity of inertia. Remarks concerning Einstein's latest hypothesis. *Koninklijke Nederlandsche Akademie van Wetenschappen Proceedings*, 19:1217–1225.

[52] de Sitter, W. (1918a). Einstein's theory of gravitation and its astronomical consequences. Third paper. *Mon. Not. Roy. Astron. Soc.*, 78:3–28.

[53] de Sitter, W. (1918b). Further remarks on the solutions of the field-equations of the Einstein's theory of gravitation. *Koninklijke Nederlandsche Akademie van Wetenschappen Proceedings*, 20:1309–1312.

[54] de Sitter, W. (1918c). On the curvature of space. *Koninklijke Nederlandsche Akademie van Wetenschappen Proceedings*, 20:229–243.

[55] Di Marco, A. (2017). Lyth Bound, eternal inflation and future cosmological missions. *Phys. Rev.*, D96(2):023511.

[56] E. Di Valentino, L. A. Anchordoqui, O. Akarsu, Y. Ali-Haimoud, L. Amendola, N. Arendse, M. Asgari, M. Ballardini, S. Basilakos and E. Battistelli, *et al.* "Snowmass2021 - Letter of interest cosmology intertwined II: The hubble constant tension," Astropart. Phys. **131** (2021), 102605

[57] Dodelson, S. (2003). *Modern cosmology*. Amsterdam, Netherlands: Academic Pr.

[58] Dodelson, S. (2017). *Gravitational Lensing*. Cambridge, UK: Cambridge University Press, 2017.

[59] Dodelson, S. and Widrow, L. M. (1994). Sterile-neutrinos as dark matter. *Phys. Rev. Lett.*, 72:17–20.

[60] Efstathiou, G., Sutherland, W. J., and Maddox, S. J. (1990). The cosmological constant and cold dark matter. *Nature*, 348:705–707.

[61] Eisenstein, D. J. et al. (2005). Detection of the Baryon Acoustic Peak in the Large-Scale Correlation Function of SDSS Luminous Red Galaxies. *Astrophys. J.*, 633:560–574.

[62] Eisenstein, D. J. and Hu, W. (1998). Baryonic features in the matter transfer function. *Astrophys. J.*, 496:605.

[63] Etherington, I. M. H. (1933). On the Definition of Distance in General Relativity. *Philosophical Magazine*, 15.

[64] Fabris, J. C. and Velten, H. (2012). Neo-Newtonian cosmology: An intermediate step towards General Relativity. *RBEF*, 4302.

[65] Fixsen, D. J., Cheng, E. S., Gales, J. M., Mather, J. C., Shafer, R. A., and Wright, E. L. (1996). The Cosmic Microwave Background spectrum from the full COBE FIRAS data set. *Astrophys. J.*, 473:576.

[66] Friedmann, A. (1922). Ueber die Kruemmung des Raumes . *Z. Phys.*, 10:377–386.

[67] Friedmann, A. (1924). Ueber die Moeglichkeit einer Welt mit konstanter negativer Kruemmung des Raumes. *Z. Phys.*, 21:326–332.

[68] Gaskins, J. M. (2016). A review of indirect searches for particle dark matter. *Contemp. Phys.*, 57(4):496–525.

[69] Gell-Mann, M., Ramond, P., and Slansky, R. (1979). Complex Spinors and Unified Theories. *Conf. Proc.*, C790927:315–321.

[70] Giblin, J. T., Mertens, J. B., and Starkman, G. D. (2016). Observable Deviations from Homogeneity in an Inhomogeneous Universe. *Astrophys. J.*, 833(2):247.

[71] Gorini, V., Kamenshchik, A. Y., Moschella, U., Piattella, O. F., and Starobinsky, A. A. (2008). Gauge-invariant analysis of perturbations in Chaplygin gas unified models of dark matter and dark energy. *JCAP*, 0802:016.

[72] Grad, H. (1958). Principles of the kinetic theory of gases. In *Thermodynamik der Gase/Thermodynamics of Gases*, pages 205–294. Springer.

[73] Grieb, J. N. et al. (2017). The clustering of galaxies in the completed SDSS-III Baryon Oscillation Spectroscopic Survey: Cosmological implications of the Fourier space wedges of the final sample. *Mon. Not. Roy. Astron. Soc.*, 467(2):2085–2112.

[74] Griffiths, D. J. (2017). *Introduction to Electrodynamics*. Cambridge, UK: Cambridge University Press.

[75] Guth, A. H. (1981). The Inflationary Universe: A Possible Solution to the Horizon and Flatness Problems. *Phys. Rev.*, D23:347–356.

[76] Harrison, E. R. (1965). Cosmology without general relativity. *Annals of Physics*, 35:437–446.

[77] Hawking, S. W. (1966). Perturbations of an expanding universe. *Astrophys. J.*, 145:544–554.

[78] Hogg, D. W. (1999). Distance measures in cosmology.

[79] Hu, W. and Sugiyama, N. (1996). Small scale cosmological perturbations: An Analytic approach. *Astrophys. J.*, 471:542–570.

[80] Hu, W. and White, M. J. (1997). CMB anisotropies: Total angular momentum method. *Phys. Rev.*, D56:596–615.

[81] Huang, K. (1987). *Statistical Mechanics, 2nd Edition*. Wiley-VCH.

[82] Hubble, E. (1929). A relation between distance and radial velocity among extra-galactic nebulae. *Proc. Nat. Acad. Sci.*, 15:168–173.

[83] Hwang, J.-c. and Noh, H. (2013). Newtonian Hydrodynamics with General Relativistic Pressure. *JCAP*, 1310:054.

[84] Jackson, J. D. (1998). *Classical Electrodynamics, 3rd Edition*. Wiley-VCH.

[85] Jordan, P., Ehlers, J., and Kundt, W. (2009). Republication of: Exact solutions of the field equations of the general theory of relativity. *General Relativity and Gravitation*, 41(9):2191–2280.

[86] Kaiser, N. (1983). Small-angle anisotropy of the microwave background radiation in the adiabatic theory. *MNRAS*, 202:1169–1180.

[87] Kaiser, N. (1984). On the Spatial correlations of Abell clusters. *Astrophys. J.*, 284:L9–L12.

[88] Kiefer, C. and Polarski, D. (2009). Why do cosmological perturbations look classical to us? *Adv. Sci. Lett.*, 2:164–173.

[89] Kirby, E. N., Bullock, J. S., Boylan-Kolchin, M., Kaplinghat, M., and Cohen, J. G. (2014). The dynamics of isolated Local Group galaxies. *Mon. Not. Roy. Astron. Soc.*, 439(1):1015–1027.

[90] Klypin, A. A., Kravtsov, A. V., Valenzuela, O., and Prada, F. (1999). Where are the missing Galactic satellites? *Astrophys. J.*, 522:82–92.

[91] Kodama, H. and Sasaki, M. (1984). Cosmological Perturbation Theory. *Prog. Theor. Phys. Suppl.*, 78:1–166.

[92] Kolb, E. W. and Turner, M. S. (1990). The Early Universe. *Front. Phys.*, 69:1–547.

[93] Kollmeier, J. A., Zasowski, G., Rix, H.-W., Johns, M., Anderson, S. F., Drory, N., Johnson, J. A., Pogge, R. W., Bird, J. C., Blanc, G. A., Brownstein, J. R., Crane, J. D., De Lee, N. M., Klaene, M. A., Kreckel, K., MacDonald, N., Merloni, A., Ness, M. K., O'Brien, T., Sanchez-Gallego, J. R., Sayres, C. C., Shen, Y., Thakar, A. R., Tkachenko, A., Aerts, C., Blanton, M. R., Eisenstein, D. J., Holtzman, J. A., Maoz, D., Nandra, K., Rockosi, C., Weinberg, D. H., Bovy, J., Casey, A. R., Chaname, J., Clerc, N., Conroy, C., Eracleous, M., Gänsicke, B. T., Hekker, S., Horne, K., Kauffmann, J., McQuinn, K. B. W., Pellegrini, E. W., Schinnerer, E., Schlafly, E. F., Schwope, A. D., Seibert, M., Teske, J. K., and van Saders, J. L. (2017). SDSS-V: Pioneering Panoptic Spectroscopy. *ArXiv e-prints*.

[94] Kosowsky, A. (1996). Cosmic microwave background polarization. *Annals Phys.*, 246:49–85.

[95] Landau, L. D. and Lifschits, E. M. (1975). *The Classical Theory of Fields*, volume Volume 2 of *Course of Theoretical Physics*. Pergamon Press, Oxford.

[96] Landau, L. D. and Lifshits, E. M. (1991). *Quantum Mechanics*, volume v.3 of *Course of Theoretical Physics*. Butterworth-Heinemann, Oxford.

[97] Lemaitre, G. (1927). A Homogeneous Universe of Constant Mass and Growing Radius Accounting for the Radial Velocity of Extragalactic Nebulae. *Annales Soc. Sci. Brux. Ser. I Sci. Math. Astron. Phys.*, A47:49–59.

[98] Lemaitre, G. (1931). The Expanding Universe. *Mon. Not. Roy. Astron. Soc.*, 91:490–501.

[99] Lemaître, G. (1997). The expanding universe. *Gen. Rel. Grav.*, 29:641–680.

[100] Lesgourgues, J. (2011). The Cosmic Linear Anisotropy Solving System (CLASS) I: Overview.

[101] Lesgourgues, J. and Pastor, S. (2006). Massive neutrinos and cosmology. *Phys. Rept.*, 429:307–379.

[102] Liddle, A. R., Parsons, P., and Barrow, J. D. (1994). Formalizing the slow roll approximation in inflation. *Phys. Rev.*, D50:7222–7232.

[103] Lifshitz, E. (1946). On the Gravitational stability of the expanding universe. *J. Phys. (USSR)*, 10:116.

[104] Lifshitz, E. M. and Khalatnikov, I. M. (1963). Investigations in relativistic cosmology. *Adv. Phys.*, 12:185–249.

[105] Lima, J. A. S., Zanchin, V., and Brandenberger, R. H. (1997). On the Newtonian cosmology equations with pressure. *Mon. Not. Roy. Astron. Soc.*, 291:L1–L4.

[106] Linde, A. (2017). On the problem of initial conditions for inflation. In *Black Holes, Gravitational Waves and Spacetime Singularities Rome, Italy, May 9-12, 2017*.

[107] Linde, A. D. (1982). A New Inflationary Universe Scenario: A Possible Solution of the Horizon, Flatness, Homogeneity, Isotropy and Primordial Monopole Problems. *Phys. Lett.*, 108B:389–393.

[108] Liu, J., Chen, X., and Ji, X. (2017). Current status of direct dark matter detection experiments. *Nature Phys.*, 13(3):212–216.

[109] Lovell, M. R., Eke, V., Frenk, C. S., Gao, L., Jenkins, A., Theuns, T., Wang, J., White, D. M., Boyarsky, A., and Ruchayskiy, O. (2012). The Haloes of Bright Satellite Galaxies in a Warm Dark Matter Universe. *Mon. Not. Roy. Astron. Soc.*, 420:2318–2324.

[110] Lukash, V. N. (1980). Production of phonons in an isotropic universe. *Sov. Phys. JETP*, 52:807–814. [Zh. Eksp. Teor. Fiz.79,1601(1980)].

[111] Lyth, D. H. (1997). What would we learn by detecting a gravitational wave signal in the cosmic microwave background anisotropy? *Phys. Rev. Lett.*, 78:1861–1863.

[112] Lyth, D. H. and Liddle, A. R. (2009). *The primordial density perturbation: Cosmology, inflation and the origin of structure*.

[113] Ma, C.-P. and Bertschinger, E. (1995). Cosmological perturbation theory in the synchronous and conformal Newtonian gauges. *Astrophys. J.*, 455:7–25.

[114] Maartens, R. (1996). Causal thermodynamics in relativity.

[115] Macciò, A. V., Mainini, R., Penzo, C., and Bonometto, S. A. (2015). Strongly Coupled Dark Energy Cosmologies: preserving LCDM success and easing low scale problems II - Cosmological simulations. *Mon. Not. Roy. Astron. Soc.*, 453:1371–1378.

[116] Macciò, A. V., Paduroiu, S., Anderhalden, D., Schneider, A., and Moore, B. (2012). Cores in warm dark matter haloes: a Catch 22 problem. *Mon. Not. Roy. Astron. Soc.*, 424:1105–1112.

[117] Maddox, S. J., Efstathiou, G., Sutherland, W. J., and Loveday, J. (1990). Galaxy correlations on large scales. *Mon. Not. Roy. Astron. Soc.*, 242:43–49.

[118] Malik, K. A. and Matravers, D. R. (2013). Comments on gauge-invariance in cosmology. *Gen. Rel. Grav.*, 45:1989–2001.

[119] Marra, V., Amendola, L., Sawicki, I., and Valkenburg, W. (2013). Cosmic variance and the measurement of the local Hubble parameter. *Phys. Rev. Lett.*, 110(24):241305.

[120] Martin, J. (2012). Everything You Always Wanted To Know About The Cosmological Constant Problem (But Were Afraid To Ask). *Comptes Rendus Physique*, 13:566–665.

[121] Martin, J., Ringeval, C., Trotta, R., and Vennin, V. (2014). The Best Inflationary Models After Planck. *JCAP*, 1403:039.

[122] McCrea, W. H. (1951). Relativity Theory and the Creation of Matter. *Proceedings of the Royal Society of London Series A*, 206:562–575.

[123] McCrea, W. H. and Milne, E. A. (1934). Newtonian Universes and the curvature of space. *The Quarterly Journal of Mathematics*, 5.

[124] McVittie, G. C. (1962). Appendix to The Change of Redshift and Apparent Luminosity of Galaxies due to the Deceleration of Selected Expanding Universes. *The Astrophysical Journal*, 136:334.

[125] Meszaros, P. (1974). The behaviour of point masses in an expanding cosmological substratum. *Astron. Astrophys.*, 37:225–228.

[126] Milne, E. A. (1934). A Newtonian expanding Universe. *The Quarterly Journal of Mathematics*, 5.

[127] Milne, E. A. (1935). *Relativity, gravitation and world-structure*. Oxford, The Clarendon press.

[128] Moffat, J. W. and Toth, V. T. (2011). Comment on "The Real Problem with MOND" by Scott Dodelson, arXiv:1112.1320. *ArXiv e-prints*.

[129] Moore, B. (1994). Evidence against dissipationless dark matter from observations of galaxy haloes. *Nature*, 370:629.

[130] Muñoz, J. B., Kovetz, E. D., Raccanelli, A., Kamionkowski, M., and Silk, J. (2017). Towards a measurement of the spectral runnings. *JCAP*, 1705:032.

[131] Mukhanov, V. (2005). *Physical foundations of cosmology*. Cambridge, UK: Univ. Pr.

[132] Mukhanov, V. F. (1985). Gravitational Instability of the Universe Filled with a Scalar Field. *JETP Lett.*, 41:493–496. [Pisma Zh. Eksp. Teor. Fiz.41,402(1985)].

[133] Mukhanov, V. F. (2004). CMB-slow, or how to estimate cosmological parameters by hand. *Int. J. Theor. Phys.*, 43:623–668.

[134] Mukhanov, V. F., Feldman, H. A., and Brandenberger, R. H. (1992). Theory of cosmological perturbations. Part 1. Classical perturbations. Part 2. Quantum theory of perturbations. Part 3. Extensions. *Phys. Rept.*, 215:203–333.

[135] Newman, E. T. and Penrose, R. (1966). Note on the Bondi-Metzner-Sachs group. *J. Math. Phys.*, 7:863–870.

[136] Novello, M. and Bergliaffa, S. E. P. (2008). Bouncing Cosmologies. *Phys. Rept.*, 463:127–213.

[137] Olbers, W. (1826). Edinburgh new phil. *J*, 1:141.

[138] Peccei, R. D. and Quinn, H. R. (1977). CP Conservation in the Presence of Instantons. *Phys. Rev. Lett.*, 38:1440–1443.

[139] Peebles, P. J. E. (1968). Recombination of the Primeval Plasma. *Astrophys. J.*, 153:1.

[140] Peebles, P. J. E. (1980). *The large-scale structure of the universe*. Princeton university press.

[141] Peebles, P. J. E. and Yu, J. T. (1970). Primeval adiabatic perturbation in an expanding universe. *Astrophys. J.*, 162:815–836.

[142] Penzias, A. A. and Wilson, R. W. (1965). A Measurement of excess antenna temperature at 4080- Mc/s. *Astrophys. J.*, 142:419–421.

[143] Percival, W. J. et al. (2007). The shape of the SDSS DR5 galaxy power spectrum. *Astrophys. J.*, 657:645–663.

[144] Perlmutter, S. et al. (1999). Measurements of Omega and Lambda from 42 High-Redshift Supernovae. *Astrophys. J.*, 517:565–586.

[145] Piattella, O. F., Casarini, L., Fabris, J. C., and de Freitas Pacheco, J. A. (2016). Dark matter velocity dispersion effects on CMB and matter power spectra. *JCAP*, 1602(02):024.

[146] Piattella, O. F. and Giani, L. (2017). Redshift drift of gravitational lensing. *Phys. Rev.*, D95(10):101301.

[147] Piattella, O. F., Martins, D. L. A., and Casarini, L. (2014). Sub-horizon evolution of cold dark matter perturbations through dark matter-dark energy equivalence epoch. *JCAP*, 1410(10):031.

[148] Piattella, O. F., Rodrigues, D. C., Fabris, J. C., and de Freitas Pacheco, J. A. (2013). Evolution of the phase-space density and the Jeans scale for dark matter derivedfrom the Vlasov-Einstein equation. *JCAP*, 1311:002.

[149] Polnarev, A. G. (1985). Polarization and Anisotropy Induced in the Microwave Background by Cosmological Gravitational Waves. *Soviet Astronomy*, 29:607–613.

[150] Profumo, S. (2017). *An Introduction to Particle Dark Matter*. Advanced textbooks in physics. World Scientific.

[151] Profumo, S., Sigurdson, K., and Kamionkowski, M. (2006). What mass are the smallest protohalos? *Phys. Rev. Lett.*, 97:031301.

[152] Racah, G. (1942). Theory of complex spectra. ii. *Physical Review*, 62(9-10):438.

[153] Riess, A. G. et al. (1998). Observational Evidence from Supernovae for an Accelerating Universe and a Cosmological Constant. *Astron. J.*, 116:1009–1038.

[154] Robertson, H. P. (1935). Kinematics and World-Structure. *Astrophys. J.*, 82:284.

[155] Robertson, H. P. (1936). Kinematics and World-Structure III. *Astrophys. J.*, 83:257.

[156] Ryden, B. (2003). *Introduction to cosmology*. San Francisco, USA: Addison-Wesley (2003) 244 p.

[157] Sachs, R. K. and Wolfe, A. M. (1967). Perturbations of a cosmological model and angular variations of the microwave background. *Astrophys. J.*, 147:73–90.

[158] Sandage, A. (1958). Current Problems in the Extragalactic Distance Scale. *ApJ*, 127:513.

[159] Sandage, A. (1962). The Change of Redshift and Apparent Luminosity of Galaxies due to the Deceleration of Selected Expanding Universes. *The Astrophysical Journal*, 136:319.

[160] Sarkar, S. and Pandey, B. (2016). An information theory based search for homogeneity on the largest accessible scale. *Mon. Not. Roy. Astron. Soc.*, 463(1):L12–L16.

[161] Sasaki, M. (1986). Large Scale Quantum Fluctuations in the Inflationary Universe. *Prog. Theor. Phys.*, 76:1036.

[162] Schneider, A., Anderhalden, D., Macciò, A., and Diemand, J. (2014). Warm dark matter does not do better than cold dark matter in solving small-scale inconsistencies. *Mon. Not. Roy. Astron. Soc.*, 441:6.

[163] Schutz, B. F. (1985). *A First Course In General Relativity*. Cambridge, Uk: Univ. Pr.

[164] Schwarz, D. J., Copi, C. J., Huterer, D., and Starkman, G. D. (2016). CMB Anomalies after Planck. *Class. Quant. Grav.*, 33(18):184001.

[165] Sciama, D. W. (2012). *The unity of the universe*. Courier Corporation.

[166] Seljak, U. and Zaldarriaga, M. (1996). A Line of sight integration approach to cosmic microwave background anisotropies. *Astrophys. J.*, 469:437–444.

[167] Silk, J. (1967). Fluctuations in the primordial fireball. *Nature*, 215(5106):1155–1156.

[168] Silk, J. et al. (2010). *Particle Dark Matter: Observations, Models and Searches*. Cambridge Univ. Press, Cambridge.

[169] Slipher, V. M. (1917). Nebulae. *Proc. Am. Phil. Soc.*, 56:403–409.

[170] Smoot, G. F. et al. (1992). Structure in the COBE differential microwave radiometer first year maps. *Astrophys. J.*, 396:L1–L5.

[171] Sofue, Y. and Rubin, V. (2001). Rotation curves of spiral galaxies. *Ann. Rev. Astron. Astrophys.*, 39:137–174.

[172] Sofue, Y., Tutui, Y., Honma, M., Tomita, A., Takamiya, T., Koda, J., and Takeda, Y. (1999). Central rotation curves of spiral galaxies. *Astrophys. J.*, 523:136.

[173] Sotiriou, T. P. and Faraoni, V. (2010). f(R) Theories Of Gravity. *Rev. Mod. Phys.*, 82:451–497.

[174] Spergel, D. N. and Steinhardt, P. J. (2000). Observational evidence for selfinteracting cold dark matter. *Phys. Rev. Lett.*, 84:3760–3763.

[175] Starobinsky, A. A. (1979). Spectrum of relict gravitational radiation and the early state of the universe. *JETP Lett.*, 30:682–685. [Pisma Zh. Eksp. Teor. Fiz.30,719(1979)].

[176] Stewart, J. M. (1990). Perturbations of Friedmann-Robertson-Walker cosmological models. *Class. Quant. Grav.*, 7:1169–1180.

[177] Stewart, J. M. and Walker, M. (1974). Perturbations of spacetimes in general relativity. *Proc. Roy. Soc. Lond.*, A341:49–74.

[178] Tram, T. and Lesgourgues, J. (2013). Optimal polarisation equations in FLRW universes. *JCAP*, 1310:002.

[179] Trotta, R. (2017). Bayesian Methods in Cosmology.

[180] Tsujikawa, S. (2014). Distinguishing between inflationary models from cosmic microwave background. *PTEP*, 2014(6):06B104.

[181] Vagnozzi, Sunny (2020). Overview of Physical Cosmology. *Springer International Publishing*, Pg. 37–63.

[182] Valkenburg, W., Marra, V., and Clarkson, C. (2014). Testing the Copernican principle by constraining spatial homogeneity. *Mon. Not. Roy. Astron. Soc.*, 438:L6–L10.

[183] van den Bergh, S. (2011). The Curious Case of Lemaître's Equation No. 24. *JRASC*, 105:151.

[184] Velten, H. E. S., vom Marttens, R. F., and Zimdahl, W. (2014). Aspects of the cosmological "coincidence problem". *Eur. Phys. J.*, C74(11):3160.

[185] Verde, L., Protopapas, P., and Jimenez, R. (2013). Planck and the local Universe: Quantifying the tension. *Phys. Dark Univ.*, 2:166–175.

[186] Viel, M., Becker, G. D., Bolton, J. S., and Haehnelt, M. G. (2013). Warm dark matter as a solution to the small scale crisis: New constraints from high redshift Lyman-α forest data. *Phys. Rev.*, D88:043502.

[187] Vogelsberger, M., Zavala, J., Simpson, C., and Jenkins, A. (2014). Dwarf galaxies in CDM and SIDM with baryons: observational probes of the nature of dark matter. *Mon. Not. Roy. Astron. Soc.*, 444:3684.

[188] Wagoner, R. V. (1973). Big bang nucleosynthesis revisited. *Astrophys. J.*, 179:343–360.

[189] Walker, A. G. (1937). On milne's theory of world-structure. *Proceedings of the London Mathematical Society*, 2(1):90–127.

[190] Wands, D., Malik, K. A., Lyth, D. H., and Liddle, A. R. (2000). A New approach to the evolution of cosmological perturbations on large scales. *Phys. Rev.*, D62:043527.

[191] Wands, D., Piattella, O. F., and Casarini, L. (2016). Physics of the Cosmic Microwave Background Radiation. *Astrophys. Space Sci. Proc.*, 45:3–39.

[192] Warren, M. S., Abazajian, K., Holz, D. E., and Teodoro, L. (2006). Precision determination of the mass function of dark matter halos. *Astrophys. J.*, 646:881–885.

[193] Way, M. J. and Nussbaumer, H. (2011). Lemaître's Hubble relationship. *Phys. Today*, 64N8:8.

[194] Weinberg, S. (1972). *Gravitation and Cosmology: Principles and Applications of the General Theory of Relativity*. Wiley - New York.

[195] Weinberg, S. (1989). The cosmological constant problem. *Reviews of Modern Physics*, 61:1–23.

[196] Weinberg, S. (1992). *Dreams of a final theory: The Search for the fundamental laws of nature*.

[197] Weinberg, S. (2002). Cosmological fluctuations of short wavelength. *Astrophys. J.*, 581:810–816.

[198] Weinberg, S. (2005). *The Quantum theory of fields. Vol. 1: Foundations*. Cambridge University Press.

[199] Weinberg, S. (2006). A No-Truncation Approach to Cosmic Microwave Background Anisotropies. *Phys. Rev.*, D74:063517.

[200] Weinberg, S. (2008). *Cosmology*. Oxford, UK: Oxford Univ. Pr.

[201] Weinberg, S. (2013). *The quantum theory of fields. Vol. 2: Modern applications*. Cambridge University Press.

[202] Weinberg, S. (2015). *Lectures on Quantum Mechanics*. Cambridge University Press.

[203] Wilczek, F. (2015). Particle physics: A weighty mass difference. *Nature*, 520:303–304.

[204] Williams, R. E., Blacker, B., Dickinson, M., Dixon, W. V. D., Ferguson, H. C., Fruchter, A. S., Giavalisco, M., Gilliland, R. L., Heyer, I., Katsanis, R., Levay, Z., Lucas, R. A., McElroy, D. B., Petro, L., Postman, M., Adorf, H.-M., and Hook, R. (1996). The Hubble Deep Field: Observations, Data Reduction, and Galaxy Photometry. *AJ*, 112:1335.

[205] Wilson, M. L. and Silk, J. (1981). On the Anisotropy of the cosomological background matter and radiation distribution. 1. The Radiation anisotropy in a spatially flat universe. *Astrophys. J.*, 243:14–25.

[206] Wu, K. K. S., Lahav, O., and Rees, M. J. (1999). The large-scale smoothness of the Universe. *Nature*, 397:225–230. [,19(1998)].

[207] Zeldovich, Y. B. (1984). Structure of the Universe. *Astrophysics and Space Physics Reviews*, 3:1.

[208] Zimdahl, W. (1996). Bulk viscous cosmology. *Phys. Rev.*, D53:5483–5493.

[209] Zlatev, I., Wang, L.-M., and Steinhardt, P. J. (1999). Quintessence, Cosmic Coincidence, and the Cosmological Constant. *Phys. Rev. Lett.*, 82:896–899.

[210] Zwicky, F. (1933).

---

[211] Betts S. et al., Development of a Relic Neutrino Detection Experiment at PTOLEMY: Princeton Tritium Observatory for Light, Early-Universe, Massive-Neutrino Yield (2013). [arXiv:1307.4738].

[212] Follin B., Knox L., Millea M., Pan, Z., 2015, Phys. Rev. Lett. 115, 091301. [arXiv:1503.07863]

[213] Ade P.A.R. et al., 2016, A & A, 594, A13, Planck collaboration. [arXiv:1502.01589]

[214] Archidiacono M., Calabrese E., Melchiorri A., 2011, Phys.Rev. D, 84, 123008. [arXiv:1109.2767]

[215] Archidiacono M., Giusarma E., Melchiorri A., Mena O., 2012, Phys.Rev. D, 86, 043509. [arXiv:1206.0109]

[216] Diamanti R., Giusarma E., Mena O., Archidiacono M., Melchiorri A., 2013, Phys.Rev. D, 87, 063509. [arXiv:1212.6007]

[217] Archidiacono M., Giusarma, E., Melchiorri A., and Mena O., 2013, Phys.Rev. D, 87, 103519. [arXiv:1303.0143]

[218] Gerbino M., Valentino E.D., Said, N., 2013, Phys.Rev. D, 88, 063538. [arXiv:1304.7400]

[219] Trotta R., Melchiorri A., 2005, Phys. Rev. Lett., 95, 011305. [arXiv:astro-ph/0412066]

[220] Krauss L.M., Long A.J., 2016, JCAP, 07, 002. [arXiv:1604.00886]

[221] Sellentin E., Durrer R., 2015, Phys. Rev. D, 92, 063012. [arXiv:1412.6427]

[222] Audren B. et al., 2015, JCAP, 03, 036. [arXiv:1412.5948]

[223] Hu W., 1998, Astrophys. J., 506, 485. [arXiv:astro-ph/9801234]

[224] Hu W., Eisenstein D.J., Tegmark M., White M.J., 1999 Phys. Rev. D, 59, 023512. [arXiv:astro-ph/9806362]

[225] Mangano. G, Miele. G, Pastor. S, Pisanti.O, Sarikas. S, 2012, Phys. Lett. B 708 1. [arXiv:1110.4335]

[226] Castorina. E et al., 2012, Phys. Rev. D 86 023517. [arXiv:1204.2510]

[227] Ma C.P., Bertschinger E., 1995, Astrophys. J., 7, 455. [astro-ph/9506072]

[228] Lewis A., Challinor A., 2002, Phys.Rev. D, 66, 023531. [arXiv:astro-ph/0203507]

[229] Shoji M., Komatsu E., 2010, Phys.Rev. D, 81, 123516. [arXiv:1003.0942]

[230] Lesgourgues J., Tram T., 2011, JCAP, 1109, 032. [arXiv:1104.2935]

[231] Beutler F. et al., 2011, MNRAS, 416, 3017. [arXiv:1106.3366]

[232] Ross A.J., Samushia L., Howlett C., Percival W.J., Burden A., Manera M., 2015, MNRAS, 449, 835. [arXiv:1409.3242]

[233] Anderson L. et al., 2014, MNRAS, 441, 24. [arXiv:1312.4877]

[234] Font-Ribera A. et al., 2014, JCAP, 5, 27. [arXiv:1311.1767]

[235] Nunes R.C., Pan S., Saridakis E.N., 2016, Phys. Rev. D, 94, 023508. [arXiv:1503.04113]

[236] Bernal J. L, Verde. L, Cuesta A. J., 2016, JCAP 02 059. [arXiv:1511.03049]

[237] Ruiz E. J and D. Huterer, 2015, Phys. Rev. D 91 6,063009. [arXiv:1410.5832]

[238] Tinker J.L. et al., 2012, Astrophys. J., 745, 16. [arXiv:1104.1635]

[239] Rozo E. et al., 2010, Astrophys. J., 708, 645. [arXiv:0902.3702]

[240] Henry J.P. et al., 2009, Astrophys. J., 691, 1307. [arXiv:0809.3832]

[241] Benson B.A. et al., 2013, Astrophys. J., 763, 147. [arXiv:1112.5435]

[242] Hajian A. et al., 2013, JCAP, 11, 64. [arXiv:1309.3282]

[243] Ade et al. P.A.R., 2010, MNRAS, 406, 1759. [arXiv:0909.3098]

[244] Ade et al. P.A.R, 2014, A&A 571 A20. [arXiv:1303.5080]

[245] Vikhlinin A. et al., 2009, Astrophys. J., 692, 1060. [arXiv:0812.2720].

[246] Heymans C. et al., 2013, MNRAS, 432, 2433. [arXiv:1303.1808]

[247] Gelman A., Rubin D., 1992, Inference from iterative simulation using multiple sequences, Statistical Science, 7, 457

[248] Oldengott I. M., Rampf C., Wong Y. Y. Y., 2015, JCAP, 1504, 04, 016. [arXiv:1409.1577]

[249] Smith T.L., Das S., Zahn O., 2012, Phys. Rev. D, 85, 023001. [arXiv:1105.3246]

[250] Wilkinson R.J., Boehm C., Lesgourgues J., 2014, JCAP, 05, 011. [arXiv:1401.7597]

[251] Archidiacono M. et al., 2016, JCAP, 08, 067. [arXiv:1606.07673]

[252] Valentino E.D., Melchiorri A., Mena, O., 2013, JCAP, 1311, 018. [arXiv:1304.5981]

[253] Weinberg S., 2013, Phys. Rev. Lett., 110, 241301. [arXiv:1305.1971]

[254] Kitching T. D, Verde L., Heavens A. F, Jimenez R., Mon. Not. Roy. Astron. Soc., 2016, 459 1. [arXiv:1602.02960]

[255] Valentino E.D., Melchiorri A., Silk J., 2016, Phys. Lett. B, 761. [arXiv:1606.00634]

[256] Valentino E.D., Melchiorri A., Linder E.V., Silk J., 2017, Phys. Rev. D, 96, 023523. [arXiv:1704.00762]

[257] Kumar S., Nunes R.C., 2016, Phys. Rev. D, 94, 123511. [arXiv:1608.02454]

[258] Kumar S., Nunes R.C., 2017, to appear in Phys. Rev. D. [arXiv:1702.02143]

[259] Yang W., Nunes R. C, Pan S., Mota D. M., 2017, Phys. Rev. D 95, 103522. [arXiv:1703.02556].

[260] Abazajian K.N., Beacom J.F., Bell N.F., 2002, Phys. Rev. D, 66, 013008, astro-ph/0203442

[261] Abazajian K.N. et al., 2015, Astropart. Phys., 63, 66, arXiv:1309.5383

[262] Abazajian, K. N., Adshead, P., Ahmed, Z., et al. 2016, arXiv:1610.02743

[263] Affleck I. and Dine M., Nucl. Phys. B 249, 361 (1985)

[264] Ali-Haimoud Y. and Bird S., MNRAS 428 (2013) 3375. arXiv:1209.0461

[265] Allison R., Caucal P., Calabrese E., Dunkley J., Louis T., 2015, Phys. Rev. D, 92, 123535. arXiv:1509.07471

[266] Audren B., Lesgourgues J., Benabed K., Prunet S., 2013, Journal of Cosmology and Astro-Particle Physics, 02, 001. arXiv:1210.7183

[267] Barenboim G., Kinney W. H., Park W.-I., 2017, Phys. Rev. D, 95, 43506. arXiv:1609.01584

[268] Barenboim G., Park W.-I., 2017, Journal of Cosmology and Astro-Particle Physics, 2017, 48. arXiv:1703.08258

[269] Blas D., Lesgourgues J., Tram T., 2011, Journal of Cosmology and Astro-Particle Physics, 07, 034. arXiv:1104.2933

[270] Brinckmann, T., Hooper, D. C., Archidiacono, M., Lesgourgues, J., & Sprenger, T. 2018, Journal of Cosmology and Astro-Particle Physics, 59. arXiv:1808.05955

[271] Canetti, L., Drewes, M., & Shaposhnikov, M. 2012, New Journal of Physics, 14, 095012. arXiv:1204.4186

[272] Capparelli, L., Di Valentino, E., Melchiorri, A., & Chluba, J. 2018, Phys. Rev. D, 97, 063519. arXiv:1712.06965

[273] Caramete A., Popa L.A., 2014, Journal of Cosmology and Astro-Particle Physics, 02, 012. arXiv:1311.3856

[274] Casas A., Cheng W.Y. and Gelmini G., 1999, Nucl. Phys. B, 538, 297. arXiv:hep-ph/9709289

[275] Castorina, E., França, U., Lattanzi, M., et al. 2012, Phys. Rev. D, 86, 023517, arXiv:1204.2510

[276] Chen, X., Fu, C., Galan, J., et al. 2017, Science China Physics, Mechanics, and Astronomy, 60, 61011, arXiv:1610.08883

[277] Choudhury, S. R., & Choubey, S. 2018, Journal of Cosmology and Astro-Particle Physics, 17. arXiv:1806.10832

[278] Cooke R., Pettini M., Jorgenson R. A., MurphyM. T. and Steidel C. C., Astrophys. J., 781, 2014, 31. arXiv:1308.3240

[279] de Salas, P. F., & Pastor, S. 2016, Journal of Cosmology and Astro-Particle Physics, 7, 051. arXiv:1606.06986

[280] Di Valentino, E., Melchiorri, A., Fantaye, Y., & Heavens, A. 2018, Phys. Rev. D, 98, 063508, arXiv:1808.09201

[281] Di Valentino, E., Brinckmann, T., Gerbino, M., et al. 2018b, Journal of Cosmology and Astro-Particle Physics, 4, 017. arXiv:1612.00021

[282] Dolgov A.D., 2002, Phys. Rept., 370, 333. arXiv:hep-ph/0202122

[283] Dolgov A. D., Hansen S. H., Pastor S., Petcov S. T., Raffelt G. G., Semikoz D. V., 2002, Nuclear Physics B, 632, 363. arXiv:hep-ph/0201287

[284] Finelli, F., Bucher, M., Achúcarro, A., et al. 2018, Journal of Cosmology and Astro-Particle Physics, 4, 016. arXiv:1612.08270

[285] Freese K., Kolb E.W., and Turner M.S., Phys. Rev. D, 27, 1689 (1983)

[286] Giusarma, E., Corsi, M., Archidiacono, M., et al. 2011, Phys. Rev. D, 83, 115023

[287] Giusarma, E., Vagnozzi, S., Ho, S., et al. 2018, arXiv:1802.08694

[288] Hu W., Scott D., Sugiyama N., White M., 1995, Phys. Rev. D, 52, 5498, astro-ph/9505043

[289] Ichiki K., Yamaguchi M., Yokoyama J., 2007, Phys. Rev D, 75, 084017, hep-ph/0611121

[290] Kang, H.-S., & Steigman, G. 1992, Nuclear Physics B, 372, 494

[291] Kinney W.H., Riotto A., 1999, Phys. Rev. Lett., 83, 3366, hep-ph/9903459

[292] Lattanzi M., Ruffni R., Vereshchagin G.V., 2005, Phys. Rev. D, 72, 063003, astro-ph/0509079

[293] Lesgourgues J., Pastor S., 1999, Phys. Rev. D, 60, 103521, arXiv:hep-ph/9904411

[294] Lesgourgues J., Pastor S., Phys. Rept., 429, 307, arXiv:astro-ph/0603494

[295] Lesgourgues J., Mangano G., Miele G., Pastor S., 2013, Neutrino Cosmology, Cambridge University Press

[296] Li, E.-K., Zhang, H., Du, M., Zhou, Z.-H., & Xu, L. 2018, Journal of Cosmology and Astro-Particle Physics, 8, 042, arXiv:1703.01554

[297] Lorenz, C. S., Calabrese, E., & Alonso, D. 2017, Phys. Rev. D, 96, 043510, arXiv:1706.00730

[298] Mangano G., Miele G., Pastor S., Pisanti O. and Sarikas S., Phys. Lett. B, 708 (2012) 1. arXiv:1110.4335

[299] Mishra-Sharma, S., Alonso, D., & Dunkley, J. 2018, Phys. Rev. D, 97, 123544. arXiv:1803.07561

[300] Nunes R.C., & Bonilla A. 2018, Mon. Non. Roy. Astron. Soc., 473, 4404. arXiv:1710.10264

[301] Oldengott I. M and Schwarz D. J, 2017, Europhys. Lett., 119, 29001. arXiv:1706.01705

[302] Pastor S., Pinto T. and Raffelt G. G., Phys. Rev. Lett., 102 (2009) 241302. arXiv:0808.3137

[303] Planck Collaboration, Aghanim, N., Akrami, Y., et al. 2018, arXiv:1807.06209

[304] Popa L.A., Vasile A., 2008, Journal of Cosmology and Astro-Particle Physics, 06, 028, arXiv:0804.2971

[305] Riess A.G. et al., 2016, Astrophys. J., 826, 56, arXiv:1604.01424

[306] Sarkar, S. 1996, Reports on Progress in Physics, 59, 1493. arXiv:hep-ph/9602260

[307] Schwarz, D. J., & Stuke, M. 2009, Journal of Cosmology and Astro-Particle Physics, 11, 025. arXiv:0906.3434

[308] Schwarz D. J. and Stuke M., 2013, New J. Phys. 15 033021. arXiv:1211.6721

[309] Semikoz, V. B., Sokoloff, D. D., & Valle, J. W. F. 2009, Phys. Rev. D., 80, 083510. arXiv:0905.3365

[310] Serpico P.D., Raffelt G.G., 2005, Phys. Rev. D, 71, 127301, astro-ph/0506162

[311] Simha V., Steigman G., 2008, Journal of Cosmology and Astro-Particle Physics, 08, 011, arXiv:0806.0179

[312] Stuke, M., Schwarz, D. J., & Starkman, G. 2012, Journal of Cosmology and Astro-Particle Physics, 3, 040

[313] Vagnozzi S., Giusarma E., Mena O., Freese K., Gerbino M., Ho S., Lattanzi M., 2017, Phys. Rev. D, 96, 123503. arXiv:1701.08172

[314] Vagnozzi S., Brinckmann T., Archidiacono M., Freese K., Gerbino M., Lesgourgues J., Sprenger T., 2018, Journal of Cosmology and Astro-Particle Physics, 2018, 1. arXiv:1807.04672.

[315] Vagnozzi, S., Dhawan, S., Gerbino, M., et al. 2018, Phys. Rev. D, 98, 83501. arXiv:1801.08553.

[316] Wang, S., Wang, Y.-F., Xia, D.-M., & Zhang, X. 2016, Phys. Rev. D, 94, 083519, arXiv:1608.00672

[317] Wang, S., Wang, Y.-F., & Xia, D.-M. 2018, Chinese Physics C, 42, 065103, arXiv:1707.00588

[318] Wang, L.-F., Zhang, X.-N., Zhang, J.-F., & Zhang, X. 2018, Physics Letters B, 782, 87, arXiv:1802.04720

[319] Wong Y.Y., 2002, Phys. Rev. D, 66, 025015, hep-ph/0203180

[320] Yang, W., Nunes, R. C., Pan, S., & Mota, D. F. 2017, Phys. Rev. D, 95, 103522, arXiv:1703.02556

[321] Zeng, Z., Yeung, S., & Chu, M.-C. 2018, arXiv:1808.00357

[322] Cowan, C. L., Reines, F., Harrison, F. B., Kruse, H. W., McGuire, A. D. 1956. Detection of the Free Neutrino: A Confirmation. Science 124, 103–104. doi:10.1126/science.124.3212.103

[323] Danby, G. and 6 colleagues 1962. Observation of High-Energy Neutrino Reactions and the Existence of Two Kinds of Neutrinos. Physical Review Letters 9, 36–44.

[324] M. Nakamura [DONUT], "Result from DONUT: Direct observation of nu/tau interaction," Nucl. Phys. B Proc. Suppl. **77** (1999), 259-264 doi:10.1016/S0920-5632(99)00425-9doi:10.1103/PhysRevLett.9.36

[325] Weinberg, S. (2008) Cosmology, vol. 1, Oxford University Press.

[326] Pontecorvo, B. (1991) Inverse beta process. Cambridge Monogr. Part. Phys. Nucl. Phys. Cosmol., 1, 25 – 31.

[327] Bahcall, J. N. 1964. Solar Neutrinos. I. Theoretical. Physical Review Letters 12, 300–302. doi:10.1103/PhysRevLett.12.300

[328] B. T. Cleveland, T. Daily, R. Davis, Jr., J. R. Distel, K. Lande, C. K. Lee, P. S. Wildenhain and J. Ullman, "Measurement of the solar electron neutrino flux with the Homestake chlorine detector," Astrophys. J. **496** (1998), 505-526 doi:10.1086/305343

[329] T. D. Lee and C. N. Yang, "Parity Nonconservation and a Two Component Theory of the Neutrino," Phys. Rev. **105** (1957), 1671-1675 doi:10.1103/PhysRev.105.167

[330] C. S. Wu, E. Ambler, R. W. Hayward, D. D. Hoppes and R. P. Hudson, "Experimental Test of Parity Conservation in β Decay," Phys. Rev. **105** (1957), 1413-1414 doi:10.1103/PhysRev.105.1413

[331] The ALEPH Collaboration, the DELPHI Collaboration, the L3 Collaboration, the OPAL Collaboration, the SLD Collaboration, the LEP Electroweak Working Group, et al.: 2005, *arXiv e-prints*, hep-ex/0509008.

[332] Aker M., Beglarian A., Behrens J., Berlev A., Besserer U., Bieringer B., Block F., et al., 2021, arXiv, arXiv:2105.08533

[333] B. Pontecorvo, "Mesonium and anti-mesonium," Sov. Phys. JETP **6**, 429 (1957)

[334] A. De Gouvêa, I. Martinez-Soler, Y. F. Perez-Gonzalez and M. Sen, "Fundamental physics with the diffuse supernova background neutrinos," Phys. Rev. D **102** (2020), 123012 doi:10.1103/PhysRevD.102.123012 [arXiv:2007.13748 [hep-ph]].

[335] Hirata, K. and 22 colleagues 1987. Observation of a neutrino burst from the supernova SN1987A. Physical Review Letters 58, 1490–1493. doi:10.1103/PhysRevLett.58.1490

[336] Askins, M. and 80 colleagues 2020. uc(Theia): an advanced optical neutrino detector. European Physical Journal C 80. doi:10.1140/epjc/s10052-020-7977-8

[337] R. Peccei and H. Quinn, "CP Conservation in the Presence of Pseudoparticles," *Phys. Rev. Lett.* **38** (1977) 1440.

[338] S. Weinberg, "A New Light Boson?," *Phys. Rev. Lett.* **40** (1978) 223.

[339] F. Wilczek, "Problem of Strong P and T Invariance in the Presence of Instantons," *Phys. Rev. Lett.* **40** (1978) 279.

[340] A. Arvanitaki, S. Dimopoulos, S. Dubovsky, N. Kaloper, and J. March-Russell, "String Axiverse," *Phys. Rev.* **D81** (2010) 123530, arXiv:0905.4720 [hep-th].

[341] B. Holdom, "Two $U(1)$'s and Epsilon Charge Shifts," *Phys. Lett.* **166B** (1986) 196–198.

[342] K. Abazajian *et al.*, "Light Sterile Neutrinos: A White Paper," arXiv:1204.5379 [hep-ph].

[343] K. Abazajian *et al.* (CMB-S4 Collaborations), "CMB-S4 Science Book, First Edition," arXiv:1610.02743 [astro-ph.CO].

[344] B. Wallisch, *Cosmological Probes of Light Relics*. PhD thesis, University of Cambridge, 2018.

[345] G. A. Marques and A. Bernui, "Tomographic analyses of the CMB lensing and galaxy clustering to probe the linear structure growth," JCAP **05** (2020), 052 doi:10.1088/1475-7516/2020/05/052, [arXiv:1908.04854 [astro-ph.CO]].

[346] Z. Li, Y. Jing, P. Zhang, and D. Cheng, "Measurement of Redshift-Space Power Spectrum for BOSS galaxies and the Growth Rate at redshift 0.57," *Astrophys. J.* **833** no. 2, (2016) 287, arXiv:1609.03697 [astro-ph.CO].

[347] H. Gil-Marín, W. J. Percival, L. Verde, J. R. Brownstein, C.-H. Chuang, F.-S. Kitaura, S. A. Rodríguez-Torres, and M. D. Olmstead, "The clustering of galaxies in the SDSS-III Baryon Oscillation Spectroscopic Survey: RSD measurement from the power spectrum and bispectrum of the DR12 BOSS galaxies," *Mon. Not. Roy. Astron. Soc.* **465** no. 2, (2017) 1757–1788, arXiv:1606.00439 [astro-ph.CO].

[348] C. Heymans *et al.*, "KiDS-1000 Cosmology: Multi-probe weak gravitational lensing and spectroscopic galaxy clustering constraints," 7, 2020. arXiv:2007.15632 [astro-ph.CO].

[349] K. Kuijken *et al.*, "Gravitational Lensing Analysis of the Kilo Degree Survey," *Mon. Not. Roy. Astron. Soc.* **454** no. 4, (2015) 3500–3532, arXiv:1507.00738 [astro-ph.CO].

[350] H. Hildebrandt *et al.*, "KiDS-450: Cosmological parameter constraints from tomographic weak gravitational lensing," *Mon. Not. Roy. Astron. Soc.* **465** (2017) 1454, arXiv:1606.05338 [astro-ph.CO].

[351] I. Fenech Conti, R. Herbonnet, H. Hoekstra, J. Merten, L. Miller, and M. Viola, "Calibration of weak-lensing shear in the Kilo-Degree Survey," *Mon. Not. Roy. Astron. Soc.* **467** no. 2, (2017) 1627–1651, arXiv:1606.05337 [astro-ph.CO].

[352] S. Joudaki *et al.*, "KiDS-450: Testing extensions to the standard cosmological model," *Mon. Not. Roy. Astron. Soc.* **471** no. 2, (2017) 1259–1279, arXiv:1610.04606 [astro-ph.CO].

[353] S. Joudaki *et al.*, "KiDS-450 + 2dFLenS: Cosmological parameter constraints from weak gravitational lensing tomography and overlapping redshift-space galaxy clustering," *Mon. Not. Roy. Astron. Soc.* **474** no. 4, (2018) 4894–4924, arXiv:1707.06627 [astro-ph.CO].

[354] H. Hildebrandt *et al.*, "KiDS+VIKING-450: Cosmic shear tomography with optical and infrared data," *Astron. Astrophys.* **633** (2020) A69, arXiv:1812.06076 [astro-ph.CO].

[355] **DES** Collaboration, T. M. C. Abbott *et al.*, "Dark Energy Survey year 1 results: Cosmological constraints from galaxy clustering and weak lensing," *Phys. Rev.* **D98** no. 4, (2018) 043526, arXiv:1708.01530 [astro-ph.CO].

[356] **DES** Collaboration, M. A. Troxel *et al.*, "Dark Energy Survey Year 1 results: Cosmological constraints from cosmic shear," *Phys. Rev.* **D98** no. 4, (2018) 043528, arXiv:1708.01538 [astro-ph.CO].

[357] C. Heymans *et al.*, "CFHTLenS: The Canada-France-Hawaii Telescope Lensing Survey," *Mon. Not. Roy. Astron. Soc.* **427** (2012) 146, arXiv:1210.0032 [astro-ph.CO].

[358] T. Erben *et al.*, "CFHTLenS: The Canada-France-Hawaii Telescope Lensing Survey - Imaging Data and Catalogue Products," *Mon. Not. Roy. Astron. Soc.* **433** (2013) 2545, arXiv:1210.8156 [astro-ph.CO].

[359] S. Joudaki *et al.*, "CFHTLenS revisited: assessing concordance with Planck including astrophysical systematics," *Mon. Not. Roy. Astron. Soc.* **465** no. 2, (2017) 2033–2052, arXiv:1601.05786 [astro-ph.CO].

[360] **KiDS** Collaboration, M. Asgari *et al.*, "KiDS-1000 Cosmology: Cosmic shear constraints and comparison between two point statistics," 7, 2020. arXiv:2007.15633 [astro-ph.CO].

[361] N. Palanque-Delabrouille, C. Yèche, N. Schöneberg, J. Lesgourgues, M. Walther, S. Chabanier, and E. Armengaud, "Hints, neutrino bounds and WDM constraints from SDSS DR14 Lyman-α and Planck full-survey data," *JCAP* **04** (2020) 038, arXiv:1911.09073 [astro-ph.CO].

[362] S. Joudaki *et al.*, "KiDS+VIKING-450 and DES-Y1 combined: Cosmology with cosmic shear," *Astron. Astrophys.* **638** (2020) L1, arXiv:1906.09262 [astro-ph.CO].

[363] M. Asgari *et al.*, "KiDS+VIKING-450 and DES-Y1 combined: Mitigating baryon feedback uncertainty with COSEBIs," *Astron. Astrophys.* **634** (2020) A127, arXiv:1910.05336 [astro-ph.CO].

[364] T. Tröster *et al.*, "Cosmology from large-scale structure: Constraining ΛCDM with BOSS," *Astron. Astrophys.* **633** (2020) L10, arXiv:1909.11006 [astro-ph.CO].

[365] T. Hamana *et al.*, "Cosmological constraints from cosmic shear two-point correlation functions with HSC survey first-year data," *Publ. Astron. Soc. Jap.* **72** no. 1, (2020) Publications of the Astronomical Society of Japan, Volume 72, Issue 1, February 2020, 16, https://doi.org/10.1093/pasj/psz138, arXiv:1906.06041 [astro-ph.CO].

[366] E. van Uitert *et al.*, "KiDS+GAMA: cosmology constraints from a joint analysis of cosmic shear, galaxy–galaxy lensing, and angular clustering," *Mon. Not. Roy. Astron. Soc.* **476** no. 4, (2018) 4662–4689, arXiv:1706.05004 [astro-ph.CO].

[367] M. M. Ivanov, M. Simonović, and M. Zaldarriaga, "Cosmological Parameters from the BOSS Galaxy Power Spectrum," *JCAP* **05** (2020) 042, arXiv:1909.05277 [astro-ph.CO].

[368] E. Di Valentino and S. Bridle, "Exploring the Tension between Current Cosmic Microwave Background and Cosmic Shear Data," *Symmetry* **10** no. 11, (2018) 585.

[369] **ACT** Collaboration, S. Aiola *et al.*, "The Atacama Cosmology Telescope: DR4 Maps and Cosmological Parameters," arXiv:2007.07288 [astro-ph.CO].

[370] **SPT** Collaboration, J. Henning *et al.*, "Measurements of the Temperature and E-Mode Polarization of the CMB from 500 Square Degrees of SPTpol Data," *Astrophys. J.* **852** no. 2, (2018) 97, arXiv:1707.09353 [astro-ph.CO].

[371] **Planck** Collaboration, P. Ade *et al.*, "Planck 2015 results. XV. Gravitational lensing," *Astron. Astrophys.* **594** (2016) A15, arXiv:1502.01591 [astro-ph.CO].

[372] A. G. Sanchez, "Let us bury the prehistoric h: arguments against using h^{-1}Mpc units in observational cosmology," arXiv:2002.07829 [astro-ph.CO].

[373] **Planck** Collaboration, P. Ade *et al.*, "Planck 2015 results. XXVII. The Second Planck Catalogue of Sunyaev-Zeldovich Sources," *Astron. Astrophys.* **594** (2016) A27, arXiv:1502.01598 [astro-ph.CO].

[374] **Planck** Collaboration, P. Ade *et al.*, "Planck 2015 results. XXIV. Cosmology from Sunyaev-Zeldovich cluster counts," *Astron. Astrophys.* **594** (2016) A24, arXiv:1502.01597 [astro-ph.CO].

[375] **SPT** Collaboration, T. de Haan *et al.*, "Cosmological Constraints from Galaxy Clusters in the 2500 square-degree SPT-SZ Survey," *Astrophys. J.* **832** no. 1, (2016) 95, arXiv:1603.06522 [astro-ph.CO].

[376] N. Arendse *et al.*, "Cosmic dissonance: new physics or systematics behind a short sound horizon?," *Astron. Astrophys.* **639** (2020) A57, arXiv:1909.07986 [astro-ph.CO].

[377] J. C. Hill, E. McDonough, M. W. Toomey, and S. Alexander, "Early Dark Energy Does Not Restore Cosmological Concordance," arXiv:2003.07355 [astro-ph.CO].

[378] G. Benevento, W. Hu, and M. Raveri, "Can Late Dark Energy Transitions Raise the Hubble constant?," arXiv:2002.11707 [astro-ph.CO].

[379] L. Knox and M. Millea, "The Hubble Hunter's Guide," arXiv:1908.03663 [astro-ph.CO].

[380] J. Evslin, A. A. Sen, and Ruchika, "Price of shifting the Hubble constant," *Phys. Rev. D* **97** no. 10, (2018) 103511, arXiv:1711.01051 [astro-ph.CO].

[381] E. V. Linder, "Cosmic Growth and Expansion Conjoined," *Astropart. Phys.* **86** (2017) 41–45, arXiv:1610.05321 [astro-ph.CO].

[382] E. Di Valentino, E. V. Linder, and A. Melchiorri, "H_0 Ex Machina: Vacuum Metamorphosis and Beyond H_0," arXiv:2006.16291 [astro-ph.CO].

[383] N. Hamaus, A. Pisani, J.-A. Choi, G. Lavaux, B. D. Wandelt, and J. Wellera, "Precision cosmology with voids in the final BOSS data," arXiv:2007.07895 [astro-ph.CO].

[384] **DES** Collaboration, M. Troxel *et al.*, "Survey geometry and the internal consistency of recent cosmic shear measurements," *Mon. Not. Roy. Astron. Soc.* **479** no. 4, (2018) 4998–5004, arXiv:1804.10663 [astro-ph.CO].

[385] E. Di Valentino, A. Melchiorri, and J. Silk, "Beyond six parameters: extending ΛCDM," *Phys. Rev.* **D92** no. 12, (2015) 121302, arXiv:1507.06646 [astro-ph.CO].

[386] E. Di Valentino, A. Melchiorri, and J. Silk, "Reconciling Planck with the local value of H_0 in extended parameter space," *Phys. Lett.* **B761** (2016) 242–246, arXiv:1606.00634 [astro-ph.CO].

[387] S. Anand, P. Chaubal, A. Mazumdar, and S. Mohanty, "Cosmic viscosity as a remedy for tension between PLANCK and LSS data," *JCAP* **11** (2017) 005, arXiv:1708.07030 [astro-ph.CO].

[388] E. Di Valentino, A. Melchiorri, E. V. Linder, and J. Silk, "Constraining Dark Energy Dynamics in Extended Parameter Space," *Phys. Rev.* **D96** no. 2, (2017) 023523, arXiv:1704.00762 [astro-ph.CO].

[389] E. Di Valentino, A. Melchiorri, and J. Silk, "Cosmological constraints in extended parameter space from the Planck 2018 Legacy release," arXiv:1908.01391 [astro-ph.CO].

[390] E. Di Valentino, A. Melchiorri, O. Mena, and S. Vagnozzi, "Interacting dark energy after the latest Planck, DES, and H_0 measurements: an excellent solution to the H_0 and cosmic shear tensions," arXiv:1908.04281 [astro-ph.CO].

[391] E. Di Valentino, A. Melchiorri, O. Mena, and S. Vagnozzi, "Non-minimal dark sector physics and cosmological tensions," arXiv:1910.09853 [astro-ph.CO].

[392] A. Gómez-Valent and J. Solà Peracaula, "Density perturbations for running vacuum: a successful approach to structure formation and to the σ_8-tension," *Mon. Not. Roy. Astron. Soc.* **478** no. 1, (2018) 126–145, arXiv:1801.08501 [astro-ph.CO].

[393] A. Gómez-Valent and J. Solà, "Relaxing the σ_8-tension through running vacuum in the Universe," *EPL* **120** no. 3, (2017) 39001, arXiv:1711.00692 [astro-ph.CO].

[394] G. Lambiase, S. Mohanty, A. Narang, and P. Parashari, "Testing dark energy models in the light of σ_8 tension," *Eur. Phys. J. C* **79** no. 2, (2019) 141, arXiv:1804.07154 [astro-ph.CO].

[395] S. Camera, M. Martinelli, and D. Bertacca, "Does quartessence ease cosmic tensions?," *Phys. Dark Univ.* **23** (2019) 100247, arXiv:1704.06277 [astro-ph.CO].

[396] E. Di Valentino and F. R. Bouchet, "A comment on power-law inflation with a dark radiation component," *JCAP* **10** (2016) 011, arXiv:1609.00328 [astro-ph.CO].

[397] R. Burenin, "Measurements of the Matter Density Perturbation Amplitude from Cosmological Data," *Astron. Lett.* **44** no. 11, (2018) 653–663, arXiv:1806.03261 [astro-ph.CO].

[398] Z. Davari, V. Marra, and M. Malekjani, "Cosmological constrains on minimally and non-minimally coupled scalar field models," *Mon. Not. Roy. Astron. Soc.* **491** no. 2, (2020) 1920–1933, arXiv:1911.00209 [gr-qc].

[399] **Planck** Collaboration, P. A. R. Ade *et al.*, "Planck 2015 results. XIV. Dark energy and modified gravity," *Astron. Astrophys.* **594** (2016) A14, arXiv:1502.01590 [astro-ph.CO].

[400] E. Di Valentino, A. Melchiorri, and J. Silk, "Cosmological hints of modified gravity?," *Phys. Rev. D* **93** no. 2, (2016) 023513, arXiv:1509.07501 [astro-ph.CO].

[401] C.-A. Lin and M. Kilbinger, "Quantifying systematics from the shear inversion on weak-lensing peak counts," *Astron. Astrophys.* **614** (2018) A36, arXiv:1704.00258 [astro-ph.CO].

[402] R. A. Battye and A. Moss, "Evidence for Massive Neutrinos from Cosmic Microwave Background and Lensing Observations," *Phys. Rev. Lett.* **112** no. 5, (2014) 051303, arXiv:1308.5870 [astro-ph.CO].

[403] H. Böhringer and G. Chon, "Constraints on neutrino masses from the study of the nearby large-scale structure and galaxy cluster counts," *Mod. Phys. Lett. A* **31** no. 21, (2016) 1640008, arXiv:1610.02855 [astro-ph.CO].

[404] P. D. Meerburg, "Alleviating the tension at low ℓ through axion monodromy," *Phys. Rev. D* **90** no. 6, (2014) 063529, arXiv:1406.3243 [astro-ph.CO].

[405] M. M. Ivanov, E. McDonough, J. C. Hill, M. Simonović, M. W. Toomey, S. Alexander, and M. Zaldarriaga, "Constraining Early Dark Energy with Large-Scale Structure," arXiv:2006.11235 [astro-ph.CO].

[406] A. Klypin, V. Poulin, F. Prada, J. Primack, M. Kamionkowski, V. Avila-Reese, A. Rodriguez-Puebla, P. Behroozi, D. Hellinger, and T. L. Smith, "Clustering and Halo Abundances in Early Dark Energy Cosmological Models," arXiv:2006.14910 [astro-ph.CO].

[407] E. Di Valentino, C. Bøehm, E. Hivon, and F. R. Bouchet, "Reducing the H_0 and σ_8 tensions with Dark Matter-neutrino interactions," *Phys. Rev.* **D97** no. 4, (2018) 043513, arXiv:1710.02559 [astro-ph.CO].

[408] M. A. Buen-Abad, G. Marques-Tavares, and M. Schmaltz, "Non-Abelian dark matter and dark radiation," *Phys. Rev. D* **92** no. 2, (2015) 023531, arXiv:1505.03542 [hep-ph].

[409] D. Wang, "Can $f(R)$ gravity relieve H_0 and σ_8 tensions?," arXiv:2008.03966 [astro-ph.CO].

[410] A. Chudaykin, D. Gorbunov, and I. Tkachev, "Dark matter component decaying after recombination: Sensitivity to baryon acoustic oscillation and redshift space distortion probes," *Phys. Rev. D* **97** no. 8, (2018) 083508, arXiv:1711.06738 [astro-ph.CO].

[411] G. F. Abellan, R. Murgia, V. Poulin, and J. Lavalle, "Hints for decaying dark matter from S_8 measurements," arXiv:2008.09615 [astro-ph.CO].

[412] S. Heimersheim, N. Schöneberg, D. C. Hooper, and J. Lesgourgues, "Cannibalism hinders growth: Cannibal Dark Matter and the S_8 tension," arXiv:2008.08486 [astro-ph.CO].

[413] K. Jedamzik and L. Pogosian, "Relieving the Hubble tension with primordial magnetic fields," arXiv:2004.09487 [astro-ph.CO].

[414] K. Dutta, A. Roy, Ruchika, A. A. Sen, and M. Sheikh-Jabbari, "Cosmology with low-redshift observations: No signal for new physics," *Phys. Rev. D* **100** no. 10, (2019) 103501, arXiv:1908.07267 [astro-ph.CO].

[415] E. Di Valentino *et al.*, "Cosmology Intertwined I: Perspectives for the Next Decade," arXiv:2008.11283 [astro-ph.CO].

[416] E. Di Valentino *et al.*, "Cosmology Intertwined II: The Hubble Constant Tension," arXiv:2008.11284 [astro-ph.CO].

[417] E. Di Valentino *et al.*, "Cosmology Intertwined IV: The Age of the Universe and its Curvature," arXiv:2008.11286 [astro-ph.CO].

[418] E. Calabrese, A. Slosar, A. Melchiorri, G. F. Smoot, and O. Zahn, "Cosmic Microwave Weak lensing data as a test for the dark universe," *Phys. Rev.* **D77** (2008) 123531, arXiv:0803.2309 [astro-ph].

[419] **Planck** Collaboration, N. Aghanim *et al.*, "Planck 2018 results. VI. Cosmological parameters," arXiv:1807.06209 [astro-ph.CO].

[420] Z. Berezhiani, A. Dolgov, and I. Tkachev, "Reconciling Planck results with low redshift astronomical measurements," *Phys. Rev. D* **92** no. 6, (2015) 061303, arXiv:1505.03644 [astro-ph.CO].

[421] L. A. Anchordoqui, V. Barger, H. Goldberg, X. Huang, D. Marfatia, L. H. M. da Silva, and T. J. Weiler, "IceCube neutrinos, decaying dark matter, and the Hubble constant," *Phys. Rev. D* **92** no. 6, (2015) 061301, arXiv:1506.08788 [hep-ph]. [Erratum: Phys.Rev.D 94, 069901 (2016)].

[422] J. Solà Peracaula, A. Gómez-Valent, J. de Cruz Pérez, and C. Moreno-Pulido, "Brans–Dicke Gravity with a Cosmological Constant Smoothes Out ΛCDM Tensions," *Astrophys. J. Lett.* **886** no. 1, (2019) L6, arXiv:1909.02554 [astro-ph.CO].

[423] J. Solà, A. Gómez-Valent, J. de Cruz Pérez, and C. Moreno-Pulido, "Brans-Dicke cosmology with a Λ- term: a possible solution to ΛCDM tensions," arXiv:2006.04273 [astro-ph.CO].

[424] J. Solà, A. Gómez-Valent, and J. de Cruz Pérez, "Hints of dynamical vacuum energy in the expanding Universe," *Astrophys. J. Lett.* **811** (2015) L14, arXiv:1506.05793 [gr-qc].

[425] J. Solà, A. Gómez-Valent, and J. de Cruz Pérez, "Vacuum dynamics in the Universe versus a rigid Λ =const," *Int. J. Mod. Phys. A* **32** no. 19-20, (2017) 1730014, arXiv:1709.07451 [astro-ph.CO].

[426] J. Solà, A. Gómez-Valent, and J. de Cruz Pérez, "First evidence of running cosmic vacuum: challenging the concordance model," *Astrophys. J.* **836** no. 1, (2017) 43, arXiv:1602.02103 [astro-ph.CO].

[427] J. Solà Peracaula, J. de Cruz Pérez, and A. Gómez-Valent, "Possible signals of vacuum dynamics in the Universe," *Mon. Not. Roy. Astron. Soc.* **478** no. 4, (2018) 4357–4373, arXiv:1703.08218 [astro-ph.CO].

[428] J. Solà Peracaula, J. de Cruz Pérez, and A. Gómez-Valent, "Dynamical dark energy vs. Λ = const in light of observations," *EPL* **121** no. 3, (2018) 39001, arXiv:1606.00450 [gr-qc].

[429] C. Moreno-Pulido and J. Solà, "Running vacuum in quantum field theory in curved spacetime: renormalizing ρ_{vac} without $\sim m^4$ terms," *Eur. Phys. J. C* **80** no. 8, (2020) 692, arXiv:2005.03164 [gr-qc].

[430] W. Hu, D. J. Eisenstein and M. Tegmark, "Weighing neutrinos with galaxy surveys," Phys. Rev. Lett. **80** (1998), 5255-5258 doi:10.1103/PhysRevLett.80.5255, [arXiv:astro-ph/9712057 [astro-ph]]

[431] KamLAND, "Precision Measurement of Neutrino Oscillation Parameters with KamLAND", (2008), Physical Review Letters, 100, 221803

[432] Adamson P., et al., "Measurement of Neutrino Oscillations with the MINOS Detectors in the NuMI Beam", (2008), Phys. Rev. Lett., 101, 131802

[433] Turk M., 2008, in Proceedings of the 7th Python in Science Conference, Varoquaux G., Vaught T., Millman J., eds., Pasadena, CA USA, pp. 46 – 50

[434] Agarwal, S., Feldman, H. A. 2011. "The effect of massive neutrinos on the matter power spectrum". MNRAS 410, 1647–1654. doi:10.1111/j.1365-2966.2010.17546.x

[435] A.D. Dolgov, "NonGUT baryogenesis," Phys. Rept. **222** (1992) 309.

[436] A.D. Dolgov and Ya.B.Zeldovich, Uspekhi Fiz. Nauk, **130** (1980) 559; "Cosmology And Elementary Particles," Rev. Mod. Phys. **53** (1981) 1.

[437] J.A. Harvey and E.W. Kolb, "Grand Unified Theories And The Lepton Number Of The Universe," Phys. Rev. D **24** (1981) 2090.

[438] A.D. Linde, "Classical Yang-Mills Solutions, Condensation Of W Mesons And Symmetry Of Composition Of Superdense Matter," Phys. Lett. B **86** (1979) 39.

[439] H.E. Haber and H.A. Weldon, "Finite Temperature Symmetry Breaking As Bose-Einstein Condensation," Phys. Rev. D **25** (1982) 502.

[440] A. Riotto and G. Senjanović, "Supersymmetry and broken symmetries at high temperature," Phys. Rev. Lett. **79** (1997) 349 [hep-ph/9702319].

[441] J. Liu and G. Segre, "Baryon asymmetry of the universe and large lepton asymmetries," Phys. Lett. B **338** (1994) 259.

[442] B. Bajc, A. Riotto and G. Senjanović, "Large lepton number of the universe and the fate of topological defects," Phys. Rev. Lett. **81** (1998) 1355 [hep-ph/9710415].

[443] J. March-Russell, H. Murayama and A. Riotto, "The small observed baryon asymmetry from a large lepton asymmetry," JHEP **9911** (1999) 015 [hep-ph/9908396].

[444] A.D. Dolgov and D.P. Kirilova, J. Moscow Phys. Soc. **1** (1991) 217.

[445] I. Affleck and M. Dine, "A New Mechanism For Baryogenesis," Nucl. Phys. B **249** (1985) 361.

[446] A. Casas, W.Y. Cheng and G. Gelmini, "Generation of large lepton asymmetries," Nucl. Phys. B **538** (1999) 297 [hep-ph/9709289].

[447] J. McDonald, "Naturally large cosmological neutrino asymmetries in the MSSM," Phys. Rev. Lett. **84** (2000) 4798 [hep-ph/9908300].

[448] J. Madsen, "Bose condensates, big bang nucleosynthesis, and cosmological decay of a 17-keV neutrino," Phys. Rev. Lett. **69** (1992) 571.

[449] R. Foot, M.J. Thomson and R.R. Volkas, "Large neutrino asymmetries from neutrino oscillations," Phys. Rev. D **53** (1996) 5349 [hep-ph/9509327].

[450] A. D. Sakharov, "Violation of CP Invariance, C asymmetry, and baryon asymmetry of the universe," Pisma Zh. Eksp. Teor. Fiz. **5** (1967), 32-35, doi:10.1070/PU1991v034n05ABEH002497

[451] J. H. Christenson, J. W. Cronin, V. L. Fitch and R. Turlay, "Evidence for the 2π Decay of the K_2^0 Meson," Phys. Rev. Lett. **13** (1964), 138-140, doi:10.1103/PhysRevLett.13.138

[452] G. Jungman, M. Kamionkowski, A. Kosowsky, and D. N. Spergel, "*Cosmological parameter determination with microwave background maps*," Phys. Rev. **D54** (1996) 1332–1344, [astro-ph/9512139].

[453] **Planck** Collaboration, N. Aghanim *et al.*, "*Planck 2018 results. VI. Cosmological parameters*," [1807.06209].

[454] G. Mangano, G. Miele, S. Pastor, T. Pinto, O. Pisanti, and P. D. Serpico, "*Relic neutrino decoupling including flavor oscillations*," Nucl. Phys. **B729** (2005) 221–234, [hep-ph/0506164].

[455] E. Grohs, G. M. Fuller, C. T. Kishimoto, M. W. Paris, and A. Vlasenko, "*Neutrino energy transport in weak decoupling and big bang nucleosynthesis*," Phys. Rev. **D93** (2016) 083522, [1512.02205].

[456] P. F. de Salas and S. Pastor, "*Relic neutrino decoupling with flavour oscillations revisited*," JCAP **1607** (2016) 051, [1606.06986].

[457] K. N. Abazajian and M. Kaplinghat, "*Neutrino Physics from the Cosmic Microwave Background and Large-Scale Structure*," Ann. Rev. Nucl. Part. Sci. **66** no. 1, (2016) 401–420.

[458] K. Abazajian *et al.*, "*CMB-S4 Science Case, Reference Design, and Project Plan*," [1907.04473].

[459] D. Baumann, D. Green, and B. Wallisch, "*New Target for Cosmic Axion Searches*," Phys. Rev. Lett. **117** (2016) 171301, [1604.08614].

[460] S. L. Shapiro, S. A. Teukolsky, and I. Wasserman, "*Do Neutrino Rest Masses Affect Cosmological Helium Production?*," Phys. Rev. Lett. **45** (1980) 669–672.

[461] F. Antonelli, D. Fargion, and R. Konoplich, "*Right-handed Neutrino Interactions in the Early Universe*," Lett. Nuovo Cim. **32** (1981) 289.

[462] G. Steigman, K. A. Olive, and D. N. Schramm, "*Cosmological Constraints on Superweak Particles*," Phys. Rev. Lett. **43** (1979) 239–242.

[463] K. A. Olive, D. N. Schramm, and G. Steigman, "*Limits on New Superweakly Interacting Particles from Primordial Nucleosynthesis*," Nucl. Phys. **B180** (1981) 497–515.

[464] A. D. Dolgov and Ya. B. Zeldovich, "*Cosmology and Elementary Particles*," Rev. Mod. Phys. **53** (1981) 1–41.

[465] K. A. Olive, G. Steigman, and T. P. Walker, "*Primordial nucleosynthesis: Theory and observations*," Phys. Rept. **333** (2000) 389–407, [astro-ph/9905320].

[466] A. D. Dolgov, "*Neutrinos in cosmology*," Phys. Rept. **370** (2002) 333–535, [hep-ph/0202122].

[467] Z. Hou, R. Keisler, L. Knox, M. Millea, and C. Reichardt, "*How Massless Neutrinos Affect the Cosmic Microwave Background Damping Tail*," Phys. Rev. **D87** (2013) 083008, [1104.2333].

[468] B. Follin, L. Knox, M. Millea, and Z. Pan, "*First Detection of the Acoustic Oscillation Phase Shift Expected from the Cosmic Neutrino Background*," Phys. Rev. Lett. **115** (2015) 091301, [1503.07863].

[469] **SPT-3G** Collaboration, B. A. Benson *et al.*, "*SPT-3G: A Next-Generation Cosmic Microwave Background Polarization Experiment on the South Pole Telescope*," Proc. SPIE Int. Soc. Opt. Eng. **9153** (2014) 91531P, [1407.2973].

[470] **Simons Observatory** Collaboration, M. H. Abitbol *et al.*, "*The Simons Observatory: Astro2020 Decadal Project Whitepaper*," [1907.08284].

[471] P. F. de Salas, M. Lattanzi, G. Mangano, G. Miele, S. Pastor, and O. Pisanti, "*Bounds on very low reheating scenarios after Planck*," Phys. Rev. **D92** (2015) 123534, [1511.00672].

[472] R. J. Scherrer and M. S. Turner, "*Decaying Particles Do Not Heat Up the Universe*," Phys. Rev. **D31** (1985) 681.

[473] F. Bezrukov, H. Hettmansperger, and M. Lindner, "*keV sterile neutrino Dark Matter in gauge extensions of the Standard Model*," Phys. Rev. **D81** (2010) 085032, [0912.4415].

[474] M.-C. Chen, M. Ratz, and A. Trautner, "*Nonthermal cosmic neutrino background*," Phys. Rev. **D92** (2015) 123006, [1509.00481].

[475] J. Zhang and S. Zhou, "*Relic Right-handed Dirac Neutrinos and Implications for Detection of Cosmic Neutrino Background*," Nucl. Phys. **B903** (2016) 211–225, [1509.02274].

[476] G.-y. Huang and S. Zhou, "*Discriminating between thermal and nonthermal cosmic relic neutrinos through an annual modulation at PTOLEMY*," Phys. Rev. **D94** (2016) 116009, [1610.01347].

[477] **PTOLEMY** Collaboration, E. Baracchini *et al.*, "*PTOLEMY: A Proposal for Thermal Relic Detection of Massive Neutrinos and Directional Detection of MeV Dark Matter*," [1808.01892].

[478] F. del Aguila, S. Bar-Shalom, A. Soni, and J. Wudka, "*Heavy Majorana Neutrinos in the Effective Lagrangian Description: Application to Hadron Colliders*," Phys. Lett. **B670** (2009) 399–402, [0806.0876].

[479] A. Aparici, K. Kim, A. Santamaria, and J. Wudka, "*Right-handed neutrino magnetic moments*," Phys. Rev. **D80** (2009) 013010, [0904.3244].

[480] S. Bhattacharya and J. Wudka, "*Dimension-seven operators in the standard model with right handed neutrinos*," Phys. Rev. **D94** (2016) 055022, [1505.05264]. [Erratum: Phys. Rev. D95, 039904 (2017)].

[481] Y. Liao and X.-D. Ma, "*Operators up to Dimension Seven in Standard Model Effective Field Theory Extended with Sterile Neutrinos*," Phys. Rev. **D96** (2017) 015012, [1612.04527].

[482] I. Bischer and W. Rodejohann, "*General Neutrino Interactions from an Effective Field Theory Perspective*," Nucl. Phys. **B947** (2019) 114746, [1905.08699].

[483] J. Alcaide, S. Banerjee, M. Chala, and A. Titov, "*Probes of the Standard Model effective field theory extended with a right-handed neutrino*," JHEP **08** (2019) 031, [1905.11375].

[484] **KATRIN** Collaboration, M. Aker *et al.*, "*An improved upper limit on the neutrino mass from a direct kinematic method by KATRIN*," [1909.06048].

[485] **DESI** Collaboration, A. Aghamousa *et al.*, "*The DESI Experiment Part I: Science,Targeting, and Survey Design*," [1611.00036].

[486] T. Banks and N. Seiberg, "*Symmetries and Strings in Field Theory and Gravity*," Phys. Rev. **D83** (2011) 084019, [1011.5120].

[487] D. Feldman, P. Fileviez Perez, and P. Nath, "*R-parity Conservation via the Stueckelberg Mechanism: LHC and Dark Matter Signals*," JHEP **01** (2012) 038, [1109.2901].

[488] J. Heeck, "*Unbroken $B - L$ symmetry*," Phys. Lett. **B739** (2014) 256–262, [1408.6845].

[489] E. D. Carlson, "*Limits On A New $U(1)$ Coupling*," Nucl. Phys. **B286** (1987) 378–398.

[490] R. Harnik, J. Kopp, and P. A. N. Machado, "*Exploring nu Signals in Dark Matter Detectors*," JCAP **1207** (2012) 026, [1202.6073].

[491] P. Ilten, Y. Soreq, M. Williams, and W. Xue, "*Serendipity in dark photon searches*," JHEP **06** (2018) 004, [1801.04847].

[492] M. Bauer, P. Foldenauer, and J. Jaeckel, "*Hunting All the Hidden Photons*," JHEP **07** (2018) 094, [1803.05466].

[493] J. Heeck, "*Lepton Number Violation with and without Majorana Neutrinos*," in *Proceedings, 50th Rencontres de Moriond Electroweak Interactions and Unified Theories: La Thuile, Italy, March 14-21, 2015*, pp. 309–316. 2015. [1503.07708].

[494] J. Heeck and W. Rodejohann, "*Neutrinoless Quadruple Beta Decay*," EPL **103** (2013) 32001, [1306.0580].

[495] J. Heeck, "*Leptogenesis with Lepton-Number-Violating Dirac Neutrinos*," Phys. Rev. **D88** (2013) 076004, [1307.2241].

[496] V. Barger, P. Langacker, and H.-S. Lee, "*Primordial nucleosynthesis constraints on Z' properties*," Phys. Rev. **D67** (2003) 075009, [hep-ph/0302066].

[497] L. A. Anchordoqui and H. Goldberg, "*Neutrino cosmology after WMAP 7-Year data and LHC first Z' bounds*," Phys. Rev. Lett. **108** (2012) 081805, [1111.7264].

[498] L. A. Anchordoqui, H. Goldberg, and G. Steigman, "*Right-Handed Neutrinos as the Dark Radiation: Status and Forecasts for the LHC*," Phys. Lett. **B718** (2013) 1162–1165, [1211.0186].

[499] A. Solaguren-Beascoa and M. C. Gonzalez-Garcia, "*Dark Radiation Confronting LHC in Z' Models*," Phys. Lett. **B719** (2013) 121–125, [1210.6350].

[500] E. Masso and R. Toldra, "*Constraints on neutrino-neutrino interactions from primordial nucleosynthesis*," Phys. Lett. **B333** (1994) 132–134, [hep-ph/9404339].

[501] B. Ahlgren, T. Ohlsson, and S. Zhou, "*Comment on "Is Dark Matter with Long-Range Interactions a Solution to All Small-Scale Problems of Λ Cold Dark Matter Cosmology?"*," Phys. Rev. Lett. **111** (2013) 199001, [1309.0991].

[502] P. Fileviez Pérez, C. Murgui, and A. D. Plascencia, "*Neutrino-Dark Matter Connections in Gauge Theories*," Phys. Rev. **D100** (2019) 035041, [1905.06344].

[503] A. Berlin and N. Blinov, "*Thermal Dark Matter Below an MeV*," Phys. Rev. Lett. **120** (2018) 021801, [1706.07046].

[504] A. Berlin and N. Blinov, "*Thermal neutrino portal to sub-MeV dark matter*," Phys. Rev. **D99** (2019) 095030, [1807.04282].

[505] J. Redondo and G. Raffelt, "*Solar constraints on hidden photons re-visited*," JCAP **1308** (2013) 034, [1305.2920].

[506] **BaBar** Collaboration, J. P. Lees *et al.*, "*Search for a Dark Photon in e^+e^- Collisions at BaBar*," Phys. Rev. Lett. **113** (2014) 201801, [1406.2980].

[507] **LHCb** Collaboration, R. Aaij *et al.*, "*Search for Dark Photons Produced in 13 TeV pp Collisions*," Phys. Rev. Lett. **120** (2018) 061801, [1710.02867].

[508] **ATLAS** Collaboration, M. Aaboud *et al.*, "*Search for new high-mass phenomena in the dilepton final state using 36 fb^{-1} of proton-proton collision data at $\sqrt{s} = 13$ TeV with the ATLAS detector*," JHEP **10** (2017) 182, [1707.02424].

[509] M. Escudero, S. J. Witte, and N. Rius, "*The dispirited case of gauged $U(1)_{B-L}$ dark matter*," JHEP **08** (2018) 190, [1806.02823].

[510] S. Bilmis, I. Turan, T. M. Aliev, M. Deniz, L. Singh, and H. T. Wong, "*Constraints on Dark Photon from Neutrino-Electron Scattering Experiments*," Phys. Rev. **D92** (2015) 033009, [1502.07763].

[511] M. Lindner, F. S. Queiroz, W. Rodejohann, and X.-J. Xu, "*Neutrino-electron scattering: general constraints on Z' and dark photon models*," JHEP **05** (2018) 098, [1803.00060].

[512] J. D. Bjorken, R. Essig, P. Schuster, and N. Toro, "*New Fixed-Target Experiments to Search for Dark Gauge Forces*," Phys. Rev. **D80** (2009) 075018, [0906.0580].

[513] S. Andreas, C. Niebuhr, and A. Ringwald, "*New Limits on Hidden Photons from Past Electron Beam Dumps*," Phys. Rev. **D86** (2012) 095019, [1209.6083].

[514] J. Blümlein and J. Brunner, "*New Exclusion Limits on Dark Gauge Forces from Proton Bremsstrahlung in Beam-Dump Data*," Phys. Lett. **B731** (2014) 320–326, [1311.3870].

[515] J. H. Chang, R. Essig, and S. D. McDermott, "*Supernova 1987A Constraints on Sub-GeV Dark Sectors, Millicharged Particles, the QCD Axion, and an Axion-like Particle*," JHEP **09** (2018) 051, [1803.00993].

[516] M.-C. Chen, A. de Gouvea, and B. A. Dobrescu, "*Gauge Trimming of Neutrino Masses*," Phys. Rev. **D75** (2007) 055009, [hep-ph/0612017].

[517] P. D. Bolton, F. F. Deppisch, C. Hati, S. Patra, and U. Sarkar, "*Alternative formulation of left-right symmetry with $B - L$ conservation and purely Dirac neutrinos*," Phys. Rev. **D100** (2019) 035013, [1902.05802].

[518] G. Mangano and P. D. Serpico, Phys.Lett. **B701** (2011) 296–299, arXiv:1103.1261 [astro-ph.CO].

[519] G. Steigman, K. A. Olive, and D. Schramm, Phys.Rev.Lett. **43** (1979) 239–242.

[520] K. A. Olive, D. N. Schramm, and G. Steigman, Nucl.Phys. **B180** (1981) 497.

[521] V. Barger, P. Langacker, and H.-S. Lee, Phys.Rev. **D67** (2003) 075009, arXiv:hep-ph/0302066 [hep-ph].

[522] W. Rodejohann, Int.J.Mod.Phys. **E20** (2011) 1833–1930, arXiv:1106.1334 [hep-ph].

[523] K. Dick, M. Lindner, M. Ratz, and D. Wright, Phys.Rev.Lett. **84** (2000) 4039–4042, arXiv:hep-ph/9907562 [hep-ph].

[524] D. Feldman, P. Fileviez Perez, and P. Nath, JHEP **1201** (2012) 038, arXiv:1109.2901 [hep-ph].

[525] W.-Z. Feng and P. Nath, Phys.Lett. **B731** (2014) 43–50, arXiv:1312.1334 [hep-ph].

[526] T. Lee and C.-N. Yang, Phys.Rev. **98** (1955) 1501.

[527] L. Okun, Yad.Fiz. **10** (1969) 358–362.

[528] E. D. Carlson, Nucl.Phys. **B286** (1987) 378.

[529] **Particle Data Group**, J. Beringer *et al.*, Phys.Rev. **D86** (2012) 010001.

[530] M. Gonzalez-Garcia, M. Maltoni, J. Salvado, and T. Schwetz, JHEP **1212** (2012) 123, arXiv:1209.3023 [hep-ph]. Updated version from http://www.nu-fit.org.

[531] E. Stueckelberg, Helv.Phys.Acta **11** (1938) 225–244.

[532] G. 't Hooft, NATO Adv.Study Inst.Ser.B Phys. **59** (1980) 135.

[533] P. Galison and A. Manohar, Phys.Lett. **B136** (1984) 279.

[534] B. Holdom, Phys.Lett. **B166** (1986) 196.

[535] S. Tulin, Phys.Rev. **D89** (2014) 114008, arXiv:1404.4370 [hep-ph].

[536] B. Batell, M. Pospelov, and A. Ritz, Phys.Rev. **D79** (2009) 115008, arXiv:0903.0363 [hep-ph].

[537] A. E. Nelson and J. Scholtz, Phys.Rev. **D84** (2011) 103501, arXiv:1105.2812 [hep-ph].

[538] P. Arias, D. Cadamuro, M. Goodsell, J. Jaeckel, J. Redondo, *et al.*, JCAP **1206** (2012) 013, arXiv:1201.5902 [hep-ph].

[539] R. Harnik, J. Kopp, and P. A. Machado, JCAP **1207** (2012) 026, arXiv:1202.6073 [hep-ph].

[540] M. Williams, C. Burgess, A. Maharana, and F. Quevedo, JHEP **1108** (2011) 106, arXiv:1103.4556 [hep-ph].

[541] R. Essig, J. A. Jaros, W. Wester, P. H. Adrian, S. Andreas, *et al.*, arXiv:1311.0029 [hep-ph].

[542] J. Heeck and W. Rodejohann, Europhys.Lett. **103** (2013) 32001, arXiv:1306.0580 [hep-ph].

[543] J. Heeck, Phys.Rev. **D88** (2013) 076004, arXiv:1307.2241 [hep-ph].

[544] T. Wagner, S. Schlamminger, J. Gundlach, and E. Adelberger, Class.Quant.Grav. **29** (2012) 184002, arXiv:1207.2442 [gr-qc].

[545] E. Adelberger, J. Gundlach, B. Heckel, S. Hoedl, and S. Schlamminger, Prog.Part.Nucl.Phys. **62** (2009) 102–134.

[546] S.-Q. Yang, B.-F. Zhan, Q.-L. Wang, C.-G. Shao, L.-C. Tu, *et al.*, Phys.Rev.Lett. **108** (2012) 081101.

[547] M. Bordag, U. Mohideen, and V. Mostepanenko, Phys.Rept. **353** (2001) 1–205, arXiv:quant-ph/0106045 [quant-ph].

[548] R. Decca, D. Lopez, H. Chan, E. Fischbach, D. Krause, *et al.*, Phys.Rev.Lett. **94** (2005) 240401, arXiv:hep-ph/0502025 [hep-ph].

[549] A. Sushkov, W. Kim, D. Dalvit, and S. Lamoreaux, Phys.Rev.Lett. **107** (2011) 171101.

[550] Y. Pokotilovski, Phys.Atom.Nucl. **69** (2006) 924–931, arXiv:hep-ph/0601157 [hep-ph].

[551] V. Nesvizhevsky, G. Pignol, and K. Protasov, Phys.Rev. **D77** (2008) 034020, arXiv:0711.2298 [hep-ph].

[552] J. Redondo and G. Raffelt, JCAP **1308** (2013) 034, arXiv:1305.2920 [hep-ph].

[553] S. Davidson, S. Hannestad, and G. Raffelt, JHEP **0005** (2000) 003, arXiv:hep-ph/0001179 [hep-ph].

[554] H. K. Dreiner, J.-F. Fortin, J. Isern, and L. Ubaldi, Phys.Rev. **D88** (2013) 043517, arXiv:1303.7232 [hep-ph].

[555] J. B. Dent, F. Ferrer, and L. M. Krauss, arXiv:1201.2683 [astro-ph.CO].

[556] H. K. Dreiner, J.-F. Fortin, C. Hanhart, and L. Ubaldi, Phys.Rev. **D89** (2014) 105015, arXiv:1310.3826 [hep-ph].

[557] G. Raffelt and D. Seckel, Phys.Rev.Lett. **60** (1988) 1793.

[558] R. Barbieri and R. N. Mohapatra, Phys.Rev. **D39** (1989) 1229.

[559] J. Grifols and E. Masso, Nucl.Phys. **B331** (1990) 244.

[560] G. Bellini, J. Benziger, D. Bick, S. Bonetti, G. Bonfini, *et al.*, Phys.Rev.Lett. **107** (2011) 141302, arXiv:1104.1816 [hep-ex].

[561] C.-W. Chiang, G. Faisel, Y.-F. Lin, and J. Tandean, JHEP **1310** (2013) 150, arXiv:1204.6296 [hep-ph].

[562] R. Laha, B. Dasgupta, and J. F. Beacom, Phys.Rev. **D89** (2014) 093025, arXiv:1304.3460 [hep-ph].

[563] H.-S. Lee, arXiv:1408.4256 [hep-ph].

[564] **NuTeV Collaboration**, G. Zeller *et al.*, Phys.Rev.Lett. **88** (2002) 091802, arXiv:hep-ex/0110059 [hep-ex].

[565] F. Escrihuela, M. Tortola, J. Valle, and O. Miranda, Phys.Rev. **D83** (2011) 093002, arXiv:1103.1366 [hep-ph].

[566] S. Davidson, C. Pena-Garay, N. Rius, and A. Santamaria, JHEP **0303** (2003) 011, arXiv:hep-ph/0302093 [hep-ph].

[567] S. Andreas, C. Niebuhr, and A. Ringwald, Phys.Rev. **D86** (2012) 095019, arXiv:1209.6083 [hep-ph].

[568] J. D. Bjorken, R. Essig, P. Schuster, and N. Toro, Phys.Rev. **D80** (2009) 075018, arXiv:0906.0580 [hep-ph].

[569] **BaBar Collaboration**, J. Lees *et al.*, arXiv:1406.2980 [hep-ex].

[570] **APEX Collaboration**, S. Abrahamyan *et al.*, Phys.Rev.Lett. **107** (2011) 191804, arXiv:1108.2750 [hep-ex].

[571] H. Merkel, P. Achenbach, C. A. Gayoso, T. Beranek, J. Bericic, *et al.*, Phys.Rev.Lett. **112** (2014) 221802, arXiv:1404.5502 [hep-ex].

[572] G. Mangano and P. D. Serpico, Phys.Lett. **B701** (2011) 296–299, arXiv:1103.1261 [astro-ph.CO].

[573] G. Steigman, K. A. Olive, and D. Schramm, Phys.Rev.Lett. **43** (1979) 239–242.

[574] K. A. Olive, D. N. Schramm, and G. Steigman, Nucl.Phys. **B180** (1981) 497.

[575] V. Barger, P. Langacker, and H.-S. Lee, Phys.Rev. **D67** (2003) 075009, arXiv:hep-ph/0302066 [hep-ph].

[576] B. Ahlgren, T. Ohlsson, and S. Zhou, Phys.Rev.Lett. **111** (2013) 199001, arXiv:1309.0991 [hep-ph].

[577] L. A. Anchordoqui, H. Goldberg, and G. Steigman, Phys.Lett. **B718** (2013) 1162–1165, arXiv:1211.0186 [hep-ph].

[578] E. Masso and R. Toldra, Phys.Lett. **B333** (1994) 132–134, arXiv:hep-ph/9404339 [hep-ph].

[579] **ATLAS Collaboration**, G. Aad *et al.*, arXiv:1405.4123 [hep-ex].

[580] M. S. Carena, A. Daleo, B. A. Dobrescu, and T. M. Tait, Phys.Rev. **D70** (2004) 093009, arXiv:hep-ph/0408098 [hep-ph].

[581] **ALEPH, DELPHI, L3, OPAL, LEP Electroweak**, S. Schael *et al.*, Phys.Rept. **532** (2013) 119–244, arXiv:1302.3415 [hep-ex].

[582] G. Cacciapaglia, C. Csaki, G. Marandella, and A. Strumia, Phys.Rev. **D74** (2006) 033011, arXiv:hep-ph/0604111 [hep-ph].

[583] E. Salvioni, A. Strumia, G. Villadoro, and F. Zwirner, JHEP **1003** (2010) 010, arXiv:0911.1450 [hep-ph].

[584] X. Chu, Y. Mambrini, J. Quevillon, and B. Zaldivar, JCAP **1401** (2014) 034, arXiv:1306.4677 [hep-ph].

[585] E. Salvioni, G. Villadoro, and F. Zwirner, JHEP **0911** (2009) 068, arXiv:0909.1320 [hep-ph].

[586] Moresco M., Pozzetti L., Cimatti A., Jimenez R., Maraston C., Verde L., Thomas D., et al., 2016, JCAP, 2016, 014. doi:10.1088/1475-7516/2016/05/014

[587] Alam S., Ata M., Bailey S., Beutler F., Bizyaev D., Blazek J. A., Bolton A. S., et al., 2017, MNRAS, 470, 2617. doi:10.1093/mnras/stx721

[588] Zhao G.-B., Wang Y., Saito S., Gil-Marín H., Percival W. J., Wang D., Chuang C.-H., et al., 2019, MNRAS, 482, 3497. doi:10.1093/mnras/sty2845

[589] du Mas des Bourboux H., Rich J., Font-Ribera A., de Sainte Agathe V., Farr J., Etourneau T., Le Goff J.-M., et al., 2020, ApJ, 901, 153. doi:10.3847/1538-4357/abb085

[590] du Mas des Bourboux H., Le Goff J.-M., Blomqvist M., Busca N. G., Guy J., Rich J., Yèche C., et al., 2017, A&A, 608, A130. doi:10.1051/0004-6361/201731731

[591] Scolnic D. M., Jones D. O., Rest A., Pan Y. C., Chornock R., Foley R. J., Huber M. E., et al., 2018, ApJ, 859, 101. doi:10.3847/1538-4357/aab9bb

[592] Riess A. G., Rodney S. A., Scolnic D. M., Shafer D. L., Strolger L.-G., Ferguson H. C., Postman M., et al., 2018, ApJ, 853, 126. doi:10.3847/1538-4357/aaa5a9

[593] Haridasu B. S., Lukovi ć V. V., Moresco M., Vittorio N., 2018, JCAP, 2018, 015. doi:10.1088/1475-7516/2018/10/015

[594] Mathews G. J., Kusakabe M., Kajino T., 2017, IJMPE, 26, 1741001. doi:10.1142/S0218301317410014

[595] Lees J. P., Poireau V., Tisserand V., Grauges E., Palano A., Eigen G., Stugu B., et al., 2014, PhRvL, 113, 201801. doi:10.1103/PhysRevLett.113.201801

[596] Cocco A. G., Mangano G., Messina M., 2008, JPhCS, 120, 022005. doi:10.1088/1742-6596/120/2/022005

[597] Yoshimura M., Sasao N., Tanaka M., 2015, PhRvD, 91, 063516. doi:10.1103/PhysRevD.91.063516

[598] Akhmedov E., 2019, JCAP, 2019, 031. doi:10.1088/1475-7516/2019/09/031

[599] Borsanyi, S. et al., Calculation of the axion mass based on high-temperature lattice quantum chromodynamics. 2016, Nature, 539, 69, arXiv:1606.07494.

[600] Saikawa, K. & Shirai, S., Primordial gravitational waves, precisely: The role of thermodynamics in the Standard Model. 2018, JCAP, 1805, 035, arXiv:1803.01038.

[601] Baumann, D., Green, D., & Wallisch, B., Searching for light relics with large-scale structure. 2018, JCAP, 1808, 029, arXiv:1712.08067.

[602] Planck Collaboration, Aghanim N., Akrami Y., Ashdown M., Aumont J., Baccigalupi C., Ballardini M., et al., 2020, A&A, 641, A6. doi:10.1051/0004-6361/201833910